TRANSPORTATION RESEARCH

RECORD

No. 1492

Materials and Construction

Hot-Mix Asphalt Design, Testing, Evaluation, and Performance

A peer-reviewed publication of the Transportation Research Board

TRANSPORTATION RESEARCH BOARD
NATIONAL RESEARCH COUNCIL

NATIONAL ACADEMY PRESS
WASHINGTON, D.C. 1995

Transportation Research Record 1492
ISSN 0361-1981
ISBN 0-309-06156-3
Price: $45.00

Subscriber Category
IIIB materials and construction

Printed in the United States of America

Sponsorship of Transportation Research Record 1492

GROUP 2—DESIGN AND CONSTRUCTION OF TRANSPORTATION FACILITIES
Chairman: Michael G. Katona, U.S. Air Force Armstrong Lab

Section on Bituminous
Chairman: Harold R. Paul, Louisiana Transportation Research Center

Committee on Characteristics of Nonbituminous Components of Bituminous Paving Mixtures
Chairman: Gale C. Page, Florida Department of Transportation
Secretary: H. Barry Takallou, TAK Consulting Engineers
Rod Birdsall, Joe W. Button, Douglas M. Colwill, Ervin L. Dukatz, Jr., Frank Fee, John M. Heggen, Lon S. Ingram, Ilan Ishai, Prithvi S. Kandhal, N. Paul Khosla, Kang-Won Wayne Lee, Kamyar C. Mahboub, Roger P. Northwood, John W. H. Oliver, Roger C. Olson, J. Claine Petersen, Michael W. Rouse, Russell H. Schnormeier, Scott Shuler, Anne Stonex, Ronald L. Terrel, Jack L. Van Kirk

Committee on Characteristics of Bituminous Paving Mixtures To Meet Structural Requirements
Chairman: Dallas N. Little, Texas A&M University
Dale S. Decker, Amy Epps, Kenneth W. Fults, Jim Gee, Lawrence E. Hart, Richard J. Holmgreen, Jr., Darrel V. Holmquist, Vincent C. Janoo, Y. Richard Kim, Rita B. Leahy, Kang-Won Wayne Lee, Jean-Marie Machet, Kamyar C. Mahboub, Michael S. Mamlouk, Louay N. Mohammad, Reynaldo Roque, Patrick Shields, Jack E. Stephens, Anthony Frederick Stock, Mary Stroup-Gardiner, Walter J. Tappeiner, Harold L. Von Quintus, James P. Walter, Gary C. Whited, John S. Youtcheff

Committee on General Asphalt Problems
Chairman: Byron E. Ruth, University of Florida
Secretary: Richard E. Root, Chicago Testing Laboratory, Inc.
J. Don Brock, Thomas C. Claret, Campbell Crawford, Dale S. Decker, Denis E. Donnelly, Jon A. Epps, Fred M. Fehsenfeld, Dan Flowers, Douglas A. Forstie, James G. Gehler, John E. Huffman, Thomas W. Kennedy, Raymond D. Pavlovich, Roger Pemberton, James A. Scherocman, Lawrence L. Smith, April J. Swanson, A. Haleem Tahir, Jack D. Telford

Transportation Research Board Staff
Robert E. Spicher, Director, Technical Activities
Frederick D. Hejl, Engineer of Materials and Construction
Nancy A. Ackerman, Director, Reports and Editorial Services
Naomi Kassabian, Associate Editor

Sponsorship is indicated by a footnote at the end of each paper. The organizational units, officers, and members are as of December 31, 1994.

Transportation Research Record 1492

Contents

Foreword vii

Effect of Coarse Aggregate Content on Stone Matrix Asphalt Rutting and Draindown 1
Walaa S. Mogawer and Kevin D. Stuart

Determination of Compactive Effort to Duplicate Pavement Voids for Corps of Engineers Gyratory Testing Machine 12
G. W. Maupin, Jr.

Development of Rolling Compaction Machine for Preparation of Asphalt Beam Samples 18
James S. Lai and Haroon Shami

Effect of Coarse Aggregate Content on Stone Matrix Asphalt Durability and Low-Temperature Cracking 26
Kevin D. Stuart and Walaa S. Mogawer

Development and Analysis of Laboratory Techniques for Simulating Segregation 36
Taisir S. Khedaywi and Thomas D. White

Performance Prediction for Large-Stone Mixes Using the Repetitive Simple Shear Test at Constant Height 46
John Harvey, Jorge B. Sousa, and William Crockford

Application of Digital Image Processing to Quantitative Study of Asphalt Concrete Microstructure 53
Zhong Qi Yue, William Bekking, and Isabelle Morin

Effect of Moisture Content on Measured Properties of Asphalt Mixtures 61
T. F. Fwa and C. B. Oh
DISCUSSION, *Charles MacKean*, 68
AUTHORS' CLOSURE, 69

Moisture Sensitivity Evaluation of Binder-Aggregate Mixtures 71
Shakir Shatnawi, Mahesh Nagarajaiah and John Harvey

Effects of Moisture on Surface Chemistry of Steel Slags and Steel Slag–Asphalt Paving Mixes 85
A. Coomarasamy and T. L. Walzak

Resilient Modulus Properties of Asphalt Rubber Mixes from Field Demonstration Projects in Maryland 96
M. Ayres, Jr., and M. W. Witczak

Characterization of Emulsion Aggregate Mixtures 108
John R. Anderson and Marshall R. Thompson

Laboratory Determination of Thermal Properties of Asphalt Mixtures by Transient Heat Conduction Method 118
T. F. Fwa, B. H. Low, and S. A. Tan

Fatigue Behavior of Styrene-Butadiene-Styrene Modified Asphaltic Mixtures Exposed to Low-Temperature Cyclic Aging 129
A. Othman, L. Figueroa, and H. Aglan

Comparison of Axial and Diametral Resilient Stiffness of Asphalt-Aggregate Mixes 135
Akhtarhusein A. Tayebali, John A. Deacon, and Carl L. Monismith

Tensile Versus Compressive Moduli of Asphalt Concrete 144
Punya P. Khanal and Michael S. Mamlouk

Comparison of Mix Design Concepts 151
Jorge B. Sousa, George Way, John T. Harvey, and Mickey Hines

Comparison of Marshall and Superpave Level I Mix Design for Asphalt Mixes 161
Ihab H. Hafez and Matthew W. Witczak

Correlation of Superpave $G^*/\sin\delta$ with Rutting Susceptibility from Laboratory Mixture Tests 176
Kevin D. Stuart and Richard P. Izzo
DISCUSSION, *John L. McRae,* 183
AUTHORS' CLOSURE, 183

Mix Design Methodology for a Warrantied Pavement: Case Study 184
J. Harvey, B. A. Vallerga, and C. L. Monismith

Evaluation of Hamburg Wheel-Tracking Device to Predict Moisture Damage in Hot-Mix Asphalt 193
Tim Aschenbrener

Development and Use of Georgia Loaded Wheel Tester 202
Ronald Collins, Donald Watson, and Bruce Campbell

Evaluation of Stone-on-Stone Contact in Stone-Matrix Asphalt 208
E. R. Brown and Rajib Basu Mallick

Foreword

The papers in this volume, which deal with various facets of asphalt concrete mixtures, should be of interest to engineers involved in state and local construction, design, materials, maintenance, and research, as well as contractors and materials manufacturers. The effect of compaction, segregation, and coarse aggregate properties on the performance of hot-mix asphalt is addressed. Other topics include the application of digital image processing to a quantitative study of asphalt concrete microstructure, moisture and thermal effects on the performance of hot-mix asphalt, and evaluation of fatigue, rutting, and modulus properties on hot-mix asphalt. A case study on the mix design methodology for a warrantied pavement is presented. The final topic covered is improved performance of hot-mix asphalt through new testing methods.

Effect of Coarse Aggregate Content on Stone Matrix Asphalt Rutting and Draindown

WALAA S. MOGAWER AND KEVIN D. STUART

The stone matrix asphalt (SMA) technical working group (TWG), composed of federal, state, and industry representatives, was formed in 1992. The SMA TWG developed the *SMA Model Material and Construction Guidelines*. The model suggests using 20 to 28 percent passing the 4.75-mm sieve size. The effects of coarse aggregate content on the performance and draindown characteristics of SMA mixtures was evaluated. Performance was evaluated in terms of rutting using three wheel-tracking devices: the French pavement rutting tester, the Georgia loaded-wheel tester, and the German Hamburg wheel-tracking device. Draindown was evaluated using four tests: the German draindown test, the FHWA draindown test for open-graded friction courses, a proposed draindown test developed in the Bituminous Mixtures Laboratory at the Turner-Fairbank Highway Research Center, and the National Center for Asphalt Technology draindown test. Also, the effects of using a polymer instead of a fiber as the stabilizer in the SMA mixtures were examined. Data from the draindown tests and wheel-tracking devices showed that decreasing the coarse aggregate content reduced the amount of draindown without affecting the mixture performance in terms of rutting. When using a polymer instead of a fiber, the amount of mastic that drained down increased. On the basis of the Georgia loaded-wheel tester and the Hamburg wheel-tracking device, mixtures with the polymer had significantly lower rut depths than the mixtures with fiber. On the basis of the French pavement rutting tester, mixtures with the polymer had significantly lower rates of rutting (slopes) than mixtures with the fiber, but the rut depths at the end of the test were not statistically different.

Stone matrix asphalt (SMA) is a gap-graded hot mixture that maximizes the binder and coarse aggregate contents. SMA mixtures have high proportions of coarse aggregate, binder, and mineral filler, and low proportions of middle-size aggregates compared with dense-graded mixtures. Cellulose fibers, mineral fibers, and polymers have been used as stabilizing additives to prevent draindown of the mastic before the SMA is placed and is allowed to cool (*1*).

SMA was developed in Europe more than 20 years ago. SMA mixtures in Europe have been shown through field experience to be durable and more resistant to rutting than dense-graded mixtures. More than 50 SMA pavements have been built in the United States, and additional projects have been proposed.

An SMA technical working group (TWG) composed of federal, state, and industry representatives was formed in 1992. The group assists in analyzing SMA technology and coordinating the dissemination of SMA-related information. The SMA TWG developed the *SMA Model Material and Construction Guidelines* (2). This model includes mixture, coarse and fine aggregate, stabilizer, and binder requirements for SMA mixtures. For coarse aggregates, the model suggests using 20 to 28 percent passing the 4.75-mm sieve. The model limits the 4.75-mm size fraction to a maximum of 20 percent of particles having greater than a 3:1 length-to-thickness ratio and a maximum of 5 percent of particles having greater than a 5:1 length-to-thickness ratio. The model recommends that the Los Angeles (L.A.) abrasion weight loss of the aggregate should be a maximum of 30 percent. The model also advocates the use of an aggregate with a maximum water absorption of 2 percent. Decreasing the coarse aggregate content by increasing the suggested upper limit will reduce the amount of draindown mastic in SMA mixtures. However, the effect on SMA performances of decreasing the coarse aggregate content needs to be evaluated.

W. S. Mogawer, Civil Engineering Department, University of Massachusetts Dartmouth, North Dartmouth, Mass. 02747. K. D. Stuart, FHWA, Turner-Fairbank Highway Research Center, 6300 Georgetown Pike, McLean, Va. 22101-2296.

OBJECTIVE

This paper documents Phase I of an FHWA study in which the effects of coarse aggregate content on the properties of SMA mixtures were determined. The objective of this phase was to determine the effect of coarse aggregate content on SMA draindown and performance in terms of rutting.

EXPERIMENTAL PROGRAM

To achieve the objective of this study, 12 SMA mixtures were tested. Two aggregates, three gradations, and two stabilizers were used.

Stabilizers

The two stabilizers were a cellulose fiber, Interfibe 230, and a polymer, Styrelf 1-D. The Interfibe was added at 0.3 percent by mixture mass, based on the recommendations of the supplier. Styrelf is an asphalt modified by the supplier with polymer and received in bulk form (*3*).

Asphalt

The asphalt used for preparing the mixtures with Interfibe was AC-20. This asphalt was used in Strategic Highway Research Program (SHRP) studies and was designated "ABC." The properties of AC-20 and Styrelf are presented in Table 1. Styrelf was significantly

TABLE 1 Physical Properties of the Binders

	Virgin Binder	Binder After Thin-Film Oven Test
AC-20 Binder (FHWA Code: B6090)		
Thin-Film Oven Test, percent loss		0.07
Penetration, 25 C (100g, 5s), 0.1 mm	87	60
Absolute Viscosity, 60C, dPa-s	2 042	4 349
Kinematic Viscosity, 135C, mm^2/s	480	660
Specific Gravity, 25/25C	1.038	
Solubility in Trichloroethyline, %	99.99	
Inorganic Material or Ash, percent	0.06	
Flash Point, COC, C	2.88	
	Styrelf Binder (FHWA Code: B-6096)	
Thin-Film Oven Test, percent loss		0.13
Penetration, 25 C (100g, 5s), 0.1 mm	51	39
Absolute Viscosity, 60C, dPa-s	40 958	126 826
Kinematic Viscosity, 135C, $\mu m^2/s$	2 260	3 463
Specific Gravity, 25/25C	1.026	
Solubility in Trichloroethyline, %	99.92	
Inorganic Material or Ash, percent	0.12	
Flash Point, COC, C	271	

stiffer than the AC-20 asphalt, according to capillary viscosities and penetration. The supplier modified a different AC-20 asphalt in formulating the Styrelf binder. (Note: The absolute viscosities of the Styrelf binder may not be correct. ASTM D2171 is valid for Newtonian flow, but many modified binders exhibit non-Newtonian flow at 60°C. The industry currently recommends ASTM D4957 for modified binders, but FHWA did not have the viscometer needed for the test.)

Aggregates

Crushed diabase and limestone aggregates were used in this study. The diabase was used in constructing dense-graded pavement sections tested by the accelerated loading facility at the Turner-Fairbank Highway Research Center (TFHRC). The limestone was used in the SHRP studies and was designated "RC." Aggregate properties are presented in Table 2.

Three different aggregate gradations were used. The gradations were designed to meet the SMA TWG aggregate gradation requirements and the German specifications, except for the percentages of material passing the 4.75- and 2.36-mm sieves. The three gradations were designated Gradations I, II, and III. The percent passing all sieves greater than 4.75 mm and smaller than 2.36 mm were equal for the three gradations. Gradations I, II, and III consisted of 80, 70, and 60 percent retained on the 4.75-mm sieve, respectively. The aggregate gradations are presented in Table 2 and illustrated in Figure 1.

The percent L.A. abrasion weight loss for the coarse fraction of the limestone was above the maximum percent recommended by the SMA TWG. The diabase aggregate satisfied the recommendation. Aggregates with different weight losses were included in this study to determine whether weight loss affects mixture performance.

The percent water absorptions for the three diabase gradations were below the recommended maximum of 2 percent; they were slightly greater than 1 percent. The percent water absorptions for the three limestone gradations ranged from 2.56 to 2.88 percent. This indicated that the limestone SMA mixtures would have high binder absorptions. The ramifications of not meeting the absorption specification are unknown, except that specified minimum binder contents for SMA mixtures based on mass will be easier to meet. Minimum binder contents should be based on volume. This specification was adopted from European practice, in which most aggregates have low water absorptions and absorption is a minor concern.

The percentage of aggregate particles having greater than 3:1 and 5:1 length-to-thickness, width-to-thickness, or length-to-width ratios were measured by mass and by number using 100 particles for each coarse aggregate size. The results are presented in Tables 3 and 4. The diabase aggregate did not meet the SMA TWG recommendations for flat and elongated particles in the coarse aggregate. Assuming that the recommendations are valid, there may be some breaking of the diabase aggregate particles in the hot-mixture plant or under traffic. The limestone aggregate met the recommendations.

Mixture Design

Marshall mix designs were performed to determine the optimum asphalt contents (OACs). The mixtures were designed to sustain

TABLE 2 Aggregate Properties

Sieve Size, mm	Gradation, Percent Passing I	II	III	SMA Model Specification	Based on German Spec (FHWA-RD-92-006)
19.0	100.0	100.0	100.0	100.0	100.0
12.5	95.0	95.0	95.0	85-95	90-100
9.5	68.0	68.0	68.0	75 (maximum)	34-75
4.75	20.0	30.0	40.0	20-28	23-41
2.36	17.0	22.0	26.0	16-24	18-20
1.18	16.0	16.0	16.0		15-24
0.600	14.0	14.0	14.0	12-16	12-20
0.300	12.0	12.0	12.0	12-15	10-17
0.150	10.0	10.0	10.0		9-14
0.075	9.0	9.0	9.0	8-10	8-13

	Diabase Gradation			Limestone Gradation		
	I	II	III	I	II	III
Bulk Dry Sp. Gr.	2.827	2.823	2.843	2.506	2.513	2.526
Bulk SSD Sp. Gr.	2.861	2.865	2.873	2.578	2.586	2.591
Apparent Sp. Gr.	2.916	2.885	2.932	2.701	2.709	2.701
Percent Absorption	1.16	1.17	1.07	2.88	2.88	2.56

L.A. Abrasion of the Particles in the Predominate Size Fractions Above the 2.36-mm Sieve, Percent Weight Loss:

Diabase = 17.8
Limestone = 35.4

SSD: Saturated-surface dry.

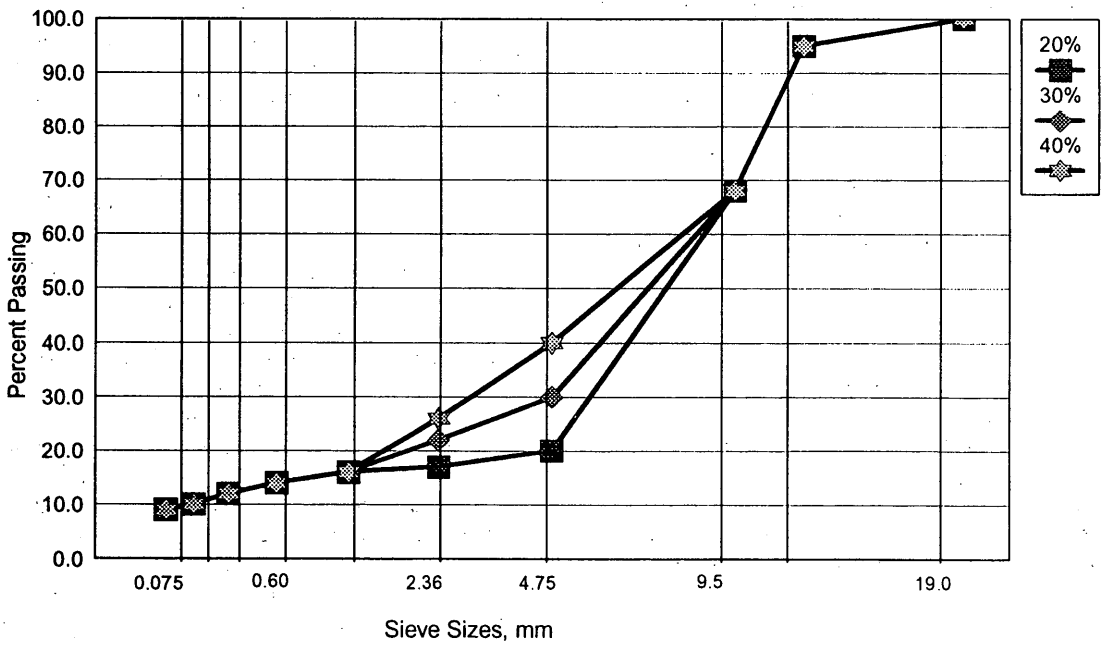

FIGURE 1 Aggregate gradations.

TABLE 3 Percent Flat and Elongated Particles

		Length to Thickness 5:1 By Mass	5:1 By Number	3:1 By Mass	3:1 By Number
Diabase	3/4 to 1/2	0.8	1	11.7	14
	1/2 to 3/8	2.3	4	25.3	28
	3/8 to #4	3.6	5	42.3	41
Limestone	3/4 to 1/2	0.0	0	11.9	14
	1/2 to 3/8	0.7	1	12.2	16
	3/8 to #4	5.3	8	23.8	29
		Width to Thickness (Flat)			
Diabase	3/4 to 1/2	0.0	0	2.0	3
	1/2 to 3/8	0.4	1	2.9	6
	3/8 to #4	0.0	0	4.5	6
Limestone	3/4 to 1/2	0.0	0	0.3	1
	1/2 to 3/8	0.0	0	1.7	3
	3/8 to #4	0.0	0	3.0	7
		Length to Width (Elongated)			
Diabase	3/4 to 1/2	0.0	0	0.0	0
	1/2 to 3/8	0.0	0	1.4	1
	3/8 to #4	0.0	0	1.3	1
Limestone	3/4 to 1/2	0.0	0	0.0	0
	1/2 to 3/8	0.0	0	0.0	0
	3/8 to #4	0.0	0	0.8	1

Note: Based on samples of 100 particles.

heavy traffic. SMA mixtures are designed in Europe for heavy traffic using 50 blows (*1*). Hence, the mixtures were compacted using 50 blows. The design air void content was 3.5 percent. The target mixing and compaction temperatures were 154°C and 143°C, respectively. Using three gradations (Gradations I, II, and III), two aggregates (diabase and limestone), and two stabilizers (Interfibe and Styrelf), 12 SMA mixtures were prepared.

The Styrelf mixture with diabase using Gradation I was eliminated from the rutting evaluation because of excessive draindown.

Draindown

The German draindown test, the FHWA draindown test for open-graded friction courses (OGFC), the 2.36-mm sieve draindown test developed in the Bituminous Mixtures Laboratory at TFHRC, and the National Center for Asphalt Technology (NCAT) draindown test were included in this study. These tests were performed to determine the effect of decreasing coarse aggregate content on draindown of the mastic, as well as the efficiency of the two stabilizers in preventing draindown.

In the German draindown test, 1 kg of mixture is prepared at the mixing temperature. The mixture is then placed into a tared, dried 800-mL glass beaker and weighed to the nearest 0.1 g. The beaker is then covered and stored for 60 min at 170°C. After storage, the mixture is removed from the beaker and placed in a tared bowl by quickly turning the beaker upside down without shaking. The final mass of the mixture is then measured and the percent draindown is calculated as

$$\text{Loss (percent)} = \frac{100\ (\text{initial sample mass} - \text{final sample mass})}{\text{initial sample mass}} \quad (1)$$

The storage temperature used in Germany is the hot-mix discharge temperature, which is much higher than temperatures used in the United States. Hence, the procedure was modified so that the compaction temperature of 143°C was used instead of 170°C.

The FHWA OGFC draindown test uses a clear Pyrex pie plate with a diameter of 203.2–228.6 mm. The mixture is placed on the Pyrex pie plate. The mixture and the plate are stored for 60 ± 1 min at 143°C. The degree of draindown is determined by comparing the amount of drained binder (viewed through the bottom of the plate) to five standard pictures having a scale of 1 to 5, representing no draindown to excessive drainage.

In the 2.36-mm sieve draindown test, a dried mixing bowl is weighed to the nearest 0.1 g. A dried 2.36-mm sieve of similar diameter is placed on top of the bowl, and 1 kg of asphalt mixture is placed on the 2.36-mm sieve immediately after mixing. The bowl,

TABLE 4 Flat and Elongated "Weighted Average" Based on Mass

Aggregate Type	Aggregate Gradation	Length to Thickness 5:1	Length to Thickness 3:1
Diabase	I	3.0	34.7
	II	2.9	33.5
	III	2.8	32.2
Limestone	I	3.4	19.1
	II	3.1	18.4
	III	2.8	17.6
		Width to Thickness	
Diabase	I	0.14	3.8
	II	0.15	3.7
	III	0.18	3.6
Limestone	I	0.00	2.4
	II	0.00	2.3
	III	0.00	2.2
		Length to Width	
Diabase	I	0.00	1.3
	II	0.00	1.2
	III	0.00	1.2
Limestone	I	0.00	0.5
	II	0.00	0.4
	III	0.00	0.4

sieve, and mixture are then covered with aluminum foil and stored for 60 ± 1 min at 143°C. After storage, the sieve is removed and the final mass of the bowl is obtained. The percent loss due to draindown is calculated as:

$$\text{Loss (percent)} = \frac{100\ (\text{final bowl mass} - \text{initial bowl mass})}{\text{initial sample mass}} \quad (2)$$

In the NCAT draindown test, the sample is placed in a wire basket that is positioned on a preweighed dry paper plate. The sample, basket, and plate are placed in a forced-air oven for 60 min at 143°C. After 60 min, the basket containing the sample is removed from the oven along with the paper plate, and the paper plate is weighed to determine the amount of draindown that occurred. The percent loss due to draindown is calculated as follows:

$$\text{Loss (percent)} = \frac{100\ (\text{final paper mass} - \text{initial paper mass})}{\text{initial sample mass}} \quad (3)$$

When this test was being performed, some particles of the mixture fell through the basket onto the paper plate. Those particles were put back into the basket before the basket was placed in the oven.

The SMA TWG recommendation of a maximum mass loss of 0.3 percent was applied to the German test, 2.36-mm sieve test, and the NCAT draindown test.

Rutting Evaluation

The French Laboratories des Ponts et Chaussees's pavement rutting tester, the Georgia loaded-wheel tester (GLWT), and the Hamburg wheel-tracking device were used to measure the rutting resistances of the mixtures.

French Pavement Rutting Tester

The French pavement rutting tester tests slabs with dimensions of 500 × 180 × 50 mm using a smooth, reciprocating, pneumatic rubber tire at 0.61 MPa and loading of 5,000 ± 50 N. The tire is 415 mm in diameter and 109 mm wide. A hydraulic jack under the slab pushes the slab upward to create the load. The machine has two reciprocating tire assemblies and tests two slabs at a time.

The slabs were fabricated using the French plate compactor. The compaction effort used in this study should provide an air void level close to the low end of the air void range that can be obtained in the field after compaction by the rollers (*3*). After the slabs were fabricated, they were cured at room temperature for 2 days. Two slabs were fabricated at the OAC for each mixture.

An initial densification of 1,000 cycles at 25°C is first applied. A cycle is two passes of the tire. The thicknesses of the slabs are measured at the end of the initial densification. These readings are con-

sidered the zero readings. The slabs are then heated to the test temperature of 60°C for 3 hr before the test begins. For a 50-mm-thick slab, the test is performed to 3,000 cycles, and the average rut depths at 30, 100, 300, 1,000, and 3,000 cycles are measured. If the average rut depth at 3,000 cycles is more than 20 percent of the slab thickness, then the mixture is considered a failure and the test is stopped (*4*). To measure the average rut depth, the machine is stopped and 15 measurements on the slab are taken—five locations along the length and three locations along the width. Slopes for different mixtures taken from log rut depth versus log cycle plots can also be compared. Rut-susceptible mixtures generally have higher slopes.

For all the SMA mixtures tested, the average percent rut depth was less than 20 percent of the slab thickness at 3,000 cycles. Therefore, it was decided to extend the test to 10,000 cycles.

Georgia Loaded-Wheel Tester

The GLWT tests a beam with dimensions 381 × 76.2 × 76.2 mm for rutting at 40.6°C. The beams are prepared by compression. Densities within 97 percent of the Marshall design density are recommended (*5*). To achieve the recommended density, a 444.8-kN load was applied and released four times rapidly and then reapplied for 6 min.

Before testing, the beams were cured for 7 days at room temperature, then cured for 24 hr at 40.6°C. After curing, each beam was loaded into the testing frame of the GLWT and initial readings were taken at the center, 50.8 mm left of center, and 50.8 mm right of center across the length of the beam. A rubber hose inflated to 0.69 MPa is positioned across the sample and a loaded wheel runs back and forth on the top of the rubber hose. When the wheel moves from right to left, the load is approximately 740 N at the center of the beam, while it is 630 N when moving left to right. The test was performed for 8,000 cycles. One cycle is defined as two passes of the wheel. Final readings were taken at the same positions as the initial readings . If the average rut depth exceeds 7.6 mm, the mixture is considered to have failed (*5*). Two beams were fabricated at the OAC for each mixture.

Hamburg Wheel-Tracking Device

The Hamburg wheel-tracking device was used to test slabs that have dimensions of 320 × 260 × 80 mm, using a smooth, reciprocating solid steel wheel. The wheel has a diameter of 203.5 mm and a width of 47.0 mm. The load is 710 N. Slabs are submerged and tested in water at 50°C. The machine has two steel wheel assemblies and tests two slabs simultaneously. The slabs were fabricated using a steel wheel roller. The slabs were cured at room temperature for 2 days. After curing, the slabs were placed in the device, and the device was filled with water until the slabs were completely immersed. When the water temperature reached 50°C, the slabs stayed immersed for 45 min before the test was performed. The machine is automated and records the deformation after each cycle. The test is performed for 20,000 passes (10,000 cycles).

The data analysis from the Hamburg wheel-tracking device includes the post-compaction consolidation, creep slope, stripping inflection point, and stripping slope as shown in Figure 2 (*6*). The post-compaction consolidation is the deformation at 1,000 passes. It is known as post-compaction consolidation because the wheel is assumed to be compacting the mixture within the 1,000 passes. The creep slope is (a) a measure of accumulation of permanent deformation caused primarily by mechanisms other than moisture damage, (b) the inverse of the rate of deformation in the linear region of the curve after post-consolidation has ended and before the stripping inflection point, and (c) the number of passes required to create a 1-mm rut depth. The stripping inflection point is the number of passes at the intersection of the creep slope and the stripping slope. It is the number of passes required to initiate stripping. The stripping slope is (a) a measure of the accumulation of permanent deformation due primarily to moisture damage, (b) the inverse of the rate of deformation after the stripping inflection point, and (c) the number of passes required to create a 1-mm rut depth from stripping (*7*).

In this study, the creep slope was measured to compare mixtures in terms of their rutting susceptibility. A higher creep slope indicates less rutting.

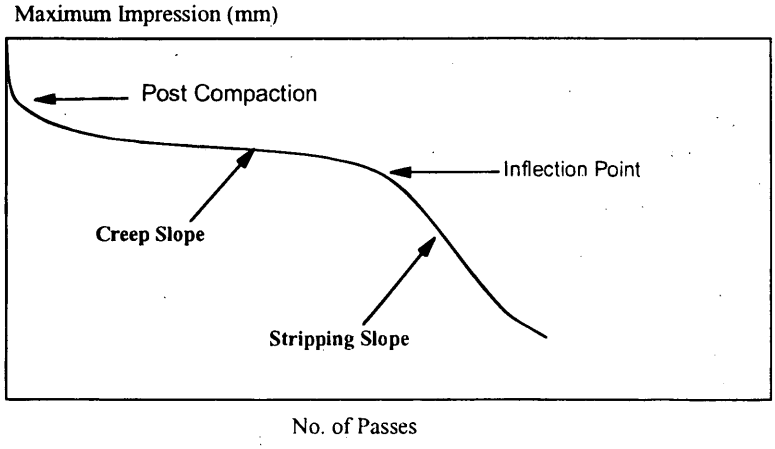

FIGURE 2 Data analysis of the results from the Hamburg Wheel-Tracking device.

RESULTS AND ANALYSIS

Mixture Design

The Marshall mixture design results are presented in Table 5. For the same gradation, the Interfibe and Styrelf mixtures with limestone had similar OAC. Also, for the same gradation the OAC of the Interfibe and Styrelf mixtures with diabase were close. There was a trend for increasing binder content and voids in mineral aggregate (VMA) with an increase in coarse aggregate. A decrease in stability and an increase in the voids filled with asphalt (VFA) were associated with this trend. The flow increased with an increase in coarse aggregate content, except for the Interfibe mixture with limestone using Gradation I. The flow and stability values were higher for Styrelf mixtures than for Interfibe mixtures. The percent binder increased more when the coarse aggregate content was increased from 70 to 80 percent than when it was increased from 60 to 70 percent. The VMAs of each SMA did not vary with the binder content, and the air voids versus binder content relationships were generally linear. Only three binder contents were used in designing the SMA mixtures.

The SMA TWG recommends a minimum of 6 percent binder by mass of mixture (2). Table 5 shows that increasing the coarse aggregate content increased the optimum asphalt content of the SMA mixtures.

The SMA TWG recommends a minimum VMA of 17. All diabase mixtures satisfied this recommendation, whereas none of the limestone mixtures did. In an associated study that is evaluating the same mixtures, extractions were performed to determine whether the Marshall hammer broke the aggregates. The extraction results showed that the increase in the amount passing the 4.75-mm sieve was higher for the limestone aggregate than for the diabase aggregate (Stuart and Mogawer, in a paper in this Record). This is due to the high L.A. abrasion weight loss of the limestone aggregate. The limestone L.A. abrasion weight loss was 35.4 percent. (The maximum recommended by the SMA TWG is 30 percent.) Because the limestone aggregate particles fractured more than the diabase particles, it was hypothesized that the lower VMAs of the

TABLE 5 Mixture Design Properties

	Diabase			Limestone		
	I	II	III	I	II	III
Interfibe Mixtures						
OAC, by mass	7.5	6.3	5.7	6.7	5.7	5.6
OAC, % by volume	17.6	15.1	13.8	14.5	12.6	12.3
Eff OAC, % by volume	16.7	14.1	13.3	12.5	10.9	10.6
Air Voids, %	3.5	3.5	3.5	3.5	3.5	3.5
VAM, %	20.2	17.7	16.8	16.1	14.4	14.0
VFA, %	80.2	80.2	79.3	78.3	75.8	75.2
Flow, 0.25 mm	17.7	17.7	14.7	18.1	19.8	17.4
Stability, N	7 819	7 819	9 000	7 633	8 404	10 498
Styrelf Mixtures						
OAC, % by mass	8.4	6.6	6.2	6.8	5.7	5.5
OAC, % by volume	19.5	15.6	14.7	14.7	12.6	12.2
Eff OAC, % by volume	18.5	14.7	13.9	12.8	10.8	10.5
Air voids, %	3.5	3.5	3.5	3.5	3.5	3.5
VMA, %	22.2	18.4	17.6	16.4	14.4	14.0
VFA, %	84.2	81.0	80.2	78.7	75.8	75.1
Flow, 0.25 mm	31.4	28.3	27.6	25.2	24.1	22.9
Stability, N	8 756	10 337	13 390	9 547	12 094	12 193

OAC: Optimal Asphalt (Binder) Content.
Eff OAC: Effective Optimum Asphalt (Binder) Content.
VMA: Voids in the Mineral Aggregate.
VFA: Voids Filled with Asphalt.

limestone mixtures were due to the greater amount of broken aggregate.

Draindown

The draindown data are presented in Table 6. It was observed that the coarse aggregate content had no effect on the draindown of mixtures prepared using Interfibe as the stabilizer, whereas mixtures prepared with Styrelf drained severely at the high coarse aggregate content (Gradation I). The six mixtures with Interfibe had low amounts of draindown and passed the four draindown tests. For mixtures prepared with either aggregate and Styrelf as a stabilizer, the German test, the 2.36-mm sieve test, and the NCAT test showed that Gradations II and III had less draindown than Gradation I.

It also was observed that the results from the four tests do not always agree.

Rutting Evaluation

French Pavement Rutting Tester

The percent air voids of the slabs are presented in Table 7. First, trial slabs were prepared and their overall air voids were measured. Then the trial slabs were cut along the wheel path, and the air voids in the wheel path were measured. This was done to determine the air voids in the wheel path before testing because they are always lower than the overall air voids. The initial air voids in the wheel path cannot be measured for the slabs to be tested.

The slabs to be tested were then prepared and their overall air voids were measured. After testing they were cut along the wheel path and their air voids in and out of the wheel paths were measured. Following the compaction sequence recommended by the manufacturer, the Interfibe and Styrelf mixtures with diabase had lower overall air voids than the Interfibe and Styrelf mixtures with limestone. The reason for this could be that the high amount of flat and elongated particles in the diabase become horizontally aligned during compaction. For the Interfibe mixtures the decreases in air voids during testing ranged from 0.4 to 2.1 percent, but there were no trends with increasing coarse aggregate content. For the Styrelf mixtures the decreases in air voids were not greater than the variability of air voids before testing. Therefore, whether the air voids decreased during testing could not be determined. It is often very difficult to obtain the desired air void level using the French compactor.

The percent rut depths are presented in Table 7. The percent rut depths of all the mixtures at the different number of passes were less than 20 percent of the specimen's thickness. Hence, all the mixtures passed.

The analysis of variance (ANOVA) statistical method at a 0.05 level of significance showed that aggregate gradation had no significant effect on the percent rut depths at 3,000 and 10,000 cycles.

TABLE 6 Draindown Test Results

	Diabase			Limestone		
	I	II	III	I	II	III
Interfibe Mixtures						
German Test, % mass loss	0.15	0.08	0.05	0.04	0.04	0.07
FHWA OGFC Test, draindown level	3	2	1	2	1	1
2.36-mm Sieve Test, % mass loss	0.00	0.00	0.00	0.00	0.00	0.00
NCAT Test, % mass loss	0.04	0.03	0.01	0.03	0.01	0.01
Styrelf Mixtures						
German Test, % mass loss	22.20	2.84	0.84	2.81	0.37	0.12
FHWA OGFC Test, draindown level	5	5	4	5	3	2
2.36-mm Sieve Test, % mass loss	8.40	1.45	0.00	3.20	0.01	0.00
NCAT Test, % mass loss	6.20	0.44	0.44	0.42	0.18	0.08

TABLE 7 (*a*) Percent Air Voids for French Pavement Rutting Tester Slabs; (*b*) French Pavement Rutting Tester Results

a)

	Diabase			Limestone		
	I	II	III	I	II	III
Interfibe Mixtures						
Overall Slab:						
Trial Specimen	4.52	4.05	5.22	5.48	4.99	6.32
Test Specimens	4.26	4.12	4.84	4.68	5.41	5.90
In Wheel Path:						
Trail Specimen	4.13	2.63	3.48	4.99	4.19	5.28
Test Specimens	2.02	2.22	2.45	3.08	3.16	3.63
Styrelf Mixtures						
Overall Slab:						
Trial Specimen	NT	2.46	1.86	4.84	5.10	4.95
Test Specimens		3.51	3.00	4.26	3.47	3.78
In Wheel Path:						
Trial Specimen		0.66	0.70	3.57	3.55	3.36
Test Specimens		1.14	1.12	2.41	1.59	1.86

b)

	Diabase			Limestone		
	I	II	III	I	II	III
Interfibe Mixtures						
% Rut Depth @ Cycle:						
30	1.3	2.1	1.2	1.2	1.5	1.0
100	2.2	2.8	1.8	1.9	2.2	1.5
300	3.4	3.3	2.4	2.4	3.1	1.9
1000	4.2	4.0	3.1	3.4	3.7	2.9
3000	5.1	4.9	4.2	5.1	4.8	3.7
10000	7.6	7.9	5.9	7.2	7.5	5.7
Slope	0.29	0.21	0.27	0.29	0.26	0.29
Styrelf Mixtures						
% Rut Depth @ Cycle:						
30	NT	3.0	3.5	1.2	2.5	2.8
100		3.7	4.6	1.4	4.2	3.5
300	NT	4.1	5.4	2.2	5.1	4.4
1000		4.9	6.4	3.1	6.3	5.3
3000		5.3	7.0	3.8	7.5	6.8
10000		6.3	7.5	5.1	9.1	7.8
Slope	0.12	0.13	0.26	0.21	0.18	1.86

NT: Not Tested.

Statistically, mixtures prepared with Styrelf had significantly lower rates of rutting than mixtures prepared using Interfibe, but the rut depths were not statistically different.

Georgia Loaded-Wheel Tester

The rut depths and air voids are presented in Table 8. The rut depths for all mixtures were less than 7.6 mm. Therefore, all of the mixtures passed.

The ANOVA statistical method at a 0.05 level of significance showed that aggregate gradation had no significant effect on the rut depth of the mixtures. Mixtures with Styrelf had significantly lower rut depths than mixtures with Interfibe.

Hamburg Wheel-Tracking Device

The creep slopes are presented in Table 9. The limestone Gradation I mixtures failed at fewer than 3,000 passes when either Interfibe or

TABLE 8 Georgia Loaded-Wheel Results

	Diabase			Limestone		
	I	II	III	I	II	III
Interfibe Mixtures						
Rut Depth, mm	6.5	5.3	4.6	4.8	3.6	4.1
Air Voids, %	3.3	4.4	3.4	4.6	3.8	4.7
Styrelf Mixtures						
Rut Depth, mm	NT	3.3	3.0	4.1	3.4	2.8
Air Voids, %		3.3	3.3	3.8	4.1	3.4

NT: Not Tested.

TABLE 9 Hamburg Wheel-Tracking Results

	Diabase			Limestone		
	I	II	III	I	II	III
Interfibe Mixtures						
Creek Slope, passes	1077	1866	1679	24.3	NT	NT
Air Voids, %	6.2	4.7	4.9	4.2		
Styrelf Mixtures						
Creep Slope, passes	NT	8333	7671	902	NT	NT
Air Voids, %		5.1	4.4	5.1		

NT: Not Tested.

Styrelf was used as the stabilizer. The steel wheel of the device crushed the limestone, causing the mixture to fail quickly. Gradations II and III were not tested because of the high amount of aggregate crushed. Statistically, gradation had no effect on the creep slopes of the Interfibe or the Styrelf mixtures with diabase. The mixtures with Styrelf had significantly higher creep slopes than the mixtures with Interfibe.

CONCLUSIONS

Mixture Design

- The air voids versus binder content relationships were generally linear for each mixture.
- The VMAs of each mixture did not vary with binder content during the mixture design.
- All diabase mixtures satisfied the SMA TWG recommendation for VMA (minimum of 17), but none of the limestone mixtures did. It was hypothesized that the lower VMAs and effective binder content by volume were due to a greater amount of aggregate being broken during compaction. However, the VMAs for the limestone mixtures were close to 17 when the coarse aggregate content was 80 percent.
- There was a trend for increasing binder content, VMA, and VFA with increasing coarse aggregate content. Associated with this trend was a decrease in stability.
- The optimum binder contents of the mixtures increased more when the coarse aggregate content increased from 70 to 80 percent than when it was increased from 60 to 70 percent.

Draindown

- The SMA mixtures with Styrelf had higher amounts of mastic draindown than the SMA mixtures with Interfibe.
- Coarse aggregate content had no effect on the draindown of mixtures prepared with Interfibe.
- Mixtures with Styrelf drained severely at high coarse aggregate content.
- The data from the German draindown test, the FHWA draindown test for OGFC, the FHWA 2.36-mm sieve draindown test developed at TFHRC, and the NCAT draindown test did not always agree.

Rutting

- Based on the GLWT and the Hamburg wheel-tracking device, the mixtures with Styrelf had significantly lower rut depths than the

mixtures with Interfibe. Based on the French pavement rutting tester, the mixtures with the Styrelf had significantly lower rates of rutting (slopes) than the mixtures with Interfibe, but the rut depths were not statistically different.

- Based on the French pavement rutting tester, GLWT, and the Hamburg wheel-tracking device, decreasing the coarse aggregate content from 80 to 60 percent had no significant effect on the rutting performance of the mixtures.

RECOMMENDATIONS

- Increasing the gap in the gradation should reduce the effects on performance of fluctuations in hot-mix plant binder contents. These effects may vary with gradation. This aspect is very important, but was not included in this study. Additional research is needed in this area.
- The diabase aggregates had more flat and elongated particles than recommended by the SMA TWG. Nevertheless, the SMA mixtures prepared with these aggregates passed the tests for rutting. Therefore, additional research on the effects of flat and elongated coarse aggregate particles on the rutting susceptibilities of SMA mixtures is needed. This should include the use of various percentages of flat and elongated particles.
- The four draindown tests did not always agree. Therefore, to determine the most applicable test, it is recommended that more SMA mixtures be tested using the four tests, and that the data be correlated to field performance.

ACKNOWLEDGMENTS

This study was funded by the Federal Highway Administration and was performed at the FHWA Turner-Fairbank Highway Research Center in McLean, Virginia.

REFERENCES

1. Stuart, K. D. *Stone Mastic Asphalt (SMA) Mixture Design*. Report FHWA-RD-92-006. FHWA, Washington, D.C., March 1992.
2. SMA Technical Working Group (sponsored by the FHWA Office of Technology Applications). *SMA Model Material and Construction Guidelines*. Jan. 1994.
3. Stuart, K. D., and P. Malmquist. Evaluation of Using Different Stabilizer in the U.S. Route 15 (Maryland) Stone Matrix Asphalt (SMA). In *Transportation Research Record 1454*, TRB, National Research Council, Washington, D.C., 1994, pp. 48–57.
4. Brosseaud, Y., J. Delorme, and R. Hiernaux. *Study of Permanent Deformations in Asphalt With the Help of the LCPC Wheel-Tracking Rutting Tester: Evaluation and Future Prospects*. TRB, National Research Council, Washington, D.C., 1993.
5. Lai, J. S. *Development of a Laboratory Rutting Resistance Testing Method for Asphalt Mixtures*. Research Project 8716, Final Report. Georgia Department of Transportation, Aug. 1989.
6. Aschenbrener, T., R. Terrel, and R. Zamora. *Comparison of the Hamburg Wheel-Tracking Device and the Environmental Conditioning Systems to Pavements of Known Stripping Performance*. Report CDOT-DTD-R-94-1, Final Report. Colorado Department of Transportation, Jan. 1994.
7. Hines, M. The Hamburg Wheel-Tracking Device. *Proceedings of the Twenty-Eighth Paving and Transportation Conference*. Civil Engineering Department, The University of New Mexico, Albuquerque, 1993.

Publication of this paper sponsored by Committee on Characteristics of Bituminous Paving Mixtures to Meet Structural Requirements.

Determination of Compactive Effort to Duplicate Pavement Voids for Corps of Engineers Gyratory Testing Machine

G. W. MAUPIN, JR.

The Corps of Engineers gyratory testing machine (GTM) has been used by various agencies to design and test asphalt mixes. Material properties such as shear strength and strain are measured during the compaction process, but a compaction process duplicating void levels in the pavement after traffic has not been clearly defined. The intent of this project was to determine the laboratory compactive effort for the GTM that duplicates the voids in pavement after it has been exposed to traffic. Samples of mix were obtained during construction of 10 field projects and tested in the laboratory with six different compactive efforts using various angles of gyration and vertical pressures. Voids were also measured in pavements immediately after construction and after several years of exposure to traffic. Regressions were then developed to allow the prediction of pavement voids from the voids obtained by the laboratory compaction procedures. A high correlation between voids obtained in the laboratory and pavement voids after several years of traffic was obtained with the GTM at two combinations of gyratory angle and vertical pressure; however, the degree of correlation was highly dependent on the inclusion of the postconstruction voids.

The gyratory testing machine (GTM) developed by the Corps of Engineers was used to design asphalt mixes for heavy-duty airfield pavements. Murfee and Manzione indicated that the GTM is still preferable to the Marshall method of mix design for pavements subjected to very heavy loads (*1*). Mississippi, Maine, and Kansas have also used the Corps GTM to analyze and design asphalt mixes.

One of the earliest models of GTM, located at Purdue University, has been used in several laboratory studies (*2,3*) from which it was concluded that bituminous mixtures can be effectively designed on the basis of their compaction and shear strain properties. The GTM can be used as a traffic simulation device to measure changes in compaction and shear strain properties of mixtures when they are placed in service, and the sensitivity of mixtures with respect to variations in gradation and asphalt content can be studied.

After considerable research using a GTM with an air roller instead of the oil-filled roller, Ruth et al. (*4*) concluded, "The gyratory compaction and densification testing procedure provides rapid assessment of a mixture's shear resistance as related to changes in asphalt content, aggregate gradation, and density." The apparatus measures the shear resistance necessary to resist rutting type deformation. Ruth et al. identified a compactive effort for the air-filled roller to simulate the density achieved by the construction process and following traffic exposure.

Virginia Transportation Research Council, 530 Edgemont Road, Charlottesville, Va. 22903.

Although the compactive effort has been identified for the air-filled roller, it has not been clearly distinguished for the oil-filled roller. Three compaction variables—angle of gyration, vertical pressure, and number of revolutions—define the compactive effort. The vertical pressure is usually taken as the tire pressure representing the traffic that will be on the mixture, commonly 827 kPa. Although an angle of gyration of 1.745×10^{-2} rad has been used considerably, lesser angles are believed to simulate traffic better. Typical values for the number of gyrations used for evaluation have been 30 and 60 revolutions; however, the developer of the equipment has indicated a preference for evaluation at a point when the rate of compaction decreases to a minimum value of 16 kg/m^3 per 100 revolutions.

The recommended compactive effort achieved by the combination of an angle of gyration of 1.745×10^{-2}, 827-kPa vertical pressure, and evaluation when the rate of compaction reaches 16 kg/m^3 per 100 revolutions was used by the author shortly after acquisition of the GTM on various mixes manufactured in Virginia. There were indications that this compactive effort was too severe. There was a need to determine what combination of compaction variables yielded densities reached in the pavement after subjection to traffic.

PURPOSE AND SCOPE

The purpose of this study was to develop a compaction procedure for the Corps of Engineers GTM that produces approximately the same void level as that reached in the pavement after it has been exposed to traffic. The study involved the sampling of mix from 10 paving projects, construction of laboratory samples with the GTM at various compactive efforts, and sampling the paving projects after exposure to traffic to determine the void level.

RESEARCH PLAN

Samples of surface mix were obtained from 10 resurfacing projects in the state of Virginia. Each of these projects was cored after 28 to 44 months to determine void levels after traffic exposure. Although some densification may continue on some of the projects, it is believed that the void level has nearly stabilized. A follow-up coring and determination of air voids will be repeated in several years to ensure that the voids have stabilized.

The samples of mix from each project were taken to the laboratory, where gyratory shear tests were performed at various levels

of compaction by varying the angle of gyration and vertical pressure. Six combinations of angle of gyration and vertical pressure were used. The angle of gyration was varied from 0.872 to 2.618 $\times 10^{-2}$ rad, and the vertical pressure was either 689 or 827 kPa. Voids total mix (VTM) values were determined on the compacted specimens.

An attempt was made to develop a correlation between the voids achieved at each compaction level and the voids in the pavement after it had been subjected to traffic. Other factors were considered in the correlations, such as total traffic and postconstruction pavement void level. The degree of correlation was the primary consideration in selecting the most satisfactory compaction level.

PROCEDURES

Sampling Mixes and Coring

An attempt was made to locate projects on primary and Interstate highways so that traffic would have a significant effect on the compaction of the pavement. The compaction by traffic to a critical level usually is the factor that results in instability and ultimate shear failure in permanent deformation types of distress. Since one of the projects was on a secondary route with very high traffic, a measurement of the amount of truck traffic was not readily available and will have to be obtained at a later date. For that reason this project was not included in the data analysis incorporating traffic for this paper.

Samples of plant mix were obtained from each project, and the location of the sampling was recorded so that cores could be taken at a later date. Pavement samples were also removed by dry-sawing immediately after construction to get an indication of the postconstruction void levels. If the pavement received insufficient compaction during construction, there would definitely be a major effect on the final void level after traffic exposure.

Laboratory Compaction

The plant mix obtained during construction was compacted in the GTM using each of the test combinations shown in Table 1. ASTM "Standard Test Method for Compaction and Shear Properties of Bituminous Mixtures by Means of the U.S. Corps of Engineers Gyratory Testing Machine (GTM)" was used to compact the specimens, with several modifications (*5*). Instead of a constant angle of gyration at 1.745 $\times 10^{-2}$ rad, it was varied from 0.872 to 2.618 $\times 10^{-2}$ rad. Also, instead of recording the shear strength and shear strain at 30 and 60 revolutions and then concluding the test, these values were recorded at regular intervals until the rate of densification decreased to 16 kg/m^3 per 100 revolutions. At this time the compaction was stopped, wall friction was measured, and the specimen was removed from the machine. Bulk specific gravities were measured and the VTM values were calculated.

Since the Marshall test method has been used by the Virginia Department of Transportation for many years, it was also used to compact the mixes to see how well it would predict the final void level of the pavement. Because these mixes were placed under what were considered to be fairly heavy traffic conditions, a 75-blow compactive effort was used. In retrospect, the current thinking of the state paving industry and departmental engineers supports a 75-blow effort only for very heavy traffic. Some of the projects that used the 75-blow effort should probably have used the 50-blow effort instead.

RESULTS

General

Table 2 gives a summary of test results for each project. The void levels achieved during the construction process before the pavement was exposed to traffic were relatively high. The only project to achieve single-digit voids was the secondary route mentioned above, which was not included in part of the analysis because of the lack of traffic data. Certainly the void level, which ranged from 10.1 to 15.0 percent in this study, should have had an influence on the magnitude of voids reached after the pavement was exposed to traffic. The "final" voids, after exposure to several years of traffic, ranged from 4.6 to 7.7 percent. The original quantity of voids was reduced on average by approximately half.

Effects of Angle of Gyration and Vertical Pressure

By comparing the voids at the different levels of compactive effort, the effect of both the gyratory angle and vertical pressure can be seen. At the lowest angle, 0.872 $\times 10^{-2}$ rad, the increase in vertical pressure from 689 to 827 kPa tends to reduce the void level.

TABLE 1 Combinations of Angle of Gyration and Vertical Pressure

Compaction Level	Angle of Gyration (Radians x 10^{-2})	Vertical Pressure (kPa)
1	0.872	689
2	0.872	827
3	1.309	827
4	1.745	689
5	1.745	827
6	2.618	689

TABLE 2 Traffic and Void Data Results

Route	Mix	Total 18 kip Equiv X 10^3	Post Const VTM	Final VTM	75-Blow Mars. VTM	VTM at Various Compactive Efforts Angle (Radians x 10^{-2})/Vertical Pressure (kPa) 0.872/689	0.872/827	1.309/827	1.745/689	1.745/827	2.618/689
58	SM-2C	137	12.2	7.2	4.7	6.3	5.5	3.2	1.9	1.7	0.6
I-64H	S-10M	877	10.3	5.5	4.4	5.6	5.9	3.7	2.4	2.4	1.2
29	SM-2C	982	10.1	4.6	5.0	6.9	6.6	3.6	2.2	1.7	2.1
01	SM-2C	513	13.3	7.6	6.1	9.4	6.6	4.3	4.9	3.0	2.0
28	SM-2C	250	15.0	7.7	5.8	8.0	6.7	4.0	2.5	2.3	1.2
I-64 NK	SM-2C	1066	13.2	7.2	5.1	6.6	6.2	3.6	2.5	2.4	1.2
I-66	SM-2C	1176	11.9	5.5	5.0	8.1	7.8	5.0	3.4	3.0	1.2
I-77	SM-2C	2160	11.1	5.6	3.2	6.4	6.0	4.1	3.1	2.4	---
I-81	SM-2C	2931	11.0	6.6	5.4	6.9	6.1	2.9	1.8	1.0	0.1
663	SM-3C	NA	7.3	3.1	4.2	4.3	5.4	3.1	1.2	1.4	0.2

TABLE 3 Multiple Regression Results

Regression (R^2)	Total ESAL x 10^7	Coefficients of Independent Variables and Constant Value for Regression Equations to Predict Final Pavement Voids: Post Const VTM	75-Blow Marshall VTM	VTM at Various GTM Compactive Efforts (Radians x 10^{-2}/kPa) 0.872/689	0.872/827	1.309/827	Constant
0.74	1.44	0.686		-0.128			-1.10
0.88	1.62	0.694			-0.668		2.12
0.86	0.61	0.673				-0.675	0.81
0.74	1.46	0.581	0.175				-1.62
0.86[a]		0.690		-0.0889			-1.29
[b]0.92[a]		0.730			-0.591		1.34
0.92[a]		0.726				-0.656	0.14
0.86[a]		0.617	0.118				-1.64

[a] The Route 663 project was included because unavailable traffic data was not necessary.
[b] Example of regression: Pavement VTM = 0.730 (Post const. voids) - 0.591 (GTM voids) +1.34

When a greater angle of 1.745×10^{-2} is used, the same magnitude of vertical pressure increase does not produce as much change in the void level. This smaller change is due to the fact that the void level is already low when this angle of compaction is used, and void level change becomes more difficult to distinguish. It is thought that the vertical pressure is analogous to the tire pressure of the traffic traveling on the pavement. Although vertical pressure may correlate with the degree of loading exerted by tires, the gyratory shear test is not an exact duplication of what takes place on the roadway. One should be careful in interpreting tests performed at different vertical pressures because one cannot be sure that a test performed at a certain vertical pressure will duplicate the behavior of the mix on the roadway exposed to the same tire pressure.

A similar comparison of voids obtained at different angles of gyration but the same vertical pressure can be seen for the tests using a vertical pressure of 827 kPa at angles of 0.872×10^{-2} and 1.309×10^{-2} rad. This small change in the angle of gyration had a significant effect on void levels.

Development of Regressions

Table 3 gives the coefficients for the multiple linear regressions developed to predict pavement voids after traffic by using voids from the gyratory shear tests. The first series was developed using 18-kip (80-kN) equivalent axle loads (ESALs) of total traffic, postconstruction voids, and voids obtained by the laboratory method as independent variables and pavement voids as the dependent variable. The second series was developed excluding traffic but including postconstruction voids and voids obtained by the laboratory method as the independent variables. It was observed that inclusion of the traffic variable tended to decrease rather than increase the degree of correlation.

This result tends to indicate that the effect of traffic was not represented properly by ESALs. Also, other factors that are not included, such as speed of traffic, may have had an overshadowing effect on the pavement voids. The regressions with angles of gyration of 0.872×10^{-2} or 1.309×10^{-2} rad and 827-kPa vertical pressure but containing no traffic variable both had high R^2 terms (0.92), indicating good correlations. The standard error of estimate was 0.48 percent voids, which is reasonable. A closer examination of the effects of the two independent variables on the degree of correlation was revealing. The postconstruction voids had a major effect on the degree of correlation that was achieved. An R^2 value of approximately 0.85 was achieved for the correlation using only postconstruction voids as an independent variable. Figures 1 and 2 compare the pavement voids on sampled projects and the voids predicted from the postconstructed voids and voids obtained with the GTM.

Before initiation of this project, the Virginia Department of Transportation began to use 75-blow Marshall designs and a higher design void content of 4 to 6 percent for the SM-2C mixes used in this field study. It has been observed that most of these mixes now are "dry," and even though rutting is no longer a problem, durability has suffered. The author also believes that the dry mixes tended to influence the degree of correlation in this study that was expected between the compaction method and the final pavement voids. The dry mixes are difficult to compact during construction; therefore, the void contents tend to be high. The high voids probably resulted in stiffening of the asphalt cement, which prevented the field mixes from reaching the void levels achieved in the laboratory with fresh asphalt. The postconstruction voids were extensive, and the asphalt

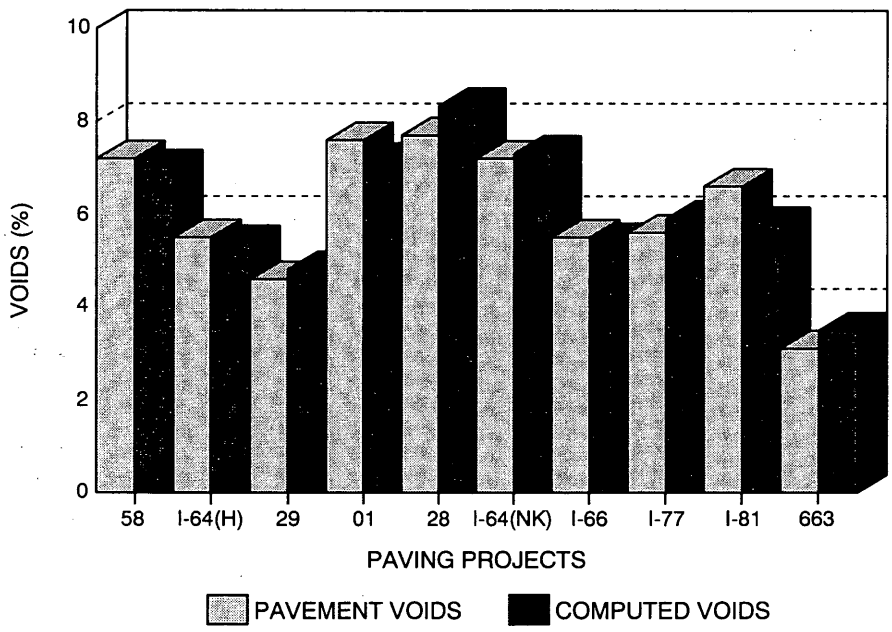

FIGURE 1 Comparison of final pavement voids and voids estimated from regression with construction voids and GTM voids at 0.872×10^{-2} rad and 827 kPa.

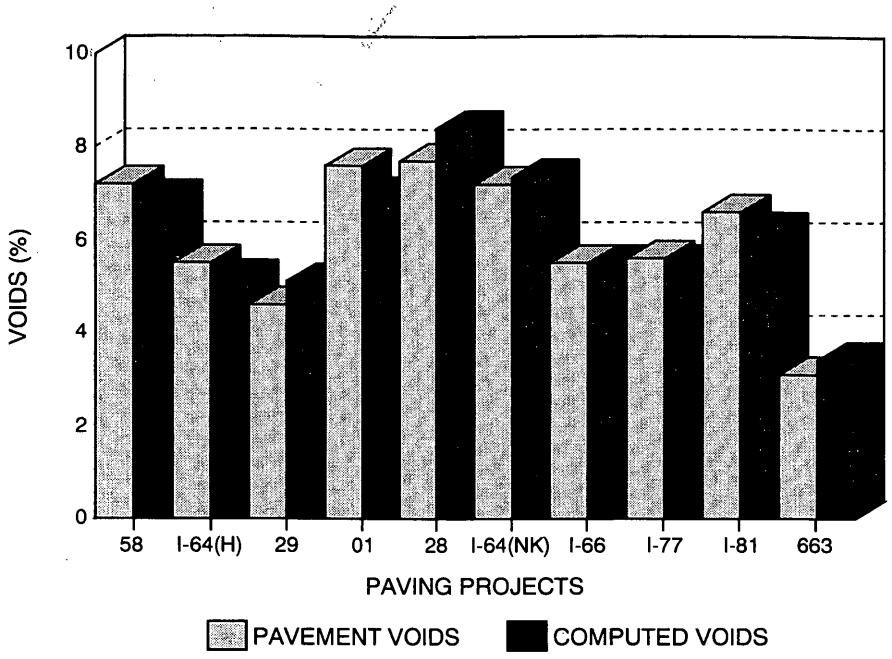

FIGURE 2 Comparison of final pavement voids and voids estimated from regression with construction voids and GTM voids at 1.309 × 10^{-2} rad and 827 kPa.

cement probably stiffened to the extent that traffic tended to compact all of the mixes about the same proportional amount, negating some of the compaction that would have been predicted by the laboratory tests.

From visual observations it appears that the voids of specimens using the gyratory shear test with an angle of 0.872 × 10^{-2} rad and 827 kPa vertical pressure most closely approximate the absolute final pavement voids. However, these results could change as additional traffic is allowed to accumulate on the sections. The correlations developed using the 75-blow Marshall voids were not quite as good as the correlations with the gyratory shear test. Figure 3 illustrates a comparison of pavement voids on

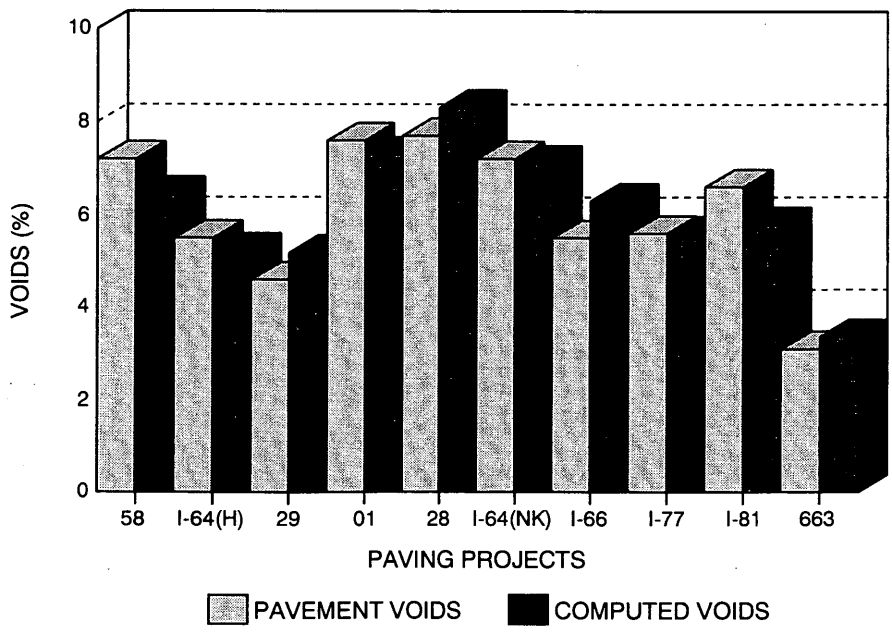

FIGURE 3 Comparison of final pavement voids and voids estimated from regression with construction voids and 75-blow Marshall voids.

the sampled projects and voids predicted by the 75-blow Marshall procedure.

CONCLUSIONS

1. A good correlation was obtained between pavement voids and voids obtained in the laboratory with the gyratory shear test; however, the degree of correlation was highly dependent on inclusion of postconstruction voids.
2. A slightly lower degree of correlation was obtained between pavement voids and voids obtained with the 75-blow Marshall compactive effort.
3. Total traffic in terms of ESALs did not aid the degree of correlation obtained, although it is known to have a significant influence on the final voids. The estimation and inclusion of traffic effects need to be refined further.

REFERENCES

1. Murfee, J., and C. W. Manzione. Construction of Rut-Resistant Asphalt Mixtures. In *Transportation Research Record 1337*, TRB, National Research Council, Washington, D.C., 1992, pp. 10–17.
2. Kumar, A., and W. H. Goetz. The Gyratory Testing Machine as a Design Tool and As an Instrument for Bituminous Mixture Evaluation. *Proc. AAPT*, Vol. 43, 1974, pp. 350–383.
3. Wood, L. E., and A. G. Altschaeffl. *Effects of Asphalt Composition and Compaction on the Performance of Asphalt Pavement Mixtures.* Report JHRP-87/7. Purdue University, West Lafayette, Ind., 1988.
4. Ruth, B. E., X. Shen, and L. H. Wang. *Gyratory Evaluation of Aggregate Blends to Determine Their Effect on Shear Resistance and Sensitivity to Asphalt Concrete.* STP 1147. ASTM, Philadelphia, Pa., 1992, pp. 252–264.
5. *Annual Book of ASTM Standards.* Volume 04.03. ASTM, Philadelphia, Pa., 1994.

Publication of this paper sponsored by Committee on Characteristics of Bituminous Paving Mixtures To Meet Structural Requirements.

Development of Rolling Compaction Machine for Preparation of Asphalt Beam Samples

JAMES S. LAI AND HAROON SHAMI

A rolling compaction machine developed for fabricating asphalt beam samples is described. The machine was developed as a part of a research program for evaluating the rutting resistance of asphalt mixes using the loaded wheel tester. The uniqueness of this machine is that the asphalt beam sample is compacted by a rolling compaction action that simulates the compaction of asphalt mixes in the field. The machine is capable of fabricating beam samples up to 375 mm long by 175 mm wide by 125 mm thick. The overall dimensions of the machine are 1.2 m long by 0.45 m deep by 1.3 m high. The machine is portable and easy to operate. The experience of the Georgia Department of Transportation through one year of extensive use of this machine has shown that it can improve quality and productivity of fabricating asphalt beam samples. Results of the bulk densities of the asphalt beam samples fabricated by this compaction machine as well as by the static compaction procedure using a universal testing machine are presented. Three types of asphalt mixes—a surface mix, a base mix, and a stone mastic asphalt mix—were used for preparing the beam samples by the different compaction methods. To evaluate the density variation in each beam sample, the density of the whole beam was first measured, the sample was then sawed in sections (sometimes as many as 12), and densities of all sections were measured. Results from three studies presented indicated that the maximum variation of density for beam samples compacted by the rolling compaction procedure was under 1.5 percent. Visual observations of all asphalt beam samples made by the three compaction methods showed that samples prepared by rolling compaction have the least amount of crushed aggregates.

A rolling compaction machine developed exclusively for fabricating asphalt concrete beam samples is described. This machine was developed as a part of the research program for evaluating the rutting resistance of asphalt mixes using the loaded wheel tester (LWT). In this testing method, asphalt beam samples conditioned at elevated temperatures (40°C) are subjected to a repeated wheel loading of controllable wheel load (450 N) and contact pressure (0.69 MPa). Rut depths developed on asphalt beam samples at the end of 8,000 cycles of load repetitions are measured and used to assess rutting characteristics of asphalt mixes. The LWT procedure was developed by Lai (*1–3*) in collaboration with the Georgia Department of Transportation (GaDOT). This procedure has been incorporated into GaDOT Standard Test Procedure GDT-115 "Method of Test for Determining Rutting Susceptibility Using the Loaded Wheel Tester" as a supplement to the Marshall mix design method for the design of asphalt mixes. This procedure has also been used by other highway agencies to evaluate rutting characteristics of asphalt mixes (*4*).

School of Civil and Environmental Engineering, Georgia Institute of Technology, Atlanta, Ga. 30332-0355.

Preparation of asphalt beam samples to required compaction densities is an integral part of the LWT procedure. Unlike the dedicated Marshall compaction apparatus for preparing Marshall samples, no standard procedure or dedicated asphalt beam sample compaction apparatus is available for preparing asphalt beam samples for LWT. Several compaction procedures, including the kneading compaction method, and different static compression procedures for preparing the asphalt beam samples were developed and tested with varying degrees of success in the course of conducting LWT studies (*1,3*). The consensus from the users of LWT, including those participating in a round robin test program of LWT (*5*), was that a dedicated compaction apparatus for preparing asphalt beam samples could significantly ease sample preparation and improve the quality of asphalt beam samples and thus the accuracy of LWT results.

The rolling compaction machine described in this paper was developed to meet this need. The machine is capable of fabricating beam samples up to 375 mm long by 175 mm wide and up to 125 mm thick, although at the present time the beam sample dimensions are set at 300 mm long by 125 mm wide by 75 cm thick. The uniqueness of this compaction machine is that the asphalt beam sample is compacted by a rolling compaction action, which is intended to simulate the compaction of asphalt mixes in the field. The machine can also compact the asphalt mix when it is in the kneading compaction mode.

REVIEW OF PREVIOUS ASPHALT BEAM SAMPLE COMPACTION PROCEDURES

Kneading Compaction Procedure

Initially the asphalt beam samples used in the LWT test were fabricated by a California kneading compactor. The loose asphalt mix was placed in the heated beam mold, and the rectangular-shaped loading foot of the kneading compactor was activated to apply controllable compressive forces on the asphalt mix in the mold. The beam mold was moved manually on the sliding track during the compaction operation to effect the uniform compaction of the beam sample. The beam was compacted in two or three lifts. After the top layer was compacted to approximately the required height, a heated thick steel plate was placed on top of the beam and high pressure was applied to compress the mix in the mold to the final required height. This sample preparation method was used for preparing the beam samples in the early studies by Lai (*1,2*) for evaluating the rutting characteristics of asphalt mixes using the LWT. This procedure has also been used to prepare asphalt beam samples for evaluating fatigue properties.

Use of the kneading compaction method to fabricate beam samples was quite time consuming. A significant amount of aggregate crushing was observed on the compacted beam samples caused by the high contact pressure of the steel kneading foot. Another drawback of this method was that a special kneading compaction machine was required that was not readily available in most of the testing laboratories.

A different type of kneading compactor called the HasDek SLAB-PAC linear kneading compactor was developed by R/H Specialty & Machine (Terre Haute, Ind.). In this compaction procedure a beam sample mold is filled with a weighed amount of asphalt mix; the mix was calculated on the basis of the desired final density and the volume of the mold. A series of 125-mm thick steel compacting plates are placed on top of the loose asphalt mix. A roller is then lowered against the steel plates to force them to press into the loose asphalt mix while the asphalt mix and the beam mold move back and forth on a sliding table (see Figure 3). By controlling the downward movements of the roller, the asphalt mix in the beam mold can be compacted to the prescribed thickness.

Static Compaction Procedure

A simplified procedure to fabricate the beam samples by static compression was developed by Lai (*3*). This procedure utilizes a compression machine to press the weighed amount of asphalt mix in a sturdy steel beam mold to the required density. This procedure is simple to perform and is readily implementable since most testing laboratories are usually equipped with some type of compression machine suitable for this procedure.

The static compaction procedure has produced satisfactory density requirements (*5*), although the procedure is viewed to be cumbersome. The other concern was that the properties of the beam samples fabricated by the static compaction procedure, such as the orientation and interlocking of aggregate particles in the beam sample, may be different from the asphalt mixtures compacted in the field. The round robin test program showed that the variability was quite high for bulk densities of beam samples fabricated by different laboratories using different static compaction machines but the same compaction procedure (*5*). However, the single-laboratory variability of beam sample densities from each participating laboratory was quite low. Results of the round robin tests and the comments from the other users strongly suggested that development of equipment with dedicated rolling type beam sample compaction is highly desirable.

French Sample Compaction Method

The French compaction machine was developed by the Laboratory Central des Ponts et Chaussées (LCPC) to prepare asphalt beam samples for wheel tracking testing to evaluate rutting of asphalt mixtures (*7*). The machine used a 415-mm diameter by 109-mm wide wheel with smooth-tread tire that can move longitudinally and laterally against the beam sample mold filled with loose asphalt mixes. The maximum size of the beam sample that can be fabricated by this machine is 600 mm long by 400 mm wide by 150 mm thick. According to the report (*7*), different compaction procedures can be used to achieve different degrees of compaction. The advantages of this compaction procedure are that (*a*) relatively large samples can be fabricated and (*b*) the resulting aggregate orientation pattern and level of void content in the asphalt beam samples will be closer to those obtained in actual pavements. The main disadvantage is probably the high cost of the equipment, which is in the neighborhood of $100,000.

ROLLING COMPACTION MACHINE DEVELOPMENT

The important considerations in the development of this compaction machine were the ability to simulate the rolling compaction action of asphalt mixes in the field, ease of beam sample fabrication, ability to fabricate asphalt beam samples with uniform and controllable densities, and the cost of the machine. The rolling compaction machine (Figures 1 and 2) has overall dimensions of 0.45 m wide by 1.20 m long by 1.30 m high. The machine is portable and can be easily moved near the asphalt batching facility.

The machine consists of the following four basic components:

- Sliding motion assembly,
- Rolling compactor assembly,
- Beam sample mold, and
- Hydraulic system and operational control.

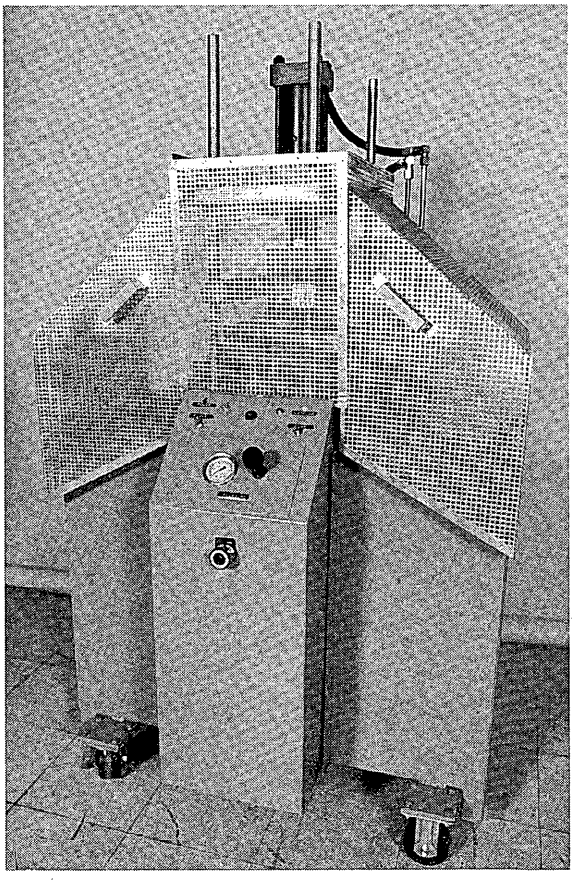

FIGURE 1 Rolling compactor.

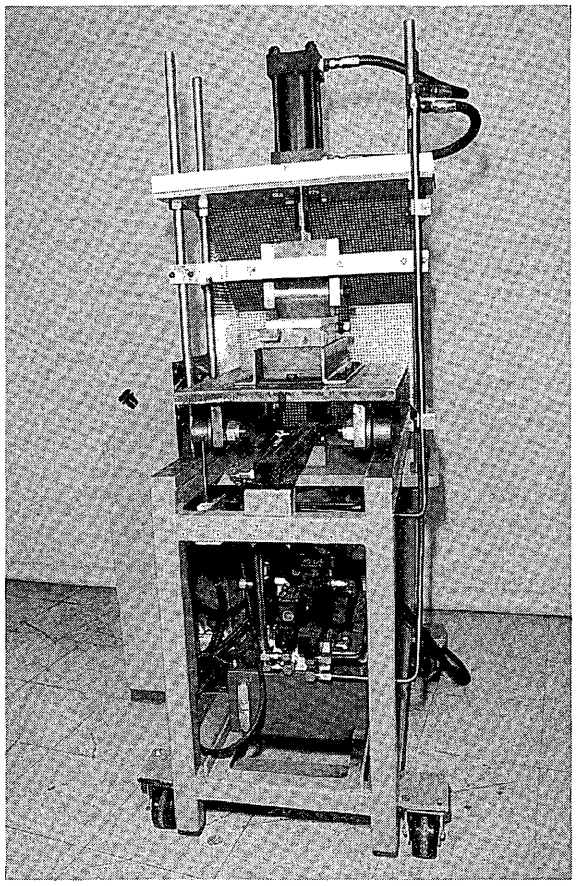

FIGURE 2 Rolling compactor (side view).

Sliding Motion Assembly

The sliding plate assembly, shown in Figure 2, consists of a 25-mm-thick steel plate 450 mm wide and 600 mm in length having four heavy-duty roller bearings attached to the bottom of the plate. The bearings are aligned longitudinally and ride on two rails. The bottom of the plate is connected to a horizontally aligned double action hydraulic cylinder. The extension and retraction action of the piston rod generates the reciprocating sliding motion of the plate. The beam sample mold restraints are on the top of the sliding plate. These removable restraints are used to secure the beam mold.

Rolling Compactor Assembly

The rolling compactor assembly generates the force for compacting the beam samples. The assembly, shown in Figures 2 and 3, consists of a load frame, a double-action hydraulic cylinder, and a compaction roller. The system is capable of applying 54 kN of force to the beam sample. Two horizontal restraining bars, one on each side of the roller clevis, are installed to restrain the horizontal movements of the roller caused by the shear force developed between the beam sample and the roller. Installation of the restraining bars is needed to minimize the wear of the cylinder bearings. During beam sample compaction, the roller exerts an adjustable vertical pressure through a nylon pad placed on top of the loose asphalt mixture in the beam mold. When the compaction roller presses against the semistiff nylon pad, it deforms and creates a curvature comparable with the curvature of a compaction roller used in the field (see Figure 4). The combined actions of the horizontal reciprocating motion of the beam mold, adjusted to approximately 3 rpm, the curvature on the nylon pad, and the vertical force from the compacting roller cause the asphalt mix confined in the beam mold to be compacted in a rolling action similar to the compaction of asphalt mixes in the field.

A kneading-type compaction similar to that of the HasDek linear kneading compactor (R/H Specialty + Machine, Terre Haute, Ind.) can easily be adapted to this compaction machine by replacing the nylon pad with a loading pad consisting of a series of loosely connected steel plates (see Figure 4).

Beam Sample Mold

Beam sample mold assembly is shown schematically in Figure 5. It includes a split mold made of a 5-mm steel plate, a loosely fitted bottom plate, and the restraints made of steel angle sections. The restraints are bolted down to the sliding plate to confine the lightweight split beam mold during compaction. Only one restraint section needs to be removed to free the beam mold. The light weight of the beam mold and ease of removing the compacted beam sample from the split beam mold make beam sample fabrication much easier than the static compaction procedure described previously.

Hydraulic System and Operational Control

A schematic diagram of the hydraulic system controlling compaction operation is shown in Figure 6. The horizontal reciprocating motion of the sliding plate is controlled by a horizontal actuator activated by an On-Off toggle switch, and the speed of the horizontal motion is adjustable by a flow control valve. When activated by the solenoid, the actuator pushes (or pulls) the sliding plate at a constant speed in one direction until it contacts the limiting switch positioned at the extreme end. When the limiting switch is activated on contact, it causes the solenoid to reverse the direction of motion of the actuator and the sliding plate to move in the opposite direction until it contacts another limiting switch positioned at the other extreme end. Thus, the sliding plate automatically slides back and forth horizontally at a constant speed within the travel length set by the limiting switches.

The movement of the compaction roller is controlled by Up and Down switches on the control panel. When the Down switch is activated, the solenoid causes the cylinder rod of the vertical actuator to extend and applies a vertical force through the roller on the nylon pad. The magnitude of the vertical force is manually controlled by a pressure regulator.

To prevent overcompaction on the asphalt beam sample, the machine is also equipped with a vertical limiting switch that controls the maximum downward movement of the compacting roller. The position of this limiting switch can be adjusted so that when the beam is compacted to the desired depth, the switch is activated and causes the vertical actuator to retract, thus preventing possible over-

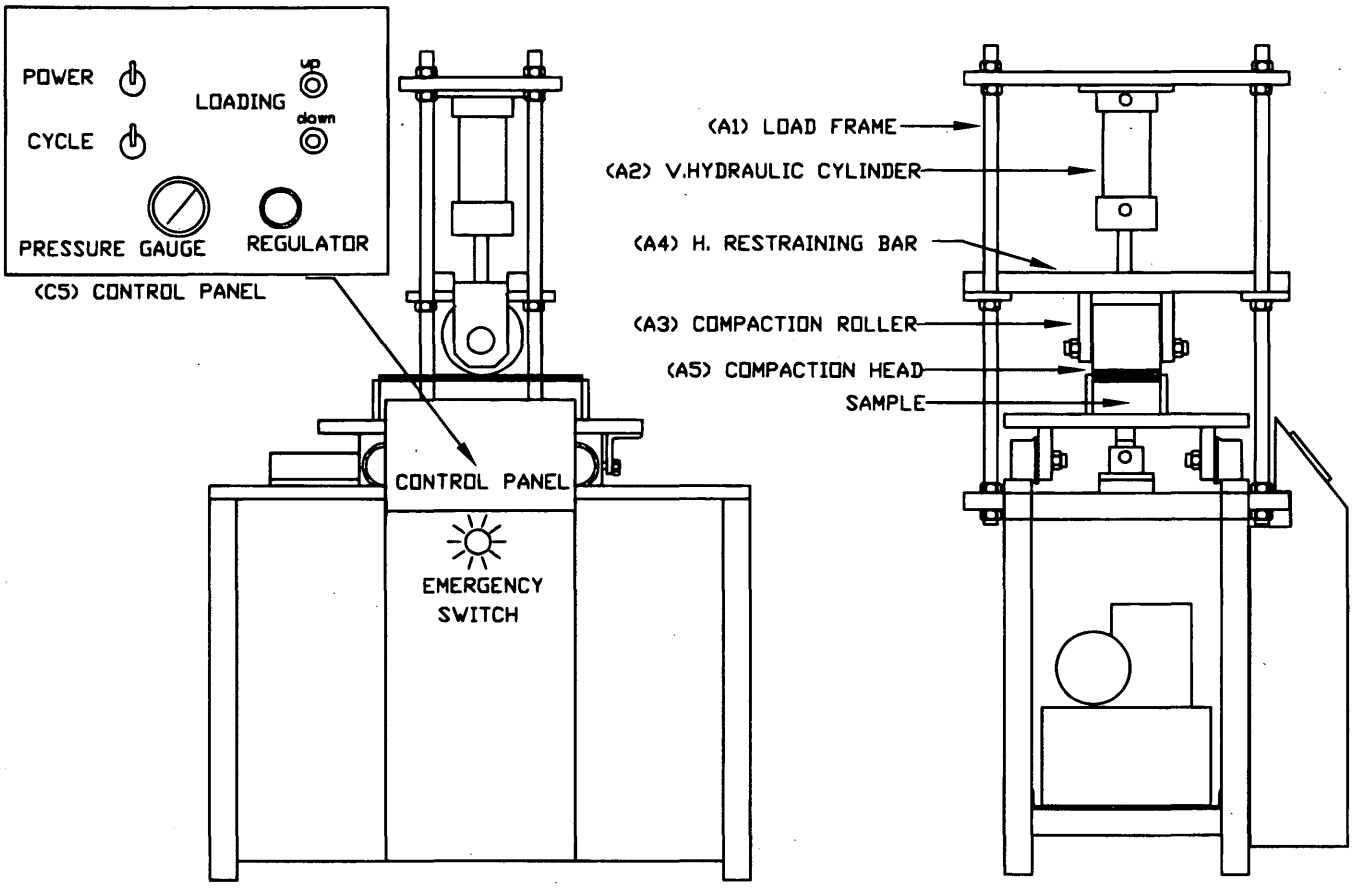

FIGURE 3 Schematic of rolling compactor.

compaction of the beam sample. Additional compaction, if needed, can be done by manually depressing and holding the Down button to cause the actuator to extend and apply the compressive force on the sample. A horizontal line inscribed on the side of the nylon pad can be used as the reference to detect uneven compaction of the beam sample. This reference line can also be used to determine the level of compaction of the beam sample. When the reference line is level with the top edge of the beam mold, the asphalt beam sample in the beam mold has been compacted to the predetermined 75-mm height. The vertical actuator can only be activated when the horizontal sliding movement of the plate is already in action. Whenever the horizontal cycle switch is turned to the Off position to stop the sliding action, the vertical actuator will automatically retract, preventing any application of compaction on the beam sample when the horizontal motion is accidentally stopped.

BEAM SAMPLE COMPACTION PROCEDURE

The procedure for using this machine to fabricate asphalt beam samples is as follows:

1. Pour the hot asphalt mix into the mold, spade the loose mixture thoroughly, and spread the mix evenly in the mold. Place the nylon pad (for rolling compaction) or the steel kneading pad (for kneading compaction) on top of the asphalt mix.
2. Secure the beam mold on the sliding plate with the restraining brackets.
3. Turn on the power, and activate the "Cycle" switch. The sliding plate will begin to make horizontal cyclic motions. Activate the "DOWN" switch to initiate the compaction, using a small force initially and gradually increasing the force to a predetermined maximum. Allow the beam sample to be compacted under the reciprocating rolling or kneading actions until the predetermined density requirement has been reached.
4. When the required compaction has been achieved, deactivate the Cycle switch, which causes the roller to retract and the sliding plate to stop at the far end. While it is still warm, remove the beam mold from the machine and extract the split beam mold (except the bottom plate) from the compacted sample.

Since the procedures for rolling compaction with the nylon pad and kneading compaction with the steel kneading pad (HasDek SLAB-PAC linear kneading compactor) are essentially the same, a comparison of these two compaction procedures was also made. The following summarizes the differences in the operational characteristics of these compaction procedures. Use of rolling compaction can occasionally develop an unevenly compacted beam sample if

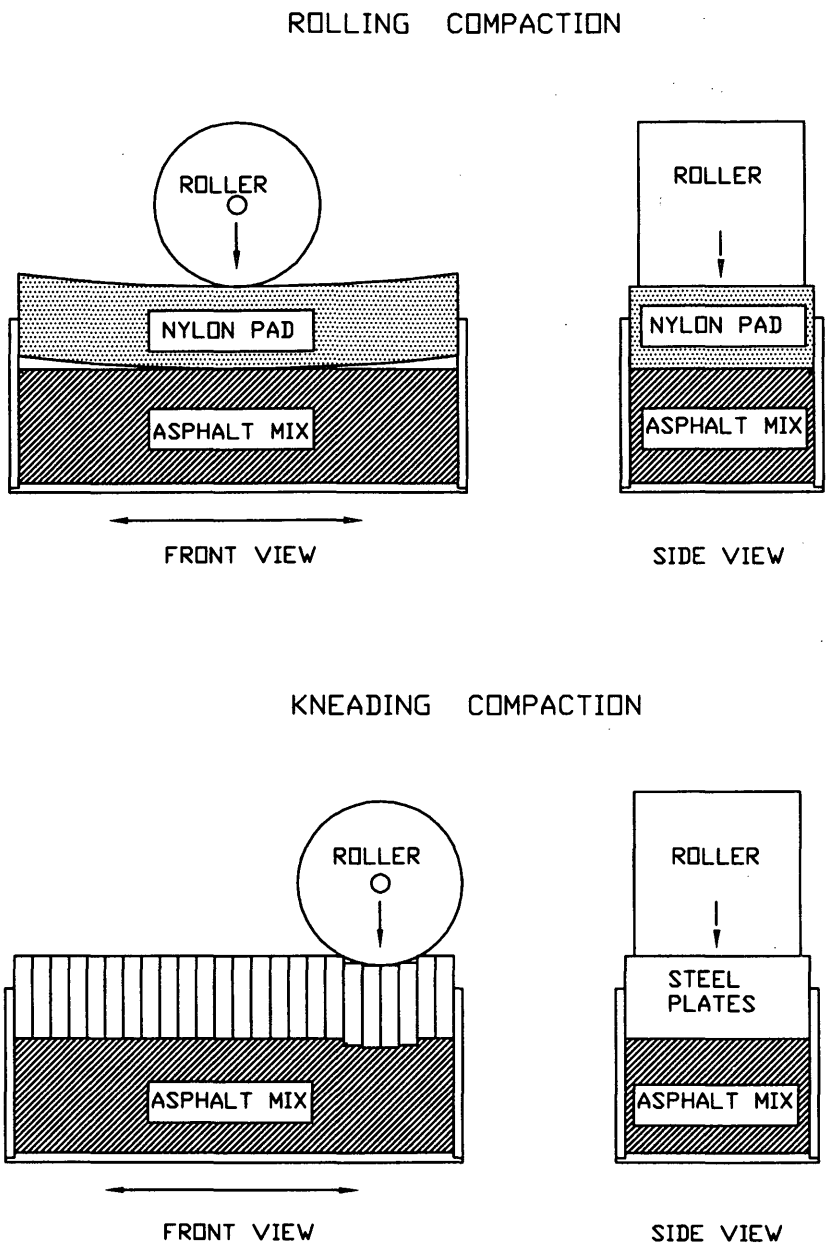

FIGURE 4 Schematics of rolling compaction and kneading compaction.

the initial compaction force applied on the loose mix is too high or if some tender asphalt mixes have low stability. The control system has the capability to allow for manual adjustment via the control switches to correct this problem. The kneading compaction procedure using the steel kneading pad minimizes this problem to a certain extent. Kneading compaction is somewhat easier to use and the compaction force can be applied faster, thus reducing the time required to compact the beam sample. These are the advantages of the kneading compaction procedure over the rolling compaction procedure. On the other hand, kneading compaction tends to cause a higher percentage of aggregates crushed in the beam sample. Also, kneading compaction does not seem to simulate field compaction of asphalt mixes as the rolling compaction procedure does. A typical time required to fabricate a beam sample, excluding the batching of asphalt mix, is about 15 and 10 min, respectively, for rolling and kneading compactions. Results of the beam densities obtained from the asphalt beam samples fabricated by these two procedures are presented in the next section.

RESULTS

The purpose of the studies presented here is to evaluate the variabilities of the beam densities within each beam sample fabricated by different compaction methods. The difference between the averaged beam densities of beam samples fabricated by different compaction methods has no significance because the level of compaction can be changed by altering the magnitude of the maximum

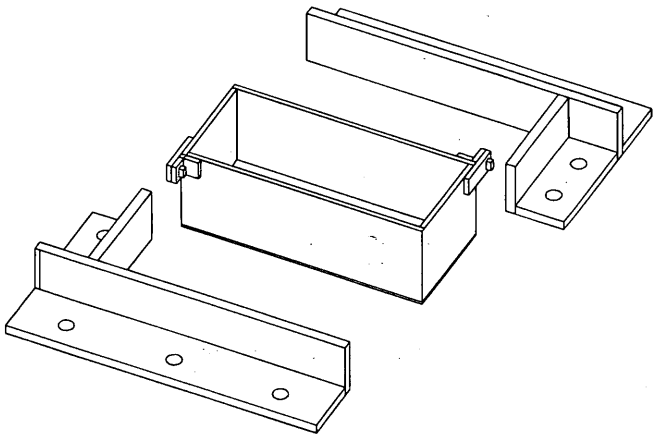

FIGURE 5 Schematic of beam mold assembly.

compaction force as well as the duration of such force applied in each compaction method.

Rolling Compaction Versus Static Compaction

Beam samples from two different mixes, a base mix (B-mix) and a stone-mastic asphalt mix (SMA-mix), were prepared by the rolling compaction procedure using the machine described in this paper and by the static compaction procedure. Two beam samples from each mix were fabricated, one by rolling compaction and one by static compaction. The following density measurements were made for each sample.

1. Determining the density of the whole beam sample;
2. Sawing the beam sample longitudinally in two halves and measuring the density of each half; and
3. Sawing half of the beam transversely in three parts identified as A, B, and C and measuring the density of each part.

Results of the density values are shown in Figure 7. The maximum density variations in the beam samples made by rolling compaction are 0.3 and 1.1 percent for the B-mix and the SMA-mix, respectively, and the maximum deviations are 1.6 and 0.9 percent for the B-mix and the SMA mix, respectively, for the beam samples made by the static compaction method. The corresponding air voids are also shown in Figure 7. For rolling compaction, a maximum force of 36 kN (8,000 lb) and 45 kN (10,000 lb) was applied for compaction of the B-mix and the SMA-mix, respectively. For static compaction, a 540-kN (120,000-lb) force was applied for both the B-mix and the SMA-mix. The significant difference in the compaction forces required between rolling compaction and static compaction indicates that in rolling compaction the contact width between the nylon pad and the asphalt mix has to be quite narrow to develop a sufficient contact pressure generated by the 36- to 45-kN

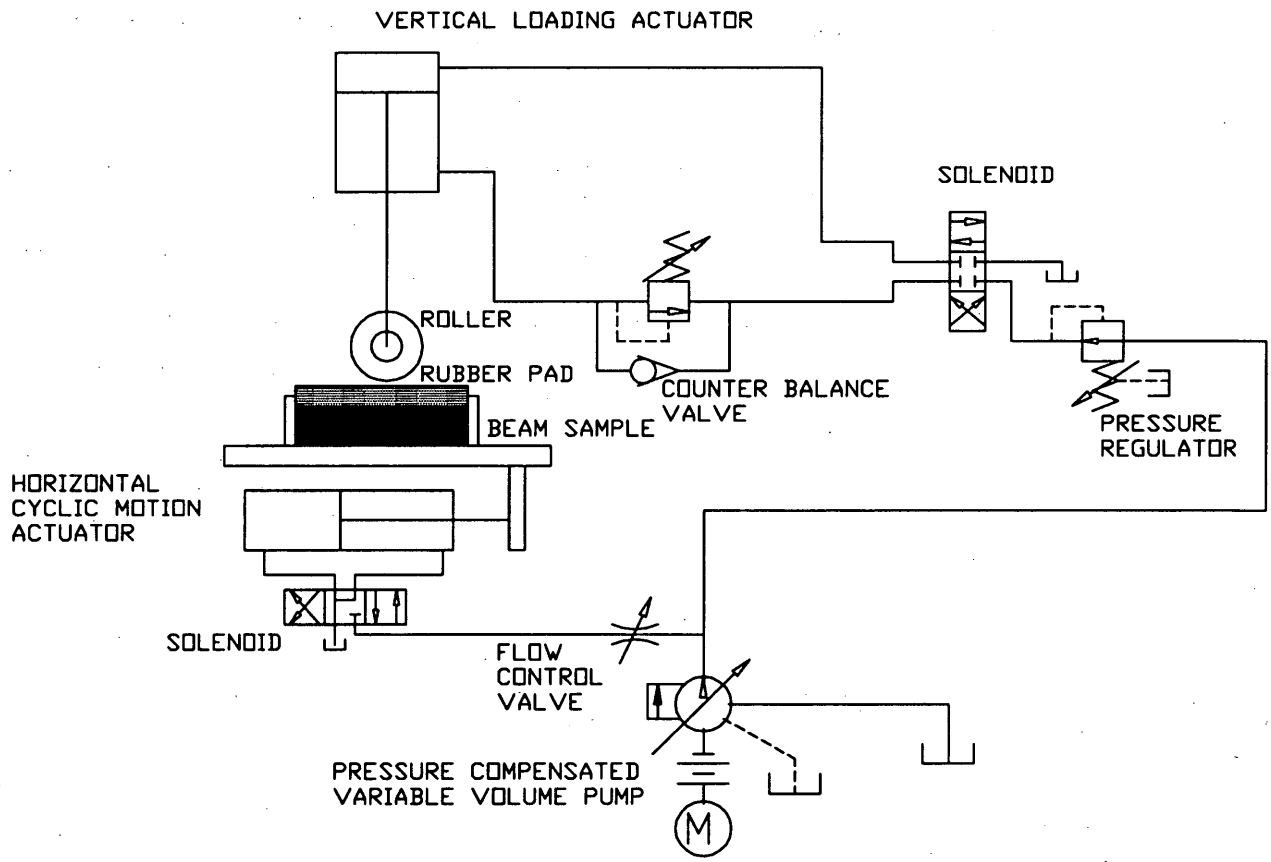

FIGURE 6 Schematic of hydraulic loading system.

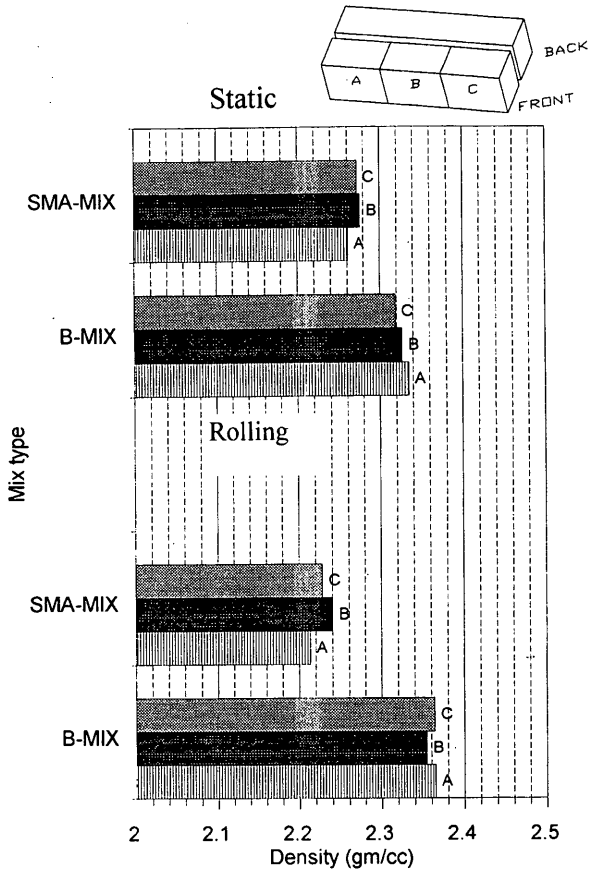

FIGURE 7 Results of rolling compaction versus static compaction.

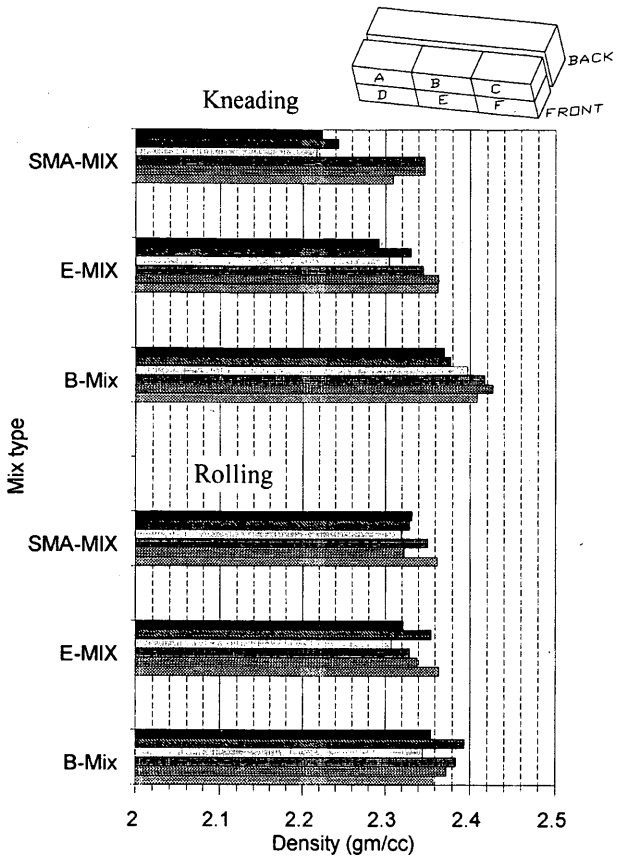

FIGURE 8 Results of rolling compaction versus kneading compaction.

force to compact the loose asphalt to the required densities. A noticeable amount of crushed aggregate particles was seen on the surfaces of the beam samples made by the static compaction method.

Rolling Compaction Versus Kneading Compaction

Three different asphalt mixes were selected in this study, a B-mix, an E-mix (surface mix), and an SMA-mix. Six beam samples were fabricated, two for each mix, with one fabricated by using the rolling compaction method and the other by using the kneading compaction method. The following density measurements were made for each beam sample.

1. The density of the entire beam sample was determined;
2. The beam samples were sawed longitudinally in two halves and the density of each half was measured; and
3. One half of the beam was sawed horizontally at mid-height and transversely into three approximately equal widths, and the bulk densities of all six sections were measured.

The results of the density measurements are shown in Figure 8. Among the beam samples fabricated by the rolling compaction method, the maximum variation of beam densities within each beam is 1.5 percent of the averaged value. There are no consistent trends of variation of the densities within beam samples. Among beam samples fabricated by the kneading compaction method, the top portions of all three beam samples have higher densities than those of the bottom portions. The difference is most noticeable for the SMA-mix where there is an average difference of 3.5 percent between the top and bottom half of the beam sample. From the visual inspection of the exposed sample surfaces, the aggregate concentration and the particle orientation were somewhat different between the upper and lower halves of the beam. Bleeding of asphalt was visible also near the bottom of the lower half of the beam samples. It was observed that many more aggregates were fractured among the beam samples fabricated by the kneading compaction method. This is not surprising as the steel plates exerted higher concentrated loads on the aggregates during the course of compaction. This type of aggregate crushing was also observed previously in the asphalt beam samples fabricated by the kneading method using the California kneading machine.

Additional asphalt beam samples were fabricated by both compaction methods, and the beam densities were measured. In this additional series of studies, each beam sample was sawed horizontally at mid-height and transversely into six approximately equal widths. Results of the density measurements of the 12 portions for each beam sample are shown in Figures 9 and 10. The densities in the beam samples fabricated by the kneading compaction method are much more consistent with the maximum deviation being 1.25 percent throughout the whole beam sample while that from the rolling compaction method exhibited more variation.

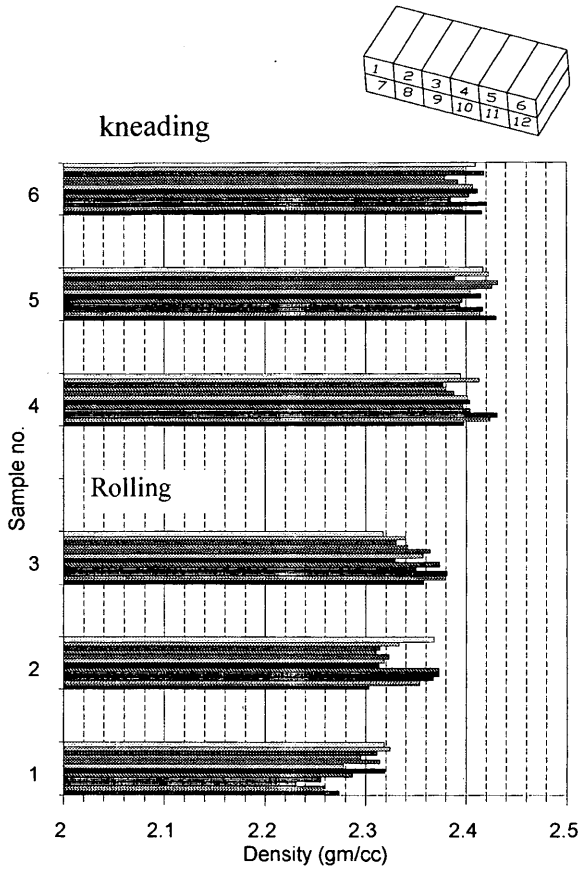

FIGURE 9 Results of rolling compaction versus kneading compaction, B-mix second testing series.

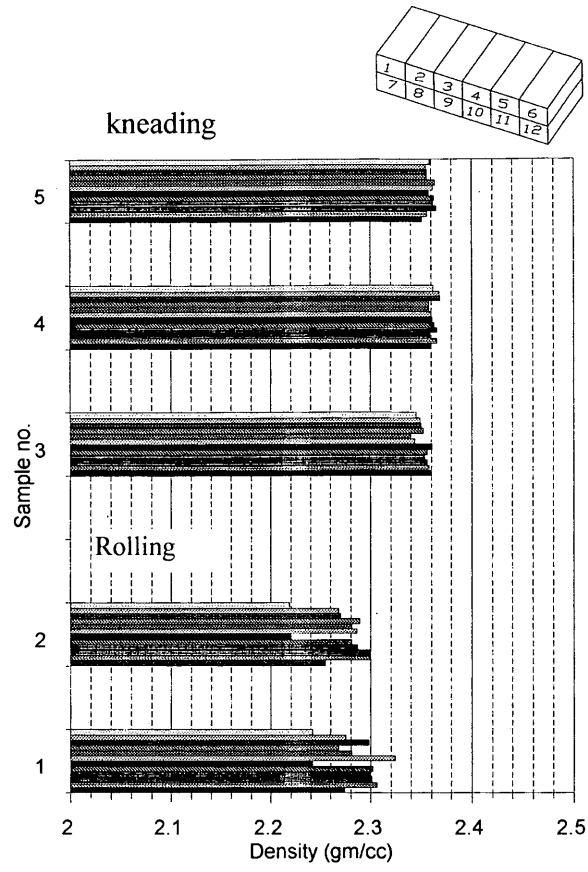

FIGURE 10 Results of rolling compaction versus kneading compaction, E-mix, second testing series.

CONCLUSIONS

The rolling compaction machine has been used extensively to fabricate asphalt beam samples for evaluating rutting characteristics of asphalt mixes since September 1993 by the Office of Materials and Research of the Georgia DOT. The experience of the Georgia DOT has shown that this machine is easier to use than the static compaction procedure, can fabricate asphalt beam samples with uniform and controllable densities, and can significantly improve the productivity of fabricating asphalt beam samples. Since the rolling compaction and the kneading compaction methods each offer certain advantages over the other, additional evaluations will be made in the future round robin evaluation program before deciding which method should be adopted as the standard procedure for fabricating asphalt beam samples.

ACKNOWLEDGMENTS

The authors gratefully acknowledged the funding provided by FHWA through GaDOT. The assistance by Ronald Collins and Lamar Caylor of the GaDOT Office of Materials and Research is greatly appreciated.

REFERENCES

1. Lai, J. S. *Development of a Simplified Test Method to Predict Rutting Characteristics of asphalt Mixes*. Research Project No. 8502, Final Report. Georgia Department of Transportation, Atlanta, July 1986.
2. Lai, J. S. *Evaluation of the Effect of Gradation of Aggregate on Rutting of Asphalt Mixes*. Research Project No. 8706, Final Report. Georgia Department of Transportation, Aug. 1988.
3. Lai, J. S., and T. M. Lee. *Use of a Loaded Wheel Testing Machine to Evaluate Rutting of Asphalt Mixes*. In *Transportation Research Record 1269*, TRB, National Research Council, Washington, D.C., 1990, pp. 116–123.
4. West, R. C., G. C. Page, and K. H. Murphy. *Evaluation of the Loaded Wheel Tester*. Research Report FL/DOT/SMO/91-391. Florida Department of Transportation, Tallahassee, Dec. 1991.
5. Lai, J. S. Results of the Round Robin Test Program for Evaluating Rutting of Asphalt Mixes Using Loaded Wheel Tester. Presented at the 72nd Annual Meeting of the Transportation Research Board, Washington, D.C., 1993.
6. Aschenbrener, T., and K. Stuart. *Comparison of Results Obtained From the French Tester With Pavements of Known Behavior*. Colorado Department of Transportation, Denver, Oct. 1992.

Publication of this paper sponsored by Committee on Characteristics of Bituminous Paving Mixtures to Meet Structural Requirements.

Effect of Coarse Aggregate Content on Stone Matrix Asphalt Durability and Low-Temperature Cracking

KEVIN D. STUART AND WALAA S. MOGAWER

The effects of coarse aggregate content on the resistance of stone matrix asphalt (SMA) mixtures to moisture damage, aging, and low-temperature cracking were evaluated. Extractions were also performed to determine whether the Marshall hammer crushed aggregates during the mixture designs. The coarse aggregate content was varied by changing the percentages of aggregate passing the 4.75- and 2.36-mm sieves. These sieves control the degree of gap in an SMA mixture. The percentages of aggregate passing the other sieve sizes were not varied. Moisture susceptibility was affected more by the type of aggregate and the type of stabilizer than by gradation, or coarse aggregate content. Decreases in long-term aging with increasing coarse aggregate content were provided by three of four sets of coarse aggregate contents. (The use of two stabilizers and two aggregate types provided the four sets of coarse aggregate contents.) However, these decreases in aging only occurred at the highest test temperatures, which were 16°C and 32°C. Long-term aging had no significant effect on the data compared with no aging at lower temperatures; therefore, coarse aggregate content could have no effect. Studies concerned with the effects of coarse aggregate content on low-temperature cracking were inconclusive. The amount of aggregate broken during compaction increased with an increase in coarse aggregate content. The cumulative percentage passing the 4.75-mm sieve increased by more than 5 percent for the gradations closest to those recommended by FHWA's *SMA Model Material and Construction Guidelines*. The increases were as great as 15.8 percent.

Stone matrix asphalts (SMAs) are gap-graded hot mixtures that maximize the coarse aggregate and binder contents (*1,2*). SMA mixtures have a high proportion of high-quality manufactured coarse aggregate, a high proportion of binder and mineral filler, and a low proportion of middle-sized aggregate as compared with dense-graded mixtures. The higher proportion of coarse aggregate in an SMA mixture provides more contact points between the coarse aggregate particles. The increase in contact points provides a high resistance to rutting and may reduce the influence of the type and amount of binder on rutting.

OBJECTIVE

This paper documents Phase II of an FHWA study in which the effects of coarse aggregate content on the properties of SMA mixtures were determined. The 4.75- and 2.36-mm sieves were used to control the degree of gap and coarse aggregate content of SMA mixtures and, together with the amount of material passing the 75-μm sieve, control the optimum binder content.

K. D. Stuart, Federal Highway Administration, Turner-Fairbank Highway Research Center, 6300 Georgetown Pike, McLean, Va. 22101-2296. W. S. Mogawer, Civil Engineering Department, University of Massachusetts—Dartmouth, North Dartmouth, Mass. 02747.

The objective of Phase I was to determine the effects of coarse aggregate content on rutting and draindown (see paper by Mogawer and Stuart in this Record). Draindown of the mastic can occur during construction. The primary use of SMA mixtures is to reduce rutting.

The objective of Phase II was to determine the effects of coarse aggregate content on moisture susceptibility, aging, low-temperature cracking, and aggregate degradation during compaction in the laboratory. The Phase I study showed that coarse aggregate content had no effect on rutting susceptibility. However, the variations in the compositions of the mixtures could affect other properties. For example, if the optimum binder content increases with an increase in coarse aggregate content, the resistance to moisture damage and aging, and possibly to low-temperature cracking, may improve.

MATERIALS

Aggregates

Crushed diabase and limestone aggregates were used. The diabase aggregate is used extensively in Northern Virginia and has been used in SMA mixtures. The limestone aggregate was used in the Strategic Highway Research Program (SHRP) and was designated "RC." Aggregate properties are given in Table 1.

The three gradations used in this study were designated Gradations I, II, and III, which consisted of 80, 70, and 60 percent aggregate retained on the 4.75-mm sieve, respectively. The gradations met both the FHWA *SMA Model Material and Construction Guidelines* (*2*) and gradation limits based on German specifications, except that the percentages passing the 4.75- and 2.36-mm sieves were allowed to vary (*1,2*). Only Gradation I met the guidelines for these two sieves. With higher coarse aggregate contents, the gap in the gradation is higher, which should increase the optimum binder content.

The Los Angeles abrasion test provided a mass loss of 17.8 percent for the diabase coarse aggregate, which was below the maximum allowable loss of 30 percent recommended by the FHWA guidelines. The limestone coarse aggregate showed a mass loss of 35.4 percent. Assuming that the recommendation of 30 percent is valid, the limestone coarse aggregate may be susceptible to degradation in the hot-mix plant or under traffic. Aggregates with different losses were included in the study to determine if mixture properties, primarily rutting and aggregate degradation during compaction, are affected by abrasion resistance.

The FHWA guidelines also recommend that no more than 20 percent by mass of the coarse aggregate particles have a length-to-

TABLE 1 Aggregate Properties

Gradations:

Sieve Size	Gradation, Percent Passing I	II	III	SMA Model Recommendation	FHWA-RD-92-006 Based on German Specifications
19.0 mm	100.0	100.0	100.0	100.0	100
12.5 mm	95.0	95.0	95.0	85-95	90-100
9.5 mm	68.0	68.0	68.0	75 (Maximum)	34-75
4.75 mm	20.0	30.0	40.0	20-28	23-41
2.36 mm	17.0	22.0	26.0	16-24	18-30
1.18 mm	16.0	16.0	16.0		15-24
600 μm	14.0	14.0	14.0	12-16	12-20
300 μm	12.0	12.0	12.0	12-15	10-17
150 μm	10.0	10.0	10.0		9-14
75 μm	9.0	9.0	9.0	8-10	8-13

Specific Gravities (SG) and Absorption:

	Diabase Gradation I	II	III	Limestone Gradation I	II	III
Bulk Dry SG	2.827	2.832	2.843	2.506	2.513	2.526
Bulk SSD SG	2.861	2.865	2.873	2.578	2.586	2.591
Apparent SG	2.916	2.885	2.932	2.701	2.709	2.701
Percent Absorption	1.16	1.17	1.07	2.88	2.88	2.56

SSD: Saturated Surface Dry.

Los Angeles Abrasions of the Particles in the Predominant Size Fractions Above the 2.36-mm Sieve, Percent Mass Loss:

Diabase Coarse Aggregate = 17.8
Limestone Coarse Aggregate = 35.4

thickness ratio greater than 3 to 1, and that no more than 5 percent of the particles have a length-to-thickness ratio greater than 5 to 1. Approximately 18 percent of the limestone coarse aggregate particles had a length-to-thickness ratio greater than 3 to 1, and 3.1 percent had one greater than 5 to 1. Approximately 33 percent of the diabase coarse aggregate particles had a length-to-thickness ratio greater than 3 to 1, but only 2.9 percent had one greater than 5 to 1. Assuming that the recommendations are valid, there may be some breaking of the diabase aggregate particles in the hot-mix plant or under traffic. Previous stockpiles of the diabase aggregate had passed the recommendation (*3*). However, the percentage of flat and elongated particles in the aggregate varies over time and with the source. It was decided to determine whether mixture properties, primarily rutting and aggregate degradation during compaction, are affected by a high number of flat and elongated particles.

Binders and Stabilizers

An AC-20 and Styrelf 1-D were used as binders. The AC-20, designated "ABC" by SHRP, was stabilized with a loose cellulose fiber named Interfibe 230. Interfibe is a domestic cellulose fiber supplied by the Interfibe Corporation (Portage, Mich.). It was added at 0.3 percent by mixture mass; this is the typical percentage used in practice.

Styrelf is an asphalt reacted with styrene-butadiene (SB) and shipped by the supplier in bulk form. It was supplied by the Koch Materials Company (Pennsauken, N.J.). Styrelf was considered to be a stabilizer in this study, although the stabilizer is the reacted SB.

MIXTURE TESTING PROGRAM

The following mixture tests were performed. The analysis of variance (ANOVA) and the *t*-test at a confidence level of 95 percent were used to evaluate the data.

- Marshall mixture design,
- Resistance to moisture damage,
  - —ASTM D 4867,
  - —Hamburg wheel-tracking device,
- Resistance to aging (Superpave Method M-007),
  - —No aging,
  - —Short-term oven aging (STOA),
  - —Long-term oven aging (LTOA),
- Resistance to low-temperature cracking,
  - —Diametral modulus (Md) at −32°C and −16°C.
  - —Indirect tensile test at −16°C,
- Aggregate degradation through extractions.

MIXTURE TEST DESCRIPTIONS

SMA Mixture Design

The SMA mixtures were designed by the 50-blow Marshall method (*2*). The optimum binder contents were based on an air void level of 3.5 percent. The target mixing and compaction temperatures were 154°C and 143°C, respectively.

The experimental design originally involved 12 mixtures consisting of two aggregate types (diabase and limestone), three grada-

tions (I, II, and III), and two stabilizers (Interfibe and Styrelf). Diabase Gradation I with Styrelf was eliminated because of excessive draindown. Specimens for this mixture could not be fabricated.

Resistance to Moisture Damage

ASTM D 4867: Effect of Moisture on Asphalt Concrete Paving Mixtures

ASTM D 4867 was one of two methods used to evaluate moisture susceptibility (*4*). Three unconditioned (dry) and three conditioned (wet) specimens were tested per mixture. Wet specimens were (*a*) vacuum-saturated with distilled water so that 55 to 80 percent of the air voids were filled with water, (*b*) subjected to a freezing cycle for 15 hr at −18.0 ± 2.0°C, (*c*) soaked in a 60°C distilled water bath for 24 hr, and (*d*) tested at 25°C along with the dry specimens. Specimens were compacted by the Marshall hammer. A target air void range of 5 to 6 percent was used because SMA mixtures are specified to have less than 6 percent air voids after compaction in the field.

The diametral modulus (M_d) and indirect tensile strength (S_t) tests were performed. The M_d's were measured using an apparatus manufactured by the Retsina Company (Oakland, Calif.). Although marketed to measure a resilient modulus, the apparatus provides a total modulus at a loading time of 0.1 sec by applying a load on the vertical diameter of a specimen and measuring the total horizontal tensile deformation. The equation used to calculate M_d is

$$M_d = \frac{P(u + 0.2734)}{tH_t} \quad (1)$$

where

M_d = diametral modulus (MPa),
P = load (N),
u = Poisson's ratio (assumed as 0.35),
t = specimen thickness (mm), and
H, S_t = total horizontal deformation (mm).

The S_t tests were performed at a loading rate of 50.8 mm/min. The equation used to compute the S_t of a specimen 101.6 mm in diameter specimen is

$$S_t = \frac{6.27P}{t} \quad (2)$$

where

S_t = indirect tensile strength (kPa),
P = load (N), and
t = thickness (mm).

The diametral modulus-retained ratio (M_dR) and tensile strength-retained ratio (TSR) were computed for each mixture in terms of percentages. A retained ratio is the average wet value divided by the average dry value.

The average percentage of visual stripping was also estimated for each mixture. Visual stripping is the percentage of area that is stripped relative to the total area of the split surfaces of the specimen.

The percent swell for each mixture, the average change in the volumes of the specimens due to moisture conditioning, was also measured. A high amount of swell indicates internal damage.

A TSR below 80 percent, an M_dR below 70 percent, and visual stripping above 10 percent are suggested criteria for considering a mixture to be susceptible to moisture damage (*5*). Swells equal to or greater than 1 percent were used as indicators of high internal damage, although a firm maximum allowable swell has not been established (*5*). These criteria were developed for dense-graded mixtures. Their applicability to SMA mixtures has not been verified.

Hamburg Wheel-Tracking Device

The Hamburg wheel-tracking device produces moisture damage by rolling a steel wheel across the surface of a slab that is submerged in water at 50°C for 20,000 passes. The device tests two slabs at a time using two reciprocating solid-steel wheels with a diameter of 203.5 mm and a width of 47.0 mm. The load is 710 N. The slabs had a length of 320 mm, a width of 260 mm, and a thickness of 80 mm.

A maximum allowable rut depth of 4 mm at 20,000 passes is used by the city of Hamburg, Germany. The Colorado Department of Transportation recommends maximum allowable rut depths of 4 mm at 10,000 passes and 10 mm at 20,000 passes, based on correlations between their test data and moisture damage in pavements (*6*).

The postcompaction consolidation, creep slope, stripping inflection point, and stripping slope can also be analyzed (*7*). Postcompaction consolidation is the deformation at 1,000 passes. It is called postcompaction consolidation because the wheel is assumed to be compacting the mixture within 1,000 passes. Creep slope is a measure of the accumulation of permanent deformation due primarily to mechanisms other than moisture damage. It is the inverse of the rate of deformation in the linear region of the curve after consolidation has ended and before the stripping inflection point. It is the number of passes required to create a 1-mm rut depth. The stripping inflection point is the number of passes at the intersection of the creep slope and the stripping slope. It is the number of passes at which moisture damage starts to dominate performance. Inflection points below 10,000 passes indicate moisture susceptibility (*6*). Stripping slope is a measure of the accumulation of permanent deformation due primarily to moisture damage. It is the inverse of the rate of deformation after the stripping inflection point. It is also the number of passes required to create a 1-mm rut depth. Higher inflection points and stripping slopes, as hypothesized, indicate less moisture damage (*7*).

Resistance to Aging (Age Hardening)

The mixtures were oven-aged according to Superpave Method M-007 (*8*). This method states that short-term oven aging (STOA) produces the average amount of aging at 6 months to 2 years of service life. Long-term oven aging (LTOA) produces the average amount of aging at approximately 10 years of service life.

For STOA, the loose mixture was placed in a forced draft oven for 4 hr at 135°C. The mixture was then compacted to an air void level of 5 to 6 percent. For LTOA, the compacted specimens were placed in a forced-draft oven for 5 days at 85°C.

M_d's were measured at −32°C, −16°C, 0°C, 16°C, and 32°C. Deformations were maintained within a range of 76 to 200 E-05 mm by varying the load. The test is virtually nondestructive in this range, and the same specimens can be tested at all temperatures. Specimens were tested at the lowest temperature first. They were stored at the test temperature for 24 hr before testing.

Surface-course mixtures with lower M_d values are more flexible and therefore more resistant to fatigue cracking. (This generalization may not be valid when modified and unmodified binders are compared. Therefore, comparisons between the SMA mixtures with Interfibe and with Styrelf should be made with caution.) Mixtures with greater resistances to aging are better able to maintain flexibility.

Resistance to Low-Temperature Cracking

The M_d and indirect tensile strength tests were used to evaluate low-temperature cracking at an air void level of 5 to 6 percent. The M_d values measured to evaluate the effects of coarse aggregate content on aging included temperatures of −32°C and −16°C. These data were also used to evaluate low-temperature cracking. A lower M_d is equated with a greater resistance to low-temperature cracking. (Like the prior hypothesis for aging, this generalization may not be valid in comparisons between modified and unmodified binders.)

Indirect tensile strength tests were performed on unaged and LTOA specimens at −16°C with a loading rate of 1.27 mm/min. Tensile strength (S_t), horizontal tensile strain at failure (e_t), and the amount of work needed to cause tensile failure were evaluated. The work is the area under the stress-strain curve from the beginning of the test until failure. Higher e_t's and higher amounts of work are associated with increased resistance to low-temperature cracking. These increases are usually accompanied by lower S_t's, although this generalization may not be true for all modified binders. The equation used to compute S_t, assuming a Poisson's ratio of 0.35, is

$$e_t = 0.0205\, H_t \quad (3)$$

where e_t is the horizontal tensile strain at failure and H_t is the total horizontal deformation in millimeters.

Aggregate Degradation

Extractions were performed to determine whether the 50-blow Marshall hammer procedure crushed the aggregates and whether degradation varied with aggregate type, aggregate gradation, or stabilizer type. A previous study showed that the Marshall hammer can break the coarse aggregate (*3*). Each mixture was compacted using 50 blows per side. The centrifuge method of extraction was used.

RESULTS AND DISCUSSION

Mixture Design

Properties at the optimum binder contents are given in Table 2. Diabase Gradation I with Styrelf was eliminated because of excessive draindown. There are two possible reasons for its erroneous binder content of 8.4 percent. First, draindown occurred during the design. Additional binder was probably needed to account for the loss due to draindown. Second, some SMA mixtures with high binder contents may contain as much as 3.5 percent encapsulated air voids. The air voids do not significantly decrease below this level as the binder content is increased.

There was a trend of increasing binder content, increasing voids in the mineral aggregate, increasing voids filled with asphalt, and decreasing stability with increasing coarse aggregate content. Gradation I had the most coarse aggregate. Gradations I and II had

TABLE 2 Mixture Design Properties

	Diabase Gradation			Limestone Gradation		
	I	II	III	I	II	III
			Interfibe Mixtures			
OAC, % by Mass	7.5	6.3	5.7	6.7	5.7	5.6
OAC, % by Volume	17.6	15.1	13.8	14.5	12.6	12.3
Eff OAC, % by Volume	16.7	14.1	13.3	12.5	10.9	10.6
Air Voids, %	3.5	3.5	3.5	3.5	3.5	3.5
VMA, %	20.2	17.7	16.8	16.1	14.4	14.0
VFA, %	80.2	80.2	79.3	78.3	75.8	75.2
Flow, 0.25 mm	18	18	15	18	20	17
Stability, N	7 819	7 819	9 000	7 633	8 404	10 498
			Styrelf Mixtures			
OAC, % by Mass	8.4	6.6	6.2	6.8	5.7	5.5
OAC, % by Volume	19.5	15.6	14.7	14.7	12.6	12.2
Eff OAC, % by Volume	18.5	14.7	13.9	12.8	10.8	10.5
Air voids, %	3.5	3.5	3.5	3.5	3.5	3.5
VMA, %	22.2	18.4	17.6	16.4	14.4	14.0
VFA, %	84.2	81.0	80.2	78.7	75.8	75.1
Flow, 0.25 mm	31	28	28	25	24	23
Stability, N	8 756	10 337	13 390	9 547	12 094	12 193

OAC: Optimal Asphalt (Binder) Content.
Eff OAC: Effective Optimum Asphalt (Binder) Content.
VMA: Voids in the Mineral Filler.
VFA: Voids Filled With Asphalt.

the larger differences in binder content. The differences in binder contents between Gradations II and III were less. The flows were not significantly affected by coarse aggregate content.

The hypothesis evaluated in this study was that as the binder content for a given aggregate type increased, the resistance to moisture damage, aging, and low-temperature cracking would improve. Therefore, Gradation I would have the greatest resistance and Gradation III, the least resistance. Gradation II should produce data closer to those for Gradation III because they had similar binder contents. Also, the limestone mixtures had lower binder contents than the diabase mixtures at equal air void levels.

Resistance to Moisture Damage

ASTM D 4867

Table 3 shows that all three diabase gradations with Interfibe had failing TSR and M_dR values, although Gradations I and II had higher retained ratios and lower percentages of swell than Gradation III. The ratios for Gradations I and II indicate a slight-to-moderate susceptibility to moisture damage. The low ratios for Gradation III indicate a high susceptibility to moisture damage. All three percentages of visual stripping show severe stripping. Table 4 shows that both diabase gradations with Styrelf passed the tests; thus, there were no differences between the two gradations in terms of moisture susceptibility.

Tables 3 and 4 show that all six limestone mixtures failed the tests and that the resistance to moisture damage was not a function of gradation. The limestone mixtures exhibited more damage than the diabase mixtures. This is probably related to aggregate type, although the limestone mixtures also had significantly lower binder contents by volume. The three limestone gradations with Styrelf exhibited less damage compared with the three limestone mixtures with Interfibe.

Overall, the data were affected more by the type of aggregate and the type of stabilizer than by gradation. The data also show that both the dry S_t and the dry M_d decreased with an increase in coarse aggregate content.

Hamburg Wheel-Tracking Device

The test results in Table 5 show that all three diabase gradations with Interfibe had stripping inflection points less than 10,000 passes and very steep stripping slopes. These data indicate a moderate-to-high susceptibility to moisture damage. The inflection points were not well defined because of rapid failure. There were no statistically significant differences between the data for the three gradations. Both diabase gradations with Styrelf passed the tests, and there were no differences between the two gradations in terms of moisture susceptibility.

These conclusions were similar to those given by ASTM D 4867 except that gradation had no effect on the wheel-tracking data for the three diabase gradations with Interfibe. The effects of the wheel-tracking device were more severe on Gradations I and II with Interfibe, based on a comparison between the wheel-tracking data and the retained ratios. However, the data from the wheel-tracking device matched the high levels of visual stripping provided by ASTM D 4867.

Only Gradation I of the limestone mixtures was tested. Both the Interfibe and Styrelf mixtures failed the test rapidly because of both moisture damage and observable crushing of the aggregate. This aggregate had a Los Angeles abrasion weight loss of 35.4 percent. Gradations II and III were not tested because of the poor performance using Gradation I, especially the observation that the aggregate was being crushed under the force of the steel wheel. The steel wheel cut the aggregate particles as it traveled back and forth. The resultant changes in gradation could not be measured because the portion of the slab that the wheel damaged was too small to obtain a representative sample; in addition, the high degree of disruption caused aggregate particles to become dislodged from the slabs. The applicability of the device for testing all mixtures is questionable.

TABLE 3 Moisture Damage Results for Interfibe Mixtures

	Diabase Gradation			Limestone Gradation		
	I	II	III	I	II	III
Tensile Strength Test at 25°C:						
Average Dry, kPa	360	444	520	446	506	570
Average Wet, kPa	261	328	252	194	216	232
Retained Ratio (TSR), %	72.5	73.9	48.5	43.5	42.7	40.7
	Fail	Fail	Fail	Fail	Fail	Fail
Diametral Modulus Test at 25°C:						
Average Dry, MPa	663	1 027	1 138	1 287	1 462	1 771
Average Wet, MPa	415	628	467	344	390	414
Retained Ratio (M_dR), %	62.6	61.1	41.0	26.7	26.7	23.4
	Fail	Fail	Fail	Fail	Fail	Fail
Average Visual Stripping, %	50	50	60	80	80	80
	Fail	Fail	Fail	Fail	Fail	Fail
Average Swell, % by Volume	0.2	-0.1	0.8	1.4	1.3	1.6
Average Air Voids, %	5.6	5.2	5.7	5.5	5.6	5.5

TABLE 4 Moisture Damage Results for Styrelf Mixtures

	Diabase Gradation			Limestone Gradation		
	I	II	III	I	II	III
Tensile Strength Test at 25°C:						
Average Dry, kPa	Not	622	667	688	792	824
Average Wet, kPa	Tested	616	654	422	511	585
Retained Ratio (TSR), %		99.0	98.1	61.3	64.5	71.0
		Pass	Pass	Fail	Fail	Fail
Diametral Modulus Test at 25°C:						
Average Dry, MPa		948	1 229	1 540	1 889	2 316
Average Wet, MPa		940	1 237	820	1 164	1 189
Retained Ratio (M_dR), %		99.2	101	53.2	61.6	51.3
		Pass	Pass	Fail	Fail	Fail
Average Visual Stripping, %		2.5	5.0	40	40	40
		Pass	Pass	Fail	Fail	Fail
Average Swell, % by Volume		-0.4	0.6	0.8	0.7	0.9
Average Air Voids, %		5.4	5.4	5.4	5.6	5.5

Resistance to Aging

The M_d's for the unaged, STOA, and LTOA specimens are given in Table 6. One specimen of diabase Gradation II and one specimen of limestone Gradation I, both containing Styrelf, fell apart during LTOA and could not be tested.

The trend at all temperatures and at all three levels of aging was that the M_d's were lowest for Gradation I. This gradation had the most coarse aggregate and highest binder contents. A firm conclusion regarding the effects of coarse aggregate content on aging could not be stated because the data were not dependent on the degree of aging. This was confirmed using ANOVAs.

To evaluate the data further, the differences in M_d between STOA and unaged, LTOA and unaged, and LTOA and STOA specimens were analyzed. These differences are given in Table 7. Differences within 15 percent of the average M_d were within the error of the test and were assigned a value of zero to facilitate the ability to observe trends and eliminate small negative values that would erroneously indicate a decrease in modulus due to aging. STOA and LTOA only provided statistically significant increases in M_d compared with unaged specimens at 16°C and 32°C. The greatest effect on a percentage basis was at 32°C.

An ANOVA performed on the Interfibe data showed that the amount of aging produced by either STOA or LTOA significantly decreased with an increase in coarse aggregate content at 16°C and 32°C. This result was found for both aggregate types. For the Styrelf mixtures, a decrease in aging with increasing coarse aggregate content was only found for the limestone aggregate after LTOA. Therefore, a decrease in long-term aging with increasing coarse aggregate content was provided by three of four sets of coarse aggregate con-

TABLE 5 Hamburg Wheel-Tracking Device Results

	Diabase Gradation			Limestone Gradation		
	I	II	III	I	II	III
			Interfibe Mixtures			
Stripping Inflection Point, Passes	8,523	9,200	8,705	Fail	NT	NT
Stripping Slope, Passes/mm	739	557	422	Fail		
Initial Air Voids, %	6.2	4.7	4.9	4.2		
			Styrelf Mixtures			
Stripping Inflection Point, Passes	NT	None	None	Fail	NT	NT
Stripping Slope, Passes/mm		None	None	Fail		
Initial Air Voids, %		5.1	4.4	5.1		

NT: Not Tested.
Fail: No Data Due to Rapid Failure.
None: No Data Due to the Absence of Moisture Damage.

TABLE 6 Aging Results Using Diametral Modulus Test

	Diabase Gradation			Limestone Gradation		
	I	II	III	I	II	III
			Interfibe Mixtures			
Unaged						
M_d at -32°C, MPa	31 000	31 400	34 700	28 900	31 600	28 600
M_d at -16°C, MPa	25 900	27 800	26 400	20 500	21 400	22 000
M_d at 0°C, MPa	13 100	15 100	15 800	11 000	11 700	13 700
M_d at 16°C, MPa	1 630	2 340	2 720	2 460	3 100	3 230
M_d at 32°C, MPa	262	365	476	519	690	724
STOA						
M_d at -32°C, MPa	33 500	39 300	38 800	28 700	29 200	29 700
M_d at -16°C, MPa	23 700	31 000	32 800	20 800	23 100	23 800
M_d at 0°C, MPa	13 200	15 200	17 900	13 000	13 900	17 600
M_d at 16°C, MPa	2 810	3 910	4 630	3 760	4 920	6 290
M_d at 32°C, MPa	519	816	1 060	977	1 410	1 770
LTOA						
M_d at -32°C, MPa	30 100	42 800	41 500	27 700	29 700	29 700
M_d at -16°C, MPa	23 000	27 900	29 000	22 100	26 200	23 300
M_d at 0°C, MPa	14 300	16 600	17 900	14 500	18 000	17 400
M_d at 16°C, MPa	2 800	4 200	5 180	6 010	7 270	8 600
M_d at 32°C, MPa	545	885	1 160	2 080	2 450	3 190
			Styrelf Mixtures			
Unaged						
M_d at -32°C, MPa	Not	42 700	33 700	28 300	31 500	31 600
M_d at -16°C, MPa	Tested	33 700	30 600	22 500	23 600	24 200
M_d at 0°C, MPa		14 100	16 000	12 300	15 000	15 300
M_d at 16°C, MPa		2 340	3 140	3 010	3 850	4 630
M_d at 32°C, MPa		427	627	731	1 090	1 160
STOA						
M_d at -32°C, MPa		44 600	43 700	28 200	29 400	34 400
M_d at -16°C, MPa		28 900	27 500	21 100	23 200	23 200
M_d at 0°C, MPa		17 500	18 700	13 200	17 000	14 800
M_d at 16°C, MPa		3 380	3 980	3 350	4 680	4 780
M_d at 32°C, MPa		696	945	786	1 240	1 440
LTOA						
M_d at -32°C, MPa		26 200	32 200	25 100	31 900	30 000
M_d at -16°C, MPa		28 300	27 000	21 500	25 400	23 200
M_d at 0°C, MPa		16 100	16 300	13 400	16 300	16 600
M_d at 16°C, MPa		4 040	4 500	4 430	6 470	7 540
M_d at 32°C, MPa		869	938	1 560	2 630	3 580

tents. A decrease in short-term aging with increasing coarse aggregate content was provided by two of four sets—both aggregates with Interfibe. (The lack of a Gradation I for the diabase aggregate with Styrelf may have hindered the analyses.)

A supplemental finding, obtained by comparing the LTOA data at 16°C and 32°C with the STOA data, was that LTOA did not significantly increase the M_d compared with STOA using the diabase aggregate. This finding was found to be statistically valid for all gradations and for both stabilizers. LTOA significantly increased the M_d's of the limestone gradations with either stabilizer. These differences could be due to the lower binder contents by volume of the limestone mixtures and to differences in aggregate surface chemistry.

Statistical analyses at 16°C and 32°C also indicated that there was less aging in the Styrelf mixtures compared with the Interfibe mixtures.

Resistance to Low-Temperature Cracking

The M_d's measured at −32°C and −16°C are shown in Table 6. The M_d's after LTOA were lowest for Gradation I, which had the most coarse aggregate and highest binder contents. Therefore, Gradation I provided the best resistance to low-temperature cracking. There were no statistical differences between Gradations II and III after LTOA. Gradation had no significant effect on the M_d's of the STOA or unaged specimens. Aggregate type and stabilizer type had no significant effect at any aging level.

The log M_d's after LTOA for each set of three gradations were plotted versus temperature so that the differences in M_d's could be converted into differences in temperature. The M_d of each Gradation I was used as the reference stiffness because it provided the best resistance to low-temperature cracking. The temperatures corresponding to this stiffness were then obtained from the plots for Gradations II and III. Gradations II and III had temperatures that were 3°C to 8°C higher than Gradation I at −16°C, and 6°C to 16°C higher at −32°C. This shows that the effect of gradation on low temperature properties can be significant.

The indirect tensile strength test data are shown in Table 8. There was a trend of decreasing tensile strength with increasing coarse aggregate content for both aggregates. This trend was statistically significant for four of eight sets of three gradations. The Styrelf mixtures had significantly higher tensile strengths than the Interfibe mixtures. However, coarse aggregate content, aggregate type, and

TABLE 7 Change in Diametral Modulus Caused By Aging

	Diabase Gradation			Limestone Gradation		
	I	II	III	I	II	III
			Interfibe Mixtures			
STOA to Unaged						
M_d at -32°C, MPa	0	7 900	0	0	0	0
M_d at -16°C, MPa	0	0	6 400	0	0	0
M_d at 0°C, MPa	0	0	0	2 000	2 200	3 900
M_d at 16°C, MPa	1 180	1 570	1 910	1 300	1 820	3 060
M_d at 32°C, MPa	257	451	580	458	720	1 050
LTOA to Unaged						
M_d at -32°C, MPa	0	11 400	6 800	0	0	0
M_d at -16°C, MPa	0	0	0	0	4 800	0
M_d at 0°C, MPa	0	0	0	3 500	6 300	3 700
M_d at 16°C, MPa	1 170	1 860	2 460	3 550	4 170	5 370
M_d at 32°C, MPa	283	520	680	1 560	1 760	2 470
LTOA to STOA						
M_d at -32°C, MPa	0	0	0	0	0	0
M_d at -16°C, MPa	0	0	0	0	0	0
M_d at 0°C, MPa	0	0	0	0	4 100	0
M_d at 16°C, MPa	0	0	0	2 250	2 350	2 310
M_d at 32°C, MPa	0	0	0	1 100	1 040	1 420
			Styrelf Mixtures			
STOA to Unaged						
M_d at -32°C, MPa	Not	0	10 000	0	0	0
M_d at -16°C, MPa	Tested	0	0	0	0	0
M_d at 0°C, MPa		3 400	0	0	0	0
M_d at 16°C, MPa		1 040	840	0	830	0
M_d at 32°C, MPa		269	318	0	0	280
LTOA to Unaged						
M_d at -32°C, MPa		0	0	0	0	0
M_d at -16°C, MPa		0	0	0	0	0
M_d at 0°C, MPa		0	0	0	0	0
M_d at 16°C, MPa		1 700	1 360	420	2 620	2 910
M_d at 32°C, MPa		442	311	829	1 540	2 420
LTOA to STOA						
M_d at -32°C, MPa		0	0	0	0	0
M_d at -16°C, MPa		0	0	0	0	0
M_d at 0°C, MPa		0	0	0	0	0
M_d at 16°C, MPa		660	520	1 080	1 790	2 760
M_d at 32°C, MPa		173	0	774	1 390	2 140

stabilizer type had no significant effect on e_t or work. The variabilities of the replicate strain measurements of each mixture were high, and well-defined tensile cracks were not obtained. The test may not be applicable to SMA mixtures.

Aggregate Degradation

The data for the Interfibe mixtures are given in Table 9. Gradation and aggregate type affected the amount of broken aggregate, but the type of stabilizer was not a factor. Compared with the gradations in Table 1, the extracted gradations show that aggregate was broken during the 50-blow Marshall mixture designs. There was an increase in broken aggregate with an increase in coarse aggregate content, and the limestone aggregate degraded more than the diabase aggregate. Diabase Gradations I and II and all three limestone gradations had an increase of more than 5 percent with the 4.75-mm sieve. The greatest increase was 15.8 percent.

The limestone gradations also had increases in the range of 2 to 3 percent with the 75-μm sieve. The diabase gradations had an increase of less than 1 percent, which matches what has been found by FHWA for dense-graded mixtures containing this aggregate. No change with the 4.75-mm sieve was found when the diabase aggregate was used in dense-graded mixtures. The amount of degradation for the limestone aggregate when used in dense-graded mixtures is not known by the authors.

The degradation of the limestone aggregate was most likely related to its lack of abrasion resistance and hardness. The limestone coarse aggregate had a Los Angeles abrasion loss of 35.4 percent; the diabase coarse aggregate had a loss of 17.8 percent. The extracted aggregates did not provide an association between the degradation of the diabase aggregate and its high number of flat and elongated particles. An examination of the extracted aggregate from diabase Gradation I with Interfibe showed that the percentage of flat and elongated particles in the aggregate did not decrease. To investigate further the effects of the percentage of flat and elongated particles, additional specimens were compacted using diabase Gradations I and II with Interfibe after the percentage of flat and elongated particles was decreased from 33 to 19 percent. The degradation shown by the change with the 4.75-mm sieve was lowered from 10.0 to 5.1 percent for Gradation I, and from 6.5 to 5.6 percent for Gradation II. The percentage of flat and elongated particles

TABLE 8 Low-Temperature Cracking Results Using Indirect Tensile Strength Test At −16°C

	Diabase Gradation			Limestone Gradation		
	I	II	III	I	II	III
			Interfibe Mixtures			
Unaged						
Tensile Strength, kPa	1030	1290	1200	900	1270	1700
Strain (× 1000)	2.20	3.80	1.90	0.60	1.20	0.60
Work, KPa	1.86	3.41	1.99	0.38	0.93	0.64
LTOA						
Tensile Strength, kPa	1100	1510	1700	1400	1500	1520
Strain (× 1000)	3.30	2.20	1.00	0.40	1.30	1.00
Work, KPa	2.47	1.98	1.32	0.48	1.36	0.83
			Styrelf Mixtures			
Unaged						
Tensile Strength, kPa	Not	1420	1590	1340	1690	1890
Strain (× 1000)	Tested	2.90	2.50	1.50	2.10	1.30
Work, KPa		2.97	3.32	1.28	2.68	1.99
LTOA						
Tensile Strength, kPa		1780	1990	1240	2110	2160
Strain (× 1000)		2.70	2.60	2.10	1.40	1.10
Work, KPa		3.94	3.83	1.11	2.00	1.69

TABLE 9 Aggregate Gradations (Percent Passing) of Interfibe Mixtures After Extractions

Sieve Size	Diabase Gradation			Limestone Gradation		
	I	II	III	I	II	III
Marshall design specimens (50 blows):						
19.0 mm	100.0	100.0	100.0	100.0	100.0	100.0
12.5 mm	93.3	94.5	94.9	95.9	95.3	96.2
9.5 mm	72.0	72.5	69.8	75.8	74.7	74.2
4.75 mm	30.0	36.5	43.2	35.8	40.8	46.8
2.36 mm	20.4	25.1	29.8	23.9	28.6	32.0
1.18 mm	17.6	18.1	18.8	20.0	21.2	21.2
600 μm	15.3	15.4	15.7	17.1	17.8	17.3
300 μm	13.3	13.4	13.6	14.8	15.3	15.0
150 μm	11.3	11.3	11.5	13.0	13.3	13.2
75 μm	9.6	9.7	9.9	11.3	11.8	11.6
JMF at 4.75 mm	20.0	30.0	40.0	20.0	30.0	40.0
JMF at 75 μm	9.0	9.0	9.0	9.0	9.0	9.0
Increase at 4.75 mm:	10.0	6.5	3.2	15.8	10.8	6.8
Increase at 75 μm:	0.6	0.7	0.9	2.3	2.8	2.6
Marshall-size specimens tested for moisture damage, aging, and low-temperature cracking (Blows ranged from 17 to 28):						
Increase at 4.75 mm:	6.8	5.9	4.2	12.3	10.0	7.7
Increase at 75 μm:	0.5	1.1	1.1	1.9	1.6	1.8
Slabs for the French Pavement Rutting Tester (Pneumatic rubber tire compaction was used to compact slabs to the design air-void level):						
Increase at 4.75 mm:	5.2	3.3	NT	6.8	4.8	NT
Increase at 75 μm:	1.3	1.6		2.7	1.8	

JMF: Proposed Job-Mix Formula.
NT: Not Tested.

appeared to have some effect on degradation, but degradation was still high using 19 percent flat and elongated particles.

Specimens with Interfibe, representing those used in other mixture tests, were also compacted and extracted. Marshall-size specimens tested for moisture damage, aging, and low-temperature cracking were compacted using blows ranging from 17 to 28. Slabs for the French pavement rutting tester (Phase I rutting study) were compacted using a rolling pneumatic rubber tire. A review of all of the data in Table 9 showed that the extracted gradations varied with the mixing and compaction procedure. Therefore, the coarse aggregate contents were not consistent throughout the study. The procedure using the rubber tire compactor degraded the aggregate less than the Marshall hammer procedure based on the aggregate passing the 4.75-mm sieve.

CONCLUSIONS

1. There was a trend of increasing binder content, increasing voids in the mineral aggregate, increasing voids filled with asphalt, and decreasing stability with increasing coarse aggregate content.
2. Moisture susceptibility was affected more by aggregate type and stabilizer type than by coarse aggregate content.
3. Short- and long-term oven aging (STOA and LTOA) only provided increases in M_d compared with unaged specimens at 16°C and 32°C. The degree of aging had no consistent effect at −32°C, −16°C, and 0°C. A decrease in long-term aging with increasing coarse aggregate content was provided by three of four sets of coarse aggregate contents at 16°C and 32°C. (The use of two stabilizers and two aggregate types provided the four sets of coarse aggregate contents.) A decrease in short-term aging with increasing coarse aggregate content was provided by two of four sets at 16°C and 32°C.
4. The low-temperature cracking studies were inconclusive. The effects of coarse aggregate content depended on the degree of aging according to the M_d's. As the degree of aging increased, there was a trend for increasing resistance to low-temperature cracking using the coarsest gradation. However, gradation had no significant effect on the indirect tensile strain at failure (S_t) or work. This test did not produce well-defined tensile cracks; thus, it may not be applicable to SMA mixtures.
5. Mixtures with Styrelf had greater resistances to aging at 16°C and 32°C and to moisture damage than mixtures with Interfibe. Low-temperature properties were not significantly affected by the type of stabilizer.
6. The amount of aggregate broken during the mixture designs increased with an increase in coarse aggregate content. The cumulative percent passing the 4.75-mm sieve increased by more than 5 percent for Gradations I and II, which were closest to the gradations recommended by the FHWA guidelines.
7. The degree of degradation also varied with the mixing and compaction procedure. A procedure using a rubber tire compactor was found to degrade the aggregates less than the Marshall hammer procedure. The coarse aggregate contents were not consistent from test to test because different mixing and compaction procedures had to be used in each test.

RECOMMENDATIONS

1. The gradations of additional SMA mixtures need to be determined after they are designed by extracting the aggregate from the compacted specimens. No guidance can be given at this time as to the acceptable amount of breakage.
2. SMA mixture design methods that do not degrade the aggregate more than in the field are needed. Aggregate degradation in mixtures containing high coarse aggregate contents has been previously observed and is the primary reason why the FHWA design procedure for open-graded friction courses is not based on an analysis of compacted specimens.
3. Additional comparisons between the Hamburg wheel-tracking device and other methods for determining moisture susceptibility, such as ASTM D 4867, are needed. The applicability of using the Hamburg wheel-tracking device to evaluate a variety of mixtures needs to be determined because the steel wheel can crush some aggregates.
4. The applicability of the Superpave LTOA procedure to conditioning SMA mixtures needs to be determined. Two specimens fell apart during LTOA.
5. Correlations between laboratory aging and field aging are needed because the conclusions of a laboratory study can be significantly affected by the degree of aging used.
6. The trend of the M_d's at all temperatures (−32°C, −16°C, 0°C, 16°C, and 32°C) was that they were lowest for Gradation I, which had the most coarse aggregate and highest binder contents, although this trend was not always statistically significant. This trend was also provided by the tensile strengths (S_t). The effect of this trend on fatigue life should be measured using bending beam tests.

REFERENCES

1. Stuart, K. D. *Stone Mastic Asphalt (SMA) Mixture Design.* FHWA Report FHWA-RD-92-006. FHWA, U.S. Department of Transportation, March 1992.
2. SMA Technical Working Group. *SMA Model Material and Construction Guidelines.* FHWA, U.S. Department of Transportation, Oct. 1992.
3. Stuart, K. ., and P. Malmquist. Evaluation of Using Different Stabilizers in the U.S. Route 15 (Maryland) Stone Matrix Asphalt (SMA). In *Transportation Research Record 1454*, TRB, National Research Council, Washington, D.C., 1994, pp. 48–57.
4. American Society for Testing and Materials. *1992 Annual Book of ASTM Standards.* Section 4, Vol. 4.03, Philadelphia, Pa., April 1992.
5. Stuart, K. D. *Evaluation of Procedures Used to Predict Moisture Damage in Asphalt Mixtures.* FHWA Reports FHWA/RD-86/090 and 091. FHWA, U.S. Department of Transportation, March and Sept. 1986.
6. Aschenbrener, T., R. Terrel, and R. Zamora. *Comparison of Hamburg Wheel-Tracking Device and the Environmental Conditioning System to Pavements of Known Stripping Performance.* CDOT-DTD-R-94-1. Colorado Department of Transportation, Denver, Jan. 1994.
7. Hines, M. The Hamburg Wheel-Tracking Device. *Proc., Twenty-Eighth Paving and Transportation Conference.* Civil Engineering Department, The University of New Mexico, Albuquerque, N.Mex., 1991.
8. Strategic Highway Research Program. *SHRP Designation: M-007, Short- and Long-Term Aging of Bituminous Mixes.* Report SHRP-A-379. National Research Council, Washington, D.C., 1994.

Publication of this paper sponsored by Committee on Characteristics of Bituminous Paving Mixtures to Meet Structural Requirements.

Development and Analysis of Laboratory Techniques for Simulating Segregation

TAISIR S. KHEDAYWI AND THOMAS D. WHITE

Objectives of this research were to develop laboratory techniques for simulating asphalt mixture segregation and determine mixture compactibility and physical properties. Segregation in asphalt concrete pavements occurs as a result of nonuniform distribution of the mixture components such as aggregate and asphalt. Mixture segregation can lead to premature pavement distress. Factors and steps in the production, transportation, and placement of asphalt mixtures associated with segregation include material type, mixture design, stockpiling and handling, plant type and operation, surge silos, truck loading and unloading, and laydown. Materials used in the study included gravel, natural sand, and an AC-20 asphalt cement. Aggregates were selected to meet the Indiana Department of Transportation specification for a No. 8 binder with a maximum aggregate size of 25.0 mm (1 in.). In order to simulate various degrees of segregation of the coarse and fine fractions, four artificially segregated asphalt mixtures were prepared in addition to the control asphalt mixture. As part of the study, specimens were compacted for the fine mixtures using the U.S. Corps of Engineers gyratory testing machine to determine the stability and compactibility indexes. Specimens were also prepared and tested using the indirect tensile test method. Slabs of the five mixtures were compacted using a laboratory linear compactor. Subsequently, these slabs were tested using the Purwheel tracking device to determine their rutting potential and moisture susceptibility. Results indicate that segregation affects the residual asphalt content, gradation, stability index, compatibility index, air voids, unit weight, indirect tensile strength, rutting potential, and moisture susceptibility of asphalt concrete mixtures.

Asphalt concrete mixture segregation in pavements occurs as a result of nonuniform distribution of the mixture components such as asphalt and aggregate. Segregation in pavements leads to premature distress such as cracking, rutting, raveling, and stripping. These distresses will affect the performance, serviceability, and structural capacity of the pavement (*1*). Segregation may result from one or a combination of the following factors: aggregate type, mixture design, stockpiling and handling, plant type and operation, truck loading and unloading, and laydown operations.

Asphalt content and gradation have a significant effect on potential for segregation. For example, a gap-graded mixture with low asphalt content is prone to segregation. Brock (*2*) described a gap-graded mixture as one that has a gradation making an S across the maximum density line.

Bryant (*3*) studied the variation of asphalt content as a result of segregation. He concluded that there was a relationship between the degree of segregation and the percentage of extracted asphalt and recommended an effort to reduce segregation because of its potential effects on asphalt mixture characteristics. Brown et al. (*4*) concluded that segregated areas are generally 8 to 15 percent coarser than nonsegregated areas on the No. 8 sieve; the voids are typically 3 to 5 percent higher; and the asphalt content is often 1 to 2 percent lower.

T. S. Khedaywi, Department of Civil Engineering, Jordan University of Science and Technology, Irbid, Jordan. T. D. White, Purdue University, 1284 Civil Engineering Building, West Lafayette, Ind. 47907-1284.

LABORATORY WORK

A laboratory study has been conducted to measure the effect of various degrees of segregation on the physical and mechanical characteristics of asphalt mixtures. A description is provided of materials and tests.

Materials

Asphalt Cement

One asphalt cement (AC-20) was used in the study which was obtained from a storage tank at Fauber Construction Company, Inc., West Lafayette, Indiana. Test results characterizing this asphalt are presented in Table 1.

Aggregate

Aggregates used in the study were gravel and sand meeting Indiana Department of Transportation (INDOT) specifications. The aggregate stockpiles were blended to meet an INDOT #8 binder gradation with a maximum aggregate size of 25.4 mm (1 in.). The gravel and sand were obtained from Vulcan Materials Company and Fairfield Builders Supply Corporation, respectively, of West Lafayette, Ind. Properties and the gradations of the aggregate are given in Tables 2 and 3.

Samples for mix design purposes were compacted using 75 blows on each side with the Marshall manual hammer. An optimum asphalt content of 4.5 percent was selected at 6 percent air voids. This is the current INDOT criterion for selecting optimum asphalt content.

Five mixes with varying degrees of segregation were evaluated in the laboratory. A mixture with a median gradation according to the specifications for INDOT #8 binder gradation and at 4.5 percent asphalt content was used as one degree of segregation (mix design). This heated mixture was sieved over a 10-mm (3/8-in.) sieve creating coarse (retained) and fine (passing) mixtures representing the extremes of segregation. Two other mixtures with intermediate degrees of segregation were produced by combining percentages of the coarse and fine material as shown (1 mm = 0.04 in.):

Mix. No.	Segregation Classification	Percentage of Material + 10 mm	− 10 mm
1	Very fine	0.0	100.0
2	Fine	24.0	76.0
3	Mix design	48.3	51.7
4	Coarse	74.0	26.0
5	Very coarse	100.0	0.0

Mixtures 1 and 5 have visible segregation. The five mixtures are shown in Figure 1.

Sample Gradation

Gradations of the extracted aggregate were determined for each segregated mixture in accordance with ASTM C 1 36. Gradations are shown in Figure 2.

Extracted Asphalt Content

Three extraction tests (ASTM D2172, Method B) were performed on each of the five segregated mixtures. The asphalt content is expressed as the mass percentage of moisture-free mixture. Figure 3(*a*) shows the extracted asphalt versus degree of segregation.

Tests

Gyratory Test

The US Corps of Engineers gyratory testing machine (GTM) was used to compact and test the five mixtures. Segregated specimens were proportioned for an approximate total weight of 1200 g. For example, a batch weight of 1275 g for Mix 2 would be proportioned as 0.24 × 1275 = 306 g of +10-mm (+3/8-in.) material and 0.76 × 1,275 = 969 g of −10 mm (−3/8 in.) material.

Each mixture combination was weighed into a separate mixing bowl. The bowls were placed in an oven and heated to a temperature between 135°C (275°F) and 149°C (300°F). When the mixture was heated, the bowl was removed from the oven and the mixture was mixed by hand with a trowel. The entire batch was placed in the GTM mold and spaded with a heated spatula 15 times around the perimeter and 10 times over the interior. The surface was smoothed to a slightly rounded shape. Temperature of the mixture immediately before compaction was not less than 135°C (275°F). The mold assembly was placed in the GTM.

Specimens were compacted and tested according to ASTM D3387. Three specimens were prepared for each mixture using a 1380-kPa (200-psi) vertical pressure, 1-degree angle of gyration, and 30, 60, and 120 revolutions. After compaction, samples were

TABLE 2 Properties of Aggregate Used

Type of Aggregate	ASTM Test Designation	Bulk Specific Gravity	Apparent Specific Gravity	Water Absorption (percent)
Gravel	C127	2.61	2.66	1.88
Sand	C128	2.60	2.72	1.77

TABLE 3 Aggregate Gradation Used

Sieve Size	Percentage Passing	Specification Limits*
25.00 mm	100	100
19.00 mm	92.5	80-98
12.50 mm	68.0	56-80
9.50 mm	51.2	43-68
No. 4	33.4	25-40
No. 8	28.0 1	4-40
No. 16	20.6	8-32
No. 30	12.8	5-24
No. 50	4.5	2-16
No. 100	0.8	0-10
No. 200	0.3	0-3

25.4 mm=1 inch

*Indiana Department Of Transportation Specification Limits

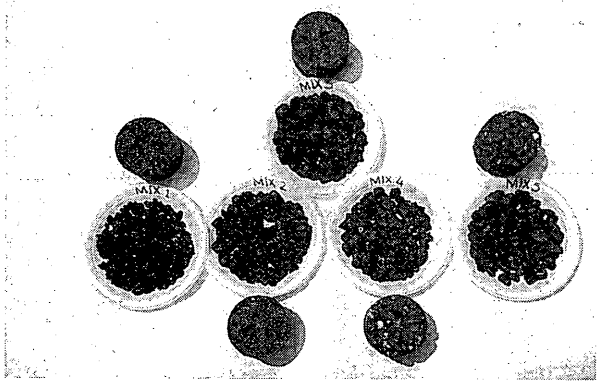

FIGURE 1 Samples from prepared mixes and specimens.

TABLE 1 Properties of Asphalt Used

Property	ASTM Test Designation	Test Result
Penetration (0.1 mm) at 25°C, 100 gm, 5 sec	D5	75
Ductility (cm) at 25°	CD113	100+
Specific gravity at 25°	CD70	1.026
Softening point (°C) (ring and ball)	D36	48
Flash point (°C)	D92	325

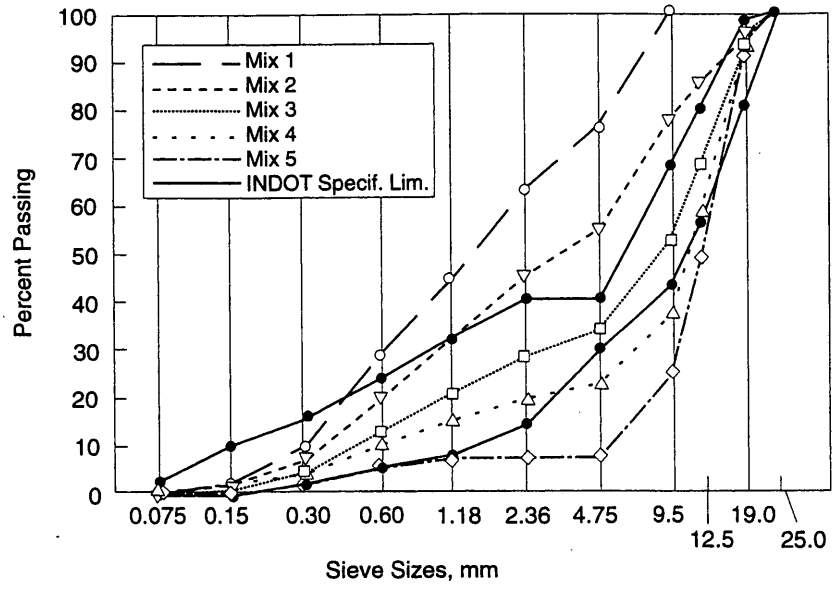

FIGURE 2 Aggregate gradations after extraction test.

removed from the mold and allowed to cool for at least 2 hr before handling.

Subsequently, the following determinations were made:

1. Unit weight (total mix),
2. Gyratory stability index (GSI):

$$\text{GSI} = \frac{\text{Minimum gyrograph band width}}{\text{Minimum intermediate gyrograph band width}} \quad (1)$$

3. Gyratory compactibility index (GCI)

$$\text{GCI} = \frac{\text{Unit weight at 30 revolutions}}{\text{Unit weight at 60 revolutions}} \quad (2)$$

4. Percent air voids of total mix.

Figures 3(*b*), 4, and 5(*a*) present the results of the above determinations.

Indirect Tensile Test

Indirect tensile tests were conducted on specimens prepared with the GTM. The compressive load was applied through a steel loading strip 12.7 mm (0.5 in.) wide with a radius equal to that of the specimen (*5*). The tensile strength was calculated using the following equation.

$$S_t = 2P/\pi tD \quad (3)$$

where:

S_t = tensile strength (kPa),
P = maximum load (kg),
t = specimen height immediately before tensile test (mm), and
D = specimen diameter (mm).

Figure 5(*b*) shows the indirect tensile test results.

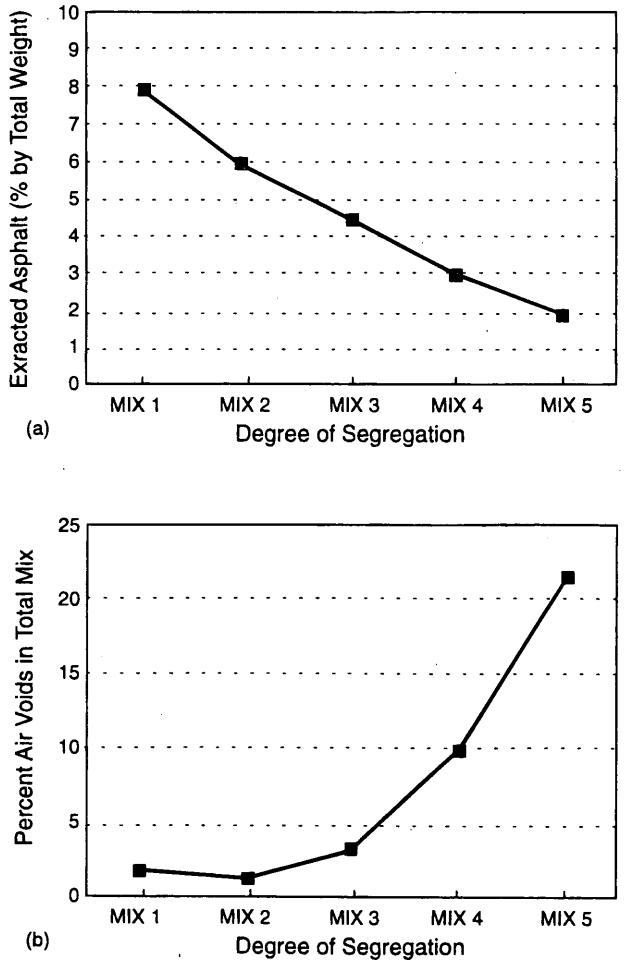

FIGURE 3 (*a*) Extracted asphalt versus degree of segregation, (*b*) percent air voids versus degree of segregation.

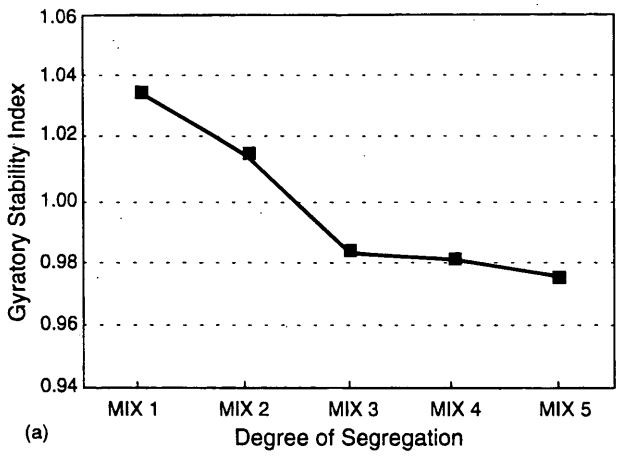

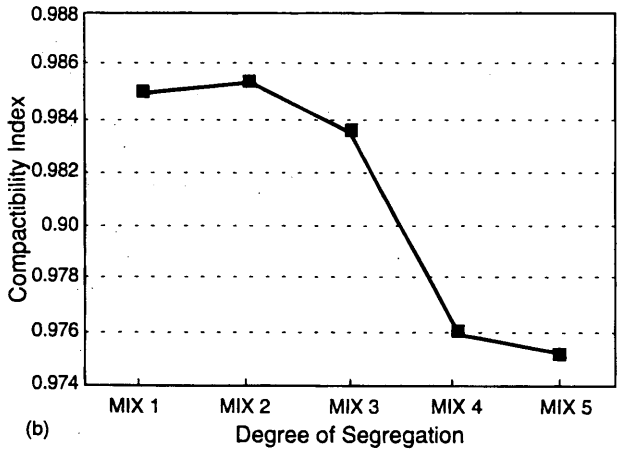

FIGURE 4 *(a)* **Stability index versus degree of segregation, *(b)* compactibility index versus degree of segregation.**

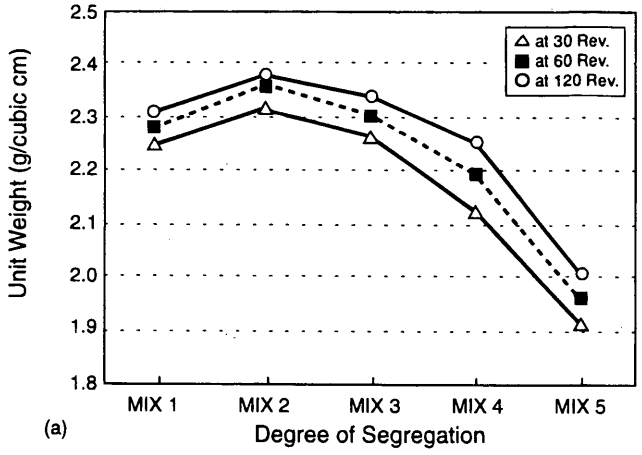

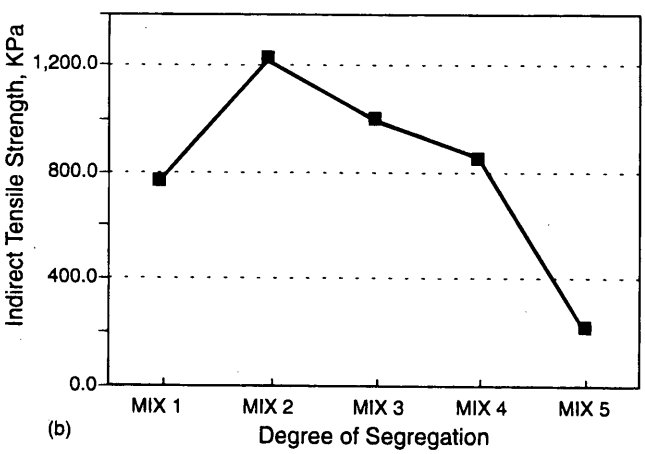

FIGURE 5 *(a)* **Unit weight versus degree of segregation, *(b)* indirect tensile strength versus degree of segregation.**

Purwheel-Tracking-Device Test

Segregated asphalt mixture resistance to permanent deformation and moisture damage was evaluated using the Purwheel tracking device (*6*).

Mixture Preparation Figure 3(*a*) was used to determine the asphalt content for each degree of segregation. An amount of aggregate and asphalt to produce a compacted slab 622.3 mm (24.5 in.) long, 304.8 mm (12.0 in.) wide, and approximately 76.2 mm (3 in.) deep was weighed into three mixing bowls. The total weights of aggregate for test mixtures 1 through 5 were 30.082 kg (66.481 lb), 31.295 kg (69.162 lb), 30.774 kg (68.011 lb), 29.695 kg (65.626 lb), and 25.625 kg (56.631 lb), respectively. Corresponding asphalt contents were 7.87, 5.87, 4.50, 2.93, and 1.87 percent. Target densities for the slabs were determined from specimens compacted with a 75-blow Marshall manual compaction effort. The mixing bowls with aggregate were placed in the oven and heated to a temperature between 135°C (275°F) and 149°C (300°F). When the aggregate was heated, asphalt was added and the combination was mixed with a mechanical mixer.

Slab Compaction For this study, slabs were compacted with a linear compactor (Figure 6). Before compaction, a filter paper was placed in the bottom of the mold. Once the aggregate and asphalt were mixed, the entire batch was placed in the compactor mold and spaded vigorously with a heated spatula. The surface of the mix was leveled and another piece of filter paper was placed on top of the mixture. Forty-nine vertical steel plates, each 12.7 mm (0.5 in.) thick, were placed vertically on top of the mix in the mold. The roller was lowered to contact the top of the steel plates. As the mold assembly moved back and forth horizontally the roller was cranked down. Moving the mold back and forth under the roller simplified keeping the roller motion parallel to the mix surface. After compaction, the steel plates were removed and the slab was allowed to cool in air. Half of the mold was detachable to facilitate removal of the slab. Subsequently, the slab was moved to a smooth, level surface until testing began. The unit weights of slabs made from Mixes 1 through 5 were 2.308 (144.0), 2.314 (144.3), 2.292 (143.0), 2.168 (135.2), and 1.929 (120.3) g/cm^3 (lb/ft^3), respectively. Corresponding air voids were 2.94, 5.51, 8.65, 14.88, and 27.45 percent.

The compacted slabs were tested with the Purwheel tracking device (Figure 7) which was fabricated in the Purdue University Central Machine Shop. Two sets of slabs were tested in replicate. The first set of slabs was tested using a steel wheel 50.8 mm (2 in.)

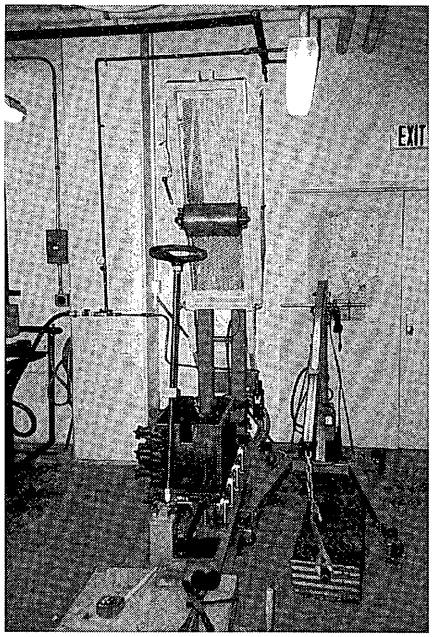

(*a*)

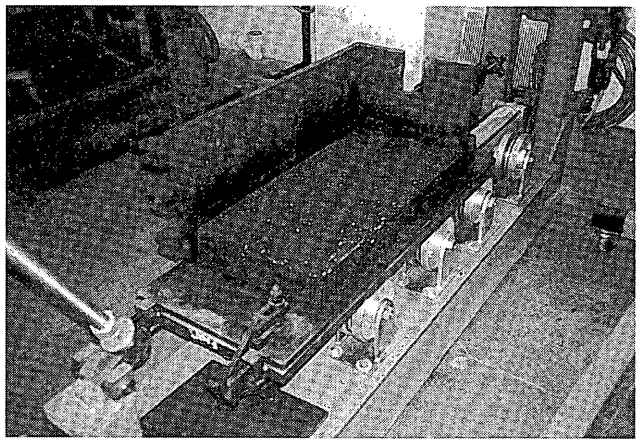

(*b*)

FIGURE 6 Purdue linear kneading compactor: (*a*) prepared for compaction; (*b*) after compaction.

wide, and the second set was tested using a steel wheel 76.2 mm (3 in.) wide. Both steel wheels were loaded to have an initial contact pressure of 827.6 kPa (120 psi). Tracking tests were conducted with the slabs submerged in water at 50°C (122°F). The wheels tracked over the slab at a velocity of 34 cm/sec (1.1 ft/sec). A software program controlled all test parameters. The vertical deformation was measured to the nearest 0.01 mm (0.00039 in.) with a linear variable differential transformer. Deformation was stored for five equally spaced points along the specimen during each pass of the wheel. The resulting deformation was displayed during the test. Tests were run for 20,000 passes, or until the average rut depth reached 25.4 mm (1 in.). Figure 8 shows slabs ready for testing and one slab after testing. Figures 9 through 15 show results of the Purwheel-tracking-device tests.

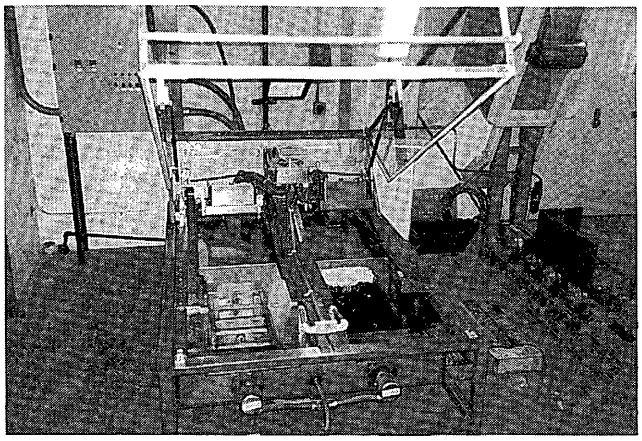

(*a*)

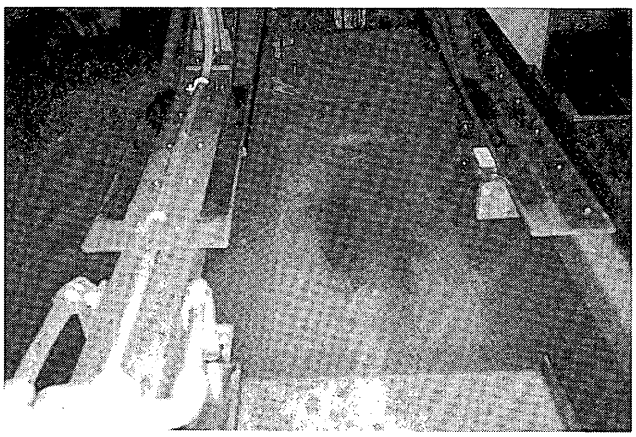

(*b*)

FIGURE 7 Purwheel tracking device: (*a*) prepared for testing; (*b*) after testing.

ANALYSIS OF RESULTS AND DISCUSSION

A number of sample preparation techniques and test procedures have been utilized in this study. The results of applying these techniques and tests are discussed.

Extracted Asphalt

Asphalt content varies with the degree of segregation as shown in Figure 3(*a*). A lower asphalt content occurs with a coarse fraction, because the larger aggregates have a smaller surface area for asphalt to coat than the fine aggregate fraction. In addition to the larger surface of the fine aggregate fraction, the fine aggregates tend to agglomerate into a mastic, which holds more asphalt.

The combination of smaller aggregate sizes and high asphalt content in Mixes 1 and 2 creates an increase in the potential for rutting. The combination of large aggregate and low asphalt content in Mixes 4 and 5 creates a potential for fatigue, raveling, thermal cracking, and stripping.

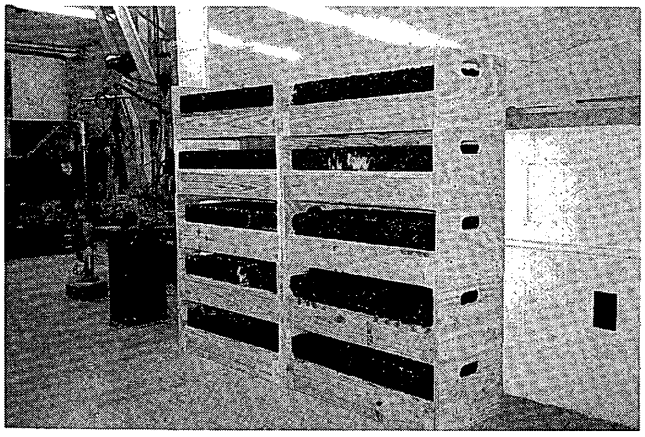

(*a*)

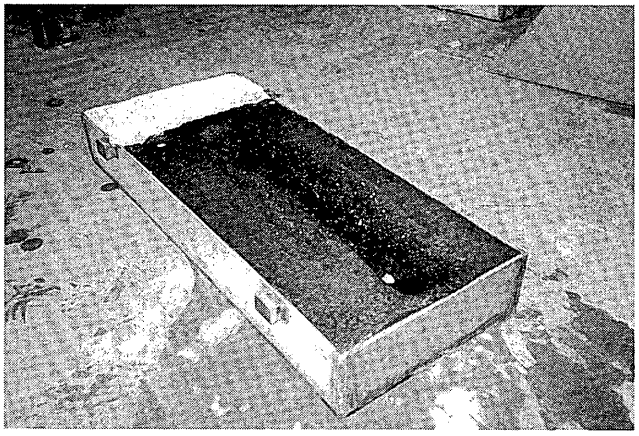

(*b*)

FIGURE 8 (*a*) Slabs ready for testing; (*b*) slab after testing.

Gradation of Extracted Aggregate

The gradations of the five segregated asphalt mixtures are shown in Figure 2. INDOT gradation limits for the #8 binder are also plotted in Figure 2 for comparison. The percentages retained on the 10-mm (3/8-in.) sieve were 0, 22.5, 48.3, 63.1, and 75.2 for Mixes 1, 2, 3, 4, and 5, respectively. A wide range of segregation was achieved by proportioning the plus and minus 10-mm (3/8-in.) fractions.

Air Voids

Air voids for each of the five mixes are presented in Figure 3(*b*). The air voids are low for Mixes 1 and 2 and increase dramatically for Mixes 4 and 5.

Gyratory Stability Index

A GSI value in excess of unity indicates a progressive increase in plasticity during densification (ASTM D3382). Since the compaction effort can be varied to simulate pavement loading conditions, an increase in this index indicates instability of the hot mix asphalt for a given loading. Figure 4(*a*) shows the effect of segregation on the GSI values of mixes in this study. There is considerable loss in stability for Mixes 1 and 2 as compared with Mixes 4 and 5, which means that the finer mixes are more plastic.

Gyratory Compactibility Index

The GCI is an indicator of the compactibility of asphalt mixtures. The closer this index approaches unity, the easier the mix is to compact. Figure 4(*b*) presents the effect of segregation on the GCI values of the five mixes; it can be seen that the GCI value decreases with an increase of coarse aggregate in the mix.

Unit Weight

Figure 5(*a*) shows the relationship between degree of segregation and unit weight of the mixes. The unit weights at 120 revolutions for the five mixtures are 2.313 (144.3), 2.381 (148.5), 2.342 (146.1), 2.248 (140.2), and 2.010 (125.4) g/cm^3 (lb/ft^3), respectively. Figure 5(*a*) also shows that the unit weight increases with increasing number of revolutions or compactive effort.

Indirect Tensile Test

The change in indirect tensile strength with degree of segregation is shown in Figure 5(*b*). It can be seen that the tensile strength increases to a maximum value and then decreases. This result is directly correlated to density.

Purwheel-Tracking-Device Test

Purwheel-tracking-device tests were carried out on all five mixes described in the section on laboratory work. When samples are tested in hot water the Purwheel tracking device measures mixture potential for permanent deformation and stripping. The advent of stripping is usually accompanied by a sudden increase in the rate of deformation; free, stripped asphalt; and flushing of the fine aggregate fraction from the mixture (7). A typical rutting curve (Figure 9) is divided into four regions: postcompaction, creep slope, stripping inflection point, and stripping slope. These regions have been described by Hines (7). Results are shown in Figures 10 through 15 for each of the five mixtures tested with both the 50.4-mm (2-in.) and 76.2-mm (3-in.) wide wheels. Table 4 shows observations of stripped and flushed fines for the five mixes.

In general, the linear compactor produced specimens with increasing and then decreasing density for different degrees of segregation starting with the very fine segregated mixture (Mix 1). Also, the air voids for the total mix show results corresponding to those for density; that is, they first decrease and then increase. Specifically, the slab densities were close to the gyratory-compacted core densities at 30 revolutions. Air voids of the slabs were higher than the gyratory cores. The maximum difference occurred for the coarse mixture (Mix 5), where the air voids were approximately 22 and 27 percent for the gyratory cores and linear compactor slabs, respectively. The slabs prepared with the linear compactor show the same relative magnitude of density and air voids as those of the gyratory-compacted cores. Results of the tests

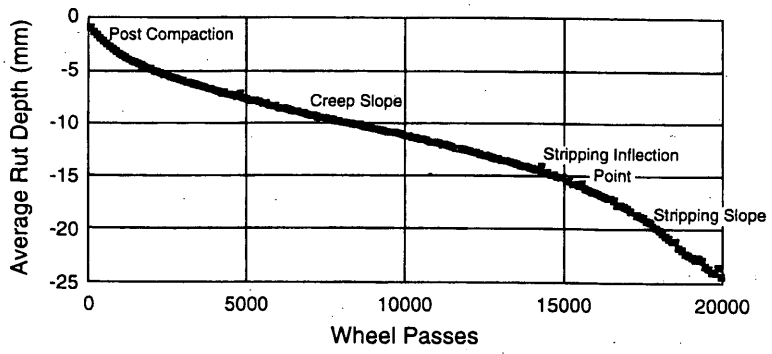

FIGURE 9 Rutting characteristics.

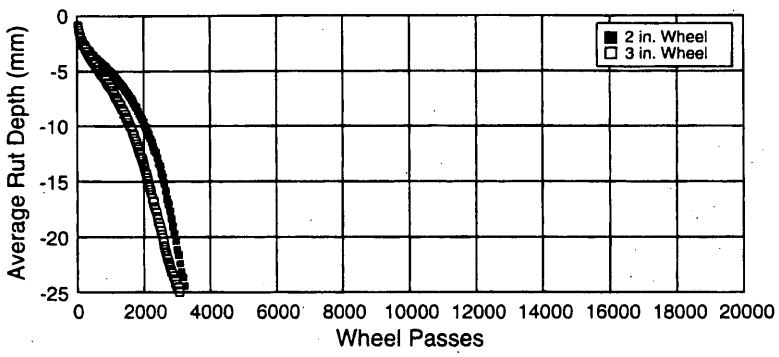

FIGURE 10 Relationship between average rut depth and number of wheel passes for Mix 1.

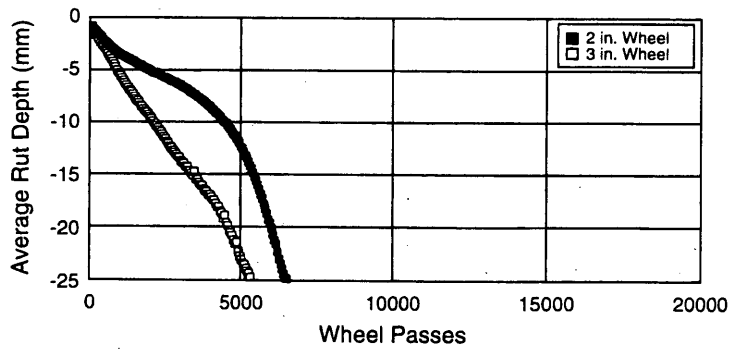

FIGURE 11 Relationship between average rut depth and number of wheel passes for Mix 2.

may be affected by the difference, but for a given test the relative results are considered to be significant.

Inverse Creep Slope

The inverse creep slope is derived from the rate of deformation in the linear region of the deformation curve, after post compaction effects have ended and before the onset of stripping (*6*). The inverse creep slope is reported in passes per millimeter. Therefore, the higher this value, the more resistant the mix is to permanent deformation.

The influence of degree of segregation on the inverse creep slope is shown in Figure 15. The inverse creep slope increases with increasing amount of coarse aggregate for Mixes 1 through 4 but is much lower for Mix 5. Figure 15 also shows that, in

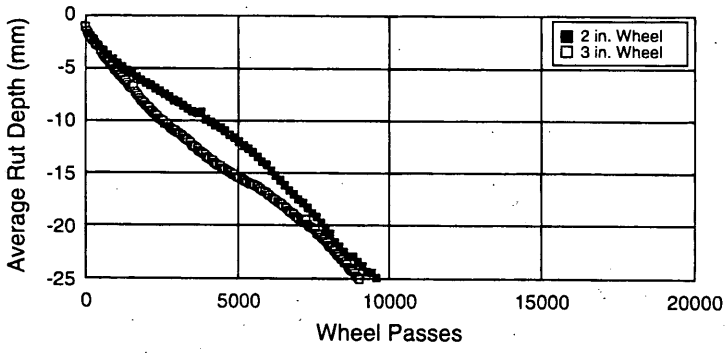

FIGURE 12 Relationship between average rut depth and number of wheel passes for Mix 3.

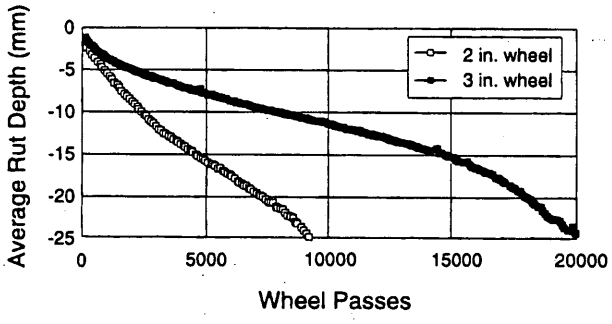

FIGURE 13 Relationship between average rut depth and number of wheel passes for Mix 4.

general, Mixes 1, 2, and 5 are more sensitive to rutting than Mixes 3 and 4.

Stripping Inflection Point

The stripping inflection point is the number of passes at the intersection of the creep slope and the stripping slope. The stripping inflection point is related to the amount of mechanical energy required to produce stripping under the test conditions. A lower stripping inflection point indicates a mixture that is likely to strip (*6*).

The influence of degree of segregation on the stripping inflection point is shown in Figure 15(*b*). The stripping inflection point first increases and then decreases with increasing amount of coarse aggregate. Mixes 1, 2, and 5 have higher potential for stripping than Mixes 3 and 4.

Inverse Stripping Slope

The inverse stripping slope is the rate of deformation in the linear region of the deformation curve after stripping begins and until the end of the test. The inverse stripping slope is related to the severity of moisture damage. The lower the inverse stripping slope, the more severe the moisture damage (*6*).

Figure 15(*c*) shows the influence of degree of segregation on the inverse stripping slope, which first increases and then decreases with increasing amount of coarse aggregate in the mix. The plot shows that Mixes 1, 2, and 5 have lower resistance to moisture damage than Mixes 3 and 4.

Summary

Figure 15 shows that for coarse Mix 4 [63.1 percent retained on 10-mm (3/8-in.) sieve] and very coarse Mix 5 [75.2 percent retained on 10-mm (3/8-in.) sieve], the values of inverse creep slope, stripping inflection point, inverse stripping slope, and passes at a 25-mm (1-in.) rut depth with the 50.4-mm (2-in.) wheel are lower than those

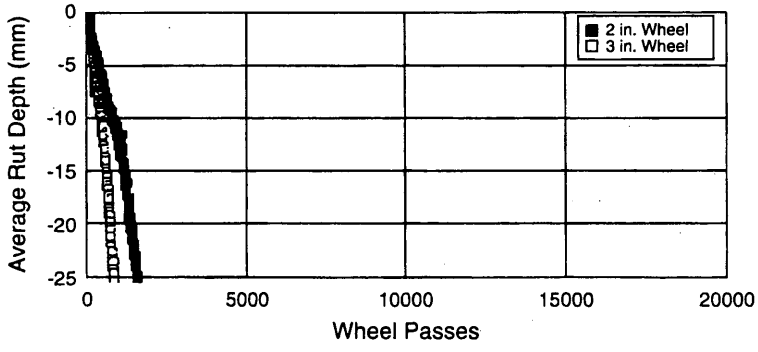

FIGURE 14 Relationship between average rut depth and number of wheel passes for Mix 5.

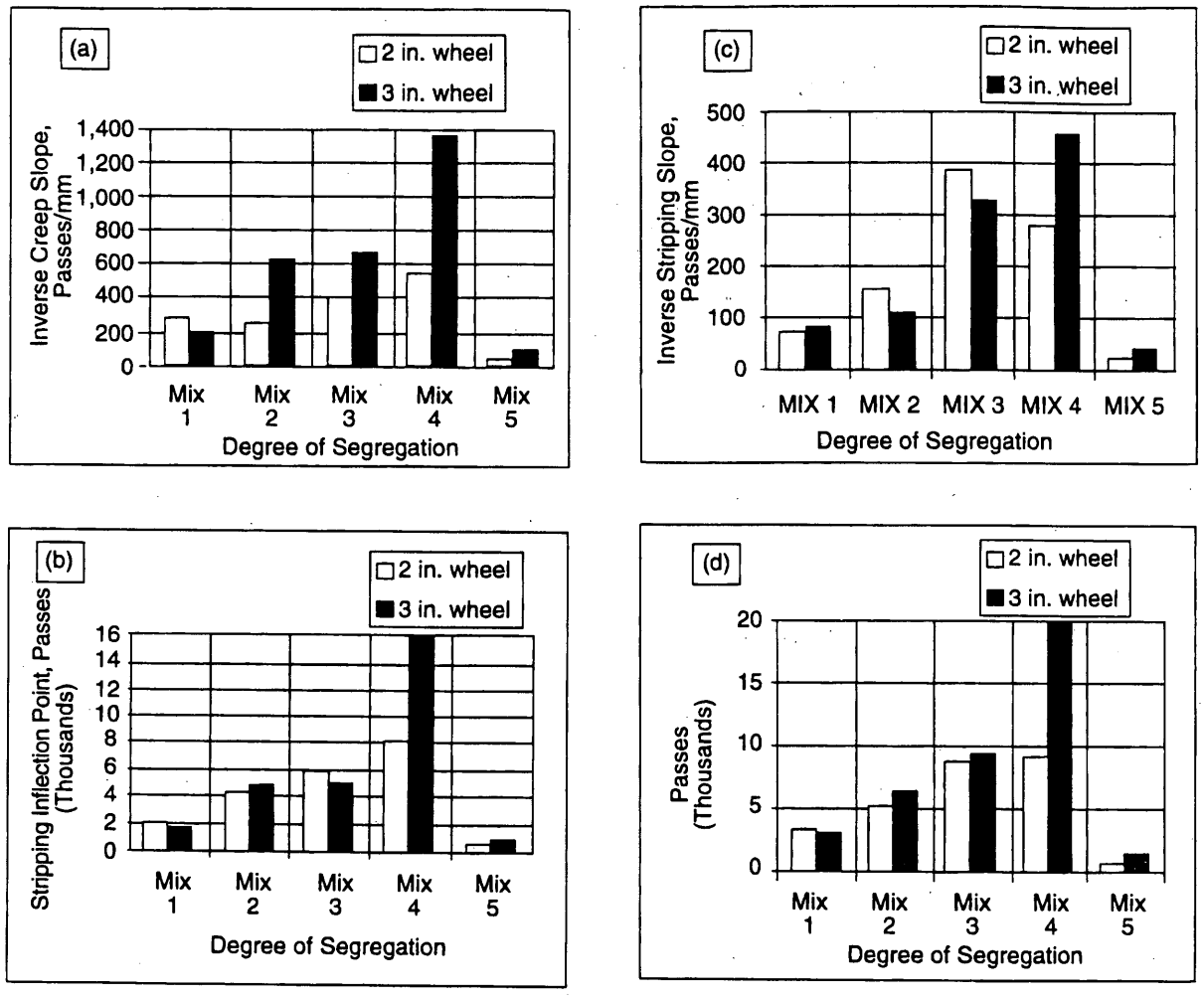

FIGURE 15 (*a*) **Creep slope versus degree of segregation;** (*b*) **stripping inflection point versus degree of segregation;** (*c*) **stripping slope versus degree of segregation;** (*d*) **passes at 2.5-mm rut depth versus degree of segregation.**

TABLE 4 Observations of Stripped Asphalt and Flushed Fines

	Free Asphalt		Flushed Fines	
Mix No.	Yes	No	Yes	No
1	x		x	
2	x		x	
3	x		x	
4	x		x	
5		x		x

values obtained with the 76.2-mm (3-in.) wheel. This result suggests that the aggregate interlock is being compromised sooner with the 50.4-mm (2-in.) wheel even though the initial contact pressure is adjusted to be the same.

The following are observations made during the Purwheel-tracking-device tests:

1. Mix 5 performed so poorly that little information could be obtained about the test or the relative merits of the 50.4-mm (2-in.) versus 76.2-mm (3-in.) wheels.
2. Mixes 1, 2, and 3 showed similar characteristics for both the 50.4-mm (2-in.) and 76.2-mm (3-in.) wheels.
3. The greatest difference in results between the 50.4-mm (2-in.) and 76.2-mm (3-in.) wheels was for Mix 4. In this case the 76.2-mm (3-in.) wheel appeared to accentuate Mix 4 characteristics. As pointed out above, any benefit was completely lost in testing Mix 5.
4. It appeared that the 76.2-mm (3-in.) wheel would be more effective in testing this type of mixture (gravel/natural sand) with a gradation as coarse as Mix 4.
5. Ultimately, a correlation with field performance of mixtures will be needed.
6. Additional tests of mixtures with other aggregates should be made and are planned.

CONCLUSIONS

On the basis of the laboratory testing performed in this study, the following conclusions were drawn:

1. As a result of segregation, the combination of fine material and excess of asphalt created a potential for rutting.
2. Laboratory samples were effectively prepared representing a wide range of potential segregation.
3. The gyratory stability index and the compactibility index decreased with increasing amount of coarse aggregate.
4. Air voids were low for segregated fine material and high for segregated coarse material.
5. Indirect tensile strength increased and then decreased with increasing amount of coarse aggregate.
6. Inverse creep slope, stripping inflection point, and inverse stripping slope increased and then decreased with increasing amount of coarse aggregate.
7. Results of Purwheel-tracking-device tests showed that for segregated bituminous mixtures containing an excess of coarse aggregate, the 50.8-mm (2-in.) wheel was more severe than the 76.2-mm (3-in.) wheel.
8. The Purdue linear compactor did not fracture the aggregate and compacted slabs to a predetermined density.

ACKNOWLEDGMENT

This research was sponsored by the Indiana Department of Transportation and the Federal Highway Administration.

REFERENCES

1. Elton, D. J. Expert System for Diagnosing Hot-Mix Asphalt Segregation. In *Transportation Research Record 1217*, TRB, National Research Council, Washington, D.C., 1989, pp. 38–45.
2. Brock, J. D. Segregation of Asphalt Mixtures. *Proc., Association of Asphalt Paving Technologists*, Vol. 55, 1986, pp. 269–277.
3. Bryant, L. J. Effect of Segregation of an Asphalt Concrete Mixture on Extracted Asphalt Percentage. *Proc., Association of Asphalt Paving Technologists*, Vol. 36, 1967, pp. 206–218.
4. Brown, E. R., R. Collins, and J. R. Brownfield. Investigation of Segregation of Asphalt Mixtures in the State of Georgia. In *Transportation Research Record 1217*, TRB, National Research Council, Washington, D.C., 1989, pp. 1–8.
5. Anagnos, J., and T. Kennedy. *Practical Method for Conducting the Indirect Tensile Test*. Research Report 98-10. Center for Highway Research, University of Texas at Austin, August 1972.
6. Habermann, J. A. *Design Features and a Preliminary Study of the Purdue Linear Compactor and the Purwheel Tracking Device*. M.S. thesis. Purdue University, West Lafayette, Ind., 1994.
7. Hines, M. The Hamburg Wheel-Tracking Device. *Proc., Twenty-Eighth Paving and Transportation Conference*, Civil Engineering Department, The University of New Mexico, Albuquerque, N.Mex., 1991.

Publication of this paper sponsored by Committee on Characteristics of Bituminous Paving Mixtures to Meet Structural Requirements.

Performance Prediction for Large-Stone Mixes Using the Repetitive Simple Shear Test at Constant Height

JOHN HARVEY, JORGE B. SOUSA, AND WILLIAM CROCKFORD

Transfer functions have been developed that permit prediction of vertical rut depth versus equivalent single axle loads in situ using the repetitive simple shear test at constant height (RSST-CH). These transfer functions are based on statistical correlation of field performance and laboratory testing of field cores from Strategic Highway Research Program General Pavement Sections, with conventional binders and gradations and 19-mm (¾ in.) maximum aggregate. A comparison is presented between measured field performance of large-stone mixes in situ and the performance predicted using the current RSST-CH transfer functions. Because of the larger aggregates contained in the mixes, the RSST-CH specimen diameter and height were increased to maintain a similar aspect ratio between the aggregate and specimen dimensions. New techniques for controlling specimen height during the test were also developed. The results of the comparison indicate that the RSST-CH and previously developed transfer functions are useful in predicting in situ rutting for large-stone mixes.

As part of the recently completed Strategic Highway Research Program Project A-003A (SHRP A-003A), test methods and analysis procedures were developed to predict the rutting performance of asphalt-aggregate mixes. For rapid prediction of rutting performance for typical mixes, the repetitive simple shear test at constant height (RSST-CH) was recommended by SHRP A-003A because it applies the primary distress mechanism responsible for rutting in the field to the laboratory specimen.

The RSST-CH is performed at a temperature at which most permanent deformation will occur at the project site. To predict the vertical rut depth in situ caused by traffic loading, transfer functions are applied to the output from the RSST-CH, which is permanent shear strain caused by simple shear load repetitions.

The transfer function relating permanent shear strain in the RSST-CH to vertical rut depth in situ is based on comparison of RSST-CH results from laboratory-prepared specimens with finite element analysis that include a nonlinear viscoelastic constitutive relation and materials properties from results of a set of tests on the same materials (*1*). A linear relation was found between permanent shear strain in the RSST-CH and vertical rut depth in the pavement.

A transfer function relating RSST-CH load repetitions to equivalent single axle loads (ESALs) in situ was developed by Sousa and Solaimanian (*2*) from statistical correlation of RSST-CH results and traffic and rut depth measurements from SHRP General Pavement Sections (GPS). The mixes in the GPS used for development of the transfer function only included 19-mm maximum aggregate, dense gradations, and conventional asphalt binders. However, because the RSST-CH measures the response of the material to the primary distress mechanism responsible for rutting, it is proposed in many cases that the use of the relation developed from the GPS can be extrapolated to large-stone mixes (LSMs) and mixes with modified binders with a reasonable degree of accuracy.

It is known that the response of asphalt-aggregate mixtures is nonlinear with respect to changes in simple shear stress in the laboratory and to changes in tire pressures and loads in situ. Successful application of the transfer function to mix types outside of the GPS data base requires that the nonlinearity not be significantly affected by binder modification or gradation changes. The portability of the transfer function must be determined through experimentation. This type of experimentation has been executed on a limited basis for asphalt-rubber hot mix with a gap-graded aggregate component, recycled asphalt pavement, stone-mastic asphalt with rubber- and polyolefin-modified binders (*3;* Harvey et al., paper in this Record), and dense-graded asphalt concrete with PBA-6 (Harvey et al., paper in this Record) and PG-70 (Sousa et al., paper in this Record) modified binders, all with successful results to date.

The results of RSST-CH testing on field cores from sections containing LSMs and control sections are presented, as well as a comparison of predicted rutting performance with in situ traffic and rut depth measurements. New techniques for the RSST-CH developed for LSMs are also described.

TEST PROCEDURE

Description of RSST-CH

The test used to evaluate the permanent shear deformation resistance of the field cores was the RSST-CH, developed as part of SHRP Project A-003A (*1*). The test was performed using the prototype Universal Testing System (UTS) device built by James Cox and Sons and in operation at the University of California at Berkeley (UCB) since 1991. The UTS has two hydraulic actuators under closed-loop digital control, one horizontal and one vertical. For the RSST-CH, the specimen is bonded to platens, which are then clamped to the actuators. The vertical actuator is used to maintain the specimen at a constant height, and the horizontal actuator applies a repetitive haversine shear stress. For this project the RSST-CH was performed using a 68.9-kPa (10-psi) shear stress, with 0.1 sec loading time followed by 0.6 sec rest period. Each specimen was subjected to approximately 10,000 load repetitions.

J. Harvey, University of California, Institute of Transportation Studies, 109 McLaughlin Hall, Berkeley, Calif. 94720. J. B. Sousa, SHRP Equipment Corporation, 1301 South 46th Street, Bldg. 158, Richmond, Calif. 94804. W. Crockford, Texas A&M University, Texas Transportation Institute, TTI/CE Building, Suite 508, College Station, Tex. 77843.

Special RSST-CH Procedures for LSMs

Applying RSST-CH procedures to LSM specimens required the use of larger specimens and modifications in the placement of the instrumentation on the specimen. The UTS was initially designed to accommodate specimens 150 mm (6 in.) in diameter with room on both sides to mount necessary instrumentation. In the original setup, a linear variable differential transformer (LVDT) was mounted on one side of the specimen to measure the shear displacement between two horizontal planes in the specimen. On the opposite side an LVDT was mounted to measure and control the distance between the top and bottom platens [see Figure 1(*a*)]. For the LSM, testing specimens 200 mm (7.75 in.) in diameter were used, each with two axial LVDTs mounted at 45 degrees from the front and back of the specimen [see Figure 1(*b*)].

Specimen Size

If the results of materials testing are to be used in mechanistic analysis or for correlation of mechanistic concepts with empirical data, it is important to select a specimen size that will provide repeatable results and allow the application of the defined state of stresses, strain, or both, for the range of materials to be compared. To obtain repeatable results in RSST-CH testing of asphalt-aggregate mixes, a specimen must be large enough so that one or two of the larger aggregates do not control the material behavior; if two large aggregates were located one on top of the other such that they bridged a large portion of the specimen height, they might cause a much different result than if they were located elsewhere. Moreover, other work has indicated that a more uniform shear stress distribution is obtained using larger-diameter specimens (*1*).

For these reasons, larger specimen dimensions are called for in the use of the RSST-CH with mixes of larger aggregates. However, to use the transfer functions developed for the smaller specimens, the larger specimens must maintain a similar state of stresses and strains, that is, constant height during testing and a similar ratio between height and diameter.

Because of the size of the stones in the LSMs, a larger specimen was selected to maintain the ratio of stone size to specimen height used for conventional gradations. Instead of the usual cylindrical specimen 150 mm in diameter by 50 mm thick (6 in. × 2 in.), specimens 200 mm by 75 mm (7.75 in. × 3 in.) were used. The 200-mm (7.75-in.)-diameter specimen is shown compared with the 150-mm (6-in.) and 100-mm (4-in.)-diameter specimens in Figure 2.

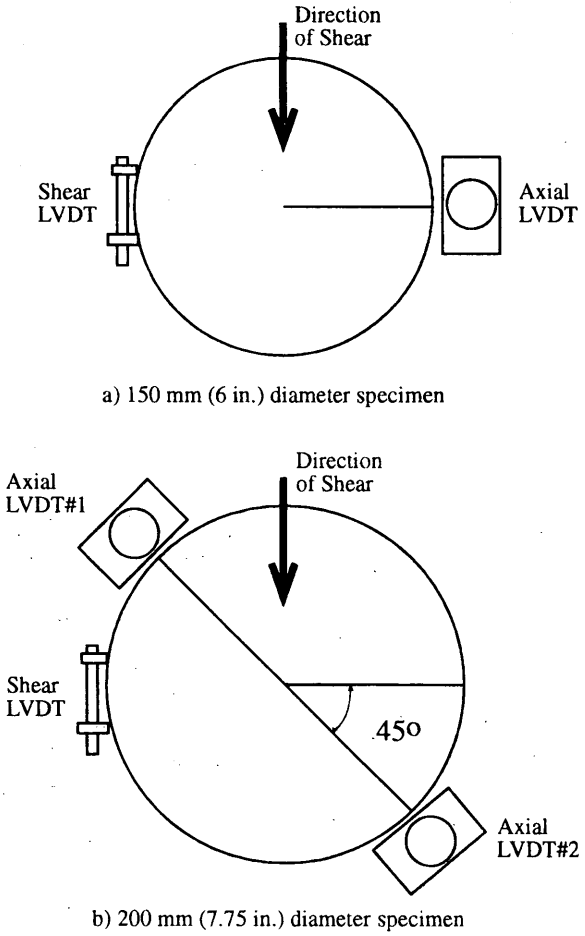

FIGURE 1 Schematic drawing of LVDT mountings on specimens.

Instrumentation

To accommodate the larger specimens, larger platens had to be manufactured by Cox and Sons. Because of a lack of space in the load frame of the prototype UTS, it was no longer possible to mount the axial LVDT on the side of the specimen. An option may have been to mount one LVDT in the front or the back of the specimen. However, in that case the software would maintain the height constant in the front or the back, not in the center as is the case with the 150-mm (6-in.)-diameter specimens typically used for the RSST-CH.

To remedy this problem, two LVDTs were mounted at 45 degrees [see Figure 1(*b*)], one in front and one in back, so that the ATS software could control the *average* readings of both LVDTs. To do this, advantage was taken of the ATS software's virtual channels feature, which permits the creation of a virtual channel with the sum, average, or difference between any two real channels. As Figure 3 shows, a virtual channel called LVDT_ave was created by assigning to it the average of the two real channels, LVDT_#1 and LVDT_#2. After this assignment, the software uses the virtual channel as if it were any other channel; it can be used as a feedback control, as a limit detector, or as a repository for data. During tests executed for this project, the virtual channel LVDT_ave was used to close the feedback loop for the vertical actuator to ensure that the center of the specimen was maintained at a constant height.

A 200-mm (7.75-in.) specimen with instrumentation is shown in Figure 4. The two LVDTs were used to control the vertical actuator (*4*). A third LVDT, to control the horizontal actuator, was mounted on the center axis of the specimen 90 degrees from the direction of shear. This arrangement prevents the LVDT from reading any possible angular movements between the platens due to the flexibility of loading frame. With this system, the center distance of the platens is kept constant, but there is no guarantee that the front and back of the specimen are maintained at a constant distance. The parallelism of the platens during testing will depend on the rigidity of the testing system.

The location of the LVDT would become irrelevant if the testing frame could be made infinitely rigid. In an effort to control

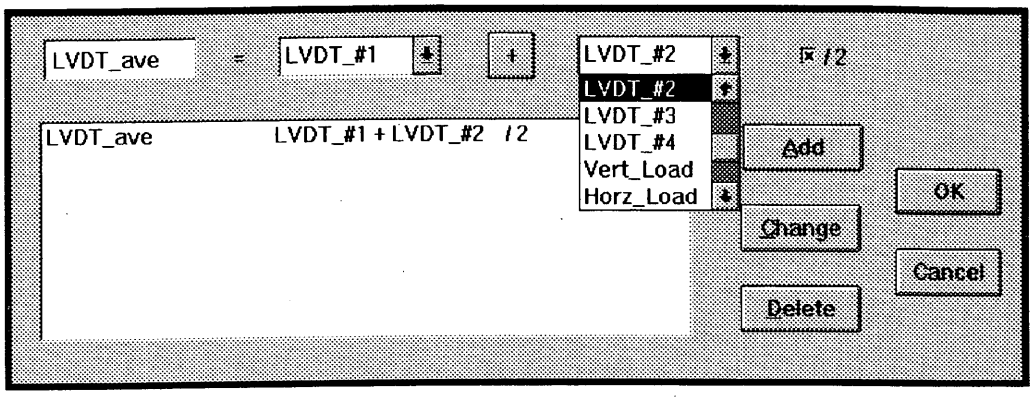

FIGURE 2 Window from ATS software used to create virtual channels.

parallelism, FHWA's request to procure the SHRP shear tester specifies that the test platens must remain parallel within ±0.00635 mm in 150 mm (±0.00025 in. in 6 in.) (*5*). Without this specification, machines of different flexibilities might yield different results. The specification for maintaining constant height requires that the change in height during a pulse be maintained below $\pm 1.3 \times 10^{-3}$ mm (5×10^{-5} in.) as recommended in AASHTO TP7 (*5*).

Selection of Test Temperature

The temperature used for testing for this project was the 7-day maximum average temperature, $T_{7daymax}$, calculated from weather station data and latitude (*6*). The calculated test temperatures are included in Table 1.

Field Cores

Cores were taken in the field at each test section. According to the records available, the cores were taken primarily in the wheel path, although it is unknown whether several were from outside the wheel path (*7*). All field cores had approximately a 200-mm (7.75-in.) diameter.

Air void contents were calculated using the bulk specific gravity determined using parafilm (*8*) and the maximum specific gravity found using the Rice method (ASTM D2041). Air void contents are shown in Table 1.

DESCRIPTION OF LSM TEST SECTIONS

The field cores tested were taken from four sites constructed between 1989 and 1992, two in Colorado and two in Wyoming, as part of a research project performed by the Texas Transportation Institute (TTI). The following site descriptions and information (from a condition survey performed in 1993) are taken from the interim report for that project (*7*). The rut depths noted in the condition survey did not distinguish between densification of the mix and plastic flow. However, it should be noted that densification and plastic flow were not measured separately on the SHRP GPS sections used for original development of the RSST-CH transfer functions (*1,2*).

FIGURE 3 Comparison of 200-mm, 150-mm, and 100-mm specimens and platens.

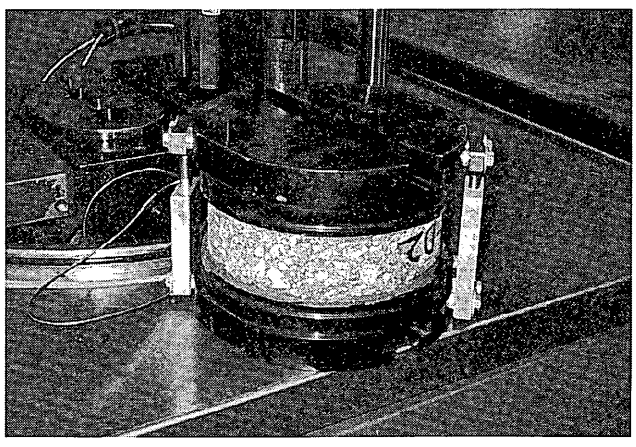

FIGURE 4 LVDT mounting on 200-mm specimen for height control (horizontal LVDT to measure shear deformation not shown).

TABLE 1. Summary of Test Information, Core Location, in Situ Rut Depth and Traffic Data, RSST-CH Results; and Predicted ESALs to in Situ Rut Depth

					In Situ Rut Depth			*RSST-CH reps*		*Predicted ESALs to in-situ rut depth*	
Specimen	Max Agg Size (mm)	Air-Voids	Depth to Layer Top (mm)	Test Temp (C)	Min Rut Depth (mm)	Max Rut Depth (mm)	ESALs to in-situ Rut Depth	to perm shear strain		log(RSST-CH) = -4.36 + 1.24log(ESAL) Equiv ESALs to Rut Depth (mm)	
Laramie, WY								1.0%	2.0%	2.5	5.0
LAA13	19.0	5.2	38	47.2	0.0	5.0	1.86E+06	2.46E+03	1.28E+04	1.78E+06	6.73E+06
LAA14	19.0	7.3	38	47.2	0.0	5.0	1.86E+06	6.66E+02	2.55E+03	6.21E+05	1.83E+06
LAB2	31.8	4.7	38	47.2	2.5	5.0	1.86E+06	1.49E+04	4.95E+04	7.63E+06	2.00E+07
LAB16	31.8	5.4	38	47.2	2.5	5.0	1.86E+06	7.98E+02	5.01E+03	7.19E+05	3.16E+06
Cedar Point, CO								1.0%	8.0%	2.5	20.0
CP34711	19.0	3.9	0	51.1	2.5	2.5	8.17E+05	5.60E+01		8.43E+04	
CP34767	19.0	1.9	0	51.1	2.5	2.5	8.17E+05	8.74E+03		4.95E+06	
CP348612	38.0	6.5	0	51.1	2.5	20.0	8.17E+05	1.19E+07	1.98E+12	1.67E+09	2.71E+13
Flagler, CO								1.0%	2.0%	2.5	5.0
FL3743	38.0	5.1	0	53.9	2.5	5.0	2.70E+05	2.19E+03	1.16E+04	1.62E+06	6.23E+06
FL3746	38.0	6.3	0	53.9	2.5	5.0	2.70E+05	5.57E+03	4.93E+04	3.44E+06	2.00E+07
FL3955	38.0	3.6	50	53.9	0.0	0.0	2.70E+05	1.98E+02		2.33E+05	
FL39514	38.0	4.1	50	53.9	0.0	0.0	2.70E+05	8.70E+01		1.20E+05	
Rock Springs, WY								1.0%		2.5	
RSA7	38.0	3.7	38	48.9	0.0	0.0	1.25E+06	2.30E+01		4.11E+04	
RSA111	38.0	5.7	38	48.9	0.0	0.0	1.25E+06	1.80E+01		3.38E+04	
RSA112	38.0	6.4	38	48.9	0.0	0.0	1.25E+06	1.05E+02		1.40E+05	

Cedar Point, Colorado

An LSM [38 mm (1.5 in.) maximum aggregate] and a control mix [19 mm (0.75 in.) maximum aggregate] were constructed at this site in the westbound lanes of Highway 70, approximately 125 km (75 mi) east of Denver. The section containing the control mix consisted of a 38-mm (1.5-in.) layer of dense-graded asphalt concrete over a 44-mm (1.75-in.)-thick dense-graded binder/leveling course. Both mixes were of the same type (Colorado Type C). The condition survey indicated extensive fatigue cracking in the overlay and rut depths less than 2.5 mm (0.1 in).

The LSM at this site was used as an 83-mm (3.75-in.)-thick surface material during the period between construction and condition survey. The surface was found to have extensive alligator cracks in the wheel paths. Rut depths ranged between 2.5 and 20 mm (0.1 and 0.8 in). The Colorado Department of Transportation has confirmed that much of the rutting occurred in the underlying layers because of water penetrating the cracked surface rather than rutting in the mix because of low permanent deformation resistance.

Both the control and LSM overlays were constructed in August 1989. The average number of daily ESALs in the design lane is approximately 571.

Flagler, Colorado

Two test sections containing LSM were investigated at this site on Interstate 70. Both were constructed in September 1991. The LSM was used as a 75-mm (3-in.)-thick surface material at Milepost 374. This section was found to have random longitudinal cracking and rut depths of 2.5 to 5 mm (0.1 to 0.2 in).

At Milepost 395 section, the LSM was placed as a 95-mm (3.75-in.)-thick layer below 50 mm (2 in.) of asphalt concrete with a 19-mm (0.75-in.) maximum aggregate (Colorado Type C) containing an asphalt-rubber binder. This section was found to have little or no rutting. The average number of daily ESALs in the design lane is 404.

Rock Springs, Wyoming

This section was in the eastbound lane of Interstate 80 east of Rock Springs. The 64 mm-(2.5-in.)-thick LSM layer on this section was placed below a 38-mm (0.75-in.)-thick seal in September 1991. The condition survey indicated no cracking or rutting. The average number of daily ESALs in the design lane is 1,870.

Laramie, Wyoming

This site included a control section on I-80 containing a 19-mm (0.75-in.) maximum aggregate asphalt concrete base course 76 mm (3 in.) thick below a 19-mm (0.75-in.)-thick wearing course. The control section had no cracking and a 2.5- to 5-mm (0.1- to 0.2-in.) rut depth.

The LSM section had the same cross section as the control section, except that the base course was an open-graded LSM with a maximum aggregate of 31.8 mm (1.25 in.). This section was found to have no cracking and a 2.5- to 5-mm (0.1- to 0.2-in.) rut depth. Both sections were constructed in July 1992. The average number of daily ESALs in the design lane is 2,550.

TEST RESULTS AND ANALYSIS

Analysis Method

The method used to make the comparison between performance predicted from laboratory testing and measured field performance is based on a statistical correlation between field measurement of rut depth, ESALs, and maximum 7-day average temperature ($T_{7daymax}$) at SHRP GPS test sites and laboratory measurement of permanent shear deformation on field cores from the same GPS sites at temperature $T_{7daymax}$ for each GPS section using repetitive simple shear loading with the specimen maintained at constant height (*2*).

To correlate these measurements, permanent shear strain from the RSST-CH was related to vertical rut depth on the basis of finite element analysis as part of SHRP Project A-003A (*1*). During a test, the permanent shear strain increases with each load application. Using the finite element analysis, permanent shear strain in the RSST-CH has been estimated to correspond to vertical rut depth in situ as follows: vertical rut depth = A permanent shear strain, where A = approximately 276 mm (11 in.) for thick lifts. The value for A was found to decrease with decreasing layer thickness (*1*).

The analysis method assumes that nearly all permanent deformation will occur in situ at temperatures approximately 5°C (9°F) below and above $T_{7daymax}$. Load repetitions (RSST-CH) to the vertical rut depth of interest are converted to ESALs using the following equation, developed from the GPS data by Sousa and Solaimanian (*2*): $\log(\text{RSST-CH load repetitions}) = -4.36 + 1.240 \cdot \log(\text{ESAL})$.

It is important to note that this relation is based on cores taken from both inside and outside the wheelpath. Increase in permanent shear deformation resistance due to densification and other effects of trafficking is important and must be partially responsible for the variance in the original results from the GPS sections and any other comparisons of actual and predicted performance, such as those found in this study. Changes in the mix are also caused by environmental factors (e.g., aging and moisture damage). The best validation of the transfer functions used for this study will occur when field performance is compared with mix design results. A few projects of that type have been completed (Harvey et al., paper in this Record; Sousa et al., paper in this Record). It is important to compare all useful data available in order to evaluate the applicability of any proposed mix design methods, bearing in mind the possible sources of bias and variance that may exist in the data.

It has been shown previously that the laboratory compaction method can have an even greater effect than densification on permanent shear deformation resistance (*9*). If the transfer functions described here are to be used effectively, the compaction method that best produces the same permanent shear deformation resistance as field cores should be used to produce specimens for mix design.

Performance Prediction and Comparison with Field Data

RSST-CH results were used with the method described previously for prediction of ESALs to a selected rut depth. The selected rut depths for this project were those measured during the condition surveys described. These results are shown in Table 1 along with the accumulated ESALs measured in situ between the time of construction and the condition survey. Except for the Cedar Point sections, the predicted performance compares reasonably well with the measured results. It bears repeating that the Cedar Point LSM

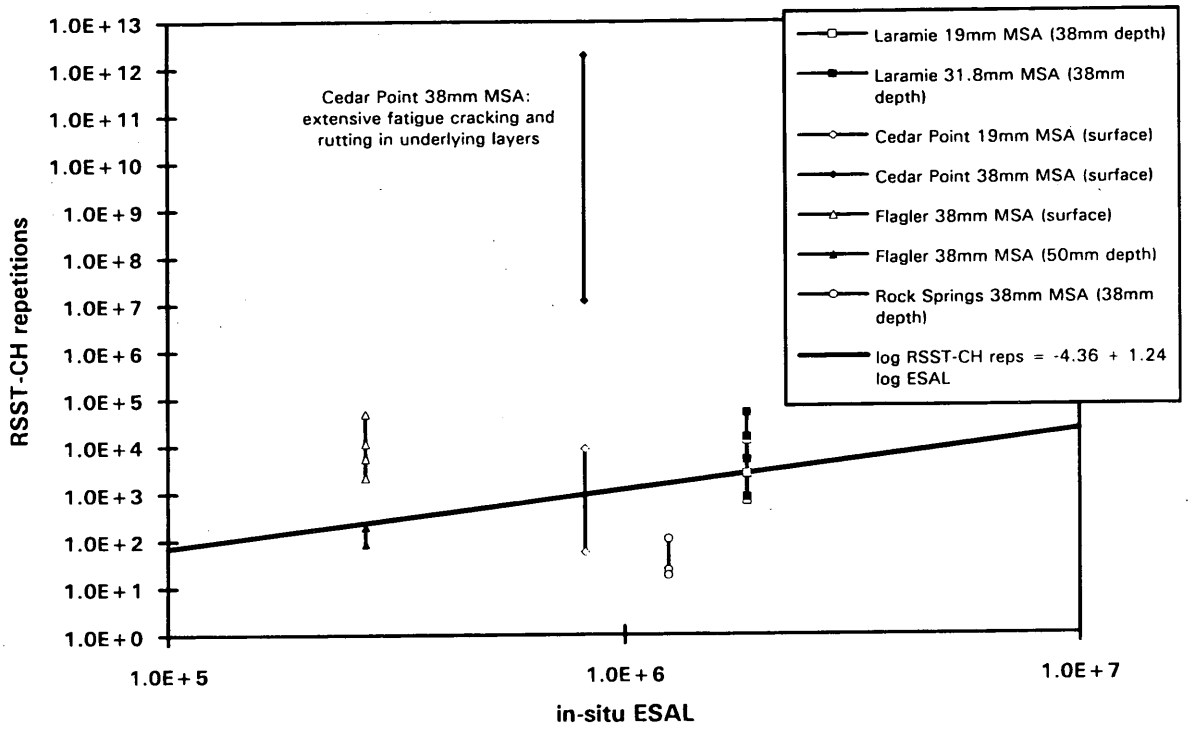

FIGURE 5 Comparison of LSM data with Sousa and Solaimanian transfer function.

sections were badly cracked and that some of the rutting observed on that section was confirmed by the Colorado Department of Transportation as having occurred in the underlying layers because of moisture passing through the cracked surface.

The Sousa and Solaimanian transfer function is shown in Figure 5, plotted with the data presented in this study. Again, except for the Cedar Point LSM, the data presented here generally fit the relation generated from the GPS site data. This indicates that the shift factor is portable to LSMs despite their lack of representation in the original GPS data base.

SUMMARY AND CONCLUSIONS

Data are presented from LSM field cores using the RSST-CH. These results, and measured in situ rut depths and ESAL data, were used to evaluate the transfer function developed by Sousa and Solaimanian. Both the RSST-CH and the Sousa and Solaimanian transfer function were developed as part of SHRP Project A-003A. New techniques for the RSST-CH developed for LSMs were also presented.

The following conclusions can be drawn from the study:

1. The new techniques developed for testing LSMs with the RSST-CH were effective and, in combination with a larger specimen, appear to result in good data for this type of mix.
2. The Sousa and Solaimanian transfer function appears to be applicable to LSMs despite having been developed from a GPS data base that did not include LSMs.

It is recommended that further validation of the RSST-CH and transfer functions for use in predicting rutting performance for asphalt-aggregate mixes be performed.

ACKNOWLEDGMENTS

The work described in this paper was performed at UCB as a subcontract to the Texas Transportation Institute, Texas A&M University, as part of NCHRP Project HR4–18. The authors would like to thank the Colorado and Wyoming departments of transportation for their efforts in obtaining cores and performance data, James Cox and Sons, Inc., for the design and fabrication of the large-size platens, and Ed Nicks for fabrication of instrumentation. The help of Clark Scheffy, Maggie Paul, and the rest of the UCB Asphalt Research Program technical staff is also appreciated.

REFERENCES

1. Sousa, J. B., et al. *Permanent Deformation Response of Asphalt-Aggregate Mixes.* Report SHRPA414. Strategic Highway Research Program, National Research Council, Washington, D.C., 1994.
2. Sousa, J. B., and M. Solaimanian. Abridged Procedure to Determine Permanent Deformation of Asphalt Concrete Pavements. In *Transportation Research Record 1448,* TRB, National Research Council, Washington, D.C., 1994, pp. 25–33.
3. Harvey, J., T. Lee, J. Sousa, J. Pak, and C. Monismith. Evaluation of Fatigue and Permanent Deformation Properties of Several Asphalt-Aggregate Field Mixes Using SHRP A-003A Equipment. In *Transportation Research Record 1454,* TRB, National Research Council, Washington, D.C., 1994, pp. 123–133.

4. Sousa, J., and C. Chan. *Computer Applications in the UCB Geotechnical Laboratories.* Geotechnical Engineering Congress, Vol. II, Geotechnical Special Publication No. 27, ASCE, 1991, pp. 531–543.
5. AASHTO. *Standard Test Method for Determining the Permanent Deformation and Fatigue Cracking Characteristics of Hot Mix Asphalt (HMA) Using the Simple Shear Test (SST) Device, Designation TP7.* AASHTO Research Implementation, Gaithersburg, Md., Dec. 1993.
6. Solaimanian, M., and T. Kennedy. Predicting Maximum Pavement Temperature Using Maximum Air Temperature and Hourly Solar Radiation. In *Transportation Research Record 1384,* TRB, National Research Council, Washington, D.C., 1994.
7. von Quintus, H., J. Daleiden, M. Sargent, J. Scherocman, W. Crockford, and J. Button. *Design and Evaluation of Large-Stone Mixes.* Interim Report, NCHRP Project 4–18, February 1993.
8. Harvey, J., J. Sousa, J. Deacon, and C. Monismith. Effects of Sample Preparation and Air-Void Measurement on Asphalt Concrete Properties. In *Transportation Research Record 1317,* TRB, National Research Council, Washington, D.C., 1992.
9. Harvey, J., C. Monismith, and J. Sousa. An Investigation of Field- and Laboratory-Compacted Asphalt-Rubber, SMA, Recycled, and Conventional Asphalt-Concrete Mixes Using SHRP Project A-003A Equipment. *Proc., the Association of Asphalt Paving Technologists,* 1994, forthcoming.

The views expressed in this paper are those of the authors only, and do not necessarily reflect those of their institutions or the project sponsor.

Publication of this paper sponsored by Committee on Characteristics of Bituminous Paving Mixtures to Meet Structural Requirements.

Application of Digital Image Processing to Quantitative Study of Asphalt Concrete Microstructure

ZHONG QI YUE, WILLIAM BEKKING, AND ISABELLE MORIN

Asphalt concrete (AC) is a strongly heterogeneous material that consists of asphalt cement, voids, fine particles, sand, and coarse aggregates. A review of the literature reveals that the investigations of AC have mainly concentrated on the macroscopic behavior of the material based on the assumption that the mixture is homogeneous. This assumption is mainly due to the extreme difficulty associated with the quantitative measurements of AC microstructure and the random nature of the aggregate distribution. This paper applies an innovative digital image-processing technique to quantify the distribution, orientation, and shape of coarse aggregates (≥2 mm) in AC mixtures. Results of the quantitative measurements of coarse aggregate distribution and shape in AC mixture are then presented and analyzed. The quantitative results of AC microstructure clearly indicate the following findings: (*a*) the microstructure characteristics of coarse aggregates in AC mixtures can be accurately measured using the digital image-processing technique; (*b*) the area gradation of aggregate cross sections by the Feret diameter gives an excellent prediction of the sieve gradation of coarse aggregates (≥2 mm) used in the design of AC mixtures; (*c*) the major cross sections of coarse aggregate particles have the tendency to lie horizontally in the mixtures; and (*d*) comparison among two laboratory and two field compaction techniques provides valuable information related to compaction quality in terms of favorable aggregate distribution within the mixtures.

Digital image processing is the term that pertains to converting video pictures into a digital form and applying various mathematical procedures to extract significant information from the picture. This information may be characteristic of cracks or potholes on a pavement surface, the microstructure of cement-based materials, the fabric of clay soils, the texture of sea ice, or the angularities and shapes of granular materials (*1–5*). Although digital image processing has been widely used in civil engineering in recent years (*6*), a literature survey indicates that the application of digital image processing to the quantitative study of microstructure of asphalt concrete (AC) mixtures is limited (*7*). In this paper, an innovative digital image-processing technique is applied to the quantitative study of the AC internal structure (called microstructure) defined by the distribution, orientation, and shape of coarse aggregate particles in the mixtures. Also, a coarse aggregate particle is considered equal to or greater than 2 mm in size. Coarse aggregates and their distribution play a key role in the stability and bearing capacity of AC mixtures.

BACKGROUND

Asphalt concrete is a heterogeneous material that consists of asphalt cement, voids, fine particles, sand, and coarse aggregates. These individual materials and components have different physical and mechanical properties and behavior. The microstructure of AC mixtures is influenced by many factors, including quality of asphalt cement, aggregate gradation and shape, and quality of compaction. It has been well recognized that the microstructure of AC plays a significant role in the mechanical properties of AC and in the resistance of AC pavements to major distresses including rutting, fatigue, thermal cracking, and low-temperature cracking (*8–15*).

Realistic characterization of the failure of AC mixtures (in the form of plastic deformation, cracking, or both) necessitates consideration of the heterogeneous nature (or the microstructure) of the materials. Mechanistic models of AC mixtures have concentrated mainly on the macroscopic behavior of AC and have been constructed on the general principles of continuum mechanics (*16–19*). In most of those mechanistic models, the composite material is always assumed to be homogeneous and isotropic, and its microstructure behavior is largely ignored. This assumption could be due to the extreme difficulty associated with the quantitative measurements of AC microstructure and the random nature of aggregate distribution. In particular, the application of fracture mechanics concepts to characterize the toughness of AC by ignoring the heterogeneity of the material and the existing flaws has had limited success (*20–24*). Practical measurement of the fracture toughness K_{IC} and J-integral for AC mixtures was difficult because those parameters are significantly affected by the material properties near a macro-crack tip. Unless the failure mechanism is properly understood and analyzed, predictions of the allowable stresses in service based on small-scale laboratory tests cannot be reliable (*25*).

Recently, attempts have been made to consider AC mixtures as two-phase composites in which the coarse aggregates are embedded into the matrix consisting of asphalt cement, fine particles, and sand (*26,27*). The matrix is regarded as a homogeneous and isotropic continuum functioning as the binder of coarse aggregates. Rothenburg et al. (*26*) presented a micromechanical modeling of AC in connection with pavement rutting problems using two-dimensional discrete element techniques. The aggregates were treated as elastic elements and the binder as linearly viscoelastic material. The microstructure of aggregate distribution in AC was simulated by numerically solving Newton's equations of motion for individual particles. Sepehr et al. (*27*) performed a finite element structure analysis of AC pavements using a fictitious microstructure of an AC layer.

Furthermore, the effects of different compaction methods on AC mixtures have been extensively examined using laboratory testing and field trials during the past decades. Consuegra et al. (*28*) demonstrated that the Texas gyratory compactor, among other laboratory compaction methods, has the ability to produce AC mixtures with engineering properties closest to those determined from

Pavements Research Group, Institute for Research in Construction, National Research Council of Canada, Ottawa, Ontario, Canada K1A 0R6.

field cores. Svec and Halim (*29*) concluded that the asphalt multi-integrated roller (AMIR) compactor can produce more homogeneous and hairline crack-free AC layers when compared with a conventional vibratory roller compactor followed by a rubber tire roller. A majority of these findings were based on macroscopic properties including specific gravity, indirect tensile strength, and resilient modulus of AC mixes. For the same mix design, differences in these properties of AC compacted using different methods are mainly due to the differences of the mixture's microstructure, in particular, the distribution and orientation of coarse aggregates.

Moreover, the microstructures of conventional hot-mix asphalt (HMA), stone mastic asphalt (SMA), and large stone asphalt mixes (LSM) are quite different. It was claimed that because of point-to-point contact or interlock of coarse aggregates, or both, SMA and LSM have better performance in resisting permanent deformation than conventional HMA (*14,30*). Based on this analysis, two questions arise: (*a*) Can the differences in the microstructure be quantitatively measured for AC mixtures compacted using different methods or with different mix design? (*b*) What are the relationships between the microstructure and the performance of AC mixtures?

OBJECTIVES AND OUTLINE

To analyze and model the performance of AC mixtures more accurately and reliably, the characteristics of the microstructure have to be measured and analyzed precisely. Recent advances in hardware and software for digital image processing and analysis are providing a powerful tool for quantitatively analyzing AC microstructure. In this paper, an innovative digital image-processing technique is introduced and used to obtain quantitative information about the geometric distributions of coarse aggregates and the shape and orientation of individual aggregate particles on cross sections of AC specimens. Although digital image processing is limited to two-dimensional measurements, three-dimensional information can be derived from these measurements if a series of layers is analyzed. The outline of the paper is as follows: (*a*) a detailed description of the digital image analysis technique used in this study, (*b*) a definition of morphological measurements of AC microstructure, (*c*) a presentation of examples of the applications to AC microstructure including the effects of different field and laboratory compaction methods, and (*d*) a summary of the main conclusions and recommendations.

DIGITAL IMAGE PROCESSING

Preparation of Plane Cross Sections

Field cores or laboratory-prepared AC specimens were cut using a circular masonry saw with a diamond-tip blade in multiple vertical or horizontal plane cross sections. The circular saw can cut a thin layer of about 3-mm thickness from a specimen. Three vertical or 10 horizontal sections can be obtained from a specimen 100 mm in diameter and 50 mm high. AC specimens were conditioned at −2°C for hardening purposes. Because the thickness between any two cuts is less than 5 mm, liquid epoxy resin was applied at the plane surface to prevent detachment of aggregates from the matrix. The epoxy resin was applied about 4 hr before cutting to allow it to gain adequate strength in accordance with the manufacturer's specifications. Sections were photographed using a camera equipped with a zoom lens and a tripod. A flash was not used because of surface reflection. A ruler was placed beneath the photographed section for scaling and calibration in the digital image processing. ISO 200 Kodacolor print film was used for developing prints. A conventional hot-asphalt mix, referred to as HL4 by the Ministry of Transportation of Ontario (MTO), was used in this study. Table 1 illustrates the aggregate gradation and MTO specification limits of the HL4 mix. More details on the HL4 mix can be obtained elsewhere (*14,24,29*).

Image Digitization

A Microteck flatbed scanner with Picture Publisher's scanning functions was used to convert pictures into digital files that can be processed by computer. The AC cross section and the ruler were scanned from a picture. The resolution of picture scanning was set to the highest practical value to increase the accuracy of measurements. Aggregates were easier to identify and could be better differentiated from the background matrix using a high value of resolution. For a black-and-white print and a color picture (4 in. × 6 in.), 300 dots per inch (dpi) and 165 dpi respectively, were used. This choice was dictated by the capacity of a 1.4-MB high-density diskette used in this study. The image was stored in a file (about 1.2 MB) with .TIF format as a series of pixels (or points). Each pixel has three digital values indicating the X and Y coordinates and grey level or color intensity. An example of the digitized image is shown

TABLE 1 Aggregate Gradation and MTO Specification Limits of HL4 Mix

Sieve Size (mm)	% Passing by Dry Mass of Aggregates		
	MTO lower limit	Sieve Analysis	MTO upper limit
19.0	100	100	100
16.0	98	98.9	100
13.2	83	94.2	95
9.50	62	78.7	82
4.75	40	51.7	67
2.36	27	38.1	66
1.18	16	28.3	60
0.600	8	20.4	47
0.300	4	11.6	27
0.150	1	4.4	10
0.075	0	2.7	6

in Figure 1(*a*), which shows the horizontal cross section of a 100-mm-diameter sample of a gyratory compacted HL4 mix. The number of gyrations was 250, the applied pressure was 0.6 MPa, and the gyratory angle was 1 degree.

An image-editing software, Picture Publisher (version 4.0), was then used to manually outline the boundaries of aggregates on the digitized image. A manual technique was used because the image analysis software cannot satisfactorily and automatically recognize whether a pixel is part of an aggregate or the asphalt matrix. The automatic recognition of aggregates produced poor results because of the slight color differences between aggregates and matrix. Using the freehand mask tool in Picture Publisher, the area of every aggregate was marked and filled with a contrasting color. Everything except the AC section and the ruler was erased. Once all aggregates were contoured, the posterize-threshold tool was used to reduce the color number to 2. One color represents the aggregates and the other represents the matrix. The greyscale of a modified image was transformed into black and white. A modified image file of about 0.6 MB was then obtained. In this modified image file, pixels of aggregates are turned on, and pixels of the matrix are turned off. This separation process required about 30 min per cross section.

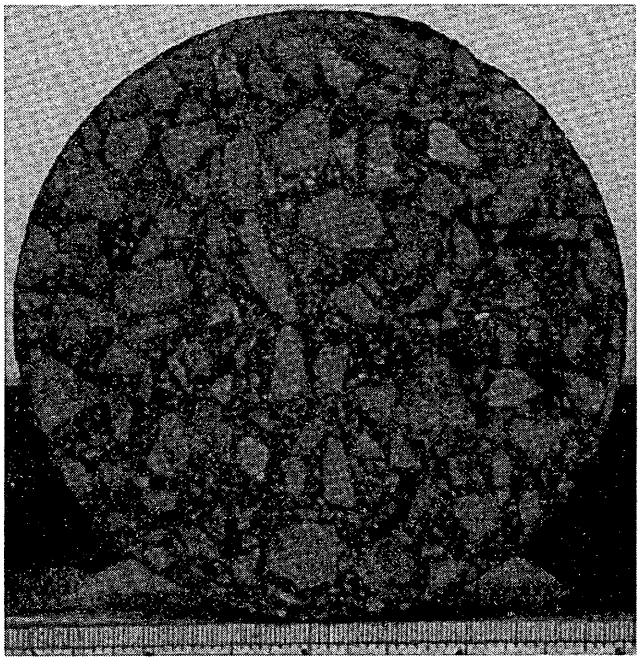

(*a*)

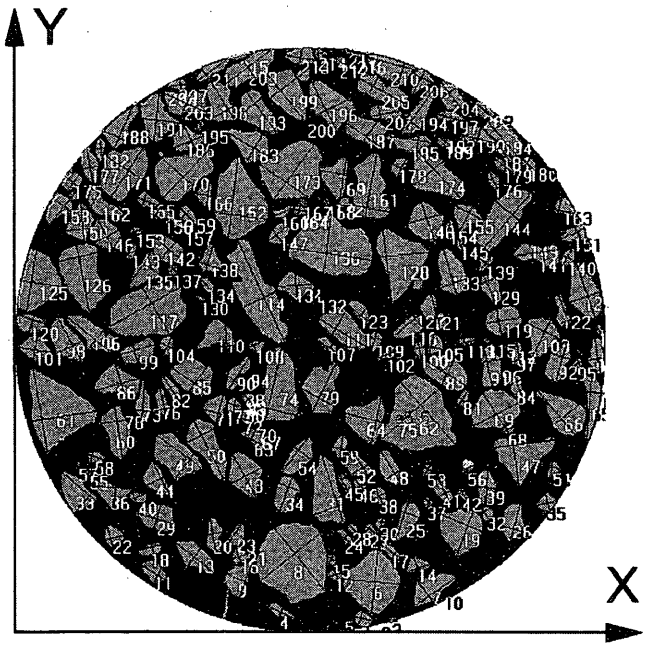

(*b*)

FIGURE 1 Digitalized images of horizontal cross section of gyratory compacted HL4 mix (100 mm in diameter). (*a*) Original image; (*b*) modified image.

Image Calculation

An image analysis statistics software called MOCHA was used to calculate the values of morphological parameters of aggregates from the modified image file. The ruler was utilized to set up the scale of the image for calculation. Two points were selected on the ruler and the actual distance was entered. A plane Cartesian coordinate system (X,Y) was automatically set up. The origin of the coordinate system is located at the lower-left corner of the image. The X-axis is along the horizontal direction on the image and the Y-axis is along the vertical direction. The calculations were performed using the automatic calculations option. The calculated values of the morphological parameters of aggregate cross sections were saved in a file with ASCII format. The modified image file was saved in either .PCX or .TIF format. Figure 1(*b*) shows an example of the modified image in Figure 1(*a*) after using Picture Publisher and MOCHA. In this MOCHA image, each aggregate has an identifying number, and the major and minor axes of each aggregate cross section are also illustrated. Table 2 presents a sample of the calculated results of the aggregate characteristics on the AC cross section in Figure 1(*a*). The aggregates listed in Table 2 can be easily identified in Figure 1(*b*). The definition of the measurements in Table 2 will be given in the next section. All the digital image processing was performed using a 66-mHz 80486 personal computer.

DEFINITIONS OF MEASUREMENT

Measurement of Aggregate Cross Section

The major axis of an aggregate cross section is defined by the greatest distance between two pixels of the boundary contour. The minor axis of an aggregate cross section is defined as the longest line that can be drawn perpendicular to the major axis. The following basic quantities can be measured automatically for an aggregate cross section: (*a*) *perimeter:* summation of all pixels forming the boundary of an aggregate cross section, (*b*) *area:* summation of all pixels contained within an aggregate cross section, (*c*) *centroid* (X_{ca}, Y_{ca}): X and Y coordinates of the binary center of mass of an aggregate cross section, (*d*) *coordinates-major axis ends:* (MaX_1, MaY_1) and (MaX_2, MaY_2), and (*e*) *coordinates-minor axis ends:* (MiX_1, MiY_1) and (MiX_2, MiY_2).

Using these basic quantities of an aggregate cross section, the following parameters can be easily calculated: (*a*) *major (or minor) axis length:* the distance between the two end points of the major

TABLE 2 Selected Results for Basic Measurements of Aggregate Distribution and Geometries on AC Cross Section of Figure 1

No.	Perimeter (mm)	Area (mm^2)	X_{ac} (mm)	Y_{ac} (mm)	MaX_1 (mm)	MaY_1 (mm)	MaX_2 (mm)	MaY_2 (mm)	MiX_1 (mm)	MiY_1 (mm)	MiX_2 (mm)	MiY_2 (mm)
8	45.22	123.20	46.71	11.54	52.02	6.59	43.41	17.22	41.21	8.43	51.11	16.30
19	26.10	41.17	74.73	16.85	74.00	12.64	76.75	20.15	71.25	19.60	78.21	16.67
43	23.08	28.62	38.47	26.01	40.48	22.35	36.45	29.49	41.40	27.29	36.27	24.73
61	43.46	88.81	6.96	37.00	5.50	29.67	3.11	44.14	13.55	36.82	2.93	35.17
66	28.21	33.85	91.77	36.45	87.37	40.30	93.60	32.97	90.12	34.62	94.33	38.10
79	27.97	36.10	51.29	40.66	49.82	36.63	53.85	44.88	47.99	40.66	53.30	37.73
126	32.44	60.39	11.36	59.53	12.46	53.49	10.26	64.66	7.33	61.91	13.74	63.38
133	21.66	26.87	73.09	59.90	74.00	56.42	71.80	63.93	75.47	58.98	71.25	57.52
136	45.66	102.67	53.12	64.11	45.98	64.11	59.90	62.10	53.12	69.79	51.84	60.08
173	36.15	77.17	46.53	76.93	43.41	72.35	50.19	81.51	49.27	72.54	41.03	78.21

(or minor) axis, or (*b*) *Feret diameter:* diameter of a fictitious circular aggregate that has the same area as the aggregate, equal to $(4 \text{ area}/\pi)^{1/2}$; (*c*) *major axis orientation:* angle between the major axis and a horizontal line (*i.e.,* the *X*-axis) on the scanned image; (*d*) *shape factor:* a measure of how nearly circular an aggregate cross section is, equal to 4π area/perimeter^2 (a perfect circle and a line have a shape factor of 1 and 0, respectively); and (*e*) *compactness:* an alternative method for assessing the degree of circularity of an aggregate cross section, given by perimeter^2/area. The compactness for a perfect circle is about 12.6 and increases to infinity for a line.

Statistical Parameters of AC Cross Sections

Using the measured data of an aggregate cross section, statistical parameters can be calculated to show the microstructure characteristics on an AC cross section. Some of these statistical parameters are defined as follows: (*a*) *area percentage:* percentage of the area occupied by aggregates over the total area of an AC cross section, (*b*) *centroid of aggregates:* the centroid of all aggregates on an AC cross section, (*c*) *eccentricity:* percentage of the distance of the centroid of aggregates to the geometric center of the AC cross section over the radius or the width of an AC cross section, and (*d*) *percentage of moment of inertia:* percentage of the summation of the moment of inertia of aggregates over the total moment of inertia of the AC cross section with respect to the *X*-axis or the *Y*-axis.

Furthermore, the following gradation analysis can be performed using the digital data of aggregates on AC cross sections.

(*a*) *Area gradation by minor axis length, Feret diameter, or major axis length:* summation of the areas of the aggregates whose minor axis lengths, Feret diameters, or major axis lengths are between 2 mm and a dimension d ($d \geq 2$ mm) over the total aggregate area, respectively. It is expressed in percentage as a function of the dimension d.

(*b*) *Number (or area) gradation by shape factor:* summation of the number (or area) of aggregates whose shape factors are between 0 and a value s ($0 \leq s \leq 1$) over the total aggregate number (or area). It is expressed in percentage as a function of the value s.

(*c*) *Number (area or compactness) gradation by orientation:* summation of the number (area or compactness) of aggregates whose major axis orientations are between -90 degrees and an angle θ (-90 degrees $\leq \theta \leq 90$ degrees) over the total aggregate number (area, or compactness). It is expressed in percentage as a function of the angle θ. The major axis orientations of aggregates are between -90 degrees and 90 degrees. The three dimensions of an aggregate cross section, i.e., minor axis length, major axis length, and Feret diameter, can be applied to the definition of coarse aggregates ($d \geq 2$ mm) on an AC cross section.

DIGITAL IMAGE RESULTS AND ANALYSIS

The preceding described digital image-processing technique will be applied to the quantitative study of AC microstructure. Two examples are presented in this paper to show the coarse aggregate distribution in AC mixtures. The first example shows the differences of coarse aggregate distribution in the horizontal and vertical cross sections of an AC mixture. The second example shows the effects of different compaction methods on the microstructure characteristics of AC mixtures. The HL4 mix was used in both examples.

Differences Between Horizontal and Vertical Cross Sections

Two gyratory compacted HL4 specimens were used in this analysis. One horizontal circular cross section (Figure 1; 100 mm in diameter) and one vertical rectangular cross section (63 mm high and 95 mm wide) were obtained from the two specimens. Using the digital image-processing technique, the basic measurements were calculated for the geometries and distributions of coarse aggregates on the two cross sections. There are, respectively, 122, 158, and 173

aggregates whose minor axis length, Feret diameter, and major axis length are ≥2 mm on the horizontal cross section. There are, respectively, 111, 160, and 197 aggregates whose minor axis length, Feret diameter, and major axis length are ≥2 mm on the vertical cross section. The selection of 2 mm as a minimum dimension in the analysis was based on the definition of coarse aggregates in sieve analysis. The proportion of area occupied by aggregates on the horizontal cross section is 40.57, 42.91, and 43.40 percent under the condition that minor axis length, Feret diameter, and major axis length, respectively, are ≥2 mm. The proportion of area occupied by aggregates on the vertical cross section is 42.35, 45.91, and 47.36 percent under the same conditions described previously.

Figure 2(*a*) shows the area gradation of aggregates by minor or major axis lengths or Feret diameter on the horizontal and vertical cross sections. The gradation of coarse aggregates using a sieve analysis (Table 1) was also plotted in Figure 2(*a*). Figure 2(*a*) shows that the area gradations by minor and major axis lengths provide the upper and lower bounds for the result of sieve analysis, and the area gradations by Feret diameter are the closest approximation of the sieve analysis. A sieve analysis gradation is determined by the lengths of the intermediate and minor principal axes of the particle itself, and a digital image gradation is based on planar aggregate cross sections with dimensions, depending on the location and orientation of the cut surface, that may be greater than or less than the particle principal axis lengths. The gradations by shape factor of aggregates on the horizontal and vertical cross sections were plotted in Figure 2(*b*) where the Feret diameters are ≥2 mm. Figure 2(*b*) clearly shows that the shape factors of the aggregates on the two cross sections are between 0.2 and 0.8. The shape factors of the aggregates on the vertical cross section are about 0.2 less than those on the horizontal cross section. This result demonstrates that the major cross sections of aggregate particles have the tendency to lie horizontally. This tendency can also be observed from the differences between the numbers and areas of aggregates whose major or minor axis lengths are ≥2 mm on the two cross sections. The differences, based on major or minor axis lengths, are 51 (173 − 122) and 86 (197 − 111) for the numbers of aggregate particles on the horizontal and vertical cross sections, respectively. The aggregate numbers on the two cross sections, based on Feret diameter, are almost the same (i.e., 158 and 160). Moreover, the total area of the horizontal cross section is 31.2 percent greater than that of the vertical cross section.

Comparison of the gradations by orientation of aggregates on the two cross sections in Figure 3 illustrates that the orientations of aggregates on the horizontal cross section are more random than those on the vertical cross section. There are almost no aggregates whose major axes are oriented in the ranges of (−90°, −80°) and (80°, 90°) (i.e., in the nearly vertical direction) on the vertical cross section. For a completely random orientation of aggregates, the gradation by orientation should be a straight line passing the lower left corner and upper right corner in Figure 3.

Effects of Compaction Methods

Two laboratory specimens prepared by different compaction techniques and two cores recovered from pavement section compacted using uniquely different field compaction equipment were analyzed in this example. The two laboratory specimens of 100 mm in diameter and 50 mm in height were compacted using gyratory and Marshall compactors. A total of 250 gyrations at a pressure of 0.6 MPa was used for the gyratory compaction with an angle of 1 degree, and 100 impact blows were applied using a standard Marshall compactor. These unusually high compaction efforts were used deliberately to show the effects of the laboratory compaction methods under extreme conditions. The two cores of 95 mm in diameter and 50 mm in height were recovered from two sections of an experimental pavement compacted 4 years ago. One section was compacted using the AMIR compactor and the other was compacted using a conventional vibratory steel roller followed by a rubber-tire roller (*29*). Six, seven, eight, and seven horizontal cross sections were analyzed for the four specimens compacted using gyratory, Marshall, AMIR, and roller compactors, respectively (see Figure 5). The total number of calculated aggregates on these cross sections is 1,009; 1,251; 1,135; and 1,067 for the specimens compacted using gyratory, Marshall, AMIR, and roller compactors, respectively. Among them, there are 877; 1,089; 941; and 924 aggregates whose Feret diameters are ≥2 mm on the cross sections

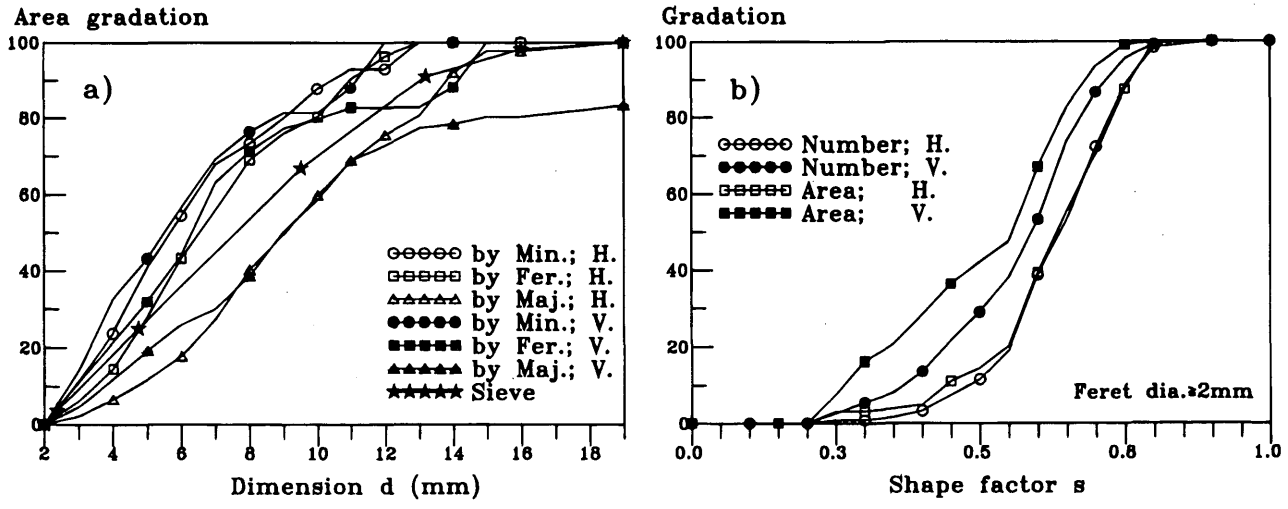

FIGURE 2 Image gradations on horizontal (*H*) and vertical (*V*) cross sections of gyratory compacted HL4 mixtures. (a) Area gradation by dimensions; (b) gradation by shape factor *s* (Feret diameter ≥2 mm).

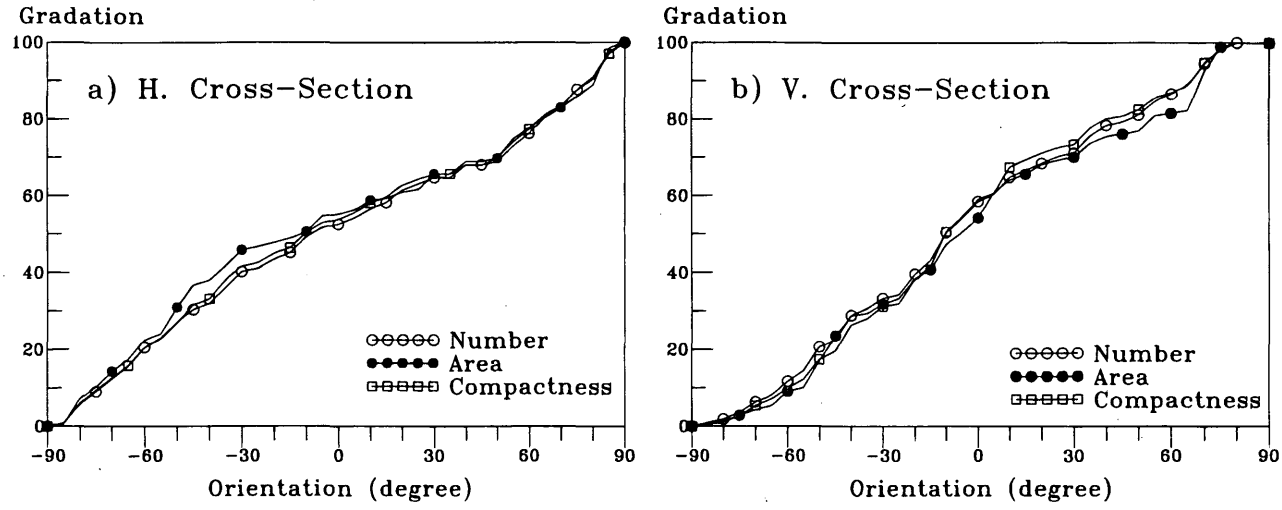

FIGURE 3 Gradation by orientation θ of aggregates on horizontal (*H*) and vertical (*V*) cross sections of gyratory compacted HL4 mixtures: Feret diameter ≥2 mm. (*a*) Horizontal cross section; (*b*) vertical cross section

of the four specimens compacted using gyratory, Marshall, AMIR, and roller compactors, respectively.

Figure 4 shows the area gradations by minor axis length, Feret diameter, or major axis length of aggregates on the horizontal cross sections of the specimens used. The sieve analysis is also plotted. The following observations can be made from these three figures.

(*a*) The area gradations by size (minor or major axis lengths, or Feret diameter) follow the same patterns and are very similar for the four specimens.

(*b*) The area gradations by the minor axis length are a little finer than that of a sieve analysis. The area gradations by the Feret diameter are the closest approximation to the sieve analysis. The area gradations by the major axis length are much coarser than that of a sieve analysis.

(*c*) The area gradation by the Feret diameter of the Marshall specimen is a little finer than that of the gyratory specimen. The area gradations by the Feret diameter of the two laboratory specimens are finer than those of the two field cores.

The first observation reflects the fact that the four specimens had the same coarse aggregate gradation of the HL4 mix. The second observation indicates that the sieve analysis gradation is determined by the lengths of the intermediate and minor principal axes of the particle itself. The third observation may be explained by aggregate breaking during the Marshall compaction of 100 impact blows.

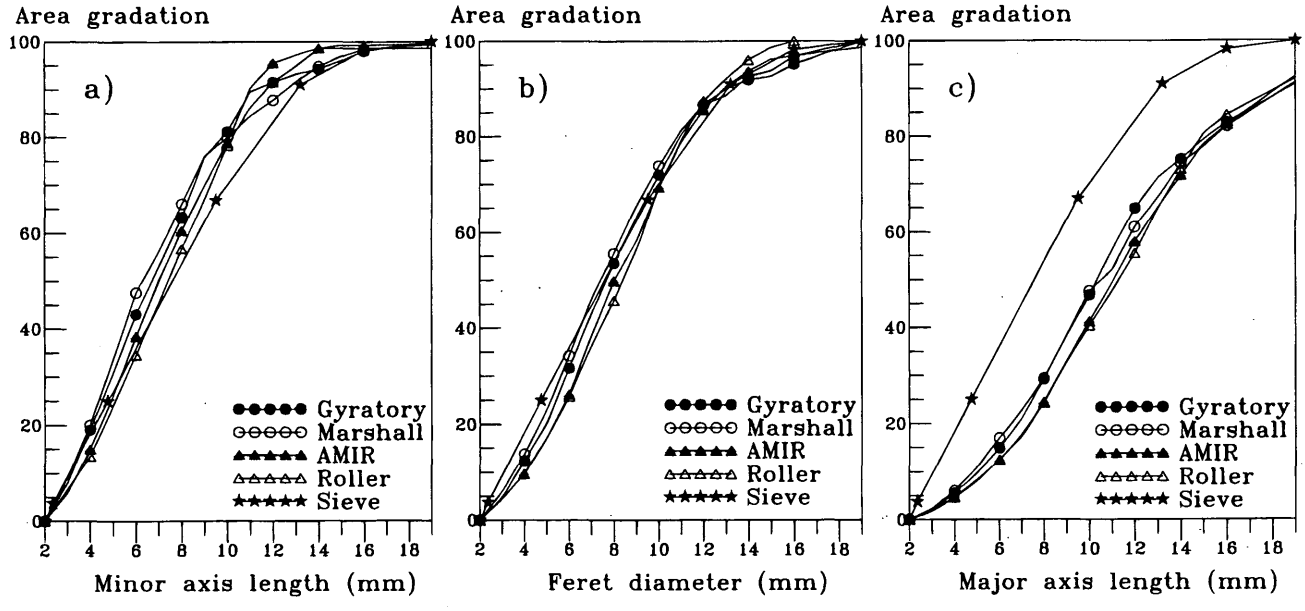

FIGURE 4 Area gradation by dimensions of HL4 mixtures compacted with gyratory, Marshall, AMIR, or steel roller compactors. (*a*) By minor axis length; (*b*) by Feret diameter; (*c*) by major axis length.

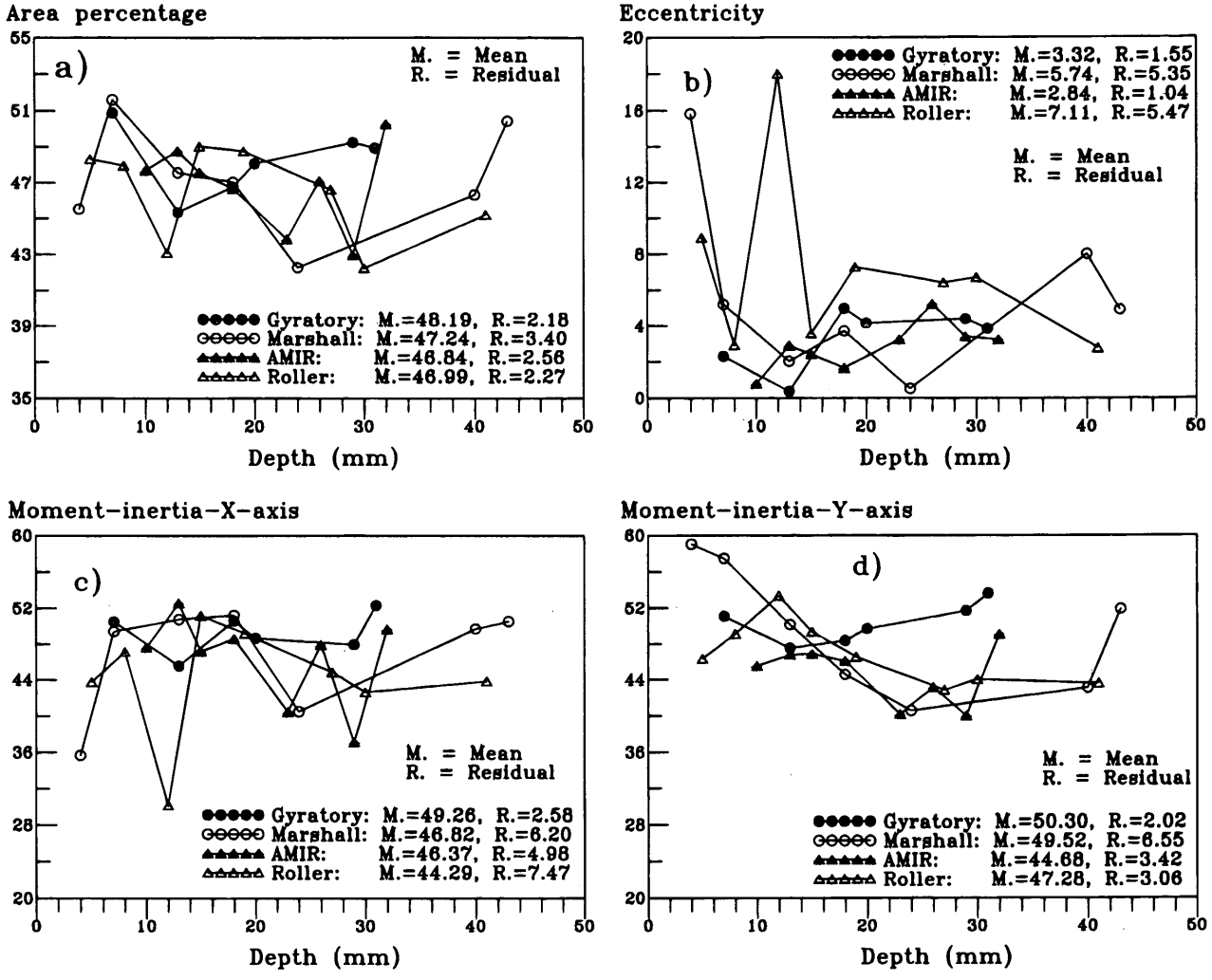

FIGURE 5 Variations of statistical parameters of aggregates on horizontal cross sections of HL4 mixtures compacted with gyratory, Marshall, AMIR, or steel roller compactors versus depth of cross sections. (*a*) Percentage of areas occupied by aggregates; (*b*) eccentricity; (*c*) percentage of moment of inertia with respect to *X* axis; (*d*) percentage of moment of inertia with respect to *Y* axis.

Figure 5 shows the vertical variations of some statistical parameters of aggregate distribution on the horizontal cross sections for the four specimens. Figure 5(*a*) shows the vertical variations of percentage areas occupied by aggregates on the horizontal cross sections. Figure 5(*b*) shows the vertical variations of eccentricity of aggregates on the horizontal cross sections. The vertical variations of percentages of moment of inertia with respect to the *X* and *Y* axes of aggregates on the horizontal cross sections were plotted in Figure 5(*c*) and (*d*), respectively. The origin of the *X* and *Y* coordinates was relocated at the center of the horizontal circular cross sections. For the two laboratory specimens, the directions of the *X* and *Y* coordinates were arbitrarily selected. For the two field specimens, the direction of the *X*-coordinate was along the longitudinal direction of the experimental asphalt pavement. The mean values and residuals of the statistical parameters are also presented in Figure 5(*c*) and (*d*). For a completely uniform distribution of aggregates in AC mixtures, there should be no vertical variation in the statistical parameters such as area percentage and percentages of moments of inertia. The moments of inertia with respect to the *X* and *Y* axes should be the same and the eccentricity should be 0. Keeping this hypothesis in mind, Figure 5 shows that the gyratory and AMIR specimens have the most homogeneous distribution of coarse aggregates. The calculation of the data in Figure 5 was based on the criterion that Feret diameter is $\geq$2 mm. Similar results can be obtained if the minor axis length ($\geq$2 mm) is used as the criterion.

CONCLUSIONS AND RECOMMENDATIONS

An innovative digital image-processing technique has been successfully applied to the quantitative study of AC microstructure. In particular, the coarse aggregates and their spatial distribution in AC mixtures can be measured and analyzed using the technique described in this paper. The results presented in this paper lead to the following preliminary conclusions and recommendations.

1. The area gradation by Feret diameter from digital image analysis gives a very good prediction of the gradation of coarse aggregates used for the mix. The Feret diameter of 2 mm can

be used as the lower limit for the definition of coarse aggregates on the plane cross sections of AC mixtures.

2. The distributions of coarse aggregates on vertical and horizontal cross sections are quite different. Aggregate cross sections are more nearly circular and more randomly oriented and have larger areas on horizontal cross sections than those on vertical cross sections of AC mixtures. This difference may contribute to AC anisotropic properties.

3. On the basis of the analysis of four specimens, it may be concluded that the gyratory and AMIR compactors can produce more uniform distribution of coarse aggregates in AC than the Marshall compactor and conventional roller compactors.

4. These preliminary findings regarding the AC microstructure characteristics (i.e., the internal structure of coarse aggregate distribution) should be further confirmed by analyzing more AC mixtures and specimens using the digital image-processing technique.

5. The measurements of aggregate distributions should be further utilized in the finite element microstructure modeling of AC mixtures.

6. The digital image-processing techniques should be applied to the quantitative study of the microstructure of different AC mixes such as SMA and LSM compacted in the laboratory or field.

ACKNOWLEDGMENTS

Deep gratitude is extended to N. K. Sinha and P. D. Barrette of the Institute for Environmental Research and Technology, NRC, Ottawa, Canada for making their digital image-processing facilities available for this investigation. I. Morin would like to thank the NRC for financial assistance during her 4-month cooperative program at the Pavements Laboratory, CSTT, NRC. The authors would also like to thank the six referees for their constructive comments, which enhanced the presentation of the paper.

REFERENCES

1. Haas, C., H. Shen, W. A. Phang, and R. Haas. Application of Image Analysis Technology to Automation of Pavement Condition Surveys. *Proc., International Transportation Congress,* Montreal, Canada, 1984, pp. C57–C73.
2. Wigan, M. R. Image Proceeding for Roads: An On-line Literature Review and Text Database Assessment. *Australian Road Research,* Vol. 15, 1985, pp. 50–55.
3. Bentz, D. P., and E. J. Garboczi. Digital-image-based Computer Modelling of Cement-based Materials. *Proc., Conference on Digital Image Processing: Techniques and Applications in Civil Engineering,* Kona, Hawaii, March 1993, pp. 44–51.
4. Yudhbir and Abedinzadeh, R. Quantification of Particle Shape and Angularity Using the Image Analyzer. *Geotechnical Testing Journal,* GTJODJ, Vol. 14, No. 3, Sept. 1991, pp. 296–308.
5. Barrette, P. D. and N. K. Sinha. Crystallographic Characterization of a Core From the Ward Hunt Shelf, Canada. *Proc., International Symposium on Snow and Related Manifestations* (*SNOW SYMP 94*), Manali, H.P., India, Sept. 1994, p. 4.
6. Frost, J. D., and J. R. Wright, (eds.). *Digital Image Processing: Techniques and Applications in Civil Engineering: Proceedings of a Conference,* Kona, Hawaii, American Society of Civil Engineers, March 1993 New York, p. 229.
7. Eriksen, K. *Microscopical Analysis of Asphalt-aggregate Mixtures Related to Pavement Performance.* Report Note 245, Danish Road Institute, Denmark, Nov. 1993, p. 17.
8. Vinson, T. S., V. C. Janoo, and R. C. G. Haas. *Summary Report Low Temperature and Thermal Fatigue Cracking.* SHRP-A/IR-90–001, National Research Council, Washington, D.C., June 1989.
9. Tangella, S. C. S. R., J. Craus, J. A. Deacon, and C. L. Monismith. *Summary Report on Fatigue Response of Asphalt Mixtures.* SHRP-A/IR-90–011, National Research Council, Washington, D.C., Feb. 1990.
10. Monismith, C. L. *Summary Report on Permanent Deformation in Asphalt Concrete,* SHRP-A/lr-91–104, National Research Council, Washington, D.C., Feb. 1991.
11. Kandhal, P. S., M. A. Khatri, and J. B. Motter. Evaluation of Particle Shape and Texture of Mineral Aggregates and Their Blends. *Proc., AAPT,* Vol. 61, Feb., 1992, pp. 217–240.
12. Servais, S. G. C., and K. I. York. The Precision of an Aggregate Particle Size and Shape Test. *Road & Transport Research,* Vol. 2, No. 2, 1993, pp. 86–97.
13. El Hussein, H. M., and A. O. A. Halim. Differential Thermal Expansion/Contraction—A Mechanical Approach to Adhesion in Asphalt Concrete. *Canadian Journal of Civil Engineering,* Vol. 20, No. 3, 1993, pp. 366–373.
14. El Hussein, H. M., and Z. Q. Yue. Criteria for Evaluation of Rutting Potential Based on Repetitive Uniaxial Compression Test. In *Transportation Research Record 1454,* TRB, National Research Council, Washington, D.C., 1994.
15. Ugh, P., and P. J. van de Loo. *Permanent Deformation of Asphalt Mixes.* Koninklijke/Shell-Laboratorium, Amsterdam, Nov. 1974.
16. Brown, S. F., and C. A. Bell. The Validity of Design Procedures for the Permanent Deformation of Asphalt Pavements. *Proc., Fourth International Conference on the Structural Design of Asphalt Pavements,* Vol.1, Ann Arbor, 1977, pp.467–482.
17. Roque, R., and B. E. Ruth. Mechanisms and Modelling of Surface Cracking in Asphalt Pavements. *Proc., AAPT,* Vol. 59, Feb., 1990, pp. 553–570.
18. Selvadurai, A. P. S., M. C. Au., and W. A . Phang. Modeling of Low Temperature Behaviour of Cracks in Asphalt Pavement Structures. *Canadian Journal of Civil Engineering,* Vol. 17, 1990, pp. 844–858.
19. Monismith, C. L. Analytically Based Asphalt Pavement Design and Rehabilitation: Theory to practice, 1962–1992. In *Transportation Research Record 1354,* TRB, National Research Council, Washington, D.C., 1992, pp. 5–26.
20. Movenzadeh, F. Asphalt Fracture. *Proc. AAPT,* Vol. 36, 1967, pp. 51–79.
21. Salam, Y. M., and C. L. Monismith. Fracture Characteristics of Asphalt Concrete. *Proc. AAPT,* Vol. 41, 1972, pp. 215–256.
22. Aglan, H., I. Shehata, L. Figueroa, and A. Othman. Structure-fracture Toughness Relationships of Asphalt Concrete Mixtures. In *Transportation Research Record 1353,* TRB, National Research Council, Washington, D.C., 1992, pp. 24–30.
23. Selvadurai, A. P. S., P. E. Joseph, and A. O. A. Halim. Evaluation of Fracture Resistance of Bituminous Materials. *Proc., Canadian Society for Civil Engineering Annual Conference,* Fredericton, N.B., 1993, Vol. 4, pp. 287–296.
24. Kim, K. W., and H. M. El Hussein. Effect of Differential Thermal Contraction on Fracture Properties of Asphalt Materials at Low Temperature. Presented at 1995 AAPT Annual Meeting, July, 1994.
25. Gdoutos, E. E. *Fracture Mechanics Criteria and Applications.* Kluwer Academic Publishers, London, 1991.
26. Rothenburg, L., A. Bogobowicz, and R. Haas. Micromechanical Modelling of Asphalt Concrete in Connection with Pavement Rutting Problems. *Proc., 7th International Conference on Asphalt Pavements,* Nottingham, UK, Vol. 1, 1991, pp. 230–245.
27. Sepehr, K., O. J. Svec, Z. Q. Yue, and H. M. El Hussein. "Finite Element Modelling of Asphalt Concrete Microstructure. In *Localized Damage III: Computer-Aided Assessment and Control, Proceedings of 3rd International Conference on Computer-Aided Assessment and Control: Localized Damage 94* (M. H. Aliabadi, A. Carpinteri, S. Kalisky, and D. J. Cartwright, eds.), Computational Mechanics Publications, Southampton, Boston, 1994, pp. 225–232.
28. Consuegra, A., D. N. Little, H. L. Von Quintus, and J. Burati. Comparative Evaluation of Laboratory Compaction Devices Based on Their Ability to Produce Mixtures with Engineering Properties Similar to Those Produced in the Field. In *Transportation Research Record 1228,* TRB, National Research Council, Washington, D.C., 1989, pp. 80–87.
29. Svec, O. J., and A. O. A. Halim. Field verification of a new asphalt compactor, AMIR. *Canadian Journal of Civil Engineering,* Vol. 18, 1991, pp. 465–471.
30. Emery, J. J., W. Schenk J. J. Carrick, J. K. Davidson, W. K. MacInnis, and J. A. Kennepohl. Stone Mastic Asphalt Trials in Ontario. In *Transportation Research Record 1427,* TRB, National Research Council, Washington, D.C., 1993, pp. 47–53.

Publication of this paper sponsored by Committee on Characteristics of Nonbituminous Components of Bituminous Paving Mixtures.

Effect of Moisture Content on Measured Properties of Asphalt Mixtures

T. F. FWA AND C. B. OH

With asphalt mixtures, the engineering properties of resilient modulus, indirect tensile strength, Marshall stability, and flow vary with the temperature at which they are measured. It is standard practice in pavement engineering to specify the measurement temperature, particularly in field measurements in which the temperature of pavement materials cannot be manually controlled. It is appropriate to focus on other field conditions that might affect the measured in situ properties of in-service pavements. The moisture content of in-service asphalt paving mixtures, which also cannot be controlled manually, is obviously another major factor to be considered. This study examines how the moisture content of an asphalt mixture influences its engineering properties, and explores whether identifying the moisture content of asphalt mixtures is necessary during measurement for proper pavement evaluation.

For easy interpretation of test results, this study involved only laboratory tests on compacted specimens prepared in the laboratory following standard procedures under controlled conditions. This arrangement offered the advantage of allowing multiple specimens to be prepared and tested under the same conditions, and made statistical assessments of the validity of the test results possible.

The steps involved in the test program were (*a*) specimen preparation, (*b*) introduction of moisture into compacted specimens, (*c*) moisture content monitoring and (*d*) evaluation by means of resilient modulus (M_R) and indirect tensile strength (*Ts*) tests. Moisture was introduced into the compacted specimens by cyclic wetting-drying treatment and 24-hr soaking in water. The effects of the two methods of moisture introduction were investigated in the study. Figure 1 shows a flow chart summarizing the test program. The details of the program are described in the following sections.

METHOD

Specimen Preparation

In this study a dense-graded asphalt mixture, which is used in Singapore for wearing courses, was used to prepare all test specimens. Its mix composition and aggregate gradation are given in Table 1. Cylindrical specimens, each 102 mm (4 in.) in diameter and approximately 64 mm (2.5 in.) in height, were prepared in accordance with the standard Marshall procedure described in ASTM D1559.

Sixty-five specimens were prepared, forming 13 groups of 5 specimens for the test program outlined in Figure 1. That is, the five specimens in a given group went through identical moisture treatment and test sequence assigned to them. All specimens were prepared to meet the local mix requirements, which limited the percent air voids to 3 to 5 percent. The bulk specific gravity of the 65 specimens varied from 2.362 to 2.404, with a mean of 2.383 and standard deviation of 0.012. The percent air voids varied from 3.07 to 4.75 percent with a mean of 3.783 percent and standard deviation of 0.573 percent.

Center for Transportation Research and Department of Civil Engineering, National University of Singapore, 10 Kent Ridge Crescent, Singapore 0511.

Grouping of Specimens

Before the specimens were grouped, all were tested for M_R in accordance with ASTM D4123 using a load of 1.6 kN (0.36 kip) applied at a frequency of 1 Hz with a loading duration equal to 400 msec. They were then arranged in decreasing order of magnitude of M_R. The first 13 specimens were randomly assigned, one each to groups 1 to 13. Next, the following 13 specimens were randomly assigned to the 13 groups, and so on. The process was repeated until all 65 specimens were assigned. Through this method of distribution, an effort was made to achieve a fair assessment of the effect of moisture content on the specimens. The 13 groups were then randomly assigned to the test program shown in Figure 1.

Moisture Treatment

One of the 13 specimen groups was randomly selected as the reference group to be tested without moisture treatment. The test results of this reference group represent properties of compacted specimens with practically 0 moisture content. The remaining 12 groups were randomly divided into two sets of 6. One set was subjected to the cyclic wetting-drying treatment and the other to 24-hr immersion. The cyclic wetting-drying treatment is an attempt to simulate the repeated wetting and drying process found in the field. This process is significant in the wet, tropical climate of Singapore, where rainfall and sunshine are abundant. In Singapore, the average number of hours each day of bright sunshine is more than 5, and the country experiences approximately 150 days of rain each year (*1*).

Cyclic Wetting-Drying Treatment

The test specimens were subjected to alternating periods of wetting and drying in an enclosed chamber. The detailed operating features of the chamber are described by the authors elsewhere (*3*). This treatment is essentially to induce moisture into the specimens. Wetting of the specimens was achieved by spraying them with tap water, at about 28°C, by means of shower heads positioned in the chamber. Drying was effected by heating using ceramic heaters after the spraying of water.

A 4-hr treatment cycle consisting of 2 hr of wetting followed by 2 hr of drying was used. The length of the wetting phase was

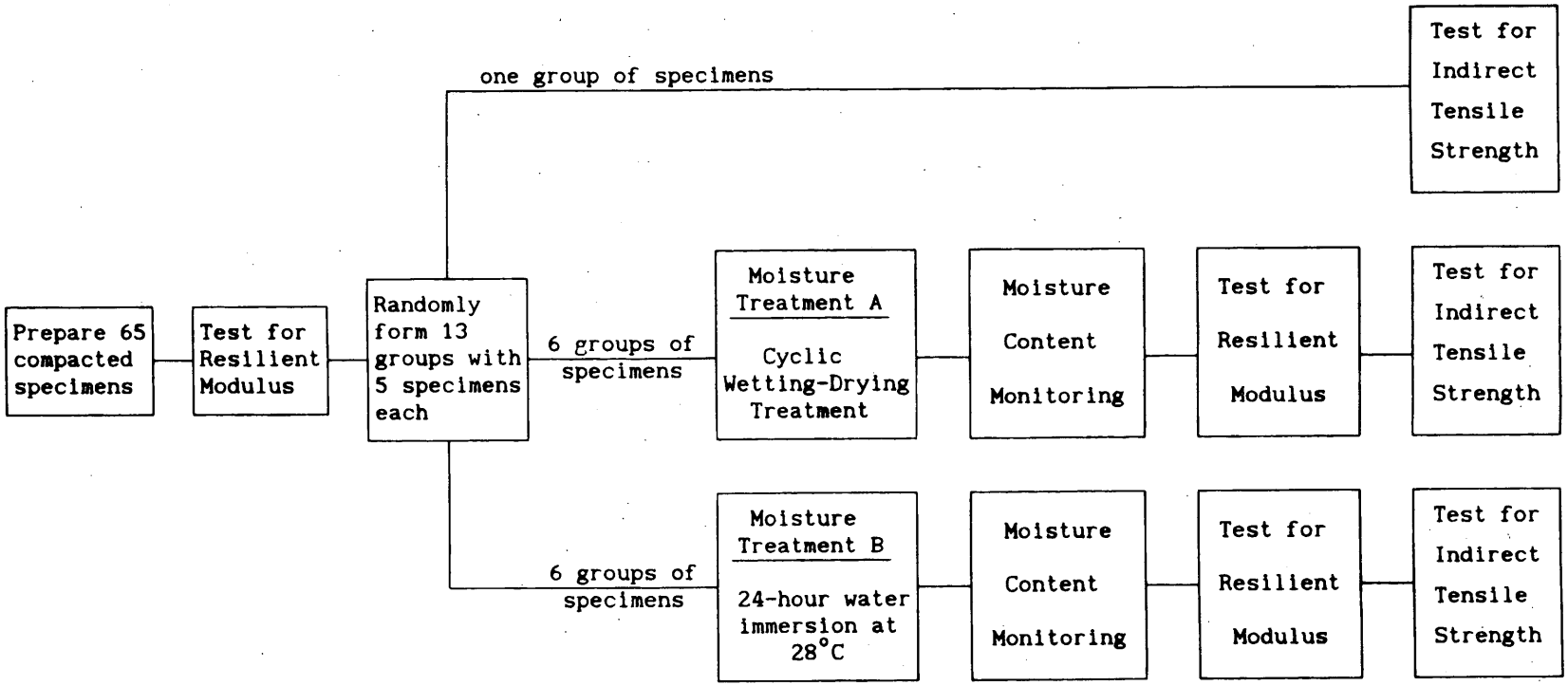

FIGURE 1 Flow diagram for test program.

TABLE 1 Mix Composition and Aggregate Gradation of Asphalt Mixture Studied

Sieve Size	19mm	13mm	9.5mm	6.4mm	3.2mm	1.2mm	0.3mm	0.075mm
Percent Passing	100	95	90	77	58	37	19	6

(a) Asphalt : Penetration grade 60/70
Binder content = 5.5% by weight of total mix

(b) Aggregate : Granite aggregates with the following gradation

selected to represent approximately the mean duration of rainfall in Singapore (*1*). The drying period was set at 2 hr to attain the desired maximum temperature of about 60°C. Previous experience (*2*) with the chamber indicates that an equilibrium moisture state in the treated specimens is reached after about 150 cycles. In the current study 150 cycles of 4-hr treatment were used, therefore taking 600 hr (or 25 days) to complete.

Water Immersion Treatment

In the water immersion treatment, compacted asphaltic specimens were placed in a broad-based container, and tap water at about 28°C was added to the container to a depth of 150 mm (6 in.). Twenty-four hr of immersion was deemed adequate, because an equilibrium moisture state could be reached within this period.

Evaluation Tests

Two mechanical properties of the test specimens, namely, M_R and *Ts*, were adopted as the basis for assessing the changes caused by the presence of moisture in the compacted specimens. M_R was determined according to the procedure outlined in ASTM D4123 using a load of 1.6 kN (0.36 kip) applied at a frequency of 1 Hz with a loading duration of 400 msec. In the *Ts* test, the rate of loading adopted was 50.8 mm/min (2 in./min). Both tests were conducted at 25°C.

Because the M_R test is nondestructive, it was performed on all specimens twice, before and after moisture treatment. It is therefore possible to compute the change in the M_R of a specimen caused by moisture treatment. Because it is practically impossible for all test specimens to have identical M_R, an appropriate parameter for assessing the effects of different moisture levels is to define the percentage of M_R retained ($R(M_R)\%$) as follows:

$$R(M_R)\% = \frac{(M_R)i}{(M_R)_o} \times 100\% \quad (1)$$

where $(M_R)_o$ is the M_R of the specimen concerned at 0 moisture content, and $(M_R)i$ is the M_R of the specimen concerned at moisture content level *i*. $R(M_R)\%$ was computed for every specimen in the 12 groups.

The *Ts* test, on the other hand, is a destructive test, and it is not possible to determine precisely the change in *Ts* caused by moisture treatment to a specimen. In this study, the change in *Ts* was estimated by comparing the average *Ts* of a group of specimens with that of the reference group. This change was expressed as the percentage *Ts* retained ($R(Ts)\%$, defined below:

$$R(Ts)\% = \frac{(Ts)i}{(Ts)_o} \times 100\% \quad (2)$$

where $(Ts)_o$ is the average *Ts* of the reference group of specimens with 0 moisture content, and $(Ts)i$ is the average *Ts* of the group of specimens with moisture content at level *i*.

MONITORING OF MOISTURE CONTENT

Measurement of Moisture Content

All test specimens prepared and compacted in accordance with ASTM D1559 were considered to have 0 moisture content. The percent air voids in each specimen was computed with the following formula:

$$\text{Percent air voids} = \frac{D - d}{D} \times 100\% \quad (3)$$

where D is the theoretical maximum density of the mixture determined in accordance with ASTM D2041, and d is the bulk density of the specimen.

A specimen was assumed to be fully saturated when all its air voids computed from Equation 3 were filled with water. Therefore, the amount of moisture in a compacted specimen at full saturation, *Ws*, was computed as the product of water density and the total air void volume of the specimen. It follows that the moisture content state of a specimen can be defined by the degree of saturation ($S\%$) given by the following equation:

$$S\% = \frac{W}{Ws} \times 100\% \quad (4)$$

where

S% = degree of saturation expressed as percent air voids filled with moisture,
w = mass of moisture in the air voids of the specimen, and
Ws = total mass of moisture in the specimen at full saturation.

The mass of moisture w in a specimen was obtained by taking the difference between the weight of the specimen before and that after moisture treatment.

Moisture Introduction by Cyclic Wetting-Drying

All six groups of specimens treated with 150 cycles of wetting-drying treatment had similar initial moisture content levels. So that the response of specimens at different moisture content levels could be studied, the six groups of specimens were assigned different drying periods after the moisture treatment. The six drying periods selected were 0 hr, 3 hr, 6 hr, 24 hr, 3 days, and 7 days, respectively.

Figure 2 shows how moisture content varies with drying periods by plotting the average $S\%$ of each group of specimens. All test

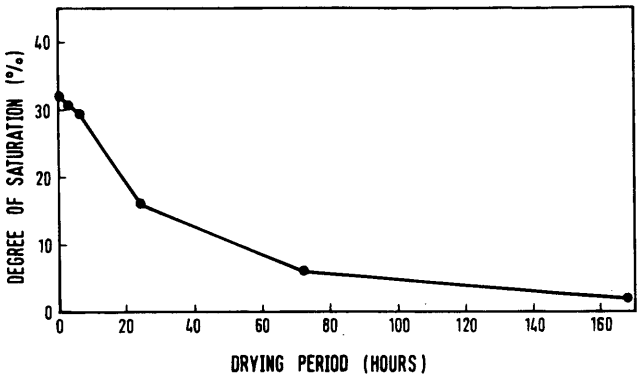

FIGURE 2 Variation of degree of saturation with drying period after cyclic wetting-drying treatment.

specimens were wiped surface dry immediately after moisture treatment using an absorbent cloth and then allowed to dry undisturbed in room conditions at about 28°C. The *S%* achieved after the cyclic wetting-drying treatment was about 32 percent. *S%* dropped to about 30.6, 29.5, and 16.4 percent after 3, 6, and 24 hr of drying, respectively. The rate of drying slowed considerably thereafter, reaching 6.3 percent after 3 days and approaching an equilibrium of about 2.2 percent after 7 days.

Moisture Introduction by Water Immersion

Six groups of specimens were subjected to 24 hr of water immersion. All test specimens were wiped surface dry immediately after the water immersion treatment and allowed to dry undisturbed in room conditions at about 28°C. The six groups of specimens went through the following six periods of drying, respectively: 0 hr, 3 hr, 6 hr, 24 hr, 3 days, and 7 days.

Figure 3 presents the variation of *S%* with drying period based on data obtained from the six groups of specimens. *S%* dropped from 55.6 percent to 52.4 percent, 50.7 percent, and 28.1 percent after drying periods of 3 hr, 6 hr, and 24 hr, respectively. At 3 days into the drying period, *S%* was found to be 11.8 percent. At 7 days into the drying period, *S%* appeared to reach an equilibrium of about 4.1 percent.

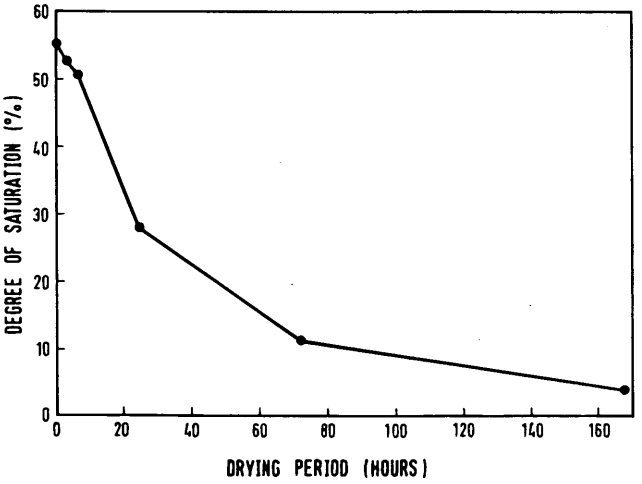

FIGURE 3 Variation of degree of saturation with drying period after 24-hr water immersion.

Compared with the cyclic wetting-drying treatment, the 24-hr water immersion was much more effective in introducing water into the compacted specimens. A degree of saturation equal to 55.6 percent was achieved after the 24-hr immersion treatment, which is 1.74 times the level produced by the cyclic wetting-drying treatment. After 7 days of drying, specimens subjected to water immersion also had higher remaining moisture content (4.1 percent degree of saturation) than those subjected to cyclic wetting-drying treatment (2.2 percent degree of saturation). It was likely that the immersion treatment enabled water to penetrate deeper into the specimens.

ANALYSIS OF TEST RESULTS

Response of Specimens Subjected to Cyclic Wetting-Drying

M_R of Specimens

The results of M_R tests are presented in Figure 4. Figure 4(*a*) plots the average M_R of each of the six groups of specimens against their drying periods. Also indicated is the average M_R of all 65 specimens at 0 moisture content (i.e., before any moisture treatment). The plot shows an inverse relationship between the presence of moisture and the M_R value measured. Specimens with higher moisture contents (i.e., with shorter drying periods) produced lower M_R values. As the moisture content decreased toward 0 with longer drying periods, the M_R measured appeared to approach the value corresponding to 0 moisture content.

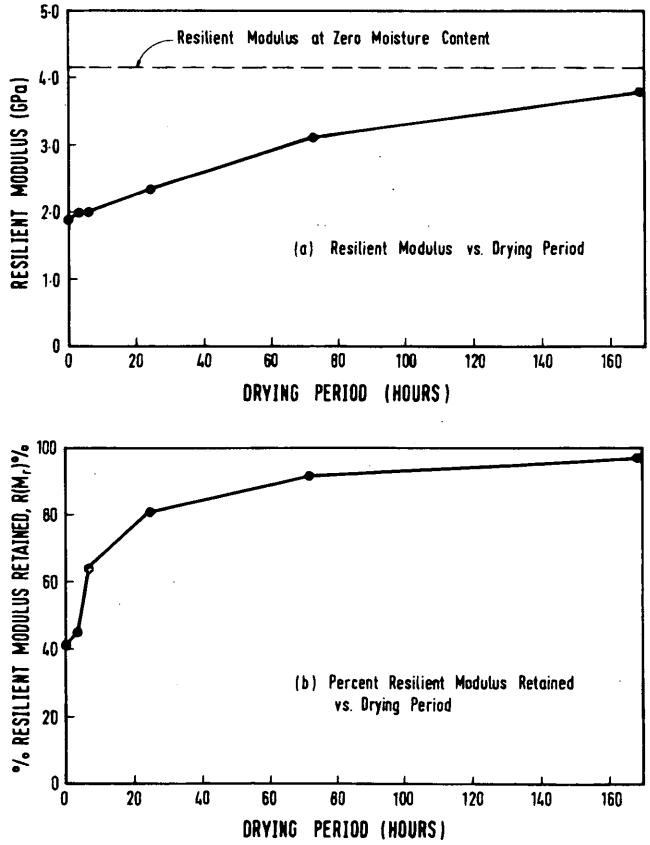

FIGURE 4 Variation of measured M_R as a function of drying period after cyclic wetting-drying treatment.

Adopting the parameter $R(M_R)\%$ defined by Equation 1, Figure 4(*b*) presents the results evaluated based on before– and after–treatment comparisons of the M_R values of individual specimens. Each point in the figure represents the mean for $R(M_R)\%$ of five specimens in a group. Although both parts of Figures 4 (*a* and *b*) indicate that specimens tended to regain their initial $(M_R)_o$ value as moisture content fell, the latter shows a more rapid increase of M_R during the first 24 hr of drying. Since Figure 4(*b*) was derived from individual $R(M_R)\%$ values, each of which was computed from the before-and-after treatment M_R of a specific specimen, it is believed that it provides a more accurate picture of the effect of moisture content.

Statistical testing of the before-and-after treatment M_R shown in Figure 4(*b*) indicated that for the four groups of specimens with drying periods of 0 hr, 3 hr, 6 hr, and 24 hr, respectively, the after-treatment M_R values were significantly lower than their corresponding before-treatment (i.e., 0 moisture content) M_R values at a 95 percent confidence level.

Figure 5 replots the results of Figure 4 in terms of $S\%$. Figure 5(*a*) and (*b*) clearly show that M_R dropped when water was introduced into the specimens, but gradually recovered as the drying process took place. In terms of the magnitude of change in M_R, the effect of moisture content on the measured values of M_R was quite significant. At $S\% = 32$ percent, the measured M_R was only about 42 percent of the $(M_R)_o$ at 0 moisture content. The corresponding M_R values measured at $S\%$ of 30.6, 29.5, 16.4, 6.3, and 2.2 percent were 45, 64, 82, 91, and 96 percent of $(M_R)_o$, respectively.

Ts of Specimens

The results of the *Ts* tests are presented in Figures 6 and 7. Figures 6(*a*) and 7(*a*) plot the average *Ts* of each of the six groups of specimens against their drying periods and degree of saturation, respectively. For comparison, the average *Ts* of the reference group of specimens (i.e., specimens with 0 moisture content) is also indicated. The plots show that the measured *Ts* was affected by the presence of moisture in a way similar to that observed for measured M_R values. The measured *Ts* values were lower for specimens with higher moisture contents (i.e., with shorter drying periods). In other words, *Ts* values varied inversely with moisture content level. *Ts* increased as the moisture content fell, and its value approached $(Ts)_o$ as the moisture content decreased toward 0.

Figures 6(*b*) and 7(*b*) present the results in terms of $R(Ts)\%$, defined by Equation 2. The plots display a similar trend of variation of *Ts* to that found in Figures 6(*a*) and 7(*a*). Statistical hypothesis tests were performed between the mean $(Ts)_o$ of the reference group and the mean *Ts* of each of the six groups with different levels of moisture content. It was found that $(Ts)_o$ was higher than the mean *Ts* of the groups with 0 hr, 3 hr, 6 hr, and 24 hr drying periods,

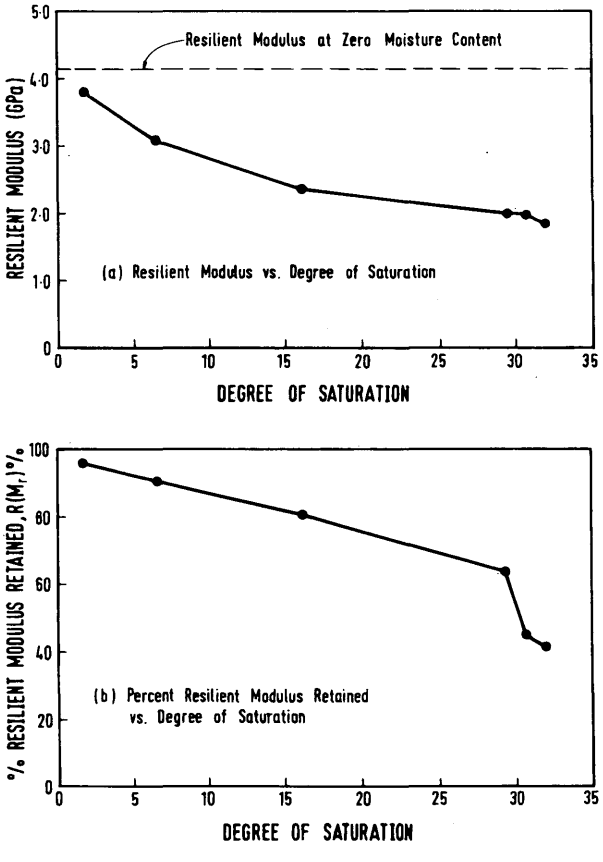

FIGURE 5 Variation of measured M_R as a function of degree of saturation after cyclic wetting-drying treatment.

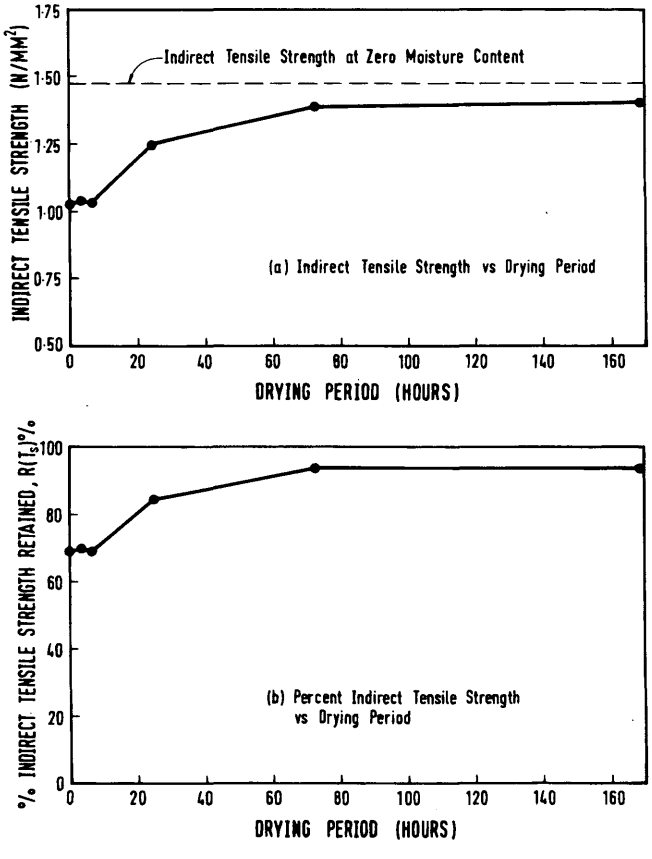

FIGURE 6 Variation of measured *Ts* as a function of drying period after cyclic wetting-drying treatment.

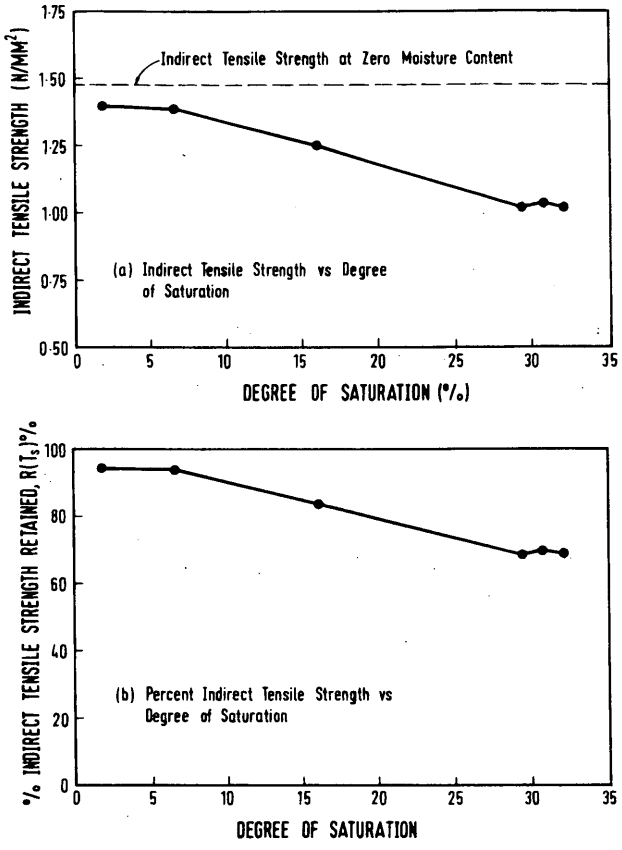

FIGURE 7 Variation of measured *Ts* as a function of degree of saturation after cyclic wetting-drying treatment.

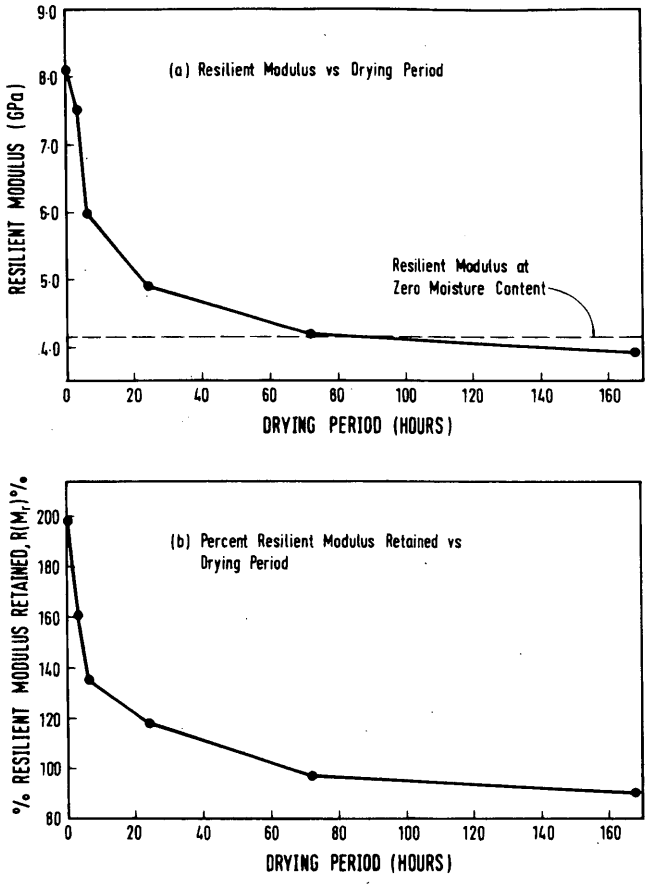

FIGURE 8 Variation of measured M_R as a function of drying period after 24-hr water immersion.

respectively, at a 95 percent confidence level. These results indicate that moisture content had a significant effect on the measured values of *Ts*. The measured *Ts* value varied from 69 percent of $(Ts)_o$ at $S\% = 32$ percent to 94 percent at $S\% = 2.2$ percent.

Response of Specimens Subjected to Water Immersion

M_R of Specimens

The M_R test results are plotted against drying periods in Figure 8(*a*) and against degree of saturation in Figure 9(*a*). It is interesting to note that compared with the M_R test results of specimens subjected to cyclic wetting-drying treatment, an opposite trend was observed in the present case. Here, the largest M_R value was obtained from the group of specimens with the highest moisture content (i.e., specimens with 0 hr of drying). As moisture content decreased for specimens with longer drying periods, the measured M_R value also decreased. The results indicate that the M_R value decreased toward $(M_R)_o$ as the moisture content approached 0.

Figures 8(*b*) and 9(*b*) present the results in terms of $R(M_R)$ percent, defined by Equation 1. It should be noted that while the data in Figures 8(*a*) and 9(*a*) were group averages of after-treatment M_R values, the results in Figures 8(*b*) and 9(*b*) are group-averaged ratios of before- and after-treatment M_R values of individual specimens. These results reaffirmed the decreasing trend of measured M_R with moisture content described in the preceding paragraph. The measured M_R values thus varied directly with moisture content, in contrast to the inverse trend observed with specimens treated by cyclic wetting and drying.

Statistical testing of the before-and-after treatment M_R measurements indicated that for specimens with drying periods of 24 hr or less, the after-treatment M_R values were significantly higher than their corresponding before-treatment (i.e., 0 moisture content) M_R values at a 95 percent confidence level. The results show that at $S\% = 55.6$ percent, the measured M_R was about two times the value of $(M_R)_o$. At $S\%$ of 52.4, 50.7, 28.1, 11.8, and 4.1 percent, the corresponding M_R values were 161, 136, 118, 97, and 91 percent of $(M_R)_o$.

Ts of Specimens

The results of *Ts* tests are summarized in Figures 10 and 11. Figures 10(*a*) and 11(*a*) plot the average *Ts* of each of the six groups of specimens against their drying periods and degree of saturation, respectively. The average *Ts* of the reference group of specimens (i.e., specimens with 0 moisture content) is also indicated in the figures. These plots show that the measured *Ts* varied directly with moisture content. The measured *Ts* values were higher for specimens with higher moisture contents (i.e., with shorter drying periods). As the moisture content decreased toward 0, the *Ts* value approached $(Ts)_o$.

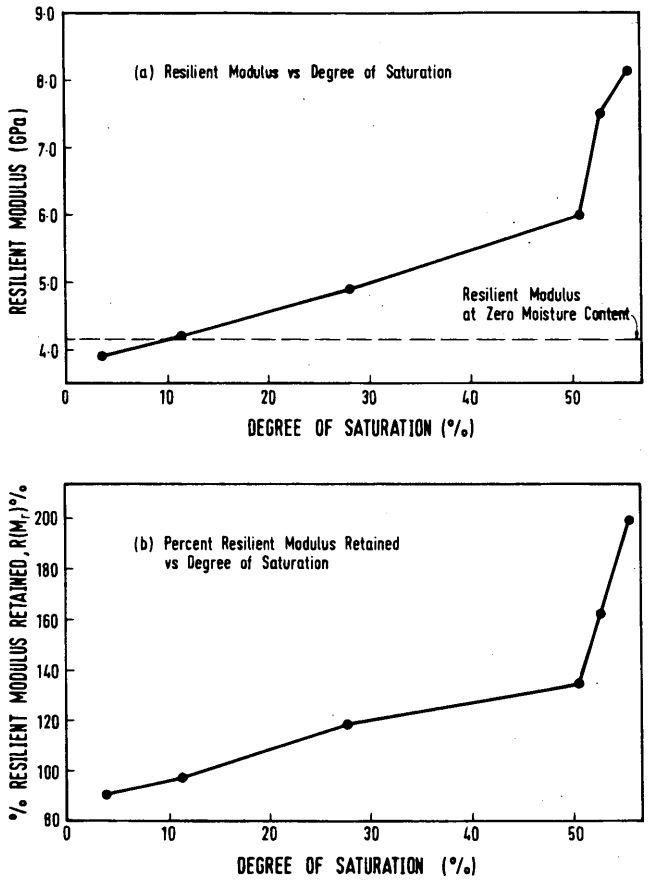

FIGURE 9 Variation of measured M_R as a function of degree of saturation after 24-hr water immersion.

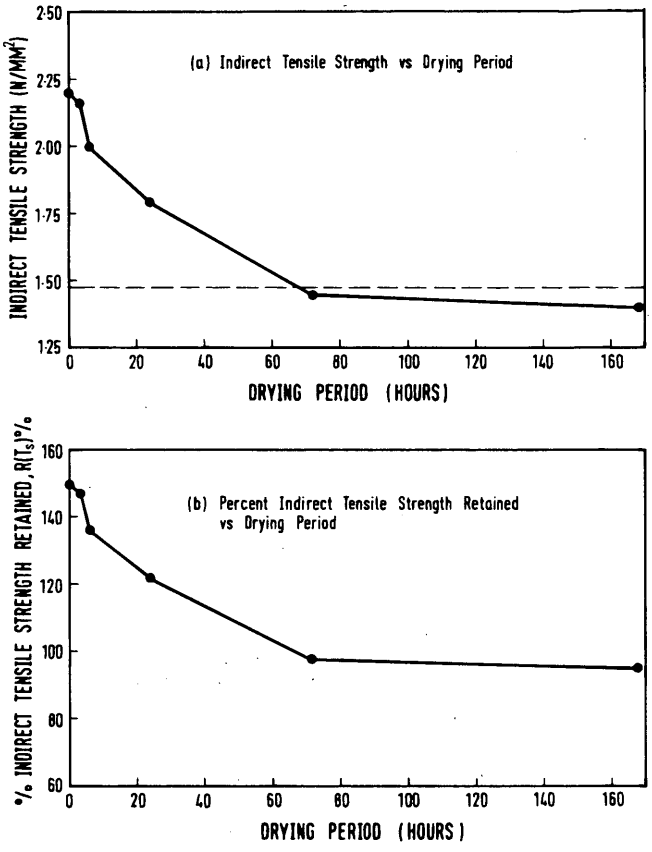

FIGURE 10 Variation of measured *Ts* as a function of drying period after 24-hr water immersion.

In Figures 10(*b*) and 11(*b*), the results are presented in terms of $R(Ts)\%$, defined by Equation 2. The plots display a similar trend of variation of *Ts* to that found in Figures 10(*a*) and 11(*a*). Statistical hypothesis tests were performed between the mean $(Ts)_o$ of the reference group and the mean *Ts* of each of the six groups with different levels of moisture content. It was found that $(Ts)_o$ was lower than the mean *Ts* of the groups with 0 hr, 3 hr, 6 hr, and 24 hr drying periods, respectively, at a 95 percent confidence level. These results confirm that moisture content had a significant effect on the measured values of *Ts*. The measured *Ts* values at *S*% of 55.6, 52.4, 50.7, 28.1, 11.8, and 4.1 percent were found to be 149, 147, 136, 122, 98, and 95 percent of $(Ts)_o$, respectively.

Statistical Analysis of Test Results

So far the analysis has clearly illustrated the significant effect of moisture content on measured properties of asphalt mixtures. In this section, statistical regression analysis is employed to examine whether, besides the moisture content, other mix properties of the specimens had any effect on the test results. The following properties of test specimens were available for the analysis: bulk density, percent air voids, and percent voids in mineral aggregate.

The analysis was performed using $R(M_R)\%$ as the dependent variable in the first instance, and $R(Ts)\%$ in the next. It was found that in both instances, the three mix properties were insignificant in explaining the changes in the dependent variables. The following regression equations were obtained:

For specimens subjected to wetting-drying treatment,

$$R(M_R)\% = 135.6 - 2.971S + 0.06621S^2 \quad R^2 = 0.603$$
$$R(Ts)\% = 81.3 + 1.343S - 0.00218S^2 \quad R^2 = 0.846$$

For specimens subjected to 24 hr immersion,

$$R(M_R)\% = 92.6 + 0.642S - 0.06677S^2 \quad R^2 = 0.754$$
$$R(Ts)\% = 103.3 + 1.629S - 0.02631S^2 \quad R^2 = 0.548$$

The results of the above analysis showing that the effect of the three mix properties was negligible are not surprising because the ranges of values of the three properties in the present study were rather narrow. All specimens studied were of the same mix prepared following the same procedure.

SUMMARY OF FINDINGS AND CONCLUSIONS

The following findings and conclusions may be drawn from the test results presented in this study.

1. Continuous 24-hr water immersion was more effective in introducing water into compacted asphaltic specimens than

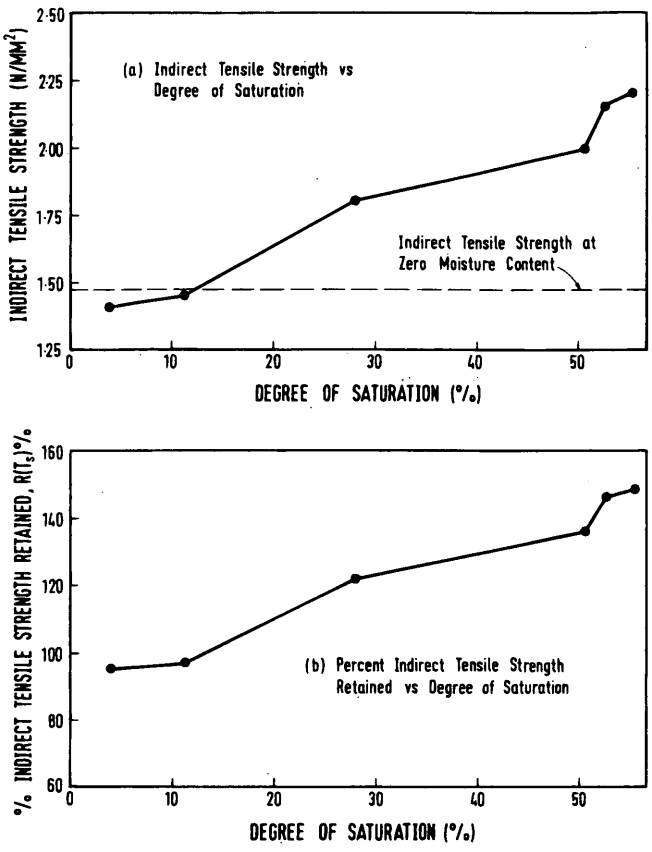

FIGURE 11 Variation of measured *Ts* as a function of degree of saturation after 24-hr water immersion.

repeated wetting-drying treatment consisting of 2-hr wetting and 2-hr drying cycles. The former achieved 55.6 percent degree of saturation, whereas the latter only achieved 32.0 percent. This suggests that prolonged immersion of pavement (e.g., during flooding) might lead to different moisture conditions than wetting of pavement by rainfall.

2. Different processes of introducing moisture into compacted asphaltic specimens could have different effects on the measured properties of the specimens. Introducing moisture by cyclic wetting-drying treatment resulted in lower measured values of M_R and *Ts* compared with the respective initial values at 0 moisture content. On the other hand, introducing moisture by water immersion led to higher values of measured M_R and *Ts*.

3. Compacted specimens treated with the two different methods of moisture treatment also behaved differently as the specimens were allowed to dry undisturbed under room condition at 28°C. For specimens subjected to cyclic wetting-drying treatment, M_R and *Ts* increased as the moisture content or the degree of saturation decreased. For specimens subjected to water immersion, M_R and *Ts* decreased as the moisture content or the degree of saturation decreased.

4. Statistical analyses confirmed the significant effect of moisture content on the measured values of M_R and *Ts*. This study shows that for a compacted dense-graded asphalt mixture, the variations of M_R and *Ts* can be expressed as a function of degree of saturation of the mixture.

5. In all the cases studied, the measured values of M_R and *Ts* approached their respective initial values measured at 0 moisture content as the moisture content decreased toward 0. These test results indicate that regardless of the moisture treatment methods applied, the loss or gain in M_R and *Ts* was only temporary. The process was reversible in the sense that the initial measured values at 0 moisture content were retained when the absorbed moisture was removed.

6. The laboratory tests indicated that, after moisture treatment, the cylindrical specimens took about 3 days of drying before their M_R and *Ts* returned to more or less their initial values at 0 moisture content. However, since the geometric dimensions of pavement and drying conditions in the field are different, the drying time needed for recovery for in-service pavements cannot not be inferred from these test results.

7. The test results showed that as the degree of saturation of test specimens fell to less than 5 percent, the measured M_R or *Ts* values were generally in the order of 95 percent or more of the initial values at 0 moisture content. In situations where the degree of saturation was higher, the difference between the measured value and the corresponding initial value at 0 moisture content could be as much as 100 percent of the latter. This suggests that one must account for the effect of moisture content in measuring the in-situ engineering properties of asphalt pavement. This is especially significant in view of the increasingly widespread use of nondestructive evaluation means, such as the falling-weight deflectometer and other deflection-based measuring techniques.

REFERENCES

1. *Summary of Observation.* Singapore Meteorological Service, Singapore, 1967–1986.
2. Fwa, T. F., and B. K. Ong, Effect of Moisture in Aggregates on Performance of Asphalt Mixtures. In *Transportation Research Record 1454*, TRB, National Research Council, Washington, D.C., 1994.

DISCUSSION

CHARLES MACKEAN
Colorado Department of Transportation, 4340 E. Louisiana Avenue, Denver, Colo. 80222.

The authors have reported increased *Ts* values for compacted hot-mix asphalt (HMA) samples that have been immersed in water for 24 hr. They imply that the moisture susceptibility tests ASTM D4867 and AASHTO T283 will not give the same results. A rapid investigation was carried out to verify the authors' results.

AASHTO AND ASTM PROCEDURES

ASTM and AASHTO differ in their treatment of samples before they are loaded. ASTM D4867–92 states, "Adjust the temperature of the dry subset by soaking in a water bath for 20 min at 77 ± 1.8°F (25 ± 1.0°C)." AASHTO T283–89 states, "The dry subset will be stored at room temperature until testing. The specimens shall be wrapped with plastic or placed in a heavy duty leak proof plastic bag. The specimens shall then be placed in a 77°F (25°C) water bath for a minimum of 2 hours and then tested as described in Section 10."

The ASTM procedure allows compacted samples to be immersed in water for 20 min, whereas the AASHTO procedure attempts to

keep the samples dry while they are submerged. The Colorado Department of Transportation (CDOT) follows AASHTO T283, which is modified as noted in the next section.

PROCEDURE

Eight hot-mix bituminous pavement samples were taken from different projects during production. The samples all contained 1 percent hydrated lime by weight of aggregate as an antistripping additive. These samples represented some of the different aggregates and binders used in Colorado.

Samples were compacted to 7 ± 1 percent air voids using a Texas gyratory compactor. The bulk specific gravity of samples is required to determine air voids. Samples were submerged in water for 3 min while their bulk specific gravity was measured. Samples were then randomly assigned to one of three treatments being compared.

The loading head speed used to test the samples is different from the speed specified in the AASHTO and ASTM procedures. AASHTO and ASTM specify loading head speeds of 2.0 in./min (50.8 mm/min). CDOT uses a loading head speed of 0.2 in./min (5.1 mm/min). The CDOT speed was used in this investigation. Lower loading head speeds result in significantly lower *Ts* values for samples. However, the *Ts* ratio remains comparable to those obtained using the AASHTO and ASTM procedures, as shown by Maupin (*1*).

Testing was performed using a Tinius Olson Super "L" hydraulic testing machine with a Model 290 digital indicating system, which displays the measured speed of the loading head. This machine allows the operator to maintain a head speed in the range of 0.19 in./min (4.8 mm/min) to 0.21 in./min (5.3 mm/min).

Three treatments were evaluated:

1. Samples stored in a 77 ± 1.8°F (25 ± 1°C) air bath for 7 days and tested dry (dry samples);
2. Samples stored in a 77 ± 1.8°F (25 ± 1°C) air bath for 6 days and submerged in 77 ± 1.8°F (25 ± 1°C) water for 24 hr and then tested wet; this treatment compares to the treatment in which the samples were submerged for 24 hr and then dried for a period of 0 hr as reported by Fwa and Oh (24 hr soak samples), and
3. Samples vacuum-saturated to 55 to 80 percent saturation and subjected to a 16 hr freeze, a 24-hr immersion in 140°F (60°C) water, and storage for 2 hr in 77°F (25°C) water and then tested as described in AASHTO T283 (Lottman samples).

Because of the preliminary nature of this investigation, only one compacted sample replicate from each HMA sample was subjected to each treatment. All samples were compacted and tested by the same highly experienced operator.

RESULTS

Table 2 shows results for the 24 samples tested. The average *Ts*'s were 403 kPa for the dry samples, 357 kPa for the 24-hr soak samples, and 343 kPa for the Lottman samples. The average tensile strength retained (TSR) values were 0.89 for the 24-hr soak treatment and 0.85 for the Lottman treatment.

Sample strengths were compared using a paired sample *t*-test. The strengths of the dry samples and the 24-hr soak samples were found to have a statistically significant difference at the 95 percent level of confidence. No statistically significant difference was found between the Lottman samples and the 24-hr soak samples at the 95 percent level of confidence.

The authors have made a valuable observation; however, there is a potential difference between the results generated by the AASHTO and ASTM test procedures for moisture susceptibility of HMA. The authors report increased *Ts* values when HMAs are exposed to moisture, whereas the *Ts* values of the mixes examined in this investigation generally decreased. Nevertheless, this investigation yielded a similar conclusion to that stated by the authors. That is, the *Ts* of samples is affected by a 24-hr soak in 77°F (25°C) water. This was shown at the 95 percent confidence level after only eight samples were tested.

This investigation is preliminary since only eight dry samples, eight 24-hr soak samples, and eight Lottman samples were tested.

This investigation found a drop in *Ts* values when samples are exposed to water. No statistical difference was found at the 95 percent level of confidence between the 24-hr soak treatment and the Lottman treatment. However, a greater number of samples may be able to show a statistically significant difference between these two treatments.

CONCLUSIONS

This investigation found that

1. Samples maintained in a dry condition did not have the same *Ts* values as samples soaked for 24 hr;
2. It would not be prudent to use the AASHTO and ASTM test methods interchangeably;
3. In general, a 24-hr soak in 77°F (25°C) water results in a reduction in the *Ts* value of samples. An exact prediction of the reduction in strength is not possible without testing individual samples, however; and
4. Further research is necessary to determine the effects of 20-min soaking at 77°F (25°C) water on the *Ts* of samples using various aggregate-binder combinations.

REFERENCE

1. Maupin, G. W. Implementation of Stripping Test for Asphaltic Concrete. In *Transportation Research Record 712*, TRB, National Research Council, Washington, D.C., 1979, pp. 8–12.

AUTHORS' CLOSURE

We thank MacKean for conducting an independent test program to verify a major conclusion reported in our study. We concluded that the presence of moisture in a laboratory-compacted asphalt mixture had a statistically significant effect on the measured M_R and *Ts* values of the mixture. The measured values of these two properties were found to vary in relation to the amount of moisture present in the air voids of the mixture.

MacKean's experiment measured the *Ts* value of (*a*) dry specimens, (*b*) specimens subjected to 24 hr of water immersion, and (*c*) specimens treated with a Lottman freeze-thaw cycle. All specimens were tested at 77 ± 1.8°F (25 ± 1°C). Since speci-

TABLE 2 Comparison of Tensile Strengths after Dry Storage, after Dry Storage Followed by Submersion in 77°F (25°C) Water for 24 hr, and after Lottman Freeze-Thaw Cycle

	'Dry' Load	'24 hour Soak'			'Lottman'		
Mix	Str.	Str.	Sat.	TSR	Str.	Sat.	TSR
1G	243	251	(20%)	1.03	230	(77%)	0.95
2B	404	369	(19%)	0.91	293	(78%)	0.73
6C	441	416	(12%)	0.94	398	(71%)	0.90
3F	471	447	(12%)	0.95	435	(76%)	0.92
2I	396	304	(*)	0.77	277	(73%)	0.70
6G	507	414	(*)	0.82	459	(68%)	0.91
1B	385	301	(17%)	0.78	298	(78%)	0.77
3E	373	353	(16%)	0.95	355	(73%)	0.95
Avg.	**403**	**357**	**(16%)**	**0.89**	**343**	**(74%)**	**0.85**

* - These saturation levels were not measured
Tensile Strength (kPa), saturation (percent), TSR:

mens of condition *c* were not examined by Mackean, we will comment only on the results related to the tests on specimens *a* and *b*.

MacKean's study concluded that "samples maintained in a dry condition did not have the same *Ts* as samples soaked for 24 hr". This conclusion confirms our findings that the presence of moisture within asphalt mixtures has a significant effect on the measured *Ts* values of the mixtures. Based on the findings of our study, it is believed that if MacKean were to include the M_R test in his experimental program, similar differences between the dry and soaked specimens would be observed.

Table 2 indicates a difference of 11.4 percent between the average measured *Ts* values of the dry and soaked specimens. The corresponding difference found in our study was about 50 percent. Besides the difference in mix types, another likely factor that contributes to this difference is the percent air voids. MacKean's specimens had 7 ± 1 percent air voids, whereas the average percent air voids in our study was 3.78 percent.

It is important to note that although we observed increased *Ts* values in the soaked specimens, MacKean's test results show reduced *Ts* values. This difference points to the complexity of the problem of partially saturated mixtures and the need for more research to understand how moisture content affects the behavior of asphalt mixtures under loads.

MacKean also concluded that "it would not be prudent to use the AASHTO and ASTM test methods interchangeably." In view of the effects of moisture content on measured *Ts* strength and M_R values, we support his recommendation. The key factor is the amount of moisture that would be gained by a specimen during the soaking process of the ASTM procedure. This effect may be negligible for some mixes but could be significant for others.

We thank MacKean for his commendable effort in verifying the test results of the paper and for sharing the results of his tests.

Publication of this paper sponsored by Committee on Characteristics of Bituminous Paving Mixtures to Meet Structural Requirements.

Moisture Sensitivity Evaluation of Binder-Aggregate Mixtures

SHAKIR SHATNAWI, MAHESH NAGARAJAIAH AND JOHN HARVEY

This study assessed the moisture sensitivity of several binder-aggregate mixtures. This assessment included an evaluation of the effect of hydrated lime on the moisture sensitivity of asphalt-concrete mixtures, the effect of variations from the optimum binder content on the moisture sensitivity of asphalt-concrete mixtures, the moisture sensitivity of asphalt-rubber mixtures, and the potential use of controlled-strain fatigue beam testing to evaluate the moisture sensitivity of asphalt-concrete mixtures. Four aggregates, three asphalt contents, and two hydrated lime contents were used for the asphalt-concrete mixtures. The asphalt-rubber mixtures included asphalt-rubber gap-graded and dense-graded hot mix. Tests performed included AASHTO T283 and the controlled-strain fatigue beam test (Strategic Highway Research Program A-003A). It was found that hydrated lime in a slurry form could be effective in reducing moisture sensitivity of asphalt-concrete mixtures. The degree of its effectiveness was found to depend on asphalt content, lime content, and aggregate source. Also, it was found that a reduction in the binder content by 0.5 percent from the optimum could adversely affect the resistance to moisture damage. AASHTO T283 results showed that the asphalt-rubber mixtures may be more sensitive to moisture than conventional dense-graded asphalt-concrete mixtures. The fatigue beam test results indicated that the test had a potential use in moisture-sensitivity evaluation. The potential parameters were the flexural stiffness ratio and the fatigue life ratio.

Moisture sensitivity is one of the major problems in asphalt-concrete pavements, potentially leading to premature pavement distress. Recently, moisture sensitivity (stripping) was identified to be the major cause of distress in a number of pavements in northern California. The distress manifested in the form of cracking (alligator, longitudinal, and transverse) with varying degrees of severity (*1*). Rutting, raveling, bleeding, and potholes also occurred at various locations. As a result of an investigation conducted by the California Department of Transportation (Caltrans), it was recommended that moisture sensitivity of asphalt concrete mixtures be evaluated using AASHTO T283 and that moisture-sensitive aggregates be treated with hydrated lime in a slurry form before mixing with asphalt to increase the moisture resistance of asphalt-concrete mixtures (*2*).

This study evaluated (*a*) the effectiveness of hydrated lime in a slurry form in minimizing the moisture sensitivity of asphalt-concrete mixtures, (*b*) the use of AASHTO T283 in assessing the moisture sensitivity of asphalt-concrete mixtures, (*c*) the effect of variations from the optimum binder content (OBC) on the moisture sensitivity of asphalt-concrete mixtures, (*d*) the moisture sensitivity of asphalt-rubber mixtures, and (*e*) the potential use of the controlled-strain fatigue beam test, Strategic Highway Research Program (SHRP) A-003A, in evaluating the moisture sensitivity of asphalt-concrete mixtures.

S. Shatnawi, California Department of Transportation, 5900 Folsom Boulevard, Sacramento, Calif. 95819. M. Nagarajaiah, 6000 J Street, Sacramento, Calif. 95819. J. Harvey, Richmond Field Station, Bldg. 480, 1301 South 46th Street, Richmond, Calif. 94804.

EXPERIMENTAL PROGRAM

The experimental program consisted of the following tests and variables.

AASHTO T283

1. Four aggregate sources: two non–moisture-sensitive and two moisture-sensitive aggregates based on field performance;
2. Three asphalt contents: the OBC as determined by Caltrans Test (CT) 367, and ± 0.5 percent variations from it (OBC −0.5 and OBC +0.5);
3. Two hydrated lime contents: 1.5 and 2.0 percent measured by dry weight of aggregate added in a slurry form (one part lime, three parts water);
4. Variable air-void levels, one at 95 percent relative compaction; and
5. Two asphalt-rubber mixtures identified as asphalt-rubber dense-graded hot mix (ARHM-DG) and asphalt-rubber gap-graded hot mix (ARHM-GG).

Controlled-Strain Fatigue Beam Test

1. Two aggregate sources (one non–moisture-sensitive and one moisture-sensitive aggregate), and
2. Two asphalt contents (OBC and OBC −0.5)

The moisture-sensitive aggregate was lime treated with 1.5 percent lime content at OBC. The specimens were compacted to 95 percent relative compaction.

MATERIALS

The four aggregate sources used in this study are identified as Kidder Creek, Clear Creek, Edsell, and Banhart. On the basis of their field performance, the Kidder Creek and Clear Creek aggregates are considered non–moisture-sensitive and the Edsell and Banhart aggregates are considered moisture-sensitive. A petrographic examination of the aggregates revealed the following:

1. Kidder Creek is composed of 75 percent metamorphic and 25 percent plutonic rocks;

2. Clear Creek is composed of 20 percent volcanic, 65 percent metavolcanic, and 10 percent plutonic rocks; and
3. Edsell and Banhart are mainly composed of andesite volcanic rock.

The gradations used for the dense-graded and the gap-graded mixes are shown in Table 1. The asphalt used in this study was AR-4000. The asphalt-rubber binder contained 17.0 percent tire rubber and 2.0 percent natural rubber (by total weight of binder).

SPECIMEN FABRICATION

The 102-mm-diameter AASHTO T283 specimens were compacted to a height of 64 mm using the California kneading compactor. The air-void levels selected for the moisture-damage specimens corresponded to 95 percent relative compaction (in-place density relative to the laboratory density) which is the minimum in-place compaction level considered satisfactory by Caltrans. Other tests were performed at different air-void levels. The air-void levels for the

TABLE 1 Mix Properties

Description	Test Method	Aggregate Source Kidder	Banhart	Clear	Edsell
Bulk Coarse Specific Gravity	CT 206	2.878	2.600	2.638	2.569
Apparent Fine Specific Gravity	CT 208	2.888	2.720	2.700	2.682
Combined Specific Gravity	AASHTO T 209	2.883	2.661	2.672	2.630
Rice Specific Gravity (DGAC)(Untreated)	AASHTO T 209	2.697	2.501	2.489	2.450
Rice Specific Gravity (DGAC)(1.5% Lime)	AASHTO T 209	-[b]	2.493	-	2.461
Rice Specific Gravity (DGAC)(2.0% Lime)	AASHTO T 209	-	2.487	-	2.448
Rice Specific Gravity (ARHM - DG)(Untreated)	AASHTO T 209	2.595	2.419	-	*[c]
Rice Specific Gravity (ARHM - GG)(Untreated)	AASHTO T 209	2.610	2.403	-	*
Percent Water Absorption (Untreated)	CT 206	0.920	1.700	1.320	1.920
Percent Asphalt Absorption (Untreated)	AASHTO T 209	0.230	0.300	0.130	0.370
Percent Asphalt Absorption (1.5% Lime)	AASHTO T 209	-	0.280	-	0.350
Percent Asphalt Absorption (2.0% Lime)	AASHTO T 209	-	0.180	-	0.210
Crushed Particles	CT 205	95%	100%	97%	100%
Sand Equivalency	CT 217	76	76	78	81
Percent Air Voids(Untreated)	CT 367	4.30%	4.21%	5.06%	4.73%
Percent Air Voids(1.5% Lime)	CT 367	-	4.36%	-	5.76%
Percent Air Voids (2.0% Lime)	CT 367	-	4.00%	-	4.80%
Percent Air Voids (SSD)(Untreated)	AASHTO T 269	6.30%	6.24%	6.76%	7.47%
Percent Air Voids (SSD)(1.5% Lime)	AASHTO T 269	-	6.46%	-	7.96%
Percent Air Voids (SSD)(2.0% Lime)	AASHTO T 269	-	5.51%	-	5.76%
Percent Air Voids (SSD)(ARHM - DG)	--[a]	2.50%	2.50%	-	*
Percent Air Voids (SSD)(ARHM - GG)	--	2.00%	2.00%	-	*
Optimum Bitumin Content (OBC)(Untreated)	CT 367	4.30%	4.70%	5.00%	5.50%
Optimum Bitumin Content (OBC)(1.5% Lime)	CT 367	-	4.70%	-	5.00%
Optimum Bitumin Content (OBC)(2.0% Lime)	CT 367	-	4.70%	-	5.00%
Optimum Binder Content (ARHM - DG)	--	6.90%	7.60%	-	*
Optimum Binder Content (ARHM - GG)	--	7.40%	8.00%	-	*

Gradation	Percent Passing					
	Gap Graded		Dense Graded			
Sieve Size (mm)	Kidder	Banhart	Kidder	Banhart	Clear	Edsell
19.0	97	100	100	100	100	100
12.5	90	91	84	86	79	84
9.50	58	67	75	70	71	75
4.75	35	32	54	52	55	55
2.36	25	22	38	37	40	36
1.18	16	18	27	29	27	24
0.60	10	14	19	23	18	15
0.30	7	8	14	13	12	11
0.15	5	6	10	9	8	8
0.075	4	4	6	6	5	6

Lime Bulk Specific Gravity = 503 kg/m^3, Asphalt Grade AR-4000
Absolute Viscosity=396.4 Pascals, Kinematic Viscosity=439 mm^2/s, Penetration=32 dmm

[a]Caltrans practice for asphalt rubber mix design.
[b]Kidder Creek and Clear Creek aggregates were not tested with lime.
[c]Edsell was not tested with rubber.

moisture-damage specimens were computed based on AASHTO T269, which uses the Rice method for maximum theoretical specific gravity (AASHTO T209) and the saturated-surface dry-bulk specific gravity (AASHTO T166).

Compaction of the beam specimens was performed using the rolling wheel compactor, which was developed at the University of California at Berkeley (UCB) during the SHRP efforts (*3*). After compaction, the beams were cut to 50 mm × 63 mm × 38 mm. This portion of the study was accomplished through a cooperative effort between Caltrans and UCB in which staff members from Caltrans performed the testing at the research laboratory of UCB with the participation and assistance of the staff from UCB.

MIX DESIGN CONSIDERATIONS

Conventional Dense-Graded Asphalt-Concrete Mixes

Without lime treatment, the OBCs for the conventional mixes containing the 19.0-mm gradations were 4.3, 5.0, 5.5, and 4.7 percent by dry weight of aggregate for Kidder Creek, Clear Creek, Edsell, and Banhart, respectively. Edsell and Banhart were then lime treated with 1.5 percent and 2.0 percent lime. After lime treatment, the OBC for Edsell decreased to 5.0 percent for both the 1.5 percent and 2.0 percent lime. The OBC for Banhart after lime treatment was the same as before lime treatment. The selection of the OBCs was based on CT 367, which requires a minimum Hveem stability of 35, slight flushing, and a minimum of 4.0 percent air voids. This test method uses the calculated air voids based on the assumption of zero asphalt absorption. The bulk specific gravity is determined according to CT 308-C, which uses the weight of the specimen in air and in water.

The air voids for Kidder Creek, Clear Creek, Edsell and Banhart at OBC were 4.30, 5.06, 4.73, and 4.21 percent using CT 367, and 6.30, 6.76, 7.47, and 6.24 percent using AASHTO T269, respectively. The air voids according to CT 367 were 2.0, 1.7, 2.74, and 2.03 percent lower than those according to AASHTO T269 for the Kidder Creek, Clear Creek, Edsell, and Banhart aggregates, respectively. From this comparison it is obvious that the current Caltrans design practice results in high air voids (according to AASHTO T269), an issue that is addressed in this paper.

Asphalt-Rubber Mixes

The mix designs for the asphalt-rubber mixes were determined according to current Caltrans practices (i.e., 2.5 percent and 2.0 percent air-void criteria for ARHM-DG and ARHM-GG, respectively, and no stability requirement). The bulk specific gravity was determined using CT 308-A. The OBCs for the ARHM-DG and ARHM-GG mixes were 6.9 percent and 7.4 percent, respectively, for Kidder Creek and 7.6 percent and 8.0 percent respectively, for Banhart.

MOISTURE CONDITIONING

AASHTO T283

The conditioning of the specimens was conducted according to AASHTO T283. In the conditioning process, the compacted specimens were stored at room temperature for a period of 72 to 96 hr. Half of the specimens were partially vacuum-saturated with water to 60 to 80 percent saturation. The conditioned specimens were put in a freezer at −18°C (0°F) for 16 hr, and then soaked in a 60°C (140°F) water bath for 24 hr. Finally, the specimens were cooled in a 25°C (77°F) water bath for 2 hr before testing.

Controlled-Strain Fatigue Beam Test

The conditioning of beam specimens was conducted in a procedure similar to that developed as part of Project SHRP A-003A (*4*), which was developed for the Moisture Conditioning System. In the conditioning process, half of the beams were vacuum-saturated with water to 60 to 80 percent. These conditioned beams were then submerged and subjected to three cycles of 5 hr at 60°C followed by 4 hr at 25°C and then one 5-hr cycle at −18°C. The saturation of the beams was maintained by wrapping them with parafilm.

PROPERTIES ANALYZED

The properties analyzed were indirect tensile strength, tensile strength ratio (TSR), flexural stiffness, flexural stiffness ratio, fatigue life, and fatigue ratio.

Indirect Tensile Strength

The indirect tensile strength, referred to hereinafter as the tensile strength, is defined as the maximum stress from a diametral vertical force that a specimen can withstand. It can be computed using the following formula:

$$\sigma t = 2000P/(\Pi t D)$$

where

σt = tensile strength (kPa),
P = maximum load carried by the specimen (N),
t = thickness of specimen (mm), and
D = diameter of specimen (mm).

TSR

The TSR, which was first suggested by Lottman (*5*), is used as a parameter to identify moisture-sensitive mixtures. The TSR is defined as the ratio of the strength of conditioned (wet) specimens to the strength of unconditioned (dry) specimens and can be expressed mathematically as

$$TSR = \sigma\tau_{wet}/\sigma\tau_{dry}$$

where

TSR = tensile strength ratio,
$\sigma\tau_{wet}$ = tensile strength of conditioned specimens, and
$\sigma\tau_{dry}$ = tensile strength of unconditioned specimens.

Flexural Stiffness

The flexural stiffness is a function of the repeated flexural stress and the strain. Recent research has suggested that for controlled-strain

testing, the effect of stiffness on fatigue life would vary (*6*). Tayebali et al. found that an increase in stiffness due to a change in asphalt type resulted in a decrease in fatigue life, whereas an increase in stiffness due to low air voids resulted in an increase in fatigue life. For controlled-stress testing, an increase in stiffness resulted in an increase in fatigue life regardless of whether it was caused by lower air voids or a change in asphalt type. The flexural stiffness ratio (FSR) was introduced as a parameter in this study. It is defined as the ratio of conditioned to unconditioned stiffness values.

$$FSR = S_{wet}/S_{dry}$$

where

FSR = flexural stiffness ratio,
S_{wet} = stiffness of conditioned specimens, and
S_{dry} = stiffness of unconditioned specimens.

Fatigue Life

Fatigue life is defined as the number of cycles to reach 50 percent of the initial flexural stiffness of the beam specimen. The fatigue life ratio was introduced as a parameter in this study:

$$FLR = FL_{wet}/FL_{dry}$$

where

FLR = fatigue life ratio,
FL_{wet} = fatigue life of conditioned specimens, and
FL_{dry} = fatigue life of unconditioned specimens.

EVALUATION OF RESULTS

The AASHTO T283 moisture-damage test results for the 95 percent relative compaction data are summarized in Table 2. To evaluate these results, two types of analysis were used: analysis of variance and *t*-test groupings. The data were first evaluated using analysis of variance to see if there were effects on tensile strength caused by variations from the OBC and changes in aggregate source, lime content, or condition (conditioned versus unconditioned strength). Table 3 shows the results of this analysis. Probabilities less than 0.05 were considered to have significant effects. Tensile strength was found to be significantly affected by variations from the OBC and changes in lime content, aggregate source and condition. After the analysis of variance, *t*-test groupings were used to show the levels at which the differences in strength occurred.

The controlled-strain fatigue beam test data were evaluated by examining the flexural stiffness and the strain-fatigue relations before and after conditioning. The FSR and FLR are two parameters that can be used in moisture-sensitivity evaluation. The evaluation of the results is described in the following section.

Effect of Variations from the OBC on Tensile Strength

Variations from the OBC affected the strength values significantly (Table 4 and Figure 1). As an example, for Kidder Creek, the tensile strength increased with the change in asphalt content from OBC −0.5 to OBC, and decreased as the asphalt content changed from OBC to OBC +0.5. For Edsell, Clear Creek and Banhart, the tensile strength generally increased with the change in asphalt content from OBC −0.5 to OBC and from OBC to OBC +0.5.

Table 4 shows the *t*-test results for all aggregates. The table shows that variations from the OBC generally produced significant differences in tensile strength values. For example, for Edsell at 1.5 percent and 2.0 percent lime contents, there were significant differences between the conditioned strength values at OBC −0.5 and OBC, and between the strength values at OBC −0.5 and OBC +0.05. However, there were fewer significant differences between the values at OBC and OBC +0.5.

Effect of Variations from the OBC on TSR

TSRs generally increased with increase in asphalt content (Table 2 and Figure 2). For example, Kidder Creek, a non–moisture-sensitive mixture, exhibited a low TSR (0.67) at the OBC −0.5 level and higher TSRs at OBC and OBC +0.5 (0.81 and 0.83, respectively). Edsell, a moisture-sensitive mixture, exhibited low TSRs at OBC −0.5 and OBC (0.52 and 0.55, respectively), and a higher TSR (0.81) at OBC +0.5. Since the TSR is a ratio between conditioned and unconditioned strength, a statistical analysis using *t*-test groupings was conducted to analyze the effect of conditioning on strength (Table 4).

Although the results showed some significant differences between the conditioned and the unconditioned specimens, fewer significant differences occurred among the lime-treated specimens. This is explained by the fact that the TSR values are high for the lime-treated specimens which means that the conditioned and unconditioned strengths are closer in values.

Effect of Aggregate Source on Tensile Strength and TSR

Tensile strength values were affected by aggregate source (Figure 1). For example, for conditioned specimens without lime treatment, Clear Creek showed the highest strength values at OBC−0.5 and OBC +0.5, and Kidder Creek had the highest strength values at OBC. There were no significant differences between Clear Creek and Kidder Creek at OBC −0.5 (Table 5). Therefore, Kidder Creek ranks highest, followed by Clear Creek, in terms of tensile strength values. Edsell had the lowest strength values at OBC −0.5 and OBC and ranks below Banhart. Banhart had the lowest strength values at OBC +0.5. There were no significant differences between Banhart and Edsell at all asphalt contents for the conditioned specimens (Table 5). Therefore, both Banhart and Edsell are expected to perform poorly. These findings agree with the reported field performance for all aggregates.

The TSRs at OBC for the different aggregates were 0.81, 0.72, 0.55 and 0.54, for Kidder Creek, Clear Creek, Edsell, and Banhart, respectively. This shows that Kidder Creek will perform best in terms of its resistance to moisture damage, followed by Clear Creek. Edsell and Banhart will perform poorly. At OBC −0.5, the TSRs are 0.67, 0.67, 0.52 and 0.43, for Kidder Creek, Clear Creek, Edsell, and Banhart, respectively. These ratios are lower than those at OBC. This shows that reducing the asphalt content results in increasing the potential for moisture damage of otherwise non–moisture-sensitive aggregates. At OBC +0.5, the TSRs were 0.83, 0.81, 0.81

TABLE 2 AASHTO T283 Moisture Damage Test Results

		95% Relative Compaction					Different Air Void Levels				
		Unconditioned		Conditioned			Unconditioned		Conditioned		
Asphalt Content	Aggregate Source	Air Voids (%)	TS[a] (kPa)[b]	Air Voids (%)	TS (kPa)	TSR[c]	Air Voids (%)	TS (kPa)	Air Voids (%)	TS (kPa)	TSR
OBC -0.5	Kidder Creek	12.88	783	12.91	526	0.67	7.77	1798	7.61	1132	0.63
OBC		10.99	1341	11.03	1084	0.81	7.19	1791	8.12	1539	0.86
OBC +0.5		9.78	926	9.48	769	0.83	7.46	1282	7.35	1086	0.85
OBC -0.5	Clear Creek	13.27	969	13.22	647	0.67	8.88	1812	8.73	1038	0.57
OBC		11.72	944	11.63	678	0.72	7.00	1955	7.01	1468	0.75
OBC +0.5		9.51	1181	9.43	955	0.81	8.03	1658	8.28	1373	0.83
OBC -0.5	Edsell	13.25	540	13.11	282	0.52	7.21	1394	7.28	1038	0.74
OBC		12.96	834	13.42	455	0.55	7.23	1773	7.32	1355	0.76
OBC +0.5		11.68	891	11.65	721	0.81	7.35	1656	7.38	1461	0.88
OBC -0.5	Edsell(1.5%)	14.63	1020	14.40	765	0.75	10.13	1424	10.13	1185	0.83
OBC		13.34	1036	13.09	981	0.95	7.28	1633	6.71	1277	0.78
OBC +0.5		11.24	1387	12.20	1056	0.76	6.89	1332	7.34	1238	0.93
OBC -0.5	Edsell(2.0%)	13.78	1171	13.69	967	0.83	7.85	1353	8.10	1164	0.86
OBC		10.61	1252	10.70	1100	0.88	7.30	1373	8.13	1254	0.91
OBC +0.5		11.80	1091	11.74	1034	0.95	6.73	1378	6.77	1286	0.93
OBC -0.5	Banhart	12.81	756	9.38	620	0.43	8.18	1632	8.00	974	0.47
OBC		10.83	967	11.44	521	0.54	9.61	1077	9.77	576	0.54
OBC +0.5		9.28	1132	12.79	714	0.55	8.08	1325	8.08	749	0.56
OBC -0.5	Banhart(1.5%)	13.02	863	12.79	714	0.83	8.80	1612	8.70	1387	0.86
OBC		11.27	856	11.33	847	0.99	7.03	1534	6.98	1546	1.01
OBC +0.5		10.90	1070	10.88	969	0.91	7.73	1387	7.80	1298	0.94
OBC -0.5	Banhart(2.0%)	12.50	756	12.71	597	0.79	6.99	1697	6.92	1656	0.98
OBC		10.31	864	10.03	898	1.04	9.40	1084	9.43	1130	1.04
OBC +0.5		9.71	902	9.44	838	0.93	8.01	1096	7.92	1020	0.93

[a]TS = Tensile Strength.

[b]1 psi = 6.89 kPa (kilo Pascals).

[c]TSR = Tensile Strength Ratio.

TABLE 3 Results of Analysis of Variance for Different Aggregates With and Without Lime

Source of Variation	Degree of Freedom	Sum Squares	Mean Squares	F Ratio	Probability
All Aggregates (without Lime)					
A	3	1043066	347689	57.44	< 0.0001
AC	2	1215864	607932	100.44	< 0.0001
C	1	1691880	1691880	279.52	< 0.0001
A*AC	6	831473	138579	22.89	< 0.0001
A*C	3	153684	51228	8.46	0.0010
AC*C	2	16155	8078	1.33	0.2729
A*AC*C	6	39832	6639	1.09	0.3780
Error	48	290530	6053		
Edsell Aggregate (with and without Lime)					
LC	2	2213824	1106912	117.03	< 0.0001
AC	2	756967	378483	40.02	< 0.0001
C	1	549643	549643	58.11	< 0.0001
LC*AC	4	221772	55443	5.86	0.0010
LC*C	2	48460	24230	2.56	0.0912
AC*C	2	3597	1798	0.19	0.8277
LC*AC*C	4	100067	25017	2.64	0.0493
Error	36	340495	9458		
Banhart Aggregate (with and without Lime)					
LC	2	250571	125286	20.49	< 0.0001
AC	2	591025	295513	48.34	< 0.0001
C	1	562428	562428	91.99	< 0.0001
LC*AC	4	84148	21037	3.44	0.0176
LC*C	2	454457	227229	37.17	< 0.0001
AC*C	2	28716	14358	2.35	0.1100
LC*AC*C	4	20142	5036	0.82	0.5188
Error	36	220093	6114		

A = Aggregate Source (Kidder Creek, Clear Creek, Edsell and Banhart)
LC = Lime content (0%, 1.5%, 2.0%)
AC = Asphalt content (OBC -0.5, OBC, OBC +0.5)
C = Condition (unconditioned and conditioned)
The level of significance is indicated by the probability of greater F.
Probabilities less than 0.05 are considered significant.

and 0.55 for Kidder Creek, Clear Creek, Edsell, and Banhart, respectively. These results show that the TSRs for Kidder Creek and Banhart did not change significantly, and TSRs increased for both Clear Creek and Edsell. This indicates that increasing asphalt content may result in increasing resistance to potential damage only in some aggregates.

Effect of Hydrated Lime on Tensile Strength and TSR

Lime treatment affected the strength values and tensile strength ratio (Table 2, Figures 1 and 2). Generally, the addition of lime increased the strength and TSR. The strength improvement in conditioned specimens caused by the addition of lime is shown in Table 6. The strength improvement was computed according to the following formula:

$$SI = [(\sigma\tau_{CL} - \sigma\tau_{CNL})/\sigma\tau_{CNL}] \times 100\%$$

where

SI = strength improvement (%),
$\sigma\tau_{CL}$ = tensile strength of conditioned lime treated specimens, and
$\sigma\tau_{CNL}$ = tensile strength of conditioned specimens without lime treatment.

The SI parameter gives a measure of the effect of lime treatment on the strength of conditioned specimens. Table 6 shows that there were strength improvements due to the addition of lime at both the 1.5 percent and 2.0 percent lime contents. For Edsell, the improvements were especially high at OBC −0.5, at which they were 171 percent and 243 percent for the 1.5 percent and 2.0 percent lime contents, respectively. At OBC the improvements were 116 percent and 142 percent for the 1.5 percent and 2.0 percent lime contents, respectively. For Banhart, the improvements were also high at OBC −0.5 where they were 120 percent and 84 percent for the 1.5 per-

TABLE 4 AASHTO T283 Results for *t*-Test Groupings at 95 percent Relative Compaction

Asphalt	Specimen	Kidder Creek		Clear Creek		Edsell		Edsell(1.5%)[c]		Edsell(2.0%)		Banhart		Banhart(1.5%)		Banhart(2.0%)	
Content	Condition	Mean[a]	T-grp[b]	Mean	T-grp	Mean	T-grp	Mean	T-grp	Mean	T-grp	Mean	T-grp	Mean	T-grp	Mean	T-grp
Comparision between Specimen conditions																	
OBC -0.5	Uncond.	783	A	969	A	540	A	1020	A	1018	A	756	A	864	A	756	A
	Cond.	526	B	648	B	283	A	765	B	857	A	324	B	714	A	597	B
OBC	Uncond.	1341	A	944	A	834	A	1036	A	1251	A	967	A	857	A	864	A
	Cond.	1084	A	678	B	455	B	981	A	1100	A	521	B	847	A	898	A
OBC +0.5	Uncond.	926	A	1180	A	891	A	1387	A	1091	A	1132	A	1070	A	903	A
	Cond.	770	A	955	B	721	A	1057	B	1034	B	620	B	969	B	838	A
Comparision between different asphalt contents																	
OBC -0.5	Uncond.	783	A	969	A	540	A	1020	A	1018	A	756	A	864	A	756	A
OBC	Uncond.	1341	B	944	A	834	B	1036	A	1251	A	967	B	857	A	864	B
OBC +0.5	Uncond.	926	C	1180	B	891	B	1387	B	1091	A	1132	B	1070	BA	903	AB
OBC -0.5	Cond.	526	A	648	A	283	A	765	A	857	A	324	A	714	A	597	A
OBC	Cond.	1084	B	678	A	455	B	981	B	1100	B	521	B	847	A	898	B
OBC +0.5	Cond.	770	C	955	B	721	C	1057	B	1034	B	620	B	969	B	838	B

[a]Values are in kilopascals (1 psi = 6.89 kPa)

[b]Groups having different designations indicate significant differences.

[c]Percentage in parentheses indicates the lime content.

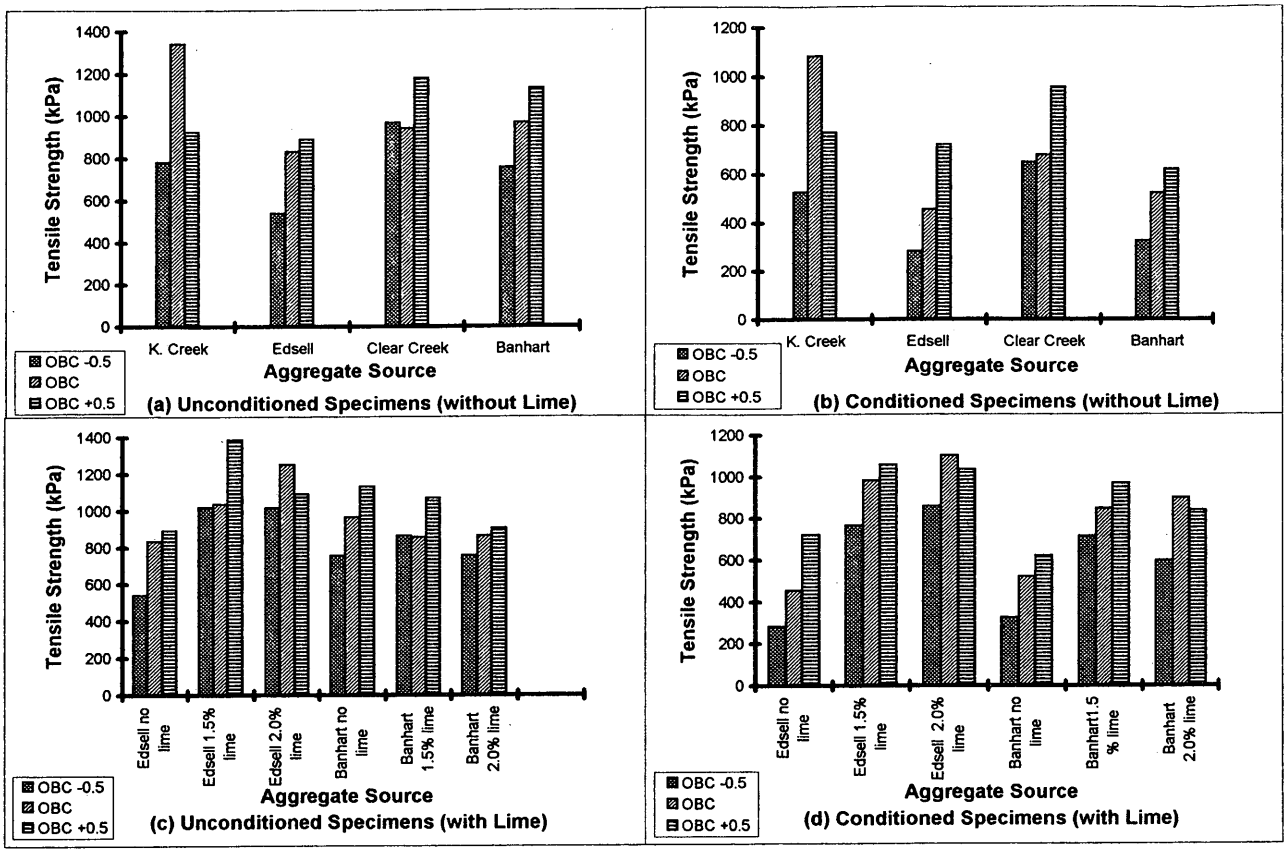

FIGURE 1 Tensile strength as a function of aggregate source and binder content.

cent and 2.0 percent lime contents, respectively. At OBC the improvements were 63 percent and 72 percent for lime contents of 1.5 percent and 2.0 percent, respectively. At OBC +0.5 there were improvements for both Banhart and Edsell but they were not as great as they were at the other asphalt contents. This shows that lime is most effective in increasing strength, especially at the lower asphalt contents where the potential for moisture sensitivity is higher.

Table 5 shows the results of the *t*-test comparing strength values at different lime contents. The table compares the strength values for Edsell and Banhart before and after lime treatment. These results show that there are significant differences between the strengths before and after lime treatment for both levels of lime content. However, there are no significant differences between strength values at 1.5 percent lime content and 2.0 percent lime content, even though the SIs for the 2.0 percent lime content were generally higher than those for the 1.5 percent lime content.

Edsell exhibited lower strength values than Banhart at OBC −0.5 and OBC, but higher strength at OBC +0.5 for the conditioned specimens. After lime treatment, Edsell exhibited higher strength values at all asphalt contents.

Table 6 shows the effect of lime treatment on the TSR values in terms of tensile strength ratio improvements (TSRIs), which were computed according to the following formula:

$$TSRI = [(TSR_{AL} - TSR_{BL})/TSR_{BL}] \times 100\%$$

where

$TSRI$ = tensile strength ratio improvement (%),
TSR_{BL} = tensile strength ratio before lime treatment, and
TSR_{AL} = tensile strength ratio after lime treatment.

Both Edsell and Banhart showed improvements. Banhart showed higher TSRI than Edsell. The TSRIs at OBC −0.5 and OBC were 44 percent and 73 percent for Edsell, and 98 percent and 83 percent for Banhart at 1.5 percent lime content, respectively. At these asphalt contents the addition of lime caused improvements in TSR. Similar patterns, with higher TSRIs, are exhibited for the 2.0 percent lime content. At OBC +0.5 the improvements were not consistent. At this asphalt content, the TSRIs for Edsell were −6 percent (no improvement) and 17 percent for the 1.5 percent and 2.0 percent lime contents, respectively, and the TSRI for the Banhart were 65 percent and 69 percent for the 1.5 percent and 2.0 percent lime contents, respectively. This supports the previous conclusion that lime treatment was most effective at lower asphalt contents.

This analysis makes it clear that treating aggregates with lime before mixing with asphalt increases the strength and the TSR. Also, because the SI and TSRI parameters give a measure of the effect of treatments such as lime, they should be used along with the TSR in moisture-sensitivity evaluation.

Effect of Air Voids on Tensile Strength and TSR

The analysis presented above was conducted at 95 percent relative compaction, at which level each mixture had a unique OBC with a

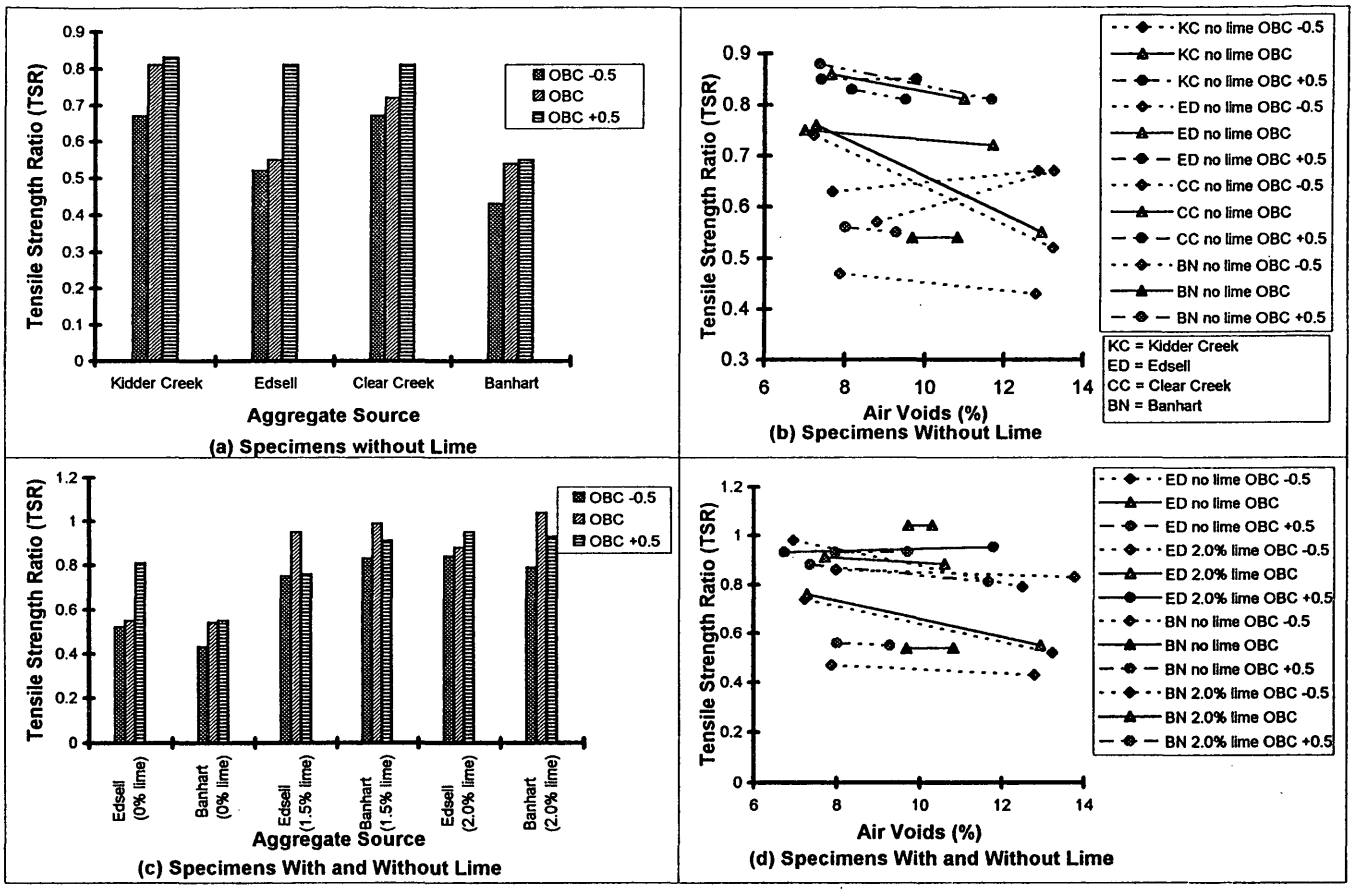

FIGURE 2 TSR as a function of aggregate source, lime content, binder content, and air voids.

unique air-void level. The variations from the OBCs also produced different levels of air voids. Therefore, the evaluated data showed a combined effect of air voids and asphalt content. These variations reflect what happens in practice in California. Other tests were conducted at different air-void levels (Table 2). Figures 2 and 3 show the effect of air voids on TSR and tensile strength. The figures show that air voids have a significant effect on tensile strength. As air voids increase, tensile strength decreases significantly. There were some decreases in the TSRs corresponding to the increases in air voids.

Effect of Using Asphalt-Rubber Binder on Tensile Strength and TSR

Table 7 contains a summary of AASHTO T283 results for the asphalt-rubber mixtures along with the conventional dense-graded asphalt-concrete (DGAC) mixtures at 95 percent relative compaction. These mixtures were compared at their OBCs. The table shows that tensile strength values for the ARHM-DG were almost equal to the DGAC mixture for Kidder Creek, and higher than the DGAC for Banhart. The strength values for ARHM-GG were significantly lower than those for DGAC and ARHM-DG mixtures. The table also shows low TSR values for the asphalt-rubber mixtures even for the non–moisture-sensitive Kidder Creek aggregate. These results indicate that there could be moisture-damage problems associated with the asphalt-rubber mixtures. However, other types of tests should be conducted to verify these findings. Tests that need to be considered include the simple shear and controlled-strain fatigue beam test (SHRP A-003A). These tests, along with field experience, will show the applicability of the AASHTO T283 test in the evaluation of the moisture sensitivity of asphalt-rubber mixes.

Evaluation of the Controlled-Strain Fatigue Beam Test

Table 8 shows the normalized results of the controlled-strain flexural beam test for different strain levels. The table shows that for the specimens that were not treated with lime, conditioning reduced both flexural stiffness and fatigue life and generally increased the phase angle. On the other hand, the lime-treated specimens showed no significant reductions in stiffness, had remarkable increases in fatigue life and exhibited reductions in phase angle as a result of conditioning. These changes indicate that when lime was present, a reaction occurred during conditioning that resulted in strengthening the binder-aggregate bond. Therefore, conditioning of the lime-treated specimens resulted in a stronger bond, instead of the weaker bond experienced with the untreated specimens. More research is needed to confirm this finding.

Table 9 shows the effect of lime on the FSR and the FLR. The table shows that for Banhart, the average FSR increased from 0.61 to 0.97 and the average FLR increased from 0.49 to 3.06 as a result

TABLE 5 Tensile Strength Data: *t*-Test Groupings Showing the Effect of Aggregate Source and Lime Content for Specific Binder Contents

Aggregate	Mean(kPa)[a]	T-Grouping[b]	Mean(kPa)	T-Grouping	Mean(kPa)	T-Grouping
	OBC -0.5		OBC		OBC +0.5	
Unconditioned Specimens without Lime						
Kidder Creek	783	A	1341	A	926	A
Edsell	540	B	834	B	891	A
Clear Creek	969	C	944	CB	1180	AB
Banhart	756	D	967	DB	1132	AB
Conditioned Specimens without Lime						
Kidder Creek	526	A	1084	A	770	A
Edsell	283	B	455	B	721	AB
Clear Creek	648	A	678	C	955	AC
Banhart	324	B	521	DB	620	ABC
Edsell Specimens with and without Lime (Unconditioned)						
Edsell no lime	540	A	834	A	891	A
Edsell 1.5% lime	1020	B	1036	B	1387	B
Edsell 2.0% lime	1018	B	1251	AB	1091	C
Edsell Specimens with and without Lime (Conditioned)						
Edsell no lime	283	A	455	A	721	A
Edsell 1.5% lime	765	B	981	B	1057	B
Edsell 2.0% lime	967	B	1100	B	1034	B
Banhart Specimens with and without Lime (Unconditioned)						
Banhart no lime	756	A	967	A	1132	A
Banhart 1.5% lime	864	B	857	A	1070	A
Banhart 2.0% lime	756	AB	864	BA	903	A
Banhart Specimens with and without Lime (Conditioned)						
Banhart no lime	324	A	521	A	620	A
Banhart 1.5% lime	714	B	847	B	969	B
Banhart 2.0% lime	597	B	898	B	838	B

[a]1 psi = 6.89 kPa

[b]Groups having different designations indicate significant differences.

TABLE 6 Tensile Strength and TSR Improvement due to the Addition of Lime for Conditioned Specimens

Asphalt Content	SI(%)	TSRI(%)	SI(%)	TSRI(%)
	Edsell with 1.5% Lime		**Edsell with 2.0% Lime**	
OBC -0.5	171	44	243	62
OBC	116	73	142	60
OBC +0.5	46	-6	43	17
	Banhart with 1.5% Lime		**Banhart with 2.0% Lime**	
OBC -0.5	120	98	84	84
OBC	63	83	72	93
OBC +0.5	56	65	35	69

of lime treatment. The table also shows that the FSRs and TSRs had similar trends in terms of their ranking of the various mixes. The strongest trends are associated with the 200-microstrain results. The FLRs were significantly lower than the FSRs and TSRs except for the lime-treated specimens. The average FLRs can be considered shift factors for the purposes of pavement modeling. The measurement of flexural stiffness before and after conditioning can be used in pavement analysis.

The strain-fatigue life relations were plotted in Figure 4 for two strain levels (200 and 300 microstrains). The figure indicates that moisture conditioning decreases fatigue life (except for the lime treated specimens) and that the mixtures at OBC −0.5 were more moisture sensitive than those at OBC.

Although the data were limited, the results indicate that the controlled-strain fatigue beam test has a potential use in moisture-sensitivity evaluation of binder-aggregate mixtures. This test mea-

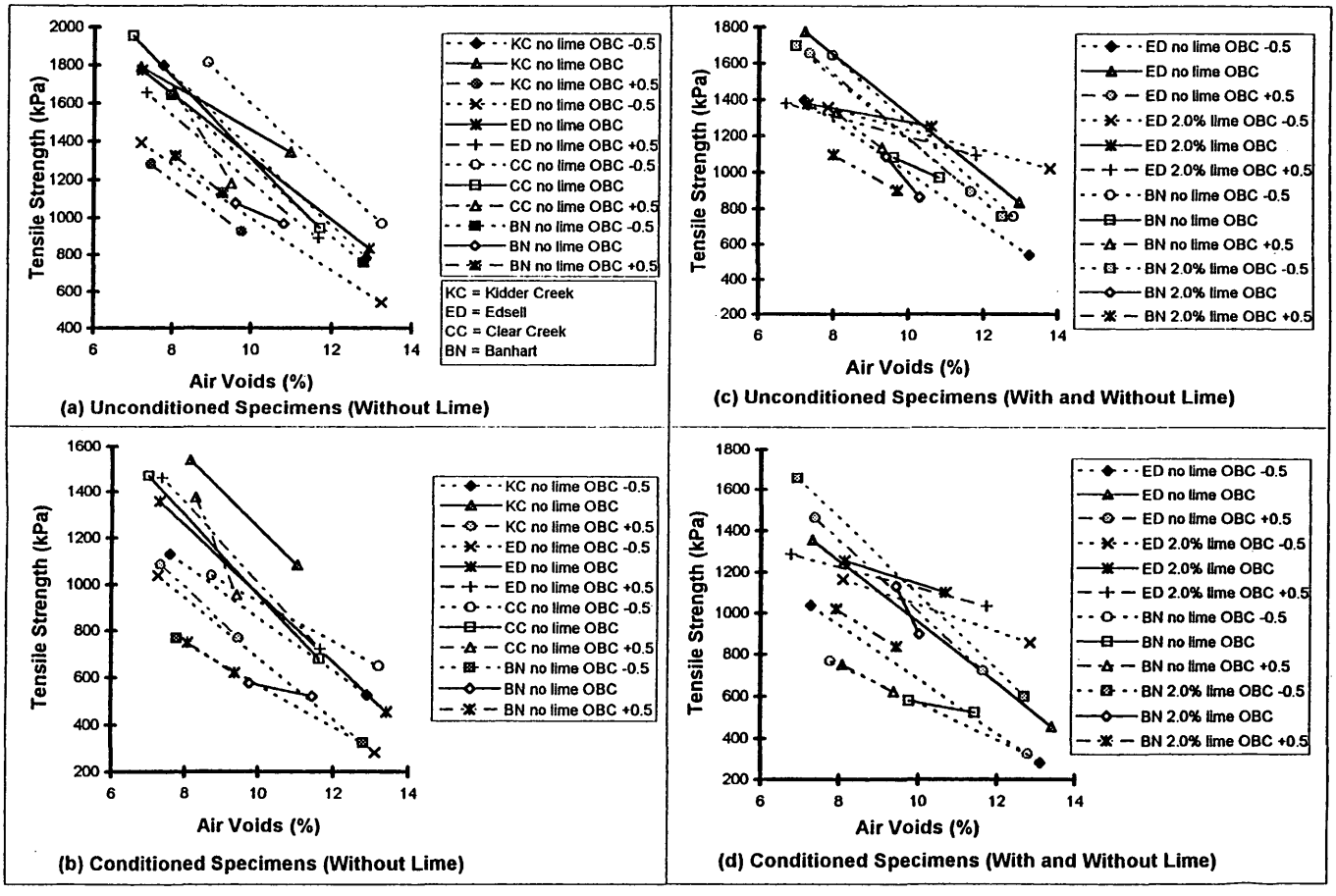

FIGURE 3 Tensile strength as a function of air voids for various aggregates.

TABLE 7 Summary of AASHTO T283 Moisture Damage Test Results for Asphalt-Rubber Mixes

Aggregate Source		Unconditioned Air Voids (%)	Unconditioned TS[a] kPa[b]	Conditioned Air Voids (%)	Conditioned TS kPa	Average TSR[c]
Kidder Creek						
DGAC		10.75	1536	10.72	1137	
		10.79	1323	10.79	1116	
		11.42	1164	11.57	999	0.81
	Mean	**10.99**	**1341**	**11.03**	**1084**	
	Std. Dev.	**0.38**	**187**	**0.47**	**74**	
ARHM DG		7.90	1392	6.74	668	
		6.60	1385	5.80	978	
		5.70	1268	5.70	785	0.60
	Mean	**6.73**	**1348**	**6.08**	**811**	
	Std. Dev.	**1.11**	**70**	**0.57**	**157**	
ARHM GG		6.30	1054	6.40	448	
		6.19	958	6.28	717	
		6.84	965	6.39	971	0.72
	Mean	**6.44**	**992**	**6.36**	**712**	
	Std. Dev.	**0.35**	**54**	**0.07**	**262**	
Banhart						
DGAC		10.99	978	10.88	593	
		11.17	965	11.95	427	
		10.33	958	11.50	544	0.54
	Mean	**10.83**	**967**	**11.44**	**521**	
	Std. Dev.	**0.44**	**11**	**0.54**	**85**	
ARHM DG		7.30	1137	7.80	503	
		7.40	1096	6.90	758	
		7.20	1123	6.90	758	0.60
	Mean	**7.30**	**1118**	**7.20**	**673**	
	Std. Dev.	**0.10**	**21**	**0.52**	**147**	
ARHM GG		6.14	861	6.14	331	
		6.66	834	5.62	537	
		6.19	847	6.91	345	0.48
	Mean	**6.33**	**847**	**6.22**	**404**	
	Std. Dev.	**0.29**	**14**	**0.65**	**116**	

[a]TS = Tensile Strength.

[b]1 psi = 6.89 kPa (kilopascals).

[c]TSR = Tensile Strength Ratio.

sures engineering properties that can be used in pavement analysis. Also, this test is an appropriate tool for moisture-sensitivity evaluation since the tension properties that relate to the binder-aggregate bond are evaluated under cyclic loading. Further evaluation and refinement of this test for moisture-sensitivity evaluation are necessary.

CONCLUSIONS

1. The modified Lottman test (AASHTO T283) appears to differentiate non–moisture-sensitive from moisture-sensitive asphalt-concrete mixtures.

2. Hydrated lime in a slurry form can be effective in increasing the moisture-damage resistance of moisture-sensitive asphalt-concrete mixtures.

3. A reduction in the binder content from the optimum by 0.5 percent may have a detrimental effect on the moisture-damage resistance of otherwise non–moisture-sensitive mixtures, and can be detrimental for moisture-sensitive mixtures.

4. Lime treatment may decrease the moisture sensitivity of asphalt-concrete mixtures that is caused by variations from the OBC.

5. Lime treatment is most effective in increasing tensile strength below the OBC where the potential for moisture sensitivity is greater.

TABLE 8 Summary of Controlled-Strain Fatigue Beam Test Results at 95 Percent Relative Compaction

Aggregate Source	Specimen Condition	Strain (μ-strain)	N_f (Cycle)	Stiffness (kPa)[a]	Phase Angle
Kidder Creek					
OBC -0.5	Unconditioned	200	69,288	4,184,490	22.76
OBC -0.5	Conditioned	200	14,214	3,013,569	27.55
OBC -0.5	Unconditioned	300	8,538	3,193,239	27.30
OBC -0.5	Conditioned	300	3,242	2,773,590	26.66
OBC	Unconditioned	200	189,481	6,791,914	21.23
OBC	Conditioned	200	54,620	5,721,300	22.64
OBC	Unconditioned	300	23,664	6,395,711	23.60
OBC	Conditioned	300	8,292	5,307,706	24.23
Banhart					
OBC -0.5	Unconditioned	200	162,846	4,920,487	20.46
OBC -0.5	Conditioned	200	30,619	2,679,190	21.82
OBC -0.5	Unconditioned	300	16,658	4,267,432	20.46
OBC -0.5	Conditioned	300	5,103	1,142,238	22.00
OBC	Unconditioned	200	110,042	5,554,236	23.28
OBC	Conditioned	200	77,417	2,734,117	27.02
OBC	Unconditioned	300	21,845	5,610,052	22.63
OBC	Conditioned	300	6,190	4,120,390	24.18
Banhart with 1.5% Lime					
OBC	Unconditioned	200	239,443	7,013,337	20.00
OBC	Conditioned	200	721,636	7,107,916	18.54
OBC	Unconditioned	300	58,877	6,885,218	20.75
OBC	Conditioned	300	182,576	6,411,558	20.22

[a]1 psi = 6.89 kPa (kilopascals).

6. In moisture-sensitivity evaluation, tensile strength, tensile SI and TSRI caused by additives should be considered as well as TSR.
7. High air voids can result in a reduction in tensile strength and TSR.
8. The controlled-strain fatigue beam test has a potential use in moisture-sensitivity evaluation. The stiffness ratio and FLR are potential parameters.
9. Asphalt-rubber mixtures (ARHM-GG and ARHM-DG) may be more moisture-sensitive than conventional dense-graded mixtures containing the same aggregate. Other tests are needed to verify this finding.

ACKNOWLEDGMENTS

This project was funded by the California Department of Transportation in cooperation with the U.S. Department of Transportation, FHWA. The authors wish to acknowledge the assistance of

TABLE 9 Moisture-Damage Parameters: TSR, FSR, and FLR

Aggregate Source	Tensile Strength Ratio	Flexural Stiffness Ratio			Fatigue Life Ratio		
		200 μ-strain	300 μ-strain	Average	200 μ-strain	300 μ-strain	Average
Kidder Creek-OBC -0.5	0.67	0.72	0.86	0.79	0.21	0.38	0.30
Kidder Creek-OBC	0.81	0.84	0.83	0.84	0.29	0.35	0.32
Banhart-OBC -0.5	0.43	0.54	0.27	0.41	0.19	0.31	0.25
Banhart-OBC	0.54	0.49	0.73	0.61	0.70	0.28	0.49
Banhart-OBC with Lime	0.99	1.01	0.93	0.97	3.01	3.10	3.06

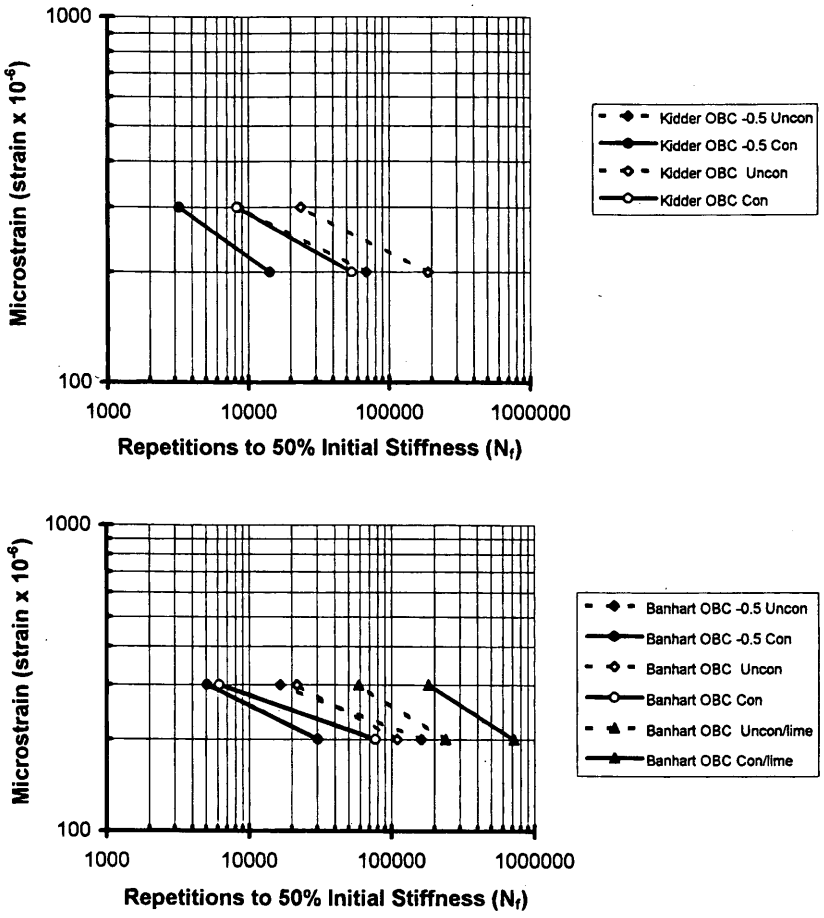

FIGURE 4 Strain-fatigue life relation at 20°C.

Jeff Rush and Regina Adams. The valuable support received from Robert Doty is greatly appreciated. Also, special thanks are due Professor Monismith, who facilitated the use of the UCB laboratory for Caltrans staff.

REFERENCES

1. Shatnawi, S R., and J. Van Kirk. Premature Asphalt Concrete Pavement Distress Caused by Moisture Induced Damage. In *Transportation Research Record 1417,* TRB, National Research Council, Washington, D.C., 1993, pp. 168–177.
2. Shatnawi, S. R. *Premature AC Pavement Distress—District 2 Investigation.* Report FHWA-CA/TL-92–07 (CALTRANS-F91TL07). California Department of Transportation, Sacramento, 1992.
3. Harvey, J., and C. L. Monismith. Effects of Laboratory Asphalt Concrete Specimen Preparation Variables on Fatigue and Permanent Deformation Results Using Strategic Highway Research Program A-003A Proposed Testing Equipment. In *Transportation Research Record 1417,* TRB, National Research Council, Washington, D.C., 1993, pp. 38–48.
4. Terrel, R. L., and S. Al-Swailmi. *Water Sensitivity of Asphalt-Aggregate Mixtures Test Development.* SHRP, National Research Council, Washington, D.C., 1992.
5. Lottman, R. P. Laboratory Test Method for Predicting Moisture Induced Damage to Asphalt Concrete. In *Transportation Research Record 843,* TRB, National Research Council, Washington, D.C., 1982, pp. 88–95.
6. Tayebali, A. A., J. A. Deacan, J. S. Coplantz, J. T. Harvey, and C. L. Monismith. Mixtures and Mode-of-Loading Effects on Fatigue Response of Asphalt-Aggregate Mixtures. *Proc., AAPT* March 1994.

Publication of this paper sponsored by Committee on Characteristics of Bituminous Paving Mixtures to Meet Structural Requirements.

Effects of Moisture on Surface Chemistry of Steel Slags and Steel Slag–Asphalt Paving Mixes

A. COOMARASAMY AND T. L. WALZAK

Random cracking and premature failure have been observed in some steel slag–asphalt pavements in Ontario. The causes of the failure were investigated. Surface chemistry and morphology of steel slags and asphalt mixes and the effect of moisture on these characteristics were studied using scanning electron microscopy, scanning electron microscopy coupled with energy-dispersive x-ray analysis, and optical microscopy. X-ray diffraction and electron microprobe analysis were used for mineralogical studies. Experiments were also performed to determine moisture uptake and volume expansivity of steel slags and steel slag–asphalt mixes. Basic oxygen furnace slags and an electric arc furnace slag were used in this investigation, and asphalt mixes were prepared from some samples. The results indicate that failure in steel slag–asphalt mixes in moist environments is due to the formation of calcium-rich deposits, mainly calcium carbonate, along the surface and the interface. This affects interfacial bonding and can cause excessive expansion of the slag leading to cracking of the mixture. This reactivity was also observed in field core samples, even after several years of service. The mineralogical data showed that the distribution and microstructure of the two main phases (an iron oxide-rich mixed oxide phase and a calcium silicate phase in steel slags) were different among the slags examined. The calcium silicate phase appears to be one of the sources responsible for the reactivity of steel slags in moist environments.

Steel slag aggregates (SSA) were first used in hot-mix asphalt (HMA) pavement in Ontario in 1969. They were used primarily as premium skid-resistant aggregates in dense friction course (DFC), open friction course (OFC), and other densely graded hot-laid asphalt pavements (*1*). Although steel slag is not used as extensively as other aggregates, there have been a number of successful applications in different highway environments. Observations of premature road surface failures, mainly in the form of random cracking, have raised concerns about the overall strategy of using steel slag–asphalt mixtures and have limited their application.

Many studies concerning use of steel slag in asphalt mixes pertained to the application of these materials and their effect on the properties and performance of the asphalt (*2,3*). Typical mix properties discussed include skid resistance, cracking behavior, and tensile characteristics. The main concern about steel slag properties is their volume expansion characteristics, primarily attributed to the amount of "free" lime (CaO) and/or magnesium oxide (MgO) present in the slag (*2,4*). In many reviews of the use of steel slag as an aggregate, its composition is given in a summary table that only outlines the expected bulk chemical composition, but the role of changes in steel slag composition and surface properties, particularly the effects of moisture on surface properties has not been addressed adequately.

Many studies of steel slag properties and composition variations originated in the steel industry (*5*). These reports provide details about specific steel-making practices and their effect on slag chemistry, but, again, surface reactivity has not been considered. A master's thesis published at McMaster University in 1981 (*6*) considered weathering reactions on aggregate surfaces and their effects on skid resistance, but unfortunately there is no detailed follow-up to this work. There appears to have been little other work on the surface chemistry of steel slags (*7*).

Some research was performed to evaluate the degree of asphalt oxidation in relation to aggregate interaction (*8*) and the effect of moisture on asphalt-aggregate mixes (*9,10*), but these studies have focused on analytical technique development or evaluation of testing methods and are not related directly to the interaction of aggregate chemistry and asphalt-aggregate interfaces.

The way in which surface chemistry changes upon exposure to environmental variables may have some effect on the interfacial adhesion properties of the steel slag. Also, the relationship between the mineralogy of steel slags and their surface reactivity has not been investigated.

The main objective of this study was to gain fundamental knowledge about the processes occurring at the steel slag surface and near-surface regions during exposure of steel slag and steel slag–asphalt mixes to various environmental variables, particularly moisture.

METHODOLOGY

Steel Slag Samples Studied

The steel slag samples examined in this study were produced by two different steel-making techniques. Samples A through E were produced in a basic oxygen furnace (BOF), whereas sample F was produced in an electric arc furnace (EAF). Three of the BOF slags (B, D, E) were typical slags from three different plants; the other two BOF slags (A, C) were experimental samples.

DFC Marshall briquettes were made from three types of BOF slags representing typical slag from two sources (B, D) and an experimental slag (A), along with a traprock reference sample, using Marshall mix design procedures. Attempts to make DFC briquettes from EAF slags were not successful because of difficulty in compacting to 3 percent air voids.

A. Coomarasamy, Ministry of Transportation, Ontario, 1201 Wilson Avenue, Downsview, Ontario, Canada M3M 1J8. T. L. Walzak, University of Western Ontario, London, Ontario, Canada N6A 5B7.

Instrumentation

Three techniques were primarily used in this study: (*a*) scanning electron microscopy coupled with energy dispersive x-ray analysis (SEM/EDX), (*b*) electron probe x-ray microanalysis (EPMA), and (*c*) x-ray diffraction (XRD). These techniques provide complementary information about material composition, morphology, and surface chemistry.

A modern SEM (Model ISI D-130) with a Noran light element EDX system capable of quantitative analysis and digital x-ray mapping available at Surface Science Western was used. The EPMA instrument used was a JEOL Superprobe 8600. A Rigaku Rotaflex Ru-200B spectrometer from the Department of Earth Sciences, University of Western Ontario (scan conditions: 2 degrees to 100 degrees (2θ) with a step size of 0.020 degrees) was used for XRD measurements.

Some Fourier transform infrared (FT-IR) measurements were also performed. These measurements were performed with a Perkin Elmer 2000 FT-IR apparatus and, in some cases, a Spectra-Tech baseline horizontal attenuated total reflectance (ATR) accessory was used. In the ATR the solid sample was pressed against a ZnSe crystal.

Sample Preparation

For all SEM analysis, the steel slag samples were mounted on sample holders using carbon paint and then coated with a thin layer of sputter-deposited gold to minimize charging effects.

For the microprobe analysis, samples of each steel slag under study were mounted in a cold mount epoxy resin (Struers Epo-Fix) and polished using standard metallographic methods to a 3-μm diamond finish. After polishing, the cross sections were coated with a thin layer of evaporated carbon and then examined using the electron microprobe.

For the XRD analysis, the slag samples were crushed (jaw crusher), placed in a ball mill, and ground by mortar and pestle to ~ 10-μm particle size. The samples were then mounted on a glass slide and placed in the diffractometer.

Bulk chemical composition of steel slag samples was determined by wet chemical analysis using a partial digestion procedure with finely ground samples. Free lime content was estimated by an ethylene glycol–methanol extraction and titration procedure. Physical properties relevant to use of steel slag as aggregate were also determined.

Moisture Uptake and Expansion Tests

Tests for percentage mass increase of steel slag caused by moisture uptake under different relative humidities were conducted in the laboratory using saturated salt solutions in desiccators maintained at ambient temperature.

A steel slag expansion test was performed according to ASTM D-4792–88. In this procedure steel slag specimens were prepared using the standard Proctor method and stainless steel molds with perforated base plates to allow for moisture movement during the immersion period. The specimens were then immersed in the water bath and maintained at 71°C ± 2°C, and the vertical expansion with time was recorded daily for 2 weeks.

Steel slag–asphalt briquettes with 8 to 10 percent air voids were also prepared to conduct HMA expansion tests (*11*).

Weathering Experiments

Two accelerated weathering experiments were performed: the first set involved only slag particles exposed to 90 to 100 percent RH at 30°C; the second set involved both asphalt Marshall briquettes and slag particles exposed to 100 percent RH at 50°C. In each experiment, each slag sample or briquette was placed in an open beaker, and the beaker was placed in the humidity chamber. In the humidity chamber the samples were observed to be continuously wet with a thin film of water but were never completely immersed.

RESULTS

Steel Slag Surface Characterization

Results of surface characterization by EDX are summarized in Table 1. The results show surprising consistency in the surface composition of the different steel slags. The sampling depth for EDX analysis is 1 to 2 μm under these conditions, so the term "surface" actually refers to the average composition to this depth below the surface. In all cases, surfaces were enriched in calcium and oxygen with varying levels of silicon, iron, aluminum, magnesium, and manganese. In most cases, surface carbon levels were below 10 wt percent. On average, surface calcium levels decreased and oxygen levels increased after washing.

Figure 1 shows a series of SEM micrographs of the surface of as-received steel Slag D (*a,b*) and the same slag after washing (*c,d*). Washing appears to have removed larger crystals from the surface, giving a more uniform topography. These changes in surface chemistry and surface morphology after washing indicate that washing effectively removed loosely attached material resulting in lower surface calcium levels. However, there is evidence of additional surface reactions, as shown by development of a network of finer crystals on the washed slag surfaces (Figure 1*d*). As with the EDX results, these changes in surface morphology were found to be consistent among the slags investigated.

Cross-Section Characterization by EPMA

Results of microprobe analysis on the slag samples are summarized in Table 2, a and c. Also, representative backscattered electron images were collected of both the bulk (i.e., slag particle interior) and the interface region; these are shown in Figure 2.

As shown in Figure 2(*a*) and (*b*), the slag was not uniform in cross section. In this case, the cross section is from steel Slag D, but with the exception of the EAF slag sample [Figure 2(*c*) and (*d*)], the observations were consistent among all slag samples examined. The backscattered images indicate at least three distinct phases in the slag: a light-colored phase [1 in Figure 2(*a*)], a dark-colored phase (*2*), and a medium-colored phase (*3*). All the slags appear to have phases 1 and 2, but only slag D exhibited phase 3. In addition to the various phases present in the bulk of the slag particles, it is clear from Figure 2(*b*) that the interface region of the slag is different again.

The results shown in Table 2(*a*) for slag D demonstrate that the light-colored phase is an iron oxide–rich phase of mixed oxides of magnesium, manganese, and calcium. In contrast, the dark phase was a calcium oxide–rich phase also high in silicon oxide, probably a form of calcium silicate. The medium phase (3) was consistent

TABLE 1 Composition of Steel Slag Surfaces by EDX Analysis

Sample	Treatment	Element (wt%)							
		Ca	Fe	Al	Si	Mg	Mn	C	O
A	MTO Washed	44.0	16.0	0.9	5.4	2.2	3.3	1.8	27.0
B	MTO Washed	32.0	4.4	1.7	6.3	2.2	1.2	5.9	47.0
C	MTO Washed	40.0	3.5	0.4	1.5	1.3	2.2	11.0	40.0
D	MTO Washed	35.0	4.9	0.6	5.0	2.5	2.0	8.2	42.0
	As Received	42.0	3.1	0.3	5.7	1.7	2.4	8.0	37.0
F	As Received	46.0	2.7	2.7	10.0	2.9	1.4	0.0	35.0

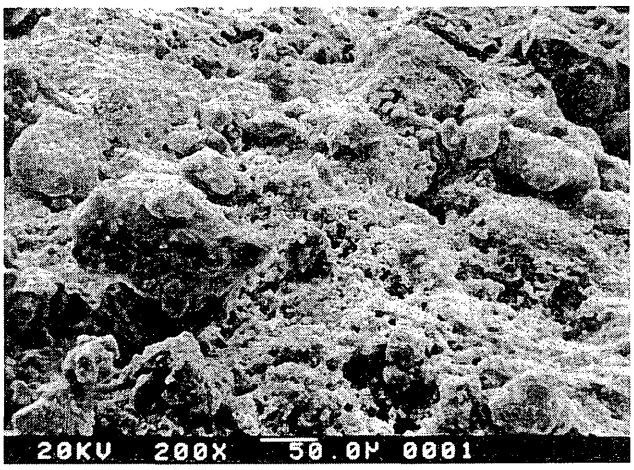

(*a*)

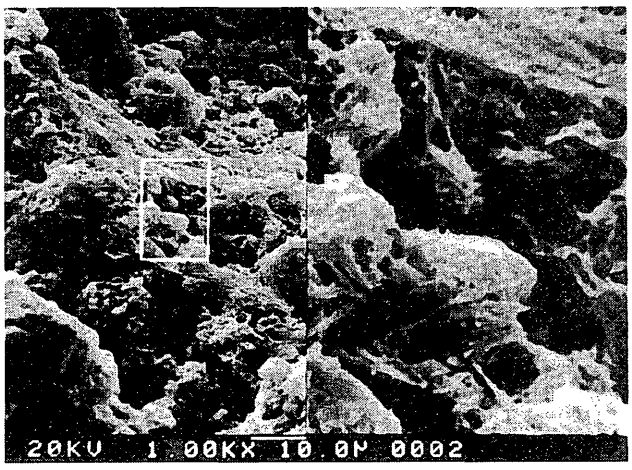

(*b*)

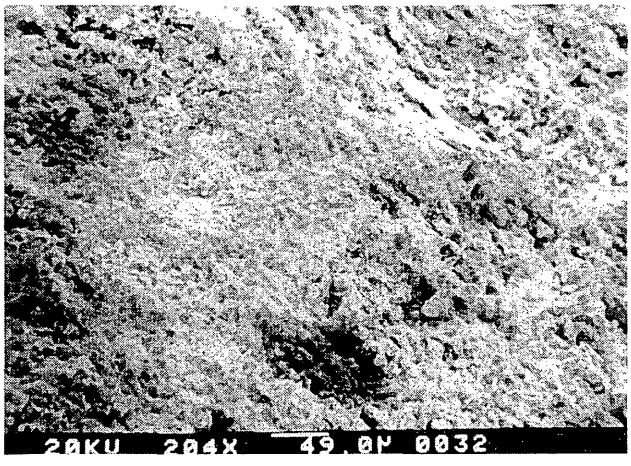

(*c*)

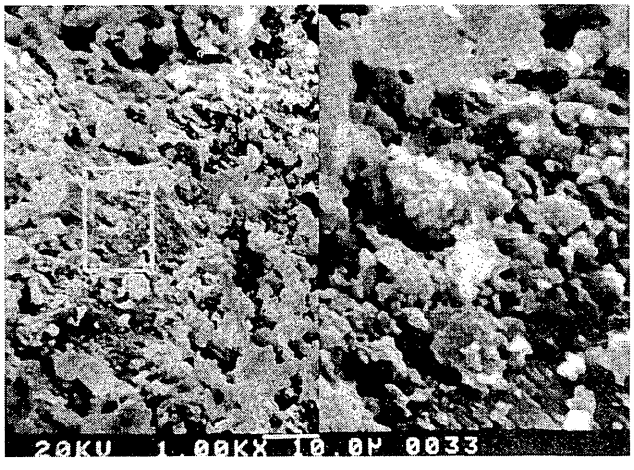

(*d*)

FIGURE 1 SEM micrographs of Slag D: (*a*) as received under low magnification; (*b*) as received under high magnification; (*c*) washed, under low magnification; (*d*) washed, under high magnification.

TABLE 2 Analysis of Steel Slag Cross Sections by Electron Microprobe

(a) *Slag D*	Constituent (wt%)						
Region/Phase	SiO_2	Al_2O_3	FeO	MgO	CaO	MnO	Other
Light #1	–	–	66.0	7.3	14.0	11.0	
Light #2	0.8	–	58.0	19.0	8.6	13.0	
Light #3	–	–	48.0	32.0	5.2	15.0	
Medium #1	2.2	2.8	45.0	0.6	45.0	1.1	TiO_2 3.0
Dark #1	32	0.3	4.6	0.7	61.0	1.6	
Dark #2	25	0.2	5.5	0.9	66.0	1.7	
Dark #3	27	0.2	4.2	1.0	67.0	1.4	
Edge #1	12.0	–	8.6	3.6	65.0	10.0	
Edge #2	32.0	0.2	4.2	0.8	60.0	2.3	
Edge #3	36.0	0.8	11.0	1.3	44.0	6.0	Cl 0.9
Edge #4	22.0	23.0	4.4	4.7	43.0	1.4	Cl 0.7
Edge #5	0.5	–	26.0	53.0	2.0	18.0	

(b) *Slag E*	Constituent (wt%)						
Region/Phase	SiO_2	Al_2O_3	FeO	MgO	CaO	MnO	Other
Light #1	1.1	3.5	44.0	0.8	44.0	3.1	TiO_2 3.1
Light #2	3.2	8.1	36.0	0.8	46.0	2.3	TiO_2 3.8
Dark #1	32.0	0.3	2.1	0.3	63.0	0.5	TiO_2 0.3
Dark #2	33.0	0.4	1.8	0.3	64.0	0.5	
Dark #3	34.0	0.2	1.2	0.5	63.0	0.5	
Edge #1	3.4	0.4	0.5	0.8	94.0	0.4	Cl 0.3
Edge #2	24.0	4.1	4.1	13.4	52.0	0.8	Cl 1.7
Edge #3	15.0	1.8	9.1	8.0	62.0	2.7	Cl 1.7
Edge #4	15.0	15.0	2.2	3.9	63.0	0.2	Cl 0.2

(c) *Slag F*	Constituent (wt%)						
Region/Phase	SiO_2	Al_2O_3	FeO	MgO	CaO	MnO	Other
Light #1	–	–	28.0	37.0	7.0	28.0	
Light #2	–	–	24.0	40.0	8.1	28.0	
Light #3	–	–	29.0	41.0	4.1	26.0	
Dark #1	38.0	0.6	0.2	3.2	58.0	–	
Dark #2	33.0	0.4	0.3	4.1	62.0	–	
Dark #3	30.0	0.4	0.2	4.5	65.0	–	

with a calcium oxide, possibly a calcium ferrite phase such as $Ca_2Fe_2O_5$ or $CaFeO_2$, which is also a constituent in the light-colored mixed oxide phase. The detailed composition, distribution, and microstructure of the primary phase was found to be different among the slags, probably a function of the type of processing to which the slag was subjected (cooling rate probably being the dominant processing difference). In some regions of the slag bulk interiors, particularly in and near internal pores, there were regions of 90 to 100 percent calcium oxide, perhaps representing a small amount of free lime in the slag. However, these regions were normally less than 1 to 2 percent of the total slag volume and were not consistently found among the slag samples.

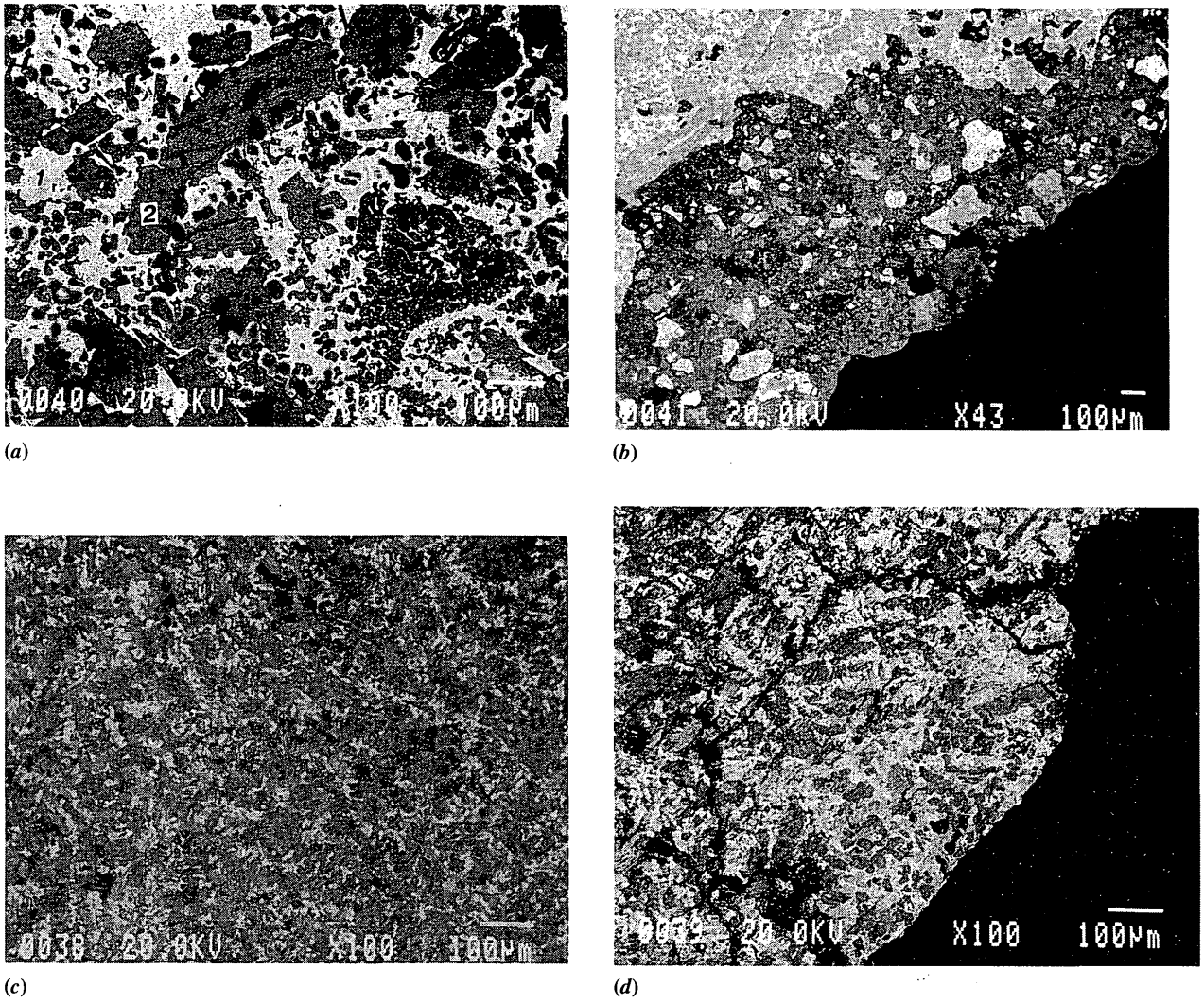

(*a*) (*b*)

(*c*) (*d*)

FIGURE 2 Backscattered electron images of steel slags: (*a*) Slag D interior, (*b*) Slag D interface, (*c*) Slag F interior, (*d*) Slag F interface.

Table 2(*a*) also shows that the interface regions (edge areas) were very different in composition. These regions exhibited more variation in composition than the two "bulk" phases but were primarily calcium-rich. As seen in Figure 2(*b*), these interface regions were quite thick, extending more than 100 μm into the interior of the slag particle. However, these regions were not uniformly distributed around the perimeter of the slag particles; for most samples, this type of nonhomogeneous outer layer made up between 20 and 80 percent of the total perimeter of the particle. This means that the surface reactivity of the slag will be controlled in part by the phases present in this layer. Some of the data, in particular the results from Slag E, Table 2(*b*), also indicated detection of chlorine in the outer interface region, further suggesting that this layer is reactive and sensitive to environmental conditions.

Slag F was the only slag sample that did not exhibit this nonuniform layer at the outer surface, [Figure 2(*c,d*)]. It is unclear why this slag should exhibit surface features different from the other samples examined, although it was the only EAF slag in this study. The microprobe data on this slag [Table 2(*c*)] also indicated that the light-colored phase (the mixed oxide phase) was lower in iron oxide and higher in MgO component compared with the BOF slags.

Chemical Composition of Steel Slags

Results of the chemical analysis and free lime content of the slags are given in Table 3(*a*); the physical properties for the aggregates are given in Table 3(*b*). Results indicate that all the BOF slags have very similar chemical composition. EAF Slag F has a lower iron oxide content and free lime content compared with the other slags.

Moisture Uptake and Expansion Test Results

Moisture Uptake

The percentage mass increases for the different steel slag fine aggregates under different relative humidities are given in Figure 3, which

TABLE 3 Steel Slag Properties: (a) Chemical and (b) Physical

(a) Component %wt.	Slag Type				
	A	B	C	D	F
% Insoluble	11.9	13.7	12.9	10.5	14.2
Fe_2O_3	26.4	23.2	19.6	28.9	18.5
Al_2O_3	7.85	11.4	8.0	4.5	15.8
CaO	45.3	44.5	44.5	41.5	45.3
MgO	9.95	6.9	10.5	11.2	3.6
Heat Loss	-1.5	-0.03	1.1	3.1	2.2
Free Lime	4.15	3.0	3.8	4.7	1.1

(b) Properties	Slag Type			
	A	B	D	F
Polished Stone Value (PSV)	60.5	61.0	63.0	61.0
Aggregate Abrasion Value (AAV)	3.6	3.5	4.2	-
Absorption	1.195	1.438	2.535	1.9
Relative Density, Bulk	3.417	3.36	3.28	3.194
Relative Density, Apparent	3.565	3.53	3.577	3.401
Wash Pass 75 μm	2.98	3.85	4.35	6.36

indicates that rate of moisture uptake is strongly dependent on relative humidity. Higher water uptake of Slag D is probably caused by relatively less abundance of well-formed crystal phases in this slag compared with other slags, a result of cooling rate differences.

Expansion Test

Results obtained for Slags A, D, F, and trap rock samples are given in Figure 4. All the slags used in this test showed volume expansion in excess of 1 percent in 1 week, which is the maximum permissible expansion recommended for highway construction materials (aggregate and fill materials). However EAF Slag F and Slag A (an experimental BOF slag) showed lower percentage expansion compared with the other two slags. These results also show that volume expansion does not necessarily correspond to the free lime content of the samples.

The HMA expansion test conducted by immersing the briquettes in water for 24 hr at 60°C revealed that all the briquettes prepared with Slags A and D also failed because of high volume expansion, which indicates that expansivity from moisture uptake/reactivity is too large to meet proposed draft specifications.

Accelerated Weathering Experiments

Slag Particle Results

In the first set of slag particle experiments it was observed that high humidity exposures at 30°C resulted in a change in surface morphology. These results show that during exposure, the surface of the slag became covered in a thick crystal-like deposit. As shown in Table 4, this change in surface morphology was accompanied by an increase in calcium levels of the surface compared with initial surface composition, given in Table 1. These calcium-rich crystals were easily removed from the surface and easily fractured. Such "weathering" products would obviously be undesirable as an interface layer for wetting with asphalt because of their fragility. These surface deposits were first observed after 10 days at 30°C. As shown in Table 4, longer exposures did not seem to change the composition of the surface deposits. This surface deposition was observed for all slags examined. The EDX spectrum obtained after aging is consistent with the presence of a calcium carbonate–type compound.

The changes in surface morphology of the slag particles after exposures to 100 percent RH at 50°C were very similar to the results obtained at 30°C. The main difference, as expected, was the rate at which surface deposits formed. As shown in Table 4, these deposits were higher in calcium. This is probably because the 50°C deposits were more uniform and thicker than the 30°C deposits, resulting in more signal from the surface layer in the former case and more signal from the underlying substrate in the latter case.

Steel Slag Marshall Briquette Results

The slag/asphalt interface before exposure was characterized by uniform coverage of aggregates with asphalt with no sign of deposits and all internal voids free of debris. After exposure periods

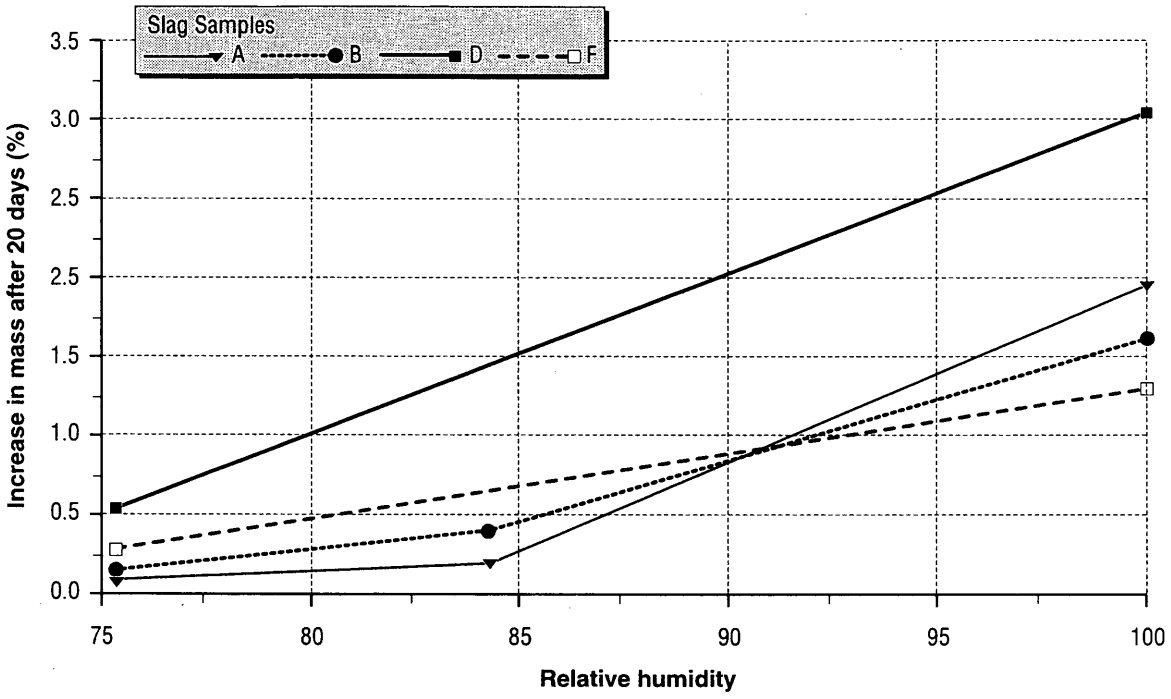

FIGURE 3 Moisture uptake of steel slags at different relative humidities.

of only 10 days at 50°C there were signs of deposits on all the exposed slag faces. These deposits were uniformly distributed across the slag surfaces and, as determined by the EDX analysis, were also calcium-rich. All the slag briquette samples examined exhibited this growth of calcium-rich material on the exposed slag surfaces. At longer exposure times, it was observed that internal voids and cracks were also becoming filled with this white crystalline deposit. It seems the calcium-rich crystals were able to form wherever a moisture film was present. This concurs with the assumption that the thin film of moisture in contact with exposed slag faces would become saturated with dissolution products from the slag. These dissolution products would then be free to move in the water phase to other locations; hence deposition would also occur within these cracks and pores.

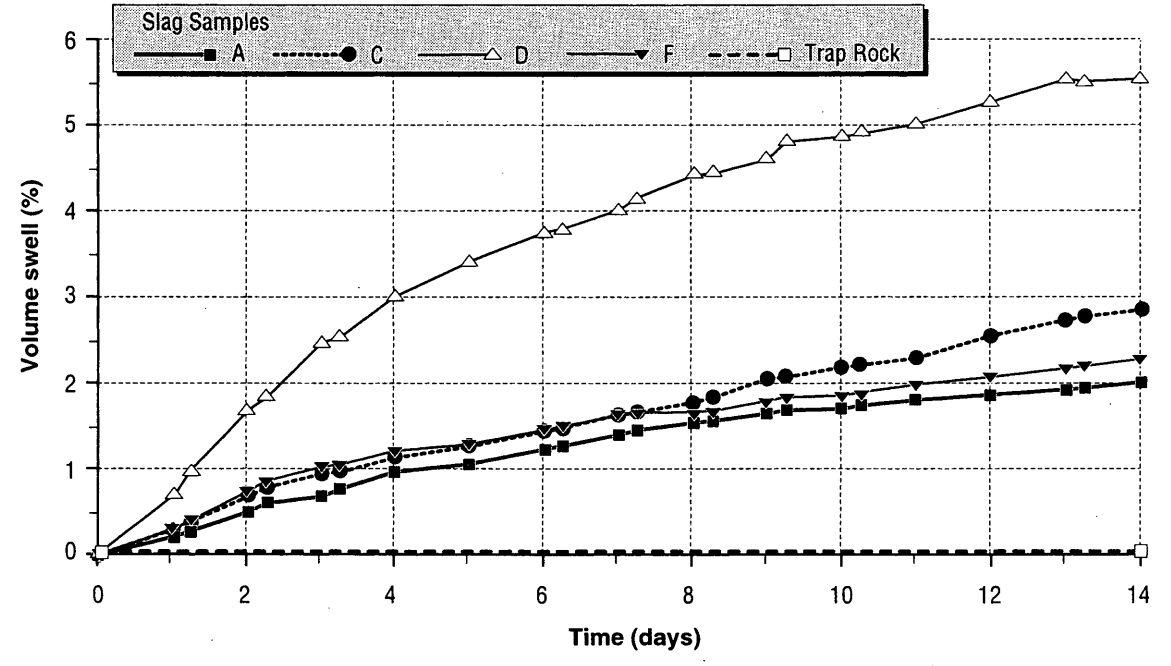

FIGURE 4 Steel slag aggregate expansion test results.

TABLE 4 Composition of Steel Slag Surfaces After Aging at 100 Percent RH as determined by EDX Analysis

Slag	Time Aged	Temp.	Element (wt%)							
	(d)	(°C)	Ca	Fe	Al	Si	Mg	Mn	C	O
A	10	30	48.0	0.0	0.0	0.6	0.0	0.0	10.0	41.0
	45	30	53.0	0.0	0.0	0.0	0.0	0.0	9.1	38.0
	10	50	67.0	0.0	0.0	0.8	0.0	0.0	11.0	21.0
B	10	30	45.0	0.0	0.0	0.0	0.0	0.0	7.9	47.0
	45	30	51.0	0.0	0.0	0.0	0.0	0.0	8.9	40.0
	10	50	75.0	0.0	0.0	0.0	0.0	0.0	4.3	21.0
C - Area 1	10	30	52.0	0.0	0.0	0.0	0.0	0.0	11.0	37.0
	45	30	55.0	0.0	0.0	1.0	0.0	0.0	10.0	34.0
	10	50	72.0	0.0	0.0	0.0	0.0	0.0	3.8	23.0
C - Area 2	10	50	34.0	0.0	0.0	0.3	0.0	0.0	19.0	48.0
D	10	30	51.0	0.0	0.0	1.0	0.0	0.0	12.0	36.0
	45	30	55.0	0.0	0.0	1.3	0.0	0.0	13.0	31.0
	10	50	71.0	0.0	0.0	1.2	0.0	0.0	8.9	19.0

These calcium-rich deposits were also observed on the top (uncut) surfaces of the briquettes wherever slag particles were present, either uncovered or only partially covered by the asphalt.

In many of the briquette samples, cracks formed after prolonged exposures (>1 month) at 50°C. The path of these cracks often progressed along the slag-asphalt interfaces, and calcium-rich deposits formed in many of the cracks. The expansion test and FT-IR results suggest that the cracks were formed because of changes in the slag volume rather than changes in the asphalt characteristics. Cracks were observed in all slag briquette samples.

The only briquette samples not exhibiting aggregate reactions (and, interestingly, no visible cracks after humidity exposures) were the briquettes made with traprock. Even after 3 months at 50°C, the aggregate-asphalt interface appeared uniform and free of defects, and all internal voids were free of deposits.

Good field core samples were characterized by slag-asphalt interfaces that appeared uniform with good adhesion and coverage, as shown in Figure 5(*a*). Also, these cross sections exhibited internal voids that were free of debris. In contrast, the cross sections of field cores that were described as having poor behavior (many cracks) exhibited slag-asphalt interfaces that had accumulated white deposits. The internal voids of these poorly behaving field cores were also filled with this white deposit (Figure 5(*b*)). EDX analysis confirmed that the deposits were very similar in composition to the surface deposits found on the briquette samples after aging.

Experiments in which cross sections of field cores were placed in the humidity chamber at 50°C also showed that both good and bad field cores exhibited some slag surface reactivity with calcium-rich deposits forming as shown in Figures 5(*c*) and (*d*). This clearly indicates that contact with moisture can still result in a reaction with the steel slag, even after it has been in service for many years, suggesting that the reactivity is probably due to the hydratable phases in steel slag, mainly the calcium silicate phase.

FT-IR Results

Samples were prepared in a manner similar to that described previously (*8*). Numerous samples of the asphalt were obtained from the interface and near-interface regions and were characterized using diffuse-reflectance FT-IR. Particular emphasis was placed on the carbonyl region (1690 to 1850 cm^{-1}), where it has been demonstrated previously that changes caused by asphalt oxidation can be observed.

Although changes were observed in the slag-asphalt interface after these weathering experiments, these did not relate to any systematic changes in the FT-IR response. In particular, no significant changes were observed in the carbonyl region of the spectrum.

Mineralogical Characterization by XRD

To summarize the major findings of the XRD analysis, the predominant mineral phases found can be separated into five categories (*12*): (a) wuestite (FeO); (b) calcium silicates (Ca_3SiO_5, Ca_2SiO_4, β-Ca_2SiO_4 (larnite), and $Ca_{54}MgAl_2Si_{16}O_{90}$); (c) calcium oxides and ferrites ($Ca_2Fe_2O_5$, $CaFeO_2$, $CaFe_3O_5$, and CaO); (d) manganese oxides ($(Mn,Mg)(Mn,Fe)_2O_4$ (hausmannite)); and (e) periclase (MgO).

The microprobe analysis indicated that the two predominant phases were a mixed oxide phase consisting of FeO, MnO, and MgO along with varying low levels of CaO and a CaO/SiO_2-rich phase. This first phase would be expected to exhibit contributions to the XRD pattern from the FeO, MgO, MnO components as well as from hausmannite. The other dominant phase observed in the cross-sectional analysis, the CaO/SiO_2-rich phase, could be anything from the various calcium silicate minerals listed in the preceding paragraph, but the ratio Ca/Si as determined by the micro-

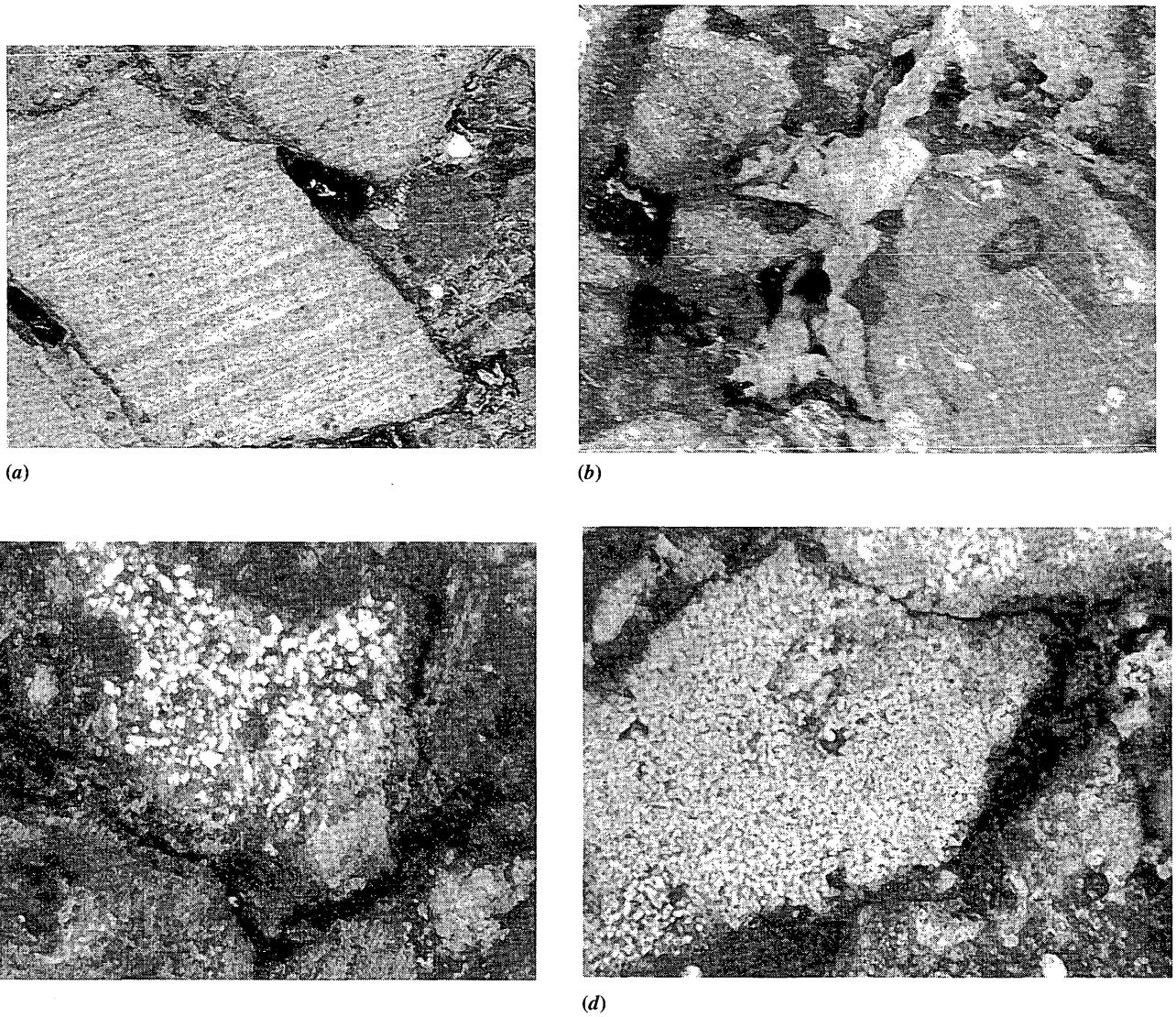

FIGURE 5 Optical micrographs of steel slag–asphalt field cores: (*a*) cross section of "good" field core, (*b*) cross section of "poor" field core, (*c*) "good" field core after aging (10 days at 50°C, 100 percent RH), (*d*) "poor" field core after aging (10 days at 50°C, 100 percent RH).

probe would indicate that it was predominantly in the form of a Ca_2SiO_4-like phase.

The XRD data indicated the presence of far more mineral phases than were implied by the microprobe analysis. This may be because the XRD data were generated from crushed bulk samples. Whereas the microprobe data were generated from discrete phase fields that may have varying composition on a local scale that was not analyzed, the XRD data were able to differentiate among the many phases present.

The mineralogical information of steel slag can also be used to examine some of the possible reactions that may occur when these materials are exposed to the accelerated weathering conditions. Some of the possible reactions involve the calcium silicates hydrating to form C-S-H gels as in portland cement or the calcium oxides forming portlandite ($Ca(OH)_2$) and goethite (FeO(OH)). Instability of steel slags has been attributed to the existence of bicalcium silicate in β-metastable form and the presence of free lime (*13*). The periclase may also be expected to hydrate and form brucite ($Mg(OH)_2$). With the presence of CO_2 in the moisture on the slag surface, there would be further formation of calcium carbonate ($CaCO_3$) from the calcium hydroxide species present.

The results obtained from both the SEM/EDX analysis of the deposits on the slag surfaces after weathering and from the slag-asphalt interface, both in-service and after weathering, show that the formation of calcium carbonate is the main reaction. From the phases present, the most likely source of the calcium would be the various calcium silicate phases detected in the slag cross sections. Another source of calcium would be the calcium-rich layer found in regions at the outer surface of many of the slag samples examined.

DISCUSSION OF RESULTS

This study has shown interesting results about the behavior of steel slags in contact with moisture. All slag samples examined exhibited formation of calcium-rich deposits (mainly calcium carbonate),

even after a relatively short exposure of 10 days at 30°C at 90 to 100 percent RH. Steel slags in asphalt briquettes also exhibited calcium-rich deposits. In many cases, cracks were observed in the briquette cross sections after aging; the path for these cracks was often along slag-asphalt interfaces that exhibited deposit formation, indicating that asphalt–steel slag bond failure had occurred.

The appearance of the slag-asphalt interface after the accelerated aging experiments was similar to the interfaces from field cores obtained from steel slag–asphalt pavements in service for several years. The deposits formed after the accelerated aging experiments were very brittle and fragile and loosely attached to the surface. The aggregate expansion test and HMA expansion test results showed substantial volume increases caused by this reactivity of the steel slags samples with moisture, a cause of premature cracking and failure.

The main concern is still the general moisture reactivity and expansivity exhibited by all the steel slag samples examined. Although the free lime content of some samples was low, the slags reacted with moisture to form calcium-rich deposits. This also indicates that even with low unreacted lime content, generally considered the main cause of swelling and premature failure at the slag-asphalt interface, if moisture is allowed to enter the system there is potential for further deterioration of the slag-asphalt bond as the moisture interacts with the steel slag. Indeed, exposure of both good and bad field core cross section samples to the humidity tests confirmed this reactivity.

There are two implications of this surface reactivity: (*a*) the ingress of moisture to the interface can displace asphalt from the interface because the slag surface is more hydrophilic than asphalt and (*b*) the fragile surface deposits that form on the steel slag during exposure to moisture may weaken the strength of the asphalt-aggregate interface. Thus, the situation may degrade both the mechanical and chemical aspects of the aggregate-asphalt bonds (*14*).

In contrast, traprock briquette samples did not exhibit the same degree of reaction with moisture. No surface deposits were observed on the aggregate surfaces, the aggregate-asphalt interface remained intact, and cracking did not occur.

The examination of prepared cross sections by EPMA and XRD analysis of bulk samples indicated that the mineralogy of the steel slags was very complex. Although there appeared to be consistency in the types of phases present, there was much variability in phase distribution in the bulk of the slag particles. The main cause of these differences is thought to be the cooling rate, which affects the mineralogy and surface characteristics and, to a lesser extent, changes in steel-making practice that determine the bulk chemistry of steel slags; batch operations also introduce variability. Also, composition of the surface zones was different from that of the bulk of the slag particles. Oxide phases based on FeO, MnO, MgO, and CaO and calcium silicate phases were predominant. XRD analysis indicated little difference in phase composition as a function of particle size. The primary source of the calcium-rich deposits formed during aging experiments appears to be the calcium silicate phases and, to a lesser extent, the mixed oxide phase containing calcium oxide. This study suggests that control of the amount and distribution of these types of phases may be a way to control the inherent reactivity of steel slag in moist environments.

Water uptake and expansion tests examine the behavior of steel slag and steel slag–asphalt mixes on a macroscopic level and should always be used to screen slag materials for potential application as aggregate. However, if the reduction in unreacted lime and the associated expansion characteristics do not prove to be the sole predictor of steel slag behavior in asphalt mixes, then a detailed study may be necessary to further optimize steel slag chemistry. The combination of EPMA examination of prepared cross sections and XRD analysis has proved effective in characterizing steel slags.

CONCLUSIONS

1. All steel slag samples used in this study exhibited surface reactivity during high humidity weathering experiments. This reactivity resulted in the formation of white crystalline surface deposits of a calcium carbonate-like compound.
2. During high-humidity exposures, steel slag briquettes also developed white deposits. In some cases cracking developed along slag-asphalt interfaces.
3. Examination of field cores indicated that slag-asphalt interfaces were characterized by the presence of white deposits containing mainly $CaCO_3$, which were similar in composition to those found in the laboratory weathering exposures.
4. Mineralogical characterization indicated that steel slags exhibited similar bulk phase composition, but the distribution (microstructure) of the slags was very different. In most cases, outer surface regions of the slag were of different composition from the slag interior. The main phases present were oxide phases based on FeO, MnO, MgO, and CaO, and calcium silicate phases. The most likely source for the calcium-rich deposits formed during humidity exposures are the calcium silicate phases present in the slags.
5. All steel slag aggregate samples showed volume expansion excessive of proposed draft specifications for aggregates in highway construction. However, BOF experimental slags studied showed reduced expansivity compared to a typical production sample, indicating that suitable processing methods may control volume expansivity of steel slags.
6. The failure mechanism observed in steel slag aggregate mixtures was attributed mainly to the excessive expansivity of steel slags due to reaction with moisture. This reactivity could be the cause of long-term degradation of the asphalt-aggregate interface in the presence of moisture.

RECOMMENDATION

The relationship between steel slag phase distribution, processing parameters (such as cooling rates), and their effects on reactivity and expansivity of steel slags should be investigated with a view to producing high quality aggregate for highway construction. This study may be extended to include modification of steel slags with other materials.

ACKNOWLEDGMENTS

The authors thank Kevin Buchaly, University of Waterloo cooperative student, and the Engineering Materials Office, for assistance in conducting expansion tests and some of the other aggregate tests; Fred Langstaff, Department of Geology, UWO, and David Kingston of Surface Science Western for assistance in EPMA and x-ray diffraction work; and the staff of Dofasco, Stelco, Lasco, Algoma, and John Emery Geotechnical Engineering Limited for providing the samples for this research. The assistance of Robert

Lockhart and Peter Lesner in the preparation of this paper is also gratefully acknowledged.

REFERENCES

1. John Emery Geotechnical Engineering Limited. *Mineral Aggregate Conservation: Reuse and Recycling Report.* Ontario Ministry of Natural Resources, Queen's Printer for Ontario, 1992, 68 pp.
2. Noureldin, A. S., and R. S. McDaniel. Evaluation of Surface Mixtures of Steel Slag and Asphalt. In *Transportation Research Record 1269,* TRB, National Research Council, Washington, D.C., 1989, pp. 133–147.
3. Emery, J. J. Slag Utilization in Pavement Construction. ASTM Special Technical Publication 774, *Extending Aggregate Resources,* ASTM, Philadelphia, 1980, pp. 95–118.
4. Geisler, J., and R. Schlosser. Investigations Concerning Structure and Properties of Steel Slags. *Third International Conference on Molten Slags and Fluxes,* June 22–29, 1988, University of Strathclyde, Glasgow, Institute of Metals, 1989.
5. Anon. *An Assessment of the Properties of BOS Slag: A Review of the Chemistry, Mineralogy and Physical Properties of the Air-Cooled BOS Slags,* British Steel Corporation, 1976.
6. Halim, R. A. *Aggregate Surface Texture Influences on Asphaltic Concrete Skid Resistance,* M.S. thesis. McMaster University, 1981.
7. Ingo, G. M., and L. Scoppio. Small-area XPS and XAES Study of Early Iron Metallurgy Slags. *Surface and Interface Analysis,* vol. 18, 1992, p. 551.
8. McKay, J. F. Study of Asphalt Aging on Aggregate Using Infrared Spectrometry, *Symposium on Chemistry and Characterization of Asphalts,* American Chemical Society, Washington, D.C., 1990 p. 496.
9. Parker, F., and E. R. Brown. Comparison of Methods for Measuring Moisture Content of Aggregate and Asphalt-Aggregate Paving Mixtures. *Journal of Testing and Evaluation,* vol. 19, 1991, p. 161.
10. Akili, W. The Effect of Moisture on Laboratory-Prepared Asphalt Mixtures, *Journal of Testing and Evaluation,* vol. 21, 1993, p. 73.
11. Ministry of Transportation Ontario. Resistance to Stripping of Asphalt Cement and Analysis of Extracted Aggregate from Bituminous Paving Mixtures, Method of Test for *Laboratory Testing Manual,* LS-283. Vol. 2, 1994.
12. Walzak, T. L. *Surface Chemistry of Steel Slags and Steel Slag-Asphalt Interaction.* Final Report. MTO Research and Development Project 22244. University of Western Ontario, 1995.
13. Panis, A. Investigation of LD Slags for Use in Road Construction (in French). *Bulletin of the International Association of Engineering Geology,* No. 30, 1984.
14. Tarrer, A. R., and V. P. Wagh, Innovative Test to Predict the Strength and Type of Aggregate Bonds. *Symposium on Chemistry and Characterization of Asphalts,* American Chemical Society, Washington, D.C., 1990, p. 361.

Publication of this paper sponsored by Committee on Characteristics of Bituminous Paving Mixtures to Meet Structural Requirements.

Resilient Modulus Properties of Asphalt Rubber Mixes from Field Demonstration Projects in Maryland

M. AYRES, JR., AND M. W. WITCZAK

Results of resilient modulus (M_r) response obtained from field cores of a newly constructed Maryland State Highway Administration demonstration project concerning the performance of asphalt rubber mixtures are presented. The test project involves over 12.5 km of US-340 and MD-140 highways, contains 30 test sections, and utilizes 14 different mixtures (1 conventional control mix and 13 rubber mixes). Six types of plant-blended wet process asphalt rubber mixtures, two types of manufacturer preblended asphalt rubber (Neste SAR and Bitumar Ecoflex), two types of dry process patented Plus Ride, and three types of a generic dry process rubber-modified mix were evaluated. The analysis of 180 field cores with the Baladi indirect test fixture with three transducers directions is presented. In addition to describing the results of the M_r test program for all of the mixtures investigated, statistical analysis of variance (ANOVA) studies were conducted to evaluate field core horizontal anisotropy, compare among the five M_r prediction models currently available, and quantify five sources of variance associated with the M_r field evaluation program. It was found that no horizontal anisotropy is present in field cores. Another study conclusion was the fact that the assumption of a Poisson's ratio value when using only horizontal or longitudinal transducers yields statistically different results for the M_r response compared with models that calculate the Poisson's ratio based on both vertical and horizontal deformations or models that use only the vertical measurements in conjunction with an assumed Poisson's ratio. Finally, the component variance analysis indicated that the largest source of variability is associated with the orientation of the diametral plane during the M_r test. This variance was found to be greater than even the within-section, between-section, and between-mix sources of variability.

Unlike many other types of solid waste, tires are not categorized as biodegradable and result in long-term disposal problems because they cannot be effectively buried or incinerated (*1*). In 1991, the Intermodal Surface Transportation Efficiency Act (ISTEA) set minimum use requirements for asphalt rubber within pavements as a partial solution to the environmental problem. However, serious technical and economical questions emerged from the basic guidelines of the legislative resolution.

To obtain answers for those questions and effectively implement the decision, several state and public agencies initiated studies on the use of rubber in pavement construction. In the state of Maryland, a project between the Maryland Department of Transportation (MDOT) and the University of Maryland (UM) was established with the primary objective of providing essential information on asphalt rubber binder characterization, mix design, and field performance.

Department of Civil Engineering, University of Maryland, College Park, Md. 20740.

Field performance is being evaluated through two demonstration projects on US-340 and MD-140 north of Baltimore. These projects involve the design, construction, testing, and monitoring of 30 sections that include both wet and dry processes in 14 different mix types. All projects were constructed between August and November 1993.

Laboratory characterization of the mixtures as actually placed is being conducted. Field cores obtained from the sections were used to establish the resilient, strength, and permanent deformation properties. This study focuses on the resilient properties of the asphalt rubber mixtures obtained from those field cores.

MIX TYPES USED

Thirteen types of asphalt rubber mixes and one conventional control were used in this study (*2*). Among these were six wet process, five dry process, and two preblended wet process mixes. The wet blend mixes were divided into two categories, one with AC-20 and the other with AC-10 type asphalt cement. Within these groups, three levels of rubber percentage—10, 15, and 20 percent—were used along with the appropriate percentage of extender oil. The dry process mixes were also divided into two groups: the patented Plus Ride and a dry generic mix developed at UM. The Plus Ride mixes were the No. 12 and No. 16 mixtures, each having 3 percent rubber. Rubber percentages of 0.75, 1.5, and 2.25 percent were used in the dry generic mixes investigated. In addition, two types of manufacturer preblended wet mixes, Neste SAR 10/10 and Bitumar (Ecoflex), were examined. Table 1 summarizes the mix design characteristics for each mix type used in the test sections.

FIELD CORING

The demonstration projects on US-340 and MD-140 consist of 30 test sections (cells). Each section is approximately 0.3 km (1,000 ft) long (*2*). The plant-mixed wet process mixtures were placed on US-340 in 14 sections. For each of the seven mix types, including a control, there were two sections. Five different dry-process mixes were laid on the eastbound lane of MD-140 in 12 sections, including two controls. Finally, the two preblended wet mixes were placed in four sections on the westbound lane of MD-140. Half of the sections constructed with the plant-mixed wet and dry processes were placed in two 38-mm (1.5-in.) lifts. The remaining sections were built in a single 38-mm (1.5-in.) layer.

Two groups of six cores each, 100 mm (4 in.) in diameter, were extracted from each test section by MDOT personnel. This resulted

TABLE 1 Mix Design Properties

Mix Process	Mix Type	Type Asphalt	Design AC (%)	Rubber (%)	Extender Oil (%)	Density Gmb (kg/m3)	Stability (N)	Flow Value (0.25 mm)	Stab/Flow Ratio (kN/mm)	Air Voids Va(%)	Voids Min. Agg. VMA (%)	Voids Filled VFB (%)
	Control	AC-20	4.8	NA	NA	2427	9679	12.2	3.17	4.0	13.3	72.0
	AC-10 rp10	AC-10	6.1	10	1.0	2393	11227	17.0	2.64	3.4	16.6	79.5
	AC-10 rp15	AC-10	6.1	15	3.0	2393	9955	17.0	2.34	3.4	16.6	79.3
Wet	AC-10 rp20	AC-10	6.3	20	7.0	2384	9701	16.0	2.43	3.6	16.5	79.5
	AC-20 rp10	AC-20	6.6	10	1.0	2379	11615	19.0	2.45	3.5	17.4	80.5
	AC-20 rp15	AC-20	6.6	15	3.0	2387	11770	20.0	2.35	3.3	17.2	80.7
	AC-20 rp20	AC-20	6.6	20	7.0	2380	10965	18.0	2.44	3.6	16.7	78.7
	G0.75	AC-20	5.4	0.75	NA	2369	8566	21.2	1.62	4.0	15.6	74.0
	G1.50	AC-20	6.5	1.5	NA	2335	6232	26.5	0.94	4.0	18.2	78.0
Dry	G2.25	AC-20	7.5	2.25	NA	2283	4363	29.0	0.60	4.0	20.8	81.9
	PR12	AC-20	7.1	3	NA	NA	NA	NA	NA	3.0	18.5	NA
	PR16	AC-20	7.5	3	NA	NA	NA	NA	NA	3.0	19.0	NA
Pre	SAR10	AC-20	5.4	10	NA	2403	7454	NA	NA	4.0	16.4	NA
Blended	ECO10	AC-20	5.1	10	NA	2420	11125	8.0	5.56	4.0	16.0	NA

TAI MS-2 Conventional AC Mix Criteria (75 blow Marsh)

Stability -	8006 N Min.
Flow -	8 to 14 (1/4 mm)
Va % -	3 to 5
Vma % -	14 Min.
Max agg. siz	25 mm
Vfa % -	65 to 75

Note: % rubber in wet and preblended mixes refer to the asphalt content

in a total of 360 core samples from the entire project. Each core group was taken from a location approximately 30 to 60 m (100 to 200 ft) from the ends of a given test section. Within each core group, the six cores were extracted as close as possible from each other. All cores were obtained at the center of the paving lane. When the coring was performed, the diameter in the direction of traffic was clearly marked to be used as a reference for load application during the laboratory tests.

The cores were processed at the UM laboratory so that only the top 38-mm (1.5-in.) lift was used for the laboratory testing. After the sawing process, the specimens were measured and weighted. Three thickness and two diameter measurements were taken from the samples. The air, water, and surface-dry weights were also defined. After the geometric and gravimetric measurements, the specimens were placed inside sealed plastic bags to avoid contact with the air before testing.

From the 360 cores, half were used to define the resilient and strength properties. The remaining specimens are being tested for permanent deformation properties and will be the subject of later reports.

LABORATORY TESTS

Equipment

A diametral (indirect) device was used to determine the resilient and strength properties of the specimens. Field cores with a 100-mm (4-in.) nominal size were tested using the Baladi fixture. An MTS closed-loop servo-hydraulic system equipped with an environmental chamber was used for the load application. The loading form applied by the hydraulic system was programmed on a 458.20 MTS controller. Actual loads were measured through a 1 360-kg (3,000-lb) capacity load cell. The environmental chamber was used to test specimens at the desired temperature level

An A/D (analog-to-digital) card was available to link the testing system to a microcomputer, converting the analog voltage signals from the load cell and linear variable differential transformers (LVDTs) into digital voltage numbers. The data acquisition and specimen property computations were automatically obtained through a PC 486-66-type computer using specific data analysis programs (*3*) developed at UM.

Resilient Modulus Test

A repetitive haversine pulse load with 0.1-sec duration and 0.9-sec dwell time was used to obtain the total and instantaneous resilient moduli. Vertical, horizontal, and longitudinal deformations were recorded through five transducers mounted on each side of the specimen, as shown schematically in Figure 1.

The prediction of the resilient moduli as well as the Poisson's ratios used five different approaches, which are functions of the number and type of LVDTs used. The computations are based on the following LVDT sequence:

1. Using only one vertical LVDT,
2. Using only the two horizontal LVDTs,
3. Using the vertical and two horizontal LVDTs,
4. Using the two longitudinal LVDTs, and
5. Statistical regression model using all five LVDTs.

The peak, instantaneous, and valley values for each cycle were determined by the software developed at UM. The series of equations related to each of the five measurement approaches previously described may be found in the Baladi indirect test fixture reference

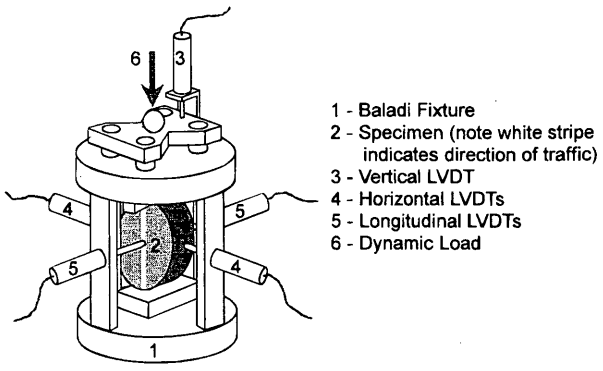

FIGURE 1 Schematic diagram of test configuration.

manual (*4*). They are not presented or discussed here because of space limitations.

TESTING AND ANALYSIS PLAN

The method used to perform the evaluation of M_r and tensile strength is based on ASTM D4123. The following overall sequence was used to test each of the cores:

1. Store the core in the environmental chamber at the test temperature 24 hr before the test;
2. Perform resilient modulus test so that the load is applied in the axis marked with the direction of traffic (0-degree orientation);
3. Perform resilient modulus test so that the load is applied transversely to the direction of traffic (90-degree orientation); and
4. Without moving the specimen from the previous position, conduct an indirect tensile strength test.

A 1-Hz cycle load was used in the dynamic tests. Each cycle consisted of a 0.1-sec load time and a 0.9-sec dwell time. The load and the number of cycles were specific and constant for each test temperature. Table 2 summarizes the test conditions at each temperature.

Three cores within a core group location were used to determine the resilient and strength properties of the mixes. The tests were performed at the three different temperatures described in Table 2. One specimen was tested at each temperature for each location, making up two cores per temperature per section. Modulus values were computed with the last five load cycles of each test. In summary, there were five repetitions for each plane and orientation test, two plane and orientation tests for each core and location, two cores and locations for each section, and two sections (except for the control, which had four sections) per mix type at each of the three different temperatures.

ANALYSIS OF RESULTS

Summary of Results

A summary of the results obtained for each test section mixture type is shown in Table 3. The values for M_r and Poisson's ratios represent the average for each mix type and each temperature. Results were computed using Prediction Model Number 3 (vertical and horizontal deformations). As indicated, each core was submitted to two M_r tests and one indirect tensile strength test. The strength tests are not reported or discussed in this paper.

Statistical Analysis

The development of the field coring plan was based upon the ability to conduct rigorous statistical data analysis in the form of an ANOVA. For the M_r analysis, it should be recognized that a total of 18,000 separate M_r predictions were obtained from the field cores (i.e., 180 cores, five repetitions per plane, two planes, five prediction equations, and two types: total and instantaneous M_r).

Horizontal Anisotropy Effect

Several prior research studies have suggested the possibility that anisotropic moduli in the horizontal direction are present in constructed pavement systems. In order to investigate this possibility statistically, M_r determinations on each core were made on two planes of the core. The 0-degree orientation was associated with the M_r response measured in the direction of traffic, whereas the 90-degree orientation was associated with the M_r response perpendicular to traffic.

In this analysis, the only statistical parameter of interest is the plane orientation effect. Because of this, a one-way ANOVA (at 5 percent level of significance) was undertaken between the 0-degree and 90-degree orientation results within each core. Table 4 summarizes the results of this analysis for each of the three test temperatures studied. Based on the results shown, it is evident that the F-statistic is lower than the critical F-value at each temperature analyzed. It can therefore be concluded that no horizontal anisotropic effect is present in field cores from the construction process. The plane-to-plane variability of M_r testing is a completely random process. As a consequence, it is not necessary to record the direction of traffic in field cores before the coring operation.

TABLE 2 Resilient Modulus Test Conditions

Temperature °C (°F)	Maximum Dynamic Load N (lb)	Total Number of Cycles
4.4 (40)	4450 (1000)	100
21.1 (70)	1335 (300)	75
37.8 (100)	312 (70)	45

TABLE 3 Laboratory Test Results—Average Values per Mix Type

Temperature (deg. C)	Mix Type	Instantaneous Mr (kPa)				Total Mr (kPa)			
		0 degree Orientation	90 degree Orientation	Average	Poisson	0 degree Orientation	90 degree Orientation	Average	Poisson
4.4	Control	4934653	5508136	5221395	0.156	4264059	4555847	4409953	0.171
	AC-10 rp10	4094463	4283399	4188932	0.215	3334135	3418880	3376508	0.271
	AC-10 rp15	4908605	4248479	4578324	0.294	3905233	3389582	3647755	0.365
	AC-10 rp20	3322248	3668465	3495356	0.106	2808004	3000645	2904324	0.157
	AC-20 rp10	4561869	4375307	4468590	0.121	3834145	3724345	3779246	0.155
	AC-20 rp15	3880141	5625756	4752948	0.239	3147519	4417350	3782438	0.266
	AC-20 rp20	3535197	4350117	3942656	0.087	3085688	3646675	3366182	0.112
	G0.75	3326344	5362036	4344190	0.103	2896454	4475513	3685983	0.117
	G1.50	4409882	4221844	4315863	0.170	3650648	3488135	3569389	0.198
	G2.25	3663117	3616108	3639615	0.174	2989233	2909873	2949552	0.208
	PR12	3170904	3090480	3130694	0.106	2611772	2544897	2578334	0.127
	PR16	3949110	4436538	4192823	0.134	3269696	3635505	3452600	0.168
	SAR10	4444562	3972355	4208459	0.134	3671881	3291902	3481893	0.171
	ECO10	3674633	3567873	3621253	0.278	2962195	2889880	2926037	0.311
21.1	Control	3278571	3621455	3450013	0.219	2608693	2793772	2701232	0.265
	AC-10 rp10	2165909	4188753	3177331	0.479	1704464	2670101	2187282	0.508
	AC-10 rp15	3039661	2717709	2878685	0.314	2213967	2073814	2143891	0.384
	AC-10 rp20	2670171	3014263	2842217	0.257	2043526	2203326	2123422	0.313
	AC-20 rp10	3474835	3205519	3340177	0.342	2516276	2418662	2467471	0.395
	AC-20 rp15	2683610	4538352	3610981	0.350	2023791	3035638	2529713	0.382
	AC-20 rp20	2563673	2841386	2702529	0.142	2030896	2250665	2140781	0.208
	G0.75	3431583	3356024	3393804	0.337	2522996	2515713	2519356	0.397
	G1.50	2909383	3248144	3078764	0.389	2070040	2312630	2194310	0.448
	G2.25	2277291	2590780	2434035	0.436	1643237	1737152	1690195	0.516
	PR12	3060318	2386110	2723214	0.249	2150064	1720516	1935289	0.299
	PR16	2255324	3171743	2713533	0.375	1674225	2071670	1872947	0.452
	SAR10	2756899	3167350	2962125	0.461	2116770	2350701	2233736	0.525
	ECO10	2673775	2675244	2674509	0.311	1953386	1968485	1960934	0.362
37.8	Control	1147706	1582365	1365036	0.152	949222	1271816	1110519	0.144
	AC-10 rp10	1086872	1675112	1380990	0.533	877648	1352560	1115105	0.525
	AC-10 rp15	1071602	1256367	1163985	0.370	879509	1053615	966560	0.406
	AC-10 rp20	1240794	904002	1072399	0.148	1017288	741199	879243	0.185
	AC-20 rp10	1603163	1248973	1426070	0.255	1198931	1023616	1111273	0.281
	AC-20 rp15	1002118	1150637	1093943	0.228	831551	975255	903613	0.246
	AC-20 rp20	980540	1596065	1304842	0.027	786552	1122426	1069340	0.065
	G0.75	1400060	1370066	1385062	0.228	1166942	1098089	1132516	0.231
	G1.50	1147562	1287766	1235664	0.155	938028	1115555	1024414	0.202
	G2.25	1035247	1077198	1056221	0.208	837540	853619	845579	0.275
	PR12	2041318	1426478	1757736	0.611	1785345	1109421	1533132	0.705
	PR16	1220112	1367620	1293790	0.446	1001055	1086768	1043926	0.508
	SAR10	1199194	983952	1091571	0.380	1026774	825589	926183	0.363
	ECO10	1163034	1035701	1093150	0.289	920826	828311	874568	0.331

Notes: Mix type specifications on Table 1
Parameters computed using vertical and horizontal transducers (Model 3)

TABLE 4 ANOVA One-Way Analysis—Total Modulus—Plane Orientation Effect

Temperature (deg. C)	Source of Variation	SS	df	MS	F	P-value	F crit
4.4	Between Planes	2.97E+10	1	2.97E+10	1.4505	0.2309	3.9215
	Within Planes	2.41E+12	118	2.05E+10			
	Total	2.44E+12	119				
21.1	Between Planes	2.59E+10	1	2.59E+10	3.0068	0.0855	3.9215
	Within Planes	1.02E+12	118	8.61E+09			
	Total	1.04E+12	119				
37.8	Between Planes	3.31E+08	1	3.31E+08	0.1428	0.7062	3.9215
	Within Planes	2.73E+11	118	2.32E+09			
	Total	2.74E+11	119				

where SS = sum of squares
df = degrees of freedom
MS = mean square
F = F-Statistic test
F crit = critical F
P-value = level of significance for which F = F crit

Note Computed values from Mr in psi

Validity of Five M_r Predictive Models

As previously noted, the M_r value can be determined by one of five different models developed by Baladi (*4*). Each of these models depends on the direction and combination of the transducers used during the test. The test fixture used in the study contained vertical, horizontal, and longitudinal transducers that allowed M_r predictions by all five equations.

The identification of the formula number and type or types of transducers used are as follows:

1. Formula 1: V (vertical transducer),
2. Formula 2: H (horizontal transducers),
3. Formula 3: V + H (vertical and horizontal transducers),
4. Formula 4: L (longitudinal transducers), and
5. Formula 5: V + H + L (all transducers).

It is very important to note that the Poisson's ratio can only be calculated in those formulas that include at least the vertical and horizontal deformations. In this case, Formulas 3 and 5 used a calculated Poisson's ratio, whereas Formulas 1, 2, and 4 used an assumed value of 0.35 across all test temperatures.

Similar to the previous analysis, the average total M_r for the last five repetitions (within plane) were computed for each of the five different predictive models. A one-way ANOVA, with 5 percent level of significance, was performed to obtain the results presented in Table 5.

In the first analysis, for each type of M_r, the groups containing the results from all five formulas were used in the ANOVA. In this case, for all temperatures, the F-statistic value is much higher than the critical F, showing that there are significant differences between results estimated by at least one of the five models studied.

The second analysis was performed with the groups representing only Formulas 1, 3, and 5. In this case the F values, as shown in Table 5, are much lower than the critical value. This demonstrates that the inclusion of Formula 2 (horizontal deformation), Formula 4 (longitudinal deformation), or both, is the cause for the significant differences obtained in the first statistical test.

A third analysis was completed with the results computed for a group containing Models 1, 2, 3, and 5. In this case the test statistics resulted in differences (F value greater than F_{crit}) at 40°F. This indicates that the inclusion of Model 4 is causing statistical differences in M_r as predicted by the four different models. Another strong indication in support of this conclusion is the analysis of the coefficients of variation (CVs) among the prediction models. Although the average CV for all three temperatures among Formulas 1, 3, and 5 is only 0.25 percent, the average value among Models 1, 2, 3, and 5 increases to 14 percent.

In a final analysis, Formulas 1, 3, 4, and 5 were also examined through an ANOVA one-way test. In this case the F values were significantly higher than the critical F across all three test temperatures. Figure 2 clearly shows the results and conclusions of this study at each of the test temperatures.

Based on the results of this analysis, it may be concluded that the use of longitudinal measurements to predict M_r is highly questionable [at least for the nominal core thicknesses of 1.5 in. (38 mm) used]. Even though Formula 5 incorporates longitudinal deformations, an analysis of this equation indicated that the major sensitivity of M_r is a result of the vertical and horizontal deformations.

Despite the lack of significant differences in the test statistics at 70°F and 100°F with prediction Model 2 (horizontal deformation only), the analysis of the CVs indicates that significantly lower variability among the prediction models is obtained when Prediction Model 2 is excluded from the group containing Formulas 1, 3, and 5.

It is therefore recommended that Formulas 1 and 3 be considered most representative as predictive models. Although the immediate benefit of Formula 1 is its simplicity because it is only necessary to measure vertical deformations, the added complexity of mounting a test apparatus to measure horizontal deformations has the advantage that it allows for the computation not only of the M_r value but of the Poisson effect as well. Though Formula 5 also satisfactorily

TABLE 5 ANOVA One-Way Analysis—Differences on Total M_r Results Obtained by Five Different Formulas

Temperature (deg.C)	Source of Variation	All Formulas					Formulas 1, 3 & 5				
		df	*MS*	*F*	*P-value*	*F crit*	*df*	*MS*	*F*	*P-value*	*F crit*
	Between Formulas	4	1.95E+12	83.8104	1.31E-48	2.3999	2	2.17E+07	0.0011	9.99E-01	3.0430
4.4	Within Formulas	320	2.32E+10				192	1.98E+10			
	Total	324					194				
	Between Formulas	4	2.14E+11	16.9759	1.53E-12	2.4022	2	7.82E+06	0.0012	9.99E-01	3.0470
21.1	Within Formulas	295	1.26E+10				177	6.47E+09			
	Total	299					179				
	Between Formulas	4	1.13E+11	35.5769	1.32E-25	2.3932	2	1.01E+07	0.0047	9.95E-01	3.0316
37.8	Within Formulas	420	3.17E+09				252	2.15E+09			
	Total	424					254				

		Formulas 1, 2, 3 & 5					Formulas 1, 3, 4 & 5				
		df	*MS*	*F*	*P-value*	*F crit*	*df*	*MS*	*F*	*P-value*	*F crit*
	Between Formulas	3	5.20E+11	22.2166	8.10E-13	2.6399	3	1.48E+12	72.0517	8.16E-34	2.6399
40	Within Formulas	256	2.34E+10				256	2.05E+10			
	Total	259					259				
	Between Formulas	3	3.07E+07	0.0039	1.00E+00	2.6428	3	2.66E+11	20.9737	4.43E-12	2.6428
70	Within Formulas	236	7.91E+09				236	1.27E+10			
	Total	239					239				
	Between Formulas	3	1.96E+09	0.8273	4.80E-01	2.6315	3	1.31E+11	40.8933	1.49E-22	2.6315
100	Within Formulas	336	2.37E+09				336	3.20E+09			
	Total	339					339				

where df = degrees of freedom
MS = mean square
F = F-Statistic test
F crit = critical F
P-value = level of significance for which F = F crit

Note Computed values from Mr in psi

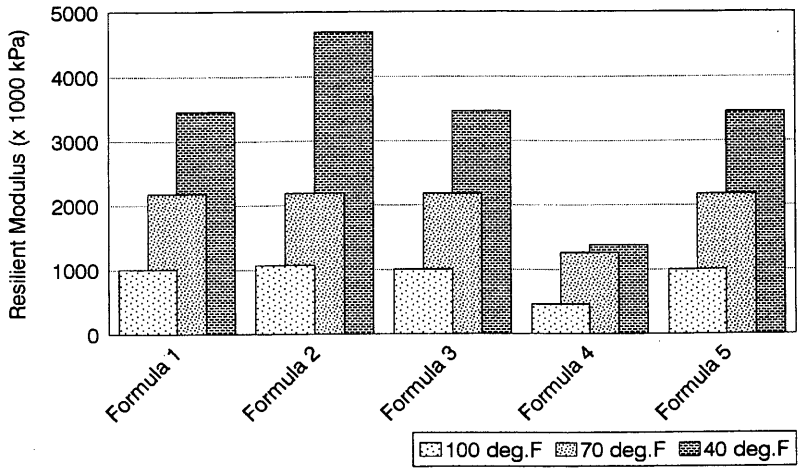

FIGURE 2 Average total resilient modulus values computed by five prediction models.

portrays both M_r and μ, no additional benefits are obtained compared with Model 3.

As a consequence of this analysis, the assumption of a Poisson's ratio value in a model that includes only vertical deformation (Formula 1) allows satisfactory M_r predictions. On the other hand, the same is not true for a model containing only horizontal measurements in the cylindrical specimen.

Analysis of Variability Components

An important element of any testing program is the quantification of the relative variability components of any measurement. Once this is accomplished, the most cost-effective and technically accurate sampling and testing program can be developed. The experimental field coring program was developed to determine estimates of the variance components associated with the field core evaluation of the M_r parameter.

This was accomplished through a five-level nested (hierarchical) ANOVA one-way balanced design model. The total variance model used is

$$\sigma^2_{\text{total}} = \sigma^2_r + \sigma^2_p + \sigma^2_c + \sigma^2_{bs} + \sigma^2_m$$

where

σ^2_r = within-plane variance associated with the number of repetitions (cycles),
σ^2_p = variance associated with the number of planes (diametrals) within a core,
σ^2_c = variance associated with the number of core locations within a given section,
σ^2_{bs} = variance associated between sections of the same mix type, and
σ^2_m = variance associated between the different mixtures used in this study.

The ANOVA was conducted separately for each test temperature for both the total and instantaneous M_r results. Table 6 summarizes the results of this analysis, and Table 7 is a summary of the variance components expressed by the CV. In the ANOVA, some negative variances are obtained. This merely indicates that the mean square for the effect level is less than that for the nested level immediately below and, as a consequence, the estimated variance is approximately 0.

A review of the average CV component values shown in Table 7 clearly indicates that the greatest source of variability in M_r measurements is associated with the plane or diametral effect within any given core. This variation can be seen to approximately six times that associated with the within-section (cores-within-section) component. In contrast, the least significant variation is associated with the number of cycles (repetitions) used to establish the M_r within a given core diametral. Finally, the variability among all of the different mixtures evaluated in this study was surprisingly low (CV_m = 2.3 and 5.8 percent). This result is discussed further in the next section.

To illustrate the application of the results obtained, classical statistical limit-of-accuracy curves were developed for a unique statistically homogeneous section. In this analysis it has been assumed (as an approximation) that the CV_i parameter is valid across all temperature ranges. With this assumption, the relationship for the limit of accuracy (R) expressed as a percentage of the true section mean can be derived from statistical principles to be

$$\left(\frac{R}{X}\right) = K_\alpha \left[\frac{CV_r^2}{n_r n_p n_c} + \frac{CV_p^2}{n_p n_c} + \frac{CV_c^2}{n_c}\right]^{\frac{1}{2}} \quad (2)$$

where

K_α = standard normal deviate,
CV_i = coefficient of variation for the ith component,
n_i = number of observations for the ith component, and
r, p, c = within-plane repetitions, between-plane and between-core (within-section) effects.

Figure 3 represents the solution of this limit-of-accuracy relationship for K_α = 1.96 (95 percent confidence); n_r = 5 cycles and CV_r = 1.5 percent, CV_p = 30 percent and CV_c = 5.0 percent. Use of

TABLE 6 ANOVA One-Way Nested Five Levels—Variance Model for M_r

Temperature deg C		Variance Component	Deg of Freedom	Sum of Squares	Mean Square	Est Comp Variance	Est Comp Std Dev
4.4	Total MR	Mix Types	13	1.7713E+12	1.3626E+11	160099563.1	12653.05
		Sections in Mix Type	14	1.8179E+12	1.2985E+11	4188147585	64715.9
		Cores in Section	28	1.2905E+12	4.609E+10	-3568756205	-
		Planes in Core	56	4.5795E+12	8.1777E+10	16351772785	127874.1
		Repetitions	448	8206237630	18317494.7	18317494.71	4279.894
	Instantaneous MR	Mix Types	13	2.4089E+12	1.853E+11	-329072664.1	-
		Sections in Mix Type	14	2.7785E+12	1.9846E+11	5974071843	77292.12
		Cores in Section	28	2.2114E+12	7.898E+10	-7098925281	-
		Planes in Core	56	8.3983E+12	1.4997E+11	29980952599	173150.1
		Repetitions	448	2.8986E+10	64700819.2	64700819.21	8043.682
21.1	Total MR	Mix Types	13	7.6086E+11	5.8528E+10	149344660.3	12220.67
		Sections in Mix Type	14	7.3575E+11	5.2554E+10	50719090.48	7121.734
		Cores in Section	28	1.4431E+12	5.1539E+10	2264713322	47589
		Planes in Core	56	1.618E+12	2.8892E+10	5774968707	75993.21
		Repetitions	448	7779400070	17364732.3	17364732.3	4167.101
	Instantaneous MR	Mix Types	13	1.0105E+12	7.7734E+10	-2320500715	-
		Sections in Mix Type	14	2.3878E+12	1.7055E+11	592487867.5	24341.07
		Cores in Section	28	4.4437E+12	1.587E+11	4760975417	68999.82
		Planes in Core	56	6.2213E+12	1.1109E+11	22210345210	149031.4
		Repetitions	448	1.9137E+10	42716199.4	42716199.36	6535.763
37.8	Total MR	Mix Types	13	2.5842E+11	1.9879E+10	259295003.9	16102.64
		Sections in Mix Type	14	1.331E+11	9506936996	7332560.273	2707.87
		Cores in Section	28	2.6209E+11	9360285791	-252889896.3	-
		Planes in Core	56	6.6579E+11	1.1889E+10	2375901778	48743.22
		Repetitions	448	4334787475	9675864.9	9675864.899	3110.605
	Instantaneous MR	Mix Types	13	3.5777E+11	2.7521E+10	159109654.7	12613.87
		Sections in Mix Type	14	2.9619E+11	2.1157E+10	299201507.4	17297.44
		Cores in Section	28	4.2483E+11	1.5173E+10	-329519810.3	-
		Planes in Core	56	1.0342E+12	1.8468E+10	3687574870	60725.41
		Repetitions	448	1.3434E+10	29987616.3	29987616.31	5476.095

* "-" represents square root of negative value
** variance values in psi (1 psi = 6.89 kPa)

these values leads to a solution that represents a fairly accurate, though approximate, analysis for M_r evaluation at any temperature or type of M_r (total or instantaneous). It should be apparent that the limit of accuracy is nearly insensitive to the M_r value used but that it is highly sensitive to the number of planes (diametrals) tested within a core. As an example, it can be observed from Figure 3 that similar accuracies (i.e., 20 percent) can be achieved either by a combination of two cores and five diametral planes per core or by five cores and two diametral planes per core. Although both testing programs yield the same accuracy, it would obviously be much more economical to select only two core locations and test each core sample in five random plane orientations.

TABLE 7 Summary of Variance Components by CV Value

Mr Type	Variance Component	CV Value at Temperature			Average CV (%)
		4.4 deg.C	21.1 deg.C	37.8 deg.C	
Total	Between mixes	2.6	3.9	10.9	5.8
	Between sections	13.2	2.3	1.8	5.8
	Cores within sections	0.0	15.0	0.0	5.0
	Planes within cores	26.0	24.0	32.9	27.6
	Repetitions within planes	0.9	1.3	2.1	1.4
Instantaneous	Between mixes	0.0	0.0	7.0	2.3
	Between sections	13.0	5.6	9.5	9.4
	Cores within sections	0.0	15.9	0.0	5.3
	Planes within cores	29.1	34.3	33.5	32.3
	Repetitions within planes	1.4	1.5	3.0	2.0

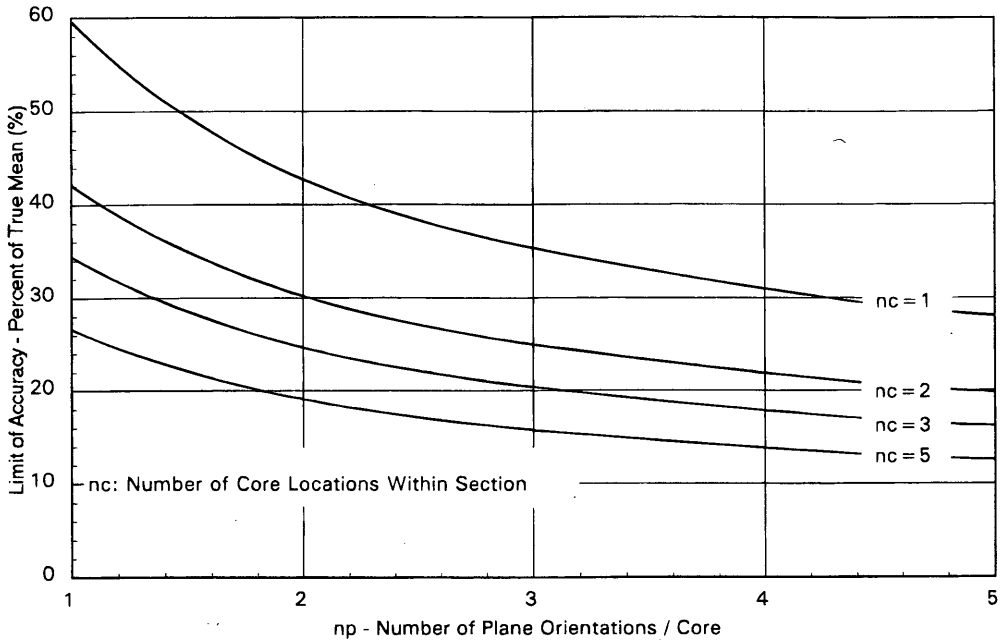

FIGURE 3 Limit of accuracy relationship for M_r evaluation of field cores.

Influence of Mixture Types

The summary of M_r results has been shown in Table 3 for the 14 different mixtures placed in the demonstration test sections. Figures 4 through 8 graphically portray these results. In Figures 4 through 6, the average instantaneous and total M_r, by mix type, are shown for each of the three test temperatures used [4.4°C (40°F), 21.1°C (70°F), and 37.8°C (100°F)]. Figures 7 and 8 show ratios of the M_r results relative to the control mix used. This control mix was an MSHA "SC" dense-graded surface course mix using a Chevron AC-20 binder.

With only a few exceptions, the control mix exhibited the largest M_r values between mixtures, M_r types, and across all temperatures. The most notable exception was both M_r responses, at 37.8°C, for the Plus Ride No. 12 mixture. Modulus ratios of 1.3 to 1.4 times the control mix were obtained.

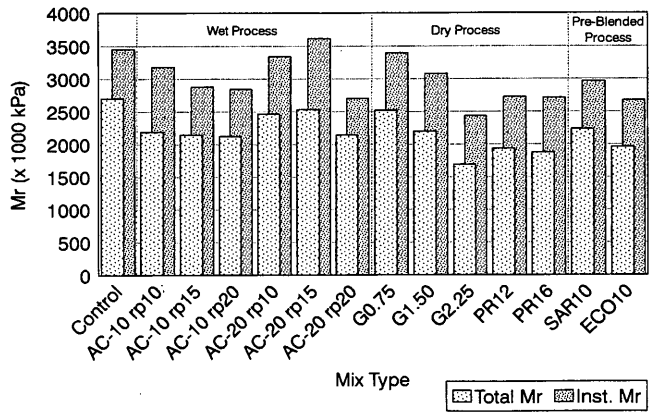

FIGURE 5 Instantaneous and total resilient modulus versus Mix Type—21.2°C.

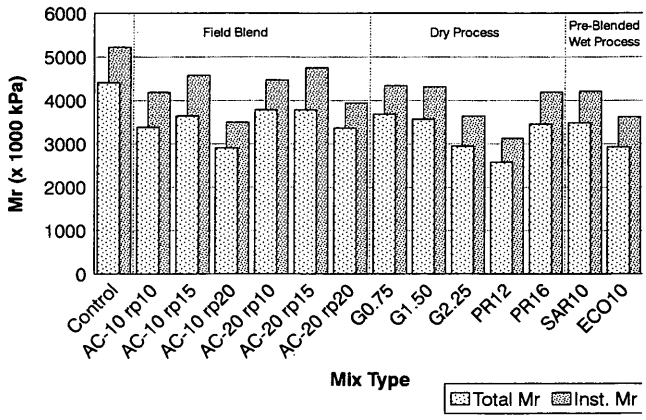

FIGURE 4 Instantaneous and total resilient modulus versus mix type—4.4°C.

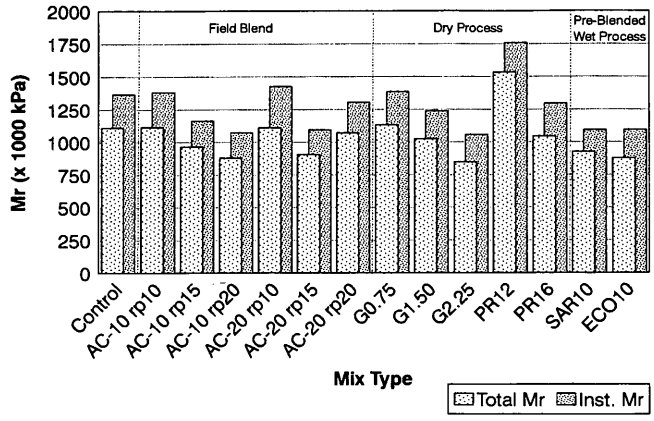

FIGURE 6 Instantaneous and total resilient modulus versus mix type—37.8°C.

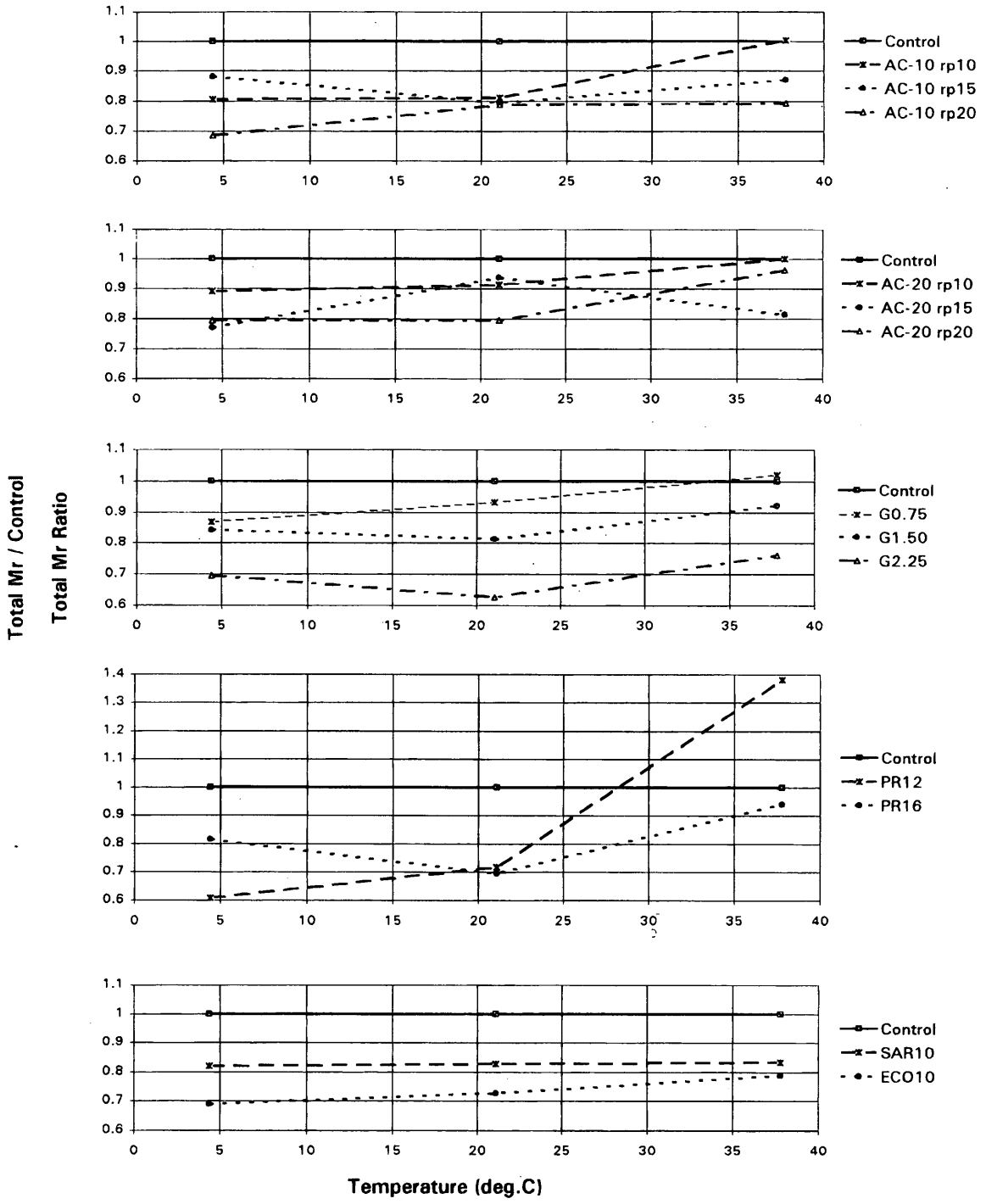

FIGURE 7 Total M_r/control total M_r ratio versus temperature.

For the field-blended wet asphalt rubber mixtures, it is difficult to observe distinct trends in the M_r value as the rubber percentage was increased from 10 to 20 percent. In general, the AC-20 blends gave slightly higher M_r values compared with comparable AC-10 field blends. Additionally, the M_r ratios were about 0.8 at the cold (4.4°C) temperature and increased with temperature to approximately 0.9 to 0.95 at the warm (37.8°C) temperature. At the cool temperature, it appeared that the maximum M_r value occurred at the 15 percent rubber additive for both the AC-10 and AC-20 blends. However at the warmest test temperature, the maximum M_r was associated with the 10 percent rubber additive for both the AC-10 and AC-20 blends.

The manufacturer preblended wet asphalt rubber mixtures (Neste SAR 10/10 and Bitumar Ecoflex) both contain 10 percent rubber additives. As shown in all the figures, the M_r ratio response was about 0.85 across all temperatures for the SAR

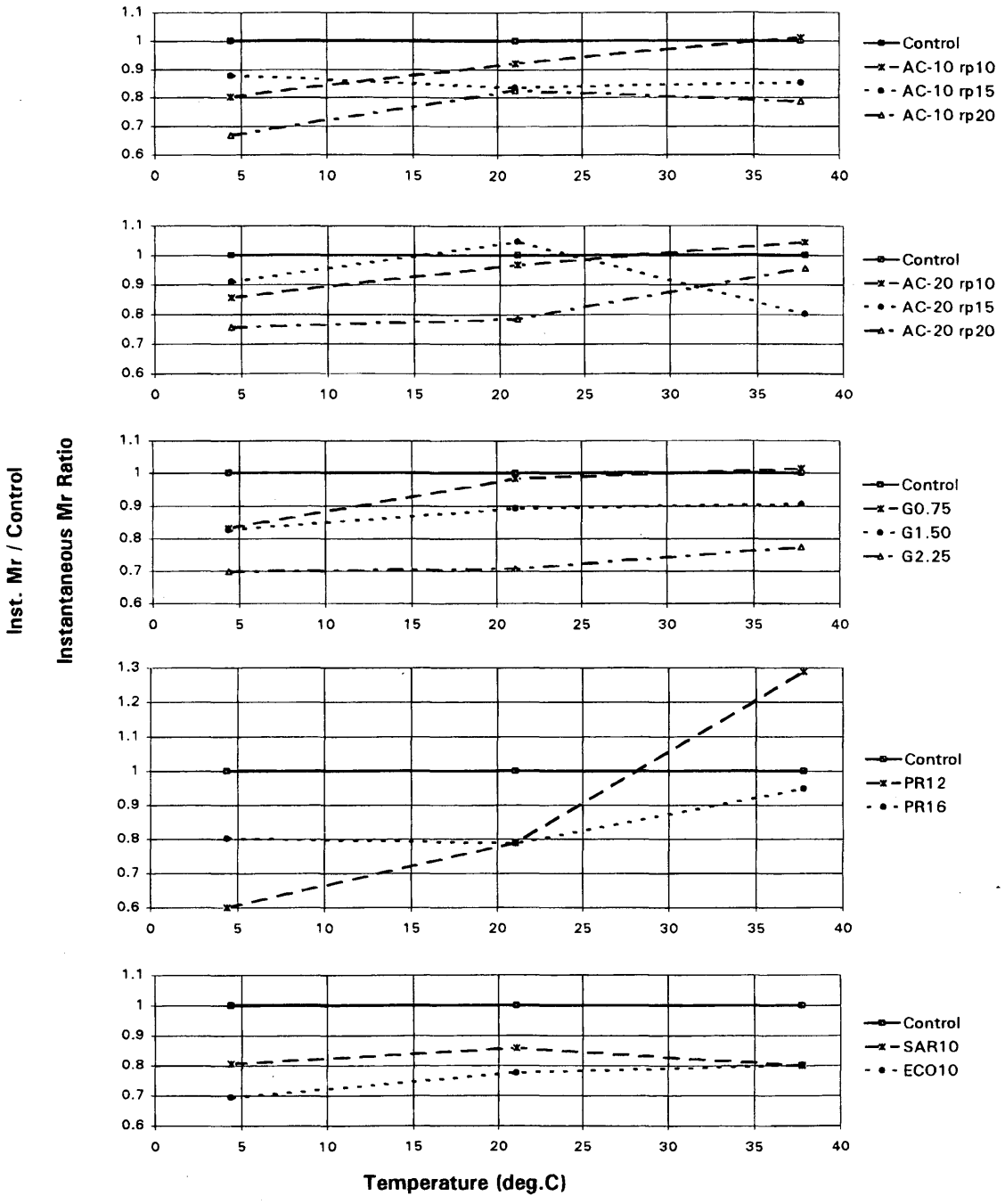

FIGURE 8 Instantaneous M_r /control instantaneous M_r ratio versus temperature.

10/10 and between 0.70 (cool) to 0.80 (warm) for the Ecoflex binder.

For the dry process generic rubber-modified mixtures, the M_r ratio generally decreased with increasing rubber content. For the 0.75 percent rubber blend, the ratio was 0.85 to 0.90 at the cool temperature and approached the control mix modulus at higher temperatures. In contrast, the 2.25 percent rubber blend had M_r ratios between 0.7 and 0.8.

The patented Plus Ride mixes, especially PR No. 12, resulted in the most significant temperature susceptibility to M_r values for all of the mixtures evaluated. The M_r ratio for PR No. 12 mix was found to be about 0.6 at the low temperature and increased to about 1.3 to 1.4 at the warm temperature. In general, PR No. 16 had a larger modulus at 4.4°C than PR No. 12. This trend was reversed at the high temperature (37.8°C) and at the intermediate temperature (21.1°C) both PR mixtures yielded equivalent modulus values.

CONCLUSIONS

The laboratory M_r responses on 180 field cores were obtained from a newly constructed field demonstration project by the Maryland State Highway Administration. This project involves the construction of over 12.5 km of highway composed of 30 separate test sections and 14 different asphalt rubber mixtures. The M_r evaluation of cores was accomplished with the Baladi indirect test fixture using vertical, horizontal, and longitudinal transducers.

Based on the analysis, the following conclusions can be drawn:

1. A statistical ANOVA showed that there is no horizontal anisotropy of the M_r response of the field cores. Thus, the M_r response is independent of the diametral (plane) orientation. As a consequence, there is no need to reference the direction of traffic on cores sampled from field sections.
2. The test analysis allowed for the prediction of five separate sets of M_r estimates, depending upon the type and combination of transducers used. Based upon an ANOVA, it was concluded that the use of only horizontal or longitudinal transducers (three core axis) to determine the M_r response gave significantly different values compared to models that include the vertical measurements. Use of either vertical or both gave statistically identical estimates of the M_r response. It is recommended that the use of both vertical and horizontal transducers be used to accurately measure both the M_r and Poisson's ratio values. For simplicity, if only the M_r response is of interest, the model that includes only vertical measurements can satisfactorily be used in conjunction with an assumed Poisson's ratio value.
3. ANOVA techniques were used to determine the magnitude of five separate variance components within the M_r test. These components are (*a*) repetitions (cycles), (*b*) plane (orientation), (*c*) within section, (*d*) between sections, and (*e*) mix types. It was found that the repetition effect had the smallest source of variation and the plane/diametral orientation had the largest source of variation.
4. Limit of accuracy curves were developed for M_r field core test results within a statistically homogeneous section using the variance (coefficient of variation) values found from the component ANOVA study. As an example, for equivalent accuracy of the M_r response, it was found that it is much more cost-effective to maximize the number of diametral planes tested within a given core relative to increasing the number of cores within a given highway project.
5. In general, the M_r response of the MSHA dense graded (AC-20) control mix resulted in the largest M_r results, across all temperatures, compared with the 13 asphalt rubber mixes investigated. The most notable exception was a Plus Ride No. 12 mix at 37.8°C (100°F) where M_r ratios (relative to the control mix) were 1.3 to 1.4. For all asphalt rubber mixtures, typical M_r ratios varied, on the average, between 0.8 and 0.9. Lower M_r ratios were normally observed at the low test temperature of 4.4°C (40°F), whereas the larger ratios occurred at the high test temperatures. M_r values were generally decreased as the percentage of rubber increased.

Although this study is devoted exclusively to discussions of the M_r response of asphalt rubber mixtures, further studies dealing with tensile strength and permanent deformation behavior are currently being conducted. These results, taken together with the results of nondestructive deflection tests, skid/friction measurements, visual condition surveys, and quality control data, will allow for a more comprehensive evaluation of the field performance of the asphalt-rubber mixtures used in the demonstration project.

ACKNOWLEDGMENTS

The authors are grateful for the technical and financial assistance provided by the Maryland Department of Transportation (SHA) for completion of the project study described in this paper.

REFERENCES

1. Witczak, M. W. *State of the Art Use of Ground Rubber in Hot Mix Asphalt.* Synthesis Report to the Maryland Department of Transportation, University of Maryland at College Park, 1991.
2. Witczak, M. W. *Field Coring and Test Plan* (Manual). Maryland State AWO-093-360-046, Maryland Department of Transportation, SHA, 1993.
3. Mirza, M. W., and M. W. Witczak. *Bituminous Mix Dynamic Material Characterization-Data Acquisition and Analysis Programs Using 45820 MTS Controller.* Program Background and Users' Guide, University of Maryland at College Park, 1994.
4. Gilson Company, Inc. *Baladi INTT Fixture—Instructions for Test Procedures, Analytical Analysis, Maintenance and System Verification* (Manual).

The views and opinions presented are those of the authors and not those of the Maryland Department of Transportation.

Publication of this paper sponsored by Committee on Characteristics of Bituminous Paving Mixtures to Meet Structural Requirements.

Characterization of Emulsion Aggregate Mixtures

JOHN R. ANDERSON AND MARSHALL R. THOMPSON

Emulsion aggregate mixtures (EAMs) are one type of low-quality cold-mixed asphalt concrete mixture. In Illinois, road-mixed and plant-mixed EAMs are used frequently as base or surface courses on low-volume rural roads (less than 1,000 average daily traffic). This research characterizes the EAM engineering properties that contribute to the observed performance of EAM pavements using laboratory testing. Dense-graded and open-graded aggregates treated with HFE-300 and CSS-1 emulsions are considered. Shear strength, repeated loading response (resilient modulus, permanent deformation), dynamic cone penetrometer, and curing effects are evaluated. The study concludes that EAMs are characterized as an improved granular material.

Emulsion aggregate mixtures (EAMs) are one type of low-quality cold-mixed asphalt concrete mixture. In Illinois, road-mixed and plant-mixed EAMs are used frequently as base or surface courses on low-volume rural roads (less than 1,000 average daily traffic). EAMs made with dense-graded and open-graded aggregates are placed frequently in 100-mm (4-in.) layers over existing pavements. Motor graders or conventional pavers are used to place the EAMs. At least a single surface treatment is generally applied before the first winter.

This study was conducted to characterize EAM engineering properties. The literature reports studies on EAM Marshall stabilities, tensile strengths, curing effects, and EAM pavement fatigue performance. This laboratory study focuses on the pertinent EAM engineering properties of shear strength, repeated load response, and dynamic cone penetrometer (DCP) indications.

LITERATURE

Research in the 1970s reported that EAM material properties improve with moisture loss. Darter et al. (*1*) reported Marshall stabilities ranging from 2 to 13 kN (500 to 3,000 lbf), depending on the emulsion type, and tensile strengths at generally less than 165 kPa (24 psi). Diametral modulus values are reported by Schmidt et al. (*2*) on the order of 1034 to 3445 MPa (150 to 500 ksi) at 23°C (73°F) after 30 days of curing.

Some researchers evaluated EAMs in a fully cured condition (*2–4*). They reported that EAMs have the "ultimate" potential to obtain diametral moduli equivalent to those of hot-mix asphalt concrete (HMAC). Research for The Asphalt Institute's thickness design manual concluded that the EAM modulus was equivalent to that of HMAC, and therefore that EAM fatigue life was equivalent to that of HMAC (*5–7*).

J. R. Anderson, Burns & McDonnell, 4800 E. 63rd Street, Kansas City, Mo. 64141. M. R. Thompson, University of Illinois at Urbana-Champaign, 1211 NCEL, MC-250, Urbana, Ill. 61801.

Walter (*8*) and Hicks et al. (*9*) reviewed the performance of 237 km (148 mi) of open-graded EAMs in the Pacific Northwest; they concluded that open-graded EAMs are more resistant to fatigue cracking than HMAC. Santucci (*6*) reported that EAM pavements with greater than 20 percent voids seldom exhibit fatigue cracking. The San Diego Road Test (*10*) reported fatigue cracking of HMAC surfaces on EAM bases. However, it was not reported whether the EAM bases developed fatigue cracks. The field performance indicates that EAMs are not characterized with a fatigue life.

PRELIMINARY FIELD STUDY

A preliminary field study was conducted to review the performance of EAM pavements in Illinois. Approximately 195 km (121 mi) of EAM pavements with ages ranging from construction day to 20 years were reviewed (*11*). Structural distresses (rutting, fatigue cracking) were rare, thus precluding a formal pavement distress survey. The lack of fatigue cracking was confirmed through interviews with experienced users (R. Beyers, Emulsicoat, Inc., Urbana, Illinois; J. Renner, Louis Marsch, Inc., Morrisonville, Illinois; B. Miteff, Koch Materials Company, Chicago, Illinois; F. Cramer, Marshall County Highway Engineer, retired, personal communication, May 28, 1993; R. Nelson, President, Advanced Asphalt, personal communication, Princeton, Illinois, May 18, 1993; D. Johnson, Crawford County Highway Superintendent; P. Koberlein, Assistant County Highway Superintendent, Sangamon County; and S. Armon, Advanced Asphalt.)

DCP tests were conducted on representative sections. The DCP provides a rapid indication of in situ shear strength. The DCP values give the penetration rate in millimeters per blow (in./blow) for each drop of an 8-kg (17.6-lb) mass.

Typical EAM pavement penetration rates were approximately 3 mm/blow (0.12 in./blow). For comparison, typical high-quality HMAC DCP penetration rates were considerably less, approximately 0.5 mm/blow (0.02 in./blow) (*11*). The lower the penetration rate, the greater the shear strength.

Further testing was conducted using the falling weight deflectometer (FWD). FWD testing was limited to sections with generally 203 mm (8 in.) or more of EAM thickness. The FWD applied a 40-kN (9,000-lbf) load to a 305-mm (12-in.)-diameter plate. Deflection sensors were placed at 305-mm (12-in.) intervals to 914 mm (36 in.).

Various algorithms are available to backcalculate subgrade modulus and approximate EAM modulus using the FWD data (*12*). However, for EAM comparisons, the actual deflections were considered more appropriate. In particular, the deflection at the center of the load $D0$ and the AREA parameter describing the deflection basin were used.

EAM *D*0's of 0.6 mm (22 mil) were typical as compared with HMAC values of 0.3 mm (12 mil) and 0.9 mm (36 mil) for untreated aggregate bases (*13,14*). The EAM AREA was 457 mm (18 in.). The EAM AREAs are between the HMAC AREA of 559 mm (22 in.) and the untreated aggregate AREA of 356 mm (14 in.) (*13,14*). EAM FWD responses are bracketed between HMAC and untreated aggregate base responses.

LABORATORY STUDY

This laboratory investigation characterized the engineering properties that contribute to the favorable FWD and DCP responses and the general lack of EAM pavement structural distresses. To adequately characterize the responses, testing was conducted on several mixes prepared from five aggregates, two emulsions, and an asphalt cement. The laboratory tests included rapid shear strength, repeated loading, and DCP.

Materials

Five aggregates were used, as indicated in Table 1. Aggregates A, B, and C were for laboratory-mixed specimens. Aggregates D and E were from plant-mixed EAM stockpiles. Dense-graded aggregates were A, B, and D; open-graded aggregates were C and E.

Aggregate A was a partially crushed gravel with nonplastic fines. Aggregates B and C were crushed dolomitic limestone with a plasticity index of 4. Aggregate D was a natural river gravel, and Aggregate E was a crushed dolomitic limestone containing chert.

The two most commonly used emulsions in Illinois, HFE-300 and CSS-1, were selected for this research. The HFE-300 contained 67.5 percent residual asphalt cement, with a penetration in excess of 300. The CSS-1 contained 62.3 percent residual asphalt cement, with a penetration of 136.

Mix Designs

Mix designs are imperative in the laboratory but are used as general guidelines in the field. NCHRP Report 259 (*15*) reviewed the Illinois and The Asphalt Institute Hveem procedures and concluded:

> [A] precise laboratory design (even if obtainable) is not critical for achieving a successful pavement. At best it can only serve as a general guideline for an initial job-mix formula with adjustments being made following evaluation . . . [of] such factors as workability, coating, plasticity, and ease of compaction.

Dense-graded aggregate EAM mix designs were conducted using the Illinois method (*16*). The coating test described in Asphalt Institute Publication MS-19 (*17*) was used for the open-graded aggregates; combinations that produced 90 to 100 percent coating were used for this research. The residual asphalt cement (ResAC) contents of the mixtures are indicated in Table 2.

To bracket the EAM properties, testing was repeated on the untreated aggregates and a low-quality hot-mixed bituminous aggregate mix (BAM). The untreated dense-graded aggregates were compacted at 100 percent of AASHTO T-99 moisture and density, which is different from the EAM moisture and density.

The BAM mixes used Aggregates A, B, and C treated with AC-5 asphalt cement, with a penetration of 141. The Marshall method of mix design, using 50 blows per side, was conducted on the BAM mixes (*18.*) Table 2 indicates the asphalt cement contents.

EAM Compaction Moisture

The literature reported that EAM properties improve with moisture loss. There are three sources of water in an EAM at mixing: hygroscopic water in the aggregate, water added to improve coating, and water in the emulsion. The sum of these three sources is the total moisture content of the mix.

TABLE 1 Aggregate Gradations

	Percent Passing				
	Lab-Mixed			Plant-Mixed	
Sieve mm	A Dense	B Dense	C Open	D Dense	E Open
38	100			100	
25	96	100	100	97	100
19		97	91		
12	75	86	45	88	40
5	51	48	4	68	2
1	35	19	3	46	
0.43	22	14	2	25	
0.15	11	10		6	
0.075	9	9	1	4	

1 mm = 0.039 in.

TABLE 2 At-Test Specimen Conditions

Aggregate	Binder Type	ResAC%[a]	% T-99 Density[b]	Moisture Content, %
A Dense Lab-Mixed	none	none	100.0	6.3
	HFE-300	4.0	92.2	2.8
	CSS-1	4.0	92.2	2.3
	AC-5	4.0	100.7	none
B Dense Lab-Mixed	none	none	100.0	7.2
	HFE-300	4.0	90.6	1.5
	CSS-1	4.0	89.2	1.8
	AC-5	4.0	102.2	none
C Open Lab-Mixed	none	none	100.0[c]	0.1
	HFE-300	3.0	100.0	1.0
	CSS-1	3.0	100.0	1.0
	AC-5	3.0	99.1	none
D Dense Field-Mix	none	none	100.0	7.7
	HFE-300	3.4	90.0	0.6
E Open Field-Mix	none	none	100.0[c]	0.1
	HFE-300	2.9	100.0	1.8

[a] Residual Asphalt Cement content, percent of dry aggregate weight.

[b] AASHTO T-99 was conducted on the untreated dense-graded aggregates; EAM and BAM densities are by weight of dry aggregate, as a percentage of the T-99 density.

[c] Open-graded untreated aggregates were compacted to a maximum density without fracturing particles. EAM and BAM densities are by weight of dry aggregate, as a percentage of the maximum density.

The Asphalt Institute recommends compaction when 50 percent of the total moisture (at mixing) has evaporated (*19*). EAMs for this research were compacted after 50 percent of the total moisture had evaporated; testing was conducted immediately following compaction. Advantages of using the "50 percent drying" criterion for EAM properties are as follows:

1. Adequate performance is assured on construction day,
2. Estimates of time to "ultimate strength" are not required for structural design, and
3. EAM pavement properties improve with curing and traffic.

Density and Voids Analysis

Density and voids analysis for EAMs requires consideration of the moisture content. The density and voids analysis equations in NCHRP 259 (*15*) using the aggregate apparent specific gravity are recommended. The NCHRP 259 equations used are as follows:

$$\text{MC\%} = \frac{\text{mass of water}}{\text{mass of dry mixture}} \times (100 + \text{AC\%}) \quad (1a)$$

$$\text{Dry agg. density} = \frac{\text{wet mix density}}{1 + \frac{\text{AC\%}}{100} + \frac{\text{MC\%}}{100}} \quad (1b)$$

$$\text{VMA\%} = \left(1 - \frac{\gamma_d}{G_{sa}\,\gamma_w}\right) 100 \quad (1c)$$

$$V_{amc}\% = \left(1 - \frac{\gamma_d}{G_{sa}\,\gamma_w} - \frac{\gamma_d\,\text{AC\%}}{100\,B\,\gamma_w}\right) 100 \quad (1d)$$

$$V_{air}\% = V_{amc}\% - \frac{\gamma_d\,\text{MC\%}}{\gamma_w} \quad (1e)$$

where

AC% = residual asphalt cement (% of dry aggregate),
MC% = moisture content (% of dry aggregate),
VMA% = voids in mineral aggregate,
V_{amc}% = air and moisture volume (%),
B = specific gravity of asphalt cement,
G_{sa} = apparent specific gravity of aggregate,
γ_w = density of water (62.4 pcf), and
γ_d = EAM dry aggregate density.

TEST PROCEDURES

Rapid shear strength and repeated loading tests were conducted on 152-mm (6-in.)-diameter by 305-mm (12-in.) cylindrical specimens under triaxial stress states. DCP tests were conducted on materials compacted in 203-mm (8-in.)-diameter by 381-mm (15-in.) cylindrical steel molds. All tests were conducted at 23°C (73°F).

Specimen Preparation

Compaction was with a full-faced pneumatic vibratory compactor, applying 134 N (30 lbf) of force per blow. The 305-mm (12-in.) triaxial specimens were compacted in five lifts; the 381-mm (15-in.) DCP specimens were compacted in six lifts.

The compacted triaxial specimens were encased in two membranes: an inner 0.8-mm (31-mil) neoprene membrane, and an outer 0.6-mm (25-mil) latex membrane. Aluminum loading platens were sealed to the specimen with the membranes and clamps. Confinement during handling was provided by a vacuum until the triaxial chamber was assembled. The triaxial chamber consisted of an aluminum base plate, lid, and an acrylic cell. After assembly, confinement was provided by compressed air.

Test Equipment

The rapid shear strength and repeated load tests (resilient modulus, permanent deformation potential) were conducted with an electrohydraulic loading apparatus manufactured by MTS Systems, Inc. (MTS). The MTS apparatus was fitted with a 44.5-kN (10-kip) ram and load cell. A function generator controlled the load pulse: either constant strain for the rapid shear test or haversine for repeated loading. A personal computer fitted with an 8-channel data translation analog:digital board triggered the MTS and recorded data. Total specimen deflections were measured using linear variable differential transducers (LVDTs).

RAPID SHEAR TEST

The rapid shear test defined the shear strength and the Mohr-Coulomb failure envelope. Three different confining pressures (σ_3) were used: 34, 103, and 207 kPa (5, 15, and 30 psi). Deviator stress ($\sigma_d = \sigma_1 - \sigma_3$) was applied axially at a constant strain rate of 38 mm (1.5 in.) per second. This rate corresponded to 5 percent strain in 400 msec. Total specimen deflections were measured using the LVDT in the loading ram.

Shear strength was defined as the maximum deviator stress. If there was no clearly defined peak stress, then the shear strength was defined as the deviator stress at 5 percent axial strain.

Using the failure deviator stresses and confining pressures, the Mohr-Coulomb failure envelope was determined by evaluating the best-fit regression line according to

$$\sigma_1 = a + b\sigma_3 \tag{2}$$

where

σ_1 = major principal stress, $\sigma_d + \sigma_3$,
σ_3 = minor principal stress (confining pressure), and
a, b = regression coefficients.

Then the cohesion (C) and angle of internal friction (ϕ) were evaluated by

$$C = \frac{a}{2\sqrt{b}} \tag{3}$$

$$\phi = \arcsin \frac{(b-1)}{(b+1)} \tag{4}$$

The relation between σ_1 and σ_3 can be expressed as

$$\sigma_1 = \sigma_3 N_\phi + 2C\sqrt{N_\phi} \tag{5}$$

where

$$N_\phi = \tan^2\left(45 + \frac{\phi}{2}\right) \tag{6}$$

This procedure has been used successfully in previous studies (*20,21*).

REPEATED LOADING TEST

Cylindrical specimens 152 mm (6 in.) diameter by 305 mm (12 in.) were subjected to various triaxial stress states that were less than the failure stress states. Haversine load pulses were applied by the MTS with a load pulse duration of 0.1 sec (10 Hz). A 0.9-sec rest period between load pulses was used. Deflections were measured using external LVDTs mounted on the loading piston.

Permanent Deformation

An indication of permanent deformation (rutting) potential was determined from analysis of the conditioning sequence of the triaxial repeated load specimens. The repeated load specimens were conditioned with 1,000 applications of 310-kPa (45-psi) deviator stress at 103-kPa (15-psi) confining pressure before resilient modulus testing. Data recorded were permanent deformation, resilient deformation, and applied deviator stress. Measurements were made at 1, 10, 50, 100, 500, and 1,000 load applications.

The model used to evaluate permanent deformation, ϵ_p%, was

$$\epsilon_p\% = AN^b \tag{7}$$

where A is the antilog of a in $\log \epsilon_p\% = a + b \log N$ and N is the number of cycles.

TABLE 3 Resilient Modulus Stress States

Deviator Stress, σ_d kPa	Confining Pressure, σ_3 kPa	Bulk Stress, θ kPa	Principal Stress Ratio, σ_1/σ_3
68.9	34.5	172.3	3
103.4	34.5	206.7	4
137.8	68.9	344.5	3
206.7	68.9	413.4	4
206.7	103.4	516.8	3
310.1	103.4	620.1	4
310.1	206.7	930.2	2.5
413.4	206.7	1033.5	3

1 kPa = 0.145 psi

Resilient Modulus

After the conditioning sequence, resilient modulus testing was conducted at various stress states. One hundred load pulses at each of the stress states in Table 3 were applied. Principal stress ratios (σ_1/σ_3) varied from 2.5 to 4.

The resilient modulus was calculated after the 100th load application at each stress state. Resilient modulus is defined as

$$E_R = \frac{\sigma_d}{\epsilon_r} \quad (8)$$

where

E_R = resilient modulus,
σ_d = applied deviator stress, and
ϵ_r = recoverable axial strain.

Linear regression of the stress-sensitive response was used to obtain a best-fit equation:

$$\log E_R = a + n \log \theta \quad (9)$$

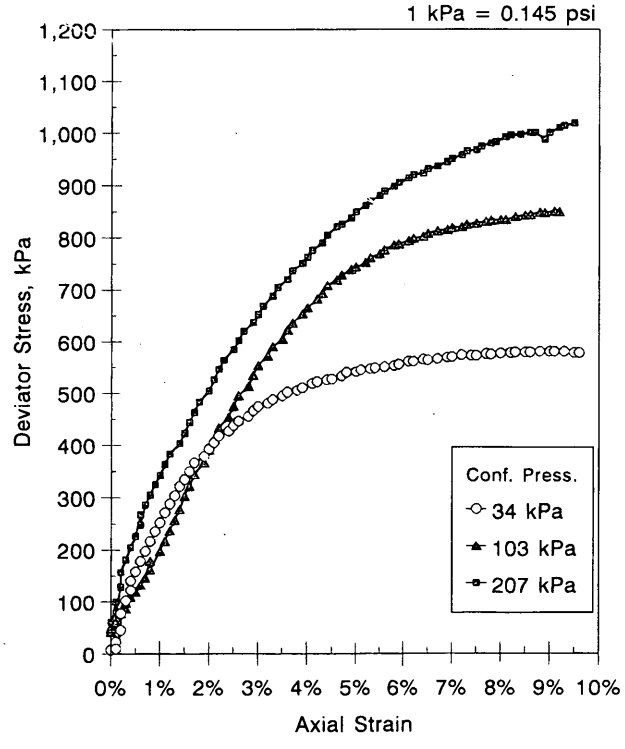

FIGURE 1 Aggregate A untreated rapid shear.

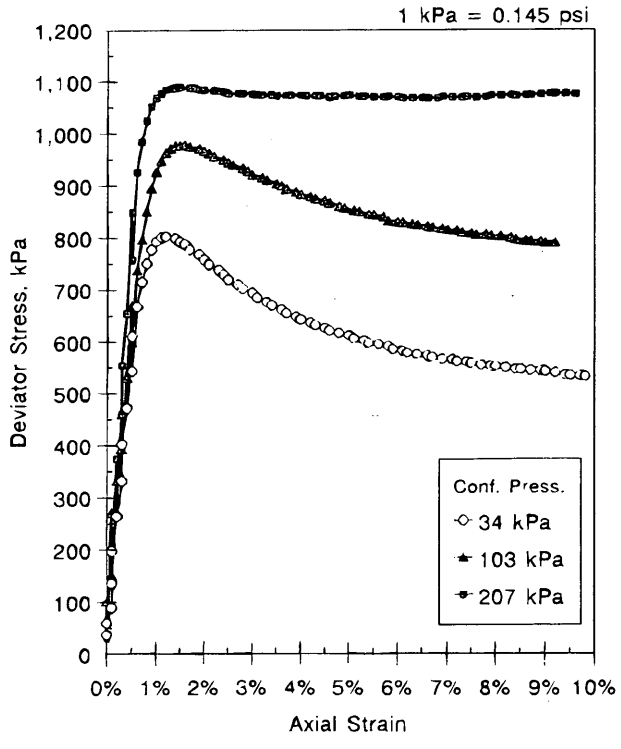

FIGURE 2 Aggregate A EAM rapid shear.

where θ = bulk stress, $\sigma_1 + \sigma_2 + \sigma_3 = \sigma_d + 3\sigma_3$, and a, n = regression coefficients.

The response was transformed into the θ model:

$$E_R = K\theta^n \quad (10)$$

where K is the antilog of a in Equation 9. The stress sensitivity is depicted by n; an n of 0 represents a constant modulus material.

DYNAMIC CONE PENETROMETER TESTS

The DCP was used to obtain a rapid indication of in situ shear strength. Ayers (*20*) presented an extensive study concerning development and prediction of shear strength of granular materials using the DCP.

DCP testing in the laboratory was performed on the untreated aggregates and EAMs in a 203-mm (8-in.)-diameter by 381-mm (15-in.) cylindrical steel mold. The rod penetration after each anvil blow is the penetration rate, which was recorded in millimeters per blow.

SHEAR STRENGTH RESULTS

Figure 1 presents the response for dense-graded untreated Aggregate A for the three confining pressures. This response is a ductile failure, a typical one for untreated aggregates. There is no defined peak; therefore, failure stress is taken at 5 percent axial strain.

Figure 2 is for the same aggregate treated with 4 percent ResAC HFE-300 emulsion. The response is initially brittle, with a ductile postpeak failure, typical for the EAMs. Comparison of Figures 1 and 2 indicates that there is no substantial shear strength difference.

To quantify the difference between ductile and brittle responses, the secant modulus (E_{sec}) was used. Secant modulus was defined as the ratio of 50 percent of the failure deviator stress to the corresponding strain. Secant modulus is generally insensitive to confining pressure (*11*); thus, the average secant modulus of the confining pressures was used to characterize the stress-strain response. Table 4 shows that all of the EAM secant moduli increase in excess of 50 percent over the untreated aggregates.

TABLE 4 Properties from Triaxial Testing

Agg.	Binder Type	Shear Strength				Repeated Load		
		ϕ° [a]	C[a] kPa	E_{secb} MPa	Shear Str.[c] kPa	K[d] MPa	n[d]	ϵ_p%[e]
A Dense	none	27.6	158	21	642	8.8	0.493	2.2
	HFE-300	26.6	241	152	893	25.7	0.414	0.4
	CSS-1	42.3	262	193	1468	73.5	0.258	0.6
	AC-5	---	---	1288	10728[f]	97.2	0.394	0.1
B Dense	none	41.0	117	103	777	11.6	0.557	1.0
	HFE-300	35.1	214	179	1009	24.4	0.440	0.4
	CSS-1	31.5	310	165	1258	53.7	0.341	0.4
	AC-5	---	---	1192	10245[f]	304.0	0.252	0.1
C Open	none	44.7	55	41	591	16.9	0.492	1.1
	HFE-300	35.4	83	131	510	19.4	0.466	3.3
	CSS-1	---	---	172	978	19.7	0.481	0.2
	AC-5	17.6	627	213	1773	168.5	0.242	0.5
D Dense	none	45.4	41	117	542	3.2	0.742	0.6
	HFE-300	38.0	172	131	927	43.5	0.365	0.4
E Open	none	41.6	69	48	579	7.4	0.597	0.5
	HFE-300	33.1	96	131	522	60.3	0.330	1.4

[a] Mohr-Coulomb friction angle, ϕ degrees, and cohesion, C.
[b] Secant modulus, E_{sec} at 50% of peak stress.
[c] Deviator stress at σ_3=69 kPa (10 psi).
[d] Resilient modulus constants, $E_R = K\theta^n$.
[e] Predicted permanent strain, $\epsilon_p\% = AN^b$, at N =1000.
[f] Unconfined compressive strength using 445kN ram.

--- Specimen tested unconfined

1 kPa = 0.145 psi

The results of the numerous shear strength tests are presented in Table 4. For comparative purposes, the predicted shear strength (deviator stress) at 69-kPa (10-psi) confining pressure was calculated using Equations 5 and 6. Several general trends are evident from a review of the shear strength responses:

1. The untreated materials generally indicate a ductile response, whereas the EAMs exhibit a brittle failure, as demonstrated by comparison of Figures 1 and 2.
2. EAMs generally have a higher cohesion than the untreated aggregates; the friction angle generally decreases by emulsion treatment.
3. The dense-graded aggregate shear strength (σ_d) is improved with emulsion addition.
4. The shear strength of the open-graded aggregate EAM with HFE-300 is slightly less than the untreated aggregates. This is attributed to the heavy volatile constituents of HFE-300 emulsion. The secant modulus is still substantially improved over the untreated aggregate.
5. EAM shear strength is substantially less than the BAM shear strength.

REPEATED LOADING RESULTS

The repeated loading sequence evaluated rutting potential and resilient modulus. EAM rutting potential is considerably less than the potential rutting of untreated aggregates (Table 4). The predicted permanent deformation after 1,000 cycles generally decreases by 60 percent or more.

The open-graded aggregate EAMs (Aggregates C and E) increased in rutting potential with addition of HFE-300 emulsion. This increase is attributed to the heavy volatile constituents of high-float emulsions. However, field performance does not suggest that significant rutting occurs in EAM pavements made with HFE-300 or CSS-1 emulsions.

Referring to Table 4, the EAMs are less stress sensitive (lower n value) than the untreated aggregates. This trend holds for the dense-graded and open-graded EAMs. In all cases, EAMs have a larger K and lower n, which contribute to an improved modulus response.

Figure 3 compares the EAM modulus parameters for the θ-model from this research. Also demonstrated is the "typical" relationship for untreated aggregates from extensive research by Rada and Witczak (*22*). The EAMs indicate an improved modulus response resulting from the improvement in the K and n parameters.

The increase in K is related to an increase in shear strength, as illustrated in Figure 4. Figures 3 and 4 include results from testing in this research and additional testing, described further by Anderson (*11*), on untreated aggregates, EAMs, and BAMs.

DCP RESULTS

Table 5 summarizes the DCP penetration rates. The responses indicate that emulsion treatment decreases the penetration rate to approximately one-third of the untreated aggregate values. Figure 5 demonstrates the average penetration rate for the top 152 mm (6 in.) for Aggregate C. At depths greater than 152 mm (6 in.) in the laboratory mold, overburden effects reduce the differences between materials.

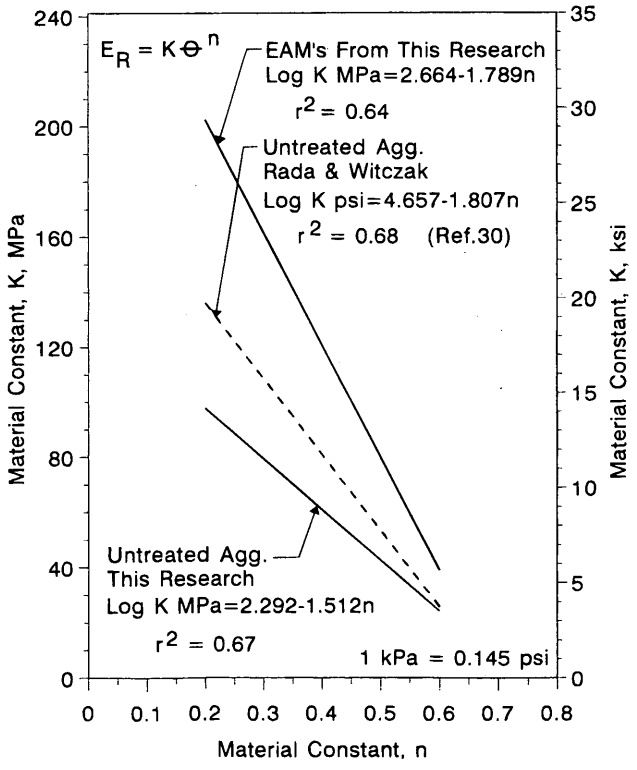

FIGURE 3 Comparison of modulus parameters.

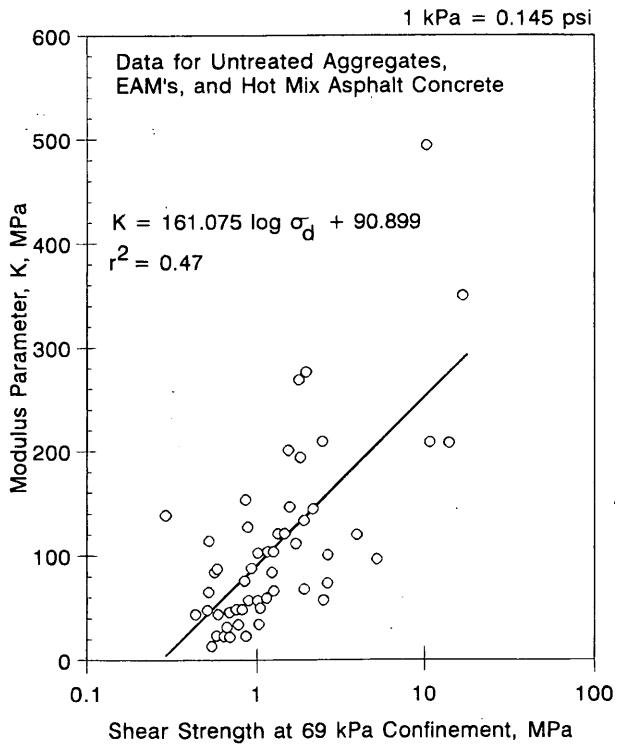

FIGURE 4 Modulus K and shear strength.

TABLE 5 Laboratory Dynamic Cone Penetrometer

Aggregate	DCP Penetration Rate, mm/blow	
	Untreated	EAM w/HFE-300
A	15	3
B	9	3
C	27	10
D	7	5
E	---	7

--- Test not conducted

1 mm = 0.039 inch

The DCP illustrates an important effect of the emulsion on a typical open-graded aggregate (Figure 5). Open-graded, untreated aggregates are dependent on aggregate interlock for strength. Confinement or cohesion, or both, is needed to maintain interparticle contact.

The cohesion required is apparently small, as 28 kPa (4 psi) was sufficient for Aggregate C (Table 4). This small amount of cohesion significantly increased the shear strength, as indicated by the penetration rate. The DCP penetration rate decreased from 76 mm (3.0 in.) to 13 mm (0.5 in.) (Figure 5). The cohesion permits open-graded EAMs to function as a stabilized pavement layer.

The relation indicated in Figure 6 can be used to convert DCP penetration rate to California bearing ratio (CBR). Figure 6 was developed from work by Kleyn (*23*) for a wide range of stabilized materials; similar correlations exist for unconfined compressive strength (*24*, *25*). The EAM penetration rates in Table 5 correlate to a CBR of approximately 100 for the dense-graded EAMs and 24 for the open-graded EAMs.

MIXING EFFECTS

Table 4 indicates the trends for the plant-mixed EAMs, Aggregates D and E. Aggregates D and E had been stockpiled for approximately 2 months before sampling and testing. The plant-mixed specimens indicate the same trends and responses as the laboratory-

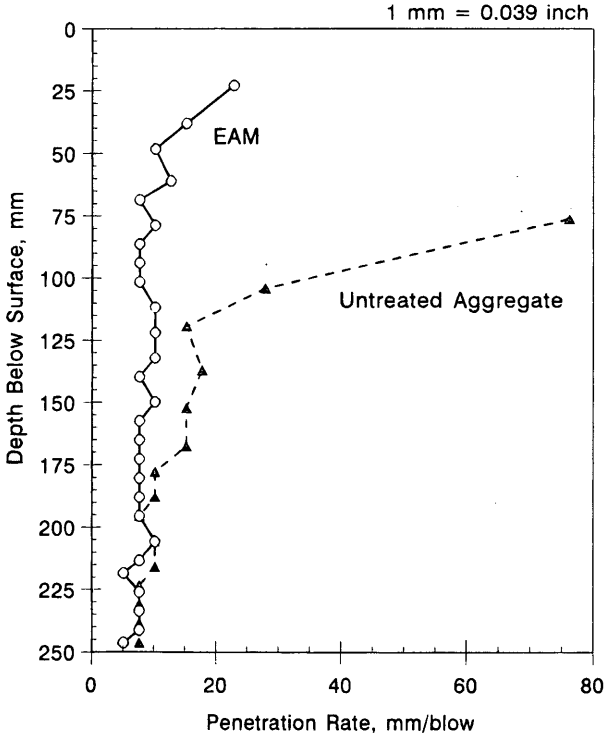

FIGURE 5 Aggregate C DCP.

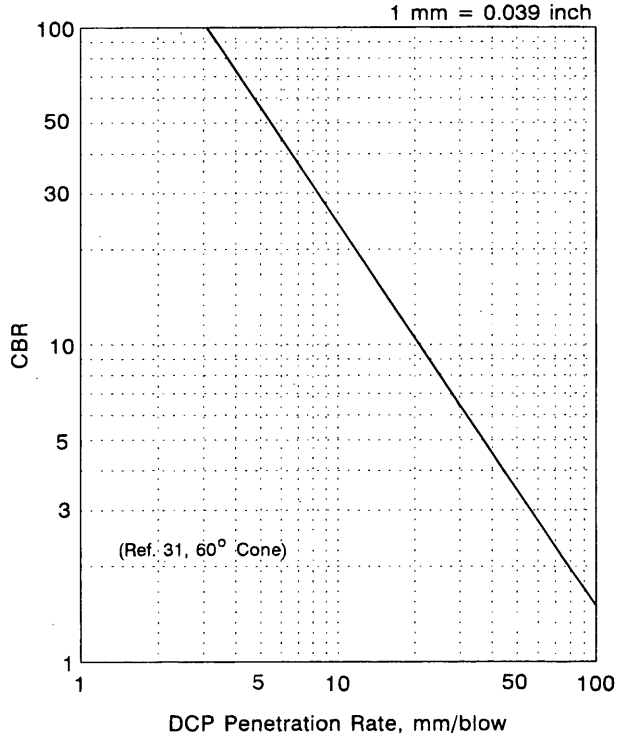

FIGURE 6 DCP-CBR conversion.

mixed specimens; emulsion improves the engineering properties of the aggregate.

BINDER EFFECTS

Table 4 indicates comparisons between HFE-300 and CSS-1. The consistent trend is that CSS-1 emulsion improves EAM shear strength and modulus response more than HFE-300. This trend is more apparent for dense-graded than open-graded EAMs. However, both types of emulsions provide acceptable EAM performance.

Table 4 also compares the EAMs with BAM-type mixes using AC-5. There is substantial improvement in all responses using asphalt cement to treat the aggregate. The BAM shear strengths are an order of magnitude greater than those of the EAMs. The modulus responses are also increased significantly, and the permanent deformation potential is reduced greatly.

To evaluate an EAM "fully cured" strength, additional specimens were compacted at the 50 percent moisture-loss condition and then cured to constant weight for several months. The curing conditions were 38°C (100°F) and 25 percent relative humidity.

Table 6 demonstrates the results of the fully cured EAM specimens. Comparison with the AC-5 results in Table 4 indicates that the EAM properties are significantly less than the BAM mixes. The important conclusion is that EAMs do not have the potential to ultimately attain properties similar to HMAC.

CONCLUSIONS

EAM properties and responses are not constant, but vary with moisture content. Tables 4–6 summarize typical EAM engineering properties at various cure conditions. Specific properties and trends that were identified are as follows:

1. EAM engineering properties improve with increased moisture loss.
2. The magnitude of EAM shear strength is not improved greatly over the untreated granular material, but the EAM secant modulus is significantly higher than the untreated aggregate.
3. Dense-graded EAM shear strength generally exceeds open-graded EAM shear strength.
4. EAM modulus is improved over the untreated aggregate modulus.
5. EAM modulus is stress hardening, that is, E_R increases with an increase in bulk stress, θ.

The obvious trend is that EAM engineering properties (shear strength, resilient modulus, secant modulus, rutting potential, DCP) improve with increased moisture loss. EAM engineering properties continue to improve with curing after compaction. However, even after curing to constant weight, EAM properties are not equivalent to those of HMAC. Thus, EAMs are displaying characteristics of an improved granular material.

TABLE 6 Fully Cured EAM Triaxial Properties

		Shear Strength				Repeated Load		
Agg.	Emulsion	ϕ^{oa}	C[a] kPa	E_{secb} MPa	Shear Str.[c] kPa	K^d MPa	n^d	ϵ_p%[e]
A Dense	HFE-300	---	---	675	2370[f]	114.2	0.313	0.1
	CSS-1	---	---	413	5126[f]	35.9	0.507	0.02
B Dense	HFE-300	36.7	427	138	1907	27.8	0.461	0.3
	CSS-1	---	---	482	3879[f]	45.4	0.501	0.1
C Open	HFE-300	37.9	324	262	1544	126.7	0.239	1.4
	CSS-1	43.5	124	200	882	65.8	0.341	1.7
D Dense	HFE-300	44.0	296	158	1709	56.2	0.354	0.2
E Open	HFE-300	32.9	34	131	290	85.9	0.247	3.6

[1] Mohr-Coulomb friction angle, ϕ degrees, and cohesion, C.
[2] Secant modulus, E_{sec} at 50% of peak stress.
[3] Deviator stress at σ_3=69 kPa (10 psi).
[4] Resilient modulus constants, $E_R = K\theta^n$.
[5] Predicted permanent strain, $\epsilon_p\% = AN^b$, at N =1000.
[6] Unconfined compressive strength using 445kN ram.

--- Specimen tested unconfined

1 kPa = 0.145 psi

ACKNOWLEDGMENT

This paper is based on research results previously developed in Project IHR-527, Mechanistic Design for Local Roads, sponsored by the Illinois Department of Transportation.

REFERENCES

1. Darter, M. I., S. R. Ahlfield, P. L. Wilkey, and R. G. Wasill. *Development Of Emulsified Asphalt-Aggregate Cold Mix Design Procedure.* IHR-505, Transportation Engineering Series No. 22. University of Illinois, Urbana, Feb. 1978.
2. Schmidt, R. J., L. E. Santucci, and L. D. Coyne. Performance Characteristics of Cement-Modified Asphalt Emulsion Mixtures. *Proc., AAPT,* Vol. 42, Feb. 1973.
3. Terrel, R. L., and C. L. Monismith. Evaluation of Asphalt-Treated Base Course Materials. *Proc., AAPT,* Vol. 37, 1968.
4. Terrel, R. L., and C. K. Wang. Early Curing Behavior of Cement-Modified Asphalt Emulsion Mixtures. *Proc., AAPT,* Vol. 42, Feb. 1973.
5. The Asphalt Institute. *Thickness Design Asphalt Pavements for Highways and Streets.* MS-1, Lexington, Ky., Feb. 1991.
6. Santucci, L. E. Thickness Design Procedure for Asphalt and Emulsified Asphalt Mixes. *Proc., 4th International Conference on Structural Design of Asphalt Pavements,* Ann Arbor, Mich., Aug. 1977.
7. The Asphalt Institute. *Research and Development of The Asphalt Institute's Thickness Design Manual (MS-1),* 9th ed. Research Report No. 82-2. Lexington, Ky., Aug. 1982.
8. Walter, J. *Development of Failure Criteria for Open-Graded Asphalt Emulsion Mixes.* Transportation Engineering Report 77-9. Department of Civil Engineering, Oregon State University, Corvallis, 1977.
9. Hicks, R. G., K. R. Valdez, D. S. Decker, and C. E. Christopher. *Performance Update of Open-Graded Emulsified Asphalt Pavements in the Pacific Northwest.* Transportation Research Report 88-7. Transportation Research Institute, Oregon State University, Corvallis, March 1988.
10. Kallas, B. F., and J. F. Shook. *San Diego County Experimental Base Project Final Report.* Research Report 77-1. The Asphalt Institute, Lexington, Ky., Nov. 1977.
11. Anderson, J. R. *Characterization of Emulsion Aggregate Mixtures.* Doctoral thesis. University of Illinois, Urbana, May 1994.
12. Thompson, M. R. ILLI-PAVE Based NDT Analysis Procedures. In *Non-Destructive Testing of Pavements and Backcalculation of Moduli,* ASTM STP 1026, Philadelphia, Nov. 1989.
13. Thompson, M. R., and K. Cation. *A Proposed Full-Depth Asphalt Concrete Thickness Design-Procedure.* Transportation Engineering Series No. 45, Illinois Cooperative Highway and Transportation Series No. 213. University of Illinois, Urbana, July 1986.
14. Elliott, R. P., and M. R. Thompson. *Mechanistic Design Concepts for Conventional Flexible Pavements.* Transportation Engineering Series No. 41, Illinois Cooperative Highway and Transportation Series No. 207. University of Illinois, Urbana, Aug. 1984.
15. *NCHRP Report 259: Design of Emulsified Asphalt Paving Mixtures.* TRB, National Research Council, Washington, D.C., 1983.
16. Illinois Department of Transportation. *Implementation Package: Emulsified Asphalt-Aggregate Mixtures-Mix Design and Design Coefficients.* Physical Research Report No. 91. Bureau of Materials and Physical Research, Springfield, Ill., April 1981.
17. *A Basic Asphalt Emulsion Manual,* 2nd ed. Manual Series No. 19. The Asphalt Institute, Lexington, Ky. (formerly College Park, Md.), 1979.
18. Willis, J. *White Paper—Testing of Class B Mixes Used in Illinois.* University of Illinois, Urbana, Aug. 1993, in preparation.
19. *Asphalt Cold Mix Manual,* 3rd ed. Manual Series No. 14. The Asphalt Institute, Lexington, Ky., 1989.
20. Ayers, M. E. *Rapid Shear Strength Evaluation of In Situ Granular Materials Utilizing the Dynamic Cone Penetrometer.* Ph.D. thesis. University of Illinois, Urbana, Oct. 1990.
21. Thompson, M. R., and K. L. Smith. Repeated Triaxial Characterization of Granular Bases. In *Transportation Research Record 1278,* TRB, National Research Council, Washington, D.C., Jan. 1990.
22. Rada, G., and M. W. Witczak. Comprehensive Evaluation of Laboratory Resilient Moduli Results for Granular Material. In *Transportation Research Record 810,* TRB, National Research Council, Washington, D.C., 1981.
23. Kleyn, E. G. *The Use of The Dynamic Cone Penetrometer (DCP).* Report L2/74. Transvaal Roads Department, Pretoria, South Africa, 1975.
24. Bester, M. D., and L. Hallat. *Dinamiese Kegelpeilstaaf (DKP) [Dynamic Cone Penetrometer (DCP)].* University of Pretoria, Pretoria, South Africa, 1977.
25. De Villiers, P. J. *Dinamiese Kegelpeilstaaf Korrelasie met Eenassigge Druksterkte. [Dynamic Cone Penetrometer Correlation with Unconfined Compressive Strength].* University of Pretoria, Pretoria, South Africa, 1980.

The contents of this paper reflect the views of the authors, who are responsible for the facts and accuracy of the data. The contents do not necessarily reflect the official views of the Illinois Department of Transportation. This paper does not constitute a standard, specification, or regulation.

Publication of this paper sponsored by Committee on Characteristics of Bituminous Paving Mixtures to Meet Structural Requirements.

Laboratory Determination of Thermal Properties of Asphalt Mixtures by Transient Heat Conduction Method

T. F. FWA, B. H. LOW, AND S. A. TAN

A laboratory procedure for determining the thermal conductivity (k) and diffusivity (α) of asphalt mixtures by means of a transient heat conduction experiment is described. It is first established that the plane wall theory of heat conduction can be applied to a finite-slab problem if the thickness-to-width ratio is kept within 0.2. The main concept of the proposed approach is to determine the k and α values that would match the theoretical temperature-time response with the measured response. Two different test procedures are studied: a vertical slab and a horizontal slab experiment. The experimental details involved in the two test procedures are described. The theoretical and measured temperature-time responses can be matched by one of the following two schemes: Scheme I matches the inflection points of the two temperature-time history curves, whereas Scheme II relies on a curve-fitting technique. Results of tests on two different dense-graded asphalt mixtures are used to evaluate the relative merits of the two experimental procedures and the two matching schemes. The results indicate that the vertical slab experiment and the Scheme I matching method yielded more accurate estimates of the k and α values. The computed values were found to compare well with reported values in the literature.

The mechanical properties of asphalt mixtures are temperature dependent, and knowledge of the temperature state in an asphalt pavement is required often in pavement thickness design (*1*), compaction of asphalt mixtures during pavement construction (*2,3*), structural evaluation of pavement (*4*), and performance analysis of pavement under traffic loads (*5,6*). It is an advantage if the engineer can determine the thermal properties of the asphalt materials used, thereby allowing the temperature state of the pavement under service conditions to be estimated with confidence. Unfortunately, thermal property determination is not a standard test in most highway laboratories and is performed rarely by highway engineers. The conventional steady-state methods of measuring thermal conductivity [such as ASTM C518 (*7*)] suffer the disadvantage that the time taken to reach thermal equilibrium may be inconveniently long for asphalt mixtures, which are poor conductors of heat. The long period to reach steady state also restricts the method's use for measurements on damp materials because of redistribution and drying of moisture within the test specimen.

A thin-slab transient heat conduction procedure developed by the authors to determine the thermal conductivity (k) and diffusivity (α) of asphalt mixtures is described. By means of the heat conduction theory for plane walls, the time history of temperature at the midpoint of a thin slab is first derived. Next, this theoretical temperature-time history is matched with experimental measurements to arrive at a pair of k and α values that provide the best fit between the theoretical and measured temperature-time responses. Two possible experimental procedures, one with a vertical slab and one with a horizontal slab, are presented. Also presented are two different temperature-time history matching schemes: one relies on matching of inflection points of the temperature-time curves, and the other on matching of temperature-time curves by means of a curve-fitting technique. The relative merits of the two experimental procedures and the two matching schemes are discussed.

Center for Transportation Research, Department of Civil Engineering, Kent Ridge, Singapore 0511, Republic of Singapore.

APPLICATION OF PLANE WALL THEORY TO THIN SLAB PROBLEM

Plane Wall Heat Conduction Theory

The theoretical time history for the temperature at the midpoint (i.e., central point of the midplane) of a finite thin slab can be derived by considering the case of an infinitely large plane wall. When a plane wall with a uniform initial temperature of T_i is immersed suddenly in a fluid medium of temperature T_f, the time history of temperature at the midplane, T, can be expressed in a nondimensional form as follows (*8*):

$$\theta = \sum_{n=1}^{\infty} C_n \exp(-\xi_n^2 F_0) \quad (1)$$

where

$$\theta = \frac{(T - T_f)}{(T_i - T_f)}$$

is the normalized midplane temperature;

$$C_n = \frac{4 \sin \xi_n}{2\xi_n + \sin(2\xi_n)}$$

ξ_n = discrete values equal to the positive roots of the following transcendental equation, $\xi_n \tan \xi_n = B_i$, where B_i is the Biot number given by hd/k, h being the convection heat transfer coefficient, d one-half of the thickness of wall, and k the thermal conductivity of wall material; and

F_0 = $(\alpha t/d^2)$ is dimensionless expression for time t, also called the Fourier number, in which α is the thermal diffusivity of the wall material.

For a plane wall with fixed thickness d subjected to a temperature differential of $(T_f - T_i)$, the relationship between normalized temperature and time (i.e., θ and F_0) is dependent on h, k, and α. It is noted that this relationship holds for the respective average values of h, k, and α over the temperature range from T_i to T_f.

Adaptation to Analysis of Thin Slab Problem

The foregoing plane wall theory can be applied in practice to study the time variation of temperature at the midpoint (i.e., central point of the midplane) of a square slab of dimension $2L \times 2L \times 2d$, provided the ratio of d/L is sufficiently small that the error involved in temperature-time response estimation is negligible.

The exact solution for the case of a square slab can be obtained by linear superposition of the plane wall solutions in the three orthogonal planes encompassing the square slab. The time history of temperature at the midpoint of a square slab is thus given by

$$\theta_{slab} = \theta_{plane\ wall\ x} \times \theta_{plane\ wall\ y} \times \theta_{plane\ wall\ z} \quad (2)$$

Figure 1 shows solutions for equations 1 and 2 obtained for different combinations of k values and d/L ratios for an air flow velocity of 10 m/sec. It was found that the computed temperature history at the midpoint of square slabs coincides with that of a plane wall ($d/L = 0$) for values of d/L up to 0.2. For d/L ratios greater than 0.2, deviations from the plane wall behavior become progressively larger. Based on these results, a limiting d/L ratio of 0.2 for square slabs was adopted in this study to ensure that the temperature variations at the midpoint of slab can be modeled using the one-dimensional plane wall theory.

EXPERIMENTAL PROCEDURES

Choice of Fluid Medium and Flow Control

It has been established that the parameters that influence the time history of temperature at the midpoint of a thin slab are the convection heat transfer coefficient h, the thermal conductivity k, and diffusivity α of the slab material. The ability to control the temperature, flow pattern, and velocity of the fluid medium, thereby maintaining a uniform heat transfer rate (hence constant h) during the test, is probably the single most important factor in the experiment to determine k and α.

Air was selected as the fluid medium, as water would not be suitable for determining k and α of damp asphalt mixtures. A high-precision temperature chamber that could control temperature stability and uniformity up to ± 0.5°C was used for the experiment. The air flow direction was horizontal, with a velocity of approximately 10 m/sec. In the present study, air velocity during the test was measured using an anemometer. As the thermal properties of asphalt materials such as k and α are known to vary with temperature (*9*), the choice of test temperatures T_i and T_f should reflect the temperature range experienced by the pavement of interest.

Specimen Preparation

Two dense-graded asphalt mixtures, designated W1 and W3 and shown with their respective mix compositions in Table 1, were tested in this study. Four slabs were prepared for each of the two mix types. Each slab measured 250 × 250 mm, with a thickness of approximately 40 mm. Each slab was compacted in two equal layers to allow thermocouples to be placed at the midplane position. One-half of the amount of the mixture was first compacted in a split steel mold by means of a static press at a pressure of 40 MPa at 135°C for 3 min. A thermocouple was placed at the midpoint before the second layer was compacted at 135°C, a pressure of 50 MPa for 5 min. The magnitudes of compaction pressure in the two stages were selected so that the densities of the two layers would be approximately equal. The average bulk density of the W1 specimens was 2.204 g/cm^3 and that of the W3 specimens was 2.254 g/cm^3. The corresponding average percentages of air voids were 7.3 and 6.6 percent.

Test Procedure

The test temperatures of $T_i = 25$°C and $T_f = 60$ C° were adopted in this study to represent the typical range of pavement temperature in the tropical climate of Singapore. Two possible test procedures were studied, as shown in Figure 2. The first one was a vertical slab

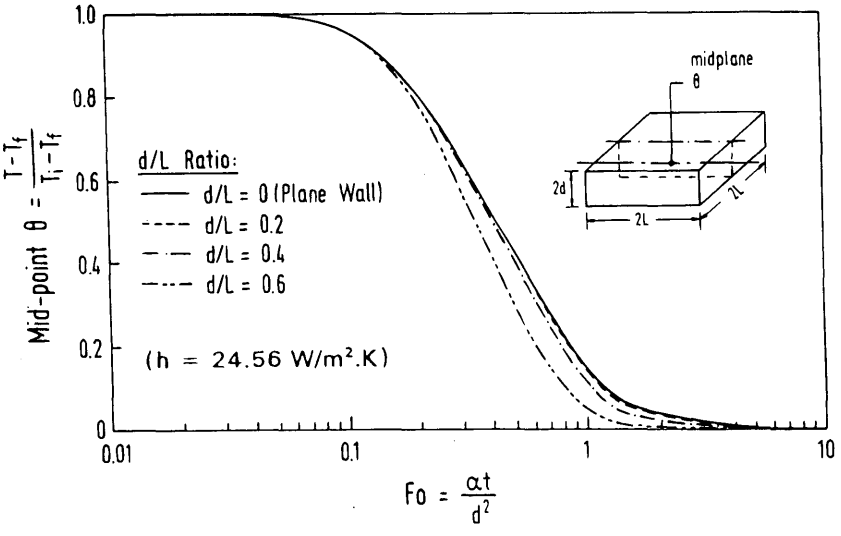

FIGURE 1 Theoretical temperature-time history curves for finite slab as a function of thickness-to-width ratio.

TABLE 1 Mix Composition of Asphalt Mixtures Tested

Mix Type	Binder Content	Aggregate size distribution (% passing)							
		19mm	13mm	9.5mm	6.4mm	3.2mm	1.2mm	0.3mm	0.075mm
W3	5.5%	100	95	90	77	58	37	19	6
W1	5.5%	100	100	100	95	74	47	27	6

Notes: (1) Granite aggregates are used in Singapore.
(2) Asphalt is of penetration grade 60/70.

experiment, in which the slab was positioned vertically in a horizontal air flow, and the second method was a horizontal slab experiment, in which the slab lay flat with its top surface exposed to the air flow.

Vertical Slab Experiment

The test slab was first placed in the temperature chamber set at T_i = 25°C. After thermal equilibrium was reached, the chamber temperature was raised to 60°C. The chamber took approximately 30 sec to achieve a uniform temperature of 60°C. The changes of temperature at the midpoint were recorded at 10-sec intervals by an automatic data recording system. For this study, the test was only necessary to be conducted up to the point at which the midpoint temperature reached 53°C.

Horizontal Slab Experiment

The test procedure was the same as that for the vertical slab experiment. The two experiments only differed in the test setup. In the horizontal slab experiment, the sides and the base of the slab were fully insulated using polyfoam. Only the top surface was exposed

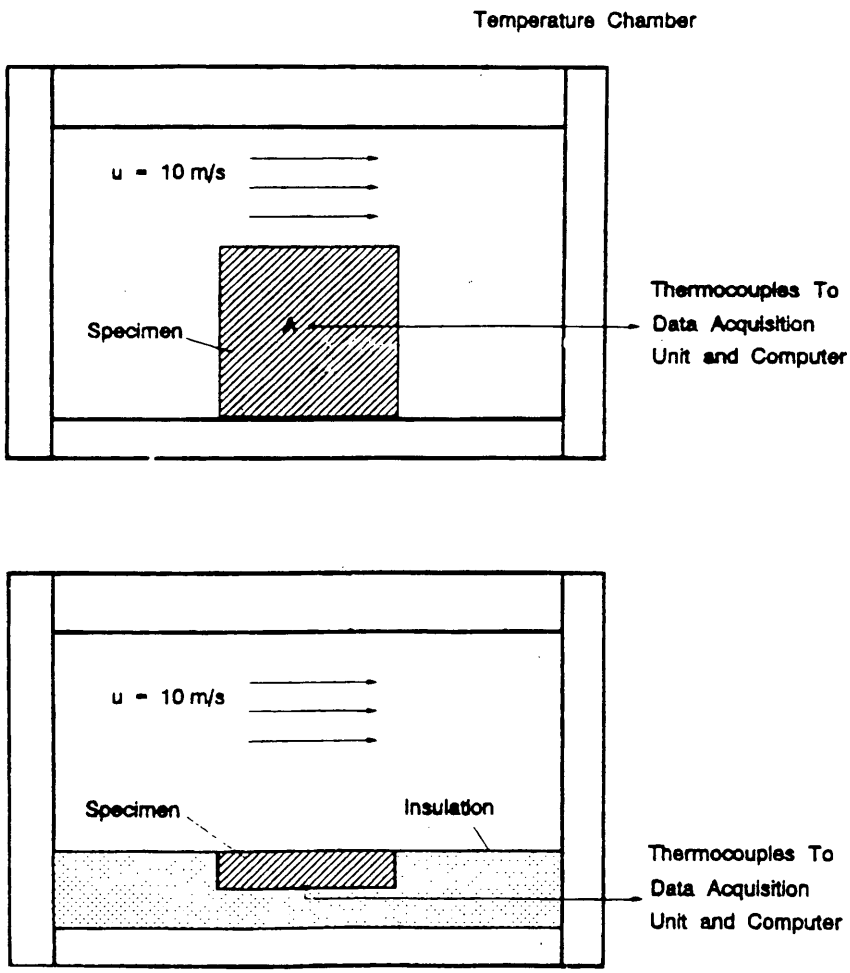

FIGURE 2 Schematic diagrams of test setup: *(a)* vertical slab experiment; *(b)* horizontal slab experiment.

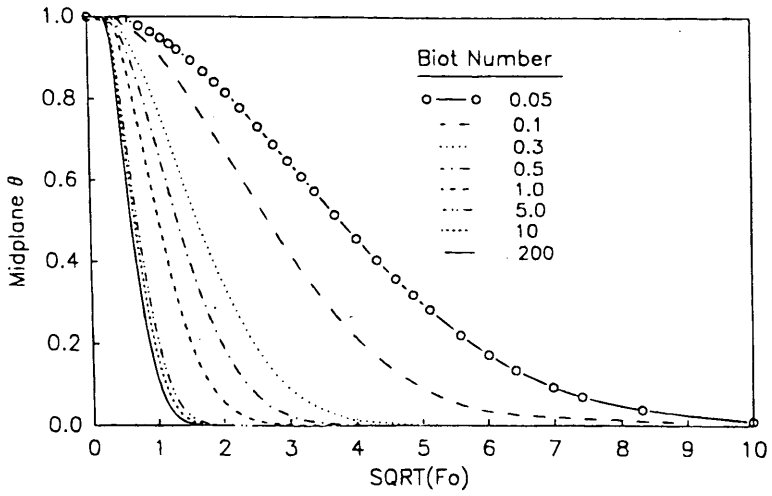

FIGURE 3 Theoretical temperature-time history curves for plane wall plotted in time scale represented by $\sqrt{F_o}$.

to the air flow. The point of temperature measurement was also different. Instead of monitoring temperature at the central point in the midplane, the thermocouple was fixed at the central point of the bottom face to measure the temperature variation at that point. It should be mentioned that this horizontal slab experiment is not constrained by the *d*/*L* restriction, and that the value of *d* to be used in the computation is 40 mm.

DETERMINATION OF *k* AND α

Scheme I

It is apparent from Figure 1 that there exists an inflection point in each of the θ versus log(F_o) curves. Figure 3 indicates that the same is also true in a θ versus $\sqrt{F_o}$ plot. The purpose of Scheme I is to determine the *k* and α values of the test material by matching the theoretical and experimental inflection points based on the θ versus $\sqrt{F_o}$ plot. The equation for a tangent to a θ versus $\sqrt{F_o}$ curve is

$$\theta = M\sqrt{F_o} + C \tag{3}$$

By substituting $F_o = \alpha t/d^2$, we have

$$\theta = M\sqrt{\frac{\alpha}{d^2}} \cdot \sqrt{t} + C \tag{4}$$

where *M* is the theoretical gradient of the θ versus $\sqrt{F_o}$ curve and *C* is the theoretical intercept of the tangent line with the θ axis for either the θ versus $\sqrt{F_o}$ or θ versus $\sqrt{t}$ curve. Equation 4 suggests that if one chooses to plot θ versus $\sqrt{t}$, then its tangent line is given by

$$\theta = m\sqrt{t} + C \tag{5}$$

with

$$m = M\sqrt{\frac{\alpha}{d^2}} \tag{6}$$

where *m* is the theoretical gradient of the θ versus $\sqrt{t}$ curve. Equation 5 provides a convenient means for estimating *m* and *C* at the inflection point from experiment by plotting measured θ against $\sqrt{t}$.

Since the coefficient of convection heat transfer (*h*) and slab thickness (2*d* for vertical slab and *d* for horizontal slab experiment) is known in conducting a transient heat conduction experiment, it is possible to derive theoretically from Equation 1 the inflection point, designated (θ*, $\sqrt{F_o}$*), and also the gradient M* and intercept C* at the inflection point for any given B_i value. For example, Table 2 gives the computed values of inflection point parameters for the experimental conditions selected for the present study.

With the above information, *k* and α of the test material can be determined in the following steps:

1. Determine from experimental data the inflection point in a θ versus $\sqrt{t}$ plot, and the gradient and intercept (designated *m** and *C**) of the tangent line at this point.
2. Knowing *C**, determine B_i and *M** from Table 2.
3. Calculate *k* and α from $k = hd/B_i$ and $\alpha = (m^*d/M^*)^2$, respectively.

To facilitate data processing and computation, a computer program has been written to calculate *k* and α based on the above procedure. It involves expressing the θ versus $\sqrt{t}$ curve as a polynomial regression equation and determining its inflection point analytically. The step-by-step procedure is shown in the flow chart in Figure 4.

Scheme II

Scheme II seeks to determine the pair of *k* and α values that gives a theoretical temperature-time history with the best fit to the measured experimental history. This is performed in this study by finding the *k* and α that minimize the discrepancies between theory and experiment over seven points of the temperature-time curve. The seven points selected were at θ values of 0.2, 0.3, 0.4, 0.5, 0.6, 0.7, and 0.8.

For a given value of *h*, theoretical plots of F_o versus $1/B_i$ produce linear relationships for constant values of θ, as depicted in Figure 5. These relationships can be represented by the following linear

TABLE 2 Theoretical *M* and *C* at Inflection Point of Temperature-Time History Curve

1/Bi	Bi	M	C	$\sqrt{F}$	θ
50.000	0.02	-0.12134	1.217079	5.014941	0.608539
10.000	0.10	-0.27114	1.232590	2.272924	0.616295
6.667	0.15	-0.32637	1.240947	1.901080	0.620473
5.000	0.20	-0.38277	1.250765	1.633795	0.625382
4.000	0.25	-0.42486	1.258857	1.481472	0.629428
3.333	0.30	-0.46774	1.267707	1.355130	0.633853
2.857	0.35	-0.50275	1.275347	1.268355	0.637672
2.500	0.40	-0.53835	1.283455	1.192036	0.641719
2.000	0.50	-0.59967	1.298131	1.082498	0.648986
1.667	0.60	-0.65399	1.311750	1.003398	0.655530
1.429	0.70	-0.70286	1.324376	0.943494	0.661227
1.250	0.80	-0.74713	1.336023	0.896794	0.665999
1.111	0.90	-0.78768	1.346796	0.859356	0.669890
1.000	1.00	-0.82485	1.356697	0.828899	0.672979
0.833	1.20	-0.88348	1.372276	0.787075	0.676906
0.714	1.40	-0.94297	1.387880	0.750949	0.679753
0.667	1.50	-0.97297	1.395625	0.734677	0.680800
0.625	1.60	-0.99389	1.400976	0.723957	0.681442
0.556	1.80	-1.03589	1.411555	0.703833	0.682455
0.500	2.00	-1.07808	1.421915	0.685262	0.683142
0.455	2.20	-1.10573	1.428584	0.673770	0.683572
0.417	2.40	-1.13343	1.435128	0.662777	0.683913
0.385	2.60	-1.16116	1.441528	0.652242	0.684169
0.357	2.80	-1.18889	1.447761	0.642128	0.684338
0.333	3.00	-1.21660	1.453804	0.632403	0.684420
0.313	3.20	-1.23125	1.456983	0.627316	0.684595
0.286	3.50	-1.25322	1.461652	0.619852	0.684835
0.250	4.00	-1.30332	1.471678	0.603624	0.684962
0.222	4.50	-1.32896	1.476642	0.595484	0.685263
0.200	5.00	-1.36240	1.482710	0.585212	0.685411
0.167	6.00	-1.40523	1.490014	0.572298	0.685798
0.143	7.00	-1.43741	1.495075	0.562765	0.686150
0.125	8.00	-1.46255	1.498743	0.555393	0.686451
0.111	9.00	-1.48272	1.501480	0.549520	0.686695
0.100	10.00	-1.49916	1.503575	0.544745	0.686912
0.067	15.00	-1.55027	1.509171	0.529947	0.687609
0.050	20.00	-1.57676	1.511442	0.522265	0.687955
0.033	30.00	-1.60382	1.513228	0.514380	0.688251
0.025	40.00	-1.61745	1.513905	0.510385	0.688382
0.020	50.00	-1.62568	1.514233	0.507960	0.688449
0.017	60.00	-1.63123	1.514411	0.506322	0.688479
0.013	80.00	-1.63807	1.514601	0.504292	0.688529
0.010	100.0	-1.64218	1.514694	0.503070	0.688558
0.000	9999.	-1.65880	1.514848	0.498107	0.688582

regression equations, all with coefficient of determination (r^2) exceeding 0.999.

At $\theta = 0.2$ $F_o = \frac{\alpha' 0.2}{d^2} = 1.62502\left(\frac{1}{B_i}\right) + 0.73506$ (7*a*)

At $\theta = 0.3$ $F_o = \frac{\alpha' 0.3}{d^2} = 1.21661\left(\frac{1}{B_i}\right) + 0.58241$ (7*b*)

At $\theta = 0.4$ $F_o = \frac{\alpha' 0.4}{d^2} = 0.92646\left(\frac{1}{B_i}\right) + 0.47838$ (7*c*)

At $\theta = 0.5$ $F_o = \frac{\alpha' 0.5}{d^2} = 0.70124\left(\frac{1}{B_i}\right) + 0.39826$ (7*d*)

At $\theta = 0.6$ $F_o = \frac{\alpha' 0.6}{d^2} = 0.51726\left(\frac{1}{B_i}\right) + 0.33242$ (7*e*)

At $\theta = 0.7$ $F_o = \frac{\alpha' 0.7}{d^2} = 0.36172\left(\frac{1}{B_i}\right) + 0.27700$ (7*f*)

At $\theta = 0.8$ $F_o = \frac{\alpha' 0.8}{d^2} = 0.22714\left(\frac{1}{B_i}\right) + 0.22752$ (7*g*)

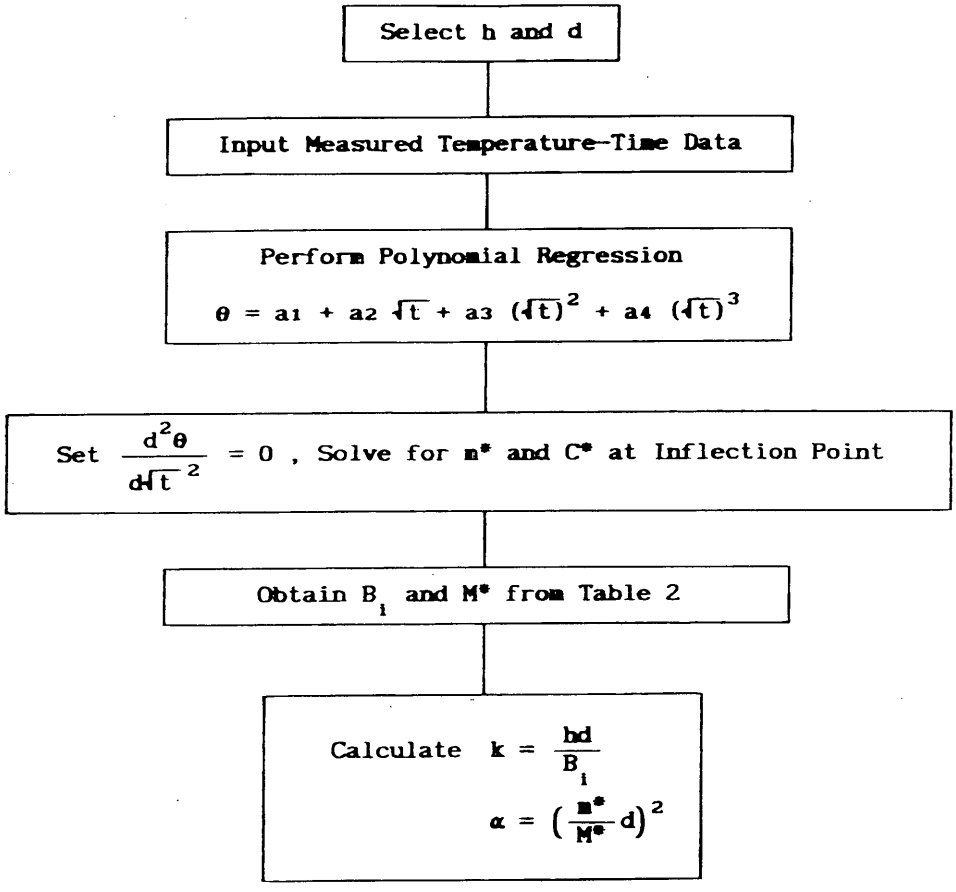

FIGURE 4 Computer program flow chart for Scheme I matching method.

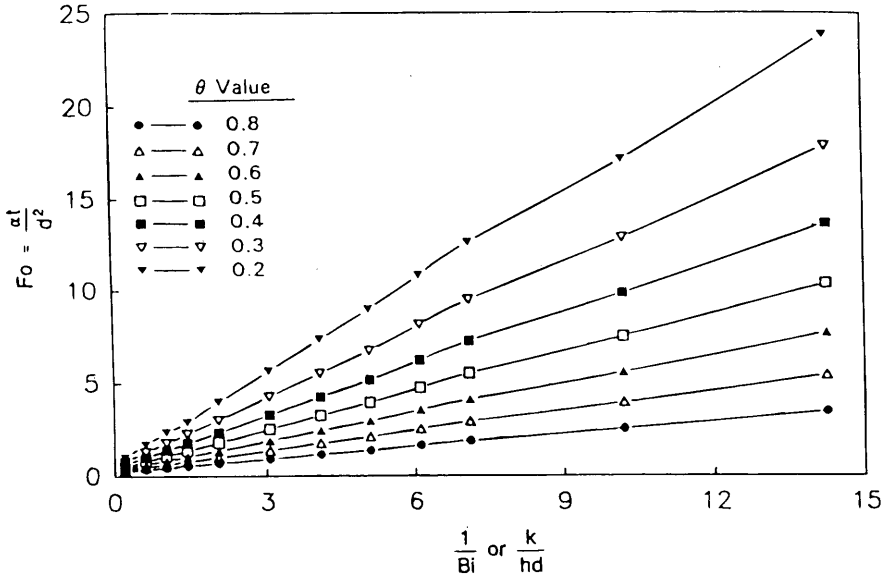

FIGURE 5 Plots of F_o versus $(1/B_i)$ for constant values of θ.

The following iterative process was adopted for estimating k and α:

1. Assume a value of k and compute one α value each from Equation 7(a-g) using experimental values of $t_{0.2}$, $t_{0.3}$, $t_{0.4}$, $t_{0.5}$, $t_{0.6}$, $t_{0.7}$, and $t_{0.8}$.
2. Compute the mean of the seven α values.
3. Using the assumed k value and the mean α value, compute the theoretical values of $t_{0.2}$, $t_{0.3}$, $t_{0.4}$, $t_{0.5}$, $t_{0.6}$, $t_{0.7}$, and $t_{0.8}$ by means of Equation 7($a-g$), respectively.
4. Repeat for other values of k and select the k value that produces the smallest error term defined as follows:

$$\text{ERROR}^2 = \sum_{0=0.2}^{0=0.8} (t_{\text{theoretical}} - t_{\text{measured}})^2 \quad (8)$$

The k values were selected incrementally from the practical range of 0.1 to 7 W/m°K. Figure 6 gives the flow chart of a computer program written to perform the above iterative computation.

EXPERIMENTAL RESULTS

The thermal conductivity k and diffusivity α of the two mix types tested are summarized in Table 3. For each of the four slabs of each mix type, at least four repeated measurements were conducted, respectively, for the vertical and horizontal slab experiments. Both Scheme I and II procedures were applied to estimate k and α. Table 3(a) also presents the k values determined by the steady-state method to serve as a reference. It is believed that k determined from the steady-state method is more accurate because the test condition can be controlled more precisely as compared with the transient methods.

Vertical Versus Horizontal Slab Experiments

Table 3(a) indicates that the horizontal slab experiment tended to produce higher k values than those by the vertical slab experiment. The same general pattern of computed α values was also observed in Table 3(b). One likely reason that led to this consistent difference was the loss of heat through the insulation material. The computa-

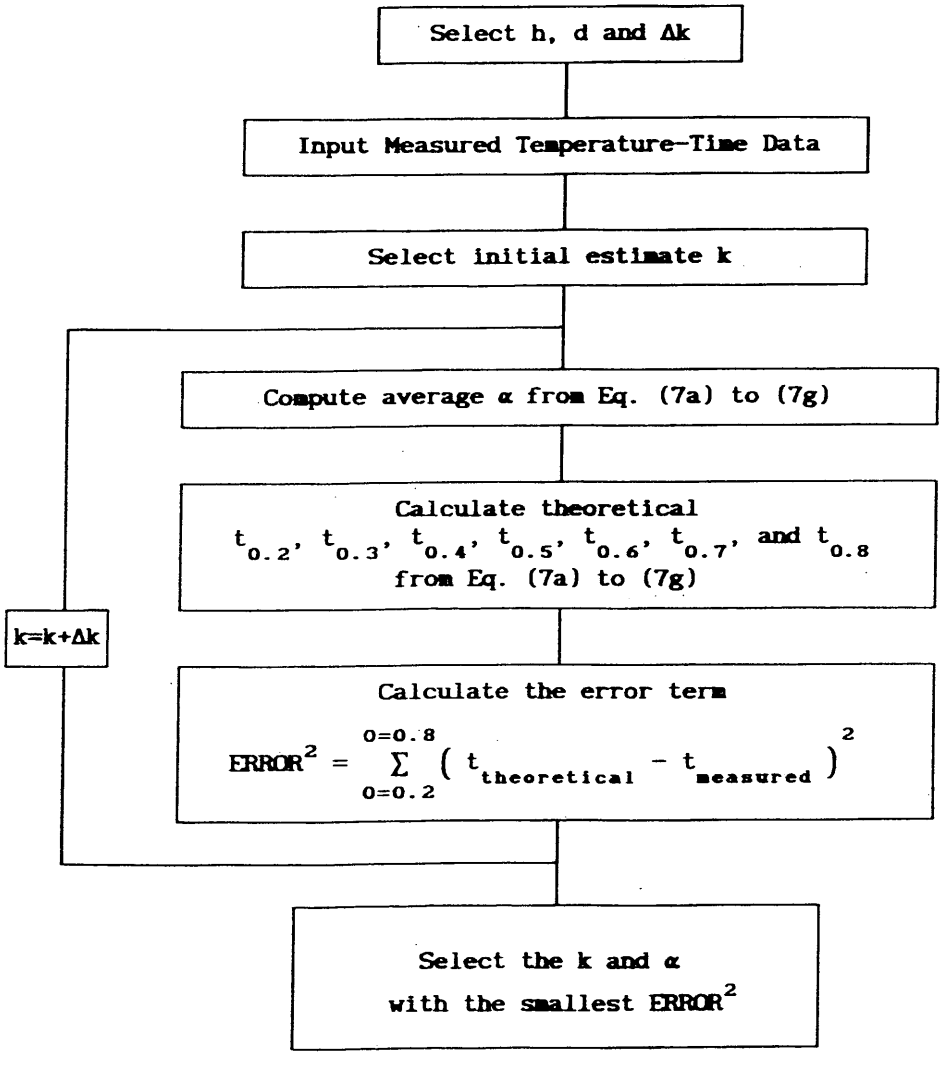

FIGURE 6 Computer program flow chart for Scheme II matching method.

TABLE 3 Values of Thermal Conductivity and Diffusivity Measured By Transient Heat Conduction Method and Steady-State Method

(a) Measured Values of Thermal Conductivity, k, in W/m°K

Asphalt Mixture	Steady State Method	Horizontal Slab		Vertical Slab	
		Scheme I	Scheme II	Scheme I	Scheme II
Mix W1	1.30	1.41	1.66	1.37	0.80
Mix W3	1.33	1.80	1.69	1.44	1.04

(b) Measured Values of Thermal Diffusivity, α, in m^2/s

Asphalt Mixture	Horizontal Slab		Vertical Slab	
	Scheme I	Scheme II	Scheme I	Scheme II
Mix W1	5.83×10^{-7}	6.78×10^{-7}	6.30×10^{-7}	4.13×10^{-7}
Mix W3	6.96×10^{-7}	6.79×10^{-7}	6.13×10^{-7}	5.11×10^{-7}

tion algorithm for the horizontal slab assumed that all heat loss was through the exposed top surface in a one-directional thermal flow from the bottom face of the slab to its top surface. However, this study was not able to determine and account for the amount of heat loss through the polyfoam material.

Compared with the values of k determined by the steady-state method, the results in Table 3(a) suggest that the vertical slab experiment produced more accurate estimates of k than the horizontal slab method. Again, this could possibly be attributed to the better representation of plane wall theory in the vertical wall experiment as compared with the horizontal slab experiment, probably due to imperfect base and side insulation in the latter.

Scheme I Versus Scheme II Matching Methods

Figure 7(a and b) demonstrates examples of Scheme I and II matching for a slab of W3 mix. As the two matching methods make use of different features of the temperature-time history curves, it is of interest to examine the relative accuracy of their results. Comparing the computed values of k by Schemes I and II in Table 3(a), it is observed that Scheme I tended to produce values closer to the k determined by the steady-state method. The only exception was the horizontal slab test on W3 mix, in which Scheme II was able to yield better k estimates. The results in Table 3(a) indicate a clear advantage of using Scheme I for the case of the vertical slab experiment.

That Scheme I produced better results in the study could possibly be explained by the temperature-time histories presented in Figure 8. Two curves for a vertical slab experiment on mix W1 are indicated: one is the measured θ-time curve from the experiment, and the other a theoretical θ-time curve derived based on the k value measured by the steady-state method. It is noted that the discrepancy between the two curves is largest in the initial one-third of the curves between θ values of 1.0 and 0.7, and smallest at the central portion between θ values of 0.4 and 0.6. The discrepancy at the initial part of the experiment must have been caused by the fact that instant change of temperature from 25°C to 60°C was not possible, and approximately 30 sec was required before the chamber temperature could reach 60°C. Scheme I computation typically covers only the portion of the curve between θ values of 0.45 and 0.75, where the discrepancy is the least. Scheme II makes use of a much wider range of the curve, thereby ending up with less accurate estimates of k values.

Requirement for Repeated Measurements

For both vertical and horizontal slab experiments, regardless of whether the Scheme I or II matching technique was used, the coefficients of variation for repeated measurements of k of a slab covered a range of approximately 6 to 24 percent, with an average of approximately 14 percent. This means that to arrive at an estimate of k within ± 10 percent of the true value with 95 percent confidence, one has to make approximately eight repeated measurements. The coefficients of variation for α measurements varied over a slightly smaller range, from approximately 5 to 21 percent. The number of repeated measurements required for k would be sufficient for α.

Comparison of the mean estimated k or α values of the four slabs of each mix type indicates considerably less variation. The W1 mix had coefficients of variation of 7.4 percent for k, and 14.2 percent for α. The corresponding values for W3 mix were 11.6 and 5.7 percent. It may thus conclude that for the two dense-graded mixes, four slabs are sufficient to achieve 95 percent confidence estimates of k and α within 10 percent of their respective true values.

Values of k and α

The test results in Table 3(a and b) indicate consistently that the W3 mix has higher thermal conductivity and diffusivity than the W1 mix. This was true for both the vertical and horizontal slab experi-

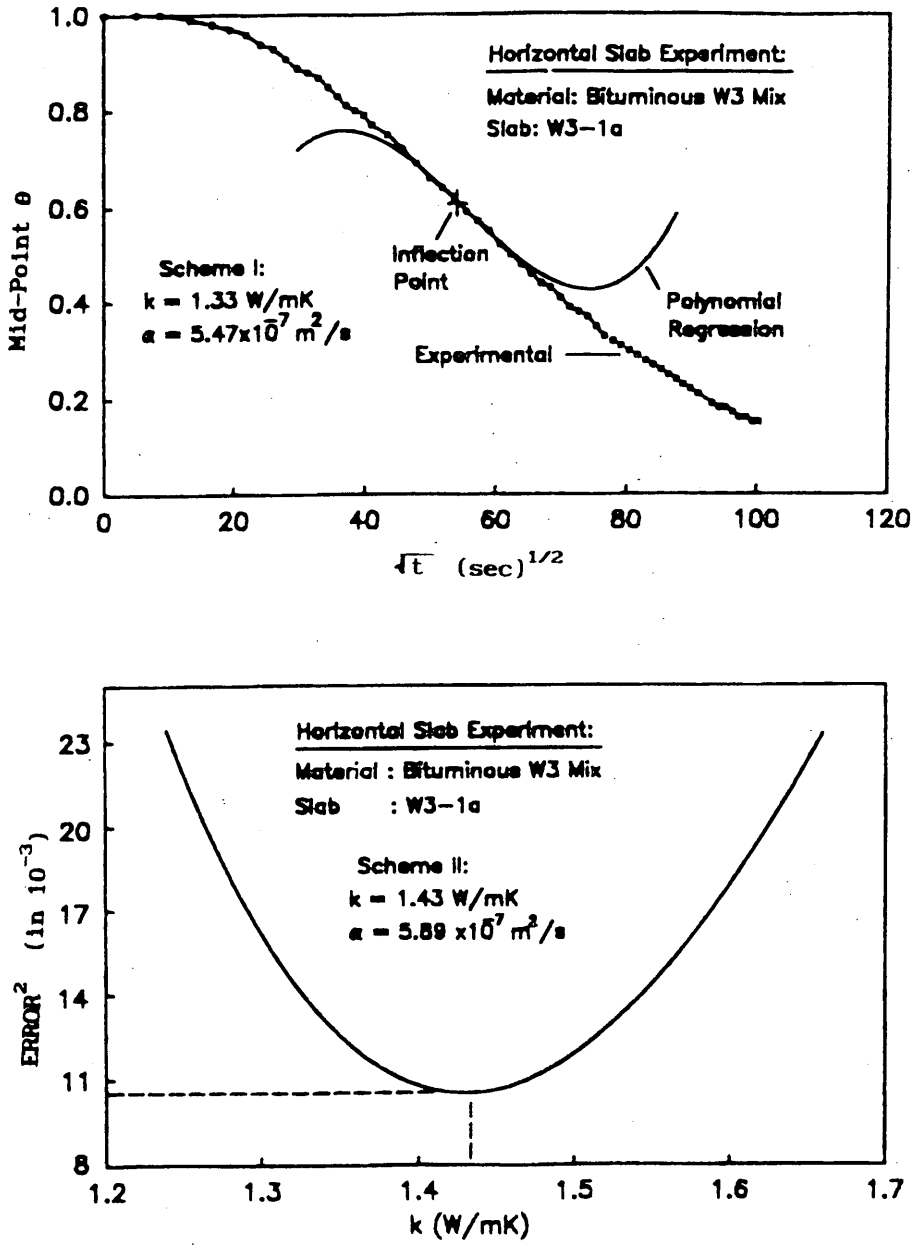

FIGURE 7 Examples illustrating Scheme I and II matching methods: (*a*) polynomial regression of experimental data in Scheme I; (*b*) determination of minimum matching error in Scheme II.

ments, regardless of whether the Scheme I or II matching method was used. Since granite aggregate with thermal conductivity in the range of 2.5 to 4.5 W/m°K (*10*) is a much better heat conductor than asphalt, which has thermal conductivity of the order of 0.6 W/m°K (8), one would expect the k and α of an asphalt mixture to be a function of the mix composition. An examination of the mix composition reveals that both the W1 and W3 mixes had the same amount of granite aggregate (94.5 percent) by weight and used the same grade of bitumen. The only differences were in the percentage of air void and the gradation of the aggregate. The W3 mix had bigger top size aggregate, higher percentage of coarse aggregate, and slightly higher percentage of air void than the W1 mix.

The values of k and α measured in this study compare well with values reported in literature, although a direct check is not possible due to differences in mix composition. Corlew and Rickson (*11*) used a value of 1.2 W/m°K for k in their analysis of temperature profiles in pavement. O'Blenis (*12*) measured in situ k of highway pavements and reported a range of 0.85 to 2.32 W/m°K, with a typical value of 1.45 W/m°K. Aldrich (*13*) applied a k value of 1.5 W/m°K to an analysis of frost penetration, and Saul (*14*) gave a value of 2.23 W/m°K for asphaltic mixtures. Barber (*15*) used a k value of 1.22 W/m°K for temperature range of 10°C to 70°C, and Solaimanian and Kennedy (*16*) used 1.46 W/m°K for approximately the same temperature range, in their respective analysis of

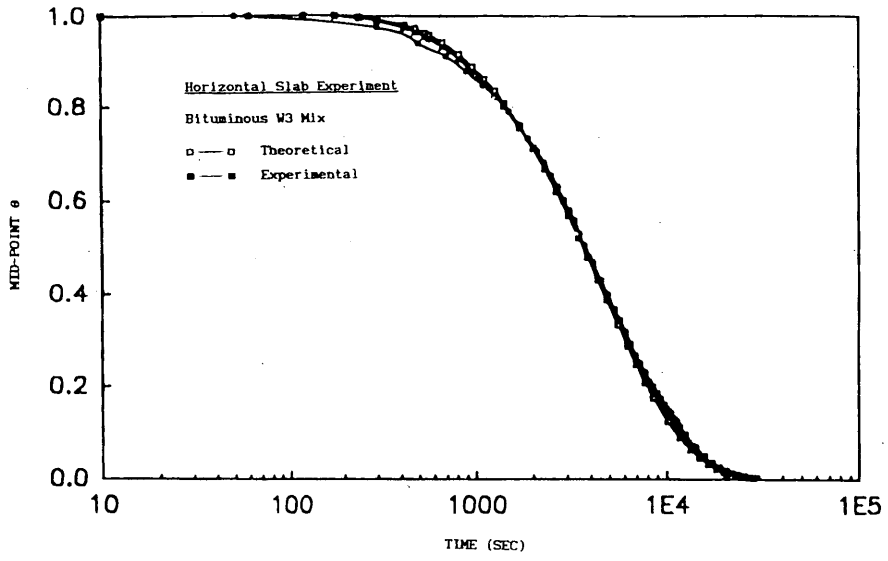

FIGURE 8 Comparison of measured temperature-time history curve from transient heat conduction experiment with theoretical temperature-time history curve plotted using k from steady-state experiment.

asphalt pavement temperature. Highter and Wall (*17*) reported that values of k for asphalt concrete ranged from 0.74 to 2.90 W/m°K after reviewing a considerable number of references regrading this property. Given the variations due to mix composition and the type of aggregate used, it maybe concluded that the values of k measured in this study are compatible with values reported in the literature.

The same conclusion can be drawn on the magnitude of α values computed in Table 3(*b*). The following values of thermal diffusivity of asphalt mixtures have been reported or measured by researchers: 4.61×10^{-7} to 11.98×10^{-7} m²/sec by O'Blenis (*12*), 11.5×10^{-7} m²/sec by Kavianipour and Beck (*9*), and 5.86×10^{-7} m²/sec by Barber (*15*) and Corlew and Rickson (*13*). The computed values of α in Table 3(*a*) are of the same order of magnitude as these reported values.

SUMMARY AND CONCLUSIONS

This study applied the plane wall heat conduction theory to the determination of thermal conductivity and diffusivity of a thin slab based on the temperature-time relationship under transient heat conduction condition. Comparisons of the theoretical temperature-time history of plane walls with those of finite slabs of different dimensions led to the conclusion that for practical applications, the plane wall theory could be applied to slabs with thickness-to-width (d/L) ratios of 0.2 or less.

Two experimental procedures, the vertical and the horizontal slab experiments, were described. Two possible schemes of matching theoretical temperature-time history to measured history for k and α determination were presented: one based on matching of inflection points, and the other based on a curve-fitting technique. Experimental results on two dense-graded mixes were used to evaluate the relative merits of the two procedures and the two matching schemes. The vertical slab experiment required more effort in specimen preparation and positioning of monitoring thermocouples. However, the horizontal slab experiment was found less accurate because of the difficulty in providing perfect insulation to the base and sides of the slab. The Scheme I method of inflection-point matching turned out to be the more desirable technique because of better matching of theoretical and measured temperature-time curves at the central portion of the curves.

For the two dense-graded mixtures studied, statistical analysis of the test results recommended that eight repeated measurements be performed to obtain with 95 percent confidence the estimates of k and α of a single test slab within 10 percent of their respective true values. To achieve the same accuracy level of k and α estimates for a dense-graded mix, the results of this study suggested that four slabs be prepared and tested. On the whole, the values of k and α measured in this study compared well with values reported in literature.

The proposed transient heat conduction method presents an attractive alternative to the conventional steady-state procedure in terms of time requirement and suitability for testing damp asphalt mixtures. It also offers the advantage that both k and α are determined simultaneously in the same experiment.

REFERENCES

1. Asphalt Institute. *Thickness Design—Asphalt Pavements for Highways and Streets.* Manual Series MS-1. 1991.
2. Dickson, E. J. The Cooling of Asphalt Layers During the Compaction Operation. *Proc., 9th Australian Road Research Board Conference,* Vol. 4, 1978, pp. 247–259.
3. Corlew, J. S., and P. F. Rickson. Methods of Calculating Temperature Profiles of Hot-Mix Asphalt Concrete as Related to the Construction of Asphalt Pavements. *Proc., Association of Asphalt Paving Technologists,* Vol. 37, 1968, pp. 101–140.
4. *AASHTO Guide for Design of Pavement Structures.* AASHTO, 1986.
5. Button, J. W., D. N. Little, B. M. Gallaway, and J. A. Epps. *NCHRP Report 268: Influence of Asphalt Temperature Susceptibility on Pavement Construction and Performance.* TRB, National Research Council, Washington, D.C., 1983.

6. Monismith, C. L. Rutting Prediction in Asphalt Concrete Pavements. In *Transportation Research Record 616,* TRB, National Research Council, Washington, D.C., 1976, pp. 2–8.
7. *ASTM Standard Test Method C518, Test Method for Steady-State Thermal Transmission Properties by Heat Flow Meter Method.* Annual Books of ASTM Standards, American Society for Testing and Materials, 1992.
8. Incropera, F. P., and D. P. DeWitt. *Fundamentals of Heat and Mass Transfer,* 3rd ed., John Wiley and Sons, Inc., New York, 1990.
9. Kavianipour, A., and J. V. Beck. Thermal Property Estimation Utilizing the Laplace Transform with Application to Asphaltic Pavement. *International Journal of Heat Transfer,* Vol. 20, 1977, pp. 259–267.
10. Kuzman, R. *Handbook of Thermodynamic Tables and Charts.* Hemisphere Publishing Corporation, Washington, D.C., 1976.
11. Corlew, J. S., and P. F. Rickson. Methods of Calculating Temperature Profiles of Hot-Mix Asphalt Concrete as Related to the Construction of Asphalt Pavements. *Proc., Association of the Asphalt Paving Technologists,* Vol. 37, 1968, pp. 101–104.
12. O'Blenis, J. D. *Thermal Properties of West Virginia Highway Materials.* MSc thesis. Department of Civil Engineering, West Virginia University, Morgantown, 1964.
13. Aldrich, H. P. Frost Penetration Below Highway and Airport Pavements. *Bulletin 135,* HRB, National Research Council, Washington, D.C., 1956.
14. Saul, R. N. J. Physical Properties of Asphaltic Bitumen. In *The Properties of Asphaltic Bitumen* (J.P.H. Pfeiffer, ed.), Chapter 2, Elsevier, New York, 1960.
15. Barber, E. S. Calculation of Maximum Pavement Temperatures from Weather Reports. *Bulletin 168,* HRB, National Research Council, Washington, D.C., 1957, pp. 1–8.
16. Solaimanian, M., and T. W. Kennedy. Predicting Maximum Pavement Surface Temperature Using Maximum Air Temperature and Hourly Solar Radiation. In *Transportation Research Record 1417,* TRB, National Research Council, Washington, D.C., 1993.
17. Highter, W. H., and D. J. Wall. Thermal Properties of Some Asphalt Concrete Mixes. In *Transportation Research Record 968,* TRB, National Research Council, Washington, D.C., 1984.

Publication of this paper sponsored by Committee on Characteristics of Bituminous Paving Mixtures to Meet Structural Requirements.

Fatigue Behavior of Styrene-Butadiene-Styrene Modified Asphaltic Mixtures Exposed to Low-Temperature Cyclic Aging

A. OTHMAN, L. FIGUEROA, AND H. AGLAN

Polymer modifiers are being considered to improve the high-temperature stiffness and low-temperature flexibility and hence the long-term performance of asphaltic mixtures. In this regard, styrene-butadiene-styrene (SBS) copolymer has received much attention. In the current research, the fatigue crack propagation resistance of an SBS-modified AC-5 mixture exposed to different durations of low-temperature thermal cycling is investigated. Beams were prepared using a constant 8 percent AC-5 asphalt by weight and 6 percent SBS as a percentage of the total binder. Aggregate gradation according to Ohio Department of Transportation Item 403 was used. Mixing and compaction were performed according to ASTM D 1559–89. A cyclic thermal aging program was performed in an environmental chamber between 21.1°C and −12°C for four different periods. The effect of thermal cycling on the fatigue resistance of the modified mixtures as determined by the modified crack layer (MCL) model was studied. A relationship between the number of thermal cycles and the specific energy of damage γ', a material parameter characteristic of the mixture's resistance to crack propagation, was established. The current investigation revealed that SBS modifier helps in maintaining a constant fatigue resistance of the mixture over a moderate number of low-temperature thermal cycles. A decrease in the fatigue resistance was observed at a higher number of thermal cycles. In addition, a dramatic improvement in the fatigue resistance of the SBS-modified AC-5 concrete mixture is seen when compared with that of the unmodified AC-5 over all durations of thermal cycling tested. The fatigue performance of the mixture as predicted from the MCL model through the specific energy of damage γ' was consistent with predictions from the conventional resilient modulus and indirect tensile tests.

The durability of asphalt pavements is greatly influenced by environmental changes during the year, especially between summer and winter and between day and night, when the daily average temperature change can be considerable. In summer, high temperatures can soften the asphalt binder and consequently reduce the stiffness of the paving mixture. At the other extreme, low temperatures in winter can stiffen the asphalt binder and reduce the flexibility of the paving mixture. As a result, thermal cracking of the pavement surface may develop, which adversely affects the performance of the paving mixture. Thus, high-temperature stiffness and low-temperature flexibility are important properties that increase the lifetime of asphalt pavements.

Various elastomer and plastomer modifiers have been sought in an attempt to address this problem. Polymer modifiers vary in function and effectiveness. Elastomers, which are at least to some extent derived from a diene chemical structure, will toughen asphalt and improve temperature viscoelastic properties. Plastomers, which come from nondiene chemicals, improve the high-temperature viscoelastic properties of softer asphalts, which have good intrinsic low-temperature properties (*1*). The properties of asphalt mixtures can be improved by selecting modifiers in the proper molecular weight range and mixing the modifiers with asphalt mixtures in an appropriate manner. In addition, these modifiers must have solubility parameters close to those of the asphalt mixtures. One of the critical factors that should be considered for better rubber-modified asphalt is the air void percentage in the total mix. The performance of a rubber-modified asphalt mixture will be improved as this percentage is reduced (*2,3*). In general, the air void percentage depends on the load capacity of the transportation facility being designed. Lower air void percentages can be obtained by increasing both the modifier and the asphalt binder content until the required value is reached (*2*).

Investigation into the effect of asphalt additives on pavement performance (*4*) has revealed that, in general, all additives improved in temperature susceptibility. Under stress control fatigue, using the phenomenological approach, which is based on the Wohler concept (*5*), these workers concluded that SBS was one of the top additives among five tested (polyethylene, Elvax, SBS, latex, and carbon black) at 0°F and 68°F. This has also been confirmed using the modified crack layer (MCL) model (*6*). However, when the mixtures containing additives were aged at 140°F for 7 days, their fatigue lifetime decreased considerably in comparison with their unaged counterparts (*4*). Under controlled displacement fatigue, using the Paris equation (*7,8*), Little et al. (*4*) also concluded that the SBS additive was considerably superior among those additives tested at 33°F. At 77°F crack branching was observed, which tends to redistribute the stress, retarding main crack growth.

The phenomenon of aging of asphalt cement has been acknowledged for a long time, and extensive research has been conducted on the effect of long-term aging on asphalt cement. However, little research has examined asphalt mixtures, and so far, no standard test methods exist (*9*). In general, studies of aging of pavements are performed by three main methods: extended heating, pressure oxidation, and ultraviolet (UV) light treatment. Aging by extended heating (*10–13*) involves an oven aging program by which pavement samples are heated to a specific temperature for a specific period. Then standard tests such as the resilient modulus test, indirect tensile tests (strain to break), and the dynamic modulus RST are performed to evaluate the effect of the laboratory aging. Pressure oxidation aging, studied by several workers (*13–15*), involves exposing heated samples of pavement to air or oxygen under pressure for a fixed time period. At the conclusion of the experiments, standard tests such as creep, resilient modulus, and fatigue are used

A. Othman and L. Figueroa, Civil Engineering Department, Case Western Reserve University, Cleveland, Ohio 44106. H. Aglan, Mechanical Engineering Department, Tuskegee University, Tuskegee, Ala. 36088.

to evaluate the effect of pressure oxidation aging on pavement. Aging by UV treatment (*10,16,17*) involves subjecting samples of pavement to UV radiation for a specific period and then performing standard tests similar to those for the extended heating and oxidative aging. Combined aging with UV and forced draft oven heating has been suggested by Tia et al. (*18*), who note that the effect of UV aging occurs at the surface although it does affect a significant depth of the pavement.

From the literature, all aging methods that have so far been used mainly involve heating the pavement to harden it through volatilization and oxidation. The main drawback of these methods is softening of the pavement samples during aging, which can lead to a loss in mechanical stability. This view is supported by Kim (*15*), who suggested that maintaining the integrity of a sample subjected to these aging methods presents a problem. Bell (*9*) stated that in some aging programs specimen confinement may be necessary to prevent collapse, and concludes that none of the aging methods used so far are clearly superior and the possibility exists for new methods.

Apparently, very little work has been done on aging using thermal cycling, which is of critical importance since it simulates the actual environmental aging cycles to which asphalt mixtures are normally exposed. Thermal cycling is known to cause transverse cracking in asphalt pavements, which considerably shortens their lifetime, particularly at low temperatures. Transverse cracking is caused by stresses from shrinkage that become greater than the tensile strength of the material (*19*). Thus, it appears that environmental aging of the pavements by low-temperature thermal cycling can test the hypothesis that polymer modifiers improve the performance of asphalt-modified pavements.

The current study evaluates styrene-butadiene-styrene (SBS) modified AC-5 mixtures. This evaluation involved aging by thermal cycling in a low-temperature regime. The performance of the modified asphalt concrete mixture was evaluated on the basis of its resistance to fatigue propagation using the MCL model. A comparison was made between the fatigue performance of the mixture with the conventional properties such as the indirect tensile strength and resilience modulus.

EXPERIMENTAL

Materials

AC-5 asphalt cement used in this study had the following physical properties: (*a*) penetration at 25°C (77°F) was 204 using ASTM D-5, (*b*) viscosity at 135°C (275°F) was 201 cSt using ASTM-2170, (*c*) viscosity at 60°C (140°F) was 461 poise using ASTM-2171, and (*d*) flash cleveland open cup using ASTM-92 was 313°C (595°F). Crushed limestone aggregate and quartzitic sand were selected for the preparation of test specimens. Ohio Department of Transportation (ODOT) Item 403 gradation was used (*20*).

Kraton D4463 (SBS), which belongs to the general group of thermoplastic elastomers, was chosen as the modifier. It was supplied in pellet form by Shell Chemical Company and requires mixing at temperatures between 160 and 193°C (320 to 380°F).

Beam Preparation

The AC-5 asphalt cement was heated alone to 149°C (300°F). The asphalt blend was prepared with 6 percent SBS by weight of the asphalt. The blend was maintained hot to a goal temperature ranging between 160 and 177°C (320 to 350°F) for at least 2 hr. It was then thoroughly mixed by means of low-shear mechanical mixer for at least 15 min to obtain a more homogenous blend. Finally, the blend was kept at a constant temperature of 163°C (325°F) until ready for use.

The required percentages of aggregate were mixed in one batch to produce asphalt concrete beams with a target unit weight of 2386 kg/m^3 (149 lb/ft^3). The aggregate mixes and the asphalt cement were heated to a temperature of about 177°C (350°F), along with the compaction mold and the mixing tools. The aggregate was then blended with the required amount of asphalt cement (8 percent of the total weight of mix) as quickly and thoroughly as possible to yield a mixture having a uniform distribution of asphalt cement. The heated mold was then filled with the heated asphalt cement–aggregate mixture. This percentage of asphalt cement corresponds to the optimum asphalt cement content as determined by the Marshall method of mix design (ASTM D 1559–89). Static compaction was then performed by applying a uniform pressure of 13.79 MPa (2000 psi) through a 0.051- × 0.38-m (2 in. × 15 in.) plate using a hydraulic press for 5 min. The overall dimensions of each beam were 0.38 m long × 0.051 m wide × 0.089 m high (15 in. × 2 in. × 3.5 in). The compacted beam was allowed to cool in the mold for a few hours before its removal. Curing was achieved by maintaining the beams at 60°C (140°F) for 1 day. All beams were then kept in a room with a controlled temperature of 21.1°C for 7 days before testing.

Thermal Aging

Beams were thermally cycled between 21.1°C and −12°C (70 to 10.4°F) in an environmental chamber. The temperature-time profile used in this study is shown on Figure 1. This profile was established initially by embedding a thermocouple in the middle of a beam. The rate of heating and cooling of the asphalt mixture was established as shown in Figure 1. A temperature plateau was maintained at the upper 21.1°C and lower −12°C temperature levels. The length of each cycle was taken as 1 day. Four durations of thermal cycling were used. These were 7, 14, 21, and 28 cycles. At least three specimens were tested at each duration period of thermal cycling used in the corresponding fatigue study. Three specimens were also fatigued without thermal cycling for comparison. Similar tests were

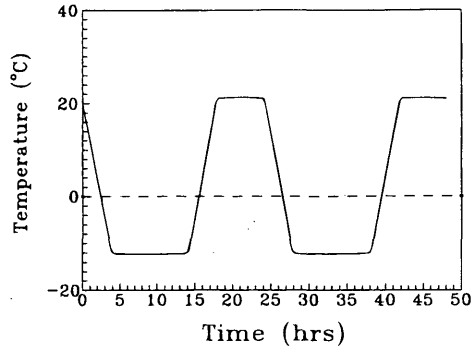

FIGURE 1 Schematic diagram of temperature-time profile for low-temperature thermal cycling program.

conducted on Marshall-sized cylindrical specimens to study the effect of thermal cycling on resilient modulus and indirect tensile failure of the SBS-modified mixture.

Fatigue Crack Propagation Tests

Four point bending fatigue crack propagation tests were performed under stress control using a repeated pneumatic flexure testing machine fitted with a 4.45-kN (1,000-lb) load cell. Tests were conducted at a constant temperature of about 21.1°C (70°F) using an invert haversine load. The load application period was 0.2 sec followed by a 2-sec rest period between repeated loads. The support span was equal to 0.26 m (10.2 in.) and the distance between the midspan loading points was 0.086 m (3.4 in.). An initial straight notch 6.4 mm (0.25 in.) deep was inserted at the middle of the specimens with a 4-mm (0.15 in.) saw that had a round tip [radius 2.4 mm (0.094 in.)]. A maximum load of 290 N (65 lb) was used with continuous cycle load applications from zero to the maximum load. A hysteresis loop (load versus deflection) was recorded at 6.4-mm (0.25 in.) intervals of crack growth using the X-Y plotter. Software was developed to digitize graphical data and to calculate pertinent areas within the load-deflection curves obtained during fatigue testing. Three specimens were fatigue-tested at four different durations of thermal cycling and three before thermal cycling, for a total of 15 beams.

RESULTS AND DISCUSSION

Fatigue Behavior

For stress-controlled fatigue, the MCL model, previously discussed in detail (*21,22*), can be expressed as

$$\left(\frac{J^*}{a}\right) = \gamma' - \beta'\left[\frac{\dot{W}_i}{a\left(\frac{da}{dN}\right)}\right] \quad (1)$$

where

J^* = energy release rate (i.e., $J^* = (\partial P/\partial a)/B$, where P is the potential energy and B is the specimen width);
a = crack length;
$\dot{W}_i$ = change in work;
da/dN = cyclic crack speed;
γ' = material parameter, characteristic of the mixture's resistance to FCP; and
β' = coefficient of energy dissipation.

The effect of thermal cycling on the fatigue resistance of the SBS-modified AC-5 mixture is examined in view of the MCL model. The crack length (a) versus the number of cycles (N) for typical specimens of the SBS modified AC-5 mixture, which were subjected to four different durations of thermal cycling, together with a typical specimen without thermal cycling are shown in Figure 2. It appears that samples subjected to 0 to 14 thermal cycles are close, with points clustering together. However, there exists a difference between their behavior when the first derivative of each curve was calculated to obtain the crack speed. Applying the crack length versus the number of cycles, the behavior of samples subjected to 21 and 28 thermal cycles shows a marked decrease in their fatigue lifetime at a faster crack propagation rate. The crack speed was calculated, to be employed in the MCL model, at intervals of crack length from the slope of each curve in Figure 2.

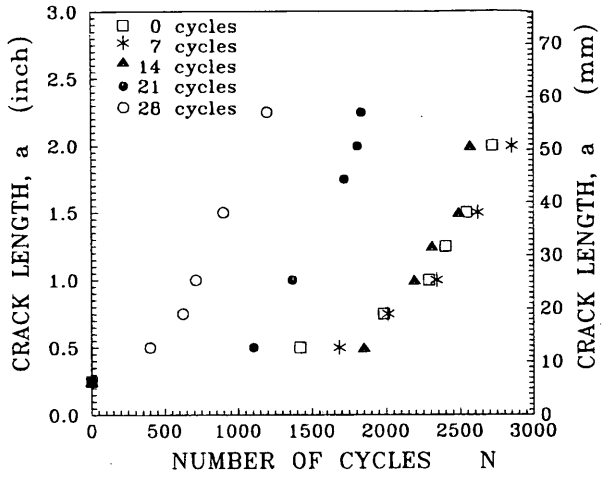

FIGURE 2 Crack length versus number of cycles for SBS-modified AC-5 asphalt concrete mixture subjected to low-temperature thermal cycling.

The energy release rate J^*, evaluated on the basis of the potential energy principle as previously reported (*23–26*), is plotted against the crack length in Figure 3. As with the lifetime curves, the effect of thermal cycling is not seen clearly until 21 and 28 cycles. The lower values of J^*, at each crack length, with increased thermal cycling are expected. However, it is interesting to note how SBS maintains its improved properties up to a certain duration of cycling, after which the improved resistance starts to drop off. Again, the value of J^* at each crack length will be employed in the present analysis to extract γ' and β' for each mixture from Equation 1.

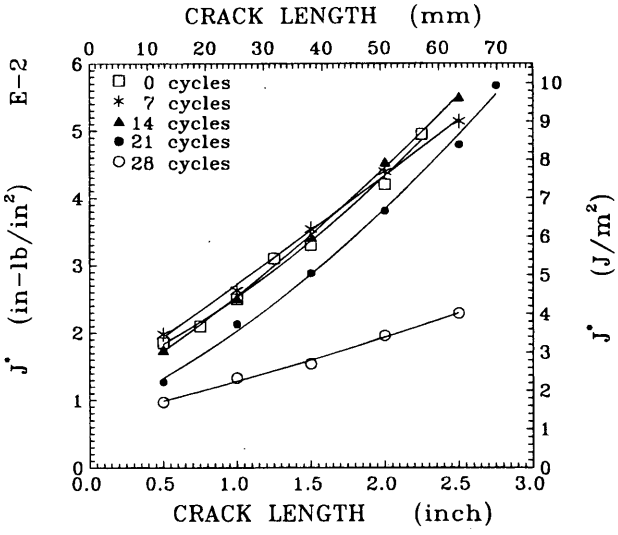

FIGURE 3 Energy release rate versus crack length for SBS modified AC-5 asphalt concrete mixture subjected to low-temperature thermal cycling.

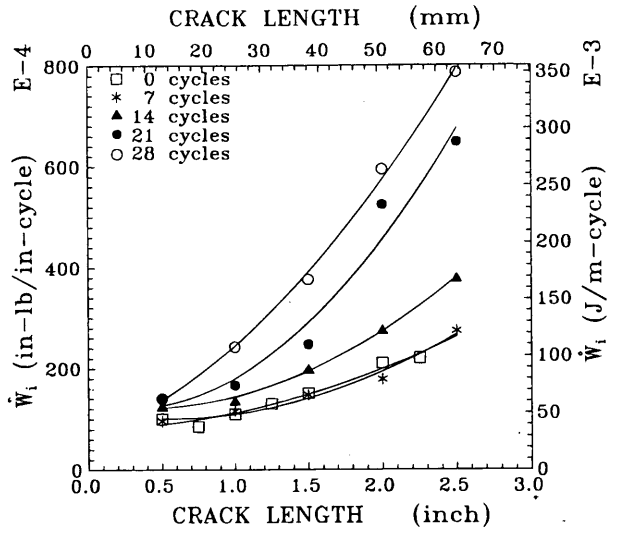

FIGURE 4 Change in work, $\dot{W}_i$, versus crack length for SBS-modified AC-5 asphalt concrete mixture subjected to low-temperature thermal cycling.

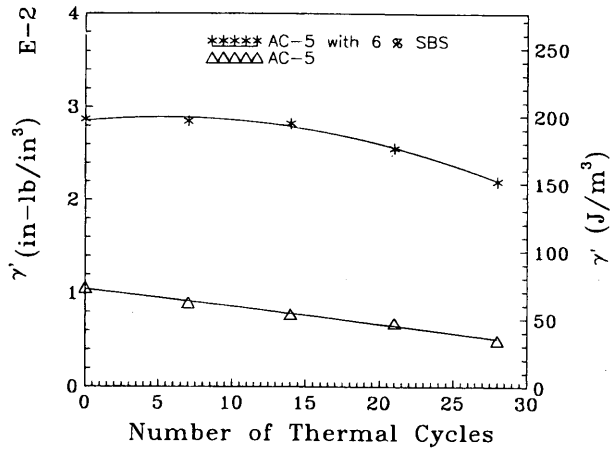

FIGURE 6 Effect of number of low-temperature thermal cycles on specific energy of damage γ' for SBS-modified AC-5 asphalt concrete mixture and unmodified AC-5.

The change in work, $\dot{W}_i$ (where $\dot{W}_i$ is the area of hysteresis loop at any crack length minus the area of hysteresis loop before crack initiation divided by the specimen thickness), versus the crack length for typical beams tested at various durations of thermal cycling (as well as beams without thermal cycling) is shown in Figure 4. The value of $\dot{W}_i$ increases with increasing number of thermal cycles. Thus, increased thermal cycling leads to the use of more work on damage formation and history-dependent dissipative processes within the active zone of the SBS-modified mixture during fatigue loading.

The previous results from a typical specimen from each duration period of thermal cycling are now plotted, on the basis of Equation 1, in order to extract γ' and β'. It is evident from Figure 5 that the experimental points for all of the mixtures make a good straight line, where γ' is the intercept and β' is the slope. The effect of thermal cycling on γ' is shown in Figure 6 for SBS-modified and unmodified AC-5 mixtures. It can be seen that γ' remains approximately constant from 0 to 14 cycles; then it decreases slightly with the increase in the number of thermal cycles for the SBS-modified mixture. This decrease in the value of γ' is indicative of reduced resistance to crack propagation. As can be seen, the addition of the SBS to the mixture greatly enhances the overall fatigue resistance over the entire duration of thermal cycling tested. In addition, the trend of a slight decrease in resistance with increased number of thermal cycles is also seen in the unmodified AC-5 mixture.

On the other hand, the coefficient of energy dissipation, β', remains constant with the increasing number of thermal cycles for the SBS-modified AC-5 concrete mixture, as seen in Figure 7. The value of β' for the unmodified AC-5 mixture was found to be higher over the entire range of thermal cycling tested. Thus, from the MCL model, a decrease in γ' with an increase in β' at all durations of ther-

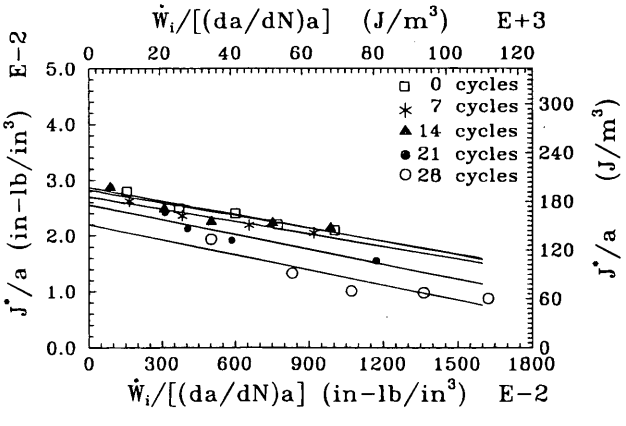

FIGURE 5 Fatigue crack propagation behavior of SBS-modified AC-5 asphalt concrete mixture subjected to various durations of low-temperature thermal cycling plotted in form of MCL model to obtain γ' and β'.

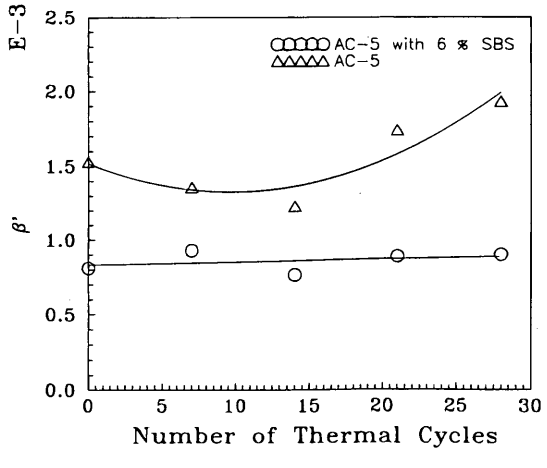

FIGURE 7 Effect of number of low-temperature thermal cycles on coefficient of energy dissipation β' for SBS-modified AC-5 asphalt concrete mixture and unmodified AC-5.

mal cycling tested indicates the fatigue resistance superiority of the SBS-modified AC-5 concrete mixture at all durations of thermal cycling tested.

The fatigue behavior of the SBS-modified mixture as assessed by the MCL model will be compared with conventional mechanical property evaluation based on the resilient modulus and indirect tensile behavior.

Resilient Modulus and Indirect Tensile Behavior

The resilient modulus tests were conducted in accord with ASTM D4123. The following equation is used to calculate the resilient modulus (M_r).

$$M_r = \frac{F(\nu + 0.2734)}{tD} \quad (2)$$

where

F = load,
ν = Poison's ratio (assumed 0.4),
t = specimen thickness, and
D = total horizontal deformations.

The average values of M_r based on three tests measured at different durations of thermal cycling for the SBS-modified AC-5 mixture and the unmodified AC-5 mixture are plotted in Figure 8. It is evident that the relationship between M_r and the number of thermal cycles is the same for the unmodified and SBS-modified AC-5 concrete mixtures up to 14 cycles after which there is a noticeable increase in the M_r of the SBS-modified mixture. The data in Figure 8 indicate that the modified mixture became less flexible as the number of thermal cycles increased, particularly after 14 thermal cycles. The unmodified AC-5 mixture exhibited a more constant increase in resilient modulus with an increase in the number of thermal cycles.

The indirect tensile behavior of specimens exposed to various numbers of thermal cycles was established in accordance with research by Kennedy and Hudson (*27*). The average compressive load versus the vertical displacement for Marshall-sized cylindrical specimens at different numbers of thermal cycles is shown in Figure 9. The maximum load increased slightly as the number of thermal cycles increased, whereas the deformation at failure as well as the deformation at maximum load were nearly constant from 0 to 7 cycles and then decreased considerably. It is also obvious from Figure 9 that the work needed to cause tensile failure, the area under the load-deformation curve, is considerably decreased with the increase in the number of thermal cycles after 7 cycles. Lower strain at failure and lower amount of work needed to cause tensile failure are associated with decreased resistance to fatigue crack propagation.

Thus, in view of the conventional resilient modulus and indirect tensile test, the resistance of the SBS-modified mixture to crack propagation is slightly decreased at increased durations of thermal cycling. This is in substantial agreement with the MCL analysis as reflected in the specific energy of damage, γ'.

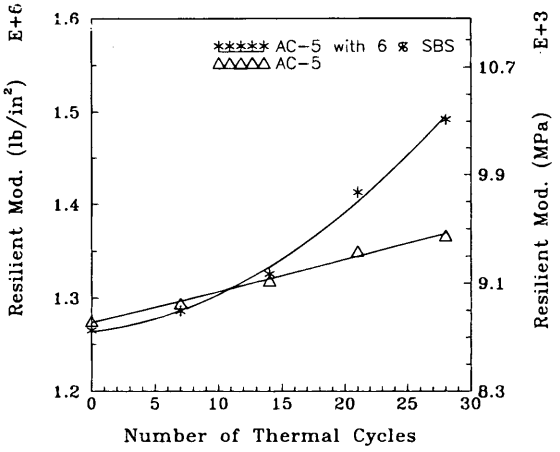

FIGURE 8 Effect of number of low-temperature thermal cycles on resilient modulus for SBS-modified AC-5 asphalt concrete mixture and unmodified AC-5.

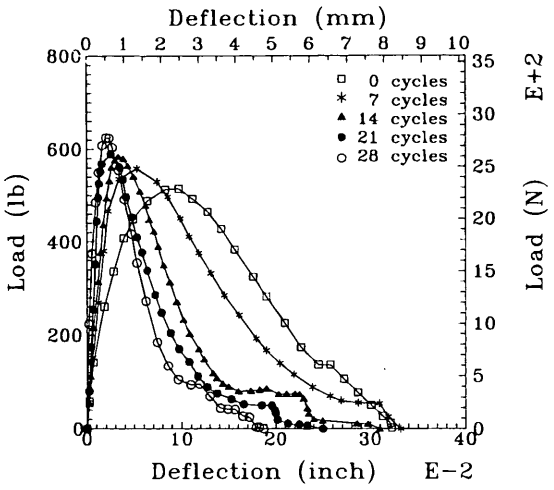

FIGURE 9 Compressive load versus horizontal deformation for indirect tensile test conducted on SBS-modified AC-5 asphalt concrete mixture subjected to various durations of low-temperature thermal cycling.

CONCLUDING REMARKS

The effect of low-temperature thermal cycling on the fatigue fracture behavior of SBS-modified AC-5 asphalt mixture was studied. Relationships between parameters controlling the fatigue fracture process, namely, the specific energy of damage γ' and the dissipative coefficient β' of the SBS mixture, and the number of thermal cycles, were established. The current study reveals that the value of γ' remains almost constant over a moderate number of thermal cycles. This can be attributed to the flexibility of the mixture induced by the SBS modifier. The value of γ' decreases at higher duration periods. The decrease in the specific energy of damage was found to accompany a nearly constant value of the dissipative coefficient β' over all durations tested. It is also noted that γ' is considerably higher and β' lower than for the unmodified AC-5 over all durations tested, indicating superior fatigue resistance to crack propagation of the SBS-modified AC-5 mixture. Exposure of the SBS-modified asphalt mixture specimens to a high number of ther-

mal cycles tends to stiffen the mixture and, in turn, reduce its fatigue resistance. However, it is still much improved over the unmodified AC-5 mixture, which also exhibits a similar reduction in resistance. The fatigue crack propagation resistance of the SBS-modified mixture predicted from the MCL model through the specific energy of damage γ' is consistent with the prediction made based on conventional resilient modulus and indirect tensile tests.

REFERENCES

1. Key Facts About Polymer Modified Asphalt. *Better Roads*, July 1989, p. 39.
2. Narusch, F. P. *Alaska Experience with Rubberized Asphalt Concrete Pavements, 1979–1982.* Division of Design and Construction, Alaska Department of Transportation and Public Facilities, Central Region, Aug. 1982.
3. Little, D. N. Performance Assessment of Binder-Rich Polyethylene Modified Asphalt Concrete Mixtures (Novophalt). Presented at the 79th Annual Meeting of Transportation Research Board, Washington, D.C., 1991.
4. Little, D. N., J. W. Button, et al. *Investigation of Asphalt Additives.* FHWA-R-D87/001. Nov. 1986.
5. Wohler A. *English Abstracts in Engineering.* Vol. II, 1871, p. 199.
6. Aglan, H., and L. Figueroa. *Structure-Fracture Toughness Relationships of Asphalt Concrete Mixtures Under Fatigue Loading.* USAE Technical Report, Dec. 1991.
7. Paris, P., and F. Erdogan. A Critical Analysis of Crack Propagation Laws, *Journal of Basic Engineering, Trans. ASME,* Vol. 85, 1963, p. 381.
8. Paris, P. C., and C. G. Sih. Stress Analysis of Cracks. In *ASTM STP 381,* American Society for Testing and Materials, 1965, pp. 30–81.
9. Bell, C. A. *Summary Report on Aging of Asphalt-Aggregate Systems.* SHRP-A/IR-89–004. Strategic Highway Research Program, National Research Council, Nov. 1989.
10. Hugo, F., and T. W. Kennedy. Surface Cracking of Asphalt Mixtures in Southern Africa. *Proc., AAPT,* Vol. 54, 1985, pp. 454–501.
11. Kemp, G. R., and N. H. Predoehl. *A Comparison of Field and Laboratory Environments on Asphalt Durability. Proc., AAPT,* Vol. 50, 1981, pp. 492–537.
12. Plancher, H., E. L. Green, and J. C. Peterson. Reduction of Oxidative Hardening of Asphalt by Treatment with Hydrated Lime—A Mechanistic Study. *Proc., AAPT,* Vol. 45, 1976, pp. 1–24.
13. Von Quintas, H., J. Scherocman, T. Kennedy, and C. S. Hughes. *NCHRP Report 338: Asphalt Aggregate Mixture Analysis System.* TRB, National Research Council, Washington, D.C., 1991.
14. Kumar, A., and W. H. Goetz. Asphalt Hardening as Affected by Film Thickness, Voids and Permeability in Asphaltic Mixtures. *Proc., AAPT,* Vol. 46, 1977, pp. 571–605.
15. Kim, O. K., C. A. Bell, J. Wilson, and G. Boyle. *Effect of Moisture and Aging on Asphalt Pavement II Fe: Part 2, Effect of Aging.* Report FHWA-OR-RD-86—1–2. FHWA, U.S. DOT, 1986.
16. Hveem, F. N., E. Zube, and J. Skog. Proposed New Tests and Specifications for Paving Grade Asphalts. *Proc. AAPT* Vol. 32, 1963, pp. 247–327.
17. Traxler, R. N. Relation Between Asphalt Composition and Hardening by Volatilization and Oxidation. *Proc. AAPT,* Vol. 30, 1961, pp. 359–377.
18. Tia, M., B. E. Ruth, C. T. Charai, J. M. Shiau, D. Richardson, and J. Williams. *Investigation of Original and In-Service Asphalt Properties for the Development of Improved Specifications: Final Phase of Testing and Analysis.* University of Florida, Gainsville, 1988.
19. Dongre, R., M. G. Sharma, and D. A. Anderson. Development of Fracture Criterion for Asphalt Mixes at Low Temperature. In *Transportation Research Record 1228,* TRB, National Research Council, Washington, D.C., 1989, pp. 94–105.
20. Ohio Department of Transportation Specification. *Construction and Materials Specifications.* State of Ohio, Columbus, Jan. 1989, p. 112.
21. Aglan, H. Evaluation of the Crack Layer Theory Employing a Linear Damage Evolution Approach. *International Journal of Damage Mechanics,* Vol. 2, 1993, p. 53.
22. Aglan, H., and L. Figueroa. A Damage Evolution Approach to Fatigue Cracking in Pavements. *Journal of Engineering Mechanics,* Vol. 119, 1993, pp. 1243–1259.
23. Aglan, H., I. Shehata, L. Figueroa, and A. Othman. Structure-Fracture Toughness Relationships of Asphalt Concrete Mixtures. In *Transportation Research Record 1353,* TRB, National Research Council, Washington, D.C., 1992 pp. 24–30.
24. Aglan H., A. Othman, L. Figueroa, and R. Rollings. Effect of Styrene-Butadiene-Styrene Modifier Percentage on the Fatigue Crack Propagation Behavior of Pavements. In *Transportation Research Record 1417,* TRB, NRC, Washington, D.C., 1993, pp. 178–186.
25. Aglan H. A. Othman, and L. Figueroa. The Specific Energy of Damage as a Fracture Toughness Criterion for Asphaltic Pavements. In *Transportation Research Record* (forthcoming).
26. H. Aglan, A. Othman, and L. Figueroa. Processing Conditions—Fracture Toughness Relationships of Asphalt Concrete Mixtures. *Journal of Materials Science,* Vol. 29, 1994, pp. 4786–4792.
27. Kennedy, J. W., and W. R. Hudson. Application of the Indirect Tensile Test to Stabilized Materials. In *Highway Research Record 235,* HRB, National Research Council, Washington, D.C., 1968, pp. 36–48.

Publication of this paper sponsored by Committee on Characteristics of Bituminous Paving Mixtures to Meet Structural Requirements.

Comparison of Axial and Diametral Resilient Stiffness of Asphalt-Aggregate Mixes

AKHTARHUSEIN A. TAYEBALI, JOHN A. DEACON, AND CARL L. MONISMITH

The stiffness of asphalt-aggregate mixes is important in determining how well a pavement performs, and is an essential property for analyzing pavement response to traffic loading. A study for stiffness determination of asphalt-aggregate mixes was conducted as a part of Project A-003A of the Strategic Highway Research Program (SHRP). Its purpose was to evaluate the sensitivity of the axial (compressive) and diametral (indirect tensile) resilient stiffness to mix and test variables and to compare the axial and diametral resilient stiffness of 16 mixes tested under various temperatures, stress levels, and loading frequencies. Results of this study indicate that both axial and diametral resilient stiffnesses are sensitive to mix and test variables, including asphalt type, aggregate type, air-void content, and temperature. However, axial and diametral testing of mixes yield different estimates of their resilient stiffnesses. Diametral resilient stiffness computed using an assumed Poisson's ratio of 0.35 generally exceeds axial resilient stiffness by an average of approximately 35 to 45 percent. SHRP Project A-003A experience suggests that the indirect tension test is not accurate for relatively weak specimens at temperatures as high as 60°C (104°F), and tension may not be reliable even at moderately high temperatures [40°C (140°F)] due to excessive vertical permanent deformation. The influence of mix and testing variables on resilient stiffness may be different depending on whether loading is in axial compression or indirect tension. By inference, differences in mix design and structural pavement design may result depending on the type of testing system used to estimate mix stiffness.

The stiffness of asphalt-aggregate mixes is important in determining how well a pavement performs and is an essential property for the analysis of pavement response to traffic loading. Although fatigue and permanent deformation tests can often be used to measure stiffness under conditions similar to those experienced by paving mixes in service, stiffness testing complements strength testing and provides essential information when results of strength tests are unavailable. Accordingly, an independent study for stiffness testing of asphalt-aggregate mixes was conducted in Project A-003A of the Strategic Highway Research Program's (SHRP's) asphalt research endeavor. Described herein are the results of axial and diametral resilient stiffness tests performed on 16 mixes. Specific objectives of this study included evaluation of the sensitivity of the axial and diametral resilient stiffnesses to mix and test variables and comparison of the axial and diametral resilient stiffness values for similar mixes tested under the same conditions. The diametral resilient stiffness value is of particular significance in this study because NCHRP investigators (*1*) recommended its use in an asphalt-aggregate mix analysis system (AAMAS) for characterization of mix stiffness at moderate temperatures 5°C to 40°C (41°F to 104°F).

A. A. Tayebali, Department of Civil Engineering, North Carolina State University, P. O. Box 7908, Raleigh, N.C. 27695–7908. J. A. Deacon, 265 Civil Engineering Building, Department of Civil Engineering, University of Kentucky, Lexington, Ky. 40506–0281. C. L. Monismith, 1301 South 46th Street, Building 452, University of California, Berkeley, Richmond Field Station, Richmond, Calif. 94804

LABORATORY TEST PROGRAM

This study of stiffness test methodologies was primarily a laboratory investigation, which included evaluation of mixes containing two core SHRP Materials Reference Library asphalts and two core aggregates. A total of 16 different mixes (combination of 2 asphalts, 2 aggregates, 2 asphalt contents and 2 air void contents) was evaluated in axial and diametral loading for a range of temperatures, stress levels, and loading frequencies (*2*). Table 1 summarizes the mix and test variables and identifies the characteristics of asphalts and aggregates used.

Axial and diametral resilient stiffness tests were conducted in accordance with ASTM D 3497 (Test Method for Dynamic Modulus of Asphalt Mixtures) and D 4123 (Test Method for Indirect Tension Test for Resilient Modulus of Bituminous Mixtures), respectively. Only total resilient stiffness (M_R) is reported in this paper.

Because resilient stiffness testing is considered nondestructive, each specimen was subjected to the full range of loading conditions at each of the test temperatures, stress levels, and loading frequencies. The high and low stress levels used during testing were adjusted according to test temperature, not only to ensure a reasonable strain reading under applied stress, but also to ensure that specimens did not experience excessive damage at the higher temperatures. Table 2 identifies the average target stress levels used at the different temperatures.

A total of 512 (16 mixes and 16 test conditions with full replication) stiffness tests was performed for the axial loading conditions, and 384 (16 mixes and 12 test conditions with full replication) for the diametral loading conditions. For both test types, specimens were fabricated using the Triaxial Institute kneading compactor. Aggregate gradation, identical for both test programs, is given in Table 3.

TEST RESULTS

Table 4 summarizes the average axial and diametral resilient stiffness values for the various materials and test conditions. The average stiffness values were computed by first partitioning the data set for each temperature according to the independent variable being

TABLE 1 Significant Mix and Test Variables for Stiffness Study

Asphalts:	2 - MRL[1] Core asphalts							
	Type	Grade	Penetration Index (PI)					
	AAK-1 AAG-1	AC-30 AR-4000	-0.5 -1.4					
Aggregates:	2 - MRL Core aggregates RB - Watsonville granite, crushed, rough surface texture RL - Chert, partially crushed, smooth surface texture							
Asphalt contents: (percent by wt. of aggregates)	2 - optimum[2] and high depending on asphalt and aggregate type							
	AAK-1				AAG-1			
	RB		RL		RB		RL	
	Opt.	High	Opt.	High	Opt.	High	Opt.	High
	5.1	5.7	4.3	5.0	4.9	5.5	4.1	4.8
Air void contents:	2 - 4±1 and 8±1 percent							
Stress levels:	2 - low and high varies with temperature							
Temperature: Axial tests Diametral tests	 4 - 0°, 20°, 40° and 60°C 3 - 0°, 20° and 40°C							
Test frequency:	2 - 1 and 0.5 Hz, pulse loading, 0.1 seconds loading time							
Number of replicates:	2							
Specimen size: Axial tests Diametral tests	 101.6 mm diameter, approximately 203.2 mm high 101.6 mm diameter, approximately 63.5 mm high							
Total number of mixes:	16							
Total No. of tests: Axial stiffness Diametral Stiffness	 512 (16 mixes, 16 test conditions, full replication) 384 (16 mixes, 12 test conditions, full replication)							

[1]SHRP Materials Reference Library
[2]Optimum by Hveem mix design method, High = optimum+0.6%

considered and then obtaining average values for all other variables. Comparison of the axial and diametral stiffness values indicates that on average the diametral stiffness is about 35 to 45 percent greater than the axial stiffness. Table 5 summarizes values for the ratio of the average resilient stiffness values measured by axial and diametral tests for the various mix and test variables. Examination of these data indicates the following:

1. At lower temperatures, specimens containing asphalt AAK-1 exhibit lower axial and diametral stiffness values than specimens containing asphalt AAG-1. At higher temperatures, specimens containing asphalt AAK-1 have higher axial stiffness values and lower diametral stiffness values than specimens containing asphalt AAG-1. Because of the differences in the temperature susceptibility characteristics of the two asphalts, it would have been expected that

TABLE 2 Target Average Stress Levels Used for Different Temperatures

Temperature	Axial		Diametral	
	Low Stress, kPa	High Stress, kPa	Low Stress, kPa	High Stress, kPa
0°C	211	419	186	357
20°C	107	213	97	188
40°C	56	109	47	95

TABLE 3 Aggregate Gradation Used

Sieve Size	Percent Passing by Weight	ASTM Spec. (D 3515)
25.0 mm	100	100
19.0 mm	95	90-100
12.5 mm	80	-
9.50 mm	68	56-80
4.75 mm	48	35-65
2.36 mm	35	23-49
1.18 mm	25	-
600 μm	17	-
300 μm	12	5-19
150 μm	8	-
75 μm	5.5	2-8

the stiffness of mixes containing asphalt AAK-1 would be higher at the higher temperature in both tests.

2. Specimens with the high asphalt content generally show higher axial resilient stiffness values than those with the low asphalt content. For diametral resilient stiffness the effect of asphalt content is reversed: specimens with the high asphalt content show lower stiffness than those with the low asphalt content.

3. Specimens containing RB aggregate show higher axial resilient stiffness values than those containing RL aggregate, except at 0°C (32°F) where the stiffness values are about the same. On the other hand, diametral stiffness values for specimens containing RB aggregate are lower than for those containing RL aggregate, except at 0°C (32°F).

4. Axial stiffness is more sensitive to air-void content than diametral stiffness.

The axial and diametral stiffness were also analyzed statistically with a general linear model (GLM) formulation as summarized in the next section.

TABLE 4 Effect of Mix and Testing Variables on Average Axial and Diametral Resilient Stiffness Values

Variable	Level	Average Axial Resilient Stiffness, MPa			Average Diametral Resilient Stiffness, MPa		
		0°C	20°C	40°C	0°C	20°C	40°C
Asphalt Type	AAK-1	11,868	3,333	545	16,215	4,223	667
	AAG-1	17,940	6,224	524	24,495	8,556	876
Asphalt Content	Optimum	14,697	4,575	538	21,390	7,176	849
	High	15,111	4,982	531	19,320	5,548	697
Aggregate Type	Granite (RB)	15,111	5,223	587	21,597	6,093	718
	Chert (RL)	14,697	4,333	483	19,113	6,652	828
Air Voids	Low	17,733	6,044	704	23,184	7,314	952
	High	12,075	3,512	366	17,457	5,423	591
Stress Level	Low	14,904	4,816	545	20,355	6,541	814
	High	14,904	4,740	531	20,355	6,210	731
Frequency	Low	14,835	4,685	524	20,217	6,320	807
	High	14,973	4,871	545	20,493	6,424	738
Repeats	First	15,042	4,713	531	19,941	6,044	773
	Second	14,766	4,844	538	20,769	6,700	773
Average		14,904	4,775	538	20,355	6,376	773

TABLE 5 Ratio of Resilient Stiffness Values for Axial and Diametral Tests

Variable	Ratio	0°C		20°C		40°C	
		Axial	Diametral	Axial	Diametral	Axial	Diametral
Asphalt Type	AAK-1 /AAG-1	0.66	0.66	0.54	0.49	1.03	0.76
Asphalt Content	Low/High	0.97	1.11	0.92	1.29	1.01	1.22
Aggregate	RB/RL	1.03	1.13	1.21	0.91	1.22	0.87
Air Voids	Low/High	1.47	1.32	1.72	1.34	1.93	1.61
Stress	Low/High	1.00	1.00	1.02	1.05	1.03	1.11
Frequency	Low/High	0.99	0.99	0.96	0.98	0.95	1.09
Repeats	First/Second	1.02	0.96	0.97	0.90	0.98	1.00
Ratio of average diametral to axial resilient stiffness		1.37		1.35		1.45	
Percent difference		37		35		45	

Statistical Analysis of Test Results

The main purpose of the statistical analysis was to determine the sensitivity of stiffness to mix and test variables. Two responses were examined, the logarithm of the resilient stiffness and the ratio of the diametral stiffness to the axial stiffness. Independent variables in the GLMs included all seven of the mix and test variables, together with all two-factor interactions among them. Accordingly, a linear model of the following type was utilized for the GLM:

$$\begin{aligned} Y_i = \mu &+ \alpha_0 \cdot \text{Asph} + \alpha_1 \cdot \text{Aggr} + \alpha_2 \cdot \%\text{Asph} + \alpha_3 \cdot \text{Voids} \\ &+ \alpha_4 \cdot \text{Temp} + \alpha_5 \cdot \text{Stress} + \alpha_6 \cdot \text{Freq} + \alpha_7 \cdot \text{Asph} \cdot \text{Aggr} \\ &+ \alpha_8 \cdot \text{Asph} \cdot \%\text{Asph} + \alpha_9 \cdot \text{Asph} \cdot \text{Voids} + \alpha_{10} \cdot \text{Asph} \cdot \text{Temp} \\ &+ \alpha_{11} \cdot \text{Asph} \cdot \text{Freq} + \alpha_{12} \cdot \text{Asph} \cdot \text{Stress} + \alpha_{13} \cdot \text{Aggr} \cdot \%\text{Asph} \\ &+ \alpha_{14} \cdot \text{Aggr} \cdot \text{Voids} + \alpha_{15} \cdot \text{Aggr} \cdot \text{Temp} + \alpha_{16} \cdot \text{Aggr} \cdot \text{Stress} \\ &+ \alpha_{17} \cdot \text{Aggr} \cdot \text{Freq} + \alpha_{18} \cdot \%\text{Asph} \cdot \text{Voids} + \alpha_{19} \cdot \%\text{Asph} \cdot \text{Temp} \\ &+ \alpha_{20} \cdot \%\text{Asph} \cdot \text{Stress} + \alpha_{21} \cdot \%\text{Asph} \cdot \text{Freq} \\ &+ \alpha_{22} \cdot \text{Voids} \cdot \text{Temp} + \alpha_{23} \cdot \text{Voids} \cdot \text{Stress} + \alpha_{24} \cdot \text{Voids} \cdot \text{Freq} \\ &+ \alpha_{25} \cdot \text{Temp} \cdot \text{Stress} + \alpha_{26} \cdot \text{Temp} \cdot \text{Freq} \\ &+ \alpha_{27} \cdot \text{Stress} \cdot \text{Freq} \end{aligned} \quad (1)$$

where

Y_1 = response variable, log stiffness,
Y_2 = ratio of diametral stiffness to axial stiffness,
μ = constant (grand mean),
α_i = model coefficients,
Asph = asphalt type,
Aggr = aggregate type,
%Asph = asphalt content,
Voids = percent air voids,
Temp = temperature,
Stress = stress, and
Freq = frequency.

The test method itself (axial or diametral), together with its interactions with other factors, was added to the GLM for modeling the logarithm of resilient stiffness. All independent variables were represented as discrete, binary quantities with the exception of temperature, which was treated as a continuous variable. Summary statistics from this modeling are presented in Table 6. Table 7 identifies by a "Yes" those effects found to be statistically significant at the 95 percent probability level. This means that there is a 5 percent or smaller chance that there actually was no effect in cases for which an effect was observed.

As indicated by the coefficient of determination, the GLM fit closely to the resilient stiffness data. The coefficient of variation of 28.7 percent compares favorably with the 16.7 percent to 36.6 percent range from stiffness measurements taken during the SHRP A-003A compaction study and reported elsewhere (*3*). Although the GLM fit to the ratio data was less accurate, many one-factor and two-factor effects were statistically significant. This means that some of the effects measured by axial test are quite different from the effects measured by diametral test. Such differences could have serious implications for the evaluation of mix effects in a comprehensive AAMAS.

The effects of asphalt type and air-void content on resilient stiffness are illustrated by Figure 1 and Table 8. For the high-temperature testing (Figure 1), there appears to be little distinction between asphalt AAK-1 and AAG-1 based on axial resilient stiffness. At the same time, the ratio of diametral stiffness to axial stiffness is quite different for the two asphalts, varying between 0.75 and 3.25. This variation indicates that the effect of asphalt type on diametral stiffness differs considerably from its effects on axial resilient stiffness. Table 8 confirms that asphalts effect on average axial stiffness at 40°C (104°F) is small and statistically insignificant at the 95 percent level, but its effect on diametral stiffness is much larger and statistically significant. Different results are obtained at lower temperatures as shown in Table 8. At these temperatures it appears that the effect of asphalt type on axial and diametral stiffness is the same, even though the magnitude of the stiffness values is different for the two tests.

One explanation for the differences in the effect of asphalt types on axial and diametral stiffness measurements is that in axial testing at high temperatures, deformations are relatively large and asphalt effects are less important than aggregate effects. At low

TABLE 6 Summary Statistics from GLM Modeling

Statistic	Resilient Stiffness (Ln psi)	Ratio of Diametral Stiffness to Axial Stiffness
Coefficient of Determination (R^2)	0.962	0.587
Root Mean Square Error	0.281	0.281
Coefficient of Variation (%)	28.7	19.4

temperatures, deformations are relatively small and aggregate influence becomes much less pronounced. In diametral testing at high temperatures, on the other hand, stiffness is measured in tension, and larger deformations do not produce more interparticle contact. Therefore, asphalt effects remain more important than aggregate effects.

Mix stiffness is an important feature of the mix analysis and design system. The above illustration underscores the fact that mix-design decisions involving fundamental mix properties might well be influenced by the type of stiffness test.

Effect of Poisson's Ratio

As reported earlier, diametral stiffness values are about 35 to 45 percent higher than corresponding axial stiffness values. Diametral

TABLE 7 Statistically Significant Effects in Stiffness Testing

Effect	Resilient Stiffness	Ratio of Diametral Stiffness to Axial Stiffness
Asphalt Type (Asph)	Yes	
Asphalt Content (%Asph)		Yes
Aggregate Type (Aggr)		
Air Voids (%Voids)	Yes	Yes
Stress Level (Stress)		
Loading Frequency (Freq)		
Temperature (Temp)	Yes	
Type of Test (Test)	Yes	N/A
Asph x % Asph		Yes
Asph x Aggr		
Asph x % Voids		Yes
Asph x Stress		
Asph x Freq		
Asph x Temp	Yes	Yes
Asph x Test	Yes	N/A
% Asph x Aggr		
% Asph x % Voids		
% Asph x Stress		
% Asph x Freq		
% Asph x Temp	Yes	
% Asph x Test		N/A
Aggr x % Voids		Yes
Aggr x Stress		
Aggr x Freq		
Aggr x Temp	Yes	Yes
Aggr x Test	Yes	N/A
% Voids x Stress		Yes
% Voids x Freq		
% Voids x Temp	Yes	Yes
% Voids x Test	Yes	N/A
Stress x Freq		
Stress x Temp	Yes	
Stress x Test		N/A
Freq x Temp		Yes
Freq x Test		N/A
Temp x Test		N/A

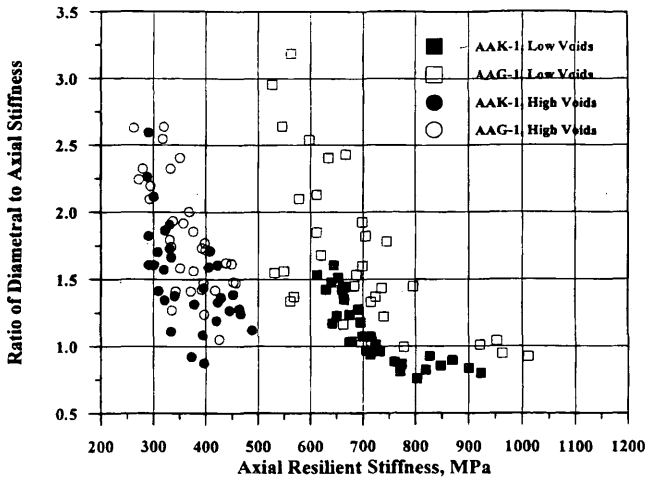

FIGURE 1 Effect of asphalt type and air-void content on resilient stiffness measurements at 40°C.

resilient stiffness values in this study were computed using the following expression *(4–6)*:

$$M_R = \frac{P\,(0.27 + \nu)}{(Ht)} \tag{2}$$

where

P = load,
H = total resilient horizontal deformation,
t = specimen height, and
ν = Poisson's ratio.

Because of difficulty in accurately measuring the resilient vertical deformation from which the Poisson's ratio is calculated, the Poisson's ratio is often assumed to be 0.35. This convention has been adopted for most of the diametral stiffness values reported herein. However, a few computations of diametral stiffness were made using values for Poisson's ratio of 0.1 and 0.2, thought to be representative of behavior at higher loading frequencies and lower temperatures. The diametral stiffness value based on a Poisson's ratio of 0.1 is about 60 percent of the value obtained using a Poisson's ratio of 0.35, as illustrated in Table 9.

Because of the demonstrated sensitivity of diametral resilient stiffness to the assumed value of Poisson's ratio, it was of interest to determine whether axial and diametral results might converge if Poisson's ratios other than 0.35 were used in the computations. Through a trial-and-error process, Poisson's ratios were found for which average axial and diametral stiffnesses were identical. These ratios are summarized in Table 10.

The variation among these ratios is extremely small, and the patterns that were anticipated—lower ratios at cooler temperatures and higher frequencies—were not demonstrated. It is concluded that the observed differences between axial and diametral stiffnesses cannot be logically explained by assumptions about the values of Poisson's ratio.

Poisson's ratio was also a subject of inquiry in the NCHRP investigation *(1)*. When computing Poisson's ratio based on measurements of resilient deformation, both vertical and horizontal, the investigators found extreme variations and concluded that many of the computed ratios were unrealistic and impractical. They attributed this to inappropriateness of linear elastic theory in deriving the expression for the Poisson's ratio. The investigators recommended assuming, not measuring, Poisson's ratio for routine mix design.

In summary, Poisson's ratio cannot be accurately determined from the vertical and horizontal deformations that are measured in indirect tension tests, either because of excessive deformations that may occur in the vicinity of the loading platens and that influence vertical deformation measurements or because of the inappropriateness of linear elastic theory. Moreover, it appears that diametral stiffnesses determined at temperatures below 20°C (68°F) should be

TABLE 8 Illustrative Effect of Test Method on Mix Stiffness

Temperature	Mix	Axial Testing		Diametral Testing	
		Average Resilient Stiffness (MPa)	Statistically Significant Difference?	Average Resilient Stiffness (MPa)	Statistically Significant Difference?
40°C	AAK-1, Low Voids	722	No	793	Yes
	AAG-1, Low Voids	691		1,112	
	AAK-1, High Voids	368	No	542	Yes
	AAG-1, High Voids	363		639	
20°C	AAK-1, Low Voids	4,397	Yes	4,597	Yes
	AAG-1, Low Voids	7,687		10,012	
	AAK-1, High Voids	2,267	Yes	3,847	Yes
	AAG-1, High Voids	4,759		6,997	
0°C	AAK-1, Low Voids	14,490	Yes	18,347	Yes
	AAG-1, Low Voids	20,948		28,083	
	AAK-1, High Voids	9,287	Yes	14,062	Yes
	AAG-1, High Voids	14,897		20,921	

TABLE 9 Example Effect of Poisson's Ratio on Diametral Resilient Stiffness in Megapascals at 0°C Testing Temperature

Test Number	Height, mm	Load, kg	Horizontal Deformation mm	Poisson's Ratio		
				0.10	0.20	0.35
1	66.3	201	0.0013	8,625	10,971	14,490
2	66.3	182	0.0011	8,832	11,178	14,766
3	66.3	388	0.0025	8,487	10,764	14,214
4	66.3	382	0.0024	8,625	10,971	14,490
5	65.0	193	0.0014	7,590	9,591	12,696
6	65.0	172	0.0012	7,797	9,867	13,040
7	65.0	384	0.0029	7,383	9,384	12,350
8	65.0	355	0.0026	7,521	9,591	12,627
Average				8,073	10,281	13,593

computed using values of Poisson's ratio somewhat less than the 0.35 that is normally assumed.

High-Temperature Resilient Stiffnesses

Axial testing was also conducted at 60°C (140°F). During this study, specimens with high air-void contents, especially those containing asphalt AAG-1 and RL aggregate, were observed to undergo excessive plastic (permanent) deformations. Nevertheless, these specimens exhibited relatively larger resilient stiffnesses than ones in which smaller levels of plastic deformation were observed, that is, those specimens containing asphalt AAK-1 and RB aggregate. Table 11 shows the average axial resilient stiffnesses at 60°C (140°F). It may be noted that at this temperature specimens containing AAG-1 asphalt and RB aggregate show lower stiffness values than those containing AAG-1 asphalt and RL aggregate. In addition, the axial stiffness value is higher at higher stress levels than at lower stress levels. It will be noted that higher stress levels result in more plastic (permanent) deformation.

One explanation for these effects is that when a specimen undergoes excessive plastic deformation, the resilient (elastic or recoverable) strain appears to be smaller, because the specimen does not fully recover during the unloading period. Because the resilient stiffness is computed as the ratio of the applied stress to resilient strain, weak specimens (which experience high plastic strain and thus low resilient strain) exhibit apparently higher stiffness values. Figure 2 shows the trace of the axial deformation versus time (number of repetitions) for a relatively weak specimen. It can be seen that the specimen does not fully recover during the unloading phase of the cycle. It will also be noted that the magnitude of the plastic deformation in just 10 cycles is approximately four to five times that of the resilient deformation.

Similar observations were made during diametral testing at 40°C (104°F). At this temperature most of the specimens, especially those with the high air-void content, experienced large plastic deformations at relatively low stress levels (41 to 69 kPa) and at low numbers of repetitions (fewer than 25 to 50). Many of these specimens showed extensive cracking and shear failures (punching) near the loading strips. Due to the extensive distress existing in specimens at this temperature, the diametral testing that had originally been planned for 60°C (140°F) was not performed. It was expected that, at this high temperature, weak specimens (such as those containing high air voids, asphalt AAG-1, and RL aggregate) would fail just from handling, even before testing could be initiated.

Figures 3 and 4 show the vertical and horizontal deformations, respectively, in a diametral test versus time (number of load repetitions) for a relatively weak specimen tested at 40°C (104°F). It should be noted that both plots show extensive accumulation of permanent strain. It should also be noted that in just 11 load repetitions the vertical plastic deformation is about 0.71 mm, whereas the horizontal plastic deformation is about 0.015 mm. The ratio of vertical to horizontal plastic deformation is approximately 50, suggesting extensive localized failure (punching) near the loading strip.

SUMMARY

The comparison of uniaxial compression and indirect tension testing of asphalt-aggregate mixes in this study has revealed the following points:

TABLE 10 Poisson's Ratio for Identical Axial and Diametral Stiffness

Frequency (Hz)	Temperature		
	0°C	20°C	40°C
0.5	0.19	0.16	0.13
1.0	0.18	0.17	0.19

TABLE 11 Effect of Mix and Testing Variables on Average Axial Stiffness at 60°C

Variable	Level	Air Voids	Granite (RB)		Chert (RL)	
			Average Stress kPa	Resilient Stiffness MPa	Average Stress kPa	Resilient Stiffness MPa
Asphalt Type	AAK-1	Low	46.2	201	48.3	190
		High	44.9	145	37.3	150
	AAG-1	Low	44.9	159	28.3	168
		High	45.5	137	29.7	144
Asphalt Content	Optimum	Low	45.5	184	39.3	176
		High	44.9	150	27.6	140
	High	Low	45.5	176	37.3	182
		High	45.5	132	39.3	155
Stress Level	Low	Low	33.8	169	26.9	173
		High	33.1	127	24.2	138
	High	Low	57.3	190	49.7	185
		High	58.0	155	43.5	157
Frequency	Low	Low	45.5	182	38.0	178
		High	45.5	142	33.8	148
	High	Low	45.5	180	38.6	180
		High	45.5	141	33.1	146
Repeats	First	Low	46.2	176	38.6	190
		High	45.5	132	34.5	157
	Second	Low	44.9	184	38.0	167
		High	45.5	150	32.4	138

1. Both axial and diametral stiffnesses are sensitive to the mix and test variables (asphalt type, aggregate type, air void content and temperature). The low and high stress levels and loading frequencies selected in this study did not significantly affect mix stiffness. The variation of asphalt content in the tested mixes was small; as a result, the observed effects of asphalt content on mix stiffness were relatively small.

2. In general, axial and diametral testing of asphalt-aggregate mixes yield different estimates of their resilient stiffness values. Average diametral resilient stiffness values computed using an assumed Poisson's ratio of 0.35 generally exceed average axial resilient stiffness values by approximately 35 to 45 percent. For individual specimens, diametral resilient stiffness values range from a low of approximately 50 per-

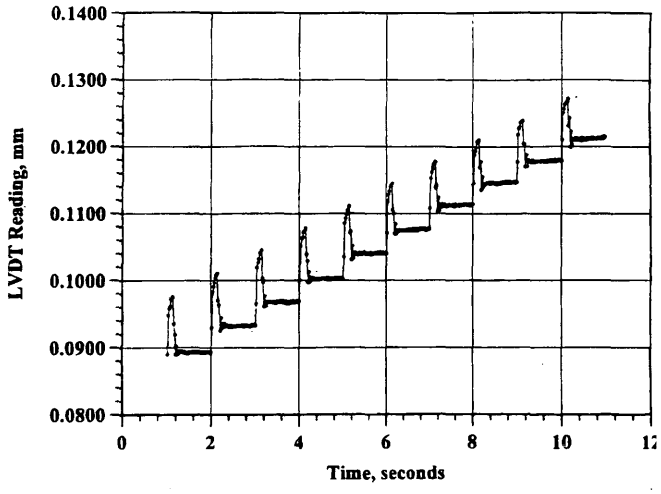

FIGURE 2 Example trace of axial deformation versus time under axial compressive testing.

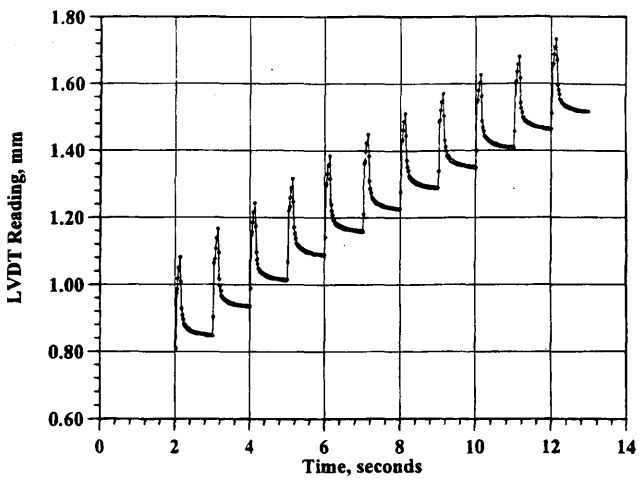

FIGURE 3 Example trace of vertical deformation versus time under diametral testing.

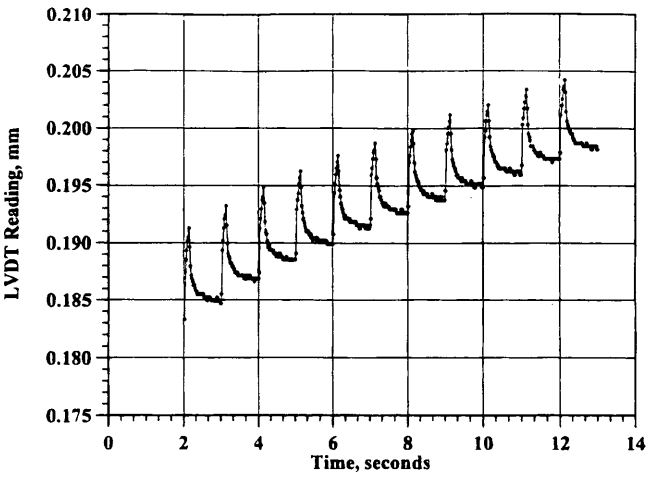

FIGURE 4 Example trace of horizontal deformation versus time under diametral testing.

cent of axial stiffness values to a high of approximately 350 percent.

3. Mix and test effects on resilient stiffness may differ according to whether loading is by axial compression or indirect tension. For example, one asphalt may appear superior if axial testing is employed, while another may appear superior with diametral testing. Such differences in effects on stiffness values arise for various reasons: (*a*) axial test results reflect greater response to shear (aggregate effects), while diametral test results reflect greater response to tension (asphalt effects); and (*b*) under conditions of larger deformations (high temperatures), the larger deformations in the axial test lead to more interparticle contact and, hence, larger stiffness, while larger deformations in the diametral tests may result in less interparticle contact. Such differences could have serious implications for the evaluation of mix effects in a comprehensive asphalt-aggregate mix-design and mix-analysis system.

4. Poisson's ratio, needed to determine resilient stiffness in diametral testing, cannot be accurately determined in the diametral test and must be assumed based on measurements obtained with other test systems. Observed differences between axial and diametral stiffnesses could not be logically explained by assuming the value of Poisson's ratio to be 0.35. Because Poisson's ratio must be assumed, diametral stiffnesses are likely to be less reliable than axial stiffnesses. Diametral stiffness values determined at temperatures below 20°C (68°F) should be computed using values of Poisson's ratio somewhat less than the 0.35 that is normally assumed.

5. Diametral stiffness cannot be accurately measured at high temperatures [60°C (140°F)]. Tests are not reliable even at moderately high temperatures [40°C (104°F)] due to excessive vertical permanent deformation. The SHRP A-003A laboratory experience suggests that weak specimens cannot be tested at temperatures as high as 60°C (140°F). NCHRP investigators also urge caution in "measuring the resilient modulus of elasticity and other properties at higher test temperatures using indirect tensile testing techniques" (*1*). Although they include 60°C (140°F) in their recommended test regime, the large permanent deformations observed in the SHRP A-003A testing cast serious doubt about the reliability of measurements at such temperatures. It seems more effective to limit indirect tension testing for resilient stiffness measurements to temperatures not greatly in excess of 20°C (68°F).

In summary, the indirect tension test appears to be suitable for determining the resilient stiffness of mixes only at low temperatures (and presumably at short loading times as well). At low temperatures, the behavior of asphalt-aggregate mixes is for the most part linearly elastic. However, the stiffness should be measured this way only if Poisson's ratio has been determined with sufficient accuracy from other types of tests.

ACKNOWLEDGMENTS

This study was conducted as part SHRP Project A-003A. This project, entitled "Performance Related Testing and Measuring of Asphalt-Aggregate Interactions and Mixtures," was conducted principally by the Institute of Transportation Studies of the University of California, Berkeley. SHRP is a unit of the National Research Council that was authorized by Section 128 of the Surface Transportation and Uniform Relocation Assistance Act of 1987.

REFERENCES

1. Von Quintus, H. L., J. A. Scherocman, C. S. Hughes, and T. W. Kennedy. *NCHRP Report 338: Asphalt-Aggregate Mixture Analysis System. TRB,* National Research Council, Washington, D.C., 1991.
2. Tayebali, A. A., B. W. Tsai, and C. L. Monismith. *Stiffness of Asphalt-Aggregate Mixes.* SHRP Project A-003A, Asphalt Research Program, Institute of Transportation Studies, University of California, Berkeley, April 1993.
3. Sousa, J. B., J. Harvey, L. Painter, J. A. Deacon, and C. L. Monismith. *Evaluation of Laboratory Procedures for Compacting Asphalt-Aggregate Mixtures.* SHRP-A/UWP-91-523, SHRP, National Research Council, Washington, D.C., 1991.
4. Kennedy, T. W. Characterization of Asphalt Pavement Materials Using the Indirect Tensile Tests. *Proc., Association of Asphalt Paving Technologists,* Vol. 46, 1977, pp. 132–150.
5. Vinson, T. Fundamentals of Resilient Modulus Testing. *Proceedings of the Workshop on Resilient Modulus Testing,* Oregon State University, Corvallis, 1989.
6. Roberts, F. L., P. S. Kandhal, E. R. Brown, D. Y. Lee, and T. W. Kennedy. *Hot Mix Asphalt Materials, Mixture Design and Construction.* NAPA Education Foundation, Lanham, Md., 1992, pp. 227–229.

This paper presents the views of the authors only and is not necessarily reflective of the views of the National Research Council, SHRP, or SHRP's sponsor. The results reported herein are not necessarily in agreement with the results of other SHRP research activities. They are reported to stimulate review and discussion within the research community.

Publication of this paper sponsored by Committee on Characteristics of Bituminous Paving Mixtures to Meet Structural Requirements.

Tensile Versus Compressive Moduli of Asphalt Concrete

PUNYA P. KHANAL AND MICHAEL S. MAMLOUK

A laboratory investigation was performed to evaluate the modulus of asphalt concrete in compression and tension. Five modes of loading, namely, quasi-static compressive, quasi-static tensile, harmonic compressive, harmonic tensile, and alternate compressive tensile loads, were used at three temperatures of 5°C, 25°C, and 40°C (41°F, 77°F, and 104°F). At 5°C, the tensile and compressive moduli were very close but at higher temperatures, the compressive modulus was always higher. These results were used in the multilayer elastic program ELSYM5 to study the effect on the stress and strain distributions of varying the modulus of asphalt concrete. A simple bimodular analysis was used in which the compressive modulus was used for the top half of the asphalt layer and the tensile modulus for the bottom half of the layer. The multilayer analysis indicates that the incorporation of the tensile modulus in the analysis gives results different from those obtained using a single compressive modulus, resulting usually in the increased predicted fatigue and rutting lives. This suggests that the use of a bimodular method of analysis that can distinguish between compressive and tensile stresses and use the appropriate modulus accordingly is more rational and provides more realistic predictions of flexible pavement responses than single-modular methods.

Material characterization is an integral part of the pavement design and analysis process and should be related to the method of design or analysis used. Since pavement is a complex structure consisting of a number of materials with different properties, perfect mathematical description of the structure and a unique characterization of the material may not be possible. All characterization methods, therefore, use some simplifying assumptions to make the problem mathematically amenable.

Most structural response models based on layered theory do not consider the heterogeneity of the asphalt concrete material. They are mostly based on linear elastic or linear viscoelastic theory. In the linear elastic theory, the material in each layer is assumed to be homogeneous, isotropic, and linear elastic. Such material can be fully characterized by two elastic parameters such as the modulus and Poisson's ratio. The viscoelastic theory considers also the time rate of stresses and strains in the asphalt concrete layer, but the assumptions of homogeneity and isotropy are still considered valid. Since asphalt concrete consists of aggregates and an asphalt binder with two distinct properties, the assumptions of homogeneity and isotropy may not be valid. One way of considering such heterogeneity of asphalt concrete is to use two different modulus values for tension and compression rather than using a single modulus value.

The use of a single modulus value for asphalt concrete would be justified if the asphalt concrete layer under the action of the traffic loads underwent either tensile stress only or compressive stress only throughout the thickness of the layer. This would also be justified if the asphalt concrete had the same modulus values in both tension and compression. Neither of these cases is true. The asphalt concrete layer under the action of vehicular loads is partly in tension and partly in compression. Figure 1 shows the pattern of stresses and strains developed in the pavement system when a vehicle travels over a smooth pavement surface (*1*). The figure shows that the pavement layers are mostly subjected to compression, while tension is developed mostly at the bottom of stiff asphalt layers. Also, it was reported as early as the 1960s that the material behaves differently in tension and in compression (*2,3*). It is therefore more realistic to use different modulus values for asphalt concrete in tension and in compression in the analysis and design of pavements.

No standard method of material characterization is currently available to determine moduli and Poisson's ratios of asphalt concrete in both tension and compression. Also, the influence of using different modulus values for tension and compression on basic pavement design parameters is not known. More work is needed on this subject to evaluate these strength parameters for asphalt concrete under different loading and temperature conditions, which forms the basis of the present study.

OBJECTIVE

The objective of this study is to evaluate the modulus and Poisson's ratio of asphalt concrete under different loading and temperature conditions. Tensile and compressive parameters under static and dynamic conditions are determined in the laboratory. The effect on critical pavement design parameters of using such parameters is also determined.

NATURE OF ASPHALT CONCRETE RESPONSE

Asphalt concrete consists of aggregate particles coated with asphalt binder as illustrated in Figure 2. When the material is subjected to compression, compressive strength is developed because of the resistance to the shear stresses of both the aggregate interlock and the stiffness of the asphalt binder. For asphalt concrete in tension, the effect of the aggregate interlock is almost nonexistent, while the asphalt binder plays an important role in the tensile resistance of asphalt concrete. Therefore, it seems logical to expect asphalt concrete to have different behaviors in tension and in compression. Also, since the stiffness of the asphalt binder is largely affected by temperature and the aggregate stiffness is not, the difference between the tensile and compressive responses is expected to be different at different temperatures.

The task of material characterization is made complicated by the effect of rate dependency, environmental conditions, state of stress,

P. P. Khanal, Applied Paving Technology, Inc., 1339 Allston, Houston, Tex. 77008. M. S. Mamlouk, Department of Civil Engineering, Arizona State University, Tempe, Ariz. 85287.

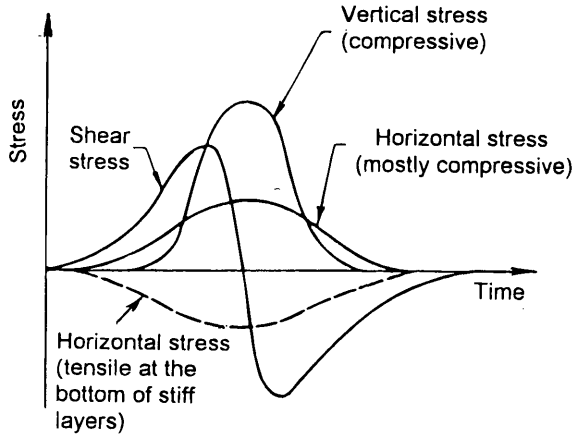

FIGURE 1 Pattern of stresses and strains developed in the pavement system under a wheel load moving on a smooth pavement surface.

and age on the properties and response of asphalt concrete. Thus, using simple assumptions in the characterization of the paving materials may not produce accurate results. Although not impossible, exact laboratory simulation of in situ conditions may be prohibitive both in time and in cost. Thus, all characterization techniques for paving materials are by necessity a compromise between rigor and practically. As such, laboratory test methods often use simplifications with the object of reproducing only those aspects of the in situ conditions that are likely to be most significant. Usually, the compromise is based on the average or limiting conditions that are believed to be critical with respect to pavement behavior.

Different modes of loading have been used by different researchers to characterize asphalt concrete in the laboratory, for example, direct tension, direct compression, and a combination of tension and compression such as the case of the diametral resilient modulus test. Also, both static and dynamic (harmonic and pulsating) loads have been used. The diametral resilient modulus test has been extensively used lately in many studies including the SHRP Long-Term Pavement Performance (LTPP) study. However, problems with the accuracy and reproducibility of such tests have been encountered.

The bimodular nature of asphalt concrete has been investigated by many researchers. Hargett and Johnson (*4*) found the compressive strength of asphalt concrete to be about 10 times the tensile strength. Kallas (*5*) conducted repeated load dynamic tests to investigate the dynamic modulus of the asphalt concrete in tension, tension-compression, and compression. He found that the dynamic modulus values under tension and tension-compression were as low as one-half of the dynamic compression modulus. Kennedy et al. (*6*) reported the permanent strain relationships for the triaxial tensile test and indirect tension test to be similar but both of them to be significantly different from those for the triaxial compression tests.

Von Quintas et al. (*7*) found the unconfined compression and indirect tensile resilient moduli not to be much different at low temperatures. However, the two modulus values were found to diverge greatly at higher temperatures. Bonaquist et al. (*8*) measured compressive and tensile moduli over a range of temperatures and frequencies and found greater dynamic compressive modulus values than indirect tensile modulus values. They also found the modulus-versus-temperature relationships to be different for different test procedures. Mamlouk (*9*) showed that the indirect tensile modulus was different than the moduli of compressive load types. He suggested refining the multilayer elastic analysis by using appropriate modulus values depending on whether the material is in tension or in compression. This seems rational because the asphalt concrete surface in pavement is partly in tension and partly in compression. If the tension and compression moduli differ significantly, then neither the compressive nor the tensile modulus alone would truly represent the asphalt concrete layer in the field.

LABORATORY TESTING AND RESULTS

In this study 35 hot-mix asphalt concrete cylindrical specimens were prepared, 102 mm (4 in.) in diameter and 203 mm (8 in.) in length. They were prepared using the California kneading compaction according to ASTM D3496. A dense aggregate gradation was used with a maximum size of 12.5 mm (1/2 in.) as shown in Table 1. An AC-40 asphalt cement was used with a content of 5.3 percent by weight of aggregate, which was the optimum asphalt content following the Marshall mix design procedure. The asphalt cement had the following properties:

1. Penetration: at 25°C, 100 g, 5 sec = 35;
2. Absolute viscosity = 3500 poise;
3. Kinematic viscosity = 350 cSt;
4. Ductility > 85 cm; and
5. Absolute viscosity after RTFO test = 8000 poise.

During compaction the number of blows was adjusted by trial and error to obtain the same bulk specific gravity as Marshall specimens. The average bulk specific gravity (saturated surface-

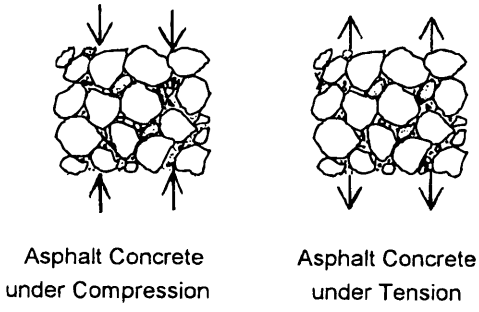

FIGURE 2 Asphalt concrete under compression and tension.

TABLE 1 Aggregate Gradation Used in Study

Sieve Size, mm (in.)	Percent Passing
12.5 (1/2)	100
9.5 (3/8)	85
4.75 (No. 4)	60
2.36 (No. 8)	49
1.18 (No. 16)	36
0.60 (No. 30)	24
0.30 (No. 50)	13
0.15 (No. 100)	7
0.075 (No. 200)	4

dry) of specimens was 2.319. Specimens were then grouped into five groups with the same average bulk specific gravity of each group.

Five laboratory tests were performed with the following loading conditions as illustrated in Figure 3:

1. Quasi-static axial compression with a rate of loading of 4.45 kN/sec (1,000 lb/sec). The maximum stress applied was approximately 275 kPa (40 psi).
2. Quasi-static axial tension with a rate of loading of 4.45 kN/sec (1,000 lb/sec). The maximum stress applied was approximately 275 kPa (40 psi).
3. Harmonic axial compression with a frequency of 3 Hz and a peak-to-peak stress of 275 kPa (40 psi) and a seating stress of about 35 kPa (5 psi).
4. Harmonic axial tension with a frequency of 3 Hz and a peak-to-peak stress of 275 kPa (40 psi) and a seating stress of about 35 kPa (5 psi).
5. Harmonic axial tension-compression with a frequency of 3 Hz and a peak-to-peak stress of 550 kPa (80 psi).

Seven different specimens were tested using each of these loading conditions, although not all the tests were successful due to minor problems with the machine and/or the measuring devices. Tests were performed at temperatures of 5°C, 25°C and 40°C (41°F, 77°F, and 104°F). Since the tests were nondestructive, each specimen was tested at the three test temperatures starting with the lowest temperature and ending with the highest temperature.

The arrangement of the linear variable differential transducers (LVDTs) attached to the test specimen inside the temperature-controlled chamber is shown in Figure 4. Two vertical spring-loaded LVDTs were attached to the specimen using clamps fixed to the specimen with epoxy. A 102-mm (4-in.) gauge length was used in the middle of the specimen height in order to reduce the "end effect." In addition, two horizontal spring-loaded LVDTs were attached to vertical posts and made contact with the specimen at two opposite sides at midheight. The bases of the specimen were fixed to the top and bottom loading heads of the machine with epoxy using the concrete capping device (ASTM C617). Since very small deformations were expected to be measured, proper specimen alignment and LVDT attachment were ensured. Also, care was taken to select the proper size and accuracy of LVDTs to ensure accurate measurements.

An electrohydraulic closed-loop machine equipped with an environmental chamber was used for testing. The machine was controlled by a microcomputer. Before testing, the LVDTs and the load cell were calibrated. During the test, the load and deformations were continuously recorded.

In case of quasi-static loading, the stress-strain relation was either linear or slightly nonlinear. The modulus was computed as the secant modulus of the stress-strain curve at 275 kPa (40 psi). The Poisson's ratio was computed as the negative of the ratio between the horizontal and vertical strains at 275 kPa (40 psi). In case of either compressive or tensile harmonic loading, the dynamic modulus was computed by dividing the stress amplitude by the strain

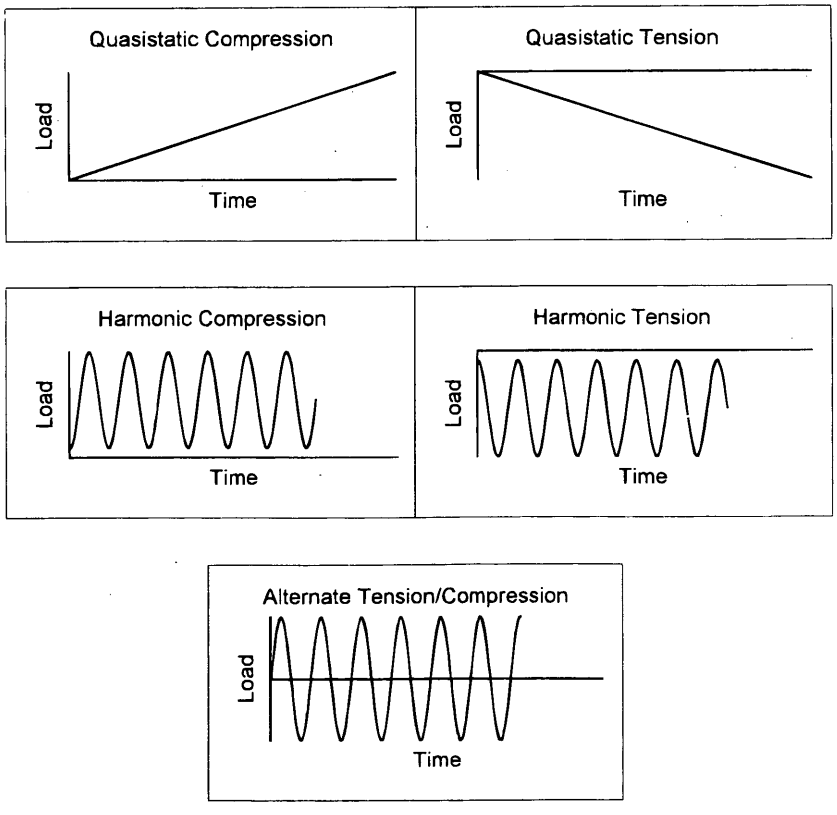

FIGURE 3 Load patterns used in the laboratory testing.

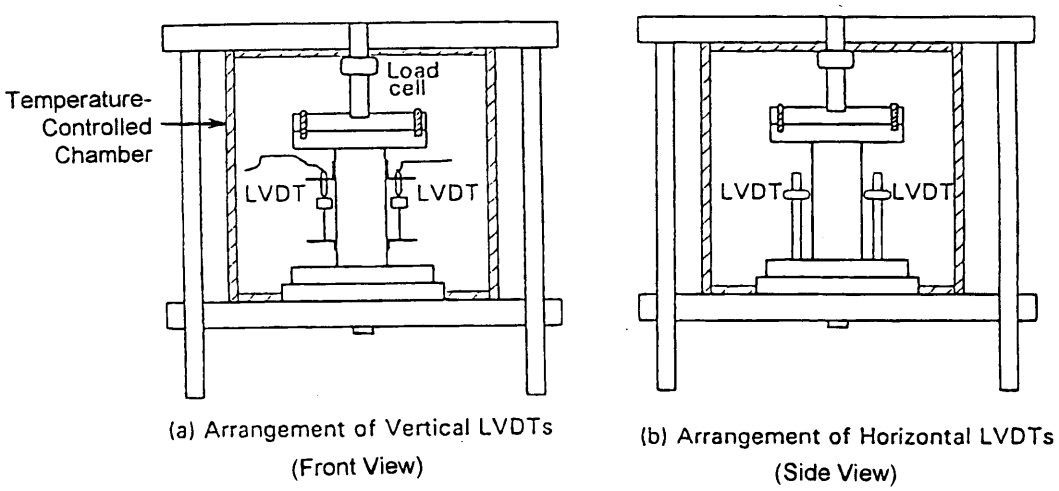

FIGURE 4 Schematic diagram of specimen and LVDT setup.

amplitude (ASTM D3497). For the alternate tension and compression test, separate tensile and compressive moduli were determined by dividing the stress amplitude by the strain amplitude in each case. The Poisson's ratio was computed as the negative of the ratio between the horizontal and vertical strain amplitudes. Table 2 shows the average modulus values for different loading conditions and test temperatures. The table shows that the modulus values are within the typical range of values obtained by other researchers. However, Poisson's ratio results were not reliable. Most Poisson's ratios were quite low and inconsistent. This problem has been reported in several studies.

TABLE 2 Average Modulus Values at Different Loading Conditions and Test Temperatures

Test Type		5°C	25°C	40°C
Quasi-Static Compression		14704	4258	676
Quasi-Static Tension		10681	3632	266
Harmonic Compression		13558	6156	1741
Harmonic Tension		14534	4250	619
Alternate	Compression	14202	6896	1378
	Tension	16457	6259	910

ANALYSIS OF LABORATORY RESULTS

Figure 5 shows a plot of mean modulus values given in Table 2. It can be seen from Figure 5 that increasing the temperature decreases the modulus for all modes of loading. Comparing the tensile and compressive moduli at each temperature shows that at 5°C (41°F), the mean tensile modulus values were slightly higher than the cor-

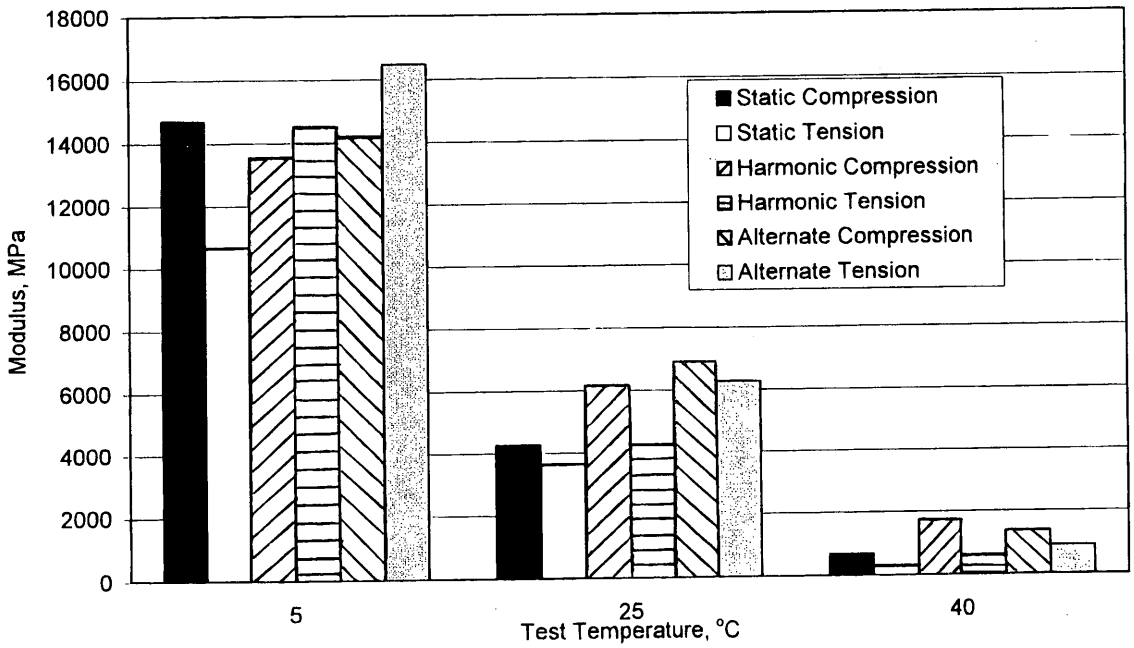

FIGURE 5 Modulus values at different test temperatures.

responding compressive values except in the quasi-static case. In general, the tension and compression modulus values were close to each other and did not follow any specific trend. At low temperatures, the asphalt binder has a high stiffness, which contributes significantly to the stiffness, and hence the modulus, of the asphalt aggregate mixture. Thus, at low temperatures, asphalt concrete seems to behave similarly in tension and in compression.

At 25°C (77°F), the mean compressive modulus values were higher than the corresponding tensile modulus values for all loading conditions. The maximum difference between the two moduli was in the harmonic tensile and compressive loading case in which the average compressive modulus was about 1.5 times the average tensile modulus. The smallest difference was in the alternate tension-compression loading case in which the compressive modulus was only about 10 percent higher than the corresponding tensile modulus.

At 40°C (104°F), however, there was a great difference between the tensile and compressive modulus values. The compression modulus was about three times as high as the tension modulus in both the static and harmonic loading cases, whereas it was about 50 percent higher in the alternate tension-compression loading mode.

The reason for obtaining tensile modulus values lower than the corresponding compressive values at high temperatures can be explained by the fact that the tensile stiffness of the mixture is contributed mostly by the tensile resistance of the asphalt binder, whereas aggregate particles contribute very little. Since the stiffness of the asphalt binder is largely reduced at high temperatures, the tensile modulus of the asphalt concrete is also reduced. On the other hand, most of the load is carried by the aggregate particles when the mixture is subjected to compression, whereas the asphalt binder has little contribution. Hence, at high temperatures the compressive modulus is not largely reduced when compared to the tensile modulus.

This clearly indicates that asphalt concrete does not behave similarly in tension and in compression, especially at high temperatures. Although it may be logical to consider similar tensile and compressive moduli at low temperatures, the assumption of similar moduli at higher temperatures is not valid. This is also demonstrated by the analysis of variance (ANOVA) statistical tests that were conducted to evaluate the significance of loading conditions and test temperatures on the modulus values. A level of significance of 5 percent was used in this study. The ANOVA results indicate that both test temperature and loading condition are significant. As expected, the most significant factor was the test temperature.

ANALYSIS OF FIELD CONDITIONS

The ELSYM5 multilayer elastic computer program (*10*) was used to evaluate the stress distribution within the asphalt layer under typical field conditions. Critical parameters such as the tensile strain at the bottom of the asphalt layer and the compressive strain at the top of subgrade were also computed. Three typical flexible pavement sections were considered and designated thin, medium thickness, and thick with layer thickness as shown in Table 3. The subgrade was assumed to have a semiinfinite thickness. The laboratory obtained tensile and compressive moduli of asphalt concrete at the three temperatures of 5°C, 25°C, and 40°C obtained by harmonic loadings were used in the analysis. The moduli of base, subbase, and subgrade materials were assumed to be 550, 275, and 140 MPa (80, 40, and 20 ksi), respectively. Poisson's ratios for asphalt concrete

TABLE 3 Layer Thicknesses of Analyzed Pavement Sections

Layer Type	Layer Thickness, mm (in.)		
	Thin	Medium	Thick
Asphalt Concrete	51 (2)	152 (6)	254 (10)
Base	102 (4)	152 (6)	203 (8)
Subbase	102 (4)	203 (8)	305 (12)

were assumed to be 0.30, 0.35, and 0.40 at 5, 25, and 40°C, respectively. Poisson's ratios measured during the laboratory testing were not used because they were unreliable. Poisson's ratios for base, subbase, and subgrade were assumed to be 0.35, 0.35, and 0.45, respectively. A circular uniformly distributed load with a 40-kN (9-kip) magnitude and a 690-kPa (100-psi) intensity was used.

Two methods of analysis were used for all three pavement sections. In the first method, only the compressive modulus of asphalt concrete was used for the whole thickness of the asphalt concrete layer. In the second method, the asphalt concrete layer was divided into two halves, with the top half assigned the compressive modulus and the bottom half the tensile modulus. Figure 6 shows the distribution of vertical and radial stresses in the thin pavement at three temperatures for the two methods of analysis. Similarly, Figures 7 and 8 show the corresponding results for the medium thickness and thick pavements, respectively. In all three figures, it can be seen that both radial and vertical pressure distributions at 5°C (41°F) are essentially identical for both methods of analysis.

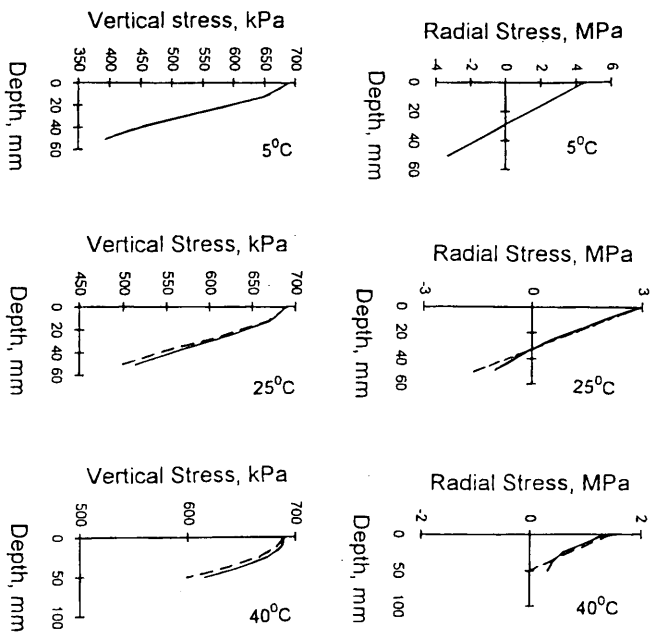

FIGURE 6 Stress distributions in thin pavements. (- - -)Method 1: compressive modulus only was used. (—)Method 2: both compressive and tensile moduli were used. Positive stresses are compression.

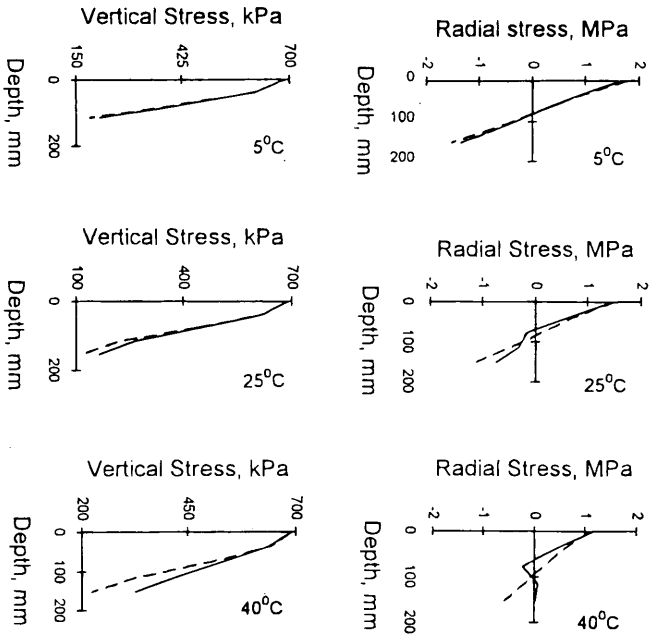

Notes:
– – – Method 1: Compressive modulus only was used
—— Method 2: Both compressive and tensile moduli were used
Positive stresses are compression

FIGURE 7 Stress distributions in medium-thickness pavements. (- - -)Method 1: compressive modulus only was used. (—)Method 2: both compressive and tensile moduli were used. Positive stresses are compression.

For the thin pavement (Figure 6) at 25°C (77°F), the tensile radial stress at the bottom of the asphalt layer was reduced by about 45 percent when the bimodular method of analysis was used. The vertical pressure distribution, however, did not change much throughout the asphalt layer. At 40°C (104°F) the compressive modulus method produced a small tensile radial stress at the bottom of the asphalt layer, whereas the use of the bimodular analysis produced a compressive radial stress. At 25°C the use of the bimodular analysis increased the tensile strain at the bottom of the asphalt layer by about 7 percent whereas at 40°C it was reduced by 40 percent. For all temperatures, there was no significant difference in the vertical deformation at the top of the subgrade.

For the medium-thickness pavement (Figure 7) at 25°C, the tensile radial stress at the bottom of the asphalt layer was reduced by about 30 percent when the bimodular analysis was used as compared with the case of using the compressive modulus only. The vertical stresses throughout the layer, however, remained practically unchanged. At 40°C the compression-only analysis gave a tensile radial stress at the bottom of the asphalt concrete layer but the tension-compression moduli combination gave a compressive radial stress. At all temperatures, the use of bimodular analysis caused a reduction in the tensile radial strain at the bottom of the asphalt layer as well as the vertical deformation on top of the subgrade. The reduction ranged from 5 to 35 percent.

For the thick pavement (Figure 8) at 25°C, the tensile radial stress at the bottom of the asphalt concrete layer was reduced by about 28 percent when the bimodular method of analysis was used as compared with the case of using the compressive modulus value only. At 40°C the combination of tension and compression moduli gave a very small compressive radial stress at the bottom of the asphalt

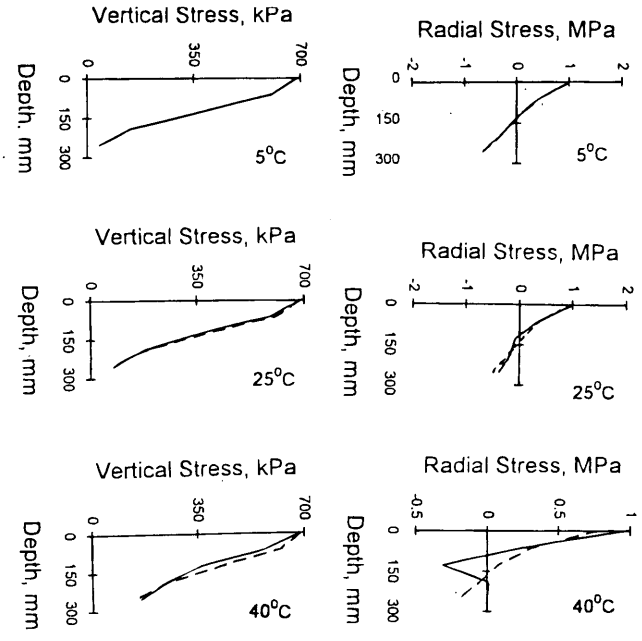

Notes:
– – – Method 1: Compressive modulus only was used
—— Method 2: Both compressive and tensile moduli were used
Positive stresses are compression

FIGURE 8 Stress distributions in thick pavements. (---)Method 1: compressive modulus only was used. (—)Method 2: both compressive and tensile moduli were used. Positive stresses are compression.

layer but induced a tensile radial stress in the middepth of the asphalt layer. This was also observed in the medium-thickness pavement section. The use of the bimodular analysis caused a slight increase (varying from 5 to 10 percent) in the radial tensile strain at the bottom of the asphalt layer as well as the displacement on top of the subgrade.

CONCLUSIONS

Based on the observations obtained from the laboratory measurements and the multilayer elastic analysis, the following conclusions can be drawn:

1. Asphalt concrete resists tensile and compressive stresses differently because of the different contributions of asphalt and aggregates to the tensile and compressive stiffnesses. Also, since the stiffness of the asphalt binder is largely affected by temperature whereas the aggregate stiffness is not affected, the difference between the tensile and compressive moduli is typically different at different temperatures.
2. Asphalt concrete has similar moduli in tension and compression at low temperatures, but those moduli are different at high temperatures. The difference between the tensile and compressive moduli becomes more significant when the temperature increases.
3. At high temperatures the tensile modulus is always lower than the compressive modulus, with the tensile modulus in some cases as low as one-third of the compressive value.
4. Since the asphalt concrete layer undergoes both tensile and compressive stresses while the tensile and compressive moduli are typically different, more accurate results can be obtained when the appropriate modulus is used in multilayer elastic analyses.
5. When both compressive and tensile moduli were used in the top and bottom halves of the asphalt concrete layer, respectively, there was no significant change in the vertical compressive stresses in most cases but the radial tensile stress at the bottom of the layer was lower than that obtained by using the compressive modulus only. The reduction was about 45 percent in the case of thin pavements and up to about 28 percent in the case of thick pavements.
6. The use of the bimodular analysis causes a reduction in the tensile strain at the bottom of the AC layer as well as the vertical compressive strain on top of the subgrade of medium thickness pavements at all three temperatures. This means it increases the predicted fatigue life as well as the rutting life of the pavement structure.
7. Further research could provide a pavement analysis method that would be able to distinguish between compressive and tensile locations within the asphalt concrete layer and use the appropriate modulus at different locations. An iterative procedure could be used for this purpose.

ACKNOWLEDGMENTS

The authors would like to thank the Department of Civil Engineering and the Center for Advanced Transportation Systems Research at Arizona State University for making their facilities available to this study.

REFERENCES

1. Brown, S. F. Material Characteristics for Analytical Pavement Design. In *Developments in Highway Pavement Engineering - 1.* (Peter S. Pell ed.) London, 1977, pp. 41–92.
2. Monismith, C. L., and K. E. Secor. Viscoelastic Behavior of Asphalt Concrete Pavements. *Proc., International Conference on the Structural Design of Asphalt Pavements,* Ann Arbor, Mich. 1962, pp. 476–498.
3. Pister, K. S., and R. A Westman. Analysis of Viscoelastic Pavements Subjected to Moving Loads. *Proc., Intl. Conf. on the Structural Design of Asphalt Pavements,* Ann Arbor, Mich. 1962, pp. 522–529.
4. Hargett, E. R., and E. E. Johnson. Strength Properties of Bituminous Concrete Tested Tension and Compression. *Proc., Highway Research Board,* Vol. 40, 1961, pp. 430–440.
5. Kallas, B. . Dynamic Modulus of Asphalt Concrete in Tension and Tension-Compression. *Proc., Association of Asphalt Paving Technologists,* Vol. 39, 1970, pp. 1–20.
6. Kennedy, T. W., A. S. Adedmila, and R. Haas. Material Characterization for Asphalt Pavement Structural Design Systems. *Proc., 4th International Conference on the Structural Design of Asphalt Pavements,* Vol. II, Ann Arbor, Mich. 1977, pp. 346–353.
7. Von Quintas, H. L., J. . Rauhut, and T. . Kennedy. Comparisons of Asphalt Concrete Stiffness as Measured by Various Testing Techniques. *Proc., Association of Asphalt Paving Technologists,* Vol. 51, 1982, pp. 35–49.
8. Bonaquist, R., D. A. Anderson, and E. Fernando. Relationship Between Moduli Measured in the Laboratory and Field Deflection Measurements. *Proc., Association of Asphalt Paving Technologists,* Vol. 55, 1986, pp. 419–448.
9. Mamlouk, M. S. Rational Concept in Relating Lab Testing to Pavement Analysis. *Proc., 7th International Conference in Asphalt Pavements,* Vol. 1, Nottingham, England, 1992, pp. 124–140.
10. Kapperman, S., G. Tiller, and M. Tseng. *ELSYM5 Interactive Version, User's Manual.* SRA Technologies, Inc., Arlington, Va., July 1985.

Publication of this paper sponsored by Committee on Characteristics of Bituminous Paving Mixtures To Meet Structural Requirements.

Comparison of Mix Design Concepts

JORGE B. SOUSA, GEORGE WAY, JOHN T. HARVEY, AND MICKEY HINES

Three mix design methods currently available to industry were used to select the asphalt content for a mix used on an overlay placed in November 1993 on Interstate 17 near Phoenix, Arizona. The methods used were Marshall, Superpave Level I, and a performance-based procedure developed during the SHRP-A003A research project using the results of the repetitive simple shear test at constant height and the flexural bending beam test. The mix, with the asphalt content selected based on the method derived in Project SHRP-A003A, was further evaluated by the Hamburg wheel tracking device. The results of a condition survey performed on the actual pavement several months after construction, are presented.

During the Strategic Highway Research Program (SHRP) several new concepts and test methods were developed to evaluate mix performance in the mix design stage. The Arizona Department of Transportation (ADOT) decided to evaluate some of these methods by placing two 1-mi test sections 6 mi north of Phoenix on Interstate 17 near the Pioneer Living Museum exit. Construction took place in November 1993. The primary purpose of the test sections was to evaluate new SHRP materials requirements and tests for mineral aggregate, asphalt, and hot-mix asphaltic concrete (HMAC) by designing and building a 75-mm (3-in.) HMAC inlay that could sustain 10 million design equivalent single axle loads (ESALs) in the 10-year design period. The major design criterion was to limit permanent deformation in the mix so that the rut depth over the life of the project would be less than 10 mm (0.4 in.). The asphalt content was selected using a performance-based mix design developed during Project SHRP-A003A. The field mix was then evaluated by the Marshall method as currently used by ADOT and by the Superpave Level I procedure (*1*). Further evaluation of the selected mix was made using the Hamburg wheel tracking device.

MIX DESIGN CONCEPTS

The goal of a mix design procedure is to combine aggregates and binder into a mix that is able to satisfy desired levels of performance. The definition of performance can be quite broad. With improvements in technology, the concept of mix design has changed. Current methods can be categorized on the basis level of complexity and ability to predict performance:

- **Level 1:** fabrication of specimens under a given set of conditions to determine their volumetric characteristics. Aggregate and binder characteristics are based on prior experience. Asphalt content is based on compactability data. This is basically the approach followed by Superpave Level I.
- **Level 2:** fabrication of specimens under a given set of conditions and execution of a test to measure a reduced set of specimen properties. Limits are set on those variables based on prior experience. Asphalt content is based on limits, ranges, or extreme values of the variables evaluated. This is basically the concept followed by the Marshall method.
- **Level 3:** determination of some fundamental properties using specimens that have undergone specific preconditioning. Performance is predicted on the basis of statistical correlations between laboratory results obtained under a given set of conditions and field observations. Asphalt content can be selected based on desired pavement performance in fatigue and permanent deformation. This is achievable with the current state of knowledge and is basically the approach proposed by some other reseachers (2–7) and used by Superpave Level III (*1*).
- **Level 4:** determination of fundamental properties of the mix (and/or components) and evolution of those properties with time, aging, strain and stress levels, and moisture. Prediction of behavior is made through an elaborate set of computer simulations. This approach is beyond the current state of knowledge. Asphalt content would be selected based on predicted pavement performance, which would be very close to actual performance.

Given that Level 4 is not readily applicable at this time, the other three concepts were addressed.

Volumetric Method—Superpave Level I Mix Design

The Superpave Level I volumetric design is similar in concept to historical volumetric mix design methods. No direct measurements are made of mixture mechanical properties and no prediction of performance is made (*8*). It differs from the Marshall method in that no test is performed on the mix at temperatures representative of those encountered in the field at which permanent deformation occurs. It also differs in that the design conditions vary with location and traffic. However, for a given set of conditions the compaction effort is the same for all mixes. Within Level I concepts the maximum number of gyrations is expected to be representative of compaction levels that lead to design life density. Given that all measurements are executed at the compaction temperature, this procedure could be used to evaluate compactability of the mix.

Volumetric mix design includes compaction using a gyratory compactor that monitors increase in density with increasing compactive effort. Compaction specimens are required to be mixed and compacted under equiviscous temperature conditions corresponding to 0.170 Pa·sec and 0.280 Pa·sec, respectively (*1*).

After short-term aging, the loose mix is ready for compaction with the Superpave gyratory compactor (SGC). The vertical pres-

J. B. Sousa, SHRP Equipment Corporation, Richmond Field Station, Bldg 155, 1301 South 46th Street, Richmond, Calif. 94804. G. Way, Arizona Department of Transportation, 206 S. 17th Avenue, Phoenix, Ariz. 85007. J. T. Harvey, Richmond Field Station, Building 480, 1301 South 46th Street, Richmond, Calif. 94708. M. Hines, Koch Materials Company, 400 N. 70th Street, P.O. Box 1507, Terre Haute, Ind. 47808.

sure is set at 0.6 MPa and the angle of gyration is 1.25 degrees. The number of gyrations per minute is 30. Three gyration levels are of interest: design number (N_{des}), initial number (N_{ini}), and maximum number (N_{max}). Relationships were developed between those values. The design number of gyrations ranges from 68 to 172 as a function of climate and traffic level. The value 68 is used for selection with design levels of less than 300,000 and average design high air temperatures below 39°C, whereas 172 is used for traffic levels above 100 million ESALs and corresponding temperatures above 44°C.

The compaction data are analyzed by computing the estimated bulk specific gravity, corrected bulk specific gravity, and corrected percentage of maximum theoretical specific gravity ($\%G_{mm}$) for each desired gyration. The volumetric properties are calculated at the design number of gyrations for each trial asphalt binder content. From these data points, the designer can generate graphs of air void content, VMA (voids in mineral aggregate), and VFA voids filled with asphalt) versus asphalt binder content. Several criteria should be observed. The target air void content should be 4 percent, VMA values are a function of the nominal maximum particle size (for instance, for a 19-mm nominal size, VMA should be higher than 13 percent), and VFA values depend on traffic level (for instance, for a project with 10 million ESALs the range is 65 to 75 percent). Furthermore, the $\%G_{mm}$ at N_{ini} should be less than 89 percent and the $\%G_{mm}$ at N_{max} should be less than 98 percent.

It can be observed from this procedure that binder type should have no effect on the development of gyratory compaction data because the compaction procedure is based on equiviscous temperature conditions. As such, selection of binder content should become independent of binder type. Conceptually, a standard binder could be specified to execute the compaction curves. Within Superpave Level I methodology, binder grade selection is independent of compaction curve data, and there is absolutely no need to execute the compaction curves with the same binder that will eventually be used in the field. It can also be observed that compaction data (air void content as a function of the number of gyrations) are a function of the angle of gyration, number of gyrations per minute, and axial pressure for the gyratory compactor. Small changes in any of these parameters can have a significant impact on the compaction data and criteria.

In addition to these mix criteria, Superpave Level I has asphalt binder criteria (from AASHTO MP-1, performance-graded specifications), aggregate quality criteria (coarse aggregate angularity, fine aggregate angularity, flat/elongated particles, and sand equivalent), combined aggregate gradation requirements (based on the nominal maximum particle size of the mixture), and moisture sensitivity criteria. Within Superpave concepts this mix design is intended to perform as a system, and subtracting any of these components could result in mixtures designed with unacceptable performance properties. On the other hand, it is possible that mixes that do not satisfy all these criteria may perform very well.

Marshall Mix Design Method

The basic concept of the Marshall mix design method is the selection of asphalt content based on optimization or limits for several variables that are not direct measures of performance. On the one hand, there is a volumetric evaluation based on specimens fabricated under a given set of conditions with a given level of compaction energy. The preset compaction energy is expected to produce density levels similar to those imposed by trafficking. After compaction, specimen VMA, VFA, and air void content measurements are reported and evaluated against a given set of allowable values. On the other hand, a test is executed at 60°C (140°F), which is assumed to be a temperature representative of that typically encountered in the pavement at which permanent deformation is likely to occur. From the test, specific parameters are measured (e.g., Marshall stability and flow). For instance, minimum Marshall values are set in the specification criteria. It should be noted that in this approach changing binder type can result in the selection of a different asphalt content as long as the viscosity of the binder at 60°C.

Performance-Based Mix Design Method

The objective of the performance-based mix design method is to establish the appropriate amount of asphalt content in a mix that will simulataneously satisfy the rut resistance and fatigue cracking requirements for a given set of conditions (e.g., traffic and environment). Figure 1 shows the process in which two mixes, A and B, are evaluated and compared with the design requirements. Mix A would satisfy the requirements, whereas Mix B would not. To evaluate rut and fatigue cracking resistance of the mixes, tests developed during Project SHRP-A003A were used. These tests are executed in conditions most critical for the distress mechanism being evaluated. For instance, the repetitive simple shear test at constant height (RSST-CH), developed to evaluate permanent deformation of the mix, should be executed at high temperatures representative of those encountered in the top 5 cm (2 in.) of the pavement during the warmest days of the year (*2*). The four-point flexural bending beam fatigue test should be executed at temperatures around 20°C, where the conditions that cause fatigue cracking are generally most severe (*7*). The effects of aging and moisture on the mix are addressed as they affect performance. Furthermore, it is recognized that air void content changes according to traffic densification, and tests are executed accordingly. For instance, for dense-graded mixes, the RSST-CH should be executed at air void contents of approximately 3 to 4 percent, where the mix is most resistant to accumulation of permanent deformation due to shear stresses. It is assumed that rutting is only likely to occur when the mix drops below that air void content range. However, successful performance-based approaches to mix design require that compaction in the laboratory yield specimens with performance properties identical to those obtained from field cores (*9*).

Using this performance-based approach, there is no need to set explicit limits on volumetric characteristics. If a mix does not meet a particular value of VMA or VFA, but still has the desired performance at the expected in situ volumetric characteristics, it would be

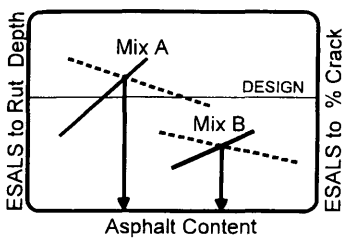

FIGURE 1 Performance-based mix design concept.

acceptable. The selection of asphalt content is based on the desired level of performance for each mode of distress. For instance, in this framework a change of asphalt type, even within the same binder grade, can affect the predictions of fatigue life.

MATERIALS

A modified binder was used for this project (*10*) to satisfy the PG70-10 grade recommended for the location. The aggregate used in the mix design stage was a crushed river gravel, and contained larger fractions with rounded faces, whereas the smaller fractions exhibited all crushed faces. Portland cement (1.0 percent by dry weight of aggregate) was used to reduce moisture sensitivity in the mix. Aggregate fractions were combined in order to meet the ADOT standard gradation.

This mix design gradation conforms with the Superpave guidelines as shown in Figure 2. It also satisfied all binder and aggregate recommendations of Superpave. However, during construction the gradation was changed and a larger percentage of crushed material was used, with 95 percent crushed on one face and 90 percent on two faces. The fine aggregate was 100 percent mechanically crushed. It can be seen in Figure 2 that the field gradation passes through the Superpave restricted zone.

PERFORMANCE-BASED LABORATORY MIX DESIGN

Permanent Deformation Evaluation

Selection of Test Temperature

It has been ADOT's experience that most rutting develops when summer temperatures are above normal. To minimize the possibility of this occurrence, the RSST-CH temperature was carefully selected. The average 7-day maximum surface pavement temperature at the site is 68.1°C (154.6°F) with a standard deviation, based on records for 42 years, of 1.7°C (3.0°F) (obtained from the SHRP project data base). From these values the temperature at the critical depth for shear deformation, 50 mm (2 in.), was computed to be 61.3°C (142.3°F). Considering that a high reliability is desired, so that this temperature is not exceeded, two standard deviations were added (approximately 0.98 percent reliability) to that value, resulting in a test temperature of 65°C (149°F).

Test Results

The RSST-CH testing was performed at the University of California, Berkeley (UC-Berkeley) Soils and Bituminous Materials Laboratory. The results were analyzed following concepts presented previously (*2,3*). Essentially, a correlation was made between the number of cycles in the RSST-CH to reach a given permanent shear strain and the number of ESALs that cause the equivalent rut depth. The relationship between permanent shear strain and rut depth is given by

$$\text{Rut depth (mm)} = 279 \times \text{maximum permanent shear strain} \quad (1)$$

The relationship between the number of cycles in the RSST-CH and ESALs in the field is given by

$$\text{Log (cycles)} = -4.36 + 1.24 \log (\text{ESAL}) \quad (2)$$

A summary of the actual results is shown in Figure 2. Air void contents were measured with parafilm (wp) and unsealed (np) (*11–13*) based on the Rice maximum specific density (ASTM D2041).

Asphalt contents used were 4.0, 4.5, and 5.0 percent by weight of aggregate. Rolling-wheel-compacted specimens were fabricated to air void contents of approximately 3.2 and 6.6 percent. All specimens were subjected to short-term oven aging (STOA) to simulate

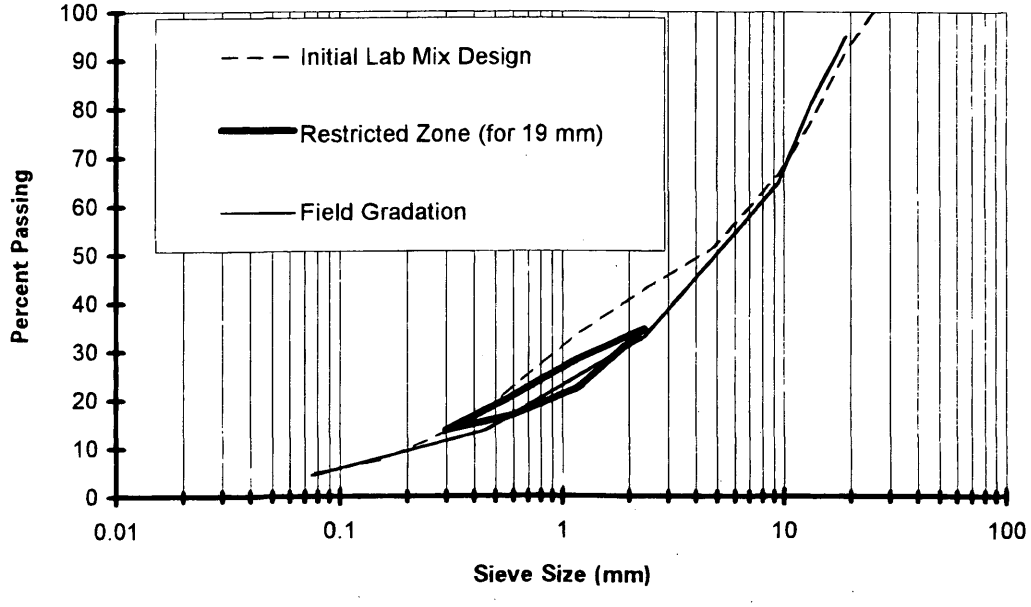

FIGURE 2 Initial laboratory mix design gradation and Superpave guidelines.

plant aging (*14*). Some of the specimens were also subjected to long-term oven aging (LTOA) to simulate long-term aging in the field (*14*). In addition, a few specimens subjected to STOA were conditioned in a moisture conditioning system (MCS) (*3*), which is an adaptation from the ECS concept (*15*).

The test results and corresponding analysis are presented in Figure 3. In general, it can be observed that low air void content specimens exhibit significantly higher resistance to permanent deformation because they can sustain higher number of ESALs before reaching the design rut depth. It can also be observed that shear resistance in low air void content specimens increases with decreasing asphalt content. The results also indicate that the mixture is not very sensitive to moisture damage, although some shear strength is lost during the moisture-conditioning process. As expected, the mix exhibits increased shear resistance with aging. The effects of the aging conditioning seem more pronounced on specimens with higher air void contents.

A multiplier of 8.97, used with the RSST-CH results here, will result in a design with a 95 percent reliability level (*3–5*). This multiplier accounts for variability in test results. Consequently, to ensure with 95 percent reliability that the RSST-CH permanent shear strain will not exceed 3.6 percent [equivalent to a 10-mm (0.4-in.) rut depth] before the expected 10 million-ESALs design criterion, a design criterion of 89.7 million ESALs should be used. Therefore, all considerations regarding asphalt concrete selection should be made at this level of traffic. This level is indicated by the 95 percent reliability design level (see Figure 5).

Selection of AC Content

Selection of the binder content of a mix depends on many factors, including resistance to permanent deformation, fatigue, raveling, and aging. It will be presented later that fatigue life was not the critical criterion for this pavement section. One of the major concerns in the design of this section was to limit permanent deformation by proper selection of aggregate, gradation, asphalt type, and content. Figure 3 shows the variation of the number of ESALs to reach a 10-mm (0.4-in.) rut depth as a function of the asphalt content for different air void contents and conditioning processes. It can be observed that depending on the conditioning process, at a 95 percent reliability level, one could select an asphalt content in a range between 4.1 and 4.6 percent. To be on the conservative side, and considering that rutting is likely to occur in the first or second summer, aging of the mix to resist permanent deformation was used. Therefore, the acceptable asphalt content range (at the 95 percent level) drops to 4.1 to 4.3 percent. Taking into consideration that asphalt content control in the field varies within ± 0.2 percent, an asphalt content of 4.2 percent was selected. In the worst scenario where 4.4 percent was placed, the mix would still be able to perform (especially if one takes aging into consideration).

Fatigue Evaluation

To evaluate the change in fatigue resistance with asphalt content, the four-point bending fatigue test (SHRP-M009 protocol) was selected. Beams were fabricated and tested using the new equipment (*7,16*), developed by SHRP-A003A. Two asphalt contents were selected for this analysis, 4.0 and 5.0 percent, to bracket the range of possible asphalt contents. The target air void content was 4.0 percent. Tests were executed under strain control at 20°C (68°F) and at 10-Hz sinusoidal loading. Failure is defined as the number of cycles at which the stiffness has fallen to 50 percent of its initial value. Fatigue results can be related to field performance by means of appropriate shift factors. For design, a multiplier of 10 was based on cracks in 10 percent of the wheelpaths. The corresponding fatigue curves are presented in Figure 4.

It can be seen that asphalt content affects fatigue performance considerably. As expected, fatigue resistance is improved with

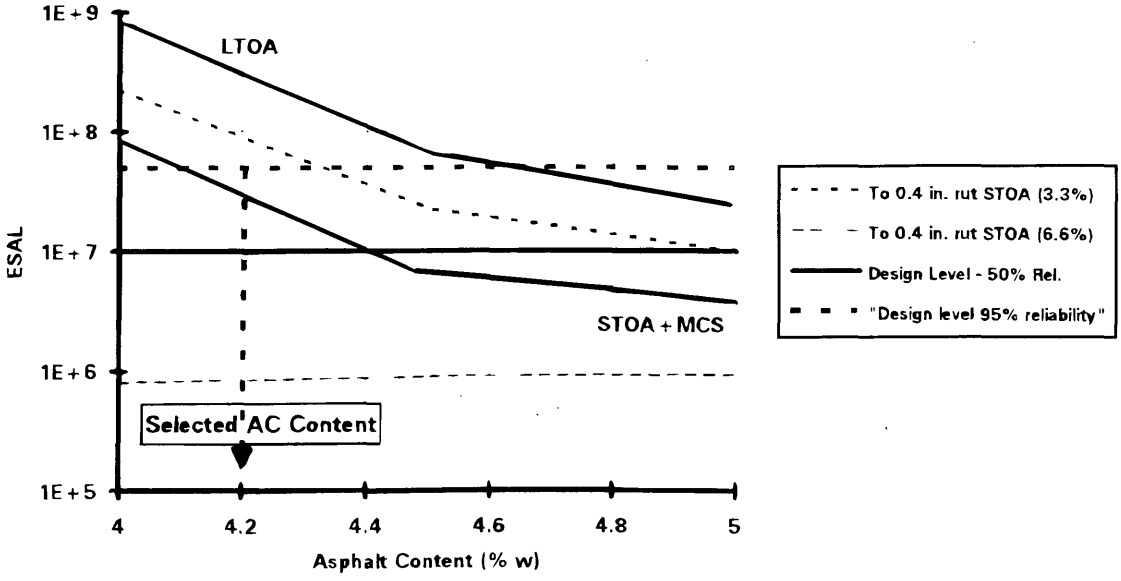

FIGURE 3 Variation of number of ESALs to reach 0.4-in. (10-mm) rut depth with asphalt content for mix used in Arizona Deer Valley: mix design RSST-CH at 65°C and 32 percent void content.

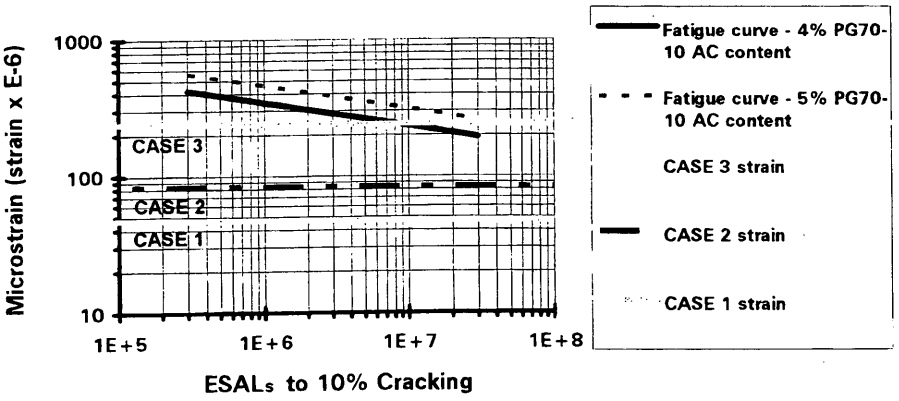

FIGURE 4 Fatigue curves for 4 and 5 percent asphalt contents.

increased asphalt content. However, to select an asphalt content that would insure adequate fatigue life, the strain level in the field must be determined. This evaluation is detailed elsewhere (*10*).

Before investigating the fatigue life of the overlay being placed, it was necessary to determine the structural characteristics of the existing pavement. This is traditionally done using back-calculation methods and falling weight deflectometer (FWD) data (*17*). Layer thickness and FWD data used in this study were provided by the ADOT. The purpose of this analysis was to have an indication of the expected fatigue life of the overlay.

From the back-calculation analysis, layer moduli were determined for a representative pavement section. Three scenarios were considered, Case 1, Case 2, and Case 3, and computations were made using elastic layer theory (ELSYM) to evaluate the magnitude of the strain level due to future pavement degradation caused by moisture effects and fatigue cracking. In Case 3 the moduli of the existing AC layer would be reduced by a factor of 10. This was considered the worst possible scenario. Cases 1 and 2 were considered more realistic with less severe material degradation (i.e., higher moduli for the existing layer and for the future condition of the new layer). It can be observed that the 10 million-ESAL design life is not reached, even in the worst-case scenario. Therefore, project fatigue life would not constrain the selection of asphalt content for this project.

It is recognized that in some cases fatigue cracks in the overlay might be due to shear fatigue instead of flexural fatigue. However, criteria have not yet been developed for shear fatigue of asphalt concrete, and it is reasonable to assume that improvements in flexural fatigue performance may be directly correlated with shear fatigue performance.

EVALUATION OF FIELD MIX WITH RSST-CH

Field cores were taken to the laboratory and tested under the same conditions as specimens cored from the rolling wheel slabs during the mix design stage. The results are presented in Figure 5. It can be observed that the cores from the field exhibit better performance than expected. The improved performance has been attributed (*10*) to gradation change (see Figure 2), better aggregate crushing, and also to more binder aging in the field than was simulated by the STOA procedure used in the laboratory mix design. It has been demonstrated (*9,10*) that the results obtained from this field mix when compacted with the rolling wheel compactor match the results obtained from the field cores, thus eliminating the possibility of differences due to compaction method (Figure 6). Although the laboratory mix was not prepared at the 4.2 percent asphalt content (by weight of aggregate) with the initial gradation, it is reasonable to expect that the behavior of such a mix would be between that of the mixes with 4.0 and 4.5 percent binder contents.

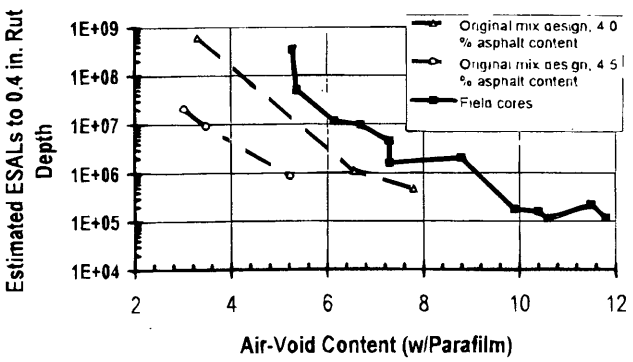

FIGURE 5 Comparison between predictions obtained from laboratory mix and those from field cores.

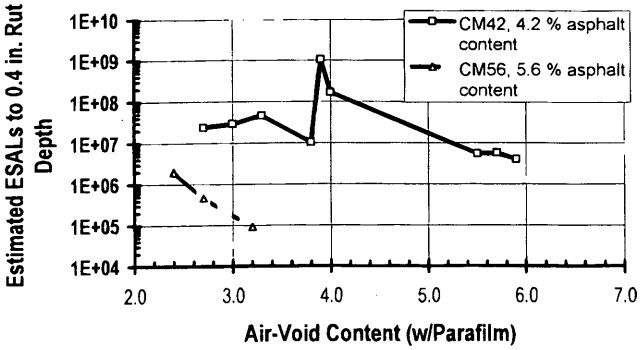

FIGURE 6 Comparison of performance of RSST-CH between mix with 5.6 percent asphalt content and another with 4.2 percent (by weight of aggregate).

EVALUATION USING SUPERPAVE LEVEL I MIX ANALYSIS

The Superpave Level I mix design was executed at the Asphalt Institute (AI), initially using the field mix (*18*). The samples were heated to 146°C for compaction in the SGC. Two samples were compacted to the maximum number of gyrations suggested by Superpave for the traffic and paving location. For I-17 in Phoenix, that corresponded to 220 gyrations (N_{max}), with 9 and 135 gyrations being the respective values for initial (N_{ini}) and design (N_{des}) compaction levels. After compaction, the two specimens were tested to determine the bulk specific gravity of the compacted mixture. From these data, the properties of the mix were determined on the basis of air void contents measured with parafilm and unsealed. The average air void content at 135 gyrations was 7.6 and 6.3 percent with and without parafilm, respectively.

The combined aggregate specific gravity was calculated as 2.655. This specific gravity would yield an average VMA of 13.5 percent at N_{des}. The mix design criteria for a 19.0-mm nominal mixture with an expected design traffic of 10 million ESALs, as well as the average mixture properties, are indicated in Table 1.

As can be seen from Table 1, the field mixture would not meet the requirements for a Superpave Level I mixture. In particular, the air void contents are too high at 4.0 percent asphalt binder content (by weight of mix), and the percent VFA is too low. As part of the Level I mix design procedure, this mixture normally would be evaluated against other aggregate gradations by mathematically adjusting the asphalt binder content to an amount that would result in 4 percent air voids. The air void criterion is the most critical. In the Superpave Level I mix design system, all mixtures are designed to achieve 4 percent air voids.

As a first approximation, the 4.0 percent air void content requirement (without parafilm) could be satisfied by a mix with about 1.0 percent more asphalt content. Once mixtures are normalized to the same air void level, the aggregate structures can be properly com-

TABLE 1 Compacted Mixture Properties from Actual Field Mix Results at 4.2 Percent Asphalt Binder and Estimates from Mix with 5.2 Percent and Actual Specimen with 5.1 Percent Asphalt Binder

Property	Results Field Mix	Estimated Mix Properties from Field Mix.	Actual Mix Properties from lab SGC specimen	Criteria
%Asphalt Binder (by wt. of aggregate)	4.2%	5.2%	5.1%	n/a
%Air Voids @ N_{design} = 135 gyrations	6.3% (without parafilm) 7.6% (with parafilm)	4.0% (no parafilm)	3.7% (no parafilm)	4.0% (no parafilm)
%VMA @ N_{design} = 135 gyrations	13.5%(without parafilm)	13.0%	12.9%	≥13.0% min.
%VFA @ N_{design} = 135 gyrations	53.3%(without parafilm)	69.2%	71.3%	65-75%
Dust-Asphalt Ratio	not available	not available	not available	0.6-1.2
%G_{mm} @ $N_{initial}$ = 9 gyrations	85.4%(without parafilm)	87.7%	89.0%	<89%
%G_{mm} @ $N_{maximum}$ = 220 gyrations	94.8%(without parafilm)	97.1%	97.3%	<98%

pared. Table 1 indicates the mixture properties at the estimated design asphalt binder content.

It can be observed that on the basis of these estimated properties, the compacted mix with the higher asphalt content would meet all Level I criteria; however, it would be considered marginally failing on both percent VMA and percentG_{mm} at N_{ini}. If this mixture had been part of a Superpave Level I trial blend analysis, an alternative aggregate structure (different combination or source of aggregates) could have been considered to improve the VMA requirements. A mix was fabricated in the laboratory with a 5.1 percent asphalt content using the field mix gradation. The mix was aged and compacted following Superpave Level I procedures. The results are also presented in Table 1 and corroborate the expected results.

A 7.6 percent air void content (with parafilm) was obtained at the design number of gyrations for the actual field mix. If, instead of using the air void content unsealed, one would consider air void content measurements with parafilm as being more representative (11–13), then the mixture would require approximately 1.4 percent more asphalt binder or a change in aggregate or aggregate gradation. Although this is not a direct application of Superpave Level I, this was the first criterion used to estimate the asphalt content of a mix with the given gradation that would satisfy Superpave Level I requirements. If time had permitted, specimens would have also been compacted with an asphalt content of 5.1 or 5.2 percent.

Specimens were fabricated at UC-Berkeley with the rolling wheel compactor at 5.6 percent (4.2 + 1.4 percent) asphalt content. The purpose of this exercise was to evaluate the mix performance with the RSST-CH at this asphalt content, representative of an asphalt content required to achieve 4 percent air voids (with parafilm) by the Superpave Level I procedure. Specimens were fabricated in the laboratory with the field gradation at 5.6 percent asphalt content (specimens labelled as CM56) and 4.2 percent asphalt content (specimens labeled as CM42) with the rolling wheel compactor. The results of the RSST-CH are presented in Figure 6. It can be observed that asphalt content has a strong effect on mix performance. At 5.6 percent it is very unlikely, within the performance-based procedure concepts, that the CM56 mix would satisfy the design requirements (i.e., it would be likely that a rut depth higher than 10 mm would develop before the 10 million design ESALs). Although not as dramatic, it is also likely that a mix with a 5.2 percent asphalt content (by weight of aggregate) would not satisfy the design requirements.

These results indicate that within Superpave Level I procedures, volumetric and densification properties obtained from the field mix are identical to those obtained from laboratory-prepared mix. They also indicate that the criteria used by Superpave to estimate Level I properties at different asphalt contents based on results at one asphalt content are quite accurate.

It can then be concluded that the 4.2 percent asphalt content used for the I-17 project does not satisfy Superpave Level I requirements. Those requirements would be marginally satisfied with an asphalt content of 5.1 to 5.2 percent (by weight of aggregate): however, the field mix gradation crosses the restricted zone suggested in the Superpave guidelines and as such would not be recommended as part of a Superpave Level I design. Nevertheless, if this mix were used with an asphalt content of 5.1 percent, the RSST-CH results indicate that it would likely exhibit unacceptable premature permanent deformation.

EVALUATION USING MARSHALL MIX DESIGN

From 1969 to 1983, the 75-blow Marshall test was used to monitor construction of HMAC by ADOT. In 1983 the Marshall test was adopted as the HMAC mix design test by ADOT. Currently, the Marshall test criteria include a minimum Marshall stability of 3,000 lb for Interstate highways. Marshall flow must be between 8 and 16. The VMA range is 14.5 to 17 percent, and the HMAC air void range is 5.8 to 6.2 percent. Marshall design criteria are monitored and controlled during construction by taking four samples per lot. For each sample, three Marshall specimens are compacted and tested. In addition, a Rice test (ASTM D2041) is performed to determine the maximum theoretical density (MTD) for each of the four Marshall samples. Marshall stability and flow, as well as Marshall bulk density and air void content, are also determined for each specimen.

The results of the Marshall analysis for the field mix and cores indicated Marshall stabilities of 5,044 and 3,760 lb and air voids of 6.2 percent and 6.9 percent, respectively. The ADOT field cores had 8.5 percent air void content on average. The VMA was 13.8 percent with a VFA value of 71.6 percent. As can be seen, the design Marshall stabilities were quite high and the field stabilities were also very high, which is indicative of a very stable mix.

EVALUATION OF FIELD MIX USING HAMBURG WHEEL TEST TRACK

Field cores 400 mm (12 in.) in diameter were taken from the pavement overlay, shipped to the Terre Haute Koch laboratory, mounted in the Hamburg wheel tracking device, and tested at 50°C (122°F) under water. One core was tested at 55°C (131°F) following Colorado Department of Transportation recommendations for PG 70 binders (*19*). The Koch laboratory has tested cores from all over the nation in the Hamburg wheel tracking device. Figure 7 shows the range of results of all 157 cores tested in the equipment as well as the results from the cores from I-17. The percentile rankings for the cores were 94 to 95 percent. The Colorado DOT's Eurolab has correlated results from the Hamburg wheel tracking test to the known performance of 20 asphalt pavements (*19*). Based on their experience, the 50th-percentile curve represents a "high maintenance" pavement, and the curve at the 90th percentile would be considered "good," corresponding to a pavement lasting 10 to 15 years. These results indicate that the mix as evaluated by this method is very resistant to ruts and stripping.

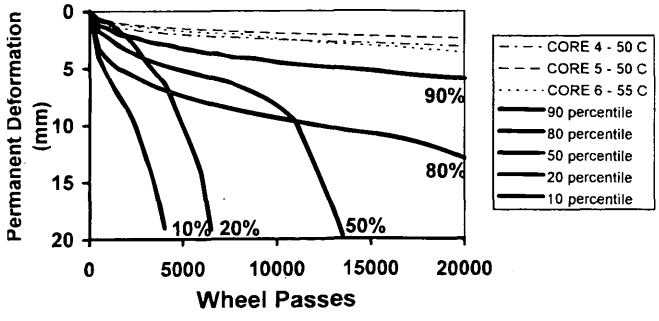

FIGURE 7 Hamburg wheel test track results compared with percentile ratings from other mixes from the United States.

EVALUATION OF FIELD PERFORMANCE

In July 1994, rut depths were measured by a K. J. Lan 690 DNC electronic profilometer at 33.3-m (100-ft) intervals. Rut depth measurements with this device are representative of a 1.5-m (5-ft) straightedge placed across each wheel path, with the recorded value being approximately equal to the average of the two wheel path ruts.

The average 7-day maximum air temperature reached 46°C (116.6°F) previous to the rut depth measurements, which would correspond to a temperature of 61.2°C (142.1°F) at 50-mm (2-in.) depth. This temperature is identical to the average [61.3°C(142.3°F)] obtained from 42 years of temperature records. The average rut depth measured in the section where field quality control took place was 1.5 mm (0.06 in.). This is indicative of good performance based on ADOT experience, where most of the mixes that fail do so in the first summer.

COMPARISON BETWEEN FIELD AND LABORATORY COMPACTION METHODS

The differences in mix design methods are not only a result of the evaluation method used but also of the compaction method employed in specimen fabrication. To identify which laboratory compaction method creates an aggregate structure most similar to that obtained in the field, specimens were prepared by compacting field mix with the following compaction methods: UC-Berkeley rolling wheel, California kneading, Texas gyratory, SHRP gyratory Reinhart (Asphalt Institute), SHRP gyratory Reinhart (FHWA field trailer), and Marshall hammer (Arizona DOT). These specimens were tested using the RSST-CH at UC-Berkeley with the prototype of the SHRP shear machine (also known as the universal testing machine), along with field cores from the section where the field mix was taken.

Using a SHRP gyratory compactor by another manufacturer additional specimens were prepared by the Asphalt Institute using a laboratory mix with the same gradation and asphalt content as the field mix. These specimens were then tested at the Asphalt Institute using the commercial version of the SHRP shear tester manufactured by Cox and Sons.

The rolling wheel, kneading, and Texas gyratory specimens were all cored and cut to their final dimensions from larger compacted masses. The SHRP gyratory and Marshall hammer specimens were cut to their final heights but had as-compacted diametral perimeters. The results of testing to a 2 percent permanent shear strain using the RSST-CH are plotted in Figure 7.

The data indicate that the rolling wheel compactor best duplicated the permanent shear deformation resistance of the field cores. The Texas gyratory specimens had somewhat less resistance than the field cores, whereas the kneading specimens had somewhat more resistance. Note that if the kneading-compacted specimens had lower air void content, higher shear resistance would be expected. The SHRP gyratory and Marshall specimens had much more resistance than the field cores. In addition, the Marshall specimens could not be compacted to the same low air void contents as the other specimens.

Three different SHRP gyratory compactors were used in this study. The specimens fabricated by those compactors were tested using two different shear machines. It must be noted (see Figure 7) that the results are quite similar, indicating good reproducibility of the compaction equipment and of the testing equipment.

It is important to note that differences were found between the results obtained from field mix with laboratory compaction and laboratory mix compacted with the rolling wheel compactor (see Figure 5). Those results suggested that the STOA aging procedures used in this project [4 hr at 135°C (275°F)] might not be representative of the aging occurring in the mix conditions in Arizona. However, the test results obtained from specimens compacted using the SHRP gyratory prepared with field mix and laboratory mix did not show any differences (see Figure 8). The most likely reason for this is the fact that the aggregate structure created by the SHRP gyratory overwhelms all other effects.

SUMMARY AND RECOMMENDATIONS

This paper presents a case study where performance-related tests developed by Project SHRP-A003A were used in the mix design process. The performance-based mix design system used is derived from SHRP-A003A findings and uses the RSST-CH to evaluate the rutting propensity of the mix. It uses the results of flexural bending beam tests in an analysis system to evaluate site-specific structural pavement fatigue life. Based on these concepts, an asphalt content of 4.2 percent by weight of aggregate was selected, and two test sections 1.6-km (1 mi) long were constructed in Phoenix, Arizona, in November 1993. The field mix and cores were then subjected to a Marshall mix design evaluation. The results indicated that according to that methodology, the mix would be very stable.

The mix was also evaluated based on Superpave Level I design concepts. The mix would not be acceptable within the Superpave framework because the field mix gradation crosses the restricted zone for a 19-mm nominal size. Furthermore, results from the gyratory compactor indicated that the mix would require about 1.0 percent more asphalt content to satisfy the 4.0 percent air void requirement. Tests were executed with 5.6 percent asphalt content (by weight of aggregate) with the RSST-CH, and based on the performance-based mix design system, the mix with higher asphalt would likely exhibit premature rutting.

Cores from the field were also subjected to the Hamburg wheel test track; the results showed that the mix satisfies the requirements associated with that equipment, indicating a mix with high resistance to rutting and to stripping. Preliminary field observation over one summer, with temperatures above normal, indicated that the mix is performing well, with virtually no rutting.

Comparisons of performance between several laboratory compaction methods and field cores over a wide range of air void contents revealed that the rolling wheel compactor produces specimens that have permanent deformation performance properties similar to those of field cores.

It appears that the mix selected will be able to satisfy the design requirements. It should therefore be asked why Superpave Level I is not capturing the good performance of this mix. Initially, Level I mix designs were proposed for traffic levels lower than 1 million ESALs (*10*); however, the Superpave manual now recommends Superpave Level I for traffic levels higher than 100 million ESALs.

One could consider that Superpave Level I might be more conservative because it would have rejected this mix. However, the

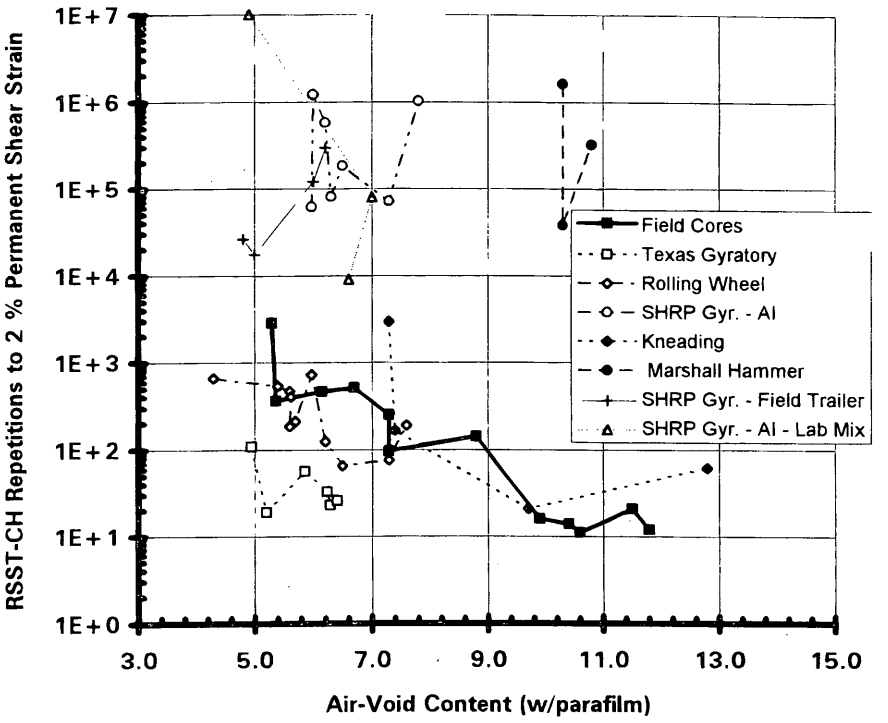

FIGURE 8 Comparison of results of RSST-CH tests for different compaction methods.

main criterion for rejection was the gradation crossing the gradation-restricted zone. Except for that reason, the mix could be considered marginally acceptable with a 5.1 to 5.2 percent asphalt content (by weight of aggregate). At those asphalt contents the predictions from the performance-based mix design system suggest that the mix would likely exhibit permanent deformation. Furthermore, ADOT experience would avoid using such high asphalt contents in that pavement section.

It is therefore recommended that performance-based mix design concepts be evaluated for implementation and that further evaluation be made in conditions similar to those presented in this paper before the Superpave Level I mix design is implemented for high-volume roads without the corresponding performance-related tests proposed in Superpave Level III. With this consideration, ADOT now has two projects under contract to further evaluate SHRP aggregate asphalt and mix design recommendations, and another project is planned for 1995.

ACKNOWLEDGMENT

The authors express their appreciation for the collaboration and efforts of the following: Mark Bouldin of Applied Paving Technology; Carl Monismith, Tom Mills, and Clark Scheffy from the University of California at Berkeley; Douglas Forstie, Larry Scofield, and Julio Alvarado from the Arizona Department of Transportation; Robert McGennis and Mike Anderson of the Asphalt Institute; FNF Construction Company and its construction crew; and Bernard A. Vallerga from B. A. Vallerga. Inc. Mike Anderson's critical review of the draft of this paper is acknowledged, recognized, and appreciated.

REFERENCES

1. Cominsky, R. J. *The SUPERPAVE Mix Design Manual for New Construction and Overlays.* Report SHRP-A-407. Strategic Highway Research Program, National Research Council, Washington, D.C., 1994.
2. Sousa, J. B. *Asphalt-Aggregate Mix Design using the Simple Shear Test (Constant Height). Proc. AAPT,* Vol. 62, 1994.
3. Sousa, J. B, J. Harvey, M. G. Bouldin, and A. Azevedo. *Application of SHRP Mix Performance-Based Specifications.* In *Transportation Research Record 1454,* TRB, National Research Council, Washington, D.C., 1994.
4. Sousa, J., J. Deacon, S. Weissman, J. Harvey, C. Monismith, R. Leahy, G. Paulsen, and J. Coplantz. *Permanent Deformation Response of Asphalt-Aggrgate Mixes.* Report SHRP-A-415. Strategic Highway Research Program, National Research Council, Washington, D.C., 1994.
5. Deacon, J., A. Tayebali, J. Coplantz, F. Finn, and C. Monismith. *Fatigue Response of Asphalt-Aggregate Mixtures—Part III—Mixture Design and Analysis.* Report SHRP A-003A. University of California at Berkeley, May 1993.
6. Tayebali, A., J. Deacon, J. Coplantz, J. Harvey, and C. Monismith. Mixture and Mode-of-Loading effects on Fatigue Response of Asphalt-Aggregate Mixtures. Presented at Annual Meeting of the Association of Asphalt Paving Technologists, St. Louis, Mo., March 1994.
7. Tayebali, A., et al. *Fatigue Response of Asphalt- Aggragte Mixes.* Report SHRP-A-404. Strategic Highway Research Program, National Research Council, Washington, D.C., 1994.
8. Huber, G. A. SUPERPAVE: The Software System. *Proceedings of the Strategic Highway Research Program and Traffic Safety on Two Continents.* The Hague, Netherlands, Sept. 22–24, 1993, Nr 1A, Part 3, 1994.
9. Harvey, J., C. L. Monismith, and J. B., Sousa. An Investigation of Field and Laboratory Compacted Asphalt Rubber, SMA, Recycled and Conventional Asphalt Concrete Mixes using SHRP-A003A Equipment. *Proc. AAPT* (in preparation).
10. Sousa, J. B. *Mix Design for a Test Section on I–17 at Valley-Pioneer Road Using SHRP PermaMix Design Concepts.* Arizona Department of Transportation, Dec. 1993.

11. Harvey, J., K. Eriksen, J. Sousa, and C. L. Monismith. *Effects of Laboratory Specimen Preparation on Aggregate-Asphalt Structure Air-Void Content Measurement, and Repetitive Simple Shear Test-Constant Height Results.* In *Transportation Research Record 1454 TRB,* National Research Council, Washington, D.C., 1994.
12. Harvey, J., J. Sousa, J. Deacon, and C. L. Monismith. Effects of Sample Preparation and Air-Void Measurement on Asphalt Concrete Properties. In *Transportation Research Record 1317.* TRB, National Research Council, Washington, D.C., 1991.
13. Harvey, J., T. Mills, C. Scheffy, J. Sousa, and C. L. Monismith. An Evaluation of Several Asphalt Concrete Specimen Air-Void Content Measurement Techniques. *ASTM Journal of Testing and Evaluation,* Sept. 1994.
14. Bell, C., Y. Abwahab, M. E. Cristi, and D. A. Sosnovske. *Selection of Laboratory Aging Procedures for Asphalt-Aggregate Mixtures.* Report SHRP-A-383, Strategic Highway Research Program, National Research Council, Washington, D.C., 1994.
15. Terrel, R., and S. Al-wailmi. *Water Sensitivity of Asphalt-Aggregate Mixes: Test Selection.* Report SHRP-A-403. National Research Council, Washington, D.C., 1994.
16. Sousa, J. B., A. Tayebali, J. Harvey, P. Hendricks, and C. Monismith. Sensitivity of Strategic Highway Research Program A-003A Testing Equipment to Mix Design Parameters for Permanent Deformation and Fatigue. In *Transportation Research Record 1384.* TRB, National Research Council, Washington, D.C., 1993, pp. 69–79.
17. Brown, S. F., W. S Tam, and J. M. Brunton. Structural Evaluation and Overlay Design: Analysis and Implementation. *Proc., Sixth International Conference on the Structural Design of Asphalt Pavements,* Ann Arbor, Michigan, Vol. 1, 1987, pp. 1013–1028.
18. Anderson, M. R. *SUPERPAVE Level I Mixture Analysis: Arizona IH-17.* Arizona Department of Transportation, Lexington, Ky. April 1994.
19. Aschenbrener, T., R. L. Terrel, and R. Zamora. *Comparison of the Hamburg Wheel Tracking Device and the Environmental Conditioning System to Pavements of Known Stripping Performance.* Report No. CDOT-DTD-R-94-1, Colorado Department of Transportation, Jan. 1994.

Publication of this paper sponsored by Committee on Characteristics of Bituminous Paving Mixtures To Meet Structural Requirements.

Comparison of Marshall and Superpave Level I Mix Design for Asphalt Mixes

IHAB H. HAFEZ AND MATTHEW W. WITCZAK

Mix designs were conducted on 20 different mixtures categorized as: (*a*) conventional, (*b*) wet process asphalt rubber (manufacturer preblended), (*c*) dry process rubber asphalt, (*d*) polymer modified mixes, and (*e*) wet-process asphalt rubber (plant-blended). These designs were developed using both the Marshall procedure and the Superpave gyratory Level I procedure. A comparison between the design asphalt contents results obtained by the two procedures is presented. The Superpave designs were conducted at a traffic level compared to traffic for the 75-blow Marshall procedure and for three climatic regions representative of cool to warm conditions. Major problems were encountered with the Superpave gyratory approach for five mixtures within the dry-process rubber asphalt groups. These problems appear to be related to the high resiliency of the rubber aggregate during the gyratory compaction process coupled with time-dependent swell of these mixtures directly after compaction. It is concluded that the Superpave Level I mix design approach is not applicable to those mixtures. For the other four groups of mixtures studied, differences between the binder contents from the Marshall and Superpave were found to be a function of the group type. Differences in design content obtained from the Superpave gyratory were found to be about 1.0 percent more asphalt as the climatic regions went from warm to cool conditions. This finding was true for all types of mixtures studied. In general, the conventional mixtures and manufacturer-preblended rubber asphalts gave similar design values between the Marshall and "warm" Superpave climatic region and the contrast is true for the plant-blended rubber asphalt. In contrast, 0.5 percent to 0.8 percent less asphalt was found for the Superpave design, in warm conditions, compared to the Marshall design for the polymer modified asphalts investigated.

The main objective of the laboratory mix design process for asphalt mixtures is to determine the combination of binder and aggregate that, when properly constructed, will yield an asphalt mixture that will withstand loading and environmental distress throughout the intended design and performance period.

The two most common mix design procedures used in the United States are the Marshall and Hveem procedures, with the former being the most widely used. In 1993, the Strategic Highway Research Program (SHRP) introduced the Superpave laboratory mix design procedure, which is based on a gyratory compaction device (*1*). Conceptually, the Superpave laboratory testing procedure is intended to be applicable for all types of asphalt mixtures: virgin and recycled hot mixtures, with or without modified binders even though SHRP research almost universally focused on conventional asphalt mixtures and binders.

The Superpave mix design procedure recommends three distinct hierarchical levels of design, termed Level I, II, and III, which are dependent on the anticipated traffic volume. Also, under each design level, the influence of the project site climatic conditions (related to design air temperature) are also combined in the mix design process. Table 1 presents Superpave guidelines for the number of design gyrations to be used under design Level I for different design air temperatures and traffic [equivalent single axle loads (ESALs)]. These design gyrations, coupled with the specific mixture gyratory densification curves developed for each mix under different asphalt contents, can be used to determine the design asphalt content. The final design asphalt (binder) content will depend on traffic level and environmental conditions.

In contrast to the proposed Superpave gyratory mix design approach, the Marshall mix design uses an impact hammer to achieve the design level of compaction (air voids) as a basis for establishing the design asphalt content. The compaction energy is controlled by the number of blows the specimen will be subjected to in the compaction process. The majority of agencies using the Marshall specify 35-, 50-, or 75-blow compaction consistent with the anticipated traffic level ($\leq 10^4$, $10^4 - 10^6$, $>10^6$, respectively). For this widely used mix design process, it can be recognized that the final design asphalt (binder) content will only depend on traffic level.

STUDY OBJECTIVES

The major objectives of this study were twofold. The first objective was to obtain quantitative information on the difference in design asphalt contents determined by the Marshall design and SHRP-Superpave gyratory Level I procedure for a variety of mixtures. The second objective was to develop a preliminary assessment of the applicability of the Superpave Level I design to several types of nonconventional (rubber and polymer modified) mixtures.

It should be clearly recognized that the pursuit of these objectives should not be misconstrued to show that the final design asphalt contents from one approach are much better than another as this can only be accomplished by a rigorous lab study encompassing more fundamental test procedures (e.g., moduli, permanent deformation, fatigue) on a given mix, at a unique combination of air-asphalt binder percentage. This study provides, for the first time, some knowledge of the anticipated differences in design asphalt content between the two major compaction processes evaluated. Because of the limited number of the mixtures evaluated, it is hoped, however, that other agencies will conduct similar studies to broaden the data base, results, and implications of this study.

MIXTURES INVESTIGATED

A total of 20 different mixtures were evaluated in the comparative mix design study. These mixtures have been classified into the five major groups identified in Table 2. The major groups investigated were: *(a)* Group 1—conventional mixtures, *(b)* Group 2—wet

I. H. Hafez, University of Maryland, College Park, Md. 20742. M. W. Witczak, University of Maryland, College Park, Md. 20742.

TABLE 1 Superpave Design Number of Gyrations (*I*)

Traffic	Average Design Air Temperature (^{0} C)					
(ESALs)	≤ 34	35 - 36	37 - 38	39 - 40	41 - 42	43 - 44
$< 3x10^5$	50	59	68	74	78	82
$< 1x10^6$	55	65	76	83	88	93
$< 3x10^6$	61	73	86	95	100	105
$< 1x10^7$	67	81	96	106	113	119
$< 3x10^7$	74	92	109	121	128	135
$< 1x10^8$	84	105	126	139	146	153
$\geq 1x10^8$	93	118	143	158	165	172

process asphalt rubber (manufacturer preblended), *(c)* Group 3—dry process rubber asphalt, *(d)* Group 4—polymer modified, and *(e)* Group 5—wet process asphalt rubber (plant blended).

For all mixtures investigated, the aggregate type, source, stockpile gradations, and maximum nominal size were identical except for the two Plus Ride mixtures. A Maryland State Highway Administration (MSHA) dense aggregate grading with maximum nominal size of 12.5 mm (½ in.) were used for all mixes except the Plus Ride mixtures where an open grading was used with a maximum nominal size of 12.5 mm (½ in.) and 19.0 mm (¾ in.) for Plus Ride No. 12 and No. 16, respectively. Table 3 summarizes the job mix gradation for all of the mixes studied.

TABLE 2 Summary of Asphalt Mixtures Group Evaluated

Group	Description	Mix Identification	UM Project
1	Conventional	Chevron AC-20	MSHA Rubber Project
		Neste AC-20	Neste Oil Study
		Conoco AC120/150	DuPont Study
2	Wet Process Asphalt Rubber	Neste SAR 10/5	Neste Oil Study
	(Manufacturer Preblended)	Neste SAR 10/10	MSHA Rubber Project
		Ecoflex (Bitumar)	MSHA Rubber Project
3	Dry Process Rubber Asphalt	Generic: Chevron AC-20 (1% R)	MSHA Rubber Project
		Generic: Chevron AC-20 (2% R)	MSHA Rubber Project
		Generic: Chevron AC-20 (3% R)	MSHA Rubber Project
		Plus Ride No 12 (3% R)	MSHA Rubber Project
		Plus Ride No.16 (3% R)	MSHA Rubber Project
4	Polymer Modified	Neste EVALAST	Neste Oil Study
		ELVALOY (Con 120/150 + 1.5% Mod)	DuPont Study
		ELVALOY (Con 120/150 + 2.0% Mod)	DuPont Study
5	Wet Process Asphalt Rubber	Citgo AC-10 (0% EO + 10% CR)	MSHA Rubber Project
	(Plant Blended)	Citgo AC-10 (3% EO + 15% CR)	MSHA Rubber Project
		Citgo AC-10 (7% EO + 20% CR)	MSHA Rubber Project
		Citgo AC-20 (0% EO + 10% CR)	MSHA Rubber Project
		Citgo AC-20 (3% EO + 15% CR)	MSHA Rubber Project
		Citgo AC-20 (7% EO + 20% CR)	MSHA Rubber Project

TABLE 3 Summary of Mix Aggregate Properties

Sieve	Job Mix Gradation (% Pass)		
mm (#)	All Mixes	Plus Ride No. 12	Plus Ride No. 16
25.40 (1")	100.0	100.0	100.0
19.00 (3/4")	100.0	100.0	96.0
12.70 (1/2")	96.0	94.0	67 0
9.50 (3/8")	82.0	69.0	50 0
4.75 (#4)	58.4	28.0	32.0
2.36 (#8)	40.9	20.0	23.0
1.18 (#16)	24.0	17.0	18.0
0.60 (#30)	14.7	16.0	15.0
0.30 (#50)	9.1	15.0	14.0
0.15 (#100)	5.5	14 0	12 0
0.75 (#200)	5.5	11 0	9.2
S.G (C.A)	2.637	2.711	2 722
S.G (F.A)	2.647	2.669	2.698
S.G (M.F)	2.760	2.788	2.819
Bulk S.G. (Combined)	2.661	2.712	2.725

SELECTION OF MIXING AND COMPACTION TEMPERATURES

Laboratory mixing and compaction temperatures for all mixtures were selected in accordance with viscosity criteria stated by the Asphalt Institute in MS-2 *(2)*. For each mix, the same mix/compaction temperatures were used for both the Marshall and Superpave Level I mix design procedures. Mixing temperatures were selected at a binder viscosity range of 150 to 190 cS while the compaction temperature range corresponded to a binder viscosity range of 250 to 310 cS. Viscosity-temperature relationships for each binder were developed using the relationship:

$$\log \log \eta \text{ (cp)} = A_i + VTS_i \log T_R$$

where:

η (cp) = viscosity in centipoise,
T_R = temperature in degrees Rankine, and
A_i, VTS_i = regression constants.

In general, these binder relationships were developed from penetration data at: 4.0°C (39.2°F), 10°C (50°F), 25°C (77°F), and 32.2°C (90°F); softening point; kinematic, and absolute viscosity tests as well as Brookfield viscosity results. A summary of the binder A_i and VTS_i values as well as the resulting mixing and compaction temperatures is shown in Table 4.

MARSHALL MIX DESIGN

Test Procedure

The Marshall test method, as described in The Asphalt Institute (TAI) manual (MS-2) (2), was used to select the "optimum/design" binder contents for all the mixes investigated in this study. Some modifications were made for the use of the Marshall procedure on the dry process asphalt rubber mixes (Group 3). For all mixtures investigated in this study, three to four different binder content percentages were selected for the Marshall stability analysis. Binder percentages progressed in 1.0 percent increments to cover an air void range between 3.0 percent to 5.0 percent, with three replicates at each binder content. The aggregates were first combined in general accordance with the Job Mix Formula (JMF) and then manually separated according to sieve sizes after blending. The specific amount required for each size was then calculated to form an aggregate blend of 1,200 g conforming as close as possible to the JMF.

For the asphalt rubber dry processed mixes, crumb rubber was added to the hot aggregate at the calculated mixing temperature and according to its percentage in the total mix. The binder, at the calculated mixing temperature, was then added to the aggregate/aggregate rubber blend by an amount according to its percent in the mix. The mix was then wet-mixed for about 2 minutes at the mixing temperature to ensure that the aggregate/rubber particles were completely and uniformly coated by the binder.

TABLE 4 Summary of Binder A_i, VTS_i Parameters

Mix Type	Binder	A	VTS	Mixing Temp (°F)	Compaction Temp (°F)
Conventional	Chevron AC-20	10.72596	-3.59598	310	290
	Neste AC-20	10.93286	-3.67221	305	285
	Conoco 120/150	11.22030	-3.78738	285	265
Wet Process Asphalt Rubber (Manufacturer Preblended)	Neste SAR 10/5	9.21569	-3.05231	340	320
	Neste SAR 10/10	9.49318	-3.14280	350	330
	Ecoflex (Bitumar)	10.06920	-3.35609	325	305
Dry Process Rubber Asphalt	Generic: Chevron AC-20 (1%, 2%, 3% R)	10.72596	-3.59598	310	290
	Plus Ride No. 12 & No. 16	10.72596	-3.59598	310	290
Polymer Modified	Neste EVALAST	8.70081	-2.84582	400	375
	ELVALOY (Conoco 120/150 + 1.5% Modifier)	10.31936	-3.45168	310	290
	ELVALOY (Conoco 120/150 + 2.0% Modifier)	9.41115	-3.11800	345	325
Wet Process Asphalt Rubber (Plant Blended)	Citgo AC-10 (0% EO + 10% CR)	8.42568	-2.75490	390	370
	Citgo AC-10 (3% EO + 15% CR)	7.29285	-2.34103	460	435
	Citgo AC-10 (7% EO + 20% CR)	7.33291	-2.35572	455	430
	Citgo AC-20 (0% EO + 10% CR)	8.42707	-2.75691	385	365
	Citgo AC-20 (3% EO + 15% CR)	7.94432	-2.58102	410	390
	Citgo AC-20 (7% EO + 20% CR)	6.80774	-2.16188	510	475

Upon mixing, the loose mixture was then placed in an oven, at 160°C (320°F), for 1 hour. This aging process simulated the short-term aging during mixing and laydown conditions. After that, samples were compacted, at the calculated compaction temperature, using an automatic Marshall hammer with 75 blows per side. To prevent expansion of the dry-process, rubber-compacted mixes in the molds during the cooling period, two plugs were placed under and above the specimen in the molds, and then a 10-lb (minimum) weight was placed on the specimen. After the specimens cooled to room temperature, they were removed from the molds and their height and weight in air and in water were recorded. The specimens were then immersed in a water bath maintained at 140°F (60°C). After 30 to 40 min, they were removed from the water bath and tested immediately using the Marshall apparatus. Stability and the flow values were recorded. Bulk density, specific gravity, voids (air), voids in mineral aggregate, voids filled with asphalt, and the stability/flow values were calculated for each specimen and the average for the replicates at the same binder content were also calculated.

Selection of Design Binder Contents

Design binder contents were selected, for each mixture, at air void levels of 3.0 percent, 4.0 percent, and 5.0 percent. These results, for the 75-blow Marshall study, are shown in Table 5. From this table, it can be observed that only insignificant changes are shown for the Group I (conventional) mixtures. For the Group 2 (asphalt rubber manufacturer preblends), asphalt contents for the two 10 percent rubber blends (SAR 10/10 and Ecoflex) are essentially the same and are about 0.5 percent more than the 5 percent rubber preblended (SAR 10/5).

The dry process rubber asphalt generic mixtures shown in Group 3 indicate that the demand for the total asphalt content, at any air void level, is increased by approximately 1.3 to 1.7 percent for each 1 percent increment of rubber (see also Chevron AC-20); Group 1 (conventional) for 0 percent rubber. For the Group 4 polymer-modified mixtures, the asphalt contents are about 0.3 percent more for the EVALAST modifier and are about 0.7 percent more for the DuPont ELVALOY mixtures.

For the Group 5 (asphalt rubber plant-blended), it was observed that for the mixtures using the AC-10 binder there is no significant difference in the design binder content as the percent of the rubber increases from 10 percent to 20 percent at any air void level. In contrast, mixes prepared with the AC-20 resulted in design binder contents being increased by about 0.1 percent for each 1 percent increase of rubber.

SHRP-GYRATORY COMPACTION

Test Procedure

The Superpave Level I mix design method requires specimen compaction with a gyratory compactor capable of providing a con-

TABLE 5 Summary of Design Asphalt Content (Marshall)

Group	Description	Mix Identification	A.C. at Temp./Vair		
			Va – 3%	Va = 4%	Va = 5%
1	**Conventional**	Chevron AC - 20	5.1	4.8	4 4
		Neste AC - 20	5.1	4.7	4.3
		Conoco AC 120/150	5.1	4.8	4 4
2	**Wet Process**	Neste SAR 10/5	5.3	4.7	4.3
	(Manufacturer Preblended)	Neste SAR 10/10	5.8	5 3	4.7
		Ecoflex (Bitumar)	5.7	5.3	4.8
3	**Dry Process Rubber Asphalt**	Generic Chevron AC-20 (1% R)	6.2	5.7	5.5
		Generic. Chevron AC-20 (2% R)	8.0	7.3	6.8
		Generic: Chevron AC-20 (3% R)	9.0	8.2	7.7
		Pluse Ride No. 12 (3% R)	10.0	8.9	7.5
		Pluse Ride No. 16 (3% R)	7 4	6 4	-
4	**Polymer Modified**	Neste EVALAST	5.5	5.1	4.6
		ELVALOY (Conoco 120/150 + 1.5% Mod)	5.8	5.3	4.8
		ELVALOY (Conoco 120/150 + 2.0% Mod)	5.9	5.5	5.1
5	**Wet Process**	Citgo AC-10 (0% EO + 10% CR)	6.6	5.9	5 4
	(Plant Blended)	Citgo AC-10 (3% EO + 15% CR)	6.6	6.1	5.6
		Citgo AC-10 (7% EO + 20% CR)	7.0	5 9	5.4
		Citgo AC-20 (0% EO + 10% CR)	6.0	5.7	5.3
		Citgo AC-20 (3% EO + 15% CR)	6.3	5.9	5.7
		Citgo AC-20 (7% EO + 20% CR)	7.0	6.7	6.4

solidation pressure of 0.60 MPa with an angle of gyration of 1.25 degrees and speed of gyration of 30.0 rpm. Cylindrical molds are also required to accommodate specimen sizes of 100 mm to 150 mm in diameter and with height ranges of 60 to 100 mm and 90 to 150 mm, respectively. The gyratory compactor can continuously monitor the increase in specimen density (expressed as a percent of its theoretical maximum specific gravity) with increasing compactive effort. For all mixes investigated in this study, specimens were compacted in the 100-mm diameter mold using a Rainhart gyratory compactor up to 200 gyrations. Two replicates were prepared at each of the three binder contents used in the Marshall mix design. Also, mixing and compaction temperatures were maintained the same as those used in the Marshall tests. Specimen height versus number of gyrations were saved in computer files to generate the corrected density curves.

Uncorrected Density Curves

The density can be computed at any point in the compaction process from the weight of the specimen and its height. This is termed the uncorrected density (C_{ux}).

$$C_{ux} = \frac{w}{\frac{\pi d^2 H}{4}} \times \frac{1}{G_{mm}}$$

where

w = the weight of the specimen, gm;
H = the height of the specimen at any number of gyrations, cm;
d = the diameter of the specimen, cm; and
G_{mm} = the theoretical maximum specific gravity of the tested specimen.

To generate final densification curves, the uncorrected values of the theoretical maximum specific gravity must be corrected using the final height recorded at the end of compaction (H_{eoc}) and the measured bulk specific gravity of the specimen after the end of compaction (G_{mb}).

Corrected Density Curves

After the compaction of the specimens, the final heights were recorded and the bulk specific gravities were measured in accordance with AASHTO T-166. The corrected density (C_{cx}) at any number of gyrations is calculated as follows:

$$C_{cx} = C_{ux} \times \frac{G_{mb}}{\frac{\pi d^2 H_{eoc}}{w}}$$

Figure 1 represents the typical densification curves obtained for a conventional mix (AC-20 Chevron) under 4.0 percent, 5.0 per-

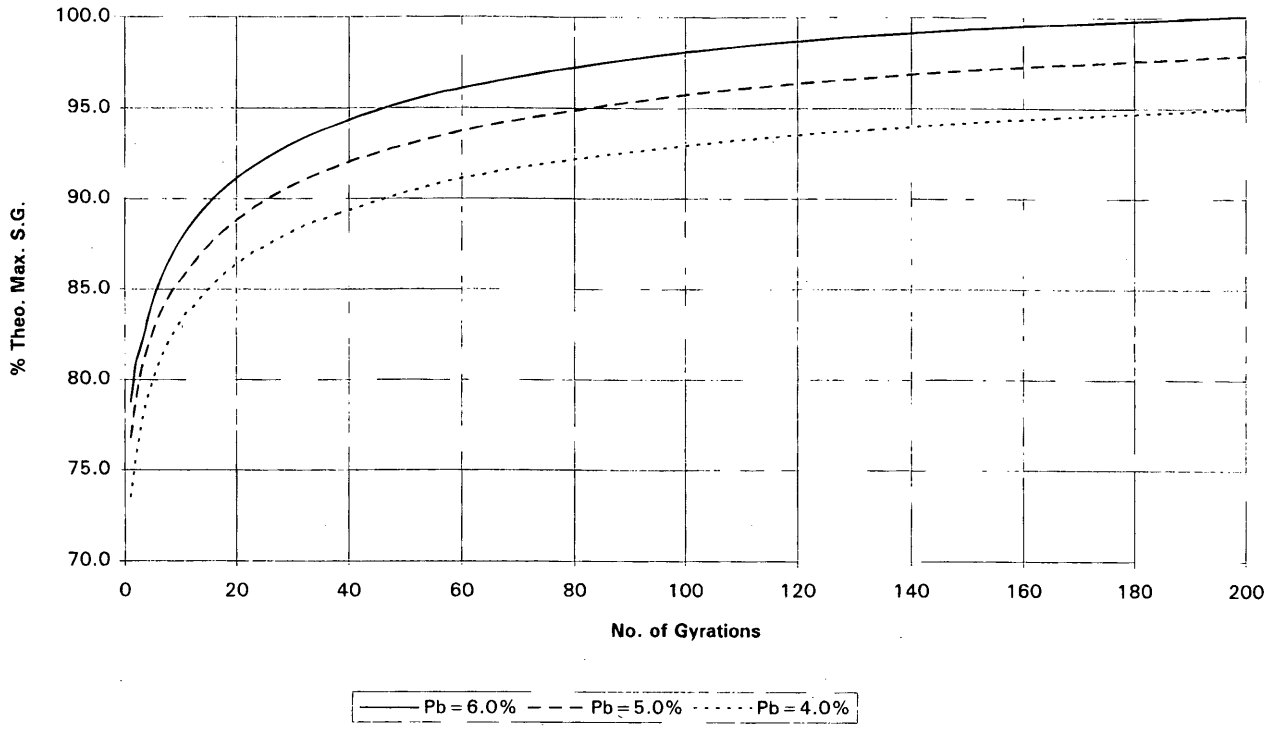

FIGURE 1 Percent of theoretical maximum specific gravity versus number of gyrations under different asphalt content with Pr = 0.0 percent (AC-20 Chevron).

cent, and 6.0 percent binder content. Each curve in this figure represents the average corrected density values for two replicates at the same binder content.

Selection of Design Binder Contents

The first step to determine the design binder content was to select a traffic level expected on the pavement as well as the average design air temperature for the pavement site. Once these two factors are selected, the design number of gyrations (N_{design}) can be determined from Table 1. The design binder content will be the one that produces a densification curve passing through 96.0 percent of theoretical maximum specific gravity (i.e., V_a = 4.0 percent at the design number of gyrations).

In this study, a traffic level less than 1×10^7 ESALs was selected in order to be consistent with the 75-blow Marshall traffic level ($>1 \times 10^6$ EAL). Ranges of the design air temperature were selected to represent different climatic conditions. These design air temperatures were ≤34°C, 37°C to 39°C, and 43°C to 44°C. The corresponding N_{design} values from Table 1 were 67, 96, and 119 number of gyrations. In addition, in lieu of simply determining the design binder content at one level of V_a = 4.0 percent binder contents were also evaluated at the 3.0, 4.0, and 5.0 percent air void levels conducted for the Marshall analysis. The summary of these results is shown in Table 6.

Table 6 summarizes design asphalt contents for mixtures in Groups 1, 2, 4, and 5. These values are not shown for Group 3 (dry process rubber asphalt) mixtures. Significant problems were found with these mixtures, with the Superpave gyratory device. These problems preclude their applicability with Superpave gyratory device and design specifications to select design asphalt contents under the Level I approach. A more detailed discussion of these findings is presented in ensuing sections of this paper.

COMPARISON BETWEEN MARSHALL AND SUPERPAVE RESULTS

Approach

Tables 5 and 6 provide summaries of the design binder content for the Marshall and Superpave gyratory procedures. These results are shown for V_a = 3.0, 4.0, and 5.0 percent. Marshall results are based on 75-blow, while the gyratory designs have been selected to represent a comparable traffic level to the 75-blow compaction and at three levels of temperature to simulate cool (≤34°C), moderate (37°C to 38°C), and warm (43°C to 44°C) climatic regions.

The comparison of the design asphalt contents is presented in two approaches. The first approach uses the difference in asphalt contents between the Superpave Level I and Marshall. This parameter is referred to as the d(AC) value or:

d(AC) = AC Percent (Superpave) − AC Percent (Marshall)

The second approach was to determine the equivalent number of gyrations, for the 75-blow Marshall results, that when used in the Superpave procedure will yield the same design binder content as determined by the Marshall approach. This parameter is referred to as the N_{eq} value. Using the information shown in Tables 5 and 6,

TABLE 6 Summary of Design Asphalt Content (Superpave Level I)

Group	Description	Mix Identification	Va (%)	A.C. at Temp./Vair		
				34 °C	37 - 38 °C	43 - 44 °C
1	**Conventional**	Chevron AC - 20	3.0	-	5.6	5.3
			4.0	5.8	5.2	4.9
			5.0	5.3	4.8	4.5
		Neste AC - 20	3.0	-	5.4	5.1
			4.0	5.6	5.0	4.7
			5.0	5.1	4.6	4.3
		Conoco AC 120/150	3.0	5.9	5.5	5.3
			4.0	5.6	5.2	4.9
			5.0	5.3	4.6	-
2	**Wet Process (Manufacturer Preblended)**	Neste SAR 10/5	3.0	-	5.7	5.4
			4.0	6.0	5.2	4.9
			5.0	5.4	4.7	4.5
		Neste SAR 10/10	3.0	-	-	5.8
			4.0	-	5.6	5.3
			5.0	5.7	5.1	4.7
		Ecoflex (Bitumar)	3.0	-	5.7	5.4
			4.0	5.8	5.3	5.0
			5.0	5.4	4.8	4.5
4	**Polymer Modified**	Neste EVALAST	3.0	-	5.5	5.1
			4.0	5.9	4.9	4.6
			5.0	5.1	4.4	4.1
		ELVALOY (Conoco 120/150 + 1.5% Mod)	3.0	5.7	5.2	5.0
			4.0	5.3	4.8	4.5
			5.0	5.0	4.4	4.1
		ELVALOY (Conoco 120/150 + 2.0% Mod)	3.0	-	5.7	5.1
			4.0	-	4.9	4.7
			5.0	5.2	4.6	4.4
5	**Wet Process (Plant Blended)**	Citgo AC-10 (0% EO + 10% CR)	3.0	6.8	6.0	5.7
			4.0	6.2	5.6	5.3
			5.0	5.7	5.2	-
		Citgo AC-10 (3% EO + 15% CR)	3.0	-	6.5	6.1
			4.0	6.6	5.9	5.6
			5.0	6.1	5.4	5.1
		Citgo AC-10 (7% EO + 20% CR)	3.0	-	7.0	6.4
			4.0	7.1	6.2	5.7
			5.0	6.3	5.4	-
		Citgo AC-20 (0% EO + 10% CR)	3.0	-	6.6	6.2
			4.0	6.8	6.0	5.0
			5.0	6.2	-	-
		Citgo AC-20 (3% EO + 15% CR)	3.0	-	5.8	5.2
			4.0	6.0	5.1	-
			5.0	5.3	-	-
		Citgo AC-20 (7% EO + 20% CR)	3.0	7.2	6.5	5.9
			4.0	6.6	5.6	-
			5.0	6.0	-	-

Table 7 is a summary of the d(AC) and N_{eq} values for the mixtures evaluated in Group 1, 2, 4, and 5. Figure 2 presents the d(AC) results, and Figure 3 shows the N_{eq} values obtained in the comparison study.

Results

As noted in Table 7 and Figures 2 and 3, mix subgroups have been developed for the Group 2, Group 4, and Group 5 categories to facilitate the ensuing discussions. Based on an examination of the information shown, the following conclusions can be drawn.

For each specific mixture evaluated, there is little (if any) variation of the d(AC) values, within a given mix, at the three levels of V_a examined. This implies that the d(AC) is independent of the target air void level used to establish the design binder content (within the normal V_a design range of 3 to 5 percent).

As would be expected, the Superpave design asphalt content is increased as the design climatic condition becomes cooler (i.e., less asphalt is required for warmer conditions). This finding was observed for all mixtures evaluated. Quite interestingly, the increase in design asphalt content by the Superpave, between the warm (43/44°C) and cool (≤34°C) condition, is equivalent to nearly 1.0 percent more asphalt irrespective of the mix type and group (i.e., this finding is true for conventional, wet blend rubber

TABLE 7 Summary of Design Binder Comparison Analysis

Group	Description	Mix Identification	Design Va (%)	d(AC) Value*			Marshall Neq
				Cool	Mod	Warm	
1	**Conventional**	Chevron AC - 20	3.0	-	0.5	0.2	138
			4.0	1.0	0.4	0.1	140
			5.0	0.9	0.4	0.1	148
		Neste AC - 20	3.0	-	0.3	0.0	120
			4.0	0.9	0.3	0.0	128
			5.0	0.8	0.3	0.0	124
		Conoco AC 120/150	3.0	0.8	0.4	0.2	145
			4.0	0.8	0.4	0.1	122
			5.0	0.9	0.2	-	104
		Group Average		**0.9**	**0.4**	**0.1**	**130**
2	**Wet Process (Manufacturer Preblended)**	Neste SAR 10/5	3.0	-	0.4	0.1	127
			4.0	1.3	0.5	0.2	142
			5.0	1.1	0.4	0.2	152
		Neste SAR 10/10	3.0	-	-	0.0	124
			4.0	-	0.3	0.0	120
			5.0	1.0	0.4	0.0	128
		Subgroup Average		**1.1**	**0.4**	**0.1**	**132**
2	**Wet Process (Manufacturer Preblended)**	Ecoflex (Bitumar)	3.0	-	0.0	-0.3	133
			4.0	0.5	0.0	-0.3	122
			5.0	0.6	0.0	-	130
		Subgroup Average		**0.6**	**0.0**	**-0.3**	**131**
4	**Polymer Modified**	Neste EVALAST	3.0	-	0.0	-0.4	104
			4.0	0.8	-0.2	-0.5	89
			5.0	0.5	-0.2	-0.5	84
		Subgroup Average		**0.7**	**-0.1**	**-0.5**	**92**
		ELVALOY (Conoco 120/150 + 1.5% Mod)	3.0	-0.1	-0.6	-0.8	68
			4.0	0.0	-0.5	-0.8	72
			5.0	0.2	-0.4	-0.7	77
		ELVALOY (Conoco 120/150 + 2.0% Mod)	3.0	-	-0.2	-0.8	91
			4.0	-	-0.6	-0.8	80
			5.0	0.1	-0.5	-0.7	67
		Sugroup Average		**0.1**	**-0.5**	**-0.8**	**76**
5	**Wet Process (Plant Blended)**	Citgo AC-10 (0% EO + 10% CR)	3.0	0.2	-0.6	-0.9	76
			4.0	0.3	-0.3	-0.6	87
			5.0	0.3	-0.2	-	87
		Citgo AC-10 (3% EO + 15% CR)	3.0	-	-0.1	-0.5	96
			4.0	0.5	-0.2	-0.5	88
			5.0	0.5	-0.2	-0.5	93
		Citgo AC-10 (7% EO + 20% CR)	3.0	-	0.0	-0.6	96
			4.0	1.2	0.3	-0.2	107
			5.0	0.9	0.0	-	98
		Citgo AC-20 (0% EO + 10% CR)	3.0	-	0.6	0.2	124
			4.0	1.1	0.3	-0.7	103
			5.0	0.9	-	-	86
		Citgo AC-20 (3% EO + 15% CR)	3.0	-	0.5	-1.1	116
			4.0	0.1	-0.8	-	68
			5.0	-0.4	-	-	70
		Citgo AC-20 (7% EO + 20% CR)	3.0	0.2	-0.5	-1.1	76
			4.0	-0.1	-1.1	-	66
			5.0	-0.4	-	-	60
		Group Average		**0.4**	**-0.2**	**-0.6**	**89**

* a. d(AC) Value = AC% (SUPERPAVE) - AC % (Marshall)
b. SUPERPAVE Climatic Regions
Cool : Temp $\leq$ 34 ^{o}C ; N_{des} = 67
Mod : Temp = 37 - 38 ^{o}C ; N_{des} = 96
Warm : Temp = 43 - 44 ^{o}C ; N_{des} = 119

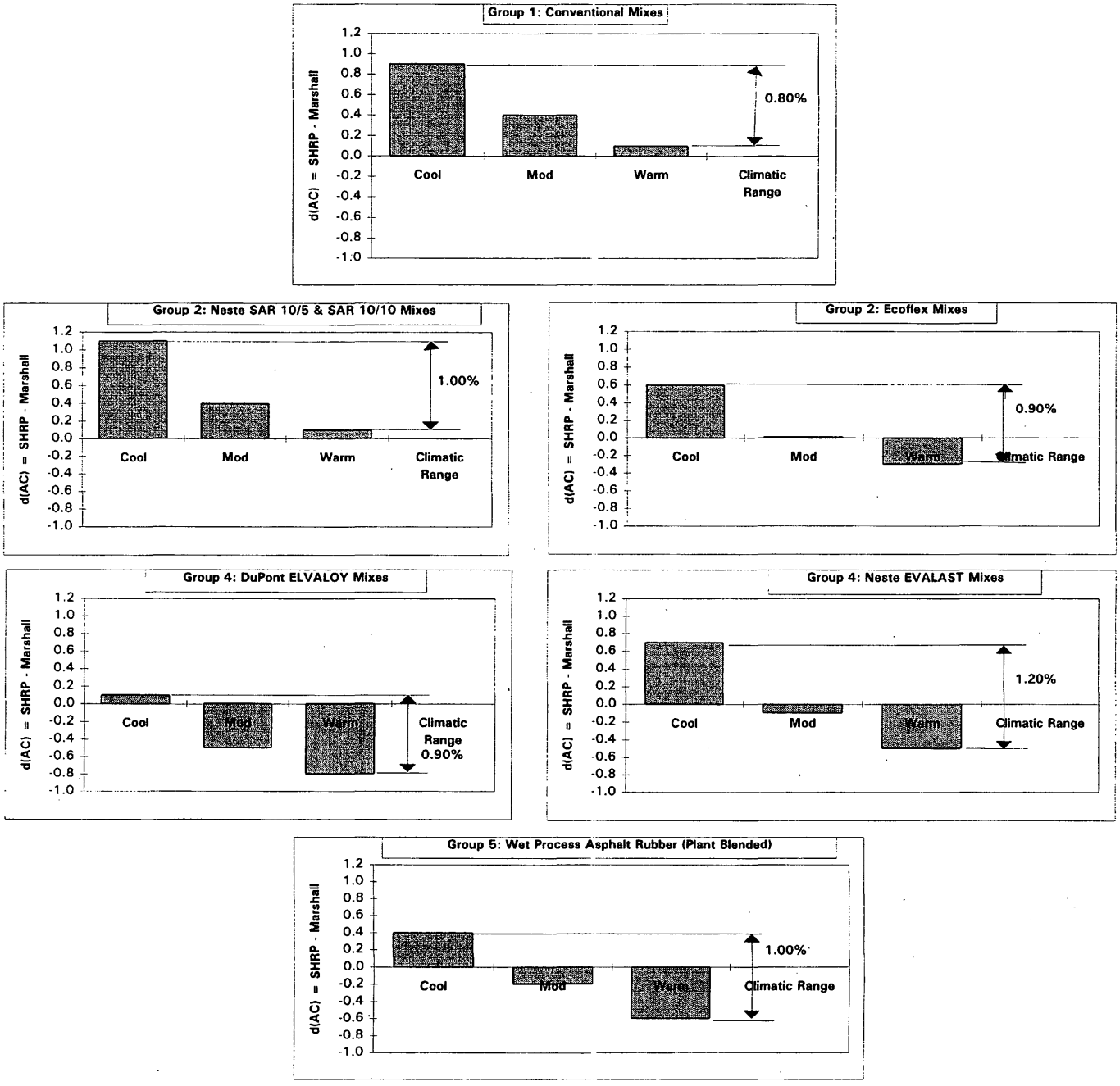

FIGURE 2 Design AC percent differences (Superpave − Marshall) for mix groups evaluated.

(manufacturer-preblended and plant-blended) and polymer-modified asphalt mixtures).

Within a given Superpave climatic region, there are no consistent trends in the d(AC) values between the various groups (subgroups) identified. In general, the d(AC)-climatic trends for the two Neste SAR (wet process-manufacturer preblends) are very similar to those found for all three of the conventional (Group 1) mixes studied. For the warm Superpave region, Level I design asphalt contents are almost equivalent to those found by the Marshall procedure. In contrast, for the cold Superpave region, the Superpave designs require about 1.0 percent more binder content than Marshall designs.

The Ecoflex (Bitumar) wet asphalt rubber binder appeared to be intermediate in d(AC) values to the conventional (Group 1) and polymer modified (Group 4) mixtures. Both polymer modified subgroups (DuPont Elvaloy and Neste Evalast) resulted in Superpave asphalt contents that were significantly less (−0.5 to −0.8 percent), for the warm Superpave condition, compared to Marshall derived asphalt contents.

Within a given Superpave climatic region, the wet process plant-blended mix (Group 5) d(AC) values are dependent on the rubber percent and the binder type. For mixes prepared with AC-10 binders, the d(AC) value increases as the rubber percent increases and the converse is true for the mixes prepared using AC-20 binder.

The average N_{eq} values for the conventional (Group 1), wet-blend SAR and wet-blend Ecoflex (Group 2) were found to be 130, 132, and 128, respectively. This implies that the probable response of the

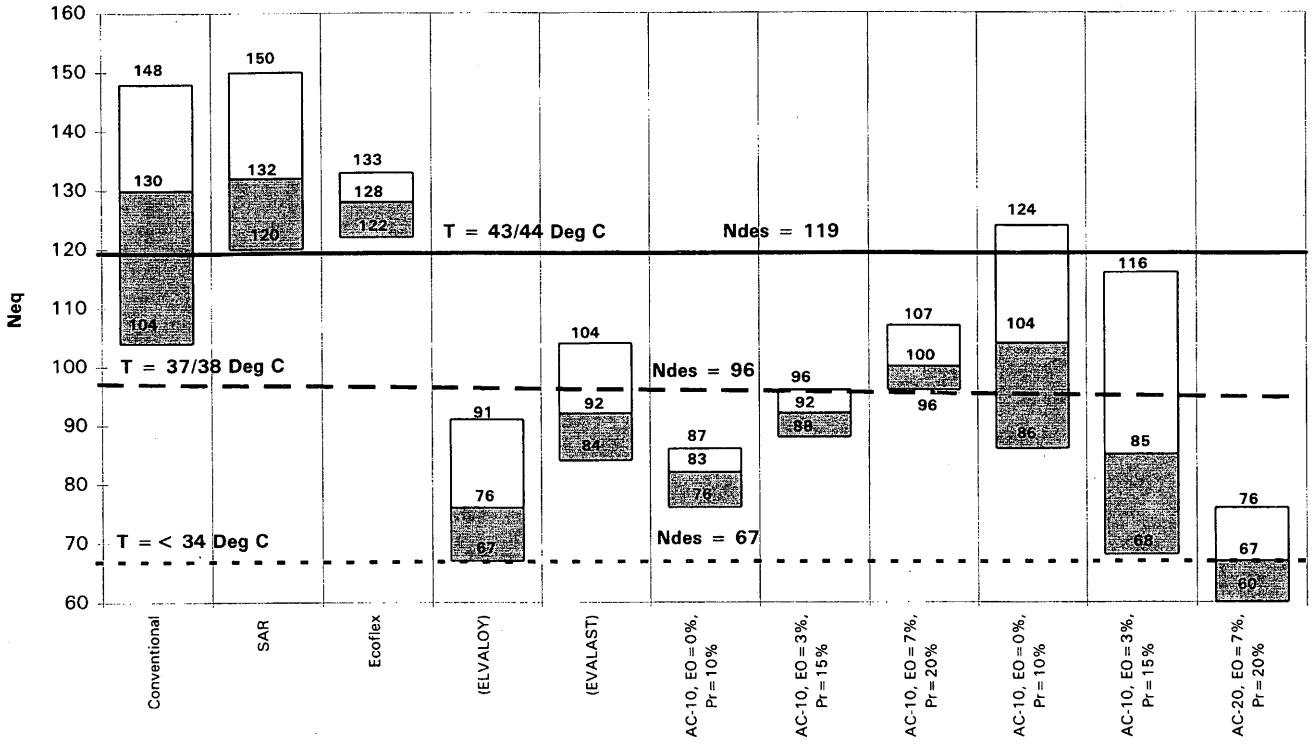

FIGURE 3 Equivalent number of gyrations for mixes investigated.

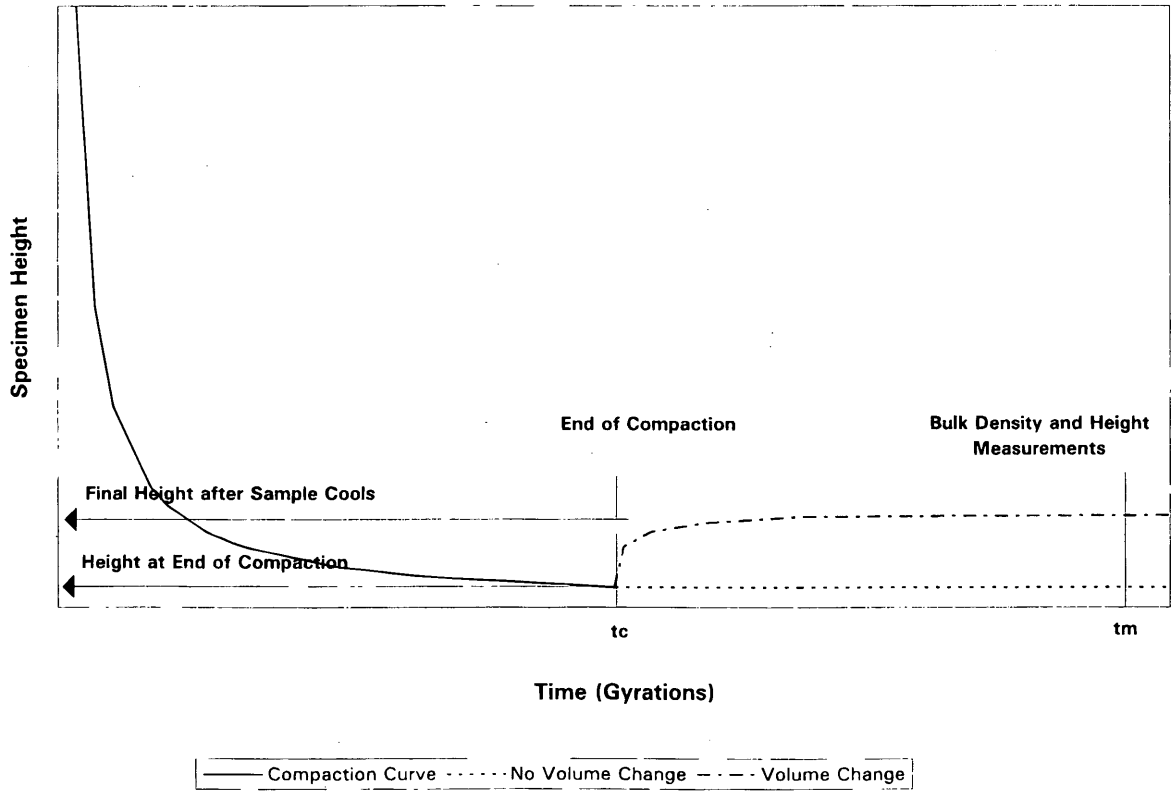

FIGURE 4 Variation of sample height during and after Superpave gyratory compaction.

wet blends investigated is not dissimilar to conventional mixtures. The overall average of these groups (N_{eq} = 130) is not greatly different from the Superpave design gyration value, for warm climatic conditions, of N_{eq} = 119. In contrast, the polymer-modified materials (Elvaloy and Evalast) resulted in N_{eq} values of 76 and 92, respectively, indicating that equivalent Superpave and Marshall design binder contents occur for colder Superpave climatic regions. This finding was also observed for the Group 5 (wet process plant-blended) as the overall average of N_{eq} was 89 and the subgroup averages ranged between 67 and 104, depending on the rubber percent and the binder type.

GYRATORY BEHAVIOR OF DRY PROCESS RUBBER ASPHALT MIXTURES

General Problem Discussion

As noted in Table 2, the study of the Group 3 (dry process rubber asphalt mixtures) involved the Marshall and Superpave Level I analysis of five separate mixtures (three generic mixes developed at the UMD and two Plus-Ride mixes). Several major obstacles developed with the implementation of the Superpave Level I approach for the Group 3 mixtures that have led the authors to conclude that the Superpave approach is not appropriate to select design binder contents for the Group 3 mixtures.

These problems and limitations regarding the Superpave approach are a direct result of two unique properties of the dry rubber asphalt mixtures. The first property of these mixtures is related to the highly resilient nature of the rubber particles used as aggregate within the mix. During the gyratory compaction process, the change in sample height (i.e., volumetric change) is primarily an elastic compression because of the high resilience of the rubber particles themselves. After the gyratory process is complete, a significant instantaneous rebound may occur in the specimen. This process is best viewed as having the gyratory device simply compact a series of elastic springs.

The second characteristic of these mixtures is related to the swelling of the sample after the compaction process stops. This positive (increase) volume change is a time dependent phenomena whose magnitude is related to the complex interaction of rubber type/gradation, percentage of rubber as well as asphalt cement, and the temperature during the compaction process.

These two volumetric change properties of the Group 3 mixtures are directly responsible for the inaccurate interpretation of lab results for use with the Superpave Level I mix design procedure currently used (especially the N_{gyr} criteria of Table 1). The schematic influence of this volume change is shown in Figure 4. Directly after compaction, if the mix has *no* volume change potential, the height of the specimen (and subsequently the measurement of the sample bulk density) is identical to end of compaction conditions. If the specimen exhibits volume change, the final height at the end of compaction and the measured bulk-specific gravity after the sample cools cannot be used to correct the density curves (i.e., obtain C_{cx}) because the specimen volumes differ between the G_{mb} measurement and the end of compaction process. Thus, even though "corrections" can be computed, they will always be in error and consequently provide erroneous plots of gyrations versus air voids (or percent of maximum theoretical gravity). In contrast, accurate estimates of the densification curve can be obtained for mixtures with little to no volume change after the compaction process.

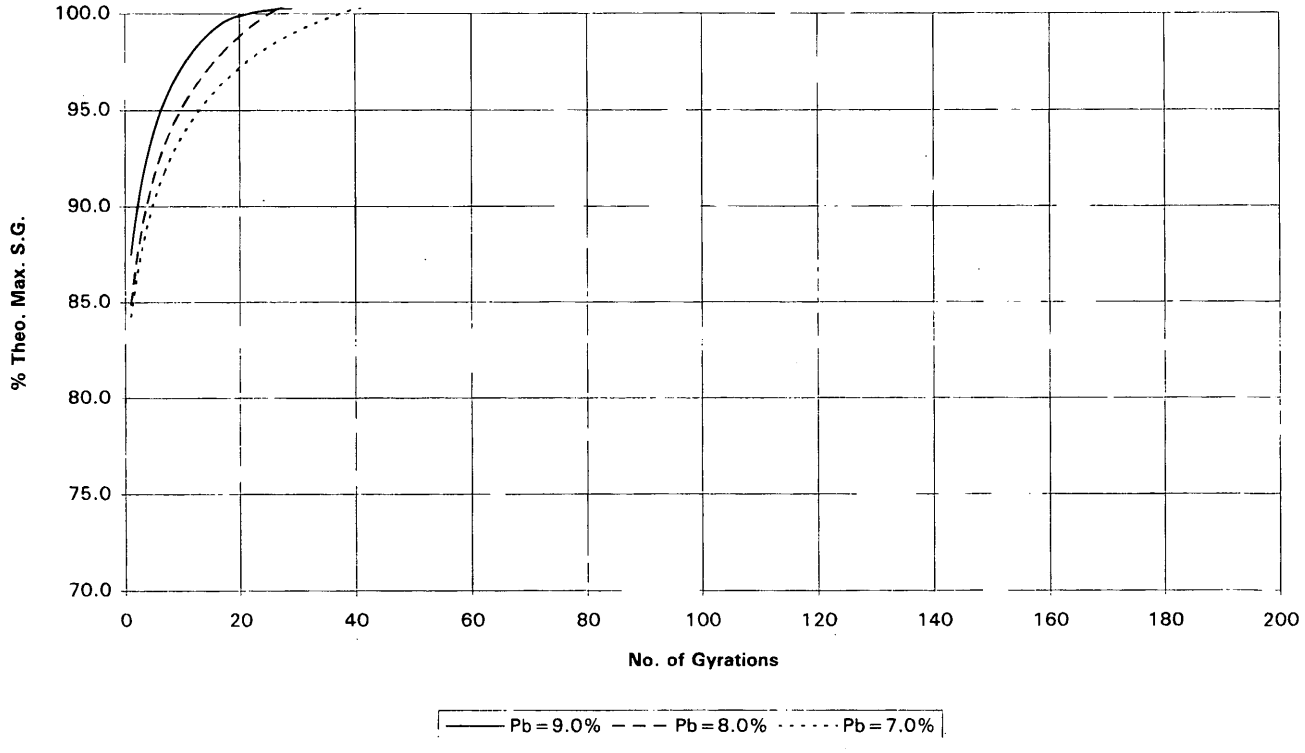

FIGURE 5 Percent of theoretical maximum specific gravity versus number of gyrations under different asphalt content (Plus Ride No. 12).

TABLE 8 Equivalent Marshall Gyrations for Group 3—Dry Process Rubber Asphalt Mixes

Group	Description	Mix Identification	Va (%)	AC % Marshall	Marshall Neq
3	Dry Process Rubber Asphalt	Generic: Chevron AC-20 (1% R)	3.0	6.2	72
			4.0	5.7	71
			5.0	5.5	59
		Group Average			**67**
		Generic: Chevron AC-20 (2% R)	3.0	8.0	23
			4.0	7.3	22
			5.0	6.8	21
		Group Average			**22**
		Generic: Chevron AC-20 (3% R)	3.0	9.0	16
			4.0	8.2	10
			5.0	7.7	13
		Group Average			**13**
		Plus Ride No. 12 (3% R)	3.0	10.0	6
			4.0	8.9	8
			5.0	7.5	11
		Group Average			**8**
		Plus Ride No. 16 (3% R)	3.0	7.4	14
			4.0	6.4	16
			5.0	-	-
		Group Average			**15**

Typical Results

Figure 5 illustrates results of the "corrected" densification curves for the PLUS RIDE No. 12 mixture at three binder contents. All five of the Group 3 mixtures evaluated resulted in very similar types of relationships. The difference in gyratory response for this mix is quite obvious in comparison to the Group 1 (conventional) mix response shown in Figure 1. As a general rule, the "computed" (erroneous) maximum theoretical density was achieved within 20 to 50 gyrations for all 15 mix-binder content combinations evaluated in Group 3. As noted, the major reason associated with the rapid "densification" of dry rubber asphalt mixtures is caused by the large resilient (elastic) deformations within the rubber particles themselves and not by permanent densification of the specimen from the compaction process.

The inapplicability of the Superpave densification curves developed for all five mixtures in Group 3 can also be viewed relative to the N'_{eq} parameter introduced in the previous section of this paper. Table 8 summarizes for the Group 3 mixtures, the Marshall design asphalt content and the equivalent Superpave gyratory repetitions necessary to achieve equivalent binder contents. Of special importance is that each of the five mixtures was successfully placed in MSHA field demonstration projects during the fall of 1993 at design Marshall asphalt contents shown in the table at air voids between 3 and 4 percent. The Superpave N_{eq} values (average) (67, 22, 13, 8, and 15) are nowhere near the Table 1 (Superpave) recommendations of N_{des} = 67, 96, and 119 to represent the various gyratory climatic regions used in this study. In fact, the difference is so large that it was impossible to obtain design binder contents for all five mixtures from the Superpave criterion shown in Table 1.

To evaluate the influence of the time-dependent volume change increase immediately after the gyratory compaction process, the gyratory machine itself determined the time-dependent height change observed during the volume change process. This process involved the preparation of an additional replicate, at each binder content, and compacting the specimens in the gyratory device to 200 gyrations. At the end of compaction, the ram pressure was released to a zero level and the height of the specimen recorded at various time increments (generally 10 measurements during the first 30 min, starting at 30 sec, 1 to 2 hr, 3 to 4 hr, and 16 to 20 hr).

The measurement of volume change was computed by two approaches using the process to obtain the G_{mb} values. In the "confined" approach, the specimens were left in the gyratory mold for 16 to 20 hr after the end of the compaction process. Bulk density measurements were obtained on the specimen after completion of the volume change measurements. For the "unconfined" approach, samples were extruded from the molds after about 1.5 hr from the end of the compaction and allowed to expand volumetrically for 16 hr before the bulk gravity was measured.

Figure 6 illustrates a typical volume change (as denoted by the air voids) pattern measured during the study. The combined influence of the nearly instantaneous and time-dependent swell pattern on this mix is clearly shown. A volume change equivalent to an air void change, dV_a, of nearly 6.0 percent was observed.

Figure 7 graphically summarizes the average dV_a values (computed by both the "confined" and "unconfined" approaches) for *all* mixtures and binder contents evaluated and not limited to the Group 3 mixtures. While dV_a values were recorded for Groups 1, 2, and 4, their magnitude is not considered to be significant relative to the dV_a values obtained on the Group 3 (dry-process rubber asphalt) mix-

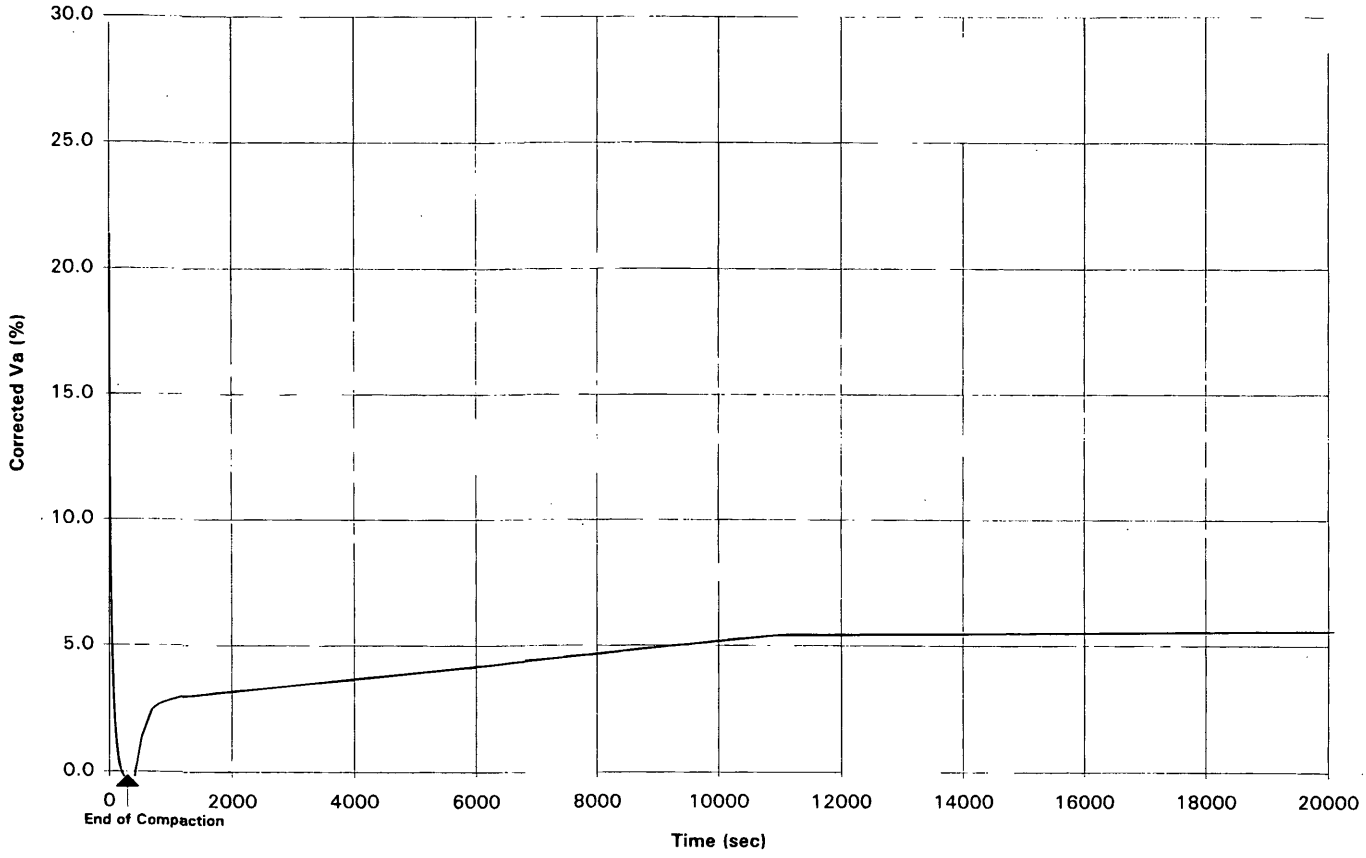

FIGURE 6 Corrected air voids versus time (rubber modified asphalt mixtures with Pb = 7.0 percent and Pr = 2.0 percent.

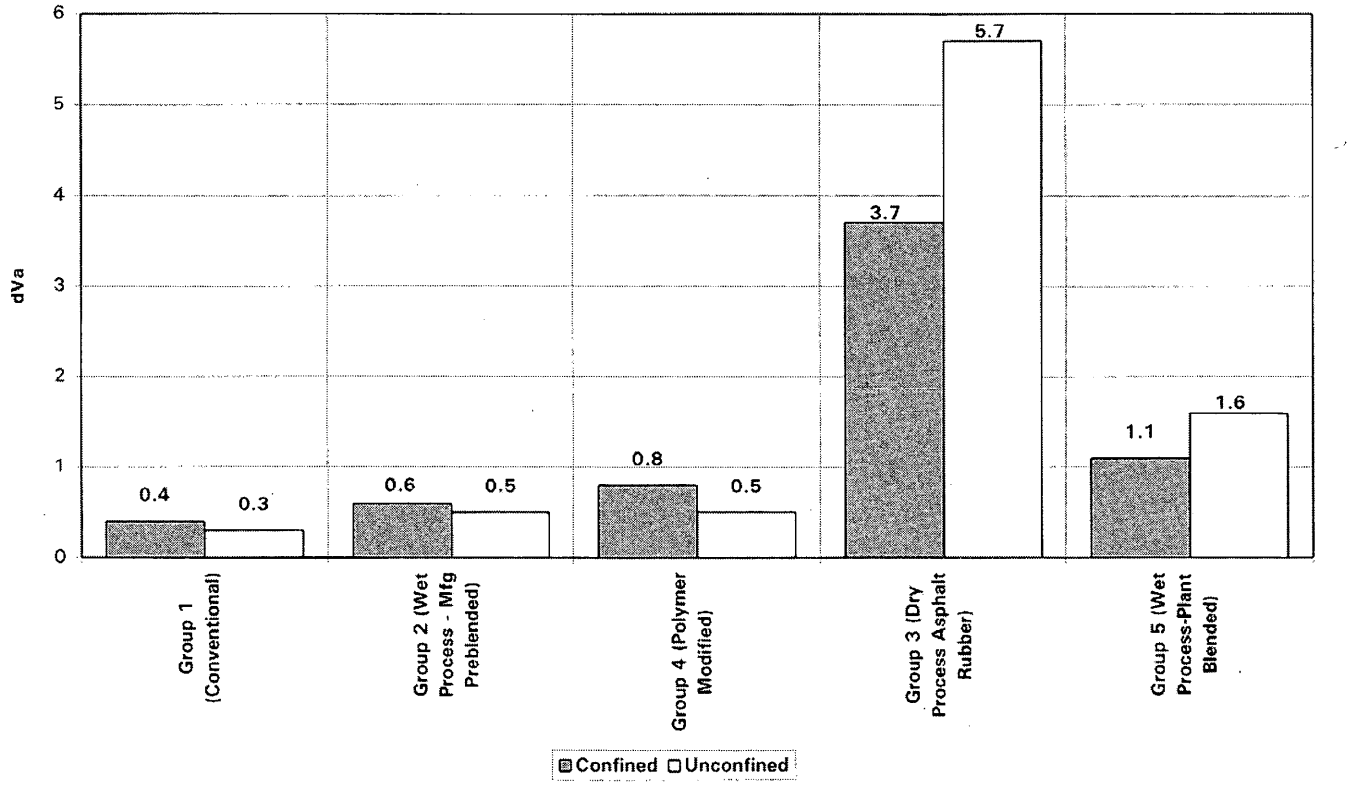

FIGURE 7 Average volume change (dV_a) values after gyratory compaction by major mix groups.

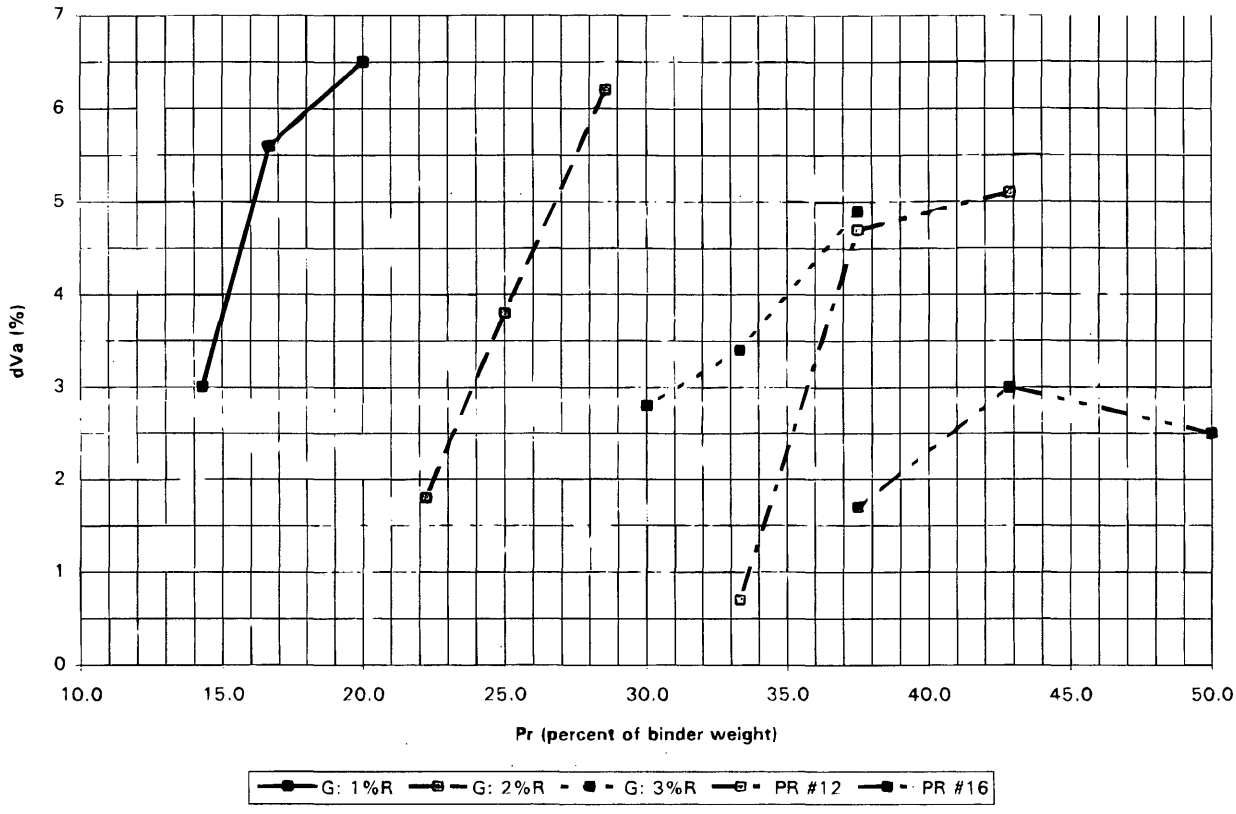

FIGURE 8 Increase in air voids after gyratory compaction versus rubber percent (by binder weight) for Group 3 mixtures—confined condition.

tures. The Group 5 (wet-process plant-blended) mixtures exhibited intermediate volume change between these two categories of groups discussed. While their volume change magnitudes are nowhere near those recorded for Group 3, they are 2 to 3 times the magnitude of Group 1, 2, and 4; therefore, these mixtures should also be considered suspect relative to the Superpave interpretation.

Figure 8 shows the relationship between dV_a and rubber percentage (by binder weight) for all five mixtures within Group 3. Within any given mix, the dV_a is shown to greatly increase as the rubber percentage is increased (*i.e.,* binder content is decreased). Or, at a given rubber percent (by total mix weight) the dV_a (volume change) is decreased with increasing asphalt content.

SUMMARY AND CONCLUSIONS

This study focused on the comparison of Asphalt Mix designs between the 75-blow Marshall and Superpave gyratory Level I approach. A total of 20 different mixtures were evaluated and categorized into five major mix groups. Based on the results of this study the following conclusions have been developed.

1. Of the five mix groups evaluated, it is the conclusion of the authors that the Superpave gyratory Level I design cannot be used to evaluate dry-process rubber asphalt mixtures. The reasons for this are due to the high resilience of the rubber particles during the compaction process and the time dependent swelling, after compaction, of these mixtures. This suggests, that problems with the Superpave approach implementation may occur on any mixture possessing these abnormal characteristics.

2. The design process for all other mixtures investigated, except for the wet-process plant-blended mixes where slightly higher swelling was observed, posed no similar type of problem and demonstrated the potential advantages and benefits of the Superpave gyratory approach.

3. Relative to the comparison of design asphalt content differences between both mix design procedures, it was found that:

   a. Within any specific mix type, the difference in asphalt contents between approaches is independent of the target air void level selected (V_a = 3.0 to 5.0 percent) to develop the design value.

   b. As the Superpave climatic regions changes from warm to cool, an increase of approximately 1.0 percent more asphalt will be required from the Level I approach. This finding was found to be true for all mix types/groups studied.

   c. Within a given Superpave climatic region, no consistent trends in design asphalt contents, between the type of mix design procedure used, were found between mixtures. In general, design asphalt contents for the conventional and wet process (manufacturer-preblended) asphalt rubber mixes were equivalent between the Marshall and the warm Superpave climatic region while the converse was true for the wet process (plant blended) asphalt rubber mixes. For identical traffic and climatic conditions, the Superpave Level I designs for polymer modified mixtures were about 0.5 percent to 0.8 percent less than the Marshall analysis.

ACKNOWLEDGMENTS

This research has been conducted under a research grant from the Maryland State Highway Administration to the University of Maryland under MSHA Study No. AW0-94–368–046, *Development of Demonstration Projects With Scrap Tire Rubber in Highway Pavements Within the State of Maryland.* The authors are indebted to MSHA for their technical and financial assistance. The contents of this paper reflect the views and opinions of only the authors and do not reflect the official views or policies of MSHA.

REFERENCES

1. Strategic Highway Research Program (SHRP) *The Superpave Mix Design Manual for New Construction and Overlays.* National Research Council, March 1993.
2. Asphalt Institute Manual Series No. 2 (MS-2). *Mix Design Methods for Asphalt Concrete and Other Hot-Mix Types.* 6th ed. Lexington, Ky., 1993.

Publication of this paper sponsored by Committee on Characteristics of Bituminous Paving Mixtures to Meet Structural Requirements.

Correlation of Superpave $G^*/\sin\delta$ with Rutting Susceptibility from Laboratory Mixture Tests

KEVIN D. STUART AND RICHARD P. IZZO

The objective of this study was to compare the Superpave $G^*/\sin\delta$ of five binders with the rutting parameters given by laboratory mixture tests. Superpave uses the $G^*/\sin\delta$ from the dynamic shear rheometer to specify binders according to rutting susceptibility. The conventional designations for the five binders are AC-5, AC-10, AC-20, Novophalt, and Styrelf 1-D. All five binders were used in a surface mixture having a nominal maximum aggregate size of 19.0 mm. The AC-5 and AC-20 binders were also used in a base mixture having a nominal maximum aggregate size of 37.5 mm to determine whether the effects of binder type on rutting susceptibility varies with maximum aggregate size. The data showed that binders with higher $G^*/\sin\delta$ produce mixtures less susceptible to rutting. The Georgia loaded-wheel tester provided a very good relationship between $G^*/\sin\delta$ and rutting susceptibility. The French pavement rutting tester and Hamburg wheel-tracking device provided reasonably good relationships. The main discrepancy for these latter two devices was that even though the Styrelf mixture had a very low susceptibility to rutting, the data suggest that the rut depths are slightly high compared with the $G^*/\sin\delta$ of the binder. The data also showed that increased maximum aggregate size did not significantly reduce the effects of binder type on rutting susceptibility. The Marshall stabilities and flows and the gyratory testing machine data did not differentiate between the mixtures according to rutting susceptibility; therefore, there were no relationships between these tests and $G^*/\sin\delta$.

The FHWA is validating Superpave (*Sup*erior *Per*forming Asphalt *Pave*ments) binder tests and specifications, Superpave mixture tests and performance models, and other accelerated laboratory tests for mixtures. Pavements were constructed at the Turner-Fairbank Highway Research Center (TFHRC) in McLean, Virginia, to assist in validating the tests for rutting and fatigue cracking. The pavements are being tested by the Accelerated Loading Facility (ALF).

The pavement testing facility consists of 12 lanes with two nominal maximum aggregate sizes and five binders. Each lane consists of one full-depth mixture. The binders are AC-5, AC-10, AC-20, Novophalt, and Styrelf 1-D. The mixtures consist of a surface aggregate blend and a base aggregate blend. The surface mixtures include all five binders. The base mixtures include only AC-5 and AC-20. The purpose of including a base mixture is to determine whether the effects of binder type on rutting vary with the maximum aggregate size.

The five surface mixtures were designed to meet the 1991 Virginia Department of Transportation specification for SM-3B mixtures, whereas the two base mixtures were designed to meet a modification of the specification for BM-3 mixtures. Uniform gradations and binder contents were used in each type of mixture in order to investigate the effects of binder properties on rutting and fatigue cracking. The aggregates and binders used in the pavements are stockpiled at TFHRC. These materials are used to produce laboratory samples for testing.

Quality control and quality assurance (QC/QA) testing was conducted by the paving contractor and FHWA to ensure that the specifications of the project were met. Samples of the five binders were obtained during the mixture designs from the terminal immediately before shipping, from the hot-mix plant after they arrived from the terminal, and daily during construction. These samples were tested to ensure that the properties of the binders did not change while they were being used. Two samples of each plant-produced mixture per lift were taken during construction. The aggregate gradations, percent natural sand, percent binder, and maximum specific gravities were determined. Specimens were also compacted for voids analyses during construction. Nuclear density tests and 72 cores taken after construction were used to determine the air void content. This information was essential for duplicating the average properties of the ALF pavements using the stockpiled materials. A separate report documenting the QC/QA testing will be published.

The initial data from the research project are presented in this paper. The Superpave binder specification uses the $G^*/\sin\delta$ from the dynamic shear rheometer (DSR) determined after subjecting a binder to the rolling thin-film oven test (RTFOT) to specify a binder according to rutting susceptibility. The first phase of the research project is concerned with how well the $G^*/\sin\delta$ parameter agrees with rutting parameters given by laboratory mixture tests. Besides the mixture tests presented in this paper, the Superpave shear tester and the NCHRP asphalt-aggregate mixture analysis system (AAMAS) will also be evaluated (*1*). Eventually, the results will be compared with ALF pavement performance. A correlation between $G^*/\sin\delta$ and rutting susceptibility will enable asphalt paving technologists to classify binders according to performance. This will lead to longer-lasting pavements and lower maintenance costs.

OBJECTIVES

The primary objective of this study was to determine whether the Superpave $G^*/\sin\delta$ ranks binders the same as laboratory mixture tests for rutting. Comparisons among the mixture tests were also included. A second objective was to determine whether the effects of binder type on rutting susceptibility vary with maximum aggregate size.

K. D. Stuart, Federal Highway Administration, Turner-Fairbank Highway Research Center, 6300 Georgetown Pike, McLean, Va. 22101–2296. R. P. Izzo, Civil and Environmental Engineering Department, University of Rhode Island, Kingston, RI. 02881. Current Address: Materials Division, Texas Transportation Institute, Texas A&M University, College Station, Tex. 77843.

BINDERS

Five binders were used: AC-5, AC-10, AC-20, Novophalt, and Styrelf 1-D. The AC-5, AC-10, and AC-20 were from Venezuela's Lagoven base stock. Koch Materials Company, Pennsauken, New Jersey, supplied these asphalts. The Novophalt binder was formulated by blending the Lagoven AC-10 asphalt with 5 percent low-density polyethylene by mass. A high shear mill was used for blending by Advanced Asphalt Technologies, Sterling, Virginia, at the paving contractor's hot-mix plant in Leesburg, Virginia. The Styrelf 1-D binder was formulated by reacting the Lagoven AC-20 asphalt with 4 percent styrene-butadiene by volume. Styrelf is a product of the Koch Materials Company and is shipped in bulk form. The traditional physical properties of the binders and the Superpave performance grades are given in Table 1.

Samples of the five binders were exposed to the RTFOT and tested by the DSR to determine $G^*/\sin\delta$. The DSR is used to evaluate the viscous and elastic behavior of asphalt binders by measuring the complex shear modulus (G^*) and phase angle (δ). These values are highly dependent on the temperature and frequency of loading (*2*). $G^*/\sin\delta$ was measured at temperatures of 10, 20, 30, 40, 50, 60, and 70°C and frequencies ranging from 0.1 to 10.0 rad/sec. This allowed a direct correlation of the $G^*/\sin\delta$ with the results of the mixture tests, which are performed at different temperatures and frequencies. The DSR frequencies corresponding to the mixture tests were based on 80 km/hr being equivalent to 10 rad/sec as established by the Strategic Highway Research Program (SHRP). The speeds of the mixture tests were divided by 8 to obtain the DSR frequency in rads per second. Table 2 provides all values of $G^*/\sin\delta$. Higher amounts of rutting were expected from the mixtures that used binders with lower values of $G^*/\sin\delta$.

As expected, $G^*/\sin\delta$ decreased with an increase in temperature and a decrease in frequency. The binders were ranked from lowest to highest $G^*/\sin\delta$ using statistical analyses. These rankings varied with the temperature and frequency. The rankings applicable to this study are given in the *Results and Discussion* section.

TABLE 1 Physical Properties of Binders

	AC-5	AC-10	AC-20	Novophalt	Styrelf
Original Binder					
Penetration, 25°C, 0.1 mm	172	113	73	55	47
Absolute Viscosity, 60°C, dPa·s	665	1 195	2 644	12 714	58 774
Kinematic Viscosity, 135°C, mm^2/s	256	322	476	2 184	2 484
Specific Gravity, 25/25°C	1.007	1.024	1.022	1.022	1.020
Solubility in Trichloroethylene, %	100.00	100.00	100.00	95.92	100.00
Flash Point, COC,°C	304	304	304	326	312
Thin Film Oven Residue					
Weight Loss, %	0.01	0.33	0.13	0.34	0.12
Penetration, 25°C, 0.1 mm	102	66	47	40	35
Absolute Viscosity, 60°C, dPa·s	1 758	3 223	7 173	29 844	208 185
Kinematic Viscosity, 135°C, mm^2/s	372	509	684	3 686	4 197
SUPERPAVE™ Performance Grade	58-34	58-28	64-22	76-22	82-22
Original Binder					
Temperature at a G*/sinδ of 1.00 kPa and 10 rad/s, °C	59.4	61.9	67.9	83.4	87.2
Rolling Thin Film Oven Residue					
Temperature at a G*/sinδ of 2.20 kPa and 10 rad/s, °C	59.3	65.0	70.2	79.3	88.0
Rolling Thin Film Oven/Pressure Aging Vessel Residue					
Temperature at a G*sinδ of 5 000 kPa and 10 rad/s, °C	9.1	14.5	17.3	26.0	24.8
Temperature at a Creep Stiffness (S) of 300 MPa and 60 s, °C	-26.9	-22.1	-19.8	-20.2	-20.9
Temperature at an m-value of 0.30 and 60 s, °C	-25.3	-20.3	-17.1	-13.4	-17.4

TABLE 2 Determination of $G^*/\sin\delta$ in Pascals at Different Temperatures and Frequencies

Temp. (°C)	AC-5	AC-10	AC-20	Novophalt	Styrelf
G/sinδ at w=10.0 rad/s, Standard Frequency for the DSR:*					
10	5 172 000	11 990 000	17 880 000	33 050 000	22 340 000
20	862 000	2 001 000	3 074 000	7 587 000	5 055 000
30	173 100	386 600	666 300	1 478 000	1 036 000
40	38 640	82 800	159 900	379 300	268 100
50	7 528	15 880	30 660	94 330	74 590
60	2 096	4 202	7 897	27 200	28 120
70	653	1 238	2 226	8 381	11 260
G/sinδ at w=2.25 rad/s, Frequency for the ALF Machine:*					
10	2 240 000	5 364 000	8 335 000	16 860 000	10 970 000
20	351 800	833 500	1 383 000	3 387 000	2 270 000
30	62 220	143 900	267 700	626 300	460 200
40	11 910	26 350	54 470	151 000	116 300
50	2 057	4 446	9 002	32 550	31 140
60	526	1 084	2 100	8 393	11 390
70	155	299	549	2 376	4 378
G/sinδ at w=0.875 rad/s, Frequency for the French Pavement Rutting Tester:*					
10	1 276 000	3 111 000	4 954 000	10 630 000	6 822 000
20	182 100	461 000	796 200	1 967 000	1 345 000
30	30 900	73 360	141 800	348 700	270 500
40	5 382	12 210	26 240	81 020	67 480
50	856	1 926	3 911	15 790	17 790
60	212	442	871	3 789	6 338
70	61	118	219	1 022	2 357
G/sinδ at w=0.125 rad/s, Frequency for the Georgia Loaded Wheel Tester, German Hamburg Wheel Tracking Device, and Gyratory Testing Machine:*					
10	346 000	873 800	1 437 000	3 629 000	2 332 000
20	50 080	118 500	216 500	567 400	421 200
30	6 358	16 100	33 210	94 120	84 440
40	899	2 215	5 060	21 000	20 600
50	130	348	635	3 128	5 232
60	28	60	124	661	1 750
70	8	16	29	167	589

AGGREGATES

All five binders were used in a surface mixture; the AC-5 and AC-20 binders were also used in a base mixture. The surface mixtures consisted of No. 68 diabase, No. 10 diabase, and natural sand. The base mixtures consisted of No. 357 diabase, No. 8 diabase, No. 10 diabase, and natural sand. The diabase aggregates used in the surface mixtures were supplied by Virginia Trap Rock, Leesburg, Virginia. The diabase aggregates used in the base mixtures were supplied by Luck Stone Corporation, Leesburg, Virginia. To eliminate moisture damage, 1 percent hydrated lime was added to both mixtures. The natural sand was supplied by Solite Corporation, Fredricksburg, Virginia. The hydrated lime was supplied by Chemston, Strasburg, Virginia.

The aggregates used in the laboratory mixtures were blended to meet the average gradations of the plant-produced mixtures. The gradations are shown in Tables 3 and 4. The target gradations are the gradations of the plant-produced mixtures. The nominal maximum aggregate sizes for the surface and base mixtures are 19.0 and 37.5 mm.

MIXTURE TESTING PROGRAM

The following mixture properties were determined:

- Marshall mixture properties at 60°C.
- French pavement rutting tester at 60°C, including the percent rut depth at 300, 1,000, 3,000, 10,000, and 30,000 cycles;

TABLE 3 Aggregate Properties for the SM-3B Surface Mixtures

Aggregate Gradations, Percent Passing:

Sieve Size (mm)	61% No. 68 Diabase	30% No. 10 Diabase	8% Natural Sand	1% Hydrated Lime	Target	Blend
25.0	100.0				100.0	100.0
19.0	97.9				98.7	98.7
12.5	60.7				76.0	76.0
9.5	37.7	100.0	100.0		62.0	62.0
4.75	9.2	99.2	95.8		44.0	44.0
2.36	2.2	75.6	88.2		32.5	32.1
1.18	1.7	52.5	74.8		23.5	23.8
0.600	1.4	37.8	46.0		17.5	16.9
0.300	1.3	27.9	14.1		11.5	11.3
0.150	1.1	19.6	4.8		8.0	7.9
0.075	0.9	12.5	2.9	100.0	5.1	5.5

The diabase aggregates were from Virginia Trap Rock.

Specific Gravities and Percent Absorption:

Bulk Dry	2.943	2.914	2.565		2.892
Bulk SSD	2.962	2.945	2.601		2.916
Apparent	2.999	3.007	2.659	2.262	2.961
% Abs	0.6	1.1	1.4		0.8

Bulk Dry = Bulk-Dry Specific Gravity.
Bulk SSD = Bulk-Saturated-Surface-Dry Specific Gravity.
Apparent = Apparent Specific Gravity.
% Abs = Percent Water Absorption.

and the slope of the relationship between log rut depth and log cycles.

- Georgia loaded-wheel tester (GLWT) at 40.6°C, including the rut depth at 8,000 cycles.
- Hamburg wheel-tracking device to 20,000 passes at 50°C, including the creep slope.
- U.S. Corps of Engineers gyratory testing machine (GTM) at 60°C, including the maximum static shear strength (Sg), gyratory stability index (GSI), gyratory elastoplastic index (GEPI), and the refusal air void level.

The target air void level for the specimens was 8 ± 1 percent, except for the Marshall specimens. The surface mixtures had a binder content of 4.85 percent by mixture mass. The base mixtures had a binder content of 4.0 percent. These levels duplicated the average air void level and binder contents of the pavements.

The data were analyzed by comparing rankings of the average test values, comparing rankings given by Fisher's least significant difference (LSD) statistical procedure, and by performing regressions. Fisher's LSD determines which averages are not significantly different from other averages. Groups of averages that are not significantly different are formed. These groups are ranked from highest to lowest. Fisher's LSD is performed in conjunction with an analysis of variance at a 95 percent confidence level.

TABLE 4 Aggregate Properties for BM-3 Base Mixtures

Aggregate Gradations, Percent Passing:

Sieve Size (mm)	41% No. 357 Diabase	15% No. 8 Diabase	38% No. 10 Diabase	5% Natural Sand	1% Hydrated Lime	Target	Blend
37.5	100.0					100.0	100.0
25.0	64.9					85.6	85.6
19.0	36.3					73.9	73.9
12.5	14.9	100.0				65.1	65.1
9.5	5.5	85.0	100.0	100.0		59.0	59.0
4.75	3.0	25.3	96.8	95.8		47.6	47.6
2.36	1.8	2.7	68.0	88.2		32.5	32.4
1.18	1.6	2.0	47.5	74.8		24.0	23.7
0.600	1.4	1.5	34.3	46.0		17.4	17.1
0.300	1.2	1.2	24.9	14.1		12.3	11.8
0.150	1.1	0.9	17.3	4.8		8.0	8.4
0.075	0.8	0.8	11.5	2.9	100.0	5.7	6.0

The diabase aggregates were from Luck Stone Corporation.

Specific Gravities and Percent Absorption:

Bulk Dry	2.971	2.956	2.894	2.565		2.907
Bulk SSD	2.984	2.981	2.935	2.601		2.934
Apparent	3.013	3.030	3.017	2.659	2.262	2.987
% Abs	0.5	0.8	1.4	1.4		0.9

Bulk Dry = Bulk-Dry Specific Gravity.
Bulk SSD = Bulk-Saturated-Surface-Dry Specific Gravity.
Apparent = Apparent Specific Gravity.
% Abs = Percent Water Absorption.

AGING STUDY

Superpave recommends that loose mixtures be oven-aged for 4 hr at 135°C before compaction (*3*). This process is termed short-term oven aging (STOA). The SHRP final report states that STOA produces the average amount of aging at 6 months to 2 years of service life. In order to better simulate the degree of aging that occurred during plant production of the ALF mixtures, an aging study was performed.

The study consisted of aging laboratory mixtures for various periods of time, extracting and recovering the binders from these mixtures and from ALF pavement cores, and performing three Superpave binder tests on the recovered binders. The laboratory aging periods were 0, 1, 2, and 4 hr. Three replicate samples were prepared for each aging period. The mixtures consisted of the surface mixture with AC-5, the base mixture with AC-5, and the surface mixture with AC-20. Cores were taken from four ALF pavements constructed with these mixtures, including two pavements with the AC-20 as a check on pavement-to-pavement variability. The recovered binders were tested by the DSR at 10, 30, 50, and 70°C; by the bending beam rheometer (BBR) at −24°C; and by the Brookfield viscometer at 135°C. Three binder tests were performed to fully examine the capability of simulating hot-mix plant aging using a forced draft oven, even though the pavements were only to be tested in the range of 10 to 60°C. All three tests should provide the same aging period if oven aging duplicates plant aging and provides the same binder chemistry. The testing program was also developed to show which of the Superpave binder parameters are most sensitive to aging.

The recovered binder properties from the aged laboratory mixtures were plotted with respect to the aging period. A regression was performed to generate a second-order polynomial equation. The aging periods required to duplicate the properties of the binders in the ALF pavements were computed for each binder and test. The differences among the data for the two AC-20 pavements were not significant; thus, averaged data were evaluated.

The results are given in Table 5. The DSR provided aging periods up to 2.5 hr and an average of 1.3 hr. The BBR stiffnesses provided no definitive conclusions. The BBR slopes provided aging periods greater than or equal to 3 hr, but the data varied very little with the aging period. The Brookfield viscosities indicated that 2.3 hr was needed for the AC-20 mixture. However, the AC-5 binders recovered from the laboratory mixtures were stiffer than the AC-5 binders recovered from the cores, even at an aging period of 0 hr.

Overall, the required oven-aging period depended on the mixture type and the binder test performed. A previous study found that the absolute viscosity at 60°C and penetration at 25°C can also give different oven-aging periods for a given mixture (*1*). This indicates that oven aging may not effectively simulate hot-mix plant aging. An aging period of 2 hr was used as a compromise.

TABLE 5 STOA Data

Binder/ Mixture Type	Laboratory Aging Period (h) 0	1	2	4	Req'd Pavement Core Property	Req'd Lab Aging (h)
Average G (Pa) at w=10 rad/s Determined by the Dynamic Shear Rheometer:*						
AC-5 Surface						
at 10°C	2 974 000	2 682 000	4 192 000	4 422 000	3 181 000	1.3
at 30°C	118 500	110 300	181 500	221 800	125 800	1.2
at 50°C	7 062	6 798	10 930	14 760	7 319	1.1
at 70°C	630	627	916	1 301	626	1.0
AC-5 Base						
at 10°C	2 990 000	4 295 000	5 546 000	5 516 000	3 453 000	0.3
at 30°C	97 360	152 900	211 900	246 100	144 600	0.7
at 50°C	5 234	8 462	12 120	15 150	8 534	0.9
at 70°C	464	726	1 038	1 284	709	0.8
AC-20 Surface						
at 10°C	8 359 000	8 922 000	10 730 000	11 580 000	9 827 000	1.4
at 30°C	302 800	372 900	423 600	585 300	455 800	2.4
at 50°C	15 690	20 810	22 750	35 240	26 210	2.5
at 70°C	1 160	1 549	1 650	2 526	1 868	2.4
Average Creep Stiffness, S, (MPa) at 60 s and -24°C Determined by the Bending Beam Rheometer:						
AC-5 Surface	92	98	124	110	139	ND
AC-5 Base	139	183	218	206	165	0.6
AC-20 Surface	284	286	312	353	333	2.5
Average Slope, m, of Log Creep Stiffness vs. Log Time at 60 s and -24°C Determined by the Bending Beam Rheometer:						
AC-5 Surface	0.40	0.40	0.38	0.36	0.36	4.0
AC-5 Base	0.38	0.37	0.36	0.34	0.35	3.0
AC-20 Surface	0.33	0.31	0.31	0.29	0.30	3.0
Average Absolute Viscosity (Pa-s) at 135°C Determined by the Brookfield Viscometer:						
AC-5 Surface	0.36	0.33	0.41	0.44	0.29	< 0
AC-5 Base	0.34	0.49	0.65	0.64	0.31	< 0
AC-20 Surface	0.45	0.51	0.52	0.63	0.55	2.3

ND = No data. A laboratory aging period could not be predicted from the data.

MIXTURE TEST DESCRIPTIONS

Marshall Mixture Properties

Marshall mixture properties were determined to verify whether the mixtures fabricated from the stockpiled materials were equivalent to the plant-produced mixtures and to evaluate the relationship between $G^*/\sin\delta$ and Marshall stability and flow.

Surface mixtures were compacted by the 75-blow Marshall method (*4*). Base mixtures were compacted using 112 blows (*5*). These blows are used to compact mixtures subjected to heavy traffic levels. The diameter and height of the surface mixture specimens were 101.6 and 63.5 mm. The base mixture specimens were 152.4 by 95.3 mm.

French Pavement Rutting Tester

The French (Laboratoire Central des Ponts et Chaussées) pavement rutting tester evaluates a slab for permanent deformation at 60°C (*6*). Each slab is 500 mm long, 180 mm wide, and 100 mm thick. The French plate compactor was used to compact the slabs; this machine employs a reciprocating, pneumatic rubber tire. The AC-5, AC-10, AC-20, Novophalt, and Styrelf surface mixtures had average air void levels of 8.4, 7.1, 7.3, 8.1, and 8.4 percent, respectively. The two base mixtures were not tested because the test method is not valid for mixtures with nominal maximum aggregate sizes greater than 20 mm.

The French pavement rutting tester tests two slabs simultaneously using two reciprocating pneumatic rubber tires that have a diameter of 415 mm and a width of 109 mm. They are inflated to 600 ± 30 kPa. The tires are always at a fixed elevation. Hydraulic jacks underneath the slabs push them upward to provide the load of 5,000 ± 50 N. Approximately 67 cycles are applied per minute. One cycle is defined as two passes of the tire. Slabs are tested in their molds.

Initially, 1,000 cycles are applied at 25°C to densify the mixture and to provide a smoother surface. The height of each slab is then calculated by averaging measurements taken at 15 positions using a depth gauge with an accuracy of 0.1 mm. This average height is considered the initial height, or point of zero rut depth. The slabs are then heated to 60°C for 12 hr. The test is started and the rut depth in each slab is measured at 300, 1,000, 3,000, 10,000, and 30,000 cycles. A mixture is acceptable if the average rut depth at 30,000 cycles is less than or equal to 10 mm. Slopes for different mixtures taken from log rut depth versus log cycle plots can also be compared. Rut-susceptible mixtures generally have higher slopes.

GLWT

The GLWT tests a beam for permanent deformation at 40.6°C (*6*). Each beam was 320 mm long, 120 mm wide, and 80 mm thick. Replicate beams were fabricated by compacting a slab and sawing it in half. The slabs had a length of 320 mm, a width of 260 mm, and a thickness of 80 mm. Each slab was compacted in two lifts using a vibratory hammer. A steel wheel roller was then used until the surface of the specimen was flat. The AC-5, AC-10, AC-20, Novophalt, and Styrelf surface mixtures had average air void levels of 7.0, 7.5, 7.1, 7.2, and 7.3 percent, respectively. The AC-5 and AC-20 base mixtures had average air void levels of 7.0 and 7.7 percent. Air void levels closer to the 8 percent target level were not obtainable. Attempts to increase the air void levels led to increased porosity around the edges and sides of the slabs.

The sides of the beam are confined by steel plates during testing except for the top 12.7 mm. A stiff rubber hose pressurized at 690 kPa with air is positioned across the top of the beam, and a loaded steel wheel runs back and forth on top of this hose for 8,000 cycles to create a rut. One cycle is defined as two passes of the wheel.

The load on the beam changes with the direction of travel. When the wheel is moving from right to left (viewed from the front of the machine), the load is approximately 740 N at the center of the beam, whereas the load is 630 N when the wheel is moving from left to right. Across the central region of the beam where the deformations are recorded, each of these loads has a variation of less than 5 percent. The load varies because the two arms that connect the wheel to the motor undergo a circular action at the motor. This "locomotion effect" shifts the distribution of the load during the test.

Deformations are measured at the center of the beam 51 mm left of center and 51 mm right of center. If the average rut depth exceeds 7.6 mm, the mixture is considered susceptible to rutting by the Georgia Department of Transportation.

Hamburg Wheel-Tracking Device

The Hamburg wheel-tracking device measures the combined effects of rutting and moisture damage by rolling a steel wheel across the surface of a slab that is submerged in water at 50°C (*6*). Slabs having a length of 320 mm, a width of 260 mm, and a thickness of 80 mm were tested. The slabs were compacted by the same method used to compact the slabs for the GLWT. The AC-5, AC-10, AC-

20, Novophalt, and Styrelf surface mixtures had average air void levels of 7.3, 6.9, 7.1, 7.4, and 7.4 percent, respectively. The AC-5 and AC-20 base mixtures had average air void levels of 6.3 and 7.0 percent. Air void levels closer to the 8 percent target level were not obtainable.

The device tests two slabs simultaneously using two reciprocating solid steel wheels that have a diameter of 203.5 mm and a width of 47.0 mm. The load is 710 N. Each wheel rolls 230 mm before reversing in direction, and the device operates at 53 ± 2 passes/min. The standard maximum number of passes is 20,000. The data from this device are customarily reported versus passes rather than versus cycles; a cycle is two passes.

A maximum allowable rut depth of 4 mm at 20,000 passes is used in Hamburg, Germany. The Colorado Department of Transportation (CDOT) recommends a maximum allowable rut depth of 10 mm at 20,000 passes (*7*). The rut depth in each slab is measured automatically and continuously by a linear variable differential transformer that has an accuracy of 0.01 mm.

The data analysis from the Hamburg wheel-tracking device includes the postcompaction consolidation, creep and stripping slopes, and stripping inflection point (*8*). The postcompaction consolidation, or the deformation at 1,000 passes, is so called because the steel wheel is compacting the mix early in the test. The creep slope relates to rutting primarily from plastic flow. It is the number of passes required to create a 1-mm rut depth. The stripping inflection point is the number of passes at the intersection of the creep slope and the stripping slope. It is the number of passes at which stripping starts to dominate performance. The stripping slope is a measure of the accumulation of rutting primarily due to moisture damage. It is the number of passes required to create a 1-mm rut depth after the stripping inflection point.

In this study, the creep slopes were used to compare the mixtures in terms of rutting. Higher creep slopes (passes per 1-mm rut depth) indicate less rutting. The postcompaction consolidations were also determined for informational purposes.

U.S. Corps of Engineers GTM

Shear susceptibility was measured using the static shear strength (Sg), gyratory stability index (GSI), gyratory elastoplastic index (GEPI), and refusal air void levels provided by the GTM, Model 8A-6B-4C. The GTM is a combination compaction and plane strain shear testing machine that applies stresses simulating pavement conditions.

The GTM was operated in accordance with NCHRP AAMAS with one modification. The NCHRP AAMAS procedure is based on ASTM D 3387 (*1*). The diameter and height of each specimen were 152.4 mm. A vertical pressure of 0.83 MPa, a 0.012-rad gyratory angle, and the GTM oil-filled roller were used. NCHRP AAMAS specifies a 0.035-rad gyratory angle; however, 0.012-rad angle was used because FHWA studies of previous pavements tested by the ALF indicated that this angle provided closer agreement between the GTM refusal densities and ultimate pavement densities. The 0.035-rad angle was found to be too high.

The GSI is the ratio of the maximum angle that occurs at the end of the test to the minimum intermediate angle. It is a measure of shear susceptibility at the refusal density. The minimum intermediate angle is the smallest angle that occurs after the compaction process has started. The GSI at 300 revolutions is close to 1.0 for a stable mixture and is significantly above 1.1 for an unstable mixture (*9*). When designing a mixture, the manufacturer states that the optimum binder content should be less than the binder content at the point at which the GSI begins to exceed 1.0. The GSI and the Sg are the principal GTM parameters used to evaluate rutting susceptibility.

The GEPI is the ratio of the minimum intermediate angle to the initial machine angle set by the operator. A GEPI of 1.0 indicates high internal friction. A GEPI significantly above 1.0 indicates lower internal friction, generally resulting from the use of rounded aggregates or from moisture damage. The manufacturer suggests using an acceptable range of 1.0 to 1.5.

The mixtures were first compacted to an 8 ± 1 percent air void level at 135°C. They were cooled to 60°C in an oven for 3 hr and then compacted and tested to their refusal densities. A trace of the gyratory angle versus number of revolutions was obtained to determine the maximum and minimum intermediate angles.

RESULTS AND DISCUSSION

Mixture Design

The Marshall data are given in Table 6 along with the gradations collected during construction, these data indicated that the plant-produced mixtures and the laboratory mixtures were essentially the same. For example, the air voids ranged from 2.5 to 4.1 percent for the plant-produced mixtures and from 2.9 to 4.3 percent for the laboratory mixtures.

The Marshall data were compared with the $G^*/\sin\delta$ at 60°C and a frequency of 0.125 rad/sec. The frequency of the Marshall test is approximately 0.00038 rad/sec, but 0.1 rad/sec was the lowest frequency used in the DSR test, and extrapolation could produce significant error. In order to combine the data from the surface mixtures with the data from the base mixtures, the stabilities of the base mixtures were reduced by a factor of 2.25 and the flows by a factor of 1.5. These factors theoretically account for the difference in the specimen size.

TABLE 6 Marshall Mixture Properties

Mixture Type	Binder Type	Optimum Binder Content (%)	MSG	Stability (N)	Flow, (0.25-mm)	Air Voids (%)	VMA (%)	VFA (%)
Properties of Plant-Produced Mixtures:								
Surface	AC-5	4.80	2.683	12 422	15.0	2.8	14.1	80.2
Surface	AC-10	4.80	2.691	13 046	15.8	2.7	13.8	80.4
Surface	AC-20	4.90	2.688	15 248	16.5	2.5	13.8	81.7
Surface	Novophalt	4.70	2.686	16 573	20.8	4.1	15.1	72.8
Surface	Styrelf	4.90	2.684	19 794	16.4	3.4	14.7	76.9
Base	AC-5	4.00	2.746	13 678	13.5	2.5	11.6	78.4
Base	AC-20	4.10	2.755	16 442	13.3	3.4	12.2	72.1
Properties of Laboratory-Prepared Mixtures:								
Surface	AC 5	4.85	2.699	11 565	14.5	3.0	13.9	78.4
Surface	AC-10	4.85	2.707	12 047	14.6	3.6	14.1	74.5
Surface	AC-20	4.85	2.706	11 232	17.6	2.9	13.5	78.5
Surface	Novophalt	4.85	2.699	16 125	16.8	4.2	14.9	71.8
Surface	Styrelf	4.85	2.701	18 536	22.8	4.0	14.7	72.8
Base	AC-5	4.00	2.750	13 295	12.8	4.3	13.1	67.2
Base	AC 20	4.00	2.750	14 168	12.4	4.2	13.0	67.7

Note: The stabilities of the base mixtures have been divided by 2.25, and the flows by 1.5, to account for the differences in specimen size.

Compaction Temperatures:	*Marshall Design Blows Per Side:*
AC-5 = 121°C	Surface = 75
AC-10 = 127°C	Base = 112
AC-20 = 135°C	
Novophalt = 141°C	
Styrelf = 141°C	

MSG = Maximum Specific Gravity of the Mixture.
VMA = Voids in the Mineral Aggregate.
VFA = Voids Filled with Asphalt.

The ranking of the average $G^*/\sin\delta$ at 60°C and 0.125 rad/sec from lowest to highest was AC-5, AC-10, AC-20, Novophalt, and Styrelf. The ranking of average stabilities from lowest to highest for the plant-produced surface mixtures was AC-5, AC-10, AC-20, Novophalt, and Styrelf. These two rankings matched each other. The ranking using the laboratory surface mixtures was AC-20, AC-5, AC-10, Novophalt, and Styrelf. This ranking did not match the $G^*/\sin\delta$ as well as the ranking provided by the plant-produced surface mixtures.

Fisher's LSD did not provide rankings that clearly separated the stabilities of either the plant-produced or laboratory surface mixtures. Rankings that clearly separated the stabilities after combing the surface mixtures with the base mixtures were not provided either. The differences among the average stabilities of the mixtures were small compared with the variabilities of the replicate measurements. The effect of aggregate size was also not discernable.

In summary, the analyses based on a comparison of averages indicated a trend of increasing stability with increasing $G^*/\sin\delta$, but the statistical analyses indicated that stability cannot be used to predict rutting performance. There were no significant differences between most of the stabilities. Furthermore, the stabilities of all mixtures were above the minimum stability of 8006 N required for heavy traffic levels.

Rankings that clearly separated the flows did not exist. The differences among the average Marshall flows of the mixtures were very small compared with the variabilities of the replicate measurements.

TABLE 7 Rutting Performance Based on Accelerated Laboratory Testing

	Surface Mixture					Base Mixture	
	AC-5	AC-10	AC-20	Novophalt	Styrelf	AC-5	AC-20
French Pavement Rutting Tester at 60°C and 0.875 rad/s:							
Cycles:	*Percent Rut Depths:*						
300	2.97	2.98	2.59	1.44	1.84	NA	NA
1,000	3.79	3.99	3.21	1.67	2.22		
3,000	4.93	5.33	4.09	2.17	2.95		
10,000	8.23	9.23	4.90	2.38	3.25		
30,000	15.50	13.77	6.38	2.60	3.74		
Slope	0.35	0.34	0.19	0.14	0.16		
$G^*/\sin\delta$, Pa	212	442	871	3 789	6 338		
Georgia Loaded-Wheel Tester at 40°C, 0.125 rad/s, and 8,000 cycles:							
Rut Depth, mm	7.38	5.38	3.72	1.42	1.67	6.29	3.46
$G^*/\sin\delta$, Pa	899	2 215	5 060	21 000	20 600	899	5 060
Hamburg Wheel-Tracking Device at 50°C and 0.125 rad/s:							
Post CC, mm	ND	3.70	3.36	0.87	1.45	4.26	2.03
Rut Depth, mm	>30	>30	8.5	1.9	2.6	>30	8.6
Creep Slope	296	634	6 224	24 594	17 947	468	3 781
$G^*/\sin\delta$, Pa	130	348	635	3 128	5 232	130	635
Post CC is the post compaction consolidation. Rut Depths are at 20,000 passes. Creep Slope is passes per 1-mm rut depth.							
Gyratory Testing Machine at 60°C and 0.125 rad/s:							
Sg, kPa	370	430	370	370	370	400	410
GSI	1.10	1.14	1.16	0.97	1.10	1.09	0.98
GEPI	1.14	1.18	1.02	0.84	1.10	1.07	0.83
Refusal Air-Void Level, %	2.13	2.03	3.30	5.91	5.97	4.20	5.46
$G^*/\sin\delta$, Pa	26	60	124	661	1 750	28	124

NA = Test is not applicable for mixtures with aggregate greater than 20 mm.
ND = No data because the mixture failed too rapidly.

French Pavement Rutting Tester

The French pavement rutting tester data are given in Table 7. The AC-5 and AC-10 surface mixtures exceeded the 10-mm maximum allowable rut depth at 30,000 cycles; the other three mixtures met the criterion.

The ranking of the average $G^*/\sin\delta$ at 60°C and a frequency of 0.875 rad/sec from lowest to highest was AC-5, AC-10, AC-20, Novophalt, and Styrelf. The ranking of the average percent rut depths from highest to lowest was AC-5, AC-10, AC-20, Styrelf, and Novophalt. These two rankings provided reversals for the Styrelf and Novophalt binders. The slopes provided the same ranking as the percent rut depths.

Fisher's LSD divided the $G^*/\sin\delta$ into four groups: (*a*) AC-5 and AC-10, (*b*) AC-20, (*c*) Novophalt, and (*d*) Styrelf. The rut depths divided into three groups: (*a*) AC-5 and AC-10, (*b*) AC-20 and Styrelf, and (*c*) Styrelf and Novophalt. The slopes produced the same three groups. The analyses suggest that the $G^*/\sin\delta$ for Styrelf is high compared with its percent rut depth and slope.

Regressions between the $G^*/\sin\delta$ and the percent rut depths, slopes, and inverse slopes provided poor r^2 values of 0.62, 0.57, and 0.62, respectively. The inverse slopes were evaluated because the slopes from the Hamburg wheel-tracking device are inverse slopes.

Georgia Loaded-Wheel Tester

The GLWT data are given in Table 7. All of the mixtures met the 7.60-mm maximum allowable rut depth at 8,000 cycles.

The ranking of the average $G^*/\sin\delta$ at 40°C and a frequency of 0.125 rad/sec from lowest to highest was AC-5, AC-10, AC-20, Styrelf, and Novophalt. The ranking of the average rut depths for the surface mixtures from highest to lowest was AC-5, AC-10, AC-20, Styrelf, and Novophalt. These two rankings are identical. The rut depths for the two base mixtures agreed with their corresponding $G^*/\sin\delta$.

Fisher's LSD divided the $G^*/\sin\delta$ into four groups: (*a*) AC-5, (*b*) AC-10, (*c*) AC-20, and (*d*) Styrelf and Novophalt. The rut depths divided into four groups: (*a*) AC-5 surface and AC-5 base, (*b*) AC-10 surface and AC-5 base, (*c*) AC-20 surface and AC-20 base, and (*d*) Styrelf and Novophalt. These two rankings are identical using the surface mixture data. The only discrepancy between the two rankings was that the AC-5 base mixture ranked with both the AC-5 and AC-10 surface mixtures according to the rut depths. However, the true effect of maximum aggregate size based on pavement performance is not known; therefore, there may or may not be a real discrepancy.

Regressions between the $G^*/\sin\delta$ and the rut depths provided a good r^2 value of 0.84 for the surface mixtures, and a fair r^2 value of 0.79 for the surface and base mixtures combined. However, these r^2 values may be artificially high because of the large gap between the $G^*/\sin\delta$ of the unmodified and modified binders. The regressions and Fisher's LSD both indicated that aggregate size had little effect on rutting performance.

Hamburg Wheel-Tracking Device

The Hamburg wheel-tracking device data are given in Table 7. The AC-5, AC-10, and AC-20 surface mixtures and the AC-5 and AC-20 base mixtures exceeded the maximum allowable rut depth of 4

mm at 20,000 passes used in Hamburg, Germany. The AC-5 and AC-10 surface mixtures and the AC-5 base mixture exceeded the maximum allowable rut depth of 10 mm at 20,000 passes used by CDOT. No moisture damage was observed in any of the slabs; therefore, the $G^*/\sin\delta$ could be directly compared with the creep slopes. The $G^*/\sin\delta$ could not be compared with the rut depths at 20,000 passes because of the limitation that the device cannot measure rut depths deeper than 30 mm.

The ranking of the average $G^*/\sin\delta$ at 50°C and a frequency of 0.125 rad/sec from lowest to highest was AC-5, AC-10, AC-20, Novophalt, and Styrelf. The ranking of the average creep slopes for the surface mixtures from lowest to highest was AC-5, AC-10, AC-20, Styrelf, and Novophalt. These two rankings provided reversals for the Styrelf and Novophalt binders. The creep slopes for the two base mixtures agreed with their corresponding $G^*/\sin\delta$.

Fisher's LSD divided the $G^*/\sin\delta$ into three groups: (*a*) AC-5, AC-10, and AC-20, (*b*) Novophalt, and (*c*) Styrelf. The creep slopes divided into three groups: (*a*) AC-5 surface and base, AC-10 surface, and AC-20 surface and base; (*b*) AC-20 surface and Styrelf; and (*c*) Styrelf and Novophalt. The analysis suggests that the $G^*/\sin\delta$ for Styrelf is high compared with its creep slope.

Regressions between the $G^*/\sin\delta$ and the creep slopes provided a fair r^2 value of 0.70 for the surface mixtures and a fair r^2 value of 0.74 for the surface and base mixtures combined. However, these r^2 values may be artificially high because of the large gap between the data of the unmodified and modified binders. Regressions between the $G^*/\sin\delta$ and the slopes in terms of rut depth per pass were very poor. Aggregate size had little effect on rutting performance.

Fisher's LSD did not provide rankings that clearly separated the postcompaction consolidations of the mixtures. The AC-5 surface mixture failed rapidly; therefore, a postcompaction consolidation could not be determined.

Gyratory Testing Machine

The GTM data are given in Table 7. Relationships between $G^*/\sin\delta$ and Sg, GSI, and the GEPI were not found. There was very little variation in each parameter from mixture to mixture. The refusal air voids had the highest amount of variation. Regressions between $G^*/\sin\delta$ and the refusal air voids provided a fair r^2 value of 0.70 for the surface mixtures and a poor r^2 value of 0.42 for the surface and base mixtures combined.

Regressions Between the Wheel-Tracking Machines

A regression between the rut depths from the GLWT and the French pavement rutting tester for the five surface mixtures provided a very good r^2 value of 0.95. Regressions between the creep slopes from the Hamburg wheel-tracking device and the rut depths from the GLWT and French pavement rutting tester for the five surface mixtures provided good r^2 values of 0.85 and 0.83. Regressions between the Hamburg wheel-tracking device and the GLWT for the surface and base mixtures combined provided a fair r^2 value of 0.78.

CONCLUSIONS

1. An oven-aging period of 2 hr was needed to simulate the average degree of aging that occurred during plant production of the ALF mixtures. However, the data indicated that oven aging may not effectively simulate hot-mix plant aging.
2. As expected, the $G^*/\sin\delta$ of the binders increased as frequency increased or temperature decreased.
3. The study incorporated five binders, and it was assumed that this would provide five levels of $G^*/\sin\delta$, but the statistical analyses indicated that some binders had $G^*/\sin\delta$ that were not statistically different from others. This reduced the experiment to three or four groups of binders. How binders statistically group together can vary with temperature and frequency.
4. The Marshall stabilities and flows and the GTM parameters did not differentiate the mixtures according to rutting susceptibility.
5. The French pavement rutting tester, GLWT, and Hamburg wheel-tracking device differentiated the surface mixtures. The rut depths varied with the type of binder.
6. The GLWT and Hamburg wheel-tracking device did not differentiate the AC-5 surface mixture from the AC-5 base mixture or the AC-20 surface mixture from the AC-20 base mixture. Increased maximum aggregate size did not significantly reduce the rut depths or the influence of binder type on rutting susceptibility.
7. A general correlation between $G^*/\sin\delta$ and rutting susceptibility is that a binder with a higher $G^*/\sin\delta$ will provide a mixture that has a lower rutting susceptibility. However, the degree of correlation varied with the mixture test. The GLWT at 40°C provided a very good relationship. The French pavement rutting tester at 60°C and Hamburg wheel-tracking device at 50°C provide reasonably good relationships. The main discrepancy in these latter two devices was that even though the Styrelf mixture had a very low susceptibility to rutting, the data suggest that the rut depths are slightly high compared with the $G^*/\sin\delta$ of the binder. (The GLWT may also provide this discrepancy if the test were to be performed at 50°C or 60°C. The data in Table 2 at a frequency of 0.125 rad/sec show that the $G^*/\sin\delta$ of Styrelf becomes higher than that of Novophalt above 40°C.)

RECOMMENDATIONS

1. The results of this study should be compared with ALF pavement performances. The initial pavement tests indicate low amounts of rutting in the Novophalt and Styrelf surface mixtures; high amounts of rutting in the AC-5, AC-10, and AC-20 surface mixtures; and lower amounts of rutting in the AC-5 and AC-20 base mixtures compared with the AC-5 and AC-20 surface mixtures. The data from the GLWT and Hamburg wheel-tracking device do not agree with this last observation.
2. The reversals provided by the Styrelf and Novophalt binders should be evaluated.
3. Additional binders should be tested to develop firm relationships between $G^*/\sin\delta$ and the rutting parameters given by laboratory mixture tests.

ACKNOWLEDGMENTS

This study was performed at the FHWA TFHRC in McLean, Va. Laboratory testing and analysis was assisted by Naga Shashidhar, Susan Needham, Frank Davis, and Scott Parobeck of EBA Engineering Inc. EBA Engineering provides on-site laboratory support services for the TFHRC Pavements and Materials Laboratories.

REFERENCES

1. Von Quintus, H. L., J. A. Scherocman, C. S. Hughes, and T. W. Kennedy. *NCHRP Report 338: Asphalt-Aggregate Mixture Analysis System.* TRB, National Research Council, Washington, D.C., 1991.
2. *Background of SHRP Asphalt Binder Test Methods.* National Asphalt Training Center Demonstration Project 101. Asphalt Institute Research Center, Lexington, Ky., 1993.
3. Strategic Highway Research Program. *SHRP Designation: M-007, Short- and Long-Term Aging of Bituminous Mixes.* Report SHRP-A-379. National Research Council, Washington, D.C., 1994.
4. *Mix Design Methods for Asphalt Concrete and Other Hot-Mix Types.* Manual Series No.2 (MS-2). Asphalt Institute, Lexington, Ky., 1988.
5. *Proposed Standard Test Method for Resistance to Plastic Flow of Bituminous Mixtures Using Marshall Apparatus (6 inch-Diameter Specimen).* Draft No. 8. ASTM, Philadelphia, Pa., Dec. 1992.
6. Aschenbrener, T., and K. D. Stuart. *Description of the Demonstration of European Testing Equipment for Hot Mix Asphalt Pavement.* CDOT-DTD-R-92-10. Colorado Department of Transportation, Denver, Sept. 1992.
7. Aschenbrener, T., R. Terrel, and R. Zamora. *Comparison of Hamburg Wheel-Tracking Device and the Environmental Conditioning System to Pavements of Known Stripping Performance.* CDOT-DTD-R-94-1. Colorado Department of Transportation, Denver, Jan. 1994.
8. Hines, M. The Hamburg Wheel-Tracking Device. *Proc., 28th Paving and Transportation Conference,* University of New Mexico, Albuquerque, 1991.
9. Roberts, F. L., P. S. Kandhal, E. R. Brown, D. Y. Lee, and T. W. Kennedy. *Hot Mix Asphalt Materials, Mixture Design, and Construction.* National Asphalt Pavement Association (NAPA) Education Foundation, Lanham, Md., 1991.

DISCUSSION

JOHN L. MCRAE
Engineering Developments Company Inc., Vicksburg, Miss. 39181.

The objective of the Corps of Engineers gyratory testing machine and method is to design an essentially rut-free pavement for whatever design stress is anticipated. The GTM procedure states, "In no case, however, should a bitumen content be selected that will be high enough to cause more than a faint spreading of the gyrograph trace." By this analysis, all of these mixtures except the Novophalt contain an excessive amount of asphalt and would be expected to rut if subjected to the 120-psi vertical stress employed in the GTM test. Please note that although the rutting test results show some rutting for all mixes, the least amount occurred for the Novophalt in each instance.

Referring to Table 7, the GEPI values are in error since the GEPI cannot be less than 1. The GEPI is defined as the ratio of the minimum intermediate gyrograph band width to the initial gyratory angle (i.e., the machine setting). Obviously the gyrograph, which is a recording of the gyratory angle, cannot be less than the machine angle controlled by the upper and lower rollers. It is not immediately evident how this error could occur.

Gyrographs for different aggregate types are also shown in order to illustrate how the gyrograph responds to the stress-strain properties of the material. The gyrograph is a recording of shear strain; the wider the gyrograph, the flatter the stress-strain curve. There is no question that S is a direct measure of plain strain simple shear and the fact that S is practically constant for these tests means that it is largely reflecting the internal friction of the aggregate, which is the same for all mixes. Any difference brought about by changes in the bitumen will more likely be reflected by changes in cohesion (not internal friction) and would be reflected in a Mohr's-type diagram, which can be readily prepared from the GTM results if $S\delta$ is plotted against increments of vertical stress.

Even more important would be changes observed in densification rate and recovery properties when using the GTM as a traffic simulator employing the air-filled upper roller in conjunction with cyclic loading (*1*).

REFERENCE

1. McRae, J. L. Asphaltic Concrete Pavements and Constituent Materials. In *Highway Research Record 361,* HRB, National Research Council, Washington, D.C., 1971.

AUTHORS' CLOSURE

McRae states that the GTM is used to produce rut-free pavements and implies that the GTM parameters should not be correlated with rut depth. The data in our paper support the second part of this statement in that no correlation was found. However, it is the first author's experience that if an asphalt mixture test cannot be used as an analysis tool because it does not discriminate mixtures with widely different levels of performance, it may not always provide the required performance when used to design a mixture. Whether the GTM is an exception to this experience needs to be shown. We have tested mixtures with 100 percent rounded coarse aggregate using the GTM. The GTM has provided optimum binder contents for the mixtures, but the GTM parameters, including shear strength, have not always indicated that the mixtures will be susceptible to rutting. Perhaps changing the applied gyratory angle would provide better results.

Concerning the errors in the reported GEPI, we have only found the GEPI to be less than 1 for a few mixtures. These low GEPI have only been obtained when testing 152.4-mm diameter specimens and not with 101.6-mm diameter specimens. Perhaps this is coincidental. GEPIs less than 1 indicate there is a problem with the procedures used to apply or calibrate the desired angle. We have tried to independently verify the applied angle using a digital protractor. This has not been successful. Repeating the calibration procedures have indicated that the machine may not be capable of measuring or applying the small angles involved at the level of accuracy that is needed.

The use of Mohr's circles and the air-filled roller are also discussed. Perhaps these would provide different results, but these alternate methods were not evaluated. We also only used a single vertical stress and a single angle. These could also be varied.

Publication of this paper sponsored by Committee on Characteristics of Bituminous Paving Mixtures to Meet Structural Requirements.

Mix Design Methodology for a Warrantied Pavement: Case Study

J. HARVEY, B. A. VALLERGA, AND C. L. MONISMITH

The application of a mix design procedure developed as part of Strategic Highway Research Program (SHRP) Project A-003A for a warrantied pavement project in California is described. Two mixes were designed for overlay of a "cracked and seated" portland cement concrete pavement, one a dense-graded asphalt concrete with a PBA-6 specification modified binder and the other an asphalt-rubber hot mix with a gap gradation. Both mixes were designed to meet rutting specifications for the pavement warranty. The mix design method considers mix performance measured using repeated load simple shear testing at constant height, traffic, site-specific temperatures, and reliability of test results and traffic predictions. The mixes were also evaluated for moisture sensitivity, using moisture-conditioning procedures developed as part of Project SHRP A-003A to determine the need for, and suitability of, using an antistripping additive. The mix design method developed in SHRP A-003A provided the contractor with a tool to predict the performance of the mix in terms of anticipated traffic during the warranty period and for site-specific temperature conditions. Both mixes were constructed as part of the overlay project in July 1993 and performed successfully during 1994.

During the 1993 construction season, the California Department of Transportation (Caltrans) decided to call for bids on state highway work using the principle of warranted pavements on several overlay construction projects. One of these projects was located on Interstate 5 north of Redding, California, running from 2 km (1.3 mi) south to 1.3 km (0.8 mi) north of the Sims Road undercrossing, hereinafter referred to as the "Sims Project." Essentially, the construction was to consist of placing two lifts of an asphalt-concrete overlay on existing portland cement concrete (PCC) pavement, which was to be "cracked and seated." Both lifts were to be 46 mm (0.15 ft) thick with the first lift to be Caltrans asphalt concrete (type A), hereinafter referred to as DGAC, and the second lift Caltrans rubberized asphalt concrete-gap graded (type G, asphalt rubber), hereinafter referred to as ARHM-GG.

The warranty was limited to the asphalt-concrete paving itself, in which the contractor was to agree to warrant the performance of the asphalt-concrete paving over a period of 5 years. Enforcement of the warranty was to be based on defined performance criteria incorporated in the special provisions of the project. Terms of the warranty are described by Vallerga (*1*).

The performance criteria include rutting, raveling, flushing, delamination, and cracking.

The contractor awarded the contract in consultation with B. A. Vallerga, Inc., and decided to use the mix design methodology developed as a part of Strategic Highway Research Program (SHRP) Project A-003A at the University of California at Berkeley (UCB) and Oregon State University (OSU). The procedure used to arrive at the designs selected for the two mixes, which have now been in service on Interstate 5 for over 1 year, is described in this paper.

J. Harvey and C. L. Monismith, Institute for Transportation Studies, 1301 S. 46th Street, Building 452, Richmond, Calif. 94804. B. A. Vallerga, BA Vallerga, Inc., 1330 Broadway, Suite 1044, Oakland, Calif. 94612.

GENERAL APPROACH

Figure 1 illustrates the framework for a comprehensive mix design and analysis system that has been proposed by the SHRP A-003A researchers (*2*). The extent of testing varies with the functional capacity of the roadway. For design situations with unusual traffic demand or unconventional materials, or both, extensive testing is recommended.

This comprehensive system consists of a series of subsystems in which the mix components, asphalt (or binder) and aggregate, and their relative proportions are selected in a step-by-step procedure to produce a mix that can be evaluated to ensure that it will attain the desired level of performance in the specific pavement section in which it is to function. Although three subsystems have been developed (to examine fatigue, permanent deformation, and low-temperature cracking), only the permanent deformation system was used in this investigation. The framework for this subsystem is briefly outlined in the following paragraphs (*3*).

Distinguishing characteristics of the permanent deformation system are shown in Table 1. For this project, the Level A procedure was selected. It involves simplified testing with the cyclic shear test at one temperature and includes the following steps, which are shown schematically in Figure 2. (It should be noted that the level A analysis system was developed using information determined from the Level B procedure, which uses a nonlinear viscoelastic three-dimensional constitutive relationship and a finite element analysis.)

The steps in the Level A procedure are as follows:

1. *Determine design requirements for reliability and performance.* The analysis system outlined here permits the designer to select a level of reliability commensurate with the pavement site for which the mix will be used. Performance requirements for permanent deformation generally call for the amount of rutting not to exceed some level, for example, 10 to 13 mm (0.4 to 0.5 in.) in order to minimize the potential for hydroplaning.
2. *Determine expected distribution of in situ temperature.* Pavement analysis in the abridged procedure requires that the mix be evaluated at the critical temperature (T_c) the temperature at which the maximum amount of permanent deformation occurs (*3*). For this mode of distress it is important to emphasize that temperatures in the upper part of the temperature range have a significant influence on the development of permanent deformation. The site-specific

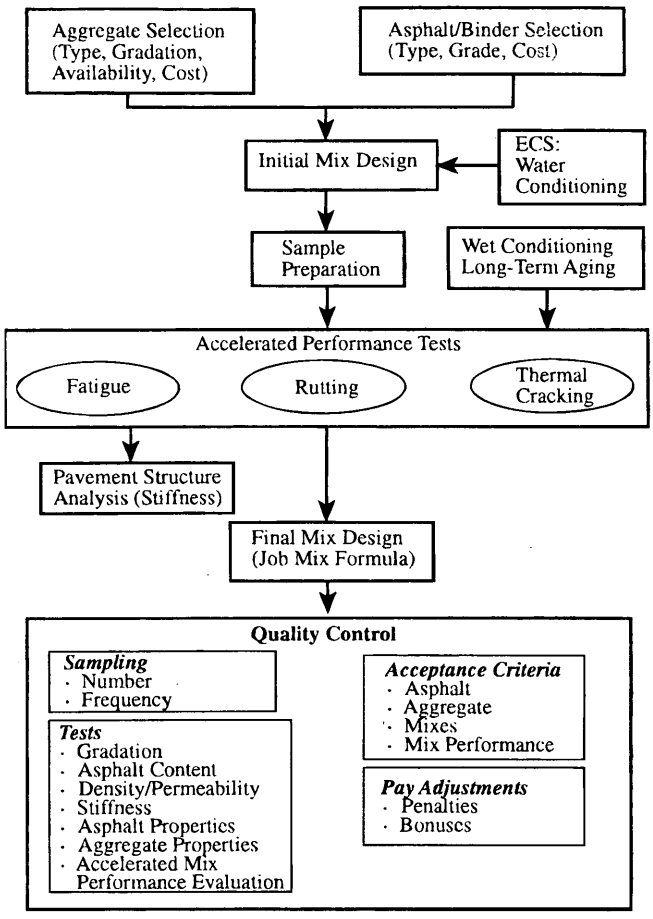

FIGURE 1 Accelerated mix performance evaluation.

critical temperature can be calculated following the procedure described by Deacon et al. (*4*). It is necessary that these computations be performed only once for a specific region or project area.

3. *Estimate design traffic demand [equivalent single axle loads (ESALs)].* For this procedure it is necessary to estimate the number of design-lane ESALs at the critical temperature using temperature conversion factors (*4*). These factors need only be computed once for specific regions.

$$\text{ESALs}_{T_c} = \text{ESALs} \cdot \text{TCF} \quad (1)$$

where TCF is the temperature conversion factor.

4. *Select trial mix.* With a binder and aggregate, a trial mix is selected. This might be done according to the Superpave methodology or by any procedure that the responsible agency considers appropriate. Changes and redesigns are evaluated at the discretion of the design (materials) engineer.

5. *Prepare test specimens and condition as required.* Cylindrical specimens 15 cm (6 in.) in diameter by 5 cm (2 in.) high are obtained from slabs prepared by rolling wheel compaction with procedures such as those used at UCB (*5–7*). These specimens are cored and then sawed so that the end surfaces are smooth and parallel.

6. *Perform cyclic shear tests.* In the level A procedure, cyclic shear tests [also referred to as repetitive simple shear test at constant height (RSST-CH)] are performed at the critical temperature, T_c, for the specific site. At this time, the recommended procedure is to use a shear stress of 69 kPa (10 psi) [associated with tire pressures of about 690 kPa (100 psi)], which is repeatedly applied with a duration of 0.1 sec and a time interval between loadings of 0.6 sec. The repeated loading is continued for 1 hr, permitting the specimen to be subjected to a total of about 5,000 stress repetitions.

7. *Determine the resistance of the trial mix to permanent deformation.* From finite element analyses it has been determined that there exists a reasonably constant ratio between the vertical rut depth obtained in representative asphalt-bound layers and the permanent shear strain obtained in the RSST-CH for the 690-kPa (100-psi) tire-loading condition (*3*). At this time N_{supply} for the given mix can be estimated using the design rut depth and the corresponding permanent shear strain from the following:

$$\text{Rut depth (in.)} = K \cdot (\gamma_p) \quad (2)$$

where (γ_p) is the permanent shear strain, and K is the conversion factor with a value of 254 to 279 (mm) [10 to 11 (in.)].It is likely that K will be somewhat dependent on the structural pavement section; that is, there may be a different conversion factor for a 10-cm (4-in.) asphalt-concrete overlay on a PCC pavement compared with a comparatively thick asphalt-concrete layer for which the factor shown in Equation 1 had been determined.

8. *Apply a shift factor to the traffic demand (ESALs).* The design traffic volume, that is, the laboratory-equivalent repetitions of the standard load, N_{demand} is determined from

$$N_{\text{demand}} = \text{ESALs}_{T_c} \cdot \text{SF} \quad (3)$$

where ESALs_{T_c} is the design ESALs adjusted to the critical temperature, T_c, and SF is the empirically determined shift factor. At

TABLE 1 Distinguishing Characteristics of Permanent-Deformation Analysis System

Variables		Level A	Level B
		Abbreviated analysis with limited cyclic shear testing	Comprehensive analysis with full testing
Testing	Type	Cyclic shear	Constant height simple shear, uniaxial strain, volumetric shear frequency sweep (with damage evaluation)
	Temperature	Critical temperature, T_c	40°C with frequency sweeps at 4°, 20°, 40°, and 60°C
In-Situ Conditions	Traffic	Equivalent ESALs at T_c, 85th percentile tire pressure	ESALs by temperature class, 85th percentile tire pressure
	Structure	Critical shear stress under "standard" load at T_c	Complete stress/strain pattern from finite element analysis
	Temperature	Frequency distribution at 50 mm (2 in.) depth	Frequency distribution throughout surface layer
Analysis	Mechanistic	Finite element analysis with nonlinear viscoelastic surface properties[a]	Finite element analysis with nonlinear viscoelastic surface properties
	Damage	Preanalysis (temperature equivalency factors for design ESALs)	Integral part of finite element analysis

[a]It is possible that sufficiently accurate results for shear stress may be determined using multi-layer elastic analysis as experience is developed.

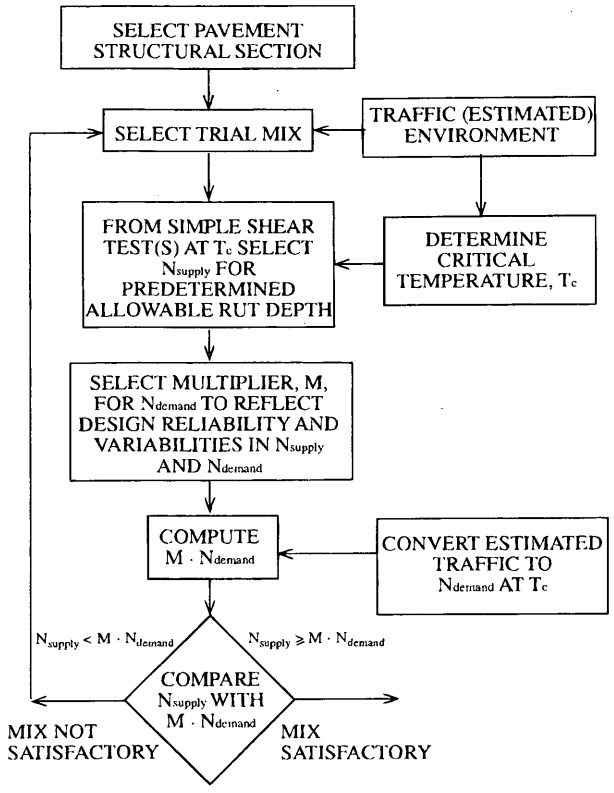

FIGURE 2 Level A mix design and analysis system.

this time, it is recommended that a shift factor of 0.04 be used. This shift factor was determined from analyses of a limited number of SHRP General Pavement Studies test sites (*3*).

9. *Compare traffic demand (N_{demand}) with mix resistance (N_{supply}).* Satisfactory performance requires that the mix resistance (N_{supply}) equal or exceed the traffic demand (N_{demand}). Accordingly a multiplier, M, is applied to N_{demand} since neither N_{supply} nor N_{demand} is known with certainty. This factor permits the incorporation of an appropriate level of design reliability as well. For a mix to be satisfactory,

$$N_{supply} \geq M \cdot N_{demand} \quad (4)$$

where M is a multiplier whose value depends on the design reliability and on the variabilities of the estimates of N_{supply} and N_{demand}, Table 2.

10. *If mix is inadequate, alter trial mix and iterate.* If the particular mix is determined to be inadequate, a number of alternatives are available to the designer, including adjusting the asphalt content, adjusting the aggregate gradation, using a modified binder, selecting another aggregate source, or making combinations of the above.

The Level A methodology can be used as a mix design procedure to select the initial binder content. Mixes can be prepared over a range in binder contents by rolling wheel compaction to the air-void content at which maximum permanent shear strain resistance occurs (about 3 percent for the mixes included in this project). For each mix the procedure described in the previous section would be followed to select N_{supply}. The mix with the highest binder content that satisfies $M \cdot N_{demand}$ (adjusted traffic) is selected for further evaluation.

PROJECT INFORMATION

The site of the Sims Project [total length of about 3.3 km (2.0 mi)] is on Interstate 5 in Shasta County, California, near the town of Castella. The site is in a mountainous area, and consisted of only the northbound lanes, which contain both flat and uphill grade (5 percent maximum) sections. The mixes were designed for an overlay to be placed on a cracked and seated PCC pavement, with the overlay structure design consisting of 46 mm (0.15 ft) of dense-graded asphalt concrete with a PBA-6 binder (DGAC-PBA6) underneath 46 mm (0.15 ft) of asphalt-rubber hot mix having a gap-graded aggregate component (ARHM-GG).

A material and workmanship warranty for a period of 5 years from the date of completion of the construction was required. The limiting rut depth could not exceed 13 mm (0.04 ft or 0.5 in.) at any time during the warranty period. It was expected that approximately 10 million 80-kN (18-kip) ESALs would traffic the design lane during that period.

Because of the thick layer of cracked and seated PCC beneath the overlay, it was calculated that fatigue cracking would not occur during the warranty period. An antistripping agent was considered for use with both mixes because water sensitivity problems have been experienced in Caltrans District 2.

SIMPLE SHEAR TEST TEMPERATURE, T_C

The temperature used for testing in the repeated load simple shear test is termed the critical temperature, T_c, and represents the temperature at a depth of 50 mm (2 in.) below the surface of the pavement. This depth has been found to be the approximate location at which maximum shear stresses occur below the edge of the tire (*3*.)

A value of T_c of 45°C (113°F) was determined for the test site according to the procedure described by Deacon et al. (*4*.)

MATERIALS AND SPECIMEN PREPARATION

Aggregate

Aggregates for both mixes were produced from the Fawndale quarry. Aggregate was received from three bins for the ARHM-GG

TABLE 2 Reliability Multipliers

Sample Size	Variance of Ln(N_{demand})	Reliability Multiplier			
		60 Percent Reliability (Z_R=0.253)	80 Percent Reliability (Z_R=0.841)	90 Percent Reliability (Z_R=1.28)	95 Percent Reliability (Z_R=1.64)
1	0.2	1.349	2.704	4.545	6.957
	0.4	1.377	2.896	5.046	7.955
	0.6	1.404	3.090	5.567	9.022
	1.0	1.455	3.480	6.673	11.381
2	0.2	1.304	2.416	3.830	5.587
	0.4	1.334	2.609	4.305	6.490
	0.6	1.363	2.802	4.797	7.456
	1.0	1.417	3.188	5.839	9.592
4	0.2	1.280	2.270	3.482	4.945
	0.4	1.312	2.464	2.946	5.805
	0.6	1.342	2.657	4.425	6.723
	1.0	1.397	3.042	5.437	8.754
8	0.2	1.267	2.197	3.313	4.640
	0.4	1.300	2.392	3.772	5.479
	0.6	1.331	2.585	4.245	6.375
	1.0	1.388	2.970	5.243	8.356

mix and four bins for the DGAC-PBA6 mix. After drying, the aggregate was batched in 7-kg (15.4-lb) samples using the following percentages (by dry weight of aggregate):

	Percent Passing	
Sieve Size	*DGAC-PBA6*	*ARHM-GG*
7/8 in.	35	45
5/8 in.	5	—
3/8 in.	21	34
Minus No. 4	39	21

Wet sieve analyses (ASTM C-117 and C-136) of the batched aggregate were performed for each mix, the results of which are presented in Table 3. It can be seen that the actual gradations were generally close to the target gradations, except for the fraction passing the 0.075-mm (No. 200) sieve for DGAC-PBA6, which was higher than the target. A higher fines content would be expected to reduce the permanent shear deformation resistance of the mix (*7*).

Mixing

DGAC-PBA6 Material

The aggregate batches were mixed with PBA-6 binder supplied by Telfer Sheldon Oil of Martinez, California. Just before mixing with the aggregate, 0.5 percent (by weight of asphalt) PaveBond PC antistripping agent was stirred into the PBA-6. Binder contents were 4.5, 5.0. 5.5, and 6.0 percent by weight of aggregate (4.3, 4.8, 5.2, 5.7 percent by weight of mix). The aggregate was heated at 152°C (305°F) for at least 2 hr before mixing. The binder was heated at the same temperature for at least 90 min before mixing.

ARHM-GG Material

The aggregate batches were mixed with asphalt-rubber binder supplied by International Surfacing Inc. (ISI) of Chandler, Arizona. Before shipment to UCB, ISI mixed 0.5 percent (by weight of binder) PaveBond PC antistripping agent into the asphalt rubber. Binder contents were 6.0, 7.0, 8.0, and 9.0 percent by weight of aggregate (5.7, 6.5, 7.4, and 8.3 percent by weight of mix). The aggregate was heated at 163°C (325°F) for at least 2 hr before mixing. The binder was heated for at least 3 hr at the same temperature before mixing.

Aging and Compaction

All mixes were short-term oven aged for 4 hr at 135°C (275°F) to simulate aging that occurs in a typical batch or drum plant (*8*). Rice maximum specific gravity tests (ASTM D2041) were performed on the mixes for each binder content.

The mixes were compacted in "ingots," each weighing approximately 20 kg (44 lb), using UCB rolling wheel compaction (*5–7*). The target air void content was 3.2 percent, as measured using parafilm. This value was selected because it appears to provide the maximum rutting resistance for the mixes included in this project and most dense-graded asphalt concrete and dense- and gap-graded asphalt-rubber mixes. If the mix can sustain the anticipated traffic at this air void content without excessive deformation, it can be concluded that satisfactory performance will be obtained in situ (*3,9*).

The compaction temperature was 141°C (285°F) for the dense-graded mixes and 146°C (295°F) for the asphalt-rubber mixes. One ingot of ARHM-GG, with an asphalt content of 6.0 percent, was compacted at 157°C (315°F) because the previous six attempts to achieve air void contents of less than 4 percent using the 146°C (295°F) compaction temperature had failed. This indicates that somewhat higher compaction temperatures are needed to compact this mix to low air void contents in the field.

After cooling overnight, the ingots were cored and cut to produce three 150-mm (6-in.) diameter, 50-mm (2-in.) tall cylindrical specimens. The specimens were tested for air void content, with the results shown in Tables 4 and 5 for the DGAC-PBA6 and ARHM-GG mixes, respectively. Only those specimens selected for testing are shown.

SIMPLE SHEAR TEST RESULTS

The cyclic shear tests were performed using the Universal Testing System developed as part of SHRP A-003A and manufactured by James Cox and Sons. For the RSST-CH, the specimen is bonded to platens that are in turn clamped to the actuators. The vertical actuator is used to maintain the specimen at a constant height, whereas

TABLE 3 Aggregate Gradations

Sieve Size mm	DGAC-PBA6 Percent Passing	Specified Percent Passing	ARHM-GG Percent Passing	Approx Target Percent Passing
26 (1 in.)	100	100	100	100
19 (3/4 in.)	98	95	98	98
13.2 (1/2 in.)	83	80	83	
9.5 (3/8 in.)	71	68	71	68
4.75 (#4)	51	48	38	34
2.36 (#8)	41	35	24	21
1.18 (#16)	29	25	16	
0.60 (#30)	19	17	10	9
0.30 (#50)	12	12	7.0	
0.15 (#100)	8.9	8	5.4	
0.075 (#200)	7.4	4	4.6	3

TABLE 4 Constant Height Simple Shear Repeated Load Tests: DGAC-PBA6 Mixes

Asphalt content by weight of aggregate — percent	Air-void content — percent	N_{supply} (at γ=0.045) $\times 10^3$	N_{supply} average $\times 10^3$
Laboratory prepared specimens			
4.5	3.9	120.4	1,015
	3.8	22.9	
	3.1	2900	
	2.6	3041	
5.0	4.2	5.1	4,973
	4.1	30.0	
	2.7	14884	
	2.5	1270	
5.5	3.3	8.8	153.5
	3.1	20.5	
	3.0	70.7	
	1.4	196.9	
	1.2	470.9	
6.0	4.2	10.4	75.1
	3.3	96.5	
	2.9	118.5	
Field Cores			
5.2	7.8	1931	1,492
	8.4	1053	
Field Mix Compacted in Laboratory			
5.2	5.5	88	57
	6.8	35	
	7.7	48	

TABLE 5 Constant Height Simple Shear Repeated Load Tests: ARHM-GG Mixes

Binder content by weight of aggregate — percent	Air-void content — percent	N_{supply} (at γ=0.045) $\times 10^3$	N_{supply} average $\times 10^3$
Laboratory prepared specimens			
6.0	2.5	4256	172.2
	2.5	2576	
	4.3	7849	
	4.4	2995	
7.0	2.9	1647	59.8
	3.0	772	
	3.9	5235	
8.0	2.8	1063	12.6
	2.9	586	
	2.9	471	
	3.4	384	
9.0	2.7	673	12.0
	3.0	781	
Field cores			
7.5	11.3	29	43.0
	12.4	57	
Field Mix Compacted in Laboratory			
7.5	9.4	29	37.2
	10.1	19	
	11.6	39	
	12.8	54	
	14.1	45	

the horizontal actuator applies a repetitive haversine shear stress. For this project, the RSST-CH was performed using a 68.9-kPa (10-psi) shear stress, with a 0.1-sec loading time followed by a 0.6-sec rest period. Each specimen was subjected to approximately 5,000 load repetitions.

During the test, the permanent shear strain increases with each load repetition. As noted earlier, permanent shear strain in the RSST-CH has been related to rut depth, according to Equation 1. For example, using a value of K equal to 279, the shear strain corresponding to a rut depth of 13 mm (0.5 in.) is 0.045 or 4.5 percent. Tables 4 and 5 summarize the number of RSST-CH repetitions to 4.5 percent permanent shear strain, N_{supply}.

BINDER CONTENT SELECTION

To select the design binder content for each mix, the procedure outlined earlier was followed.

The design traffic volume, N_{demand}, was determined from Equation 3. The design number of ESALs, adjusted to the critical temperature ($ESAL_{T_c}$), was determined by multiplying the design ESALS by the TCF for the site; in this instance a value of TCF = 0.1158 was used. A value of 0.04 was used for the shift factor, as follows:

$$N_{demand} = [(10 \times 10^6) \cdot (0.1158)] \cdot (0.04) = 46{,}230 \text{ reps}$$

To determine binder contents corresponding to different levels of reliability, N_{supply} was determined from Equation 3. Values for M were selected from Table 2 and are based on variabilities in the estimate of the natural logarithm of N_{demand} = 0.2 and a sample size of 4. Table 2 was determined for a mean square error of 0.602 from simple shear test results for one mix over a range in binder contents using Equation 5:

$$M = \exp (Z_R \cdot [\text{var}\{\ln \text{traffic estimate}\} + \text{var}\{\ln \text{RSST-CH results}\}]^{1/2} \quad (5)$$

where

R = desired confidence level,
Z_R = standard normal deviate,
var = variance, and
exp = antilog of Naperian base.

The values for M are as follows:

Reliability Level	M	$N_{demand} \times 10^5$
80	2.270	1.05
90	3.482	1.61
95	4.945	2.29

The results of the simple shear tests, Tables 4 and 5, are plotted in Figure 3 for the mixes containing the PBA-6 and asphalt-rubber binders.

These values were compared with the N_{supply} values determined from RSST-CH results for each binder content for the design rut depth [13 mm (0.5 in.)], which are also plotted in Figure 3. It can be seen that maximum binder contents of 5.4 and 5.9 percent by dry weight of aggregate for the DGAC-PBA6 and ARHM-GG mixes, respectively, would produce an asphalt concrete with 95 percent probability of not exceeding the design rut depth under the projected traffic loading of 10 million ESALs for the Sims Project.

The binder content for the DGAC-PBA6 mix determined from this analysis is approximately the same as that found acceptable from past experience with similar mixes. In contrast, the binder content for the ARHM-GG mix at this level of reliability is lower than considered acceptable for similar mixes. A 6.5 percent binder content, however, would provide N_{supply} exceeding N_{demand} with a reliability level of 80 percent.

PAST EXPERIENCE AND SELECTION OF BINDER CONTENTS

Past experience had indicated that a specified binder content of 5.2 percent by weight of dry aggregate would be successful for the same aggregate type and gradation under similar conditions. Based on the analyses presented above and past experience, a job-mix formula binder content of 5.2 percent was recommended for the mix containing the PBA-6 binder.

Limited experience (up to 4 years) on the part of advocates of asphalt-rubber binders indicated that asphalt-rubber contents of 8.1 to 8.7 percent by dry weight of aggregate have been used with no signs of excessive rutting. The calculations for the Sims Project, using air void content criteria from specimens prepared using the Hveem method (Caltrans Test 367), indicate that a binder content of 8.5 percent by dry weight of aggregate would be acceptable (although stabilometer S-values were in the range of 13 to 18, values that are considered unacceptable for conventional mixes). However, accepting the fact that limited experience has shown that asphalt-concrete mixes made with asphalt rubber can tolerate higher binder contents than asphalt-concrete mixes made with conventional asphalts, for whatever reason, a binder content of 7.5 percent by dry weight of aggregate was recommended for the ARHM-GG mix.

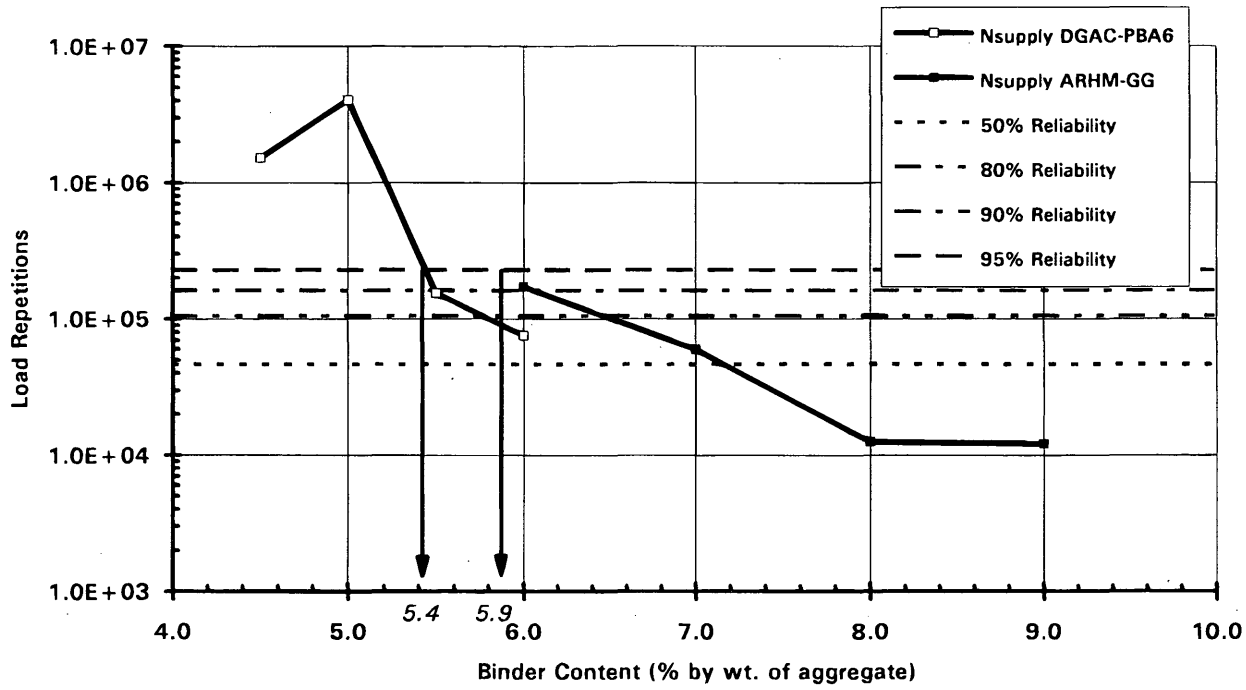

FIGURE 3 Relationship between N_{supply} (repetitions to $\gamma_p = 0.045$) and binder content for DGAC-PBA6 and ARHM-GG mixes.

MOISTURE SENSITIVITY TESTING

Moisture sensitivity of the DGAC-PBA6 and ARHM-GG mixes was evaluated at OSU using the Environmental Conditioning System, developed as part of SHRP A-003A (*10*).

Mixes were prepared with the following variations: DGAC-PBA6 mixes with 4.5 and 5.0 percent binder contents, both with and without 0.5 percent PaveBond antistripping additive; and ARHM-GG mixes with 7.0 and 8.0 percent binder contents, both with and without 0.5 percent PaveBond antistripping additive. Specimens were compacted using kneading compaction. Air void contents were approximately 8.2 ± 0.5 percent for the DGAC-PBA6 mixes and 10.6 ± 1.0 percent for the ARHM-GG mixes. These air void contents represent conditions that allow access of water into the specimens for maximum detrimental effect (*10*).

Figures 4 and 5 present the findings from the results of tests on the DGAC-PBA6 and ARHM-GG mixes, respectively. In the plots, each line connects a series of resilient moduli (M_R) ratio values obtained on a given specimen at one to four cycles of exposure in the environmental chamber of the ECS. The first three cycles consist of 6 hr in water at 60°C (140°F) followed by 4 hr in water at 25°C (77°F), and the fourth cycle consists of 6 hr in water at −18°C (0°F) followed by 4 hr in water at 25°C. The ratio values are determined by dividing the M_R after conditioning by the M_R of the original unconditioned specimen.

The results plotted in Figure 4 indicate that the use of the PaveBond additive was effective in decreasing the water sensitivity of the DGAC-PBA6 mix at both binder contents. A similar, although less effective, decrease in water sensitivity was also obtained without the additive by increasing the binder content to 5.0 percent.

The water sensitivity of the ARHM-GG mixes did not appear to be significantly affected by either binder content (7.0 and 8.0 percent) or the presence of the PaveBond antistripping additive, as can be seen in Figure 5.

On the basis of these findings, the following conclusions were drawn regarding the moisture sensitivity of the DGAC-PBA6 and ARHM-GG mixes tested:

Mix	*Binder content (%)*	*0.5% Additive*	*Moisture Sensitive?*
DGAC-PBA6	4.5	No	Yes
	4.5	Yes	No
	5.0	No	Borderline
	5.0	Yes	No
ARHM-GG	70	No	No
	70	Yes	No
	70	Yes	No
	80	No	No
	80	Yes	No

Because DGAC-PBA6 was to be placed as the lower layer of the overlay and had shown water sensitivity, it was recommended that the mix include 0.5 percent of PaveBond antistripping additive. Because the ARHM-GG mix had not shown moisture sensitivity and was to be placed as the upper layer of the overlay, it was recommended that it not include the additive; however, at the discretion of the mix producer, the additive might be included as a precautionary measure because it could significantly improve the M_R ratio values.

FIELD PERFORMANCE TO DATE

The DGAC-PBA6 and ARHM-GG mixes were placed at the site in July 1993. During 1994 no visible rutting or cracking was observed.

Two cores were taken by Caltrans outside of the wheel path after construction and tested using the RSST-CH under the same conditions used for the mix design. Those results are presented in Tables 4 and 5. It can be seen that the construction air void contents for the

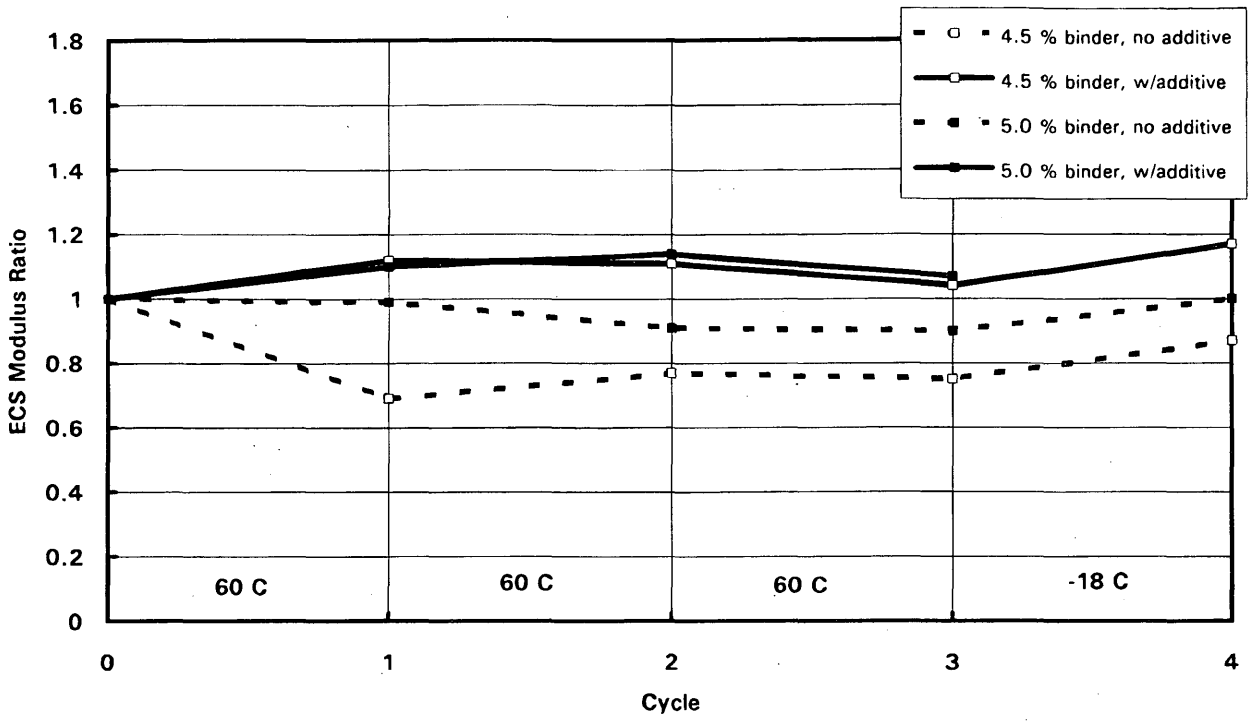

FIGURE 4 Environmental conditioning system results for DGAC-PBA6 mix.

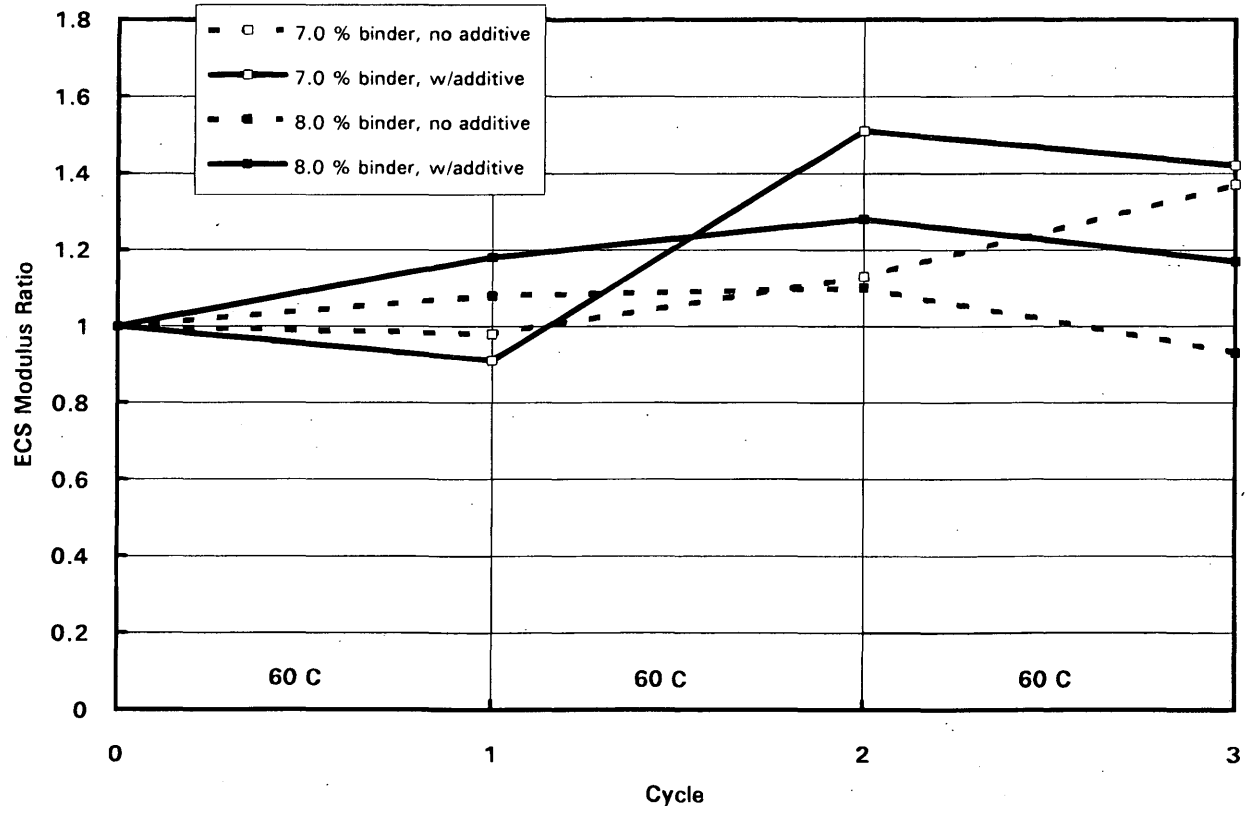

FIGURE 5 Environmental conditioning system results for ARHM-GG mix.

DGAC-PBA6 and ARHM-GG mixes were approximately 8.1 and 11.6 percent, respectively.

Field mix was also collected by Caltrans during construction, from which specimens were prepared to approximate the construction air void contents using rolling wheel compaction and tested using the RSST-CH under the same conditions used for the mix design. These results are also presented in Tables 4 and 5.

The DGAC-PBA6 results, shown plotted in Figure 6 with the original mix design data, indicate that the field cores had greater permanent shear deformation resistance than did the original mix design specimens and laboratory specimens compacted from field mix. A possible cause of the difference may be the low height of the field cores (approximately 35 to 40 mm) relative to the maximum aggregate size. The latter results correspond well with the original mix design results, considering the difference in air-void contents. It would be expected that the mix in situ would undergo additional compaction because of trafficking, resulting in higher permanent shear deformation resistance.

The ARHM-GG results, plotted in Figure 7, match well with the mix design data after accounting for the difference in air void contents. The field cores and laboratory-compacted field mix also have corresponding results.

SUMMARY

The project discussed in this paper used an application of a mix design method developed in the SHRP A-003A project. With this method, binder contents were selected for two mixes—ARHM-GG and DGAC-PBA6—that should meet the performance required by the warranty for the project.

There are a number of features of this mix design approach that differ from current procedures and that should be emphasized:

- Use of test temperature corresponding to the critical temperature for the specific site,
- Application of the primary distress mechanism for permanent deformation using the RSST-CH,
- Compaction to the critical air void content expected in the field after trafficking using a laboratory compaction procedure that produces mix characteristics similar to those produced by field compaction, and
- Use of reliability concepts that allow the mix designer to include an appropriate level of risk for the project under consideration.

In addition, the water sensitivity testing methods developed as part of the SHRP A-003A project demonstrated the suitability of, and evaluated the need for, an antistripping additive for both mixes.

It is recommended that evaluation of the mix design method presented in this paper continue by application to additional projects. Through this process the authors believe that the advantages of this methodology can be demonstrated; at the same time, further refinements can be made if required.

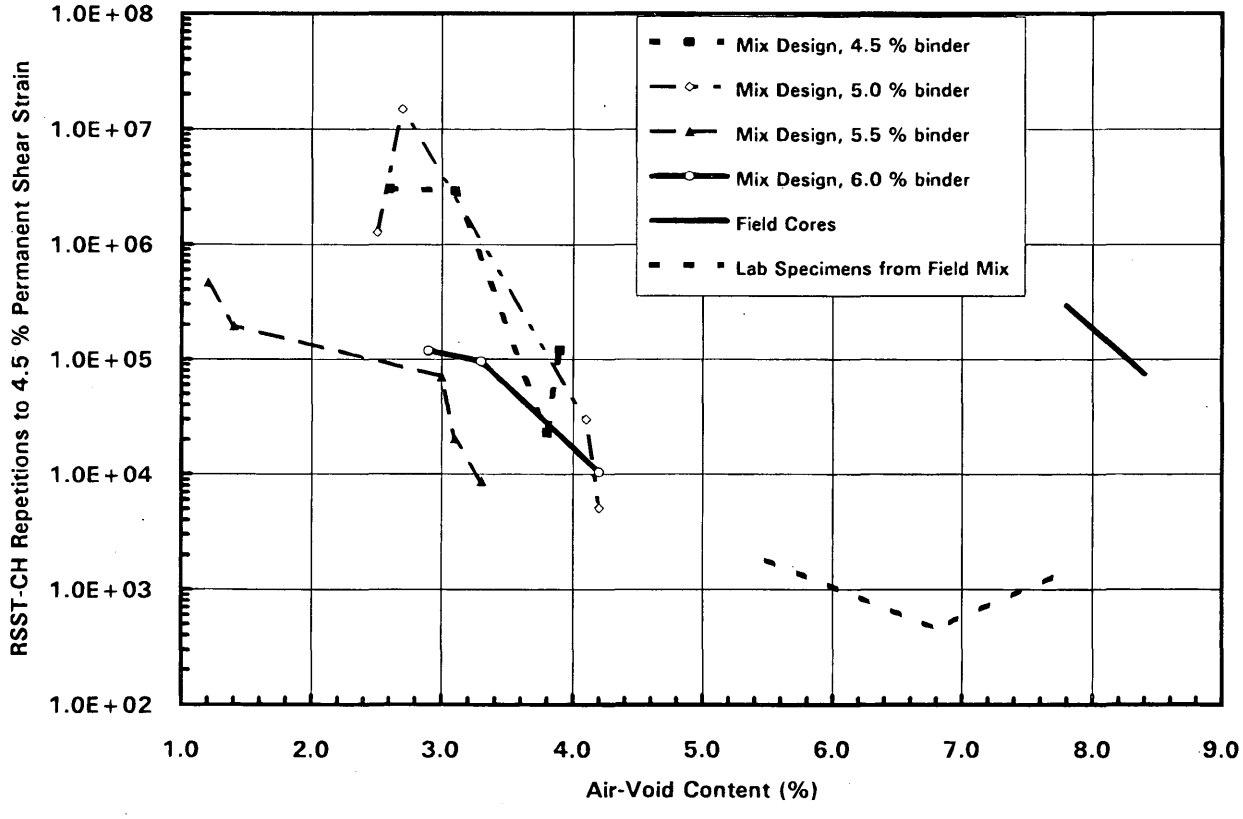

FIGURE 6 Comparison of mix design and field specimen permanent shear deformation resistance for DGAC-PBA6.

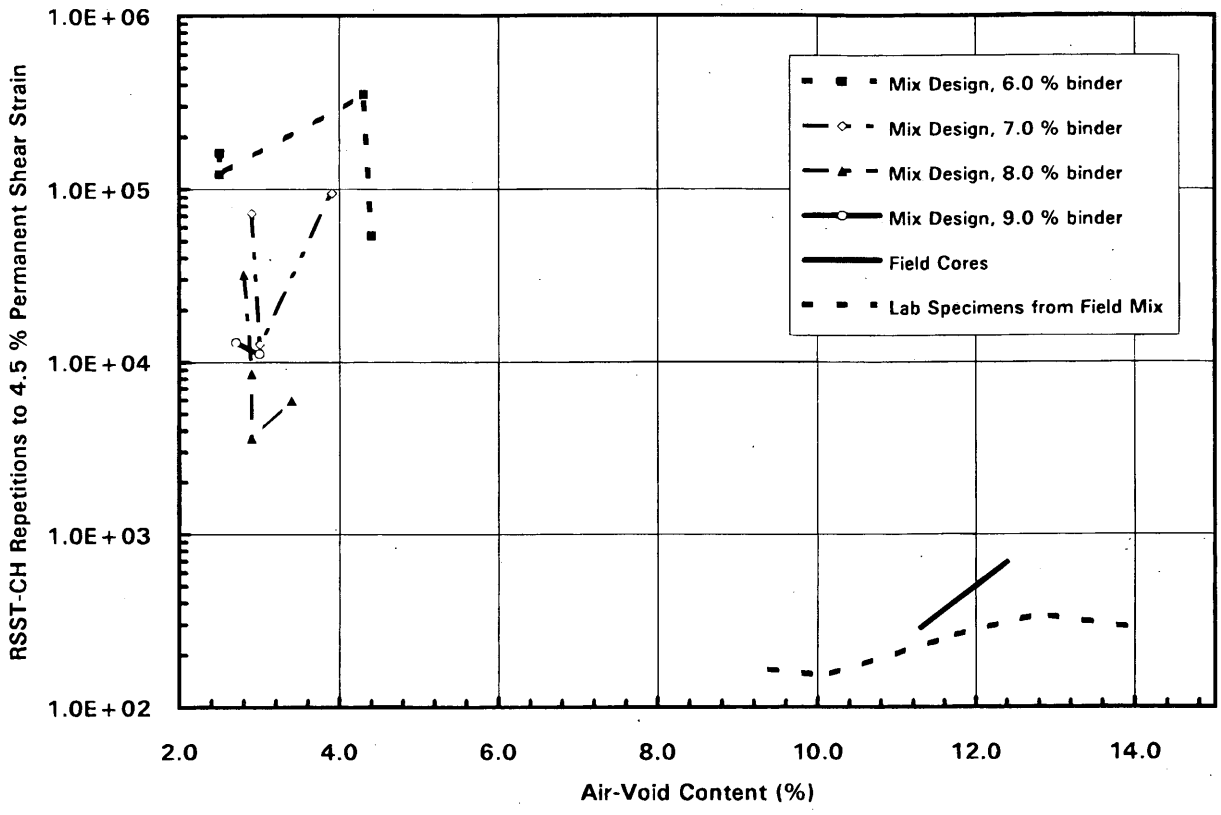

FIGURE 7 Comparison of mix design and field specimen permanent shear deformation resistance for ARHM-GG.

REFERENCES

1. Vallerga, B. A. Warrantied Pavement on an Interstate Highway in California. In *Conference Proceedings 7: Third International Conference on Managing Pavements,* TRB, National Research Council, 1995, vol. 3.
2. University of California at Berkeley, Oregon State University, Austin Research Engineers, Inc., and SWK Pavement Engineering. *Stage 1 Validation of the Relationship Between Asphalt Properties and Asphalt-Aggregate Mix Performance.* Report SHRP-A-398. Strategic Highway Research Program, National Research Council, Washington, D.C., 1994.
3. Sousa, J., et al. *Permanent Deformation Response of Asphalt-Aggregate Mixes.* Report SHRP-A-414. Strategic Highway Research Program, National Research Council, Washington, D.C., 1994.
4. Deacon, J., J. Coplantz, A. Tayebali, and C. Monismith. Temperature Considerations in Asphalt-Aggregate Mixture Analysis and Design. In *Transportation Research Record 1454,* TRB, National Research Council, Washington, D.C., 1994, pp. 97–112.
5. Harrigan E. T., et al. (ed.). *The SUPERPAVE Mix Design System Manual of Specifications, Test Methods, and Practices.* SHRP Procedure M-008. Strategic Highway Research Program, National Research Council, Washington, D.C., 1994, pp. 165–176.
6. Sousa, J., A. Tayebali, J. Harvey, P. Hendricks, and C. Monismith. Sensitivity of Strategic Highway Research Program A-003A Testing Equipment to Mix Design Parameters for Permanent Deformation and Fatigue. In *Transportation Research Record 1384,* TRB, National Research Council, Washington, D.C., 1993, pp. 80–93.
7. Harvey, J., and C. Monismith. Effects of Laboratory Asphalt Concrete Specimen Preparation Variables on Fatigue and Permanent Deformation Test Results Using Strategic Highway Research Program A-003A Proposed Testing Equipment. In *Transportation Research Record 1417,* TRB, National Research Council, Washington, D.C., 1993, pp 38–48.
8. Bell, C., A. Wieder, and M. Fellin. *Laboratory Aging of Asphalt-Aggregate Mixtures Field Validation.* Report SHRP-A-390. Strategic Highway Research Program, National Research Council, Washington, D.C., 1994.
9. Sousa, J., and M. Solaimanian. Abridged Procedure to Determine Permanent Deformation of Asphalt Concrete Pavements. In *Transportation Research Record 1448,* TRB, National Research Council, Washington, D.C., 1994.
10. Terrell, R., and S. Al-Swailmi. *Water Sensitivity of Asphalt-Aggregate Mixtures Test Development.* Report SHRP-A-403. Strategic Highway Research Program, National Research Council, Washington, D.C., 1994.

Publication of this paper sponsored by Committee on Characteristics of Bituminous Paving Mixtures to Meet Structural Requirements.

Evaluation of Hamburg Wheel-Tracking Device to Predict Moisture Damage in Hot-Mix Asphalt

TIM ASCHENBRENER

The Colorado Department of Transportation (CDOT) and FHWA's Turner-Fairbank Highway Research Center were selected to demonstrate several pieces of European equipment. The Hamburg wheel-tracking device was one of those pieces of equipment. It is used to predict moisture damage of hot-mix asphalt (HMA). This paper provides an evaluation of factors that influence the results from the Hamburg wheel-tracking device. There was excellent correlation between the Hamburg wheel-tracking device and pavements of known field performance. The Hamburg wheel-tracking device was found to be sensitive to (a) quality of aggregates, (b) asphalt cement stiffness, (c) length of short-term aging, (d) refining process or crude oil source of the asphalt cement, (e) liquid and hydrated lime antistripping treatments, and (f) compaction temperature. The Hamburg wheel-tracking device was demonstrated on two CDOT projects to improve the quality of HMA.

In September of 1990, a group of individuals representing AASHTO, FHWA, National Asphalt Pavement Association (NAPA), Strategic Highway Research Program (SHRP), Asphalt Institute (AI), and TRB participated in a 2-week tour of six European countries. Information about this tour has been published in *Report on the 1990 European Asphalt Study Tour* (*1*). Several areas for potential improvement of hot-mix asphalt (HMA) were identified, including the use of performance-related testing equipment used in several European countries. The Colorado Department of Transportation (CDOT) and FHWA's Turner-Fairbank Highway Research Center were selected to demonstrate this equipment.

The purpose of this paper is to provide an evaluation of factors that influence the results from the Hamburg wheel-tracking device.

HAMBURG WHEEL-TRACKING DEVICE

Equipment and Procedure

The Hamburg wheel-tracking device is manufactured by Helmut-Wind, Inc. of Hamburg, Germany, as shown in Figure 1; a close-up is shown in Figure 2. A pair of samples are tested simultaneously. A sample is typically 260 mm (10.2 in.) wide, 320 mm (12.6 in.) long, and 40 mm (1.6 in.) thick. Its mass is approximately 7.5 kg (16.5 lb), and the sample is compacted to 7 ± 1 percent air voids. The samples are submerged in water at 50°C (122°F), although the temperature can vary from 25°C to 70°C (77°F to 158°F). A steel wheel 47 mm (1.85 inches) wide loads the samples with 705 N (158 lb). The wheel makes 50 passes over each sample per minute. The maximum velocity of the wheel is 34 cm/sec (1.1 ft/sec) in the center of the sample. Each sample is loaded for 20,000 passes or until 20 mm of deformation occurs. Approximately 6½ hr is required for a test.

Test Results and Specifications

The results from the Hamburg wheel-tracking device include the creep slope, stripping slope, and stripping inflection point as shown in Figure 3. The results have been defined by Hines (*2*). The creep slope relates to rutting from plastic flow. It is the inverse of the rate of deformation in the linear region of the deformation curve after postcompaction effects have ended and before the onset of stripping. The stripping slope is the inverse of the rate of deformation in the linear region of the deformation curve after stripping begins and until the end of the test. It is the number of passes for each 1 mm of impression from stripping. The stripping slope is related to the severity of moisture damage. The stripping inflection point is the number of passes at the intersection of the creep slope and the stripping slope. It is related to the resistance of the HMA to moisture damage.

The city of Hamburg specifies a rut depth of less than 4 mm after 20,000 passes. A previous study (*3*) has found this specification to be very severe for pavements in Colorado. A rut depth of less than 10 mm after 20,000 passes may be more reasonable.

COMPARISON WITH PAVEMENTS OF KNOWN FIELD PERFORMANCE

Pavements of known stripping performance were tested in the Hamburg wheel-tracking device (*3*). Seven good pavements (Sites 1 to 7), five pavements requiring high maintenance (Sites 8 to 12), and eight pavements that lasted less than 1 year (Sites 13 to 20) were tested. The high-maintenance pavements are still in service after 3 to 5 years but required excessive maintenance. The pavements that lasted less than 1 year were divided into two groups.

1. Pavements that were built in layers of different materials (Sites 13 to 16) and had a unique pavement design feature, a rut-resistant composite that utilized a plant-mixed seal coat.
2. Pavements built using conventional material design practices that were not covered or "sealed" (Sites 17 to 20).

The pavements of known stripping performance were tested in the Hamburg wheel-tracking device at the 50°C test temperature. The

Colorado Department of Transportation, 4340 East Louisiana, Denver, Colo. 80222.

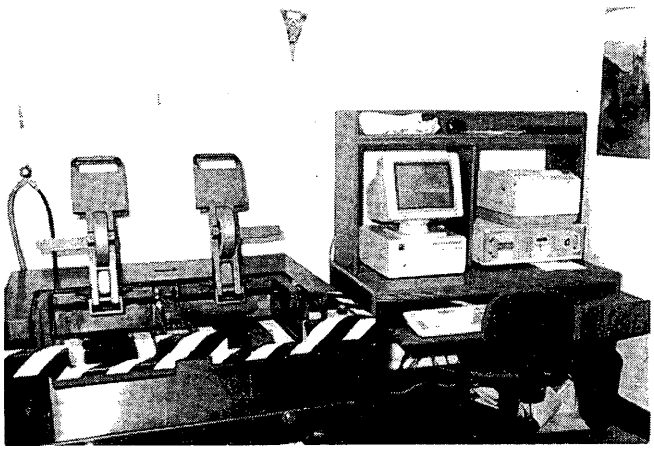

FIGURE 1 Hamburg wheel-tracking device.

stripping inflection point results are shown in Table 1. There was excellent correlation between the stripping inflection point and the known stripping performance. The good pavements (Sites 1 to 7) had stripping inflection points generally greater than 10,000 passes. The high-maintenance pavements (Sites 8 to 12) had stripping inflection points generally between 5,000 and 10,000 passes. The pavements that lasted less than 1 year (Sites 13 to 20) had stripping inflection points less than 3,000 passes. The Hamburg wheel-tracking device has the potential to discriminate between pavements of varying field stripping performance.

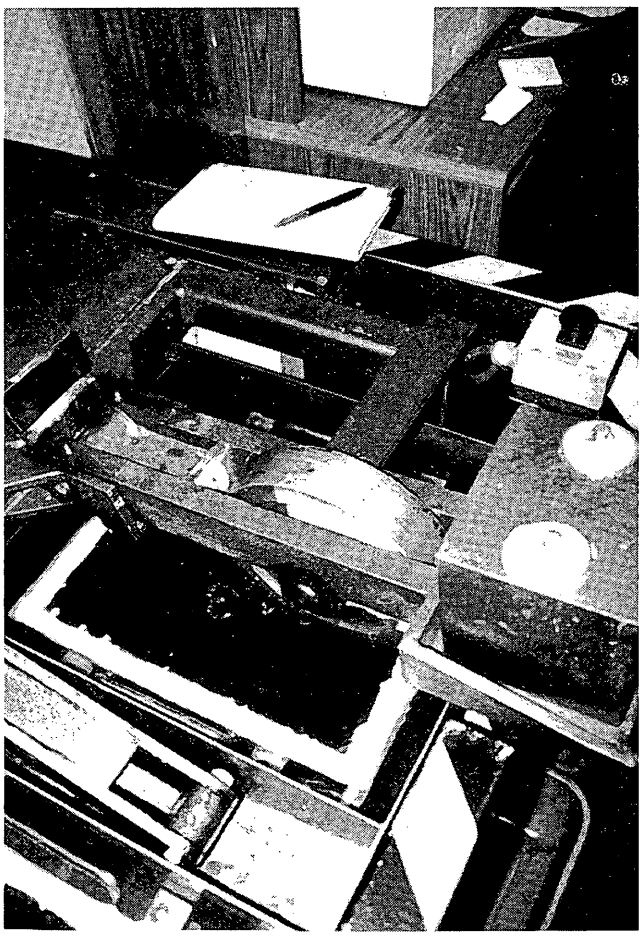

FIGURE 2 Close-up of Hamburg wheel-tracking device.

INFLUENCE OF MATERIAL PROPERTIES

Aggregate Properties

HMA from pavements of known field performance were tested, and in virtually all cases, aggregate problems were identified (*3*). Aggregate problems identified included

1. The presence of clay as identified by the methylene blue test,
2. Very high dust-to-asphalt ratios, and
3. Excessive dust coating on the aggregate.

A summary of results from these aggregate tests is shown in Table 1. Aggregate results that are considered unacceptable or marginal are enclosed in parentheses.

The methylene blue test is used to identify the quality of the material passing the 75-μm (No. 200) sieve. The test identifies deleterious clay or material with high surface activity. Test results greater than 10 mg/g are marginal and greater than 20 mg/g are unacceptable. Virtually all of the bad pavements (Sites 13 to 17, and 19 and 20) had unacceptable methylene blue values. Some of the good pavements (Sites 6 and 7) and high-maintenance pavements (Sites 8 and 9) were marginal.

The maximum dust-to-asphalt cement ratio can be defined by the quantity of 75-μm material that increases the ring-and-ball softening point (AASHTO T 53) at 11°C (*4*). All 13 of the stripping pavements except 3 (Sites 9, 13, and 17) had dust-to-asphalt cement ratios in excess of the maximum. Four of the seven good pavements (Sites 3, 4, 6, and 7) had dust-to-asphalt cement ratios less than the maximum.

The amount of dust coating the coarse aggregate was identified by dry sieving the blended aggregate over the 4.75-mm (No. 4) sieve size and then washing the material over the 4.75-mm (No. 4) sieve size. The difference in weight before and after washing was defined as the dust coating. Two pavements (Sites 17 and 18) had dust coatings of 3 percent or more.

A combination of these results is shown in Table 2. Materials that failed two of the three tests were unlikely to have good performance in the field and in the Hamburg wheel-tracking device. Materials that passed all three tests had good performance in the field and in the Hamburg wheel-tracking device.

Based on pavements of known performance, results from the Hamburg wheel-tracking device appear sensitive to aggregate properties that include: clay content, high dust-to-asphalt ratios, and dust coating on the aggregates.

Asphalt Cement Properties

Asphalt Cement Stiffness

We wanted to test asphalt cements with a variety of high-temperature properties to investigate the change in asphalt cement stiffness based on results from the Hamburg wheel-tracking device (*5*). The gradings of asphalt cement tested were three neat asphalt

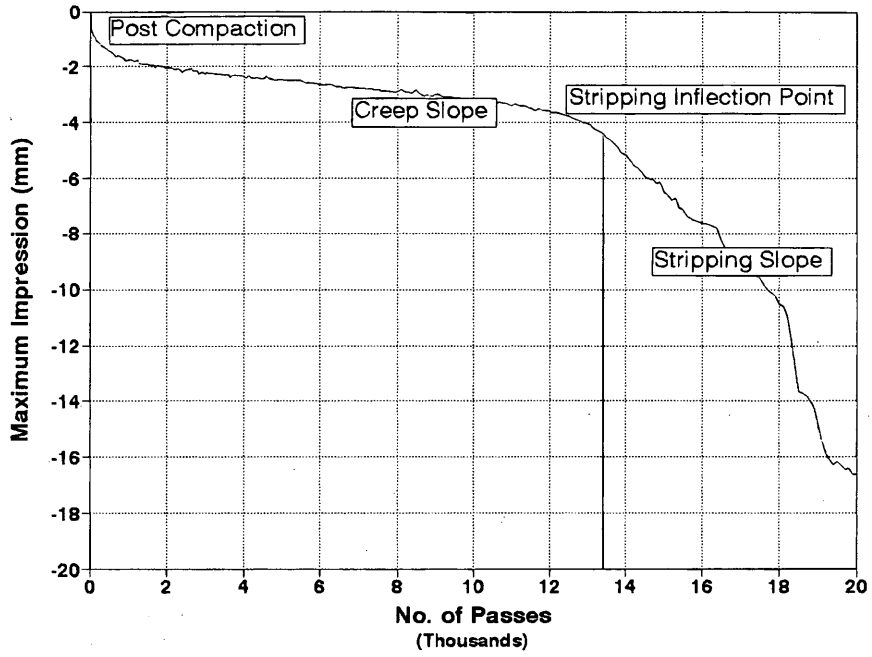

FIGURE 3 Definition of results from Hamburg wheel-tracking device.

TABLE 1 Summary of Test Results on Sites of Known Stripping Performance

Site	Methylene Blue (mg/g)	Dust:Asphalt Ratio		Dust Coating (%)	Stripping Inflection Point (Passes)
		Max.	Actual		
1	6.8	1.17	(2.01)	0.3	>20,000
2	9.5	1.18	(1.40)	0.6	>20,000
3	2.5	1.17	1.05	0.2	>20,000
4	6.4	1.34	0.99	0.2	14,200
5	5.0	1.21	(1.35)	0.4	14,500
6	(12.6)	1.48	0.92	0.3	(3,500)
7	(11.9)	1.29	0.78	0.1	>20,000
8	(13.0)	1.14	(1.67)	NT	(9,600)
9	(10.6)	1.21	0.97	0.7	(1,500)
10	8.7	1.32	(1.63)	0.2	(6,200)
11	4.3	1.24	(1.69)	0.7	>20,000
12	8.3	1.35	(1.60)	0.2	(4,600)
13	(>20)	1.19	0.94	0.5	(2,300)
14	(>20)	1.23	(1.38)	1.9	(1,500)
15	(>20)	1.20	(1.26)	NT	NT
16	(14.2)	1.29	(1.45)	0.3	(1)
17	(>20)	1.24	1.23	(3.8)	(1)
18	6.6	1.08	(1.21)	(2.8)	(2,200)
19	(>20)	0.96	(2.01)	NT	(1)
20	(>20)	1.10	(1.21)	0.5	(1)

() - Indicates Unacceptable Test Result
NT - Not Tested

TABLE 2 Ability of Tests on 75-μm Material To Predict Stripping Performance

Methylene Blue Dust:Asphalt Ratio Dust Coating	Sites of Known Performance		
	Good	High Maintenance	Less Than 1 Year
Pass All 3	2	0	0
Fail 1 of 3	5	4	1
Fail 2 of 3	0	1	7
Fail All 3	0	0	0

cements, AC-5, AC-10, and AC-20 meeting AASHTO M 226 (Table 2), and one polymer-modified asphalt cement, AC-20P, meeting AASHTO Task Force 31, Type I-D. The properties of the asphalt cements are shown in Table 3. The high-temperature performance grade (PG) of each asphalt cement as classified by SHRP is included.

Four different aggregates were mixed with each grade of asphalt cement and tested over a wide range of temperatures in the Hamburg wheel-tracking device. Table 4 shows the test temperatures required to obtain a constant stripping inflection point for each mix as the grade of asphalt cement is changed. For example, using Mix 2, an AC-5 tested at 43°C had the same stripping inflection point as an AC-20 tested at 52°C.

When one testing temperature was used and the asphalt cement stiffness was increased, the stripping inflection point occurred at a larger number of passes. When one grade of asphalt cement was used and the testing temperature was decreased, the stripping inflection point occurred at a larger number of passes. Improved moisture resistance as asphalt cement stiffness increased was expected.

In the mountainous parts of the state, softer asphalt cements are used. In the desert parts of the state, stiffer asphalt cements are used. The Hamburg wheel-tracking device should not penalize softer asphalt cements that are used in the colder parts of the state. In order to obtain the same stripping inflection point for one aggregate as the asphalt cement stiffness decreases because of environmental conditions, the test temperature should decrease.

Generally, each time the asphalt cement increases one grade in stiffness, the test temperature should increase approximately 6°C to result in the same stripping inflection point.

It was extremely interesting to compare the temperature differential required to obtain equal stripping inflection points shown in Table 4 with the temperature differential required to obtain 1 kPa stiffness from the Dynamic Shear Rheometer (DSR) shown in Table 3. The differences in high-temperature properties of each asphalt cement measured by the Hamburg wheel-tracking device were almost identical to the differences measured by the DSR.

TABLE 3 Unaged Asphalt Cement Properties

	Viscosity (60°C) (Poises)	Penetration (25°C) (dmm)	Ring & Ball Softening (°C)	DSR @ 1 kPa (°C)	High Temp. PG
AC-5	520	155	45.0	56.2	52
AC-10	1030	99	47.7	61.6	58
AC-20	1980	67	52.8	67.5	64
AC-20P	10280	74	62.2	77.4	70

TABLE 4 Test Temperatures Providing Equal Stripping Inflection Points for Various Asphalt Cement Grades

	Temperature (°C)				
	Mix 1	Mix 2	Mix 3	Mix 4	Avg.
AC-5	42	43	NP	39	41
AC-10	46	49	NP	48	48
AC-20	52	52	NP	52	52
AC-20P	NP	64	NP	58	61

NP - Not Possible to Determine
(Sample Did Not Fail or Failed Very Quickly)

TABLE 5 Recommended Testing Temperatures for Hamburg Wheel-Tracking Device

High Temperature Performance Grade (PG) °C	Viscosity Grade Meeting the High Temperature PG	Recommended Test Temperature for the Hamburg Device
46		35°C
52	AC-5	40°C
58	AC-10	45°C
64	AC-20	50°C
70*	AC-20P	55°C

* - No pavements in Colorado are at this temperature. A binder with this grade may be appropriate for locations with very heavy and slow moving traffic.

The recommended testing temperatures for the Hamburg wheel-tracking device should be selected based on the high-temperature environment the pavement will experience, as shown in Table 5. These testing temperatures should provide equal stripping inflection points for a mix as the asphalt cement grade is changed. Consideration should be given to using test temperatures 5°C lower. These temperatures would likely correspond with the city of Hamburg procedure, in which high-temperature performance asphalt cement grades of 64 or 70 and a 50°C test temperature are used.

Short-Term Aging

A study was performed to investigate the influence of short-term aging on the results from the Hamburg wheel-tracking device (*5*). The results are shown in Table 6. As short-term aging time increases, samples become more resistant to moisture damage. If allowed to short-term age for 8 hr, all of the mixtures resist moisture damage.

The increase in resistance to moisture damage as short-term aging increases is expected. This could be caused by (a) a stiffening of the asphalt cement with increased aging, (b) the development of better adhesion between the aggregate and asphalt cement with aging, or (c) a combination of the two.

Refining Process and Crude Oil Source

A study was performed to determine if the refining process or crude oil source could influence the results from the Hamburg wheel-tracking device (*6*). Four refineries provide most of the asphalt cement used by CDOT. Each refinery produced one to three different types of AC-10 or PG 58-22 grading asphalt cement. The asphalt cement properties are shown in Table 7.

The test results from the Hamburg wheel-tracking device are shown in Table 8. Each refinery was able to produce an asphalt cement that was compatible with the better aggregates (Mixes 1 and 2). Most of the asphalt cements failed in the Hamburg wheel-tracking device with the poorer aggregates (Mixes 3 and 4). Although two of the asphalt cements worked with the poorer aggregates (A1 and C2), an asphalt cement cannot be expected to overcome aggregate deficiencies.

Test results in the Hamburg wheel-tracking device are sensitive to aggregate quality. When a mix fails, the aggregate quality should be investigated. When the aggregate quality is acceptable, the refin-

TABLE 6 Deformation (mm) After 20,000 Passes Versus Short-Term Aging Period

	Deformation (mm) After 20,000 Passes			
	Short-Term Aging Period (Hours)			
Mix	0	2	4	8
1	(>20.0)	6.1	8.6	1.7
2	(>20.0)	3.3	(11.0)	1.5
3	(>20.0)	(11.8)	(13.8)	2.3
4	(>20.0)	3.5	5.5	3.1

() - Indicates Unacceptable Test Result

TABLE 7 Asphalt Cement Test Results from Various Refineries and Crude Oil Sources

Refinery	Pen. (25°C) dmm	Vis. (60°C) Poises	DSR (Tank) °C @ 1 kPa	DSR (TFOT) °C @ 2.2 kPa	Performance Grade (PG)
A1	92	1300	58.0	64.1	58-22
A2	110	940	61.7	62.1	58-22
A3	100	1060	62.4	62.7	58-22
B1	105	1030	62.1	62.3	58-22
B2	128	820	60.2	59.8	58-22
B3	103	1060	62.5	62.7	58-22
C1	100	1010	61.8	62.6	58-22
C2	90	1000	62.4	61.2	58-22
D1	87	1100	62.3	60.7	58-22
Vn	129	1040	61.7	62.1	58-22

TABLE 8 Deformation (mm) After 20,000 Passes from Various Refineries and Crude Oil Sources

	Deformation (mm) After 20,000 Passes			
Refinery	Mix 1	Mix 2	Mix 3	Mix 4
A1	9.2	7.6	(17.9)	4.2
A2	8.5	6.9	(>20.0)	(15.9)
A3	7.9	(14.8)	(12.1)	(17.6)
B1	7.2	9.2	(15.1)	(15.6)
B2	(14.8)	(>20.0)	(>20.0)	(>20.0)
B3	(14.3)	(16.7)	(16.6)	(17.4)
C1	8.4	4.0	(14.6)	(>20.0)
C2	4.4	(12.7)	5.2	5.9
D1	(>20.0)	7.3	(>20.0)	(>20.0)
Vn	(11.5)	(10.5)	(>20.0)	(>20.0)

() - Indicates Unacceptable Test Result

ing process and crude oil source should be investigated. Not all AC-10 or PG 58-22 grading asphalt cements have the same adhesion properties.

ANTISTRIPPING TREATMENT

Various Types of Antistripping Treatment

A study was performed to investigate the influence of the use of various types of antistripping additives with the Hamburg wheel-tracking device (*7*). Mixes were tested with no treatment, four different types of liquid antistripping additives, and hydrated lime.

The results are shown in Table 9. When the mixes had no treatment, the results from the Hamburg wheel-tracking device were unacceptable for Mixes 1, 2, and 3. The use of hydrated lime improved the test results dramatically for all of the mixes. Passing test results were always obtained. Mixes treated with liquid antistripping additives performed better than those with no treatment with one exception. Passing test results were obtained for some of the mixes treated with liquid antistripping additives but not with others. Mixes treated with liquid antistripping additives did not perform as well as those treated with lime but still improved the HMA.

Method of Lime Addition

A study was performed to investigate if the method of lime addition influenced the results from the Hamburg wheel-tracking device (*5*). The amount of water used for mixing and the results are summarized in Table 10.

When lime was not present, all of the mixes did poorly. When dry lime was added to dry aggregate and thoroughly mixed, there was a dramatic improvement in the results. Just the presence of lime

TABLE 9 Deformation (mm) After 20,000 Passes for Various Antistripping Treatments

	Deformation After 20,000 Passes					
			Additive A		Additive B	
Mix	No Treatment	Hydrated Lime	Type 1	Type 2	Type 1	Type 2
1	(17.0)	1.4	2.2	3.1	6.3	7.4
2	(>20.0)	2.3	8.1	8.4	5.3	(14.6)
3	(>20.0)	2.5	(13.7)	8.5	(>20.0)	(12.4)
4	8.7	2.3	6.2	4.6	5.0	4.3

() - Indicates Unacceptable Test Result

TABLE 10 Deformation (mm) After 20,000 Passes Versus Method of Lime Addition

	Deformation (mm) After 20,000 Passes				
	Method of Lime Addition				
Mix	No Lime No Water No Mellow	1% Lime No Water No Mellow	1% Lime 2% Water No Mellow	1% Lime 4% Water No Mellow	1% Lime 4% Water 3-Day Mellow
1	(>20.0)	1.5	5.9	4.6	5.7
2	(>20.0)	5.1	(13.0)	9.1	2.5
3	(>20.0)	4.5	(11.2)	5.0	4.6
4	(>20.0)	5.1	4.1	3.1	5.6

() - Indicates Unacceptable Test Result

helped significantly, regardless of moisture. The improvement did not continue as water was added. We still recommend using water when adding lime to facilitate the mixing.

COMPACTION METHODS

Field Versus Laboratory Compaction

Seven projects were selected for comparison of test results between field- and laboratory-compacted samples (*8*). Samples of loose mix were taken behind the paver and compacted in the laboratory to the same density as in the field project. The laboratory samples were compacted with the French plate compactor (pneumatic tire) and linear kneading compactor (steel wheel). Field-compacted samples were sawn from the pavement.

The comparison of test results from the Hamburg wheel-tracking device is shown in Table 11. Samples compacted with the linear kneading compactor gave slightly better results than samples compacted with the French plate compactor. In general, the samples compacted by two different methods in the laboratory performed similarly.

The field-compacted samples performed significantly worse than the laboratory-compacted samples. This might have been caused by either the additional short-term aging received by the laboratory-compacted samples or the difference in field and laboratory compaction temperatures.

The loose mix used to perform laboratory compaction had to be reheated to achieve compaction temperature. The additional heating increased the short-term aging. Additionally, the loose mix compacted in the laboratory achieved density at a much higher temperature than the field-compacted samples.

Compaction Temperature

A study was performed to investigate the influence of compaction temperature on results from the Hamburg wheel-tracking device (*7*). Samples of loose HMA were compacted in the laboratory at four different temperatures. All samples were compacted to the same percent of air voids. The results are shown in Table 12. When compaction was achieved at higher temperatures, the test results improved.

The unacceptable results at low temperatures can be explained by the following reasons: (a) aggregates break, (b) microcracks develop in the HMA, or (c) the air voids might be interconnected and not be small and dispersed. Any of these reasons or combination of reasons might explain the importance of achieving the

TABLE 11 Differences in Stripping Inflection Point (Passes) for Field- and Laboratory-Compacted Samples

Site	French vs. Kneading	French vs. Field	Kneading vs. Field
1	-2,300	3,600	5,900
2	-1,900	4,400	6,300
3	0	5,400	5,400
4	-2,600	2,600	5,200
5	0	1,500	1,500
6	0	0	0
7	0	6,800	6,800
Avg.	-970	3,470	4,440

Negative numbers indicate a stripping inflection point was higher in the second sample of the comparison.

required compaction in the field at the highest possible temperature. Short-term aging might also be a factor.

DEMONSTRATION PROJECTS

I-70 at Silverthorne

A very large project was undertaken in the fall of 1992 and summer of 1993. After a severe winter in 1992, the pavement exhibited signs of moisture damage. The Hamburg wheel-tracking device was used to improve the quality of the HMA placed in 1993 (*9*). The cost of the improvements was approximately $1.00/ton of HMA.

Two improvements were made. First, the asphalt content was increased from 5.3 percent to 5.7 percent to provide better durability. The increased asphalt content did not create rutting from permanent deformation in the Hamburg wheel-tracking device. Second, the crude oil source used for the project was changed. With a combination of these two changes, the results from the Hamburg wheel-tracking device improved dramatically. All of the aggregates were tested and found to have excellent quality; no aggregate changes were made.

I-25 at Longmont

This project was bid using the test results from the Hamburg wheel-tracking device as an incentive payment. If the HMA produced from the plant passed the Hamburg wheel-tracking test, an incentive of $1.50/ton of HMA would be awarded to the contractor. There were no provisions for disincentives for failing tests.

The contractor who was awarded the project typically used a natural sand that was not plastic but had an unacceptable methylene blue value. The contractor's typical mix did not pass the Hamburg wheel-tracking device specification. For this project, the contractor bid included an HMA that used a washed concrete sand in place of the "dirty" natural sand.

The first two samples represented 10,000 tons and passed the 10-mm specification. The contractor was awarded a bonus on this material. The final three samples failed miserably. Unfortunately, the quality control was very poor, and the contractor was shut down over 10 times and required to take corrective actions. Although the material had the potential to pass the test, a lack of a consistent and successful quality control was probably the cause of the failing tests.

TABLE 12 Deformation (mm) After 20,000 Passes for Samples Compacted at Various Temperatures

	Deformation (mm) After 20,000 Passes			
	Compaction Temperature (°C)			
Mix	66	93	121	149
1	(>20.0)	7.9	7.0	1.4
2	(>20.0)	(13.9)	(11.4)	2.3
3	(>20.0)	(>20.0)	9.2	2.5
4	(>20.0)	8.6	10.0	2.3

() - Indicates Unacceptable Test Result

CONCLUSIONS

1. The Hamburg wheel-tracking device has the potential to discriminate between pavements with known field stripping performance and several levels of severity of moisture distress.

2. Results from the Hamburg wheel-tracking device are sensitive to aggregate properties that include clay content, high dust-to-asphalt ratios, and dust coating on the aggregates. The aggregate quality is important to obtain passing results.

3. When using one testing temperature and increasing the asphalt cement stiffness, the stripping inflection point occurred at a larger number of passes. When using one grade of asphalt cement and decreasing the testing temperature, the stripping inflection point occurred at a larger number of passes. Moisture resistance improved as asphalt cement stiffness increased.

The recommended testing temperatures for the Hamburg wheel-tracking device should be selected based on the high-temperature environment the pavement will experience as shown in Table 5.

4. Results from the Hamburg wheel-tracking device are sensitive to the amount of short-term aging. As short-term aging time increases, samples become more resistant to moisture damage.

5. The results from the Hamburg wheel-tracking device are sensitive to the refining process and crude oil source. Not all AC-10 or PG 58-22 grading asphalt cements have the same adhesion properties.

6. Liquid antistripping additives improved the results from the Hamburg wheel-tracking device with some aggregates but did not improve the results with other aggregates. Hydrated lime improved the test results with all of the mixes tested.

When dry lime was added to dry aggregate and thoroughly mixed, there was a dramatic improvement in the results from the Hamburg wheel-tracking device with all aggregates. Just the presence of lime helped significantly, regardless of moisture. We still recommend using water when adding lime to facilitate the field mixing. However, additional studies should be performed to examine dry mixing.

7. Samples compacted in the laboratory with the linear kneading compactor (steel wheel) gave slightly better results than samples compacted with the French plate compactor (pneumatic tire). In general, the laboratory-compacted samples performed similarly. The field-compacted samples did significantly worse than the laboratory-compacted samples.

8. When the target density was achieved at higher temperatures, the test results from the Hamburg wheel-tracking device improved.

9. Results from the Hamburg wheel-tracking device have been used successfully on two field projects. At Silverthorne, two adjustments were made to improve an existing HMA. At Longmont, an incentive payment was used to allow an improved quality of aggregate to be used in the HMA from the beginning of the project.

10. The short-term aging of laboratory-prepared samples to match the short-term aging in the field needs to be defined. A future research study should investigate short-term aging.

ACKNOWLEDGMENTS

This study was funded with Colorado State Planning and Research funds.

The author would like to express his gratitude to the many people who made this report possible. The testing was performed by Kim Gilbert, Benja Bemelen, Cindi Moya, Nava Far, Dave Price (CDOT-Staff Materials), and J.D. Stevenson and Richard Zamora (FHWA-Colorado Division). The trial projects were successful because of cooperation from Wes Goff, Art Wilcoxon, and CDOT-Construction.

The research study panel included Byron Lord and Kevin Stuart (FHWA-Turner Fairbank Highway Research Center); Doyt Bolling (FHWA-Region 8); Jerry Cloud (FHWA-Colorado Division); Denis Donnelly, Steve Horton, and Bob LaForce (CDOT-Staff Materials); Ken Wood (CDOT-Region 4 Materials); and Donna Harmelink (CDOT-Research). The panel of Colorado experts included Bud Brakey (Brakey Consulting Engineers), Jim Fife (Western Colorado Testing), Joe Proctor (Morton International), Scott Shuler (CAPA), and Eric West (Western Mobile).

Significant insight and guidance were provided by Mickey Hines and Gayle King (Koch Materials Co.) throughout the study.

REFERENCES

1. *Report on the 1990 European Asphalt Study Tour.* AASHTO, Washington, D.C., 1991.
2. Hines, M. The Hamburg Wheel-Tracking Device. *Proceedings of the Twenty-Eighth Paving and Transportation Conference*, Civil Engineering Department, University of New Mexico, Albuquerque, New Mexico, 1991
3. Aschenbrener, T., R. L. Terrel, and R. A. Zamora. *Comparison of the Hamburg Wheel-Tracking Device and the Environmental Conditioning System to Pavements of Known Field Performance.* Colorado Department of Transportation, CDOT-DTD-R-94-1, 1994.
4. Kandhal, P. S. Evaluation of Baghouse Fines in Bituminous Paving Mixtures. Proc., *Association of Asphalt Paving Technologists*, Vol. 50, 1981, pp. 150–210.
5. Aschenbrener, T., and G. Currier. *Influence of Testing. Variables on the Results from the Hamburg Wheel-Tracking Device.* Colorado Department of Transportation, CDOT-DTD-R-93-22, 1993.
6. Aschenbrener, T. *Influence of Refining Processes and Crude Oil Sources on Results from the Hamburg Wheel-Tracking Device.* Colorado Department of Transportation, CDOT-DTD-R-94-7, 1994.
7. Aschenbrener, T., and N. Far. *Influence of Compaction Temperature and Anti-Stripping Treatment on Results from the Hamburg Wheel-Tracking Device.* Colorado Department of Transportation, CDOT-DTD-R-94-9, 1994.
8. Stevenson, J. D., and T. Aschenbrener. *Comparison of Test Results from Laboratory and Field Compacted Samples.* Colorado Department of Transportation, CDOT-DTD-R-94-3, 1994.
9. Aschenbrener, T. *I-70, Silverthorne to Copper Mountain: A Case History of the Use of European Testing Equipment.* Colorado Department of Transportation, CDOT-DTD-R-93-19, 1993.

Publication of this paper sponsored by Committee on General Asphalt Problems.

Development and Use of Georgia Loaded Wheel Tester

RONALD COLLINS, DONALD WATSON, AND BRUCE CAMPBELL

The Georgia Department of Transportation began development of a loaded wheel tester (LWT) in 1985 to better evaluate the rutting susceptibility of asphaltic concrete mixes. It has been believed throughout the industry for some time that Marshall stability tests are inadequate to accurately predict rutting potential of various mixes. With the Georgia LWT, the susceptibility of a mixture to rut can be determined in the laboratory during the design stage, and modifications to the design can be made at that time if needed. The machine can be adjusted for various weight, air pressure, and temperature conditions to simulate and test for performance under the actual field environment. The machine has been made to be a completely portable, self-contained unit with its own environmental heating chamber. Several research projects have been conducted with the Georgia LWT in order to evaluate the effect on performance of aggregate gradation, tire pressure, vehicle loading, and pavement temperature. Testing has been done on specialized mixes such as stone matrix asphalt, which shows that these mixtures are more resistant to rutting than conventional mixes even though Marshall stability test values may be lower. Asphalt mixtures produced under the Strategic Highway Research Program Level I and II volumetric design methods may still be prone to rutting. The Georgia LWT is an economical tool that can be used as a "proof tester" for properly evaluating the rutting resistance of these mixtures before they are placed on the roadway.

The Georgia loaded wheel tester (LWT) is a valuable tool that has been used by the Georgia Department of Transportation (GDOT) to assess the rutting potential of asphaltic concrete mixes. By subjecting asphaltic concrete to a loaded wheel system under repetitive loading conditions and measuring the permanent deformation induced under the wheelpath, the rutting susceptibility of the asphaltic concrete to be used in the field may be determined. This approach to assessing rutting susceptibility was thought to be much more representative of actual field conditions than the Marshall stability test currently used throughout much of the industry. In view of the complexity of the material behavior and the stress induced by traffic loading, the use of loaded wheel type testing can provide a fast and accurate means of simulating rutting at the design stage of the mix rather than waiting until the mix is in place to discover that it has a high potential for rutting.

LWT DEVELOPMENTAL RESEARCH

In order for GDOT to perform LWT research, a machine was needed. When GDOT began considering this approach in 1985, no machine was commercially available, so the Georgia Institute of Technology (Atlanta, Ga.) was contracted by GDOT to develop a LWT that would meet our needs.

Preliminary developmental work by Georgia Tech consisted of literature searches through the Highway Research Information System and draft designs. GDOT had a machine that met the base design criteria specified by Georgia Tech. This machine was previously used by GDOT for design and testing of slurry seals and was originally developed by C.R. Benedict of Benedict Slurry Seals, Inc. (Alpha, Ohio). Minor modifications to the base machine would enable Georgia Tech to perform loaded wheel research.

GDOT initiated research project No. 8503, *Development of a Simplified Test Method to Predict Rutting Characteristics of Asphalt Mixes* (*1*). The objectives of that study were to: (*a*) develop a simplified rut prediction test apparatus, (*b*) evaluate the rut prediction capability of the apparatus from the test results, and (*c*) compare the results obtained from the tests with those from creep tests and repeated load triaxial tests to evaluate rut predicting capability of the test method as compared with the other methods.

The first objective was accomplished by performing four specific tasks. All tasks involved making modifications to the base machine. First, a simple and effective means had to be devised for heating and maintaining a constant temperature in the asphaltic concrete specimens throughout the test period. After these modifications were made, the modified LWT was installed in an airtight room.

This airtight room was thermostatically controlled and heated to 35°C (95°F) with a maximum fluctuation of ±1.1°C (2°F). Georgia's mean summer temperature (hottest days) was 35°C (95°F), thus this temperature was chosen as the testing temperature.

The hard rubber wheel that was on the original machine was replaced with a 76-mm (3-in.) diameter aluminum wheel and a linear tube made of high-pressure rubber to which pressure ranging from 482 kPa (70 psi) to 827 kPa (120 psi) could be applied and controlled. The linear tube was placed stationary on top of the asphaltic concrete specimen and inflated to the desired pressure. Both ends of the tube were held in position with end clamps, which prevented the horizontal movement of the linear tube while allowing vertical flexibility. The aluminum wheel was attached to the reciprocating arm of the machine.

The next step involved developing a suitable means of holding the 76 mm x 76 mm x 381 mm (3 in. x 3 in. x 15 in.) beam sample. This specimen size was chosen because the maximum aggregate size used in Georgia asphaltic concrete mixes is slightly less than 38 mm (1 1/2 in.) and there was a need to adhere to the principle that the mixture thickness should be approximately twice that of the largest stone size in the mix. The kneading compactor to be used was already equipped for this size sample mold, and sample molds were also available that were this size. Beams to be tested were kept on flat steel plates in the test room for 24 hr at 35°C (95°F) for preconditioning.

Georgia Department of Transportation, 15 Kennedy Drive, Forest Park, Ga. 30050.

A curing and testing temperature of 35°C (95°F) was chosen to simulate the mean summertime temperature in Georgia. (Beams were initially cured at room temperature for 14 days before placement in the airtight room.) After the 24-hr period, the beams were transferred to the testing machine for testing.

Finally, GDOT needed to develop an easy and accurate means by which to measure the rutting profile on the specimens. A measuring channel was machined that would fit over the specimen so that a dial gauge could be used to measure the rutting profile.

The modifications proposed in this study were intended to produce a simplified apparatus to achieve easy and yet accurate predictions of rutting tendency of asphalt mixes.

Because the primary aim of this research was to evaluate the modified LWTs capability in predicting rutting tendencies of asphalt mixes, the initial testing was concentrated on only a few variables that were thought to be significant to potential rut development. These variables were tire pressure, testing temperature, and load.

These variables were controlled as follows:

- Tire pressure: 517 kPa (75 psi) and 689 kPa (100 psi)
- Temperature: 35°C (95°F)
- Load: 22.7 kg, 34 kg, and 45.4 kg (50 lb, 75 lb, and 100 lb, respectively)

During the test, rutting profiles of the beam were measured at predetermined numbers of repetition, such as 0, 40, 100, 400, 1000, and 4000 cycles. Results from the tests were then used to determine if the modified LWT was capable of predicting the rutting potential of asphalt mixtures.

Creep tests and repeated load triaxial tests have been shown to be capable of assessing the rutting potential of asphalt mixtures. These tests were performed in this study so that a comparison could be made between the results obtained from the use of the modified LWT and the results of these two tests.

Based on the characteristics of the results from the LWT tests and creep tests and the repeated load triaxial tests, the LWT test results seemed to produce results more in line with the rutting characteristics experienced on asphalt pavements. Originally, four mixes were chosen for this study with each mix exhibiting different degrees of rutting tendency in four different projects. Comparison between the field rutting characteristics and the magnitude of rutting from LWT tests of each mix provided a means to assess the applicability of the LWT tests in predicting the rutting potential of asphalt mixes. Unfortunately, there were many variables that hindered this effort. The differences in volumetric properties and Marshall stability and flow test results for the projects (Table 1), as well as other variables such as differences in the field compaction efforts and subsequent traffic conditions, were some of the variables that may have contributed to the differences in rutting characteristics of the four mixes in this study. Therefore, attempts to draw a conclusion on the correlation, if any, and the validity of the correlation among these four mixes in terms of the rutting observed in the field versus that from the LWT tests should be made with great caution.

In comparing the LWT with the quasi-static creep test and the repeated load triaxial test, the sample preparation and the testing for the creep test were easier to perform, whereas the repeated triaxial test was more difficult to perform. Unlike the modified LWT, which used a relatively simple loading system and deformation measuring device, the loading system and the deformation measuring device for the repeated triaxial load test used in this study were comparatively more complex.

FORMAL RESEARCH STUDIES

In July 1986, research project No. 8609, *Evaluation of Rutting Characteristics of Asphalt Mixes Using Loaded Wheel Tester* (2), was conducted by Georgia Tech for GDOT. The purposes of this study were to assess the rutting potential of six GDOT intermediate (B) type mixes and to evaluate the rutting resistance of six different modified mixes. These six mixes contained materials such as mineral fillers from Georgia Marble (Tate, Ga.), Trenton Sand Co. (Trenton, Ga.), and Sylacauga Sand (Sylacauga, Ala.). A polymer-modified asphalt cement using Kraton polymer and one handmade blend gradation to manually increase the percent of −300 μm (No. 50)-size particles were used to evaluate the importance of fine aggregate in the 300-μm (No. 50) sieve size range. The handmade gradation provided a straighter line blend between the 1.18-mm (No. 16) to 150-μm (No. 100) sieve sizes when plotted on the 0.45 power gradation chart.

GDOT found that incorporating the mineral filler from Georgia Marble Co., which has low fineness modulus and angular particle

TABLE 1 Comparison of Marshall Stability Test Results

		Stability		Flow		% Air	
Project	% AC	N	(lbs.)	mm	(.01 in.)	Voids	% VMA
IR-20(62)	6.0	8541	(1920)	3.8	(15.0)	2.89	15.13
MPC-401(73)	5.0	5262	(1183)	2.5	(9.7)	5.31	15.23
MPC-403(35) Lot 18	6.2	6032	(1356)	4.3	(17.1)	4.12	16.70
MPC-403(35) Lot 26	5.3	9181	(2064)	5.1	(19.9)	2.80	14.10

shape, into asphalt mixes improves the rutting resistance of the asphalt mixes (Table 2). It is worth noting that the Marshall stability test values of the mixes modified with 3 percent and 5 percent of this type of filler were actually lower than that of the corresponding standard mixes. Also, the benefit of using the handmade mixes over the standard mixes in improving rutting is significant (Table 3). This indicates the importance of the amount of material passing the 300-μm (No. 50) sieve and 150-μm (No. 100) sieve in the mix. The Marshall stability test values for the handmade mixes were lower than that of standard mixes. This reinforces the idea that Marshall stability test alone is inadequate to predict rutting potential of mixes.

As a result of this study, Georgia added specification requirements in January of 1987 for the No. 50 sieve into its current gradation specification requirements for all mixes.

Research Project No. 8706, *Evaluation of the Effect of Gradation of Aggregate on Rutting Characteristics of Asphalt Mixes* (*3*), was performed in early 1987. In this study, the effects of mix gradations on the rutting resistance was evaluated. Six mix gradations with aggregate top sizes ranging from 19 mm to 38 mm (¾ in. to 1½ in., respectively) were used. Also, these mix designs had amounts passing the 2.36-mm (No. 8) sieve ranging from 22 percent to 38 percent.

Results obtained from this study indicated that the modified intermediate coarse mix with a 19 mm (¾ in.) top size and 30 percent passing the 2.36-mm (No. 8) sieve substantially improved the rutting resistance when compared with the standard intermediate mix. This study also demonstrated that other aggregate characteristics such as angularity or surface texture were just as important, or more so, as gradation in reducing rutting potential.

TABLE 2 Comparison of Rutting Resistance of Mixes Containing 3 Percent and 5 Percent Mineral Filler (Georgia Marble) Versus Standard Mix

Mix Type	Rut Depth @ 2000 Cycles	
	mm	(in.)
FS	2.46	(0.097)
F3M	2.26	(0.089)
F5M	2.08	(0.082)
DS	2.31	(0.091)
D3M	2.13	(0.084)
D5M	2.11	(0.083)
CS	2.41	(0.095)
C3M	2.41	(0.095)
C5M	2.08	(0.082)

F = Limestone from Vulcan Materials at Fairmount, Georgia
D = Limestone from Vulcan Materials at Dalton, Georgia
C = Limestone from Vulcan Materials at Chattanooga, Tennessee
S = Standard or Control Mix
3M = Mixture with 3% Mineral Filler
5M = Mixture with 5% Mineral Filler

GDOT was convinced that the LWT would be beneficial in assessing the rutting susceptibility of asphalt mixes, but the machine was not a portable, self-contained unit. GDOT Research Project No. 8717, *Development of a Laboratory Rutting Resistance Testing Method for Asphalt Mixes* (*4*), was implemented in late 1987 to address this concern.

The objective of this study was to modify and improve the machine and the sample preparation method and to develop a testing procedure for using this machine. Improvements and modifications made to the LWT included the development of an environmental chamber to house the machine and to maintain a constant elevated temperature during testing. Heat strips inside the environmental chamber were used to elevate the temperature.

Modifications also included the development of a preheating box for preconditioning the test sample to the prescribed elevated temperature. Other minor modifications and improvements were made for the control and operation of the testing machine.

GDOT implemented LWT testing on a routine basis for the interstate projects and major state routes immediately. GDOT's experiences with the LWT allowed us to develop GDT-115, Method of Test for Determining Rutting Susceptibility Using the Loaded Wheel Tester. This method (implemented in 1989) defines the beam preparation procedure, beam testing procedure, and maximum rut depth allowable.

IN-HOUSE LWT STUDIES

Several "in-house" studies were performed by GDOT from 1987 to 1993. After careful consideration of in-place pavement temperatures during warm summer months, the testing temperature was increased to 40.6°C (105°F) before creating a data base. The 45.4-kg (100-lb) load and 689-kPa (100-psi) hose pressure exerts approximately 689 kPa (100 psi) of contact pressure on the sample. Also, in 1993, GDOT received a triple-track wheel tester developed by Georgia Tech. The in-house studies performed by GDOT were:

- Effects of increased temperature, load, and grade of asphalt cements on LWT Specimens (SP 92001)
- Comparison of AC-20s and 30s typically used in Georgia
- Stone matrix asphalt versus conventional mixes
- Crumb rubber versus conventional mixes

EFFECTS OF INCREASED TEMPERATURE, LOAD, AND GRADE OF ASPHALT CEMENTS ON LWT SPECIMENS

GDOT realized that in previous studies the effects of testing temperatures greater than 40.6°C (105°F) and hose pressures greater than 689 kPa (100 psi) had not been adequately researched, nor had the performance differences in asphalt cement grades (AC-10, AC-20, AC-30). So GDOT performed a research study in which the ele-

TABLE 3 Effects of Handmade Gradation on Rutting

Mix Type	Ruth Depth @ 2000 Cycles		Marshall Stability	
	mm	(in.)	N	(lbs.)
FS	2.46	(0.097)	11076	(2490)
FHM	1.83	(0.072)	9386	(2110)
DS	2.31	(0.091)	9074	(2040)
DHM	1.93	(0.076)	8674	(1950)
CS	2.41	(0.095)	8985	(2020)
CHM	2.26	(0.089)	8185	(1840)

HM = Handmade gradation

vated temperature, increased load, and different grades of asphalt cement were evaluated. It was concluded from this study that varying the hose pressure, temperature, and grades of asphalt cement yielded significant differences in rut depth.

The LWT showed that AC-20 is much more sensitive to temperature variations than AC-30 (Table 4). AC-20 Specimens were tested for an average of 4046 cycles at 48.9°C at 689 kPa (120°F at 100 psi). Testing of these samples was discontinued at this point because of excessive rutting. The rut depth was theoretically projected to 8000 cycles for comparison purposes. The average rut depth for AC-20 increased by 19 mm (0.753 in.) once the temperature was increased to 48.9°C (320°F) as compared with an increase of only 7.6 mm (0.298 in.) for AC-30. AC-10 is not used in Georgia as a hot-mix paving grade, and its use in this study was canceled because of its excessive rutting under standard conditions. Therefore, temperature change has the most pronounced effect on rut depth as determined by the conditions used in this study.

In comparison, if the temperature remained constant at 40.6°C (105°F) and the hose pressure was increased from 689 to 827 kPa (100 to 120 psi), the rut depth only increased by 7.90 mm (0.311 in.) for AC-20 and 2.57 mm (0.101 in.) for AC-30 (Table 5). This showed that increases in tire pressure have a direct effect on pavement rutting but not nearly as much as increases in pavement temperatures.

COMPARISON OF ASPHALT CEMENTS TYPICALLY USED IN GEORGIA

GDOT conducted a study in which different asphalt cements typically used in Georgia were evaluated. The objective of this study was to evaluate the contribution of AC to rutting resistance of a mix. LWT results were used for each asphalt cement and compared to determine which source of materials yields the most favorable results to rut resistance.

Loaded wheel testing by GDOT of these six asphalt cements was performed at both 40.6°C (105°F) and 48.9°C (120°F). Based on rut susceptibility and results of other physical characteristics, GDOT ranked these asphalt cements as follows:

Rank	*Code*
1	B
2	E
3	C
4	A
5	D
6	F

GDOT arranged with the National Center for Asphalt Technology (NCAT) at Auburn University to perform Strategic Highway Research Program (SHRP) binder testing on these asphalt cements. NCAT was chosen because of its proximity to GDOT's Forest Park Laboratory. NCAT concluded that all six asphalts complied with the requirements for SHRP 64-22 specifications. The RTFOT results were related more to rutting resistance than the other test conditions because this represents asphalt cement as it comes out of the asphalt plant. Also, dynamic shear numbers greater than 2.2 kPa indicate greater elasticity.

Rolling Thin-Film Oven Test

Rank	*Dynamic Shear*
1	B
2	C
3	E
4	F
5	A
6	D

The AC-30's all performed better than the AC-20's in this study. Loaded wheel test and NCAT results both agreed that asphalt "B" was the most desirable asphalt cement. This is another indication that the LWT is capable of assessing the rut susceptibility of asphalt mixes.

TABLE 4 Effects of Temperature Change on Rut Depth

Grade of AC	Test Conditions	No. of Cycles Tested	Projected Rut Depth @ 8000 Cycles	
			mm	(in.)
AC-30	40.6°C/689 kPa (105°F/100 PSI)	8000	3.33	(0.131)
AC-30	48.9°C/689 kPa (120°F/100 PSI)	8000	10.90	(0.429)
AC-20	40.6°C/689 kPa (105°F/100 PSI)	8000	4.01	(0.158)
AC-20	48.9°C/689 kPa (120°F/100 PSI)	4046	23.14	(0.911)

STONE MATRIX ASPHALT MIXES

In 1990, GDOT started experimentation with stone matrix asphalt (SMA) mixes. SMA was developed in Europe during the early 1960s. It has a high coarse aggregate content that provides resistance to deformation and efficient load distributions through stone-to-stone contact. The voids in the aggregate structure are filled with a voidless mastic composed of fine-graded, quality mineral filler and crushed fine aggregate. The SMA mix utilizes a high-asphalt cement content that requires the use of stabilizing additives such as polymers or fibers to keep the thick asphalt films from draining off the aggregate during mixing and handling. LWT results on the SMA mix cores versus the conventional mix cores from a test section on I-85 were very distinguishing. All SMA mixes had rut depths approximately one-half that of the conventional mixes.

CRUMB RUBBER

Georgia has also performed research on crumb rubber mixes versus standard mixes. A test section was placed on I-75 in Henry County that contained 6 percent crumb rubber by weight of the AC. The wet process was used to blend −180-μm (No. 80) mesh rubber with an AC-20 asphalt cement. The crumb rubber designs were more rut resistant as compared with the standard mixes. Laboratory designs showed the crumb rubber to rut one-half as much as the standard mixes −1.37 mm versus 2.64 mm (0.054 in. versus 0.104 in., respectively). Field verification of designs differed slightly for the crumb rubber. The average rut depth for beams fabricated from plant mix was 2.21 mm (0.087 in.) for the rubber and 2.62 mm (0.103 in.) for the standard mix. Average rut depths for beams cut from cores were 2.31 mm (0.091 in.) for the mix containing rubber and 2.41 mm (0.095 in.) for the standard mix.

OTHER RESEARCH

Research studies were conducted in which the LWT was used to compare different mix types and modified mixes that were being evaluated in the field. One such project was on I-75 in Whitfield County, Georgia. A test section was placed on the roadway that contained four polymer-modified asphalt cements. The performance of each section was compared with the standard mix. LWT results indicated that each modified mix would be less susceptible to rutting as compared with a standard mix.

GDOT has also worked with the FHWA to develop and improve the LWT. FHWA was interested in the LWT as a economical

TABLE 5 Effects of Pressure Changes on Rut Depth

Grade of AC	Test Conditions	No. of Cycles Tested	Projected Rut Depth @ 8000 Cycles	
			mm	(in.)
AC-30	40.6°C/689 kPa (105°F/100 PSI)	8000	5.89	(0.232)
AC-30	40.6°C/827 kPa (105°F/120 PSI)	8000	3.33	(0.131)
AC-20	40.6°C/689 kPa (105°F/100 PSI)	8000	4.01	(0.158)
AC-20	40.6°C/827 kPa (105°F/120 PSI)	6580	11.91	(0.469)

proof tester of asphaltic concrete mixes. In order to obtain a thorough unbiased assessment of the machine, the FHWA set aside funding for round-robin testing so that other states could evaluate the LWT.

Six states participated in this evaluation. At the end of the evaluation, a technical working group comprised of these states met in Georgia to discuss their findings.

One of the state agencies involved in this evaluation, the Florida Department of Transportation, compared the LWT with: (*a*) actual field performance, (*b*) gyratory shear, and (*c*) Marshall stability test. The LWT results were comparable with the actual field performance and the gyratory shear.

Overall results from this limited scope round-robin test program showed that reasonable consistency of rut-depth results from the LWT was achieved by each participating laboratory. The within-laboratory repeatability coefficient of variation was 12.7 percent. The between-laboratory variability of rut-depth results was quite high, primarily because of large variation of asphalt beam densities between laboratories.

FHWA has developed an expert task group to evaluate the performance of the LWT as an indicator of rut susceptibility. More research is currently being conducted so that more agencies can participate. Eleven agencies are now involved in this study. The round-robin testing will be conducted in two phases. Phase I of the program will evaluate the applicability of the LWT only, whereas Phase II of the program will evaluate the applicability of the rolling compactor machine together with the LWT.

TRIPLE-TRACK TESTER

GDOT now has a triple-track wheel tester that was built by Georgia Tech. It has the capability of testing three samples simultaneously. GDOT needed a machine with three sample testing capabilities so that production could be increased and more than one sample of a given design could be tested at one time.

Also, the sample size has been increased to 127 mm (5 in.) wide to better accommodate testing of coarse mixtures. It was also felt for a long time that a specimen 76 mm (3 in.) wide may not be adequate for base mixes with 38 mm (1 1/2 in.) or larger nominal top sizes. This machine compared identically with the single-track machine.

CONCLUSIONS

GDOT has been working with the LWT for several years and a lot of time, effort, and confidence has been put into this machine as an indicator of mixture rutting susceptibility.

During this 7-year period, GDOT has found that the LWT has several benefits. The first benefit is that it's a proof tester. Asphalt mix can be evaluated in the laboratory instead of under traffic, which allows pavement performance to be predicted and problem mixes identified before being placed in the field.

Another benefit of the LWT is that it can be used as a supplement to SHRP testing. SHRP Level 1 mix designs have no strength test requirements other than for moisture susceptibility testing, and the LWT may be used to proof test these designs.

Also, SHRP mix design criteria identify a forbidden zone through which mix gradations should not pass. This forbidden, or restrictive, zone needs additional study because it is not applicable in all situations. For example, the handmade gradation that was mentioned earlier passes through this zone, but the LWT showed this type of mix to have a low susceptibility to rutting.

The Georgia LWT is also economically feasible. The single-track machine may be purchased from Benedict Slurry Seal for approximately $11,000, not including compactor. The Georgia triple-track machine is being sold by Georgia Tech at a cost of approximately $35,000, including compactor. The French wheel tracker and compactor costs approximately $200,000.

The LWT can give an indication of the rut susceptibility of a mix for a relatively low cost. It can be used in conjunction with the SHRP mix design specification criteria and as a proof tester will be a good supplement to SHRP Superpave mix designs.

REFERENCES

1. Lai, J. S. *Development of a Simplified Test Method to Predict Rutting Characteristics of Asphalt Mix*. Georgia DOT Project 8503, Final Report. Georgia Department of Transportation, Forest Park, Ga., 1986.
2. Lai, J. S. *Evaluation of Rutting Characteristics of Asphalt Mixes Using Loaded-Wheel Tester*. Georgia DOT Project 8609, Final Report. Georgia Department of Transportation, Forest Park, Ga., 1986.
3. Lai, J. S. *Evaluation of the Effect of Gradation of Aggregate on Rutting Characteristics of Asphalt Mixes*. Georgia DOT Project 8706, Final Report. Georgia Department of Transportation, Forest Park, Ga., 1988.
4. Lai, J. S. *Development of a Laboratory Rutting Resistance Testing Method for Asphalt Mixes*. Georgia DOT Project 8717, Final Report. Georgia Department of Transportation, Forest Park, Ga., 1989.

Publication of this paper sponsored by Committee on General Asphalt Problems.

Evaluation of Stone-on-Stone Contact in Stone-Matrix Asphalt

E. R. BROWN AND RAJIB BASU MALLICK

The presence of stone-on-stone contact and a relatively low percentage of fine aggregate are two characteristics of stone-matrix asphalt (SMA). Although it is known that the stone skeleton in SMA is primarily responsible for its high rutting resistance, a method to quantitatively determine stone-on-stone contact has not been used in the United States. A simple laboratory method was developed to determine stone-on-stone contact in SMA with conventional hot-mix asphalt parameters such as voids in mineral aggregate, voids in coarse aggregate, and dry-rodded weight of coarse aggregate. Tests were conducted to evaluate the effect of percent passing the 4.75-mm sieve on the susceptibility of mix stability to change in void content. It was observed that mixes with a low percent passing the 4.75-mm sieve were less sensitive to low air void contents. Mixtures with a low percent passing the 4.75-mm (No. 4) sieve (30 percent or less) tended to have stone-on-stone contact.

Stone-matrix asphalt (SMA) has proven to be a rut-resistant and cost-effective surface layer material in Europe for more than 20 years. A number of SMA projects have been constructed in the United States since 1991 to evaluate its performance, and these projects will continue to be monitored for several years. Unlike conventional hot-mix asphalt (HMA), SMA mixtures are characterized as stone-on-stone contact (*1*). SMA derives its strength primarily from the stone-on-stone skeleton developed in the mix (*2–4*). The stone-on-stone skeleton is shown schematically in Figure 1, which also shows the coarse aggregate contact for an SMA gradation and the less coarse aggregate contact for a dense-graded mixture. Though there has been much discussion about SMA mixtures having stone-on-stone contact, a method needs to be selected to actually determine quantitatively whether stone-on-stone contact exists. (*5*). Also, because performance of SMA has been shown to be significantly affected by aggregate gradation (*6*), there is a need to evaluate the effect of percent passing the 4.75-mm sieve on stability of SMA mixes.

OBJECTIVE

The objectives of this study were to develop a method to measure stone-on-stone contact in SMA mixes and to evaluate the effect of stone-on-stone contact on the stability of mixes.

SCOPE

The results presented in this paper were obtained from two studies; one was conducted to evaluate stone-on-stone contact in SMA (with gravel and limestone aggregates), and the other was conducted to evaluate the effect of percent passing the 4.75-mm sieve on stability of mixes (with limestone aggregates). To evaluate stone-on-stone contact in SMA mixes, studies were carried out with gravel and limestone aggregates and 0.3 percent European cellulose fibers. Mixes were made by varying the percent of materials passing the 4.75-mm sieve, starting at 50 percent and going down to 15 percent. Two types of void were plotted against percent passing the 4.75-mm sieve: the void in mineral aggregates (VMA), and the void in coarse aggregates (VCA). VCAs were calculated in a way similar to VMAs by replacing percent of aggregates in the mix with percent of coarse aggregates in the calculation. The curves for VMA and VCA versus percent passing the 4.75-mm sieve were compared with that for the VCA obtained from the dry-rodded test of coarse aggregates to determine whether stone-on-stone contact existed.

Marshall stability was measured for gravel and limestone mixes (in the stone-on-stone contact study), and gyratory test properties were measured for limestone mixes (in the evaluation of effect of percent passing the 4.75-mm sieve). These properties were measured at different percents passing the 4.75-mm sieve and at different asphalt (air void) contents. Comparisons of changes in stability and gyratory properties with changes in air void content were made for the different mixes.

TEST PLAN

To obtain optimum resistance to rutting, it is believed that stone-on-stone contact in the coarse aggregate portion of the SMA mixture is required. In the past, stone-on-stone contact has been very subjective and has only been evaluated by visual observation from cored samples. There is a need to develop a method to quantify when stone-on-stone contact occurs to ensure that it is sufficient to provide the desired properties.

It was decided that stone-on-stone contact could be evaluated from the VMA and VCA curves. Stone-on-stone contact is considered to begin at the point at which the VCA plot begins to curve as the amount of material passing the 4.75-mm sieve is reduced. It also is considered to begin at the point at which the VMA begins to increase as the percent passing the 4.75-mm sieve is reduced. A third measure of stone-on-stone contact is when the voids in the dry-rodded condition are equal to or greater than the VCA in the SMA mixture.

Two types of aggregates, gravel and limestone, were used for this study. Coarse and fine aggregates refer to materials retained on and passing the 4.75-mm sieve, respectively. Mixes were produced with various percents of material passing the 4.75-mm sieve: 50, 40, 30, 25, 20, and 15 percent. The gradations are shown in Table 1. The binder used for the mixes was an AC-20 asphalt cement from Chevron, Inc., U.S.A. (Mobile, Ala.).

National Center for Asphalt Technology, Auburn University, Auburn, Ala. 36849.

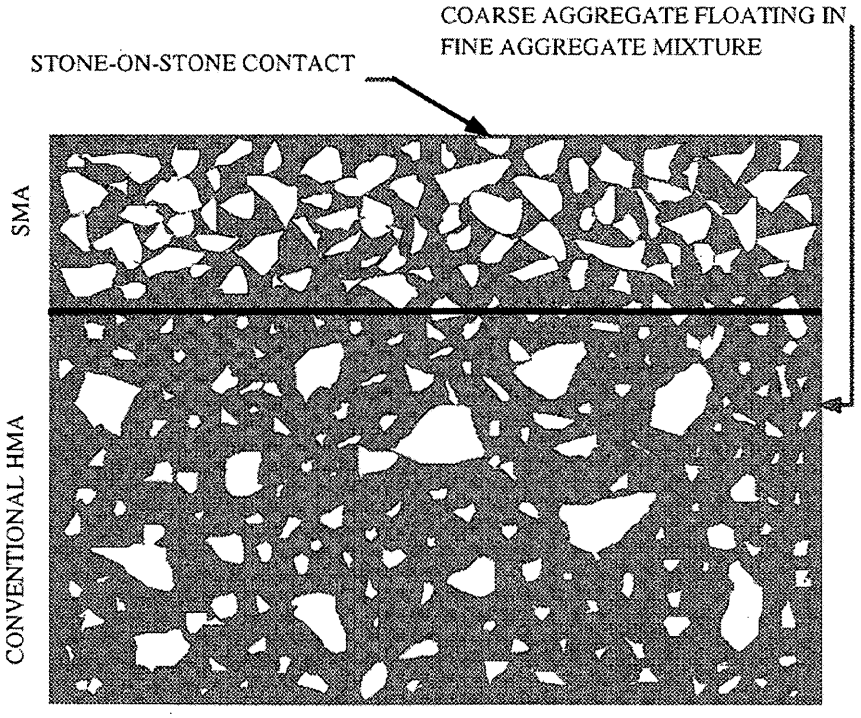

FIGURE 1 Section showing difference in stone-on-stone contact between SMA and conventional HMA.

TABLE 1 Gradation of Aggregates

Sieve Size	Percent Passing					
	MIX					
	A	B	C	D	E	F
12.5 mm (1/2 inch)	100	100	100	100	100	100
9.50 mm (3/8 inch)	75	70	65	63	60	58
4.75 mm (No. 4)	50	40	30	25	20	15
2.36 mm (No. 8)	40	32	25	21	18	15
1.18 mm (No. 16)	34	28	22	19	16	15
0.60 mm (No. 30)	30	25	20	18	15	15
0.30 mm (No. 50)	22	19	17	16	15	14
150 μm (No. 100)	15	15	14	14	13	12
75 μm (No. 200)	10.0	10.0	10.0	10.0	10.0	10.0

LIMESTONE AGGREGATES USED IN GYRATORY TESTS

Sieve Size	Percent Passing					
	MIX					
	A	B	C	D	E	F
12.5 mm (1/2 inch)	100	100	100	100	100	100
9.50 mm (3/8 inch)	83	80	78	77	74	72
4.75 mm (No. 4)	50	40	35	30	25	20
2.36 mm (No. 8)	38	30	27	24	20	16
1.18 mm (No. 16)	28	24	22	20	17	15
0.60 mm (No. 30)	22	19	16	16	14	14
0.30 mm (No. 50)	17	15	14	14	12	12
150 μm (No. 100)	12	12	11	11	11	11
75 μm (No. 200)	10.0	10.0	10.0	10.0	10.0	10.0

Samples were prepared using 0.3 percent cellulose fiber (a typical cellulose made in Europe) and agricultural lime as the filler. Mix designs were performed with the mechanical Marshall compactor (50 blows) by preparing and compacting samples with asphalt content varied in 0.5 percent increments. Three samples were made for each asphalt content. The optimum asphalt content was chosen as the asphalt content that produced 3.0 percent air voids. VMA and VCA were calculated for the compacted samples. VCA was calculated by replacing percent of aggregates in the mix (used in VMA calculations) by percent of coarse aggregates in the calculations. The equations used for calculating VMA and VCA were:

$$\text{VMA} = 100 - \frac{V_{agg}}{V_T}(100)$$

$$\text{VCA} = 100 - \frac{V_{CA}}{V_T}(100)$$

where

V_{agg} = volume of aggregate calculated using bulk specific gravity,
V_T = total volume of compacted mixture, and
V_{CA} = volume of coarse aggregate calculated using bulk specific gravity.

To measure the VCA with no fine aggregates, the coarse aggregate was placed in a container and dry rodded to maximum density in accordance with ASTM C29. The aggregates were rodded when the container was one-third full, two-thirds full, and full. The VCA in the dry-rodded condition represents stone-on-stone contact. The VMA and VCA at the optimum asphalt content were then plotted against the percent passing the 4.75-mm sieve and compared with

the VCA for a mix without any fine aggregates. The point at which the VCA in the mixture was equal to the VCA in the dry-rodded condition was the point at which it was assumed that stone-on-stone contact existed. Other measures of stone-on-stone contact were the points at which the VMA curve starts upward as the percent passing the 4.75-mm sieve is reduced, and the point at which the VCA curve began to flatten. A schematic of the test plan is shown in Figures 2 and 3.

To observe the effects of reducing the percent passing the 4.75-mm sieve, Marshall stability tests were conducted on the mixes having different asphalt contents (voids). A different set of mixes containing limestone aggregates were compacted in the Corps of Engineers gyratory testing machine (GTM) at various asphalt (air void) contents to observe the effect of percent passing the 4.75-mm sieve on the gyratory shear index (GSI) and the gyratory shear (Sg). The gradations of the limestone aggregates are shown in Table 1.

TEST RESULTS AND ANALYSIS

The results of VMA and VCA measurements for different mixes are shown in Tables 2 and 3. The variations of VMA and VCA with percent passing the 4.75-mm sieve are shown in Figures 4 and 5 for gravel and limestone, respectively. The VCA for the dry-rodded weight is also shown as an indication of the point where stone-on-stone contact begins to occur. For gravel, the VCA plot began to curve at 30 percent, the VMA curve started to increase at 30 percent (as the percent passing the 4.75-mm sieve was reduced), and the VCA of mix crossed the VCA line (dry rodded) at 26 percent. For gravel, the data show that stone-on-stone contact began at 26 to 30 percent passing the 4.75-mm sieve and was present for any percent less than 26 to 30. For limestone, the VCA plot began to curve and the VMA started to increase at 25 percent (as the percent passing the 4.75-mm sieve was reduced), whereas the VCA curve of the SMA mix crossed the VCA line (dry rodded) at 32 percent. For

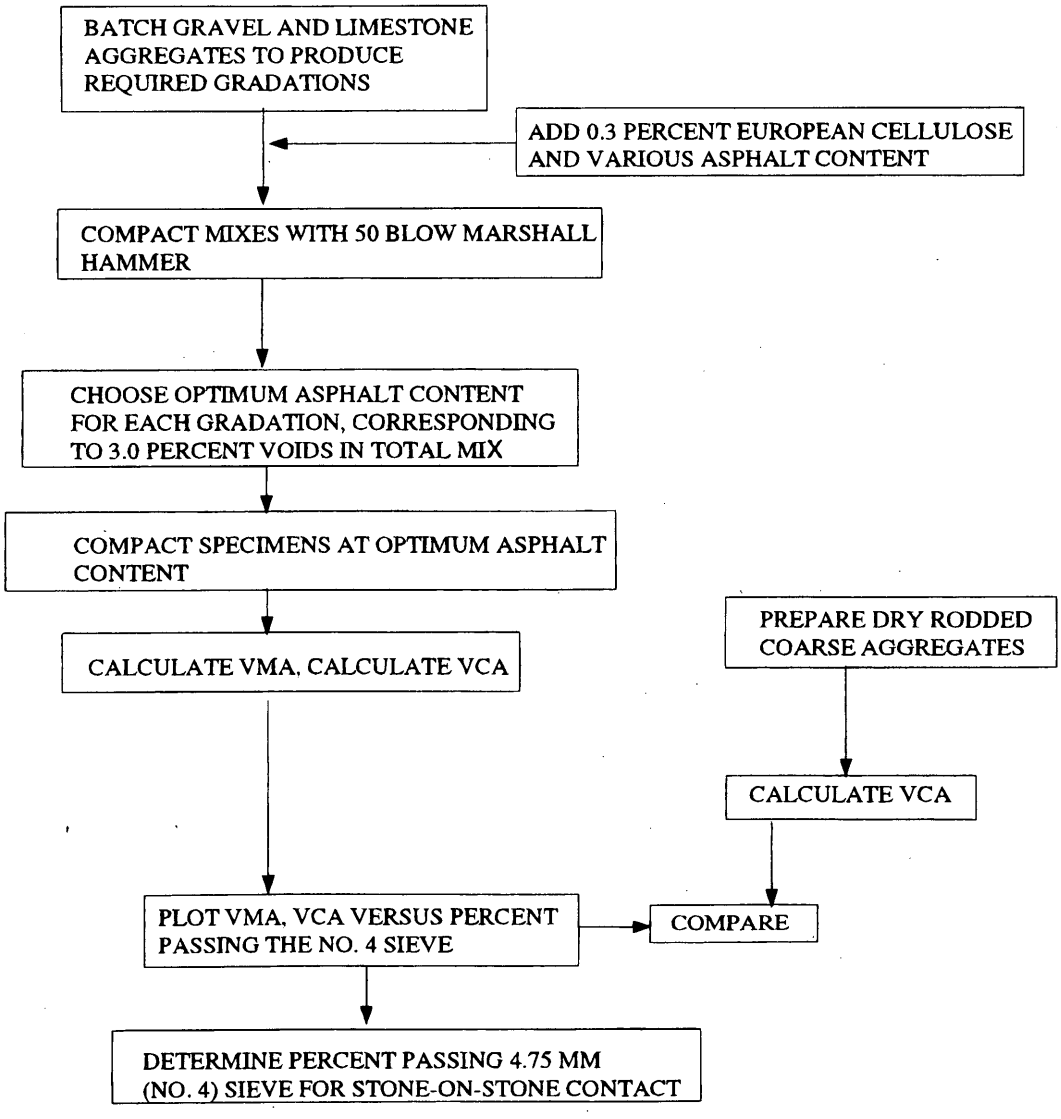

FIGURE 2 Test plan for evaluation of stone-on-stone contact.

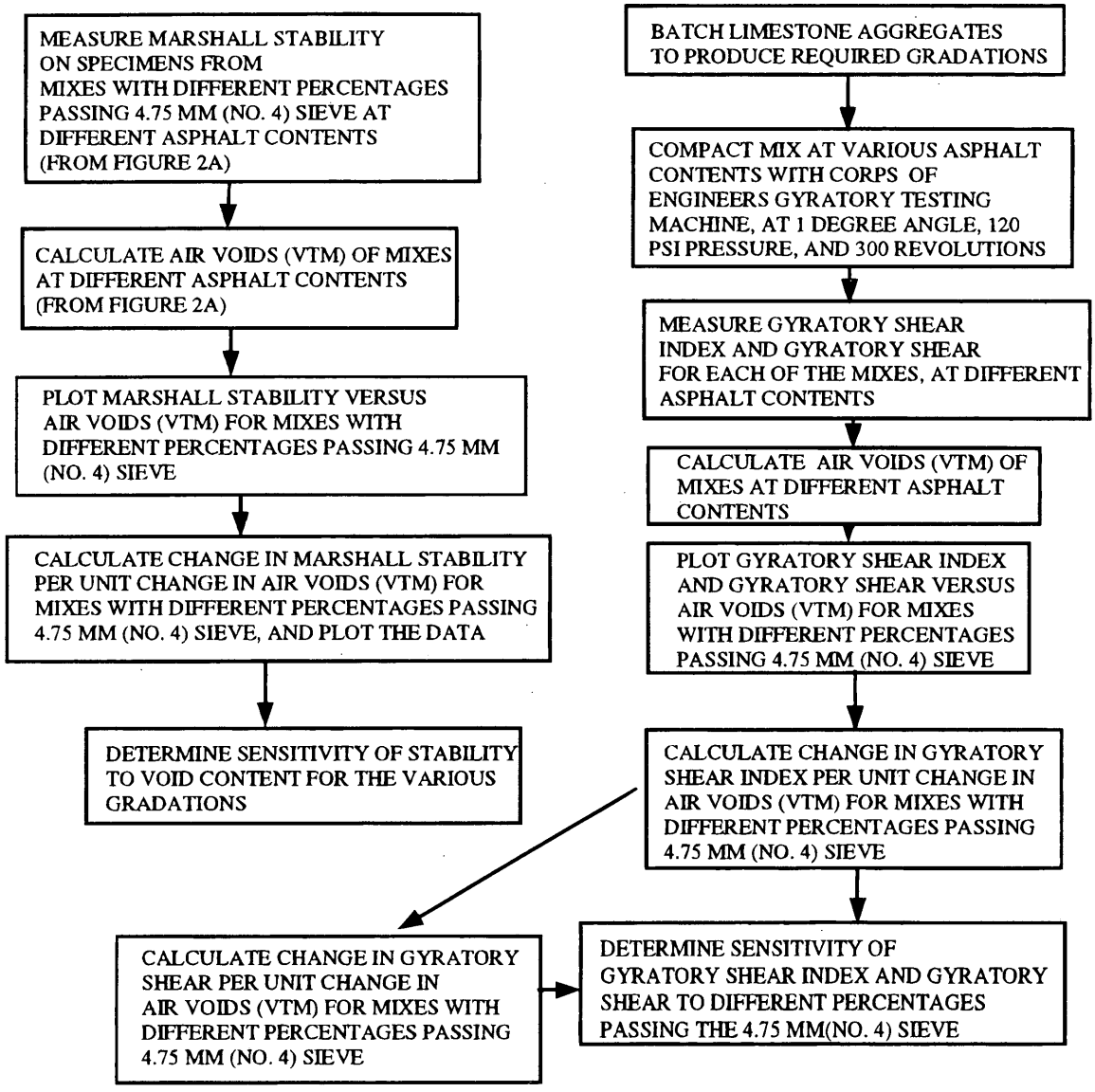

FIGURE 3 Test plan for evaluation of effect of percent passing 4.75-mm (No. 4) sieve on mix stability.

limestone, stone-on-stone contact began at 25 to 32 percent passing the 4.75-mm sieve.

The VMA content began to increase as the fine aggregate content was reduced when stone-on-stone contact began. Once coarse aggregate contact was made, a decrease in percent passing the 4.75-mm sieve did not result in an equal decrease in the VCA, and thus the VMA increased. From this point, removal of fine aggregates did not contribute to further densification of the coarse aggregate portion of the mix, and thus increased the VMA. Also, VCA in the dry-rodded condition was near the VCA for 30 percent passing (26 for gravel and 32 for limestone) the 4.75-mm sieve in both the mixes. Thus for these two mixtures, it can be assumed that stone-on-stone contact existed at less than 30 percent passing the 4.75-mm sieve and did not exist at more than 30 percent passing the 4.75-mm sieve.

The dry-rodded test seems to be a good method to determine the density of the coarse aggregate required for stone-on-stone contact. This is a simple test that can readily be conducted in most laboratories. It is believed that stone-on-stone contact occurs when the density of the coarse aggregate in the SMA mixture is equal to or higher than that measured in the dry-rodded test. This is because irrespective of the amount of fines present in a mix, the density of the rigid stone-on-stone skeleton should be approximately the same as that achieved in the dry-rodded condition. When the VCA of the dry-rodded aggregate and the density of the coarse aggregate in an SMA mix are the same, it means that the coarse aggregate in the SMA mix is at least as closely packed as that in the dry-rodded mix. Because the VCA in the dry-rodded mix represents a stone-on-stone condition, it is concluded that a similar condition exists in the SMA mix.

This study identified three possible ways to ensure stone-on-stone contact in the coarse aggregate portion of SMA mixtures. The first way was to develop a plot of VCA versus percent passing the 4.75-mm sieve. In this series of tests, the percent passing the 4.75-

TABLE 2 Summary of Volumetric and Marshall Stability Properties of Gravel Mixes

PERCENT PASSING 4.75 MM (NO. 4) SIEVE	ASPHALT CONTENT (%)	TMD	VTM	VMA	VCA	MARSHALL STABILITY (N)
50	5.0	2.435	3.4	14.0	57.0	12,298
	5.5	2.418	2.2	14.0	57.0	10,800
	6.0	2.400	1.7	14.6	57.3	8,520
	6.5	2.384	1.4	15.4	57.7	7,520
	5.1	2.431	2.9	13.8	56.9	-
40	5.0	2.435	3.6	14.2	48.5	10,213
	5.5	2.418	2.2	14.0	48.4	9,524
	6.0	2.401	1.7	14.6	48.8	7,986
	6.5	2.384	1.2	15.3	49.2	7,035
	5.2	2.429	2.9	14.0	48.4	-
30	4.5	2.449	5.1	14.6	40.2	10,169
	5.0	2.431	4.6	15.2	40.7	9,213
	5.5	2.414	3.3	15.2	40.6	7,453
	6.0	2.397	2.0	15.0	40.5	7,924
	5.4	2.418	2.8	14.4	40.1	-
25	5.7	2.414	4.0	15.9	36.9	7,613
	6.0	2.404	2.7	15.4	36.6	7,369
	6.5	2.386	2.2	16.1	37.1	7,924
	7.5	2.353	1.6	17.6	38.2	7,231
	5.9	2.407	3.2	15.6	36.7	-
20	4.5	2.446	7.5	16.9	33.5	7,582
	5.0	2.428	6.7	17.2	33.7	7,364
	5.5	2.411	5.5	17.1	33.7	7,422
	6.0	2.394	4.4	17.2	33.8	7,564
	6.6	2.374	3.9	18.1	34.4	-
15	6.0	2.409	6.7	18.7	30.9	6,987
	6.5	2.392	5.8	18.9	31.1	6,489
	7.0	2.375	5.3	19.5	31.6	6,213
	7.5	2.359	4.0	19.4	31.5	6,533
	8.0	2.343	2.9	19.5	31.5	-
DRY RODDED COARSE AGGREGATE	-	-	-	-	37.6	-

- DATA NOT AVAILABLE 1 N = 0.225 LBF

mm sieve was decreased to a point at which the straight line relationship began to curve. This curve was caused by the development of stone-on-stone contact, which prevented a closer packing of the coarse aggregate as the amount of fine aggregate was reduced. This occurred at approximately 30 percent passing the 4.75-mm sieve for the two mixtures evaluated (Figures 4 and 5).

A second method that appeared to have some possibility of identifying the occurrence of stone-on-stone contact in the coarse aggregate fraction is the VMA plot. These data can be generated at the same time as the VCA data, so no extra testing is required. As the percent passing the 4.75-mm sieve was decreased, the VMA plot was essentially flat until stone-on-stone contact began to develop; then the VMA began to increase. This increase in VMA resulted because the coarse aggregate cannot be moved closer together with a reduction in the percent of fine aggregate when stone-on-stone contact exists. This method can be used to estimate the point at which stone-on-stone contact occurs in a way similar way to the VCA method. This method also shows that stone-on-stone contact occurs at approximately 30 percent passing the 4.75-mm sieve. Both of these methods require a significant amount of testing.

A third method used in this study to measure stone-on-stone contact involved using the dry-rodded test for voids in coarse aggregate. Only coarse aggregate is used in this test, and the dry-rodded condition is a measure of stone-on-stone contact. As long as the density of the coarse aggregate in an SMA mixture is equal to or greater than the dry-rodded density, stone-on-stone contact should exist. The compacted condition of the coarse aggregate can be quantified by VCA or by the density of the coarse aggregate. This is a very simple test that involves very little time. As shown in Figures 4 and 5, this method gives about the same results as the VCA and VMA methods described previously. These methods of measuring stone-on-stone contact seem promising, but more data need to be generated, and other possible methods should be evaluated.

Effect of Percent Passing the 4.75-mm Sieve on Mixture Stability

As stone-on-stone contact is gradually achieved in a mix, with a decrease in percent passing the 4.75-mm sieve, the mix becomes

TABLE 3 Summary of Volumetric and Marshall Stability Properties of Limestone Mixes

PERCENT PASSING 4.75 MM (NO. 4) SIEVE	ASPHALT CONTENT (%)	TMD	VTM	VMA	VCA	MARSHALL STABILITY (N)
50	4.0	2.640	4.3	13.6	56.8	14,156
	4.5	2.619	3.3	13.8	56.9	12,867
	5.0	2.588	1.9	14.0	57.0	10,675
	5.5	2.567	1.1	14.5	57.3	8,511
	4.6	2.605	2.9	14.0	57.0	-
40	4.0	2.640	4.8	14.0	48.4	-
	4.5	2.619	4.0	14.5	48.7	11,480
	5.0	2.588	2.1	14.2	48.5	9,702
	4.8	2.606	3.2	14.4	48.6	-
30	4.0	2.629	5.3	14.8	40.4	9,320
	4.5	2.608	4.1	14.9	40.4	8,556
	5.0	2.588	2.9	14.9	40.4	8,013
	4.9	2.592	3.0	14.8	40.3	-
25	4.5	2.619	5.4	15.7	36.7	9,614
	5.0	2.598	3.1	14.7	36.0	8,924
	5.5	2.577	2.4	15.3	36.5	7,711
20	4.0	2.635	7.1	16.3	33.0	8,502
	4.5	2.613	5.8	16.3	33.0	8,298
	5.0	2.592	4.3	16.0	32.8	7,787
	5.5	2.572	3.2	16.2	32.9	7,542
	5.6	2.568	3.1	16.3	33.1	-
15	5.0	2.606	6.4	17.4	29.8	7,800
	5.5	2.585	5.1	17.4	29.8	7,689
	6.0	2.565	3.9	17.5	29.8	7,120
	6.5	2.545	3.3	18.0	30.3	7,342
	7.0	2.525	2.4	18.3	30.5	-
DRY RODDED COARSE AGGREGATE	-	-	-	-	42.2	-

- DATA NOT AVAILABLE

1 N = 0.225 LBF

less sensitive to a change in air voids. The presence of fines in a mix is similar to the presence of silt or clay in soil and results in a buildup of pore pressure under loading at low void contents (near saturation). However, in the case of stone-on-stone contact with a smaller amount of fines, the mix behaves more like a free-draining soil, having less pore-pressure effects. This causes the mix to be less sensitive to a change in asphalt content, just as a soil that drains freely is less sensitive to moisture content.

Marshall stability tests were conducted on the gravel and limestone mixes at different asphalt (voids) contents to observe the effect of percent passing the 4.75-mm sieve on the sensitivity of the mixes. Although Marshall stability may not be a good indicator of field stability, this test was chosen because it is a relatively simple test with which to evaluate change in stability with change in asphalt content (*7*). The results of the tests are summarized in Tables 2 and 3. Insufficient stability data were available for analysis of the limestone aggregate for 25, 30, and 40 percent passing the 4.75-mm sieve. Figures 6 and 7 show the effect of voids on Marshall stability for the different mixes. Marshall stability was observed to decrease significantly with a decrease in air void content for mixes with 50, 40, and 30 percent passing the 4.75-mm sieve. Conversely, stability remained almost constant with a change in air void content for mixes with low percent passing the 4.75-mm sieve (20 and 25 percent).

The change in stability per unit change in voids was calculated for the different mixes and plotted in Figure 8. The change in stability decreased with a decrease in percent passing the 4.75-mm sieve, indicating that mixes become less sensitive to air void content at lower percents passing the 4.75-mm sieve. For gravel, the change in stability per unit change in air voids decreased from 2300 N for 50 percent passing the 4.75-mm sieve to about 75 N for 25 percent passing the 4.75-mm sieve. Below 25 percent, the change increased slightly but remained at about 150 N per percent voids at both 20 and 15 percent passing the 4.75-mm sieve. For limestone, the change was about 1700 N per percent voids at 50 percent passing the 4.75-mm sieve and decreased to about 200 N per percent voids at 15 percent passing the 4.75-mm sieve. These data appear to confirm that 30 percent passing the 4.75-mm sieve (the point at which stone-on-stone contact occurs) is the point that separates mixtures that are sensitive to changes in voids from mixtures that are not.

GSI and Sg of Limestone Compacted in the GTM

Additional limestone mixes were compacted in the GTM at various asphalt (void) contents. The compactions were performed at 120 psi vertical pressure, 1 degree vertical angle, and 300 revolutions. Dur-

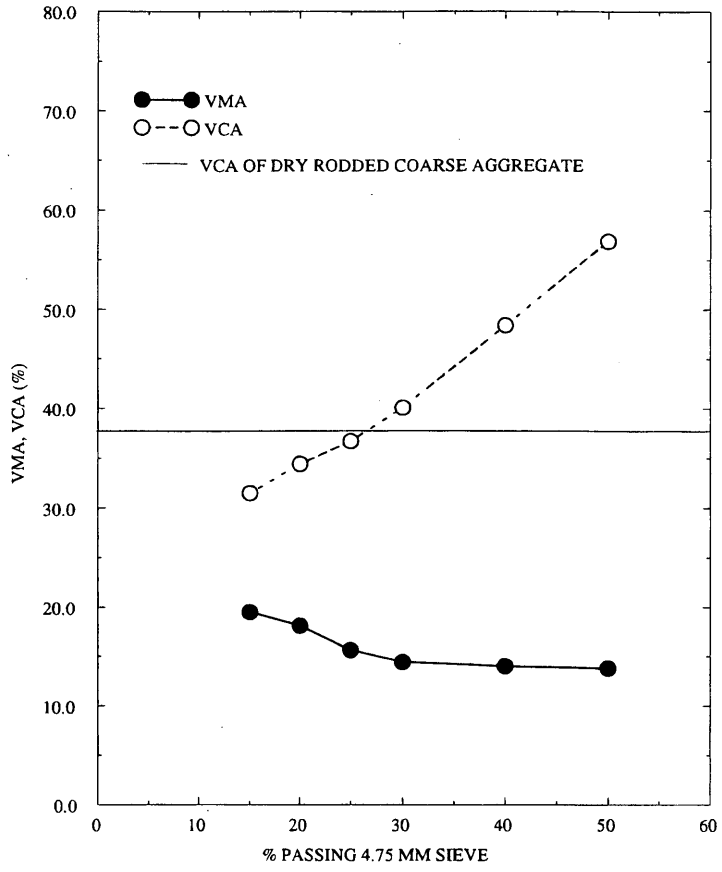

FIGURE 4 Variation of voids with percent passing 4.75-mm sieve for gravel mixes.

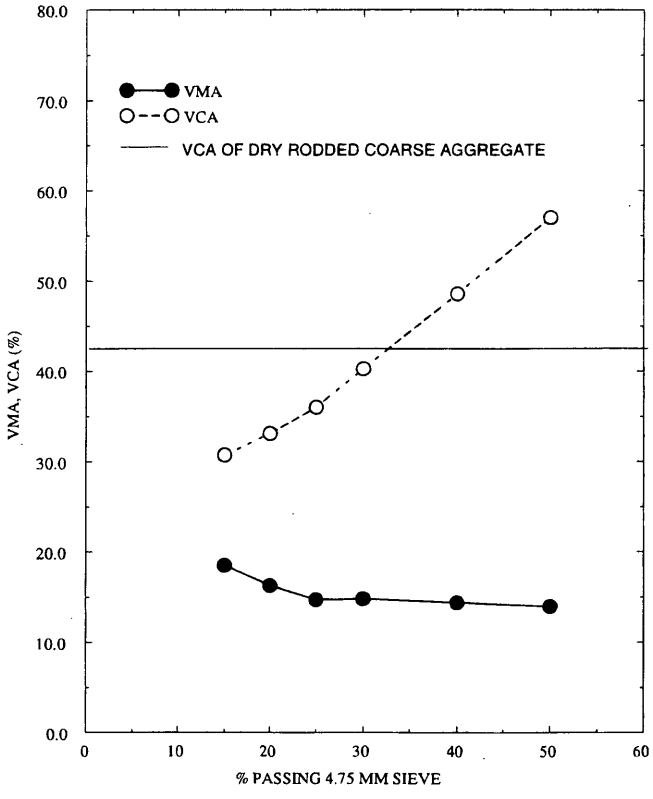

FIGURE 5 Variation of voids with percent passing 4.75-mm sieve for limestone mixes.

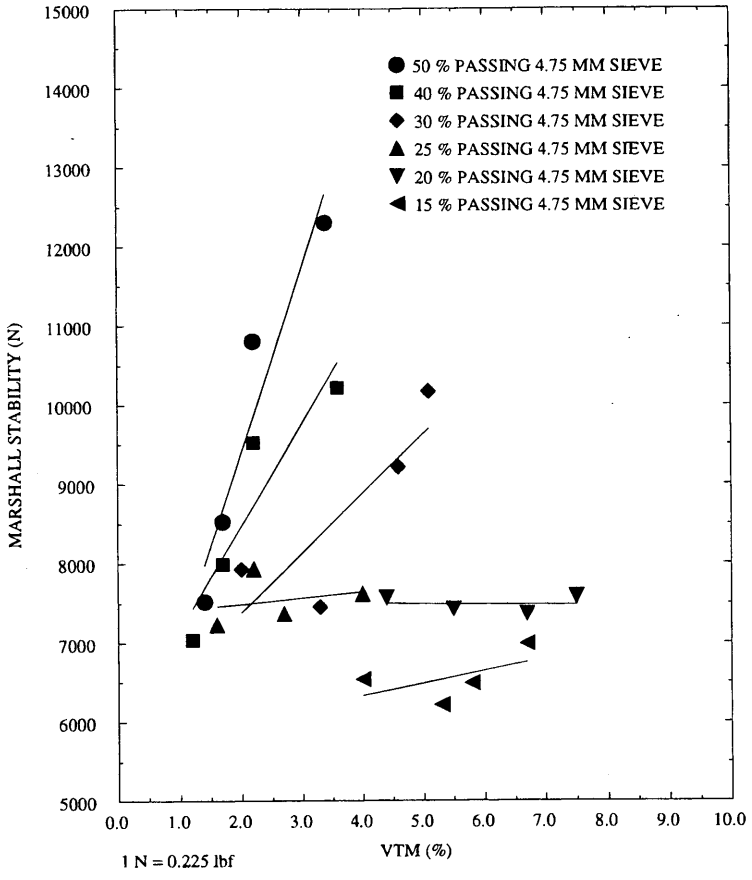

FIGURE 6 Plot of Marshall stability versus air voids for different gravel mixes.

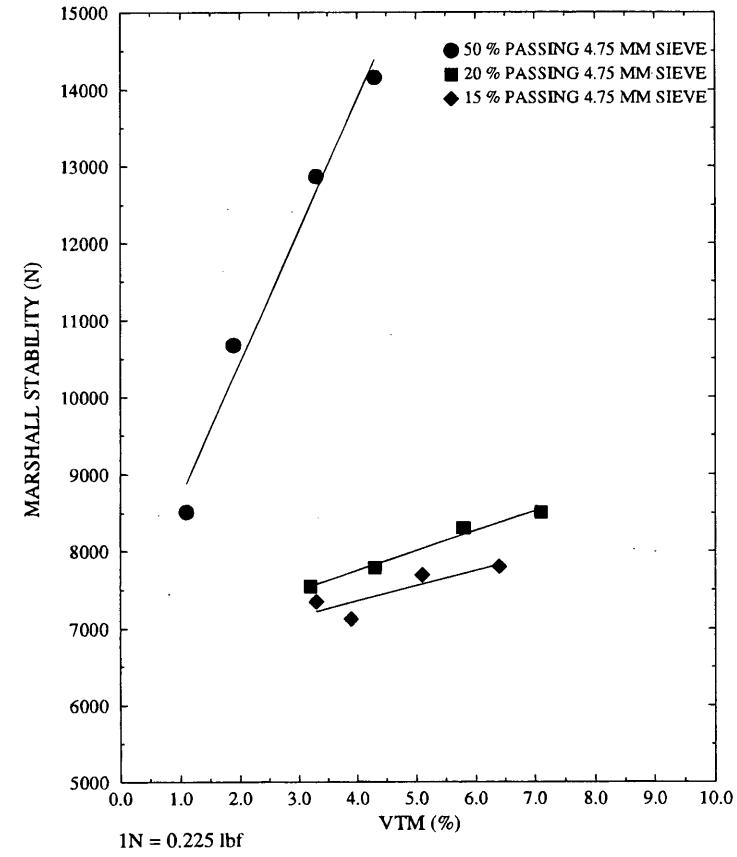

FIGURE 7 Plot of Marshall stability versus air voids for different limestone mixes.

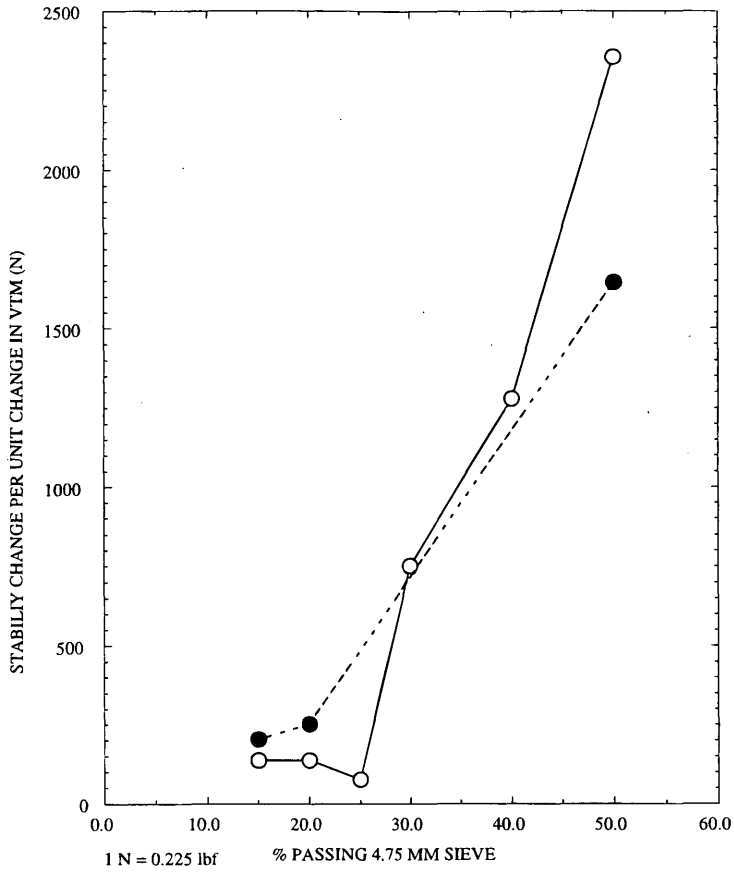

FIGURE 8 Change in Marshall stability per unit change in air void for different mixes.

ing compaction, two parameters were determined for each mix: GSI and Sg.

The GSI is a measure of mixture stability and is related to permanent deformation (*7*). It is determined by dividing the highest gyration angle by the initial angle. The gyration angle increases during compaction for unstable mixtures because of plastic flow of the HMA but does not increase significantly for stable mixtures. GSI values close to 1.0 have been shown to be typical for stable mixtures, and values significantly above 1.1 usually indicate unstable mixtures (*7*).

As the percent passing the 4.75-mm sieve is decreased, the coarse aggregates start moving closer to each other. As observed from the first phase of this study, stone-on-stone contact began to occur at 26 to 30 percent for gravel and at 25 to 32 percent for limestone. It was expected that at percents below the point of stone-on-stone contact, stability of mix would be less affected by air voids. GSI values for the mixes with different percents passing the 4.75-mm sieve and at different void contents are shown in Table 4. The results are plotted in Figure 9. The mixes with low percents passing the 4.75-mm sieve (20 and 25 percent) had GSI values very near 1 (around 1.05) at all voids contents. Mixes with 50, 40, 35, and 30 percent passing the 4.75-mm sieve showed an increase in GSI with a decrease in void content. This indicates that mixes with 30 percent and greater passing the 4.75-mm sieve became unstable at low void contents. Figure 11 shows the change in GSI values per unit change in void content. The change in GSI decreased when the percent passing the 4.75-mm sieve was decreased to 35 percent passing. The change was about 0.11 per percent voids at 50 percent, increased to about 0.12 per percent voids at 40 percent, and dropped considerably to about 0.01 per percent voids at 20 percent passing the 4.75-mm sieve.

Sg is a measure of the shear strength of the mix during compaction. This strength, measured at a high temperature [149°C (300°F)], is primarily a measure of aggregate properties because the viscosity of the asphalt is low and the mix has less cohesion (*7*). Sg values of the limestone mixes with different void contents are shown in Table 4. The results are plotted in Figure 10. The shear values decreased with a decrease in a void content for the mixes with 30, 35, 40, and 50 percent passing the 4.75-mm sieve. The Sg values dropped below 200 kPa at 3 percent and lower voids for mixes with 50 and 40 percent passing the 4.75-mm sieve. The change, although present, was less in the case of mixes with 35 and 30 percent passing the 4.75-mm sieve. However, for the mixes with low percent passing the 4.75-mm sieve (20 and 25 percent), the values remained almost constant (between 270 and 300 kPa) as the voids changed. Figure 11 shows a plot of change in Sg per unit change in void content. The change in Sg decreased with a decrease in percent passing the 4.75-mm sieve, from 66 kPa per percent voids at 40 percent to 3 kPa per percent voids at 20 percent passing the 4.75-mm sieve. It was expected that mixes with less than 30 percent passing the 4.75-mm sieve would be less sensitive to void content and hence would be able to maintain better resistance to rutting even when a gradual densification and resulting decrease in voids occurred. These data confirmed that mixtures with stone-on-stone contact are much less sensitive to air void content than mixtures without stone-on-stone contact.

TABLE 4 Summary of Gyratory Properties of Limestone Mixes

PERCENT PASSING 4.75 mm (NO. 4) SIEVE	VOIDS IN TOTAL MIX (%)	GYRATORY SHEAR INDEX	GYRATORY SHEAR (kPa)
50	0.3	1.57	17.2
	0.5	1.53	120.6
	0.8	1.43	234.3
	4.5	1.10	268.7
40	0.3	1.47	10.3
	1.3	1.26	124.0
	2.3	1.23	155.0
	3.0	1.13	199.8
35	0.3	1.45	689.0
	1.7	1.10	172.2
	1.8	1.17	258.4
	3.6	1.08	258.4
30	0.2	1.25	124.0
	1.1	1.03	251.5
	1.7	1.06	289.4
	2.5	1.01	309.4
	4.2	1.10	296.3
25	0.7	1.04	272.1
	2.0	1.00	274.2
	3.3	1.00	274.9
	4.1	1.05	289.4
20	1.0	1.04	296.3
	2.0	1.01	296.3
	3.3	1.02	292.8
	3.7	1.00	310.7

1 kPa = 0.145 psi

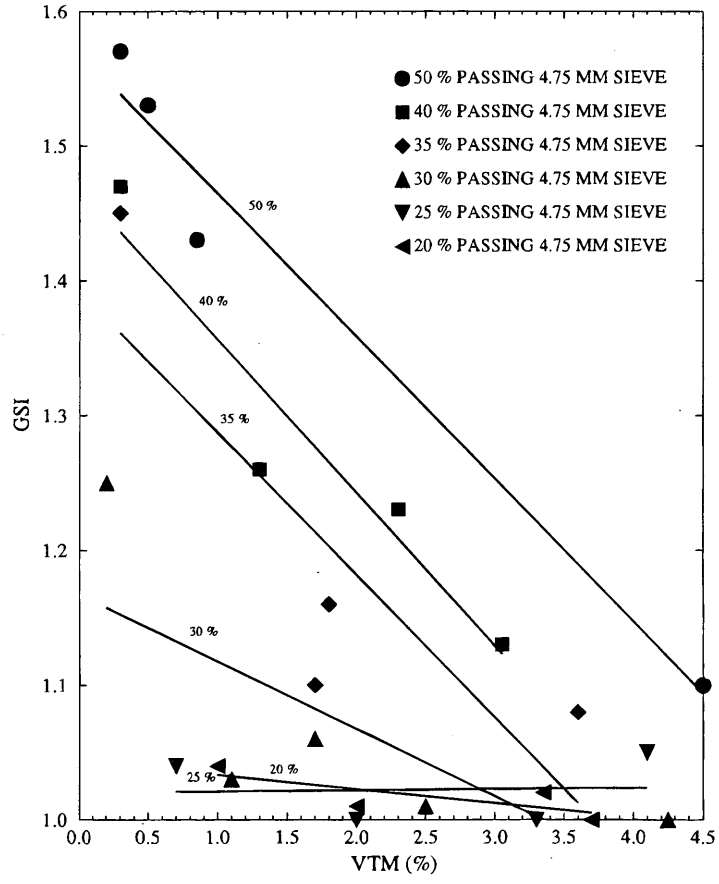

FIGURE 9 Plot of gyratory shear index (GSI) versus air voids for different mixes.

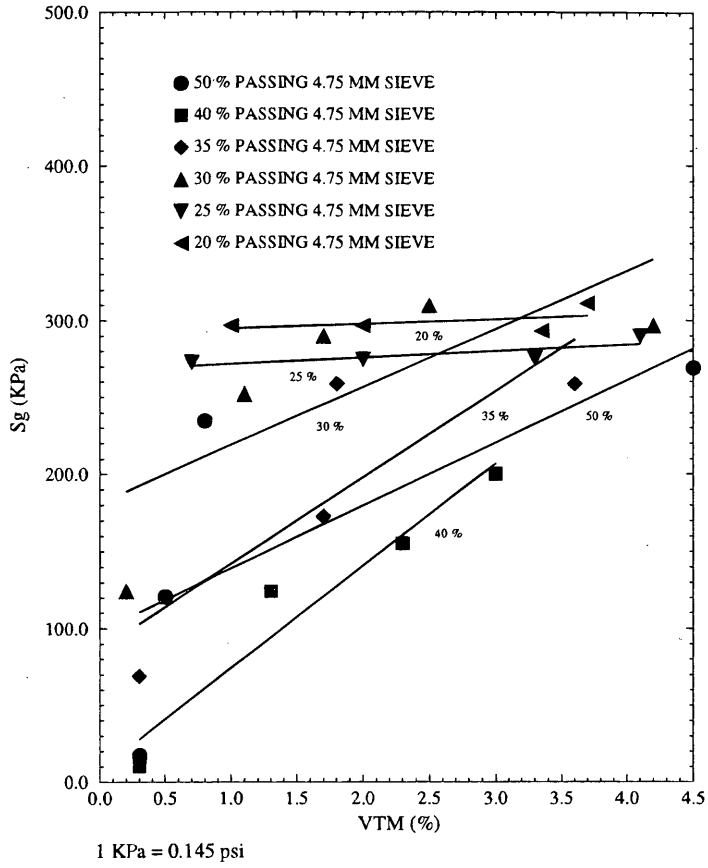

FIGURE 10 Plot of Sg versus air voids for different mixes.

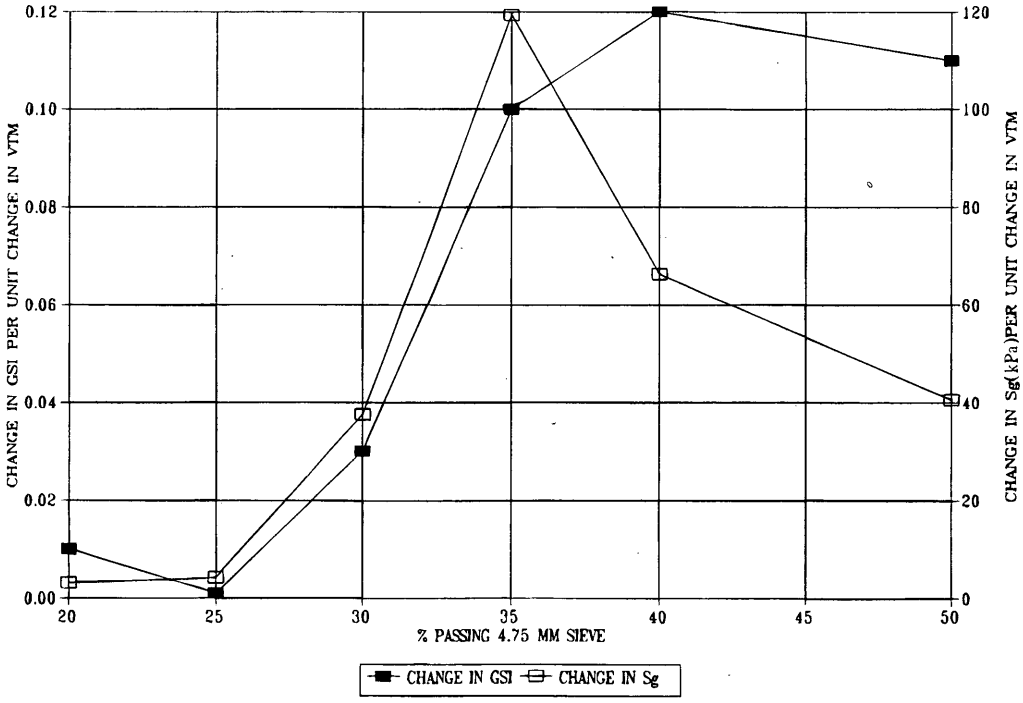

FIGURE 11 Change in GSI and Sg per unit change in air void for different mixes.

CONCLUSIONS

From the results of this study, it can be concluded that plots of VMA and VCA can be used to identify whether stone-on-stone contact exists. For the mixture evaluated in this study, stone-on-stone contact in the coarse aggregate portion began to occur at around 30 percent passing the 4.75-mm sieve. The dry-rodded test appears to be an easy way to determine the VCA necessary for stone-on-stone contact. These three methods appear to give similar results.

Stability tests indicate that mixes become less sensitive to a change in void content with a decrease in percent passing the 4.75-mm sieve and the resulting formation of stone-on-stone skeleton. As the percent passing the 4.75-mm sieve is decreased to 30 percent and lower for both gravel and limestone mixes, stone-on-stone contact occurs. These mixes with stone-on-stone contact were found to have very little or no change in stability, GSI, or gyratory shear strength with change in air voids.

REFERENCES

1. Application of European Technology for Improved Pavement Performance. Presented at meeting of the Association of Asphalt Paving Technologists, Charleston, S.C., 1992.
2. *Asphalt Technology News,* Vol. 3, No. 2, Sept. 1991.
3. Scherocman, J. A. SMA Reduces Rutting. *Better Roads*, Vol. 61, No. 11, Nov. 1991.
4. Davidson J. K., and G. J. Kennepohl. Introduction to Stone Matrix Asphalt in Ontario. Presented at meeting of the Association of Asphalt Paving Technologists, Charleston, S.C., 1992.
5. Brown, E. R., and R. Basu Mallick. *Stone Matrix Asphalt—Properties Related to Mixture Design.* Draft Report. NCAT Publication No. 94-2. Auburn University, Auburn, Ala., Feb. 1994.
6. Brown, E. R. Evaluation of Stone Mastic Asphalt Used in Michigan in 1991. In *Transportation Research Record 1427*, TRB, National Research Council, Washington, D.C., 1993, pp. 54–60.
7. Roberts, F. L., P. S. Kandhal, E. R. Brown, D-Y. Lee, and T. W. Kennedy. *Hot Mix Asphalt Materials, Mixture Design, and Construction*, 1st ed. NAPA Education Foundation, Lanham, Md., 1991.

Publication of this paper sponsored by Committee on General Asphalt Problems.